UNIVERSITY OF
BIRMINGHAM

SEISMIC EVALUATION OF VIBRO-STONE COLUMN

by

AZIMAN MADUN

A Thesis submitted to
The University of Birmingham
For the degree of
DOCTOR OF PHILOSOPHY

School of CIVIL ENGINEERING
College of ENGINEERING AND PHYSICAL SCIENCES
The University of Birmingham
May 2012

ABSTRACT

Ground improvement work is crucial in enhancing the characteristics of weak soils commonly encountered in Civil Engineering, and one such technique commonly used is vibro-stone columns. An assessment of the effectiveness of such an approach is critical to determine whether the quality of the works meets the prescribed requirements. Conventional quality testing suffers limitations including: limited coverage (both area and depth) and problems with sampling quality. Traditionally quality assurance measurements use laboratory and in-situ invasive and destructive tests. However geophysical approaches, which are typically non-invasive and non-destructive, offer a method by which improvement profiles can be measured in a cost effective way. Of these seismic surface waves have proved the most useful to assess vibro-stone columns, however, to date much of the previous work conducted has focussed on field based observations making detailed evaluation of this approach difficult. This study evaluates the application of surface waves in characterizing the properties of laterally heterogeneous soil, specifically for using in the quality control of vibro-stone column. Three models were employed which began with a simple model and extended finally to complex model: (1) concrete mortar was used to establish the method, equipment and its system, (2) pilot test on a small scale soft kaolin to adopt a model vibro-stone column and (3) main test contained a configuration of vibro-stone column in soft Oxford clay. A generic scaled-down model of vibro-stone column(s) was constructed. Measurements were conducted using different arrays of column configuration, using sand to simulate stone material. This idealized set of laboratory conditions were used to provide guidelines for the interpretation of field measurements. The phase velocity obtained from the controlled tests showed close

agreement to those reported in literature and with those generated through empirical correlations with vane shear test. The dispersive curve demonstrated an increased phase velocity with increasing wavelength for the measurements on the clay (between columns), and decreased phase velocity with increasing wavelength for the measurements on the column. More interestingly, the results showed that in the characterization of lateral non-homogeneities, the phase velocity versus wavelength relationship varies on stone columns of different diameters and densities. This illustrated that the shear modulus profiles are influenced by the effective region that spans both the lateral and depth axes, and also demonstrated how the results can be influenced by the positioning of sensors with respect to the survey target. This research demonstrates how Rayleigh waves can be used for quality assurance when constructing vibro-stone columns.

DEDICATION

For my loving mother, late father, wife, sons
(Rasimah Ahmad, Madun Ishak, Kamsiah Ahmad, Muiz, Fauzan and Irfan)
and all my teachers.

ACKNOWLEDGMENTS

I would like to acknowledge gratefully for the assistance receive from the following:

Dr Ian Jefferson for his constant supervision, guidance and encouragement which contributed to the success of the study.

Dr David N. Chapman and Professor Martin Culshaw for their opinion and advice as co-supervisors.

Mr Phillip Robert Atkins for lending his laboratory testing equipments, as well as sharing his knowledge and experience on the testing and the signal processing.

Dr Andrew Foo for helps in writing the Matlab script, setup the laboratory tests and interpretation the results.

Professor Bogdan Piwakowski, Dr. Giovanni Cascante, Chistopher Leech, Jerry Sutton for their suggestion in development the seismic surface wave for laboratory use.

Dr David Gunn and Dr Andrew Thomas for helps in my early understanding of seismic surface wave.

Professor Stewart Greenhalgh, Professor Jianghai Xia and Dr. Sebastiano Foti, for helping in interpretation of seismic surface wave results.

Ministry of Higher Education Malaysia for granting the scholarship.

Employer University Tun Hussien Onn Malaysia for permission of study leave and sponsoring family allowances.

Lab technicians' Mr Michael Vanderstam, Mr David Cope, Mr Jim White, Mr Nathan and Mr Bruce Reed for their support.

Friends in MCiB familys' and post graduate members' in room F59A (August 2007 to July 2011) for their help and support.

Finally member of family for their patience and understanding.

TABLE OF CONTENTS

LIST OF FIGURES

LIST OF TABLES

LIST OF ABBREVIATIONS

A_c/A	Area replacement ratio
A_c	Cross-sectional area of one column
ϕ	Phase angle
2-D	Two dimensional
4D	Ratio of wavelength and column diameter
A	Plan area of the unit cell attributed to a single column
A-B	Sensor pair between A and B
B	Bulk modulus
B-C	Sensor pair between B and C
BNC	Bayonet Neill-Concelman connector
C-D	Sensor pair between C and D
CPT	Cone penetration test
CSW	Continuous surface waves analysis
c_u	Undrained shear strength
d	Distance between the source and the first receiver
d_{col}	Column diameter
d_g	Stone diameter
e	Void ratio
E	Young's Modulus
E_{op}	Operational stiffness
f	Frequency
f_c	Sleeve friction
FEM	Finite element method
FFT	Fast Fourier Transform
f_n	Frequency of n (n is integer)
f_s	Sampling rate
G_{max}	Maximum or small strain shear modulus
GPR	Ground penetrating radar
G_s	Specific gravity

HEIC	High energy impact compaction
I	Current
L_{col}	Column length
LL	Liquid limit
MASW	Multi-channel analysis of surface waves
M_{max}	Constrained modulus
MSW	Multi-channel surface wave
N	SPT blow count
NI	National Instruments
PI	Plasticity index
PL	Plastic limit
PMT	Pressuremeter test
P-wave	Compression / longitudinal wave
q_c	Cone resistance
q_u	Unconfined compressive strength
r	Radius
R	Resistance
RIC	Rapid impact compaction
s	Columns spacing
SASW	Spectral analysis of surface waves
SNR	Signal-to-noise ratio
SPT	Standard penetration test
S_r	Degree of saturation
S-wave	Shear / transverse wave
V	Voltage
VSC	Vibro-replacement stone column
w	Water content
Δx	Spacing between the receivers
λ	Wave length
ω	Angular frequency ($\omega = 2\pi f$)
υ	Poisson's ratio

v_p	Compression / longitudinal wave velocity
v_s	Shear wave velocity
v_r	Rayleigh wave / phase velocity
$y_n(k)$	Time-domain signal at n discrete sample and time k
$Y_n(f)$	Spectrum of the signal at n discrete sample and frequency f
$\Delta\phi_{mn}(w)$	Phase difference between receivers m and n at frequency w.
ρ	Soil bulk density
ρ_w	Water density

Chapter 1

INTRODUCTION

1.1 Introduction

By necessity, construction developments are increasing in areas where the ground is generally of marginal quality. As a result geotechnical engineers are being challenged to provide cost effective foundation solutions, which increasingly require modification of marginal ground by improvement techniques to improve the properties of the ground (Charles, 2002). Ground improvement work is crucial in reducing the deformation of weak soils that may arise from loads imposed by civil engineering structures. The efficiency and cost effectiveness require the selection of suitable technique(s) of ground improvement for the prevailing site conditions (Serridge and Synac, 2007).

Generally ground improvement techniques are classified under a number heading. For the purposes of this thesis these are: (1) the first densification, which includes both compaction and consolidation, together with reinforcement through stiffening columns, e.g.

stone columns and (2) chemical, which includes additives such as lime and cements (Charles and Watts, 2002). The third includes the general approach using reinforcement elements, which for this thesis is considered to be a separate and distinct group, not relevant to the work presented herein. Densification through increased dry density treatment is normally suitable for gravelly, sandy and silty soils and consolidation used for clay soils. Stiffening columns are suitable for all types of soils especially for deep softer layers and are often considered to act in a reinforcing way, even though they are conducted via densification methods. It is for this reason that this approach is one of the most commonly used techniques globally (Charles and Watts, 2002). This approach can provide an economic and environmental friendly form of ground improvement technique, which enables the ground to take loads from light structural foundations such as supporting foundations for low-rise housing, industrial developments, waste treatment plants and car parks (McKelvey *et al.*, 2004).

Each ground improvement method needs to take into account the types of improvement and the deficiencies that are to be remedied. Thus, assessment of the effectiveness of ground improvement is critical to determine whether the quality of the works meets the prescribed requirements. Therefore, measurement and evaluation of the engineering properties both before and after treatment is of practical importance (Terashi and Juran, 2000). The parameters that control the quality of the ground treatment can be measured using laboratory tests. However, the process of sample retrieval required for laboratory testing often introduces additional difficulties associated with sample disturbance and the reliability of the sample as a representation of the entire site. As a result, in situ field-testing is often used as this overcomes the limitations presented by the soil sampling

process. Penetration testing, dynamic probing, field vane shear tests and loading tests are examples of conventional field-test techniques used for quality control testing. In situ zone tests using large-scale loading are one of the best indicators to characterize the foundations on improved ground. However, this method is time consuming and expensive. Moreover, load tests may only demonstrate the stiffness of the upper layers of the ground, and may not give information on the characteristics of the underlying strata (Charles and Watts, 2002).

One of the main parameter sets that can be used to predict ground deformation when loaded are the ground stiffness profiles (Matthews *et al.*, 1996; Abbiss, 2001; Moxhay *et al.*, 2008; Clayton, 2011). In addition, structures are always designed to ensure that they perform far from failure and thus operate at small strain ground deformations. Therefore, a sound knowledge of small strain stiffness is essential to make realistic predictions of deformation (Clayton, 2011). Traditionally, the measurement of stiffness profile was carried out by using a combination of laboratory and in situ, invasive field tests. However, geophysical methods, such as seismic surface wave, offer a non-intrusive and non-destructive approach to carry out these measurements. Moreover, geophysical approaches such as this provide a cost effective way to assess site conditions, while overcoming a key limitation of traditional investigative approaches.

A comparison between geophysical seismic-based techniques and conventional geotechnical load-testing methods for the measurement of the ground stiffness profile were presented by Matthews *et al.* (1995) and Clayton (2011), drawing the conclusion that geophysical testing can deliver results of significant quality. However, care is needed not

to overestimate what geophysics can achieve, by understanding geophysical techniques, in particular their limitations (Clayton *et al*., 1995). Thus, geophysical assessment of any ground improvement must be carried out with physical soundings to ensure proper calibration and validation.

Other geophysical techniques such as electrical resistivity, ground penetration radar and magnetism are useful imaging tools, but require significant skill, good knowledge on the geological model of the area and support from the borehole data to interpret the results (Crice, 2005). For example, the resistivity of soils varies depending upon soil types and moisture content. Soil resistivity is primarily controlled by the movement of charged ions in pore fluids. Hence, salinity, porosity and fluid saturation tend to dominate electrical resistivity measurements (Giao *et al.,* 2003). Meanwhile, ground penetration radar has problems in obtaining deeper results when dealing with high conductivity material such as marine clays. By contrast, seismic wave techniques, which depend on the modulus and density of the materials can be converted to very useful parameters for engineering purposes, such as elastic modulus, shear modulus and Poisson's ratio.

Seismic waves propagate in the form of body waves and surface waves, with the difference being that body waves are usually non-dispersive. In a solid and homogeneous medium, the velocity of surface waves does not fluctuate significantly as a function of the distance propagated. However, when the properties of the medium vary with depth, surface waves become dispersive such that the velocity of the propagation varies with respect to wavelength and frequency. Surface waves are also relatively less attenuated as a function of propagation distance as compared to body waves. These two characteristics make it

feasible to apply surface wave analysis for the survey of near-surface soil properties and thus in turn any changes to these properties that subsequently occur.

The conventional surface wave technique using a single pair of receivers, yield one-dimensional results of phase velocity versus depth. To resolve unknown anomalies in a laterally heterogeneous medium, it is necessary to obtain a plot of the phase velocity versus depth as well as a function of lateral distance, and hence using multi-channel receivers is more suitable. Such a method provides information with greater resolution in the lateral dimension and can therefore be used to obtain a qualitative assessment of the variability of geotechnical properties such as stiffness and strength. This enables the detection of features such as voids, fractures and soft spots. The implementation of this technique usually involves the deployment of an array of multiple receivers with the seismic source. This has been successfully demonstrated by Phillips *et al.* (2004), Nasseri-Moghaddam *et al.* (2005) and Xu and Butt (2006) for the detection of sub-surface cavities and Tallavo *et al*. (2009) for the detection of buried timber trestles.

The phase velocities obtained from the surface wave technique will convert to shear wave velocities and thus a shear modulus profile along the tested section. The cross-section of seismic wave velocities will show the lateral heterogeneities of soils due to the inclusion of columns. The key difference in this study is the lateral heterogeneity due to the columns, while being relatively homogeneous with depth. This study is aiming to evaluate seismic wave techniques for use in quality testing of stiffening columns. The method of data processing is a means to success, allowing investigation of the subsurface velocity with

alternate changes of density over short distances. In addition, seismic tests and physical tests will be calibrated for better understanding.

1.2 Research Problem

The theory developed for surface wave tests assumes a layered half space with horizontal, homogeneous and isotropic layers. As a result, the majority of surface wave applications for civil engineering are for the characterisation of layered media. In the past, the surface waves were used to evaluate the quality of stone column works laterally assuming a layered block consisting of soil and column to yield an average stiffness for both materials (Sutton and Snelling, 1998; Moxhay *et al.,* 2001; Redgers *et al.,* 2008). For this study, the surface wave test is used for quality control, which aims to assess a stiffness profile of separate materials namely that of the soil, column and the interaction between them. Thus, a better understanding of the seismic surface wave technique can be achieved in order to evaluate the stiffness profile and in particular its limitations. In the majority of applications, the heterogeneous boundaries of the medium are not known a *priori*. However, in ground improvement applications, the locations of the soil stiffening columns are often known to a good degree of accuracy in the field. The planning of the survey using this knowledge can reduce ambiguities and increase the accuracy and confidence in the measurement. Therefore, a key distinction to this application is that the locations of the soil stiffening columns are usually known, and can thus be individually assessed. However, in the case where the column location is unknown such an approach still has the potential to assess the location and properties of such columns.

1.3 Research Aim and Objectives

The aim of the study is to develop the most appropriate seismic surface wave method for attaining and utilizing data in order to investigate vertical and lateral **shear modulus**, and thus be able to evaluate the quality of ground improvement achieved when using vibro-stone columns. To achieve this aim of study, the following objectives were established:

- to identify suitable seismic surface wave equipment for laboratory scale tests,
- to develop a system for seismic surface wave testing in the laboratory,
- using this to establish an optimal surface wave testing array for data acquisition to evaluate the individual columns and non-column material,
- to identify a suitable data-processing technique in order to investigate both the spatial and vertical profiles of the phase velocity (shear modulus) in the vibro-stone column ground improvement, and,
- to understand the effect of lateral heterogeneity due to column inclusion in relation to the seismic surface wave result and the quality of the vibro-stone column.

The originalities of this research are as follows;

i. The new testing equipment and system for the seismic surface wave tests at laboratory scale has been established (see Madun *et al.*, 2010a).

ii. The seismic surface wave test for obtaining the small strain stiffness profile of column and non-column material has never before been experimented at laboratory scale; therefore

this research utilised the technique to attain and understand the stiffness change in the vertical and lateral directions of the model stone column (see Madun *et al.*, under review)

iii. This research has introduced a seismic source-receiver array to obtain a higher quality of signal-to-noise ratio for reliably assessing the quality of stone columns.

iv. This research has explained the influence of the column with respect to the dispersive curve (phase velocity profile).

1.4 Outline of thesis

Chapter 2 reviews the literature relating to the research, which includes literature on ground improvement, conventional testing methods, laboratory testing and the geophysical testing. **Chapter 3** reviews the literature relating to the use of geophysics, which includes a review on various geophysics methods and focusing on the seismic surface wave method. **Chapter 4** gives the initial testing method, which involved the development of equipment and its system for laboratory testing. The seismic surface wave experimental work began with a concrete mortar model, which involved sample preparation, and development of the test equipment and measurement procedures. **Chapter 5** presents the results of the initial test conducted on the concrete mortar. **Chapter 6** presents the geotechnical properties of materials used in the stone column model and explains the seismic surface wave testing array for the stone column tests and the data processing techniques. In **Chapter 7**, the test results are analyzed, compared to information from the literature and discussed in detail. This is followed by **Chapter 8,** which discusses the results in relation to stone column interpretation. Correlations are made between the

seismic wave results and physical test results. **Chapter 9** summarises the main conclusions from the present work. It also details recommendations for future work based on the author's experience, in the hope that further work will yield beneficial results. A complete list of **References** is included and finally, **Appendices** of relevant topics is found at the end of the thesis.

Chapter 2

GROUND IMPROVEMENT

2.1 Introduction

Ground improvement is used to avoid unacceptable movements, which may occur over the area of a proposed foundation; of particular concern is uneven soil movement. Due to its importance, development of ground improvement techniques has been continuous over the past 30 years and with many new applications being introduced. As a result, the assessment of the quality of the improvement achieved is vital especially as techniques become more sophisticated, to ensure key improvement targets and specifications are met.

2.2 Ground Improvement Techniques

Types of ground improvement can be classified in a number of ways. This thesis concentrates on densification approaches due to their popularity and these include

compaction, consolidation methods and stiffening columns (Charles, 2002), as shown in Figure 2.1. A number of the key ground improvement techniques aim to improve the bearing capacity, enhance settlement resistance, increase shear strength and, thus increase soil stiffness modulus. A detailed explanation of the various ground improvement techniques is provided by CIRIA C572 (Charles and Watts, 2002) and C573 (Mitchell and Jardine, 2002) and summarised below (see Sections 2.2.1 to 2.2.3).

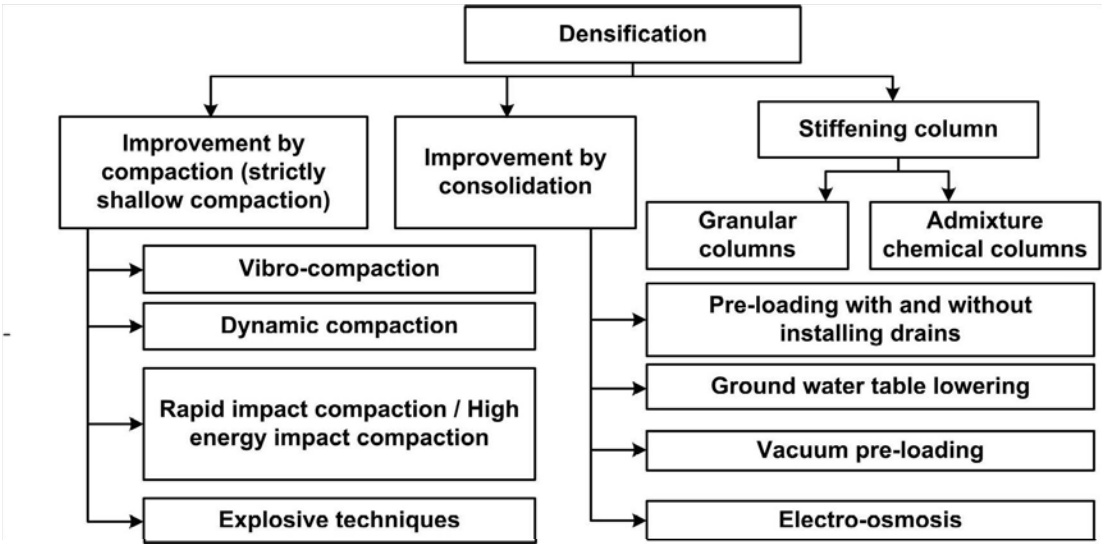

Figure 2.1: Types of ground improvements using broad densification family of approaches (Charles and Watts, 2002).

2.2.1 Densification

Densification of the ground by mechanical means is called compaction. Compaction of loose granular soils, heterogeneous soils, municipal wastes and liquefiable soils is common practice for increasing density and strength, hence reducing the volume of the

soil. This prevents excessive settlement when the treated ground is vibrated or loaded (Raju and Sondermann, 2005).

Improvement by compaction is suitable for soils that have larger particle sizes, such as gravel and sand, which allow excess pore water pressures generated during compaction to easily dissipate and, thus the soil grains can readily move closer together. In contrast, compaction in clay is only effective for shallow depths due to water retention by the soil skeleton making fine grained soils difficult to compact. Vibro-compaction is one such technique to densify coarse-grained soils (Charles and Watts, 2002). The soils are densified by the use of a vibrating probe known as a vibroflot or poker (McCabe *et al.*, 2009). The silt and clay fraction in the soil must be less than 15 to 20 % to achieve effectiveness from this method. The vibro-compaction technique is capable of penetrating down to a depth of 65 metres; thus it is commonly applied in major infrastructure projects throughout the world (Raju and Sondermann, 2005). Examples include The World and Palm Island projects off the Dubai coast (McCabe *et al.*, 2009).

Another densification technique is called dynamic compaction, which can be described as systematic tamping of the ground surface with a heavy weight dropped from a given height. Materials for which this technique is suitable include loose fills, loose sand, waste and mine tailings, collapsible soils and fine grained soils (Terashi and Juran, 2000). The final densification technique in this group includes rapid impact compaction (RIC), which uses energy from repeated blows; with compaction occurring as a result of a relatively high frequency generated from a hydraulic hammer through an anvil in a tamping foot resting directly on the ground. In addition, high energy impact compaction (HEIC) can be

used, with densification occurring as a result of an eccentric roller being towed behind a moving vehicle. However, both RIC and HEIC compact soils only to a few metres depth (Charles and Watts, 2002).

Densification improvement also includes techniques that use consolidation. The consolidation process mainly involves a combination of seepage developed due to changes in hydraulic gradients and changes in effective stress (Atkinson, 2007). For ground that consists of fine-grained soils that have low strength and low permeability, long-term settlement will cause densification if loaded by structures. Thus, these soils are expected to increase in strength and decrease in compressibility with time when loaded (Haegeman and Baertsoen, 2007). Consolidation methods consist of pre-loading with a surcharge of fill or, if required accelerated by the installation of vertical drains. In other situations, increasing the effective stress via lowering the ground water level will result in consolidation. Generally, this technique can be divided into two categories, either increase in total stress via a vertical load added by surcharge on the top of permanent fill, or increase in effective stress via lowering the ground water level achieved via drainage or vacuum pre-loading (Mitchell and Jardine, 2002).

2.2.2 Stiffening Columns

This is a technique that involves the construction of a composite system of columns of substantially greater stiffness than the surrounding soil. Two different types of columns are used to stiffen the ground: granular columns and admixture chemical columns. The creation of the granular columns uses dynamic replacement, sometimes called vibro-

replacement and also includes vibro-stone columns, formed by the replacement of soil with stronger stone materials (Charles, 2002). For the purposes of this thesis these have been classed as a densification approach due to their method of installation using vibro-flot, used also with other densification approaches. The admixture chemical stabilization column was developed in Japan in the 1970s. This method uses mixing blades and chemical additives to create an in situ column of predetermined diameter and length (Terashi and Juran, 2000). The main improvement mechanism with admixture stabilisation is via chemical reactions between the mixtures and the clay mineral, resulting in bonding of the soil particles and filling of the void spaces. The influential factors are the characteristics of the hardening agent, the characteristics of the soil, the mixing conditions, and the curing conditions. Hence, this approach has been classified separately from granular columns.

2.2.3 Vibro-stone Columns

The research repeated herein is primary aimed at examining the properties of vibro-compaction and vibro-replacement granular columns. This is because, firstly, the vibro technique is one of the world's most widely used forms of ground improvement and, secondly, because of the advantages of vibro techniques, compared with traditional techniques using the replacement of unsuitable material, which are often impractical due to economic and environmental issues (McCabe *et al.*, 2009). Therefore, ground improvement using the vibro technique can be employed to overcome this difficulty. The method has a proven record of success (Barksdale and Bachus, 1983) due to its capability to treat a wide range of weak soils from sand to clay.

For application to soil that consists of more than 85 % of coarse grained particles (larger than 63 μm) the technique known as the vibro-compaction column is used. For fine grained soils, the vibro-granular column or vibro-replacement column is used. However, the confining pressure provided by the surrounding weak soil greatly affects the bearing capacity of the stone columns. Thus, it is not suitable for very soft soils or soils with high organic content, such as peat, which have very low undrained shear strengths were the lateral support may be too small (Raju and Sondermann, 2005). Factors of three-dimensional behaviour include: the behaviour of adjacent columns, the dilation of column material (Van Impe and Madhav, 1992) and the rapid increase in the soil shear strength due to the stone column drainage effect (Guetif, *et al.*, 2007).). This rapid increase effects have resulted in the vibro-granular technique being successfully applied in much softer soils (Raju and Hoffmann, 1996).

Completed stone column projects indicate that most of the applications were on soils having an undrained shear strength around 30 kPa and only in a few cases was the strength below 15 kPa (McCabe *et al.*, 2009). For very soft soils, a technique of using geotextile coating around the column is used to obtain lateral support, thus avoiding lateral spreading of the column (Sondermann and Wehr, 2004). In other cases, a sand layer is placed on top of the soft layer, which results in some consolidation and assists in providing lateral support to the columns at the top. This has the added advantage of providing a safe working platform for the heavy equipment (Raju, 2002).

The vibro-granular columns typically consist of crushed rock or alternative material such as recycled materials, for example railway track ballast or crushed concrete (Serridge, 2005). The construction of granular columns within fine grained soils creates a composite soil mass, which has a greater average strength and stiffness, and lower compressibility than the untreated ground. As a result vibro-granular columns have been successfully applied to improve slope stability, increase bearing capacity, reduce total and differential settlement, reduce the liquefaction potential of sand and increase the rate of settlement (Raju 2002; Raju and Yandamuri, 2010).

The stiffness of the stone column is generated by the lateral stresses provided by the surrounding soil thus providing confinement of the stone column. With ultimate vertical load, the failure mechanisms of single stone columns are typically as a result of relatively low lateral support in the upper soil layer causing a bulge to occur at the depth of 2 to 3 column diameters (Barksdale and Bachus, 1983). It can also be a result of the column toe being punched into the underlying soil, such as with 'floating' foundations. Bulging causes an increase in the lateral stress within the untreated soil (Sondermann and Wehr, 2004).

The effect of stone column groups when loaded is to increase the ultimate load capacity of each of the single columns, resulting in less bulging compared with a single stone column. In the case of embankment, although strengthened by a group of stone columns, failure occurs due to the untreated soil outside the treatment zone, when the soils move laterally outward from the column area toward non-reinforced soil. This phenomenon is called 'spreading', which causes greater settlement (Tavenas *et al.*, 1979).

There are many design methods for calculating settlement of stone columns such as the equilibrium method, Priebe's method, the incremental method and the finite element method (FEM) (Barksdale and Bachus, 1983). These methods used the extended unit cell concept, which has the same conditions of loading. Priebe's method is commonly used in Europe, where the application is relatively simple as the relevant settlement ratio depends on the number and diameter of the stone columns together with the treatment depth considered (Sondermann and Wehr, 2004). The improvement factors are dependent on the angle of internal friction of the stone column, the ratio of the stone column area and the area being treated by the column material. The improvement factor indicates how many times the compression modulus increases for a grid of stone columns and to what extent the settlement will be reduced. However, there is still no acceptable design method, which can adequately account for all mechanisms that are part of the load transfer process (McKelvey *et al.*, 2004). Therefore, the use of simulation calculations by the FEM to determine the stress-deformation behaviour are recommended in the design phase (Kirsch, 2009). In addition, a trial column using load tests is highly recommended before execution of ground improvement projects to ensure an effective design (Terashi and Juran, 2000).

The vibro-replacement method consists of two approaches: the dry displacement method for soil that has low water content and the wet method for high water content. Currently, for the dry method vibrators are used to produce vibro-stone columns in fine grained soils that must be able to hold the form of the entire cavity after the vibrator has been removed. This allows for the subsequent repeated delivery and compaction of stone column material to proceed without any obstruction. The compressed air from the vibrator tip does not only flush out the drilled product but also prevents the drill-holes collapsing. For the wet

method, the use of a strong water jet injects water under high pressure to flush out loosened soil and mud rises to the surface. As a result, the cylindrical drill-holes are temporarily stable. The cavity is then filled and compacted in stages by repetitive use of the vibrator (Raju and Sondermann, 2005). However, the wet method is less commonly used in recent years due to environmental issue. Recently dry top feed or bottom feed approach of installation have been used. Figure 2.2 shows the dry process of stone column installation using both approaches.

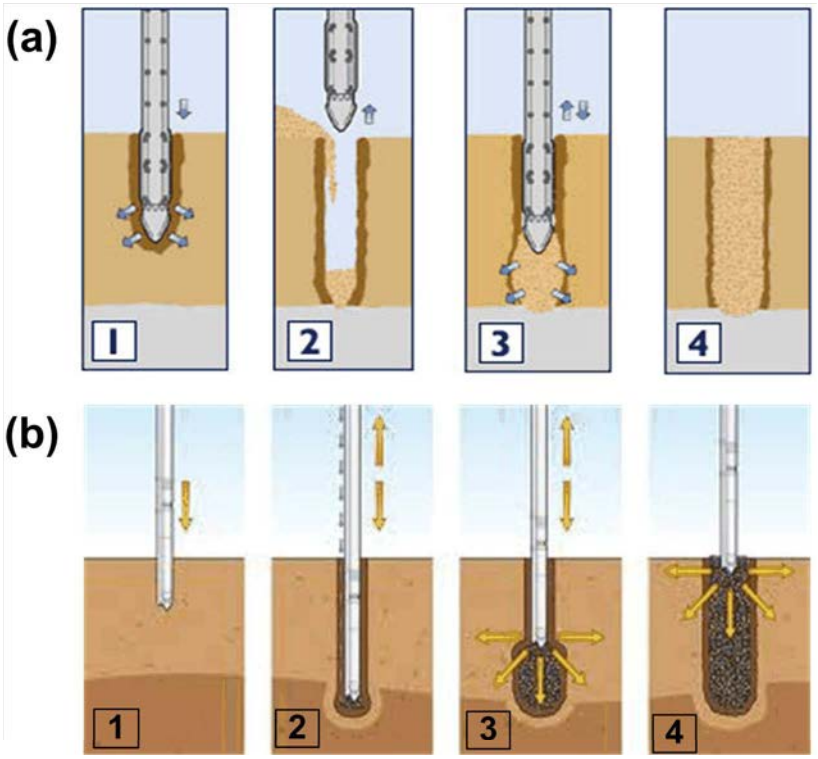

Figure 2.2: Stone column installation methods (a) the top and (b) the bottom feed of stone respectively (Raju *et al.*, 2004).

Uncertainties emerge at most of the stages of ground improvement. They could arise from the choice of the ground improvement technique, which involves identifying soil

properties as part of building the soil model. In the design stage of a stone column, uncertainty is involved in the design assumption of estimating the quantities of settlement that will occur. The process of constructing the vibro-stone columns involves issues relating to the ground, people and mechanics such as discrepancies in soil model, lack of adequate site supervision, inexperienced contractors and ineffective machinery, which could affect the quality of the vibro-stone column. Therefore, quality control is needed to ensure the design objectives are achievable.

2.3 Quality Control

In parallel with the development of new techniques of ground improvement, quality control has been developed significantly since the 1970s (Mitchell and Jardine, 2002). Quality control is important to ensure improvements are designed and produced to meet or exceed customer requirements. Quality control tests similar to site investigation tests are commonly used to verify the quality of works.

More recently, geophysical techniques have been applied in quality control tests thus enabling assessment of a greater area of improved soil. The application of geophysical techniques has been steadily growing in civil engineering studies due to the development of new geophysical testing equipment and analysis software. This has led to an increased number of field testing techniques using geophysics. Geophysical testing has significant advantages including being relatively rapid to undertake (and so more cost effective),

being non-destructive and providing representative values of soil parameters over a relatively large area (Butcher and Powell, 1995).

The quality and performance of the ground treatment methods are controlled by many factors, such as the accuracy of original soil data, precision of design tools, quality of materials used, employees' experience, construction schedule and weather (Terashi and Juran, 2000). Quality control needs appropriate specification and adequate supervision for success. Testing should be conducted at different times, including preferably before treatment, during treatment and after treatment, to understand the behaviour pre- and post-treatment.

Before treatment, site investigation is used to identify the ground engineering properties, such as load-carrying characteristics, typically using laboratory tests, in situ field tests, geophysical tests or some combination of these. In addition, when construction takes place, inspection by experienced personnel assisted by electronic devices fitted on the plant used in the improvement process, is commonly employed nowadays (Terashi and Juran, 2000). This enables the position, depths, quantities, feed rates, withdrawal and compaction times, for example, to be measured directly and allows indirect correlations to a ground's response to be determined. Post-treatment testing methods are used to assess the effectiveness of any works. Monitoring of ground improvement may be continued even after the completion using settlement markers, multilevel settlement gauges and pore water pressure monitoring to obtain the necessary information for future maintenance work (Silva, 2005; Chu and Yan, 2005). These stages of quality control are conducted through laboratory tests and in situ field tests.

2.3.1 Laboratory Tests

In laboratory testing, samples are examined according to parameters used in the design to see whether the parameters fulfil the design criteria. Laboratory testing involves retrieving soil samples from the field. An important geotechnical parameters for predicting the soil deformation is stiffness, traditionally determined using various types geotechnical apparatus, including unconfined compression tests, triaxial compression tests, bender elements or the resonant column.

The unconfined compression test and triaxial compression test are destructive tests and usually used for fine grained soils. The triaxial compression test tends to produce more usable values of soil stiffness modulus since the confining pressure stiffens the soil so that a small strain modulus can be obtained (Abdrabbo and Gaaver, 2002).

The bender elements and resonant column tests are increasingly used in the laboratory. Both tests are performed using reconstituted specimens, which have similar soil properties to the improved soil. The bender elements system allows measurement of very small strain stiffness modulus, G_{max}, by measuring the velocity of shear wave transmission through a test specimen as described by Hooker (2002) and Clayton (2011). The bender element uses a piezoelectric strip as a transmitter and receiver at both ends of a test specimen. The transmitter piezoelectric strip is connected to a waveform generator and recorded by a receiver piezoelectric strip via an oscilloscope. The shear wave can be used to calculate the value of G_{max}. To improve the reliability and repeatability of results,

Clayton *et al.* (2004) increased the number of receivers along the side of a sample as shown in Figure 2.3, therefore measuring the coherence of the received signals via cross-correlation. This enables the signal-to-noise quality to be measured as a function of frequency, thus reliability data can be assessed.

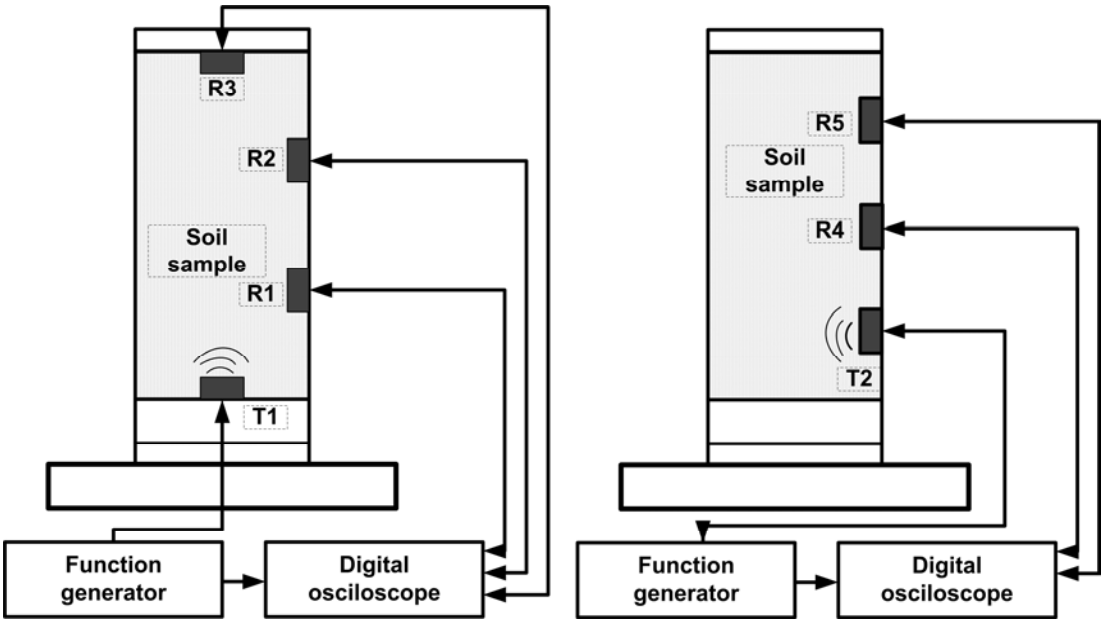

Figure 2.3: Layout of bender elements, and instrumentation, using multiple receivers to increase their reliability and repeatability (Clayton *et al.*, 2004). Note: R represents receivers and T transmitters.

The resonant column testing is similar to the bender element method and measures G_{max} for a cylindrical test specimen. One end of the test specimen is fixed and the other end is excited with a very small, sinusoidal, rotational displacement. Excitation is swept through a range of frequencies to identify the frequency at which resonance occurs. From the information about the specimen and the resonant frequency, the value of the wave propagation velocity can be derived and G_{max} calculated (Hooker, 2002).

As the stiffness modulus is a function of strain (Atkinson, 2007), the laboratory destructive tests always gives the lower bound of soil stiffness modulus compared with laboratory non-destructive tests at upper bound. This occurs due to the different strain level of measurement (see Chapter 3, Figure 3.8 and Section 3.5 for more details). In laboratory destructive tests, the unconfined compression test tends to give conservative values of soil stiffness modulus, where the stiffness modulus value is relatively small compared with the triaxial test. Meanwhile, both laboratory non-destructive tests give maximum stiffness modulus values.

2.3.2 In situ Field Tests

In situ field testing enables larger volumes of soil to be tested and so tends to be more representative of the soil mass compared with laboratory testing. In situ field tests have an advantage as samples do not need to be retrieved. For very soft clays, sands and gravels, sampling is a major problem because these materials easily change their soil structure and, as a result, produce disturbed samples. Good correlations have been produced between field tests and laboratory tests, which has led to acceptance of field techniques (Charles and Watt, 2002). For example, there was a correlation between the undrained shear strength obtained from the laboratory test on undisturbed clay samples and the cone resistance (q_c) from the cone penetration test (CPT) which was carried out in the field (Das, 2007). Of the range of in situ tests, penetration testing, dynamic probing, pressuremeter testing, field vane shear testing, plate loading testing and geophysical testing

are used for quality control; with these tests being similar to those used in conventional site investigations. On occasions, some have been modified specifically for quality control testing within ground improvements begs the question what modifications. Table 2.1 summarises the field tests used for evaluating stabilised soils (Hosoya *et al.,* 1996).

The selection of the types of quality control tests to be used is highly dependent on the cost and effectiveness of testing (Clayton *et al.,* 1995; Charles and Watts, 2002). Comparison between laboratory and in situ field test results by Bowles (1996) indicated that the soil stiffness modulus, which was measured in the in situ field test, was found to be 4 to 13 times greater than that obtained from the unconfined compression test and about 1 to 1.5 times that obtained from the triaxial undrained test. Some field quality control tests are considered as destructive tests, which involve preliminary works such as drilling or inserting instruments into the ground. The results from the field tests can be empirically correlated with the parameters, which control mass behaviour (BSI, 2005). For example, pressuremeter test results and penetration resistances are indicators of density. These empirical correlation relationships can be used to estimate other parameters such as shear strength, compressibility and stiffness (Mitchell and Jardine, 2002). A field vane shear test can be used for clayey soil, which directly measures the shear strength of the soil.

Table 2.1: Field tests for evaluating stabilised soils (Hosoya *et al.*, 1996).

Method	Test methods and results	Comment on quality control method
Sounding tests		
Standard penetration test	67.5kg hammer drops free from 750mm height and the number of blows (N-value) to penetrate 300mm are counted.	Most common method on natural soil. There is commonly correlated with unconfined compressive strength.
Dynamic cone penetration test	5kg hammer drops from 500mm height and the number of blows are counted (Nd-value) for cone to penetrate 100mm.	Easy transportation and operation. Practical for unconfined compressive strength within the range q_u of 200 to 500kPa.
Static cone penetration test	The cone penetrates at uniform speed and measures the resistance to the cone, surrounding surface friction and pore water pressure in sequence.	Applicable to measure the improvement of low strength stabilised soil but not for firm stabilised soil.
Rotary penetration test	Measure the bit pressure, torque and mud/ water pressure by a sensor at the end of the boring rod to observe the soil strength in sequence.	Greater mobility compared with core sampling and field strength can be measured. However, correlation with the unconfined compressive strength must be repeated from site to site.
P and S wave logging	Measure the velocity of P and S waves, to calculate rigidity and Poisson's ratio of stabilised soil. Two testing methods: down-hole and suspension method (source and sensors inside the borehole).	There is some correlation with unconfined compressive strength although it is not uniform. Suspension method is better to evaluate the stabilised soils
Tests utilising boreholes		
Electrical logging	Supply electric current to stabilised soil and measure current and voltage through an electrode. Then calculate the specific resistance.	The correlation with unconfined compressive strength is low.
Density logging	Measure gamma rays emitted from a probe inserted into the hole with a detector installed at a certain distance. Then convert the data into density.	Influenced by the hole diameter and water inside the hole, calibration is important. There is no correlation with unconfined compressive strength.
Loading tests		
Borehole lateral load test	Press rubber tube toward the borehole wall in stages and measure the strength and deformation modulus of stabilised soil.	Deformation modulus rather than strength is often the objective of the tests. Vertical measurement is costly so it is used as representative value of stabilised soil.
Plate loading test	Place a loading plate (round plate of 300mm in diameter) on the stabilised soil and add load in stages. Bearing capacity and deformation characteristics can be obtained directly from the load and settlement curve.	Bearing capacity and deformation characteristics can be obtained directly. However, the evaluation of stabilised soil is possible only down to a depth of 2 to 3 times of the (load) plate diameter.
Stabilised pile loading	Load on the top of the stabilised column through the load plate of the same diameter as the stabilised column. The bearing capacity characteristics are obtained from the load and settlement curve.	Bearing capacity characteristics of a stabilised column can be directly obtained. However, testing equipment is costly and the number of tests available is limited.
Non destructive test		
Integrity test	Strike the top of a stabilised column with a hammer and measure the reflected wave of the vibration using an accelerometer. Length and discontinuity of stabilised column is measure.	Simple method. However, evaluation standard for a stabilised column has not been established.
Non destructive test		
Elastic wave exploration	Emit P and S waves to measure the velocity distribution of stabilised soil. In the case of stabilised soil, measurement of S wave is preferred due to independent with the velocity of the soil water content.	Stabilised condition is measured by velocity distribution of the S wave. The measurement is made in the borehole and on the ground surface. Tomography is used to improve accuracy of the test.
Other test		
Penetration test	Use pocket type pin penetration apparatus and measure the penetration resistance of stabilised soil at the site. Then estimate the unconfined compressive strength	Easy and simple method. Many tests can be done. However, only the surface of the stabilised soil can be tested. Test of limited accuracy.

2.3.2.1 Penetration Tests

Penetration tests are used world-wide and commonly include either the dynamic Standard Penetration Test (SPT) or the static or dynamic Cone Penetration Test (CPT). The penetration tests measure the force that is needed for an open sampler or a cone to penetrate the soil. The SPT is the most common in situ test method used and is usually accompanied by other complementary measurements, field or laboratory based, for the purpose of making comparisons and establishing the relevant correlations. For overconsolidated clays in the UK, Stroud (1989) reported that SPT gave a useful guide, where extremely good correlation was obtained between the SPT blow count, N, undrained shear strength, c_u, and plasticity index, PI. The N-values reported have been well-correlated with the unconfined compressive strength obtained from laboratory tests (Kitazume, 2005). Typical correlation between the unconfined compressive strength, q_u, and the SPT N-value, is;

$$q_u = \frac{1}{4} to \frac{1}{3} N \quad \text{..... Equation 2.1}$$

The SPT is, essentially, a simple test involving the dropping of a standard hammer of known weight from a specific height. Empirical correlations are used to obtain the deformation modulus of soil. Table 2.2 shows the different empirical correlations between soil types for estimating the deformation modulus of soil from SPT N-values as reviewed by Bowles (1996).

Table 2.2: Deformation modulus of soil from SPT N-value results (Bowles, 1996).

Soil	Relationship, MPa
Sand, normally consolidated	E=6N
Sand, saturated	E=0.25(N+15)
Sand, overconsolidated	E=40+1.05N
Gravelly sand	E=1.2(N+6)
Clayey sand	E=0.32(N+15)
Silts, sandy silt, and clayey silt	E=0.3(N+6)

Note: E= modulus of soil **in drained condition**

N= numbers of blows from Standard Penetration Test (SPT)

The cone penetration test (CPT), in essence, gives a measured cone resistance, q_c, and the sleeve friction, f_c, from which the friction ratio is derived;

$$R_f = {f_c}/{q_c} \times 100\% \quad \text{..... Equation 2.2}$$

CPT is a versatile test with the capability to measure many soil properties such as pore water pressure, soil resistivity, ground vibration, small strain shear modulus, density and pressure if additional equipment is attached within the CPT cone (Clayton *et al.*, 1995). For example, Shrivastava (2007) combined the CPT with radio-isotopes to measure basic soil properties, namely density and natural water content. As a consequence, CPT has many advantages due to the real time data captured, thus saving time being more cost effective than drilling and sampling operations. Clayton *et al.*, (1995) published examples of correlations between the cone resistance, q_c, undrained shear strength, c_u, and unconfined compressive strength tests, q_u, are;

$$q_c = (15-20) \cdot c_u \quad \text{..... Equation 2.3}$$

$$c_u = {q_u}/{2} \quad \text{..... Equation 2.4}$$

The CPT technique should not be used when the ground is gravelly as this can result in the cone becoming damaged (Charles and Watts, 2002).

The pressuremeter test (PMT) is a type of penetration test that consists of a cylindrical device with a flexible membrane. The tool is operated by inserting the device into a pre-bored hole, expanding a membrane and measuring the radial displacement that occurs. The radial strain is then used to calculate the ground stiffness (Charles and Watts, 2002). However, the PMT gives horizontal ground parameters but not the vertical that are required for settlement calculations. The main disadvantage of the PMT is that it requires a pre-drilled borehole, thus making this technique costly, and the drilling destroys the fabric in the vicinity of the hole, resulting in a reduction of the soil stiffness modulus. Other types of penetration test include the field vane test, which is used to measure in situ undrained shear strength, c_u, of soft clay.

2.3.2.2 Load Tests

Load tests can give a direct measurement of the parameter that controls the mass behaviour (BSI, 2005). Therefore, they are commonly used on large projects to investigate for example the performance of vibro-stiffening columns (Sondermann and Wehr, 2004). The load test is carried out by loading a rigid plate either on a single column or on a group of columns to simulate the size and loading of real foundations. The load test is carried out to assess the in situ vertical deformation and bearing capacity of soils. The ultimate load is related to the strength achieved when there are maximum deformations. Meanwhile, the load-deformation behaviour is related to soil stiffness modulus. If a larger area is tested,

this is commonly known as a zone load tests. Zone tests are usually achieved by constructing and loading a full-size foundation or placing earth fill to simulate widespread loads. However, it is very costly and time consuming, but does gives a more realistic response of actual field condition than smaller load tests.

2.3.2.3 Geophysical Tests

Cost and time constraint factors are the main reasons why it is not easy to evaluate stabilized soils completely. Hence, quality control may only involve the laboratory testing of samples collected by site personnel or field testing for limited areas. This may lead to either an underestimate or overestimate of the strength of the stabilised system. Therefore, to achieve greater certainty of the final quality achieved, a robust quality control approach is needed that allows both pre- and post-treatment to be examined and that can be compared with the improvement specification. Geophysical methods can provide excellent resolution of spatial variability across a site before and after treatment. The main advantages with such an approach are their non-destructive, non-invasive nature and relative speed of assessment. If calibrated, details of stiffness with depth can be relatively easily obtained.

The choice of which geophysics tests to use depends on the parameters to be examined. However, obtaining the soil stiffness profile is particularly important in the ground improvement (Mitchell and Jardine, 2002). Amongst geophysical methods, the seismic method based results empirically derive geotechnical properties such as maximum shear modulus$(G_{\max})$, bulk modulus (*B)*, Young's modulus (*E)*, and Poisson's ratio (υ) (Charles

and Watts, 2002; Crice, 2005). The seismic-based techniques have proved particularly useful in determining shear modulus profile from ground treatment (Moxhay *et al.*, 2001; Redges *et al.*, 2008). See Chapter 3 for further details.

There are two methods of obtaining seismic wave data that can potentially be used for ground improvements (1) borehole methods and (2) surface methods, as shown in Figure 2.4 (Menzies, 2001). Table 2.3 explains the advantages and disadvantages of seismic-based methods. Surface wave data collection uses the surface method, which is more versatile than other methods because it is not constrained by any ground models, see Table 2.3 (b) and considered more economical in terms of field operation (Matthews *et al.*, 2000).

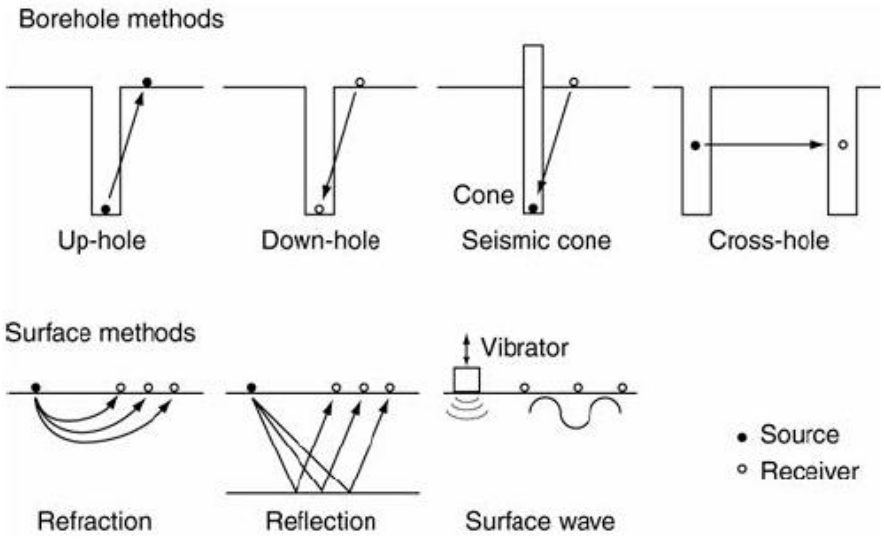

Figure 2.4: Schematic diagram showing borehole and surface methods to determine stiffness – depth profiles using seismic survey in the field (Menzies, 2001).

Table 2.3: Summary of the advantages and disadvantages of seismic-based methods, (a) boreholes methods and (b) surface methods (McDowell *et al.*, 2002).

Method	Advantages	Disadvantages
(a) Borehole method		
Up-hole	Only single hole required. Tests can be carried out in all soil and rock types. Average velocity is measured in layered materials.	Need to install plastic casing to provide stable borehole.
Down-hole	Only single hole required. Tests can be carried out in all soil and rock types. Average velocity is measured in layered materials. Higher energy sources (e.g. explosives) can be used without damaging the boreholes.	Need to install plastic casing to provide stable borehole.
Seismic cone	No borehole required; probe is pushed into the ground. Provides other geotechnical parameters in addition to stiffness. Average velocity is measured in layered materials.	Penetration limited by strength of ground. Not suitable for rock.
Cross-hole	Can detect low velocity layers, provided they are thick compared to borehole spacing. Test can be carried out in all soil and rock types. Can do imaging to show two-dimensional distributions of stiffness.	Quality of data diminishes at shallow depths. Maximum velocity is emphasized in thinly layered soils due to head wave. Expensive. Specialist processing facilities required.
(b) Surface method		
Refraction	No borehole required	Cannot detect low velocity layers below higher velocity layers. Cannot detect thin layers. Problems with interpretation of consistent velocity profile or decreasing velocity profile. Expensive; high resolution of seismic reflection is required for engineering surveys. Method only effective in layered ground.
Surface wave – Spectral analysis of surface wave (SASW) method	No borehole required. Field method is quick and relatively simple.	No selective control over the frequencies generated, therefore measurements are limited to those frequencies, which can be generated in medium by a given impulsive seismic source. It may be necessary to use a number of different impulsive energy sources.
Surface wave – Continuous surface wave (CSW) method	No borehole required. Selective frequency control of vibratory seismic source. Field method is relatively quick and simple. Preliminary result stiffness-depth profile may be viewed on site.	Depth of investigation is currently limited to about 10 m unless large lorry mounted vibrations are employed to excite low frequency.
Multi-channel Surface Wave (MSW) method	No borehole required. Field method is quick. Preliminary result stiffness-depth profile may be viewed on site. The active method (source like sledgehammer) has investigation depth shallower than 30 m and whereas the passive method (source like traffic and tidal motion) can reach a few hundred meters. Sampling redundancy due to multi receivers provides flexibility in the signal processing approach to extract the dispersion curve.	This method is more expensive comparatively with SASW and CSW as well as the use advances of electronic equipment. The signal processing technique (for example wavefield-transformation) has a tendency to average the velocity for an entire array of receivers. As a result, the small spatial soil properties change in a lateral direction will not appear.

In the soil, seismic waves propagate in the form of body waves and surface waves. The difference between the two is that body waves are usually non-dispersive. In a solid and homogeneous medium, the velocity of surface waves does not fluctuate significantly as a function of distance propagated. However, when the properties of the medium vary with depth, surface waves become dispersive such that the velocity of propagation varies with respect to wavelength or frequency. Surface waves are also relatively less attenuated as a function of propagation distance as compared to body waves. These two characteristics make it feasible to apply surface wave analysis for the survey of near-surface soil properties and, thus in turn, any changes to these properties that subsequently occur as a result of ground improvements.

2.4 Summary

There are many types of ground improvement techniques that can be applied to solving a broad spectrum of geotechnical problems. To choose which ground improvement should be applied requires detailed site investigation information. Of the suite of ground improvement approaches available, vibro flotation method are more popularly used due to their versatility. Of these vibro-stone column is very common as it is suitable to overcome the weak natural fine grained deposits, mixed made ground and ground prone to liquefaction during seismic events.

Assessment of the improvements achieved during a ground treatment process is vital to ensure success. Without this, lack of certainty and over-design commonly takes place. To

achieve greater certainty in the final treatment achieved, a robust quality assurance programme is needed that allows both pre- and post-treatment to be examined and that can be compared with the improvements specified. Traditionally, this has been achieved using physical soundings in situ, or laboratory tests. These suffer from a significant number of problems, in particular, the representative and sampling issues (as discussed in Sections 2.3.1 and 2.3.2). Geophysical methods can overcome these problems and can provide excellent resolution of spatial variability across a site before and after treatment. The chief advantages with such an approach are its non-destructive, non-invasive nature and relative speed of assessment. If calibrated, details of stiffness with depth can be relatively easily obtained.

The seismic-based techniques have proved particularly useful in determining improvement from ground treatment. Of the seismic-based approaches that demonstrate the best promise are surface wave methods. A surface wave method has a number of added advantages because it is able to assess variation both with depth and across an area in a cost effective way and so enable improvements to be examined in detail. Foti and Buther (2004) in their general report on geophysical methods applied to geotechnical engineering stated that "the potential of geophysical tests for engineering site characterization has been widely recognised, especially in recent decades. Their advantages are non invasiveness, the possibility of testing large volumes of soil, and their cost effectiveness". Cuellar (1997) list case studies from Spain and Iberian Peninsula of geotechnical applications (compacted embankment, waste landfill, rock alteration, dynamic behaviour, liquefaction of soft soils, rock fill dams, soil improvement) using surface wave test. The analytical output of surface wave studies done by Cuellar (1997) cannot be match in quality by

conventional techniques in term of equipments and labour costs. Regrettably there is total lack of information in the past literature on the information of cost between seismic surface wave (rapid, fast, less labour intensive) and conventional techniques. Furthermore, Crice (2005) and Matthews *et al* (2000) described the surface wave as the wave of the future. The use of surface wave methods to assess the advantages and limitations of ground improvement therefore has considerable scope.

Chapter 3

USE OF GEOPHYSICS

3.1 Introduction

The discipline of geophysics has developed for use in many fields such as environment, engineering, mining and archaeology where the depth of investigation required is relatively shallow (usually less than 100 m). Investigation of engineering sites, exploration for groundwater, location of buried utilities and archeological artifacts and the deeper exploration for hydrocarbons are some common examples of the application of geophysics (McDowell *et al.*, 2002). The benefit of using geophysics over conventional techniques in the geotechnical field has been discussed in Chapter 2, where geophysical tests complement conventional tests. The geophysical techniques measure the physical properties of soil, which need to relate to, and calibrate with, geotechnical properties such as moisture content, soil composition, soil strength, soil deformability, rippability and liquefaction potential. Thus, geophysical methods have the potential to be used together

with direct investigation methods integrated with them using correlations to achieve higher accuracy of the interpretations (Clayton, 2011). Thus, geophysical approaches have the potential to provide an excellent complement in any ground investigation. The following sections provide an overview of the various geophysical techniques that potential in such ground investigations, as well as for quality control in ground improvement evaluation.

3.2 Overview of Geophysical Techniques

Geophysical techniques are used to determine the physical properties of tested geo-materials. Each geophysical technique corresponds to geo-materials and geotechnical properties as summarised in Table 3.1. Therefore, it is recommended to use different geophysical techniques at the same tested location. These will give better quality of results (McDowell *et al.,* 2002). Intrusive geophysics, either via downhole or uphole methods require boreholes and, thus requires longer testing times for test preparation. Less testing preparation and fast geophysical techniques are recommended to reduce the cost. Meanwhile, to study the lateral heterogeneity site, the geophysical techniques with 2-dimensional tomography output should be incorporated in order to visualise vertical and horizontal profiles. In geotechnical engineering shallow ground is always involved, therefore geophysical techniques such as ground penetrating radar (GPR), electrical resistivity and seismic-based are frequently used because they are able to give higher spatial resolution at shallow depth (McDowell *et al.,* 2002).

Table 3.1: Relation of geophysical methods to different properties of geo-materials (Reynolds, 1997; McDowell *et al.*, 2002).

Geophysical method	Geo-material physical properties	Geotechnical properties
(1) Seismic based: refraction, reflection, surface wave methods	Elastic modulus and density	Dynamic deformation modulus (shear modulus), Poisson's ratio and differentiate soil types
(2) Electromagnetic wave based; ground electrical conductivity method, ground penetrating radar (GPR)	Conductivity, inductance, permittivity	For locating the ground water table, cavity, buried utility and soil profiles
(3) Electrical based: resistivity, induced polarization, spontaneous potential	Resistivity, capacitance, potential differences	For locating the ground water table, corrosivity of soils and differentiate soil types
(4) Gravity	Density	Deep ground profiles and cavity detection
(5) Magnetics	Magnetic susceptibility	Deep ground profiles

3.2.1 Ground penetrating radar

The ground penetrating radar (GPR) technique is an electromagnetic exploration method that transmits electromagnetic energy into the ground and records the energy that is reflected back to a receiving antenna. This method is used to determine variations in electrical conductivity with depth, usually assuming horizontal layering (McDowell *et al.*, 2002). The propagation of electromagnetic energy is attenuated due to the electrical conductivity of the material. The electromagnetic pulse is reflected by contrasts in conductivity and dielectric permittivity (Daniels *et al.*, 1988).

The selection of GPR equipment to be used is related to the set of electromagnetic properties of the geo-material and the objective of the investigation. Almost all subsurface radar systems on the market are operated at frequencies between 25 MHz and 1 GHz (McDowell *et al.,* 2002). The radar pulse frequency, magnetic permeability, electrical conductivity and permittivity of the ground control the penetration depth. The depth of investigation decreases rapidly with increasing frequency, and the greater the conductivity and permittivity of the ground the shallower the penetration of the electromagnetic pulse. Therefore, attenuation of electromagnetic radiation in wet materials shows a higher loss than in dry materials (Thomas, 2010). The magnetic permeability is generally considered negligible due to low iron contents in soils. However, as there may be occasions where soils are tested that do exhibit magnetic effects, and as even small amounts of magnetic materials such as magnetite may cause significant variations in propagation properties (Cassidy, 2007).

The GPR method has shown promise in detecting in early stage of damage and leakage from pipelines (Crocco *et al.,* 2009). The presence of higher ground water levels, however, drastically decrease the effective depth of penetration. The permittivity depends principally on the water content, where the relative permittivity is 80 for water and ranges between 2 and 6 for dry soils. Soft clay grounds contain higher water levels and so are less suitable for the utilization of the electromagnetic-based methods. On top of that, the ground conductivity survey is not able to determine the physical properties of the geo-material directly (McDowell *et al.,* 2002). The conductivity measurement from GPR is the inverse of its electrical resistivity value. Thus, the measurements from electromagnetic-based methods can be compared with results obtained from electrical resistivity methods.

3.2.2 Electrical Resistivity

The electrical resistivity method in geophysics is used to measure the conductivity and resistivity of the ground. Current is applied through one pair of electrodes and the potential difference is measured between two additional electrodes. The bulk resistivity of the medium can be calculated based on formula;

$$\rho = \frac{RA}{L} \qquad \text{Equation 3.1}$$

$$R = \frac{V}{I} \qquad \text{Equation 3.2}$$

where the ρ is the resistivity (Ωm), R is the resistance (Ω), A is the cross sectional area of medium (m^2), L is the length of medium (m), V is the voltage (V), and I is the electric current (A). A basic electrical property of all materials is shown by the ability to transmit ions. The movement of ions in electrolytic solutions, moist soils, and water-bearing rocks results in electrical conduction. The resistivity is a measure of how strongly a material opposes the flow of electrical conduction.

For soils, electrical resistivity depends on many factors such as porosity, the nature of the pore fluid, compaction of the solids, degree of saturation, particle shape and orientation, pore structure, clay content and mineralogy (Keller and Frischknecht, 1966; Garcia-Bengochea *et al.,* 1979; Arulanandan and Muraleetharan, 1988; Thevanayagam, 1993; Abu-Hassanein *et al.,* 1996). Electrical resistivity studies have been used to investigate the quality of the chemical admixture for stabilization stiffening columns (Tamura *et al.,* 2002;

Staab *et al.,* 2004). However, the relationship between resistivity and soil strength as the quality indicator has shown a very weak correlation due to the resistivity values being influenced by other parameters such as water content, pore water salinity and porosity (Staab *et al.,* 2004; Cosenza *et al.,* 2006).

3.2.3 Seismic-based methods

Seismic-based methods are the most sensitive to the physical properties of geo-materials and relatively insensitive to the chemistry of the geo-materials and their fluids (Steeples and Miller, 1990). The seismic-based techniques shake the ground producing very small strains. Thus, the soil velocities derived from the seismic-based measurements are related to soil modulus. Therefore, the seismic-based techniques can be used to derive directly the geotechnical properties that relate to strain including maximum shear modulus $(G_{\max})$, bulk modulus (*B),* Young's modulus (*E),* and Poisson's ratio (υ) (Steeples and Miller, 1990; McDowell *et al.,* 2002; Charles and Watts, 2002; Crice, 2005; Clayton, 2011).

The seismic-based techniques have proved particularly useful in determining improvement from ground treatment (Clayton *et al.,* 1995; Sutton and Snelling, 1998; Moxhay *et al.,* 2001; Jefferson *et al.,* 2008; Redges *et al.,* 2008). A comparison between seismic-based techniques and conventional geotechnical stress-strain testing for the measurement of the ground stiffness profile was presented by Matthews *et al.* (1995, 2000) and Clayton (2011), drawing the conclusion that geophysical testing can deliver results of significant quality. The seismic surface wave method is one of the seismic-based methods that is

more versatile than other methods for measuring the stiffness profile and is considered more economical in terms of field operation (Matthews *et al.*, 2000).

3.3 Seismic Waves

There are four types of elastic seismic waves, produced by impulses and all of which travel at different velocities. The four are: compression wave, called the P-wave, shear wave called the S-wave, Rayleigh wave and Love wave. P and S waves are known as body waves; Rayleigh and Love waves are surface waves as shown in Figure 3.1. A seismic wave transmits energy by vibration of soil particles in different directions. For P-waves the soil particles vibrate in the direction of wave propagation and S-waves vibrate in a direction perpendicular to the direction of wave propagation. Both waves are propagated along a hemispherical wave front; thus wave amplitude is attenuated in proportion to $1/r^2$, where r is the distance from seismic source. Surface waves are distortional stress waves that propagate near to the ground surface with a cylindrical wave front and wave amplitude attenuated in proportion to $1/\sqrt{r}$. Therefore, surface waves are less attenuated and, thus propagated over longer distances than body waves (Al-Hunaidi, 1993). Love and Rayleigh waves are surface waves that are only propagated through a solid medium with the depth of penetration being a function of their frequency and wavelength (Reynolds, 1997).

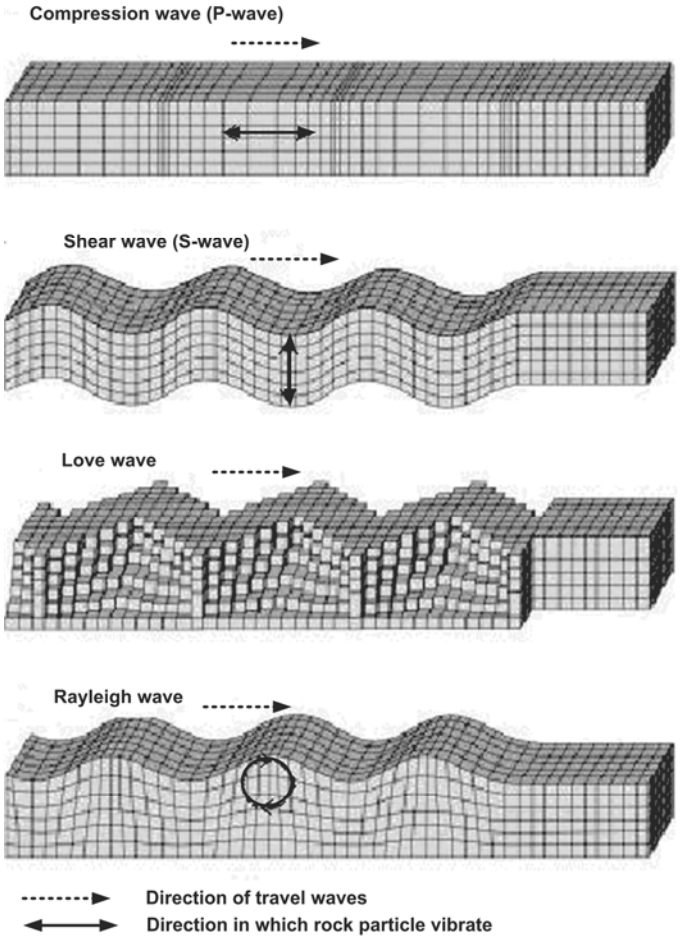

Figure 3.1: Schematic elastic wave propagation in ground (Menzies, 2001).

3.3.1 Body Waves

Elastic seismic body waves consist of two types of wave: the compressive wave (P-wave) and the shear wave (S-wave). The P-wave has the greatest velocity of the elastic seismic waves. The P-wave travels through all the media: liquids, gases and solids. Whereas, the S-wave travels slightly slower than the P-wave in solids and does not propagate through liquids and gases, as these media have no shear strength. Table 3.2 shows the typical

values of P- and S-wave for the different earth materials which illustrate key differences. The P-wave causes volumetric strains and the velocity depends on bulk density, bulk modulus and any deformation is considered to be undrained. S-waves, on the other hand, induce shear distortion in the soil without volumetric changes. The velocity of a P-wave in water is 1450 m/s. Therefore, the undrained bulk modulus of the ground is usually a combination of stiffness in both the soil and the water. In contrast, S-wave velocity in water is 0 m/s. Thus, the measured modulus is represented by the soil only. Use of S-waves is preferred when studying saturated soils because these are independent of water content (Fam and Santamarina, 1997; Matthews *et al.*, 2000). When combining P-wave and S-wave results there are advantages in distinguishing the ground water table and obtaining in situ dynamic elastic properties (Lankston, 1990).

Table 3.2: P- and S-wave typical values for different earth materials (McDowell *et al.*, 2002)

Material	P-wave velocity, m/s	S-wave velocity, m/s
Air	330	0
Water	1450	0
Sands and clays	300-1900	100-500
Glacial till	1500-2700	600-1300
Chalk	1700-3000	600-1500
Strong limestone	3000-6500	1500-3500
Weathered granite	100-3000	500-1500
Fresh granite	3000-6000	1500-3000
Slate	5000-7000	2500-3800

There are two common types of seismic survey using body waves: refraction and reflection (see Figure 3.2). The seismic refraction is based, fundamentally, on Snell's Law, which states that at the critical incident angle, a wave is refracted along the soil layer boundary before it returns to the surface. Snell's Law is;

$$Sin.i_c = V_1 / V_2 \qquad \text{Equation 3.3}$$

where i_c is the critical incident angle (degree), V_1 is the velocities of the upper layer (m/s) and V_2 is the velocities of the lower layer (m/s). The seismic refraction method requires the soil layers to increase in density with depth. The reflection method requires density contrast to reflect waves back to surface (Lankston, 1990). The seismic refraction method involves recording the travelling time of either the P-wave or S-wave energy. Thus, interpretation of the data provides layer thicknesses and seismic velocities (McDowell *et al.*, 2002). Figure 3.2 shows a diagram the difference between refraction and reflection.

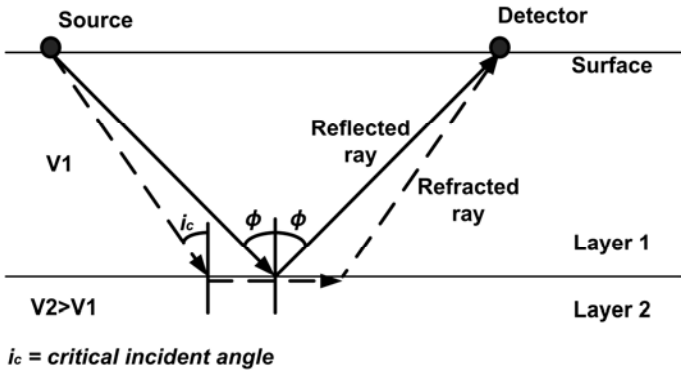

Figure 3.2: The path of refracted and reflected seismic rays in a two layer system (McDowell *et al.*, 2002)

The way in which S-waves and P-waves are generated in refraction surveying differ. Generating P-wave energy is relatively easy, either by dropping any mass vertically onto the ground surface or by using explosives to generate more P-wave energy. The generation of S-waves is more difficult. S-wave can be generated by putting energy into the ground in a direction perpendicular to the row of receivers; thus the soil particle motion will be in a perpendicular direction to the direction of wave propagation (Luna and Jadi, 2000). The perpendicular direction energy generation technique enhances the S-wave amplitude and at the same time decreases P-wave amplitude. Thus, the S-waves are easier to recognize in the seismic records (Lankston, 1990).

The seismic reflection method involves recording the seismic energy that is reflected when there is a density contrast compared with the overlying soil layer. This technique is not routinely used in civil engineering studies. However, it is used when information of a regional area is required concerning the geological structures down to depths of about 300 m (McDowell *et al.,* 2002). One of the main reasons for this is the difficulty in identifying low energy reflection arrivals in the part of the seismic record that often is 'contaminated' with refraction waves and surface waves (Steeples and Miller, 1990). Investigation of the quality of vibro-replacement stone columns using seismic refraction and reflection is difficult due to the vertical change of density resulting from the inclusion of columns. Thus, both methods have not commonly been used for assessment of quality control in stiffening columns.

Field surveys or laboratory tests can be used for these two body waves, with appropriate wave sources and receivers. The arrival times of waves are measured and converted to wave velocities. The seismic waves are directly utilised to calculate engineering

properties. From the P-wave and S-wave velocities input, the maximum shear modulus, G_{max}, the constrained modulus, M_{max} or bulk modulus, B, Young's modulus or dynamic elasticity modulus, E, and Poisson's ratio, υ, at very small strains can be calculated from the following relationships:

$$G_{\max} = \rho v_s^2 \quad \text{…….} \quad \text{Equation 3.4}$$

$$B = M_{\max} = \rho v_p^2 = \frac{E}{3(1-2\upsilon)} \quad \text{……} \quad \text{Equation.3.5}$$

$$E = 2\rho v_s^2(1+\upsilon) = \frac{\rho v_p^2(1-2\upsilon)(1+\upsilon)}{(1-\upsilon)} \quad \text{……} \quad \text{Equation 3.6}$$

$$\upsilon = \frac{\left[\left(v_s / v_p\right)^2 - 2\right]}{2\left[\left(v_p / v_s\right)^2 - 1\right]} \quad \text{……} \quad \text{Equation 3.7}$$

Where ρ is the bulk density of the soil (kg/m³), v_p is the P-wave velocity (m/s) and v_s is the S-wave velocity (m/s) (Clayton *et al.*, 1995; Menzies and Matthews, 1996; Massarsch, 2005). G_{max} can be obtained from measurements of v_s alone using equation 3.4 (Massarsch, 2005). Geo-materials have values of Poisson's ratio in the range of 0.05 for very hard rocks and nearly 0.5 for saturated unconsolidated clays (Sheriff and Geldart, 1982). According to the theory of elasticity, Young's modulus, E, and constrained modulus, M_{max}, are related to shear modulus, G_{max}, by:

$$G_{\max} = \frac{E}{2(1+\upsilon)} \quad \text{……} \quad \text{Equation 3.8}$$

$$G_{\max} = \frac{M_{\max}(1-2\upsilon)}{(1-\upsilon)} \quad \ldots\ldots\ldots\ldots \qquad \text{Equation 3.9}$$

Where υ is the Poisson's ratio, E is the Young's modulus (N/m²) and M_{max} is the.constrained modulus (N/m²).

3.3.2 Surface Waves

When the ground surface is vibrated with a vertical load, two-thirds of the energy is transformed into surface waves and propagated parallel to the ground surface (Socco and Strobbia, 2004). Rayleigh waves form as a result of interfering P and S waves at the ground surface (Xia, *et al.*, 2002). Surface waves have dispersive characteristics and, thus can be utilised to identify near-surface elastic properties. Dispersion arises because different frequencies or wavelengths travel at different depths (Reynolds, 1997). In homogeneous material, surface wave velocity does not vary with frequency. However, in layered soils with different densities, surface wave velocity varies with frequency where there is a variation in stiffness with depth (Stokoe *et al.*, 1994). This phenomenon is explained by the layering medium illustrated in Figure 3.3, where medium 1 with thickness L is overlying medium 2. The Rayleigh wavelength (λ_1) shorter than L would propagate mainly within the medium 1, thus phase velocity is representative medium 1. However, the Rayleigh wavelength (λ_2) is larger than L and this occurs as the phase velocity is influenced by the properties of both medium 1 and 2 (Rhazi *et al.*, 2002). This phenomenon is called dispersion, causing different frequencies and wavelengths to travel at different velocities.

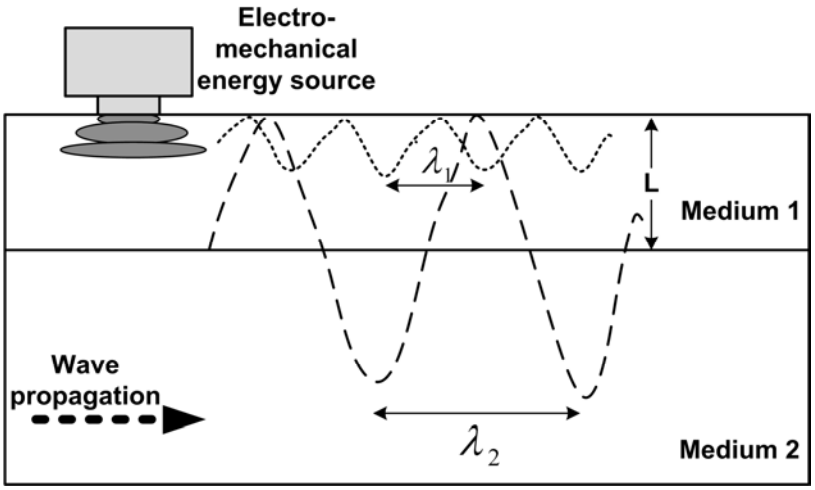

Figure 3.3: Rayleigh waves dispersion (Rhazi *et al.*, 2002)

The dispersive properties of surface waves are used to evaluate stiffness properties with depth. The Rayleigh-wavefront propagation away from the seismic source is in a cylindrical form. Meanwhile, the particles in Rayleigh waves move in elliptical trajectories whose semi major axis is perpendicular to the surface of the body and whose semi minor axis is parallel to the direction of wave propagation. The Rayleigh-wave energy is mostly concentrated in a layer of approximately one wavelength depth (Xia, *et al.*, 2004). Thus, the Rayleigh-wave phase velocity is affected by the properties of the subsurface to a depth equivalent to about one wavelength (Rhazi *et al.*, 2002).

The surface wave test methods are differentiated according to their source and receiver set-up in the field. There are three established methods for surface wave site investigation. Firstly, the Spectral Analysis of Surface Waves (SASW) method, which makes use of a transient vertical impact source. Secondly, the Continuous Surface-Wave (CSW) method uses a steady-state vibration source (Sutton and Snelling, 1998). Finally, the Multi-

channel Surface Wave (MSW) method uses multi-channel receivers and a variety of either active seismic sources, such as sledge hammers or ambient sources (Park *et al.*, 2005).

3.3.2.1 Spectral Analysis of Surface Waves

The SASW method was developed in the early 1980s, for various engineering purposes, for example, Cuellar and Valerio (1997) described it use for measuring the stiffness-depth profile of vibro-replacement stone columns; Yuan *et al.* (2008) described its use for deep mixing columns; Kim and Park (1999) described its use for the evaluation of ground densification stabilization and Ganji *et al.* (1997) outlines its use for the detection of underground obstacles.

The SASW method uses a single pair of receivers that are placed collinear with the impact point of the transient source. A series of hammer weights are needed to produce a range of frequencies. In general, heavier weights generate signals predominated by lower frequencies. The SASW recordings use a spectrum analyzer to capture signals from ground motion receivers, usually in pairs, in the time domain. The time domain data are transformed into the frequency domain. From these spectral data, the phase difference between the signals at each geophone and the coherence of the cross correlated signals can be determined. The coherence is a measure of the signal-to-noise ratio at a given frequency (Addo and Robertson, 1992). Figure 3.4 shows each step involved in the SASW method from data collection to data analysis (Luke, 1999). However, it is inevitable that certain frequencies will be missing from the spectra of these sources due to lack of precise control over the wave frequency generated using impact sources, which

may result in gaps in the stiffness profile data (Matthews *et al.*, 1996). The SASW method uses a single pair of receivers and, thus needs to be configured and reconfigured many times to sample the desired frequency range and to reduce body wave noise; therefore sometimes it is impossible to assess and distinguish signals from noise with only a pair of receivers.

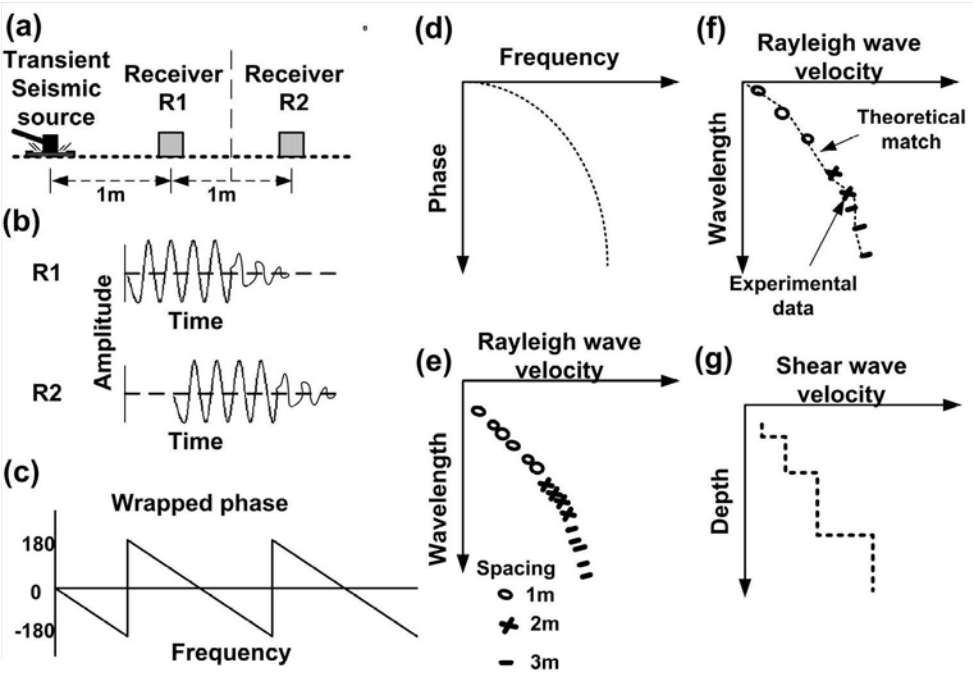

Figure 3.4: In an SASW measurement, a) source energy is applied at the ground surface; b) the resulting ground motion is detected at the receivers and digitized at the analyzer; c) the time signals are transformed to the frequency domain and the phase difference between receivers is determined; d) the phase data are unwrapped and masked to eliminate spurious components; e) the dispersion curve is generated from the unwrapped, masked phase data at several different receiver spacing; f) a theoretical dispersion curve is matched to the experimental dispersion curve to yield and g) the shear wave velocity profile for the site. (Luke, 1999).

3.3.2.2 Continuous Surface Waves

The continuous surface waves (CSW) technique uses a steady-state vibration source has increasingly been used for site characterization (Matthews *et al.*, 1996). More recently, it has been developed to determine stiffness profiles before and after ground treatment (Moxhay *et al.*, 2001). Results are shown in 1-D stiffness-depth profiles.

The seismic source uses a vibrator to produce surface wave frequencies in the range of 3 Hz to 200 Hz. A vibration source generates continuous sinusoidal waves dominated by a single frequency. To obtain greater frequency ranges and for ease of mobility, an electromechanical vibrator with a weight of less than 15 kg is recommended. However, this vibrator is not suitable for providing good quality sinusoidal waveforms at frequencies below 7 Hz. To obtain lower frequencies, heavier machinery is needed to be able to generate frequencies in the range of 3-50 Hz. Lower frequencies are related to long wavelengths and, thus provide information about deeper ground layers (Matthews *et al.*, 1996).

Using several geophones allows a best fit line to be drawn through the phase angle-distance plot, thus minimizing the influence of variations in the data. In contrast, if two geophones are used it can be difficult to obtain confidence in the results obtained. Therefore, sometimes as many as 24 receivers are used as an evolution of the CSW technique. Besides, at least two sensors are needed for the CSW test, which is arranged co-linear with the seismic source. Thus, the coherence of the cross correlated signals need to be determined for accessing the signal quality. Meanwhile, Moxhay *et al.* (2001) used 6

receivers at 2 Hz for their testing of ground improvement sites, with an additional 6 receivers used to increase the quality of data.

The CSW technique is summarised in Figure 3.5 is begun with arrangement of equipments using selective frequency (f1) and the sampling of frequencies is continued until *n* frequency (fn). The captured data are in a time domain, thus are transformed to a frequency domain. Therefore, the phase angles for each geophone are determined and plotted with distance to obtain the best fit line with assumption laterally homogeneous soil (only applicable if using more than 3 geophones). The difference phase angle between geophone pair called phase difference, is then use to calculate a phase velocities (see equation 4.7). The calculated phase velocity then divided with it respected frequency and gave the wavelength (see equation 4.9). The plot of phase velocity versus wavelength is known as dispersive curve.

The difference between the SASW and the CSW is the transient impact seismic source generated a swept frequencies meanwhile vibrator seismic source formed a single-frequency sinusoidal force respectively. The frequency is crucial in the surface wave techniques; therefore the CSW is comparatively much better than the SASW in term of the selective mono-frequency that may be used, as a result there is no frequency misses and unwanted background noise is more easily recognised, avoided and filtered in the CSW technique (Clayton, 2011). In addition, with the SASW a number of impulse energy sources are needed to generate different bands of frequencies, as a result some of the frequencies are missed due to lack of control over the wave frequency generated using impact sources (McDowell *et al.*, 2002).

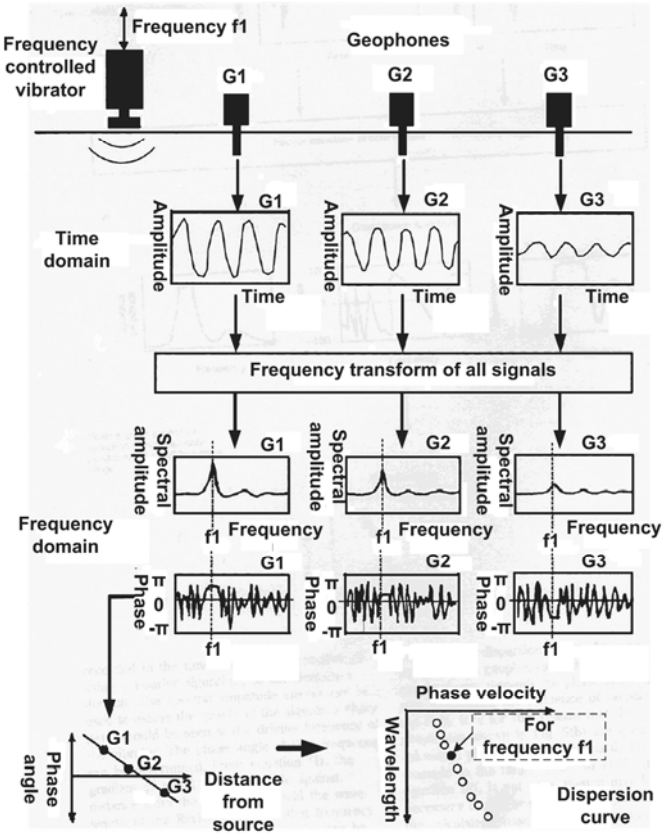

Figure 3.5: Schematic diagram showing the steps followed in the determination of the dispersive curve using the CSW technique (Matthews *et al.*, 1996).

3.3.2.3 Multi-Channel Surface Waves

The Multi-channel Surface Wave (MSW) method originated 50 years ago in Japan and was called the micro-tremor survey method (MSM). In the late 1990s, electronic equipment for the MSW was developed by the Kansas Geological Survey called multi-channel analysis of surface wave, MASW (Park *et al.*, 1999). This technique has been developed and tested for applications in civil engineering, for example, for site characterisation (Long and Donohue, 2007) and for compaction control by measuring the

decay of soil vibrations (Adam *et al.,* 2007). The approach of the MSW offers considerable advantages over conventional surface wave analysis techniques that are based upon a single transmitter-receiver pair. The method of carrying out measurements using a multiple-receiver strategy reduces survey time and allows lateral resolution to be obtained (Zywicki, 1999; Park *et al.,* 1999), while the sub-surface characterisation in both the vertical and lateral axes provide a useful 2-D representation (Socco and Strobbia, 2004). In general, the MSW has significant advantages over other surface wave techniques as all seismic wave energy, consisting of both body and surface waves, is recorded by multi-channel receivers.

MASW introduced by Park *et al.* (1999) uses many receivers, with only one shot, from which it is capable of identifying, isolating and removing noises from scattered and reflected waves during the data analysis. As a result, a best fit line can be drawn through the phase angle-distance plot, thus minimizing the influence of variations in data and allowing enhanced robustness in data processing. The entire procedure for MASW usually consists of three steps: firstly acquiring multi-channel field records, secondly extracting dispersion curves and finally, inverting these dispersion curves to obtain 1-D or 2-D shear wave velocity and depth profiles as shown in Figure 3.6. The MASW method has improved production in the field and improved characterisation of dispersion relationships by sampling the spatial wave field with multiple receivers (Park *et al.,* 2007).

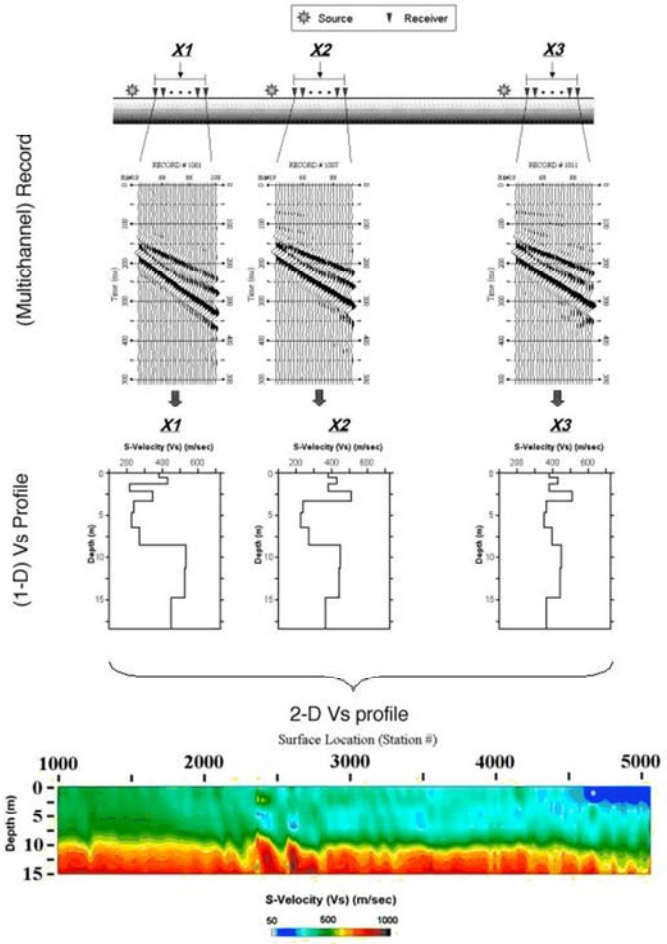

Figure 3.6: MASW field data collection by roll-along and inverting the dispersion curves to obtain 1-D or 2-D shear wave velocity and depth profiles (Park *et al.*, 2007).

The SASW and CSW techniques using a single pair of receivers yield one-dimensional results of phase velocity versus depth. To resolve anomalies in a laterally heterogeneous medium, it is necessary to obtain a plot of the phase velocity versus depth as a function of lateral distance and, hence, the MSW technique is more suitable. Such a method provides information with greater resolution in the lateral dimension and, therefore can be used to obtain a qualitative assessment of the variability of geotechnical properties such as stiffness and strength. This enables the detection of features such as voids, fractures and

soft spots (Gordon *et al.*, 1996). The implementation of this technique usually involves the deployment of an array of multiple receivers with the seismic source. It has been successfully demonstrated by, Phillips *et al.* (2004), Xu and Butt (2006) and Nasseri-Moghaddam *et al*. (2007) for the detection of sub-surface cavities and Tallavo *et al.* (2009) for the detection of buried timber trestles. Below Table 3.3 are the examples from past literature of application of MASW.

Table 3.3: Example of application of multi channel analysis of surface wave (MASW) from past literatures.

Reference	Special aspect of the research	Application	Context to this research
Park *et al.* (1998) Surface waves as a tool to image near-surface anomaly	48 channel seismograph in the field.	To obtain soil profile with simple geology stratigraphy.	For complex soil model is not relevant.
Phillips *et al.* (2004) Evaluation of horizontal homogeneity of geomaterials with the distance analysis of surface waves.	Numerical simulation in different soil conditions i.e. horizontally changes. Use of the spectral analysis of surface waves (SASW) method to evaluate the horizontal soil changes.	Lateral heterogeneity.	Relevant to this study due to suggestion on analysis the data (see Section 4.4).
Park *et al.* (2005) Combined use of active and passive surface waves.	Combines the techniques of using active seismic source (sledge hammer) and passive seismic source (ambient seismic source).	To obtain deeper layer profile	Not relevant to this study.
Xu and Butt (2006) Evaluation of MASW techniques to image steeply dipping cavities in laterally inhomogeneous terrain.	Field measurements using 12 channel seismograph. Analyses the data to obtain time delay for each channel pair.	Void detection	Indirectly relevant to this study due to time delay analysis for respective channel able to show anomalies underneath.
Nasseri-Mogaddam *et al.* (2007) Effects of underground cavities on Rayleigh waves—Field and numerical experiments.	Using 24 channel seismograph in the field. Analyses the data using the power spectrum density (PSD) technique to identify the void.	Void detection	Indirectly relevant to this study due to power spectrum density (PSD) technique for respective channel able to show anomalies underneath.
Cascante *et al.* (2008) Novel methodology for nondestructive evaluation of brick walls: fuzzy logic analysis of MASW tests.	The simultaneous measurement of the impact response using 15 accelerometers.	Brick walls evaluation	Indirectly relevant to this study viz. compare high and low phase velocity where indicated the quality of the brick wall.
Tallavo *et al.* (2008) Experimental and numerical analysis of MASW tests for detection of buried timber trestles.	Using 24 channel seismograph in the field. Plot unwrapped phase for each channel. The unwrapped phase is disturbed after the wave front passes through the timber trestle.	Buried timber trestle detection.	Relevant to this study due to plot unwrapped phase for respective channel able to show anomalies underneath (see Chapter 7).

3.4 Surface Wave Test for Ground Improvement

The majority of surface wave applications for civil engineering have been used to characterise laterally homogeneous soils and pavements (Forbriger, 2003). Because of the ability to conduct surveys quicker, this made the surface wave technique an attractive tool in assessing the effectiveness of the ground improvement work before and after treatment. These are based upon spectral analysis of surface waves (SASW), continuous surface wave analysis (CSW) and more recently, on multi-channel analysis of surface waves (MASW). Jefferson *et al.* (2008) showed how SASW can be used to assess, qualitatively, changes to ground properties laterally after vibro-replacement stone columns (VSC) treatment had taken place. Moxhay *et al.* (2001) and Redgers *et al.* (2008) applied the CSW technique to measure the stiffness-depth profile of dynamically stiffened ground and VSC, making the assumption that the columns and soils are a single block in the lateral dimension. Their results produced a profile of the average of shear-wave velocity versus depth between the stiffening columns and the surrounding soil.

Generally, the surface wave method can be separated into two main steps of data collection and signal processing for spectral analysis. For data collection, there is usually a seismic source, generating a signal $x(t)$, and multiple receivers deployed to acquire the seismic data, represented by $y_1(t)\ldots y_n(t)$ where n is the index of the array of receivers. The common options for a seismic source are usually a manually-controlled mass dropped to induce a broadband impulsive signal into the ground, or an electro-mechanical shaker controlled by a digital source. The earlier option is the simplest, while the latter allows precise control and variations of the source signal characteristics both in terms of

bandwidth and time duration. The receivers usually consist of geophones for field testing, or accelerometers in laboratory-scale testing.

The arrangement of the transmitter and receiver arrays is subject to the near- and far-offset constraints (Heisey *et al.,* 1982). These constraints are associated with the wavelength of the signals and, therefore determine the maximum and minimum frequencies that are useful for spectral analysis. The empirical rule for the near-offset constraint is recommended between the distance of the source and the first receiver, d_{min}, as a function of the surface-wave wavelength, λ, to be approximated (Al-Hunaidi, 1993; Matthews *et al.*, 1996; Park *et al.,* 1999):

$$d_{\min} > \frac{\lambda_{\max}}{3} \quad \text{..... Equation 3.10}$$

The far-offset is associated with the attenuation of the surface waves when the receiver is far away from the seismic source. This constraint is approximately:

$$d_{\max} < 2\lambda_{\min} \quad \text{.....Equation 3.11}$$

In addition, the spacing between the receivers, Δx, should be within the constraint of

$$\Delta x \approx \lambda_{\min} \quad \text{..... Equation 3.12}$$

to avoid spatial aliasing when comparing the phase between any pair of receivers. At least two surface samples should be obtained for the smallest wavelength. The spatial aliasing will cause the inaccurate evaluation of wavelength during processing (Sheriff and Geldart,

1995). λ_{max} and λ_{min} are the wavelengths corresponding to the minimum and maximum frequencies respectively.

The analysis used in such approaches assumes that the soil behaves as a layered half-space that is laterally homogeneous and isotropic. Thus, the results represent the mean velocity of the whole horizontal layer corresponding to the respective wavelength. Therefore, the majority of the stiffness profiles obtained from surface wave case studies in VSC indicate that only marginal improvement in stiffness have been achieved in the deeper layers of stone columns (Sutton and Snelling, 1998; Moxhay *et al.,* 2001; Moxhay *et al.,* 2008; Redgers *et al.,* 2008; Roy, 2010). These results are due to the surface wave tests being conducted very soon after column installation, without allowing sufficient time for pore water pressure to equilibrium to occur following treatment (Roy, 2010). This phenomenon was observed by Moxhay *et al.* (2008) which the soil improvement using VSC was progressive over time, thus stiffness generation was not detected in a deeper layer. The stiffness is higher at the shallow layer and decreased with depth and finally similar to stiffness before the treatment even though the columns lengths are longer. The phenomenon of stiffness versus time required detailed study as recommended by Roy (2010) to make a considered judgement on the applicability of the surface wave test.

Vertically layered heterogeneous soils are fairly understood in the surface wave application where the Rayleigh-wave phase velocity is affected by the properties of the subsurface to a depth equivalent to about one wavelength (Rhazi *et al*., 2002) (see Figure 3.3). The dispersive characteristics in Rayleigh wave is caused by the soil properties changed in the depth. As reviewed by Nasseri-Moghaddam (2006), lateral heterogeneities

are usually not the main consideration in applying the theories associated with surface wave analysis. An attempt was made by Tallavo *et al*. (2009) to detect buried timber trestle via investigate the spatial changes of the phase velocities. Interestingly a few sensors located in front and behind the timber trestle showed the phase velocities deviated from surrounding phase velocity because of the lateral heterogeneous effect introduced by the presence of trestle. Their results' open to the question on what shape and size is the effective region of measurement for each frequency that influenced the phase velocities. Further investigation and discussion about lateral heterogeneous is presented in the Chapter 7 and 8.

3.5 Relationship of Seismic to Geotechnical Parameters

The ground displacement prediction and their effect to the adjacent structures are important in the new era of construction especially when redevelop inner city infrastructures (Clayton, 2011). Because of the most geotechnical structures are designed to restrict ground movements and consequently the strains in the ground are usually quite small (Atkinson, 2007). Therefore, a sound knowledge of stiffness parameters at small strain is essential to make realistic predictions of the ground movements (Clayton, 2011). To obtain realistic stiffness parameters that can be used in deformation analyses is one of the most important and difficult problems in geotechnical engineering (Gordon *et al*., 1996). The sizes of strains from the finite element analyses of deformation around civil engineering structures at working loads are typically less than 0.1 %. However, the local soil strains near the edge of structures are greater than 0.1 % but will decay to zero far

from the structures. This means that in the soil stiffness will vary continuously with position and loading throughout the ground as shown in Figure 3.7. Therefore, stiffness should be measured at small strain (≈ 0.1 %) for geotechnical calculations.

Conventional measurements of soil stiffness parameters are made by conducting stress path triaxial tests in the laboratory using the triaxial test and hydraulic triaxial test. For the conventional triaxial test, it is unreliable to measure strain smaller than 0.1 %. However, using the hydraulic triaxial test it is possible to measure strain smaller than 0.01 %. To achieve 0.001 % strain reliably, an internal strain gauge should be mounted directly on the sample. It is very difficult to measure stiffness of soil at very small strain less than 0.001 % using triaxial tests by direct measurement of strains. However, the simplest way is to measure and calculate shear modulus at very small strain using the seismic shear wave velocity (Atkinson, 2007).

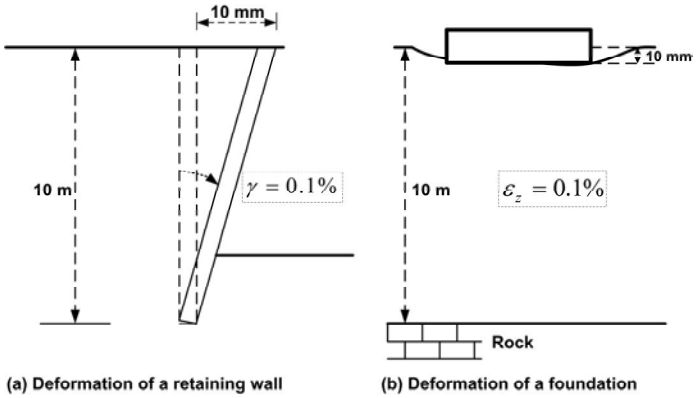

Figure 3.7: Strains at 0.1 % in the ground near typical geotechnical structures (Atkinson, 2007).

The soil modulus generated from seismic testing and geotechnical testing are at different strain levels. The strain from seismic waves is due to the shaking of soil particles at a very small range of 10^{-6} to 10^{-4} %, but for geotechnical testing in the triaxial test, for example, strain is between 0.01 and 0.001 % (Matthews *et al.*, 2000). Thus, the differences of strain measurement can yield misunderstandings in correlations. Atkinson (2007) simplified the relationship between stiffness modulus and strain as shown in Figure 3.8, where the strain increases as soil stiffness modulus decreases. In principle, there are three regions of soil stiffness: very small strain, small strain and large strain. Very small strain is a maximum and approximately constant modulus where the value corresponds to the first yield usually at 0.001 % strain. In the intermediate region, small strain, the range of stiffness changes rapidly with strain and the behaviour is highly non-linear. The third region is large strain, where the state has reached the state boundary surface, usually greater than 1 % and the soil behaviour is elasto-plastic.

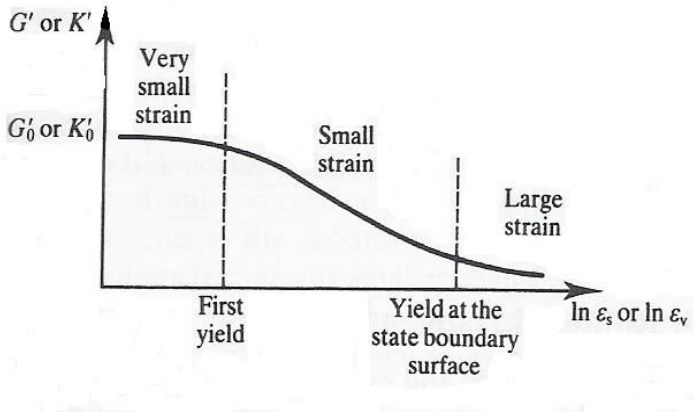

Figure 3.8: Characteristic ranges of soil stiffness modulus (Atkinson, 2007).

Stiffness means the resistance of the body to deform under applied force (Clayton, 2011). The stiffness parameters are known as Young's modulus, E, bulk modulus, B, and shear

modulus, G. The differences between them are that Young's modulus involves both the volumetric strains as well as shear distortion; bulk modulus involves strain changes in volume without change in shape, while shear modulus involves strain changes in shape without change in volume (Menzies and Matthews, 1996).

Stiffness was determined using a destructive test and a non-destructive test on different geo-materials by Clayton *et al.* (1994), Shibuya *et al.* (1995), Matthews *et al.* (1996) and Matthews *et al.* (2000). A study by Clayton *et al.* (1994) on London-Clay found that stiffnesses at 0.01 and 0.1 % strain are 0.5 and 0.2 of maximum shear modulus (G_{max}), respectively. However, the stiffness for highly fractured chalk was in the larger range between 0.93 and 2.16 of G_{max}. Shibuya *et al*. (1995) demonstrated the stiffness as well as relating it to the scale of testing. Meanwhile, Landon *et al.* (2007) showed that the stiffness changed due to sample disturbance.

The stiffness correlation study yields the concept of operational stiffness (E_{op}), where E_{op} is an expected strain level around the proposed construction structure, which is between 0.1 and 0.01 % strain (Matthews *et al.,* 2000). For soft clays, recommended operational stiffness is 0.5 of maximum stiffness (E_{op}=0.50 G_{max}), while for stiff clays and weak rocks 0.85 of maximum stiffness (E_{op}=0.85 G_{max}) is recommended. Moxhay, *et al.* (2008) and Roy (2010) made an attempt to predict the ground settlement in stone column area using stiffness profile obtained directly from the surface wave by empirically converting the very small strain to operational strain level that is experienced in actual foundation conditions.

The correlation between stiffness obtained from seismic tests and other soil parameters, such as soil strength, is also useful in the quality of ground improvement works for results correlation and calibration. For example, Mattsson *et al.* (2005) and Chan (2006) showed a strong correlation between the maximum shear modulus (G_{max}) and the undrained shear strength (c_u) of stabilised clay. The stiffness correlation must be clarified to be able to be used, due to its dependence on the clay mineralogy (Chan, 2006).

3.6 Summary

This chapter summarised the advantages of seismic-based techniques compared with other geophysical and geotechnical techniques. The seismic wave results are directly transformed to dynamic soil properties, such as the maximum shear modulus, G_{max}, the bulk modulus, B, Young's modulus, E, and Poisson's ratio, υ (Charles and Watts, 2002; Crice, 2005). The soil stiffness is a very useful parameter when analyzing the deformation of ground when it is loaded. The stiffness from a seismic wave test has different strain levels from geotechnical destructive tests such as a load test. However, the correlation of both results delivered data of significant quality. Thus, it is recommended that any geophysical assessment must be combined with direct investigation methods to ensure proper calibration.

In practice, very small strain levels are detected around the civil engineering structures like foundations, retaining walls and tunnels (Gordon *et al.*, 1996; Matthews *et al.*, 2000; Menzies, 2001; Atkinson, 2007). Normally, strain levels were between 0.01 and 0.1 %

around the civil structures (Matthews *et al.*, 2000) and decreased with distance (Atkinson, 2007). Thus, stiffness at very small strain is becoming more important for the prediction of deformation of engineering structures (Clayton, 2011). Attempts have been made to predict the deformation of foundation supported by the stone column using seismic surface wave data (Moxhay *et al.*, 2008; Roy, 2010). However the stiffness profile obtained from the surface wave testing at the stone column site yet to be understood and it was discussed in Chapter 7 and 8

The use of the seismic surface wave is one of the seismic-based methods that is more versatile than other methods and is considered more economical in terms of field operation (Matthews *et al.*, 2000). The surface waves travel near the ground surface and are less attenuated and dispersive. The dispersive characteristics only belong to the surface wave, where the frequency and wavelength vary because of the different velocities when the soils are layered. The dispersive phenomenon is used to characterize the soil properties with depth. SASW, CSW and MSW are common surface wave techniques. However, MSW is the best method due to the flexibility in the signal processing approach to extract the dispersion curve. The drawback of MSW the data processing technique has a tendency to average the velocity for an entire array of receivers. As a result, the small spatial soil properties change in a lateral direction will not appear. Therefore, the technique using each receiver pair for analysis of the velocity of the surface wave should be used. By comparing each pair of receivers' velocity, the results indicate the change of soil properties in a lateral direction.

In the majority of geophysics applications, the heterogeneous boundaries and properties of the medium are not known a priori. However, with vibro-stone columns which are man-made structures, therefore the dimensions of the columns are commonly known. It is preferred to assess the quality of the stone column individually, thus if any noncompliance column is able to identified. That was the reason in the conventional quality testing is using load test on individual column. However, the load test was too expensive to be applied on the all stone columns. The inclusion of columns created lateral heterogeneities of soil should affect the wave propagation. Therefore, in this study, the simplified models of stone columns will be constructed prior to understand the effect of the contrast in material properties in the lateral dimension in relation with Rayleigh wave properties i.e. frequency and wavelength.

Chapter 4

INITIAL TESTING METHOD

4.1 Introduction

This chapter deals with the development of small-scale seismic surface wave testing in the laboratory, used to evaluate the viability of the proposed method to investigate the quality of vibro-replacement stone columns (VSC). Due to the complexity of the VSC in the field and combined with non-homogeneity of typical natural ground conditions, it was simplified with homogeneous material and reinforced with consistent dimensions and properties of the columns. The first part of the test programme employed involved two concrete mortar blocks, one as a control and another with mild-steel columns installed to evaluate proposed test methodology. The outcomes from initial testing were subsequently used to develop the full seismic testing in natural soil, see discussion presented in Chapters 6 and 7. A pilot test was used kaolin clay bought from factory and a main test used natural soil of Oxford clay. Main test was involved stone columns configuration in larger

container, thus Oxford clay was suitable to represent natural soil as it had various clays mineralogy and also inexpensive compare to kaolin. The laboratory-scale experiments were used instead of the field tests, to allow the process of data collection to be pre-calibrated, and for true data regarding the material to be measured *a priori*.

4.2 Establishing Laboratory Seismic Surface Wave Equipment

The seismic surface wave equipment for use in the laboratory seismic tests was directly related to the material properties and the size of the test model. Figure 4.1 shows the key factors required for success of the seismic surface wave tests in the laboratory. The test apparatus, which was used for the model test, is in principle similar to that used in the field tests, but on a smaller scale. Basically, the seismic test consists of two main pieces of apparatus: the seismic source and the seismic recorder. The seismic source is generated via vertical ground motions using a point source of energy. The continuous wave is preferred rather than a transient impulse due to the intention to fully control and capture the frequency of the seismic wave. A high frequency range for the seismic receivers was selected to give more flexibility in the size of the test model. The typical model of the vibro-replacement stone columns is dimensionally scaled down, as were the seismic parameters. However, the soil properties did not require any scaling due to their insensitivity to these effects within the context of seismic characterisation (see Section 4.2.2 below).

The development of the small-scale model for seismic surface wave testing in the laboratory aimed to develop the most appropriate seismic surface wave method for attaining and utilising the data to investigate vertical and lateral stiffness and thus being able to evaluate the quality of vibro-replacement stone columns (VSC). To achieve this aim, it is necessary to investigate the suitability of the seismic equipment and its system for laboratory use. The use of seismic surface wave methods in the laboratory should have sufficient sample volume size to reduce the effect of seismic wave back-scattering, due to the model boundary together with interference by body waves. Both consequences exacerbate the signal-to-noise ratios.

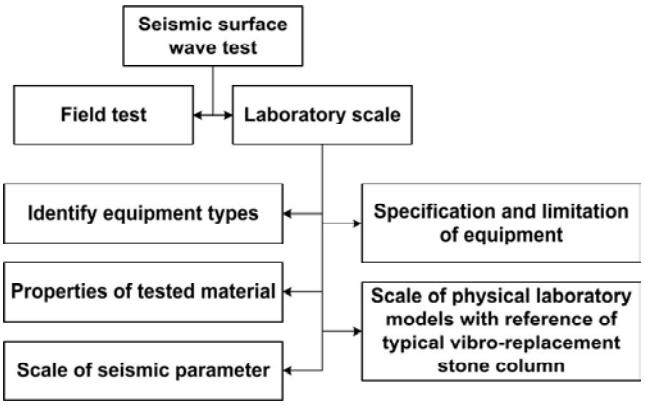

Figure 4.1: The seismic surface wave factors that contributed to the success of tests at the laboratory scale.

This study involved three steps of testing which used three different type of materials, i.e. concrete mortar, kaolin and Oxford clay which were purposely designed to (1) quantify the suitability and robustness of equipment and its systems for laboratory testing, and (2) quantify the suitability of the seismic source-receivers array to determine the lateral change of soil properties in the model of the vibro-replacement stone column. All test

materials were used in models without columns and with columns. Figure 4.2 summarises the overall testing programme that involved in the different type of materials and how it was related each other. Initial test methods employed discussed in this chapter followed by their corresponding results in Chapter 5. Following this pilot test and main test methodology were discussed in Chapter 6 with their results presented in Chapter 7.

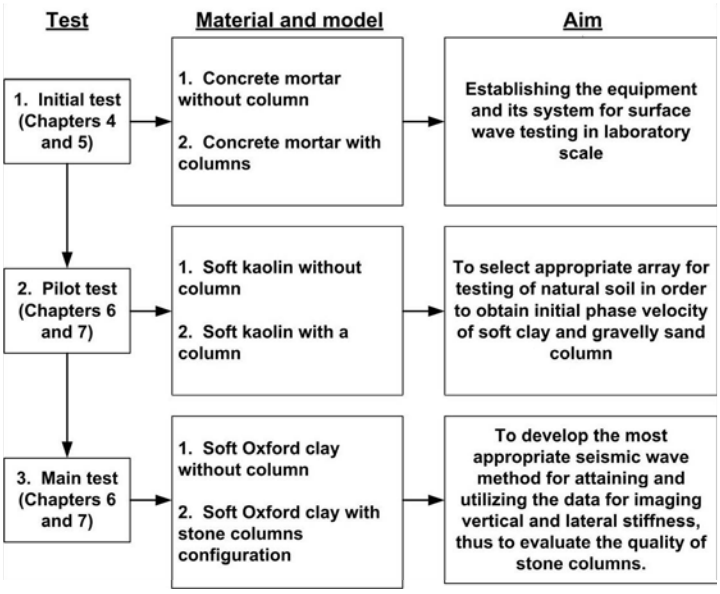

Figure 4.2: Outline details of the Initial, Pilot and Main laboratory scale model tests.

4.2.1 Seismic Surface Wave Equipment

The selection of the seismic apparatus, specification and the size of the test models has to consider the factors of time, cost and workability. The surface wave can be generated by a piezo-ceramic transducer or an electromechanical vibrator in the vertical direction used as a point energy source. In an early test development, a speaker as a seismic source was tried as a source to generate a sinusoid wave. Here the vibrated speaker diaphragm was

connected to test material using aluminium bar as shown in Figure 4.3. A tyre was used to adjust the height between diaphragm and aluminium bar and as well as to maintain it positioned. However this technique did not able to give sufficient energy due to the energy lost when the wave propagated from the diaphragm through aluminium bar and test material. As a result lower signal-to-noise ratio and gave unreliable phase velocity.

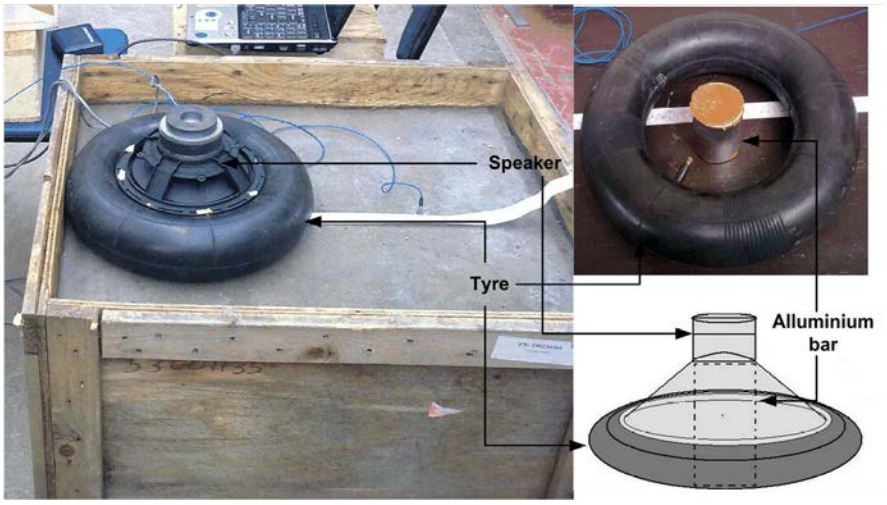

Figure 4.3: In an early test development, speaker was used to generate seismic source.

The selection of seismic sources was determined by the level of frequency and energy required for the test materials. For example, a piezo-ceramic transducer gives better energy at higher frequency rather than a electromechanical vibrator. The piezo-ceramic transducer was therefore used, which included a weight padded with acoustic absorbers to obtain better contact to the test material. Meanwhile, the electromechanical vibrator used absorber pads to support its weight and maintain its position as shown in Figure 4.4. To measure the seismic output, four piezoelectric-accelerometers and four channels of the signal conditioner were therefore used. The number of receivers deployed in a multi-channel approach was usually a compromise between the economic cost of the equipment

and the time required to conduct the survey. In addition, this was limited by the constraints of signal-to-noise ratio at the furthest receivers, beyond which the excitation source would have to be moved along with the receivers to cover an extended length or area.

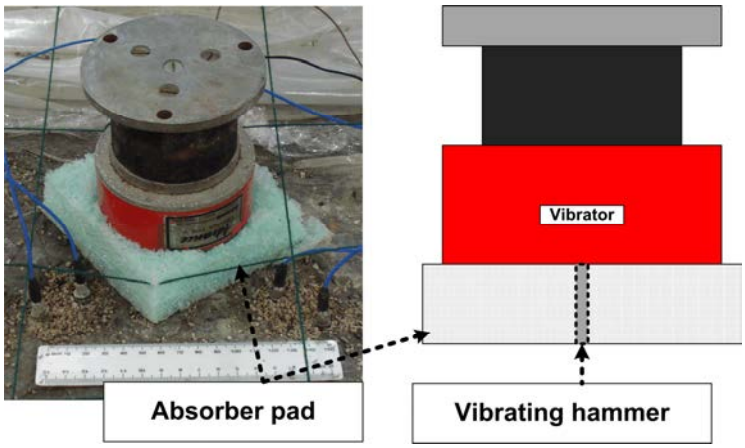

Figure 4.4: Electromechanical vibrator supported by the absorber pad to maintain it position.

The communication between the various sets of equipment was carried out using Matlab software. A script was written within the Matlab environment to conduct the experiment using a computer (see Appendix A). The computer was connected to a National Instruments data acquisition system, in which a 16-bit analogue output module (NI-9263) generated the transmission waveforms. An audio power amplifier was used to drive the seismic sources (piezo-ceramic transducer or electromechanical vibrator) with the excitation signals. On the receiver side, the sensors consisted of four piezoelectric accelerometers (ICP®, model 352C42 from PCB Piezotronics) with a frequency range of 1 Hz to 10 kHz to measure vertical ground acceleration. The accelerometers were connected

to an analogue signal conditioner (model 482C05) via a teflon cable of low-noise coaxial BNC plug model 003C10 from PCB Piezotronics. The seismic signals were then sampled by a 24-bit sigma-delta analogue-to-digital converter module (NI-9239) with a sampling rate of 50 kHz. Collected data were stored, and processed after the completion of a data acquisition session. To minimise ambient noise, the models were isolated from the ground with acoustic absorbers. Figure 4.5 summarises the equipment and its specification for use in a laboratory seismic surface wave experiment. Figure 4.6 illustrates, in general, the laboratory seismic surface wave test setup, where the seismic source is at the one end of the receivers in a linear array and Figure 4.7 shows a photograph of the equipment.

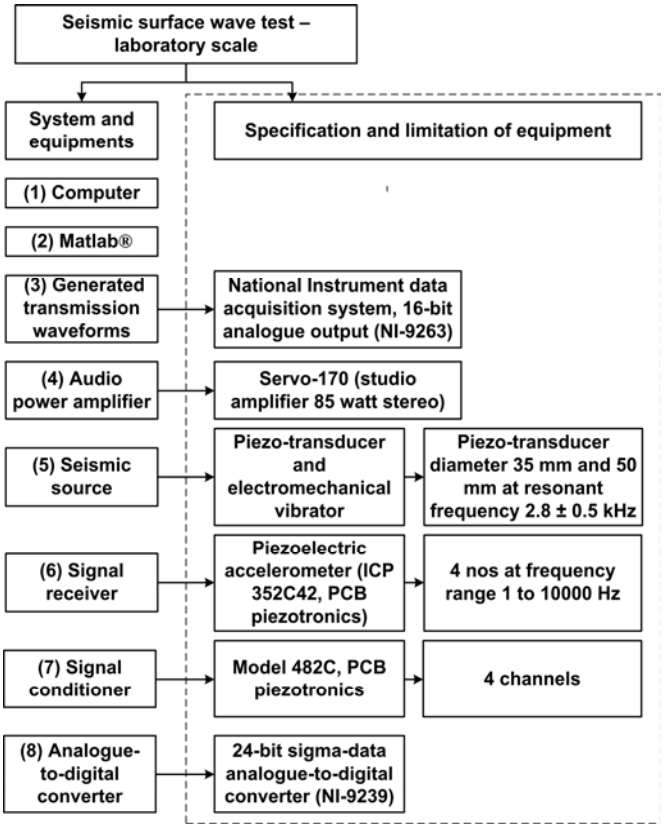

Figure 4.5: Detail of the equipment, specification for the laboratory scale seismic surface test.

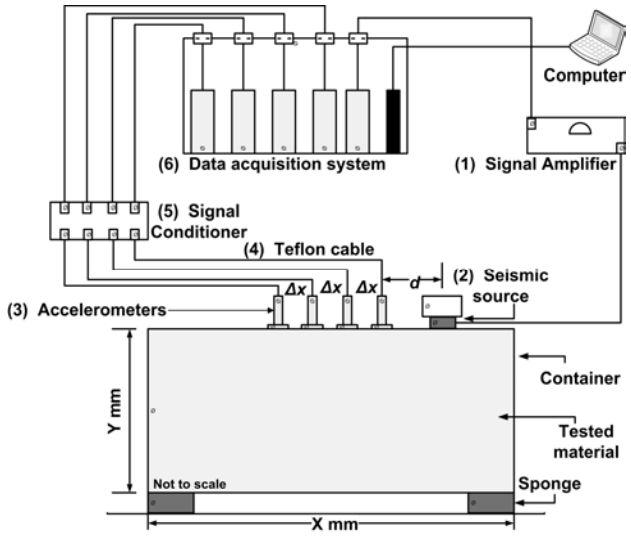

Figure 4.6: Laboratory setup for seismic surface wave test.

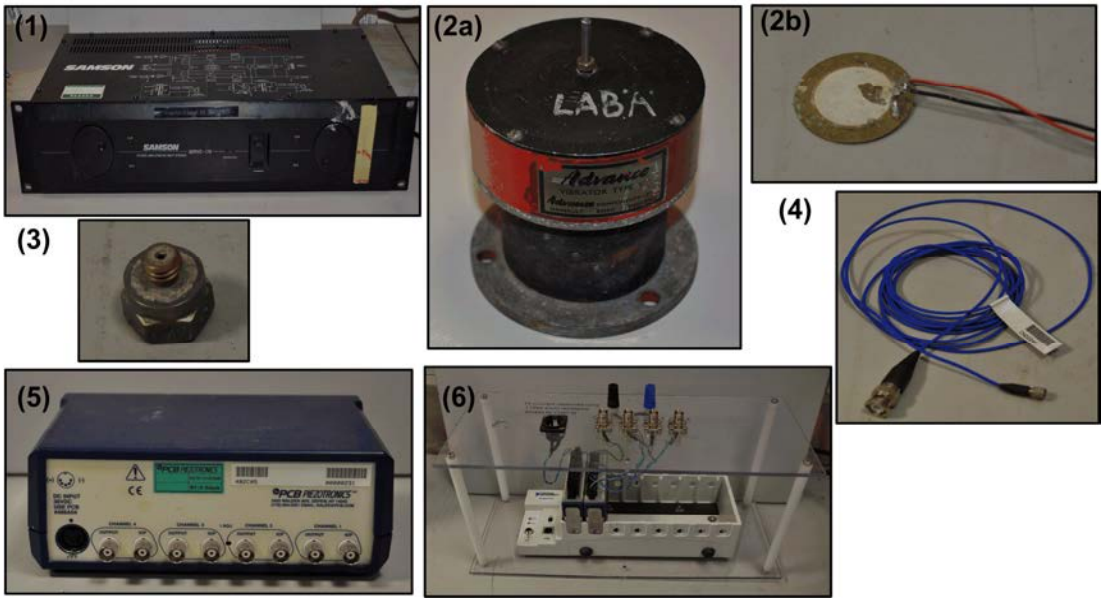

Figure 4.7: 1. Signal amplifier 2a. Electromechanical vibrator 2b. Piezo-transducer 3. Piezo-electric accelerometer 4. Teflon cable 5. Signal conditioner 6. Data acquisition system.

4.2.2 The Model of the Vibro-Replacement Stone Column

An overview of a typical vibro-replacement stone column arrangement is illustrated in Figure 4.8. A rigid footing with diameter D rests on the surface of a soft, homogenous clay bed containing a group of columns. The settlement of the footing is influenced by the following independent quantities (Hu, 1995):

h	(mm)	the penetration of the footing
c_u	(kPa)	the undrained shear strength of the soil
D	(mm)	the diameter of the footing
L_{col}	(mm)	the length of the columns
d_{col}	(mm)	the diameter of the columns
S	(mm)	the spacing between the columns
ϕ'	(degree)	angle of internal friction for column material
G_c	(kPa)	the elastic shear modulus of column material
G_s	(kPa)	the elastic shear modulus of the soil
γ_c	(kN/m³)	the unit weight of column material
γ_s	(kN/m³)	the unit weight of the soil
d_g	(mm)	the diameter of stone used in column

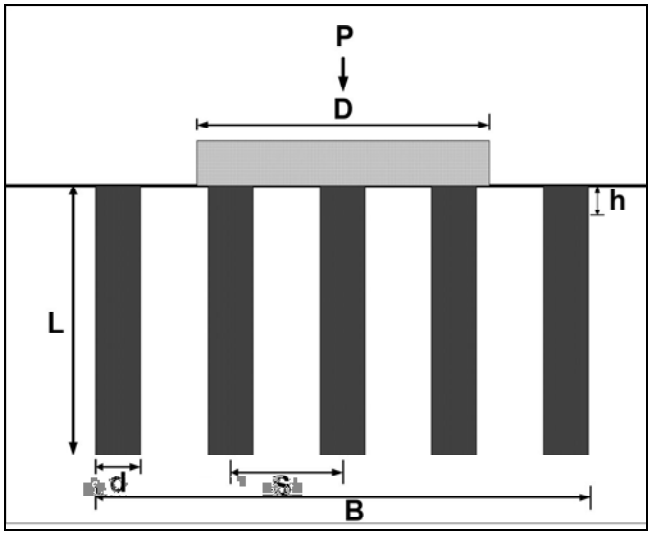

Figure 4.8: Simplified model of model stone column foundation.

To develop the most appropriate seismic wave method for imaging vertical and lateral stone column stiffness, a model was developed with all geometrical dimensions reduced by the appropriate scale factor. The scale factors of 15 to 16 were used due to the constraint of the space, the materials and the cost. The size of model and the velocity of material influenced the useful test frequency. The smaller model and higher velocity material needed a higher frequency of seismic source as well as higher receiver transducer frequency range. Despite, a larger model and lower velocity material needed lower frequency seismic source and lower receiver transducer frequency range. Thus, choosing of the scale factor and material should be designed based on availability of the seismic equipments. The physical properties of the materials remained the same as the prototype.

The dry technique of VSC construction typically used 0.28 to 0.4 m^3 per lineal metre stone backfill giving column diameter of 0.6 to 0.7 m. Meanwhile, the wet VSC technique used 0.65 to 085 m^3 per lineal metre about 0.9 to 1.04 m in diameter (Greenwood, 1970).

Figure 4.8 shows the stone column model diagrammatically. The undrained shear strength for very soft soil is below 20 kPa. Bulk modulus for dense sand and soft clay is about 30 MPa and 3 MPa, respectively (Terzaghi *et al.*, 1996). Once completed, the columns exhibit stiffness that were 10 to 20 times greater than the adjacent soil (Sonderamn and Wehr, 2004). The construction of model stone columns was planned to represent approximately typical field situations. The model of stone column was designed based on typical stone columns used in the field. According to Priebe (1995) the concentration of columns in an untreated area is referred to as the area replacement ratio, A_c/A, where A_c is the cross-sectional area of one column and *A* is the plan area of the unit cell attributed to a single column. The A_c/A is deduced from the column diameter, d_{col}, and the spacing of the columns, s;

$$\frac{A_c}{A} = c\left(\frac{d_{col}}{s}\right)^2 \qquad \text{……. Equation 4.1}$$

where *c* represent constant dependent upon the pattern of stone columns used; for a square pattern *c* is $\pi/4$ and for an equilateral triangular pattern *c* is $\pi/2\sqrt{3}$. Usually 10 to 25 % of weak soil volume is replaced by the column in low compressible site (Barksdale and Bachus, 1983). Table 4.1 summarises typical parameters of a vibro-replacement stone column in the field which consists of area replacement ratio, A_c/A, column length, L_{col}, column diameter, d_{col}, and stone diameter, d_g.

Table 4.1: Typical vibro-replacement stone column parameters (Sonderamn and Wehr, 2004).

Area replacement ratio, A_c/A %	Column length, L, m	Column diameter, d_{col}, m	Column spacing s, m	Length and diameter ratio, L_{col} / d_{col}	Stone diameter, d_g, mm	Column and stone diameter ratio, d_{col} /d_g
10 - 25	6 - 10	0.6 - 0.7 (dry technique) or 0.9 – 1.04 (wet technique)	1 - 2	10 - 20	30 – 80 (top feed) or 10 - 40 (bottom feed)	12 - 40

The physical dimensions of the models were scaled based on the actual size of vibro-replacement stone columns. The volumetric weight of the soil was not scaled since the tests were carried out in the condition of simple gravity. A reasonable similarity reached in the ratio for the geometric model stone column and typical stone columns in the field will enable the model to reveal the fundamental characteristics of wave-soil interaction in the field. The understanding revealed by the test design via this technique could be applied directly in the field with a similar ratio.

4.2.3 Construction of Model Stone Columns

The laboratory tests were devised to study the ability of seismic waves to differentiate lateral heterogeneities of properties in a controlled and known medium. At an early stage of testing, the seismic surface wave equipment and system were tested for their suitability and robustness to deliver a result. At the beginning of the test it was expected that these would be sufficient time to enable proper tuning of the equipment and system to obtain reliable data. This time may have caused significant change of the tested material

properties. Therefore, to overcome unexpected consequences in the early test, concrete mortar was used instead of natural soil. The properties of concrete mortar are reasonably constant after curing within 28 days of casting. Moreover, this approach was used by Khan *et al.* (2006) and Nasseri-Moghaddam (2006), thus the results using concrete mortar could be compared for verification.

4.3 Concrete Mortar Model

At this initial testing stage, two models consisting of concrete mortar as a control and concrete mortar with linear mild-steel bars used to simulate lateral variation properties were constructed. The second phase consisting of the model of soft natural clay with stone columns is described in Chapter 6, as part of the detailed programme of work.

4.3.1 Material and Properties

To construct the concrete mortar model, sand and cement were used. Particle size distribution was determined using the dry sieve analysis method in accordance with British Standard 1377 Part 2: 1990 (BSI, 1990). The material consists of 12 % gravel, 87 % sand and 1 % for silt. The composite curve sand is shown in Figure 4.9 (D_{50}=400 μm, D_{10}= 200 μm and D_{60}=450 μm).

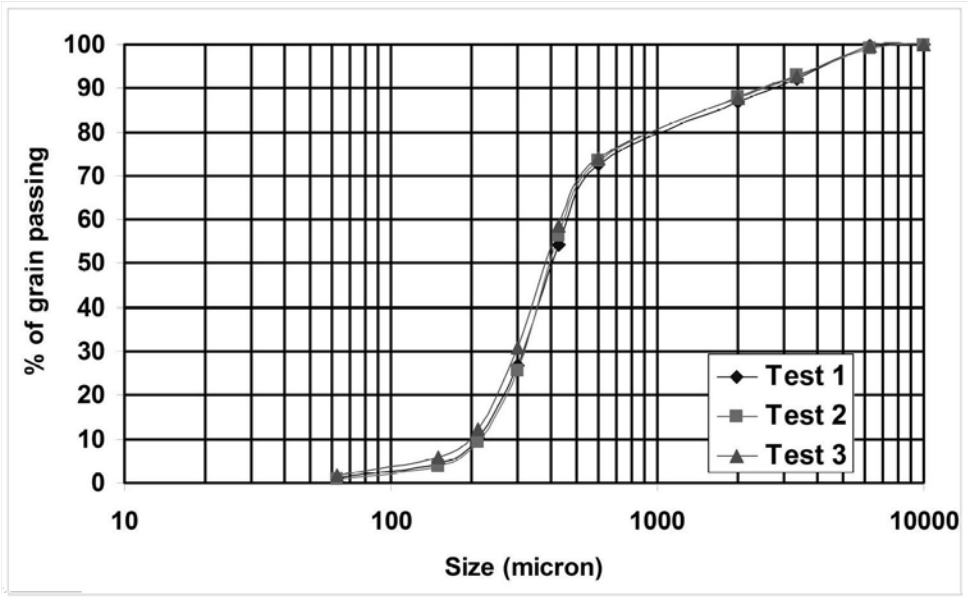

Figure 4.9: Particle size distribution of the sand used to construct the concrete mortar.

4.3.2 Experimental Setup and Calibration

For concrete mortar experimental setup, two concrete mortar blocks were constructed measuring 720 mm x 600 mm x 450 mm in length, width and depth respectively. The concrete mortar blocks were constructed using a mixture of sand with 9 % cement and 15 % water. The mixed concrete was poured into a wooden mould, then compacted using a concrete vibrator. The second block was constructed with a single line of three mild steel rods embedded before the cement-sand mixture solidified. The mixture was left to solidify for 24 hours and cured with a moist blanket to avoid surface cracking. The bulk density of concrete mortar was 2080 kg/m^3. The rods measured 38 mm in diameter, 300 mm in length and the inter-column spacing was set at 120 mm.

The dimensions of the steel columns and their spacing closely followed the ratio of the typical vibro-replacement stone columns. Although the dimensions of stone columns vary depending on circumstantial treatment requirements, typical measurements are mentioned in Table 4.1. The area replacement ratio, A_c/A, commonly used around 9 % (Barksdale and Bachus, 1983). Using this as a guideline, the steel columns were installed yielding an overall scaling factor of 16.

The concrete mortar material was chosen because its properties, such as density and moisture content, were relatively easy to control and varied insignificantly throughout the duration of the experiment. Also, the shear and surface wave velocities for concrete mortar are well documented (Khan *et al.,* 2006). The reason for using mild steel rods was to enhance the contrast of material density, thus providing a stronger variation of lateral homogeneity and subsequently aiding in the identification and analysis of the associated anomalies. The surface wave velocity in the concrete mortar block was expected to be approximately 1000 m/s (Khan *et al.,* 2006). The theoretical surface wave velocity for the mild-steel bar was calculated to be 2970 m/s using parameters of elastic modulus of 210 GPa, Poisson's ratio 0.3 and density 7850 kg/m^3, respectively (ASM International, 1993). The summary of test parameters is presented in Figure 4.10.

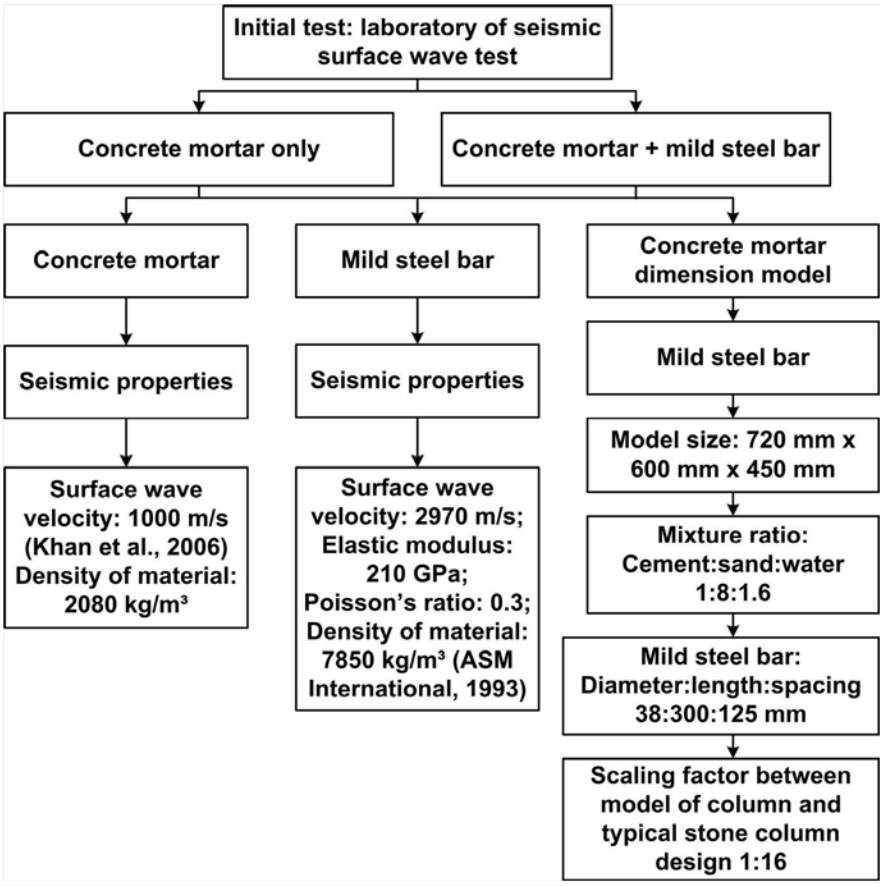

Figure 4.10: Concrete mortar test parameters.

An illustration of the laboratory setup is shown in Figure 4.11. The velocities of the surface wave for the concrete mortar and the mild-steel bar were around 1000 m/s and 2970 m/s respectively; suggesting the need of a higher frequency range. Rayleigh waves will be formed when the wavelength is smaller than half of the model depth (Zerwer *et al.*, 2000 and 2002). Therefore, the concrete mortar-mild-steel bar model needed a higher frequency, which means the piezo-ceramic transducer was more suitable to transfer high frequency energy. An audio power amplifier was used to drive the piezo-ceramic transducer with the excitation signals. The piezo-ceramic transducer was acoustically coupled to the surface using a weight padded with acoustic absorbers. A thin layer of

conductive gel was applied between the transducer and the concrete mortar surface to reduce air-voids and improve coupling. As the accelerometers' frequency range is up to 10 kHz only, the data captured will only be up to that frequency. The piezoelectric accelerometers were coupled to the surface with cyanoacrylic adhesive to obtain good coupling contact to the concrete mortar surface.

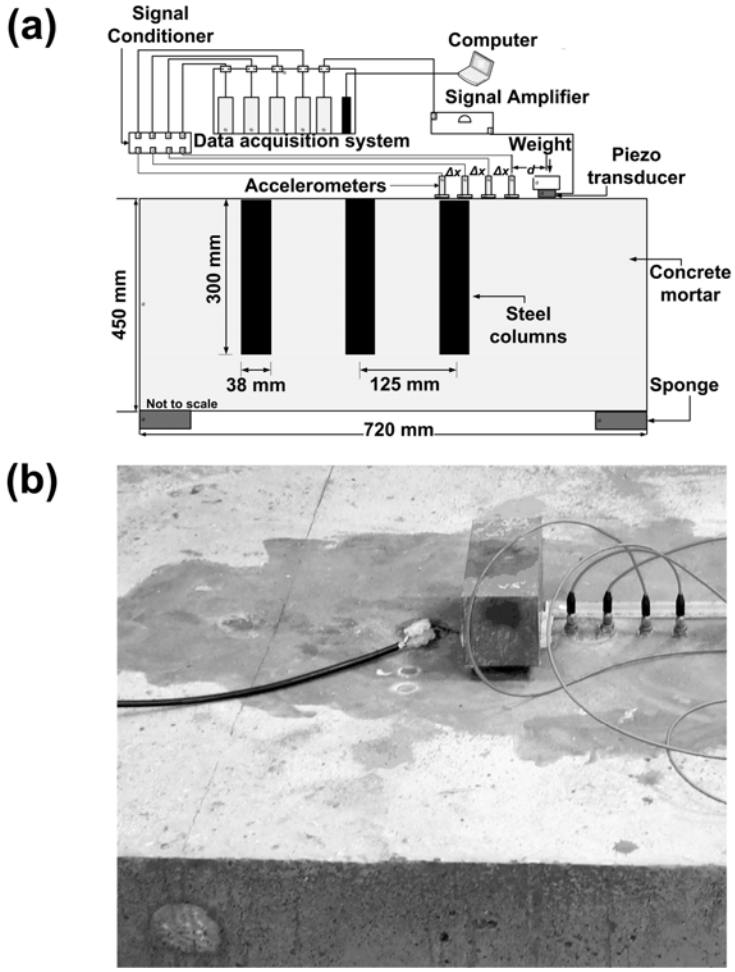

Figure 4.11: (a) Illustration of the laboratory-scaled model and equipment setup, and (b) photograph of the concrete mortar block with sensing accelerometers where the first sensor-pair on the left was located on one of the columns.

4.3.3 Experimental Procedure

The multi-channel approach used in this study is based upon a relatively small number of receiver channels. The array of receivers consisted of up to 4 piezoelectric accelerometers. The receiver array was then moved after each measurement to obtain data with a higher spatial resolution. This was repeated to extend the length of survey passing over a steel column.

The distance between the source and the first receiver, d_{min}, and the source and last receiver, d_{max}, was set as 50 mm and 125 mm. Using the constraints given in equations 3.10 and 3.11, which considers near and far offset constraint and assuming a surface wave velocity of 1000 m/s, the applicable frequency range was calculated to be between 6.7 kHz and 60 kHz, respectively. However, due to the frequency constraints of the sensing accelerometers, the upper frequency was limited to 10 kHz. The excitation waveform consisted of a 1 second continuous wave shaded with a Tukey-window to reduce spectral side-lobes and increase the dynamic range of the narrow band of interest. Using a stepped-frequency approach, the frequency of the sinusoidal wave was varied from 3 kHz up to 10 kHz with a step-size of 10 Hz. For each frequency step, 5 repetitive measurements were obtained for averaging and for the calculation of the normalised coherence.

Measurement was first performed on the block containing no steel columns to obtain a control dataset. The equipment was then set up on the concrete mortar block that contained the steel columns of diameter 38 mm. A series of measurements were performed by repeatedly moving both the excitation source and sensing accelerometers

after completing each set of measurements, until the area across the columns was surveyed. The sequence is shown in Figure 4.12. There were 15 unique lateral survey positions, and the columns were located at the 3rd, 8th and 13th of sensor pair positions respectively.

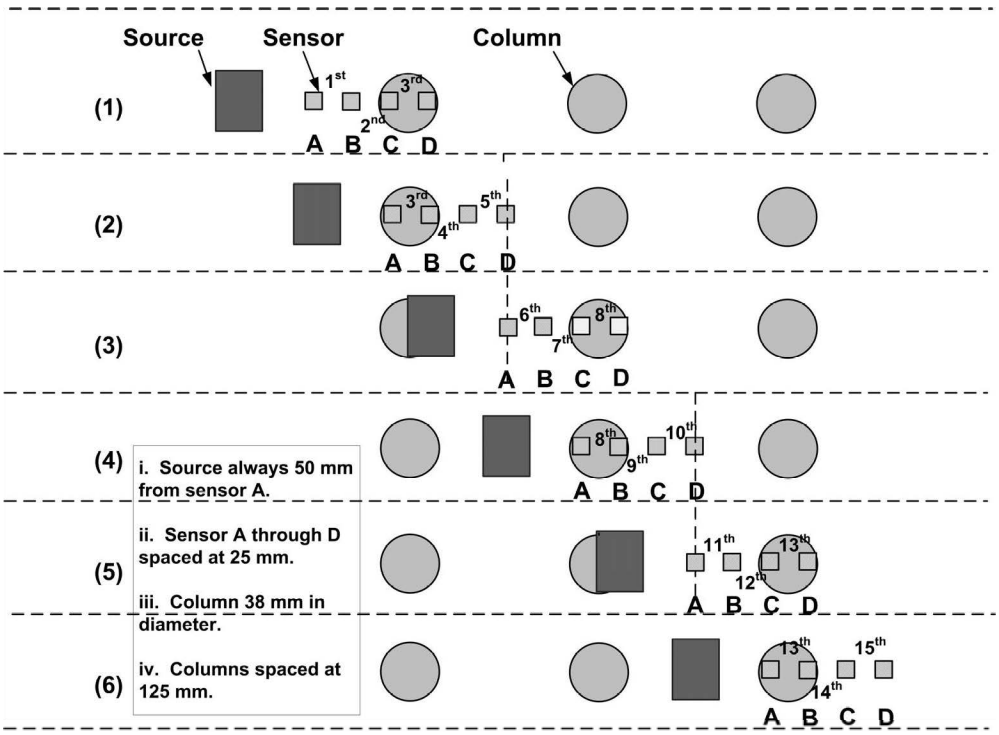

Figure 4.12: Sequence of the data collection process to survey the surface across the columns.

4.4 Method for Data Processing

Signal processing and spectral analysis techniques were applied to all surface wave data analysis in the concrete mortar (Chapter 5) and natural soil model (Chapter 7) studies. The

time-domain signals were discretely sampled, $y_n(k)$, by an analogue-to-digital converter and *N*-points were stored on a computer where the processing and the subsequent spectral analysis were carried out. To adequately capture the spectrum of the signals, the sampling rate, f_s, of the analogue-to-digital converter should be at least twice the maximum bandwidth of the signal, and usually higher in practice. The Discrete Fourier Transform (implemented using the FFT algorithm) was then applied to the signal to obtain the discrete spectrum of the signal, $Y_n(f)$:

$$Y_n(f) = \sum_{k=0}^{N-1} y_n(k) \exp(-j2\pi f\ k/N) \quad \text{..... Equation 4.2}$$

where f is the discrete frequency of the signal, $N = Tf_s$, while k and T are the discrete-time and time-duration of the signals. The signals are usually zero-padded in the time-domain prior to the application of a radix-2 FFT algorithm. As the quality of the observed phase velocity is strongly dependent upon the fidelity of the phase information, it may be necessary to observe the coherence of the received signals with respect to frequency, as a degradation of signal-to-noise ratio at a particular frequency would imply that the phase data for that frequency are unreliable. The coherence of the received signals is represented by its normalised cross-spectrum between the pairs of received signals. This allows measurement of the signal-to-noise quality as a function of frequency. In cases where the phase difference is calculated between a pair of receivers, the normalised coherence becomes a measure of variance, over multiple snapshots of time, between the received signals. The normalised coherence can then be calculated as (Ifeachor and Jervis, 1993):

$$S_{norm,mn}(f) = \frac{\sum_{p=1}^{P}\left[\left(Y_{n,p}(f) - \mu(Y_{n,p}(f))\right)\left(Y_{m,p}(f) - \mu(Y_{m,p}(f))\right)^{*}\right]}{(P-1)\sqrt{\sum_{p=1}^{P}\left|Y_{n,p}(f) - \mu(Y_{n,p}(f))\right|^{2}\sum_{p=1}^{P}\left|Y_{m,p}(f) - \mu(Y_{m,p}(f))\right|^{2}}} \quad \text{....Equation 4.3}$$

where p is the index of P, the total number of repetitive collections for each frequency step. $\mu(Y(f))$ is the mean of the complex spectrum across the repetitive collections at each step frequency f and * represents the complex conjugate operation. The signal-to-noise ratio can be calculated from the normalised coherence using

$$SNR(f) = 10\log_{10}\left(\frac{S_{norm,mn}(f)^{2}}{1 - S_{norm,mn}(f)^{2}}\right) dB \qquad \text{..... Equation 4.4}$$

The phase velocity, as a function of frequency, between any two receivers, can be calculated from their corresponding phase difference. The phase difference at a particular frequency, $\Delta\phi(w)$, is the angle of the complex spectrum value, and expressed as:

$$\Delta\phi_{mn}(f) = \tan^{-1}\left(\frac{\mathrm{Im}(S_{mn}(f))}{\mathrm{Re}(S_{mn}(f))}\right) \qquad \text{..... Equation 4.5}$$

where m and n are the receivers between which the four-quadrant phase difference is calculated. It should be noted that using only a single phase difference measurement is usually more sensitive to error from noise and interference from other modes of wave propagation. Therefore, it is recommended that if the signal-to-noise ratio is sufficiently high across reasonable bandwidths, then a best fit phase-frequency gradient is used as a method of averaging to calculate the time-delay.

The time-delay associated with the phase difference observed between the two receivers can be derived from:

$$\tau(f) = \frac{\Delta\phi(f)}{2\pi f} \qquad \ldots\ldots\ldots\ldots \quad \text{Equation 4.6}$$

The frequency-dependent phase velocity, *v(f)*, can then be obtained using the distance between the two receivers *m* and *n*, $\Delta_{mn}x$, such that:

$$v_{mn}(f) = \frac{2\pi\ f\Delta_{mn}x}{\Delta\phi_{mn}(f)} \qquad \ldots\ldots\ldots\ldots \quad \text{Equation 4.7}$$

The plot of phase velocity versus frequency is the dispersion curve. To obtain the phase velocity with respect to depth, the frequency values need to be inverted into depth. This is based upon the observation that surface waves with lower frequencies penetrate to greater depths. The process of inversion can be generally divided into three main categories (Matthews *et al.*, 1996; Menzies, 2001): approximation, iterative minimisation and finite element modelling. The approximation method is the simplest but least exact. The method is based upon the assumption that the amplitude of the surface wave is attenuated linearly as a function of depth, and can usually be represented by a direct relationship of:

$$D \approx k\lambda(f) \qquad \ldots\ldots\ldots \quad \text{Equation 4.8}$$

where the wavelength, $\lambda(f)$, is

$$\lambda(f) = \frac{v(f)}{f} \qquad \ldots\ldots\ldots\ldots \quad \text{Equation 4.9}$$

The *k* represent a constant dependent upon the tested material homogeneity and could be 0.25, 0.33, 0.5 and 1 as reviewed by Addo and Robertson (1992) and Matthews et al., (1996). The *k* values 1 and 0.5 are commonly for a vertically homogeneous site, 0.25 for stiffness increasing with depth and 0.33 as a compromise between 0.25 and 0.5 as documented in the literature (Jones, 1958; Heukolom and Foster, 1962; Ballard and Mclean, 1975; Abbiss, 1981). Meanwhile, the iterative optimisation technique is based upon the concept introduced in early work by Thomson (1950) and Haskell (1953). It is based upon iteratively optimising the parameters of the soil profile until a good match between the measured dispersion-curve and the dispersion-curve derived from the estimated soil profile is achieved. This technique is computationally intensive but offers greater accuracy in a sharply heterogeneous medium. Finite element modelling is a forward-solver technique based upon obtaining a theoretical solution to the wave propagation model through the soil. The inversion techniques deal with the assumption that the soil in layered with vertical heterogeneity and lateral homogeneity. The inversion is not applied for accessing the stiffness profile of known boundary and dimension of the model, but is sufficient of using graphical features of the dispersion curve to delineate the variations in investigated model (Rhazi *et al.*, 2002).

To date the lateral heterogeneous soil has received little treatment in the literature on the analysis of surface waves. The approximation method chosen herein was for its relative simplicity which involved consistent geometry of the model of vibro-stone column and the soil materials can be considered to be reasonably vertically homogeneous with depth relatively homogeneous (less than 2 % water content change across the soil profile), as this research involves a relatively shallow depth (30 cm and 50 cm depth for small and large

container). In context of real application Matthews *et al.* (2000) explained that if the soil density increase with depth therefore k should be 0.25 and if homogeneous soil 0.5, however so far there is no literature explained for lateral heterogeneous soil. The constant value *k* is 1 can be used when interpreting the results of the lateral heterogeneous and vertically homogeneous of column and clay. This aspect was incorporated as part of the study objectives and therefore is discussed in Chapter 7 and Chapter 8.

In a solid and homogeneous medium, the Rayleigh-wave phase velocity, v_r, can be converted into shear-wave velocity, v_s, which for an elastic medium is approximately:

$$v_s \cong \frac{1+\upsilon}{0.862+1.14\upsilon} v_r \quad \text{.....} \qquad \text{Equation 4.10}$$

where υ is a Poisson's ratio (Richart *et al.,* 1970). The maximum shear modulus of the material, G_{max}, which describes the behaviour of the ground under load (Matthews *et al.* 2000; Clayton, 2011), is related to the mass soil density, ρ, and the shear wave velocity through the relationship:

$$G_{\max} = \rho v_s^{\,2} \quad \text{.....} \qquad \text{Equation 4.11}$$

The error in maximum shear modulus arising from the approximation of the Poisson's ratio for soil and rock materials in the conversion of Rayleigh-wave phase velocity into shear wave velocity is usually less than 10% (Menzies, 2001). Using the Equation 4.10 and 4.11, the measurements of the Rayleigh-wave phase velocity enables the evaluation of the stiffness profile of the ground, as well as any associated effect of the improvement work in the near vicinity of the column.

The accuracy of the phase velocity profile is directly affected by the accuracy of phase estimation. The coherence function, such as in equation 4.3 for a stepped-frequency approach, is used to discard low quality measurements. This relies on a rigid threshold regime, where only measurements above the threshold are taken into account. As a result, all the values below the threshold are treated as equally insignificant, while the values above are likewise important. However, this may not be true and therefore may result in the suboptimal treatment of phase measurements. A weighted approach, as determined by the coherence function, is herein proposed for homogeneous material not containing columns (non-dispersive). This allows the allocation of a variable level of importance to each phase measurements. A threshold is still applied, but can now be set lower, and weighting applied to the values above this threshold. Within a layer of homogeneity, where the average of phase velocities across all the discrete depths within this layer is calculated, the weighted-mean velocity can be expressed as:

$$\bar{v} = \sum_{i=1}^{n} w_i v_i \Big/ \sum_{i=1}^{n} w_i \qquad \text{…….} \quad \text{Equation 4.12}$$

where w_n are the discrete weightings that correspond to the n measurements which exceeds the threshold. To determine a signal-quality based weighting function, it is necessary to form a relationship between the signal quality and the normalised coherence. The weighting, w_i, is thus chosen to be directly proportional to the linear form of the signal-to-noise ratio for all phase velocities exceeding the threshold, such that:

$$w(f) = \frac{S_{norm,mn}(f)^2}{1 - S_{norm,mn}(f)^2} \qquad \text{…….} \quad \text{Equation 4.13}$$

When dealing with heterogeneous soil, the step frequency approach was used while conducting the measurement to increase the signal-to-noise ratio. Signal coherence was used as indicator to obtain reliable data from the heterogeneous soil, with weighted mean not being used due to the tendency to average the whole sampling frequency. The near and far offset constraints and spatial aliasing effect (see Section 3.4, Equation 3.10, 3.11 and 3.12) which were affected by the array (distance between seismic source to first sensor and sensors spacing) were also crucial for obtained reliable phase velocity.

Chapter 5

FEASIBILITY TEST RESULT

5.1 Introduction

This chapter explains the results, limitations and conclusions from the concrete mortar model test. The outcome from the feasibility test was used to develop the surface wave tests on model of stone columns in natural soil (see discussion in Chapter 6 and 7).

5.2 Concrete Mortar Model

5.2.1 Data Processing

Every complete set of measurements contain received signals from the 4 sensing channels, spanning the frequency range of 3 kHz to 10 kHz with a step-size of 10 Hz. After the completion of each data collection session, the data were loaded into Matlab for processing. The first step was to apply an FFT on all the data to obtain the spectral

representation of the received signal. The results were a series of complex values of which the magnitude and angle, respectively, represented the spectral amplitude and phase. As a stepped-frequency transmission was implemented, the complex value corresponding to the frequency of transmission with which the received signal is associated was selected and stored. This was repeated for all the repeated transmissions at the same frequency, and then for all the frequency steps across the whole range. This yielded a new spectral series of complex FFT values as a function of the stepped frequencies. Therefore, the data were reduced to the stepped-frequency spectral representation for the 4 sensor channels, with 5 multiple sets as there were 5 repetitive snapshots for each frequency step during data acquisition.

The next step was to obtain the phase difference between the receivers. Among the 4 sensors, there were 3 phase difference measurements between adjacent sensor pairs. For each of these adjacent sensor pair, the phase difference was obtained by performing a complex conjugate multiplication in the spectral domain. For example, to obtain the phase difference between adjacent sensors A and B, the FFT of signal from sensor A was multiplied with the complex conjugate of the FFT of signal from sensor B. Since there were multiple snapshots, an average of the spectra was used in the multiplications.

5.2.2 Analysis of Results

Figure 5.1 shows the phase difference measurements obtained from the data set with no columns and from the first set of measurements with columns. In an ideal, homogeneous medium with no boundaries, the differential phase response is expected to be a linear

function of frequency. However, the result in Figure 5.1(a) shows that the measurements were corrupted by boundary reflections as well as the mutual interference between the body and surface waves; while Figure 5.1(b) demonstrates that the presence of columns introduced additional reflections due to the sharp variation in material density between the columns and the concrete mortar. This resulted in significant distortion in the phase response. Measurement from the C-D sensor pair located directly on top of the first column demonstrated the most severe distortion. This was likely to be caused by a combination of two factors, the lack of energy entering the column due to reflections and interference from reflections within the column. This was also reflected in the lack of signal coherence at the receivers over a relatively large number of frequencies.

The normalised coherence was then calculated for each of the sensor pairs using equation 4.3. The plots of normalised coherence for the case of without columns and with columns are shown in Figure 5.2. The normalised coherence is a measure of the signal quality in terms of the signal-to-noise ratio, and therefore was used as a criterion in choosing the frequencies that contained phase measurements with higher accuracy. As phase measurements are very sensitive to degradation in signal-to-noise ratio, a minimum threshold of 0.995 for the normalised coherence was applied to obtain higher accuracy of the phase difference, and the frequencies with coherence that exceeded the threshold were selected. About 30 % when without columns and 15 % with columns of the data collected were above 0.995 threshold. Higher threshold was recommended to use by Addo and Robertson (1992) to obtain high quality of data, who used the threshold larger than 0.98. Threshold 0.9 recommend and use on pilot and main test later on. However, a higher coherence was used to guage data quality.

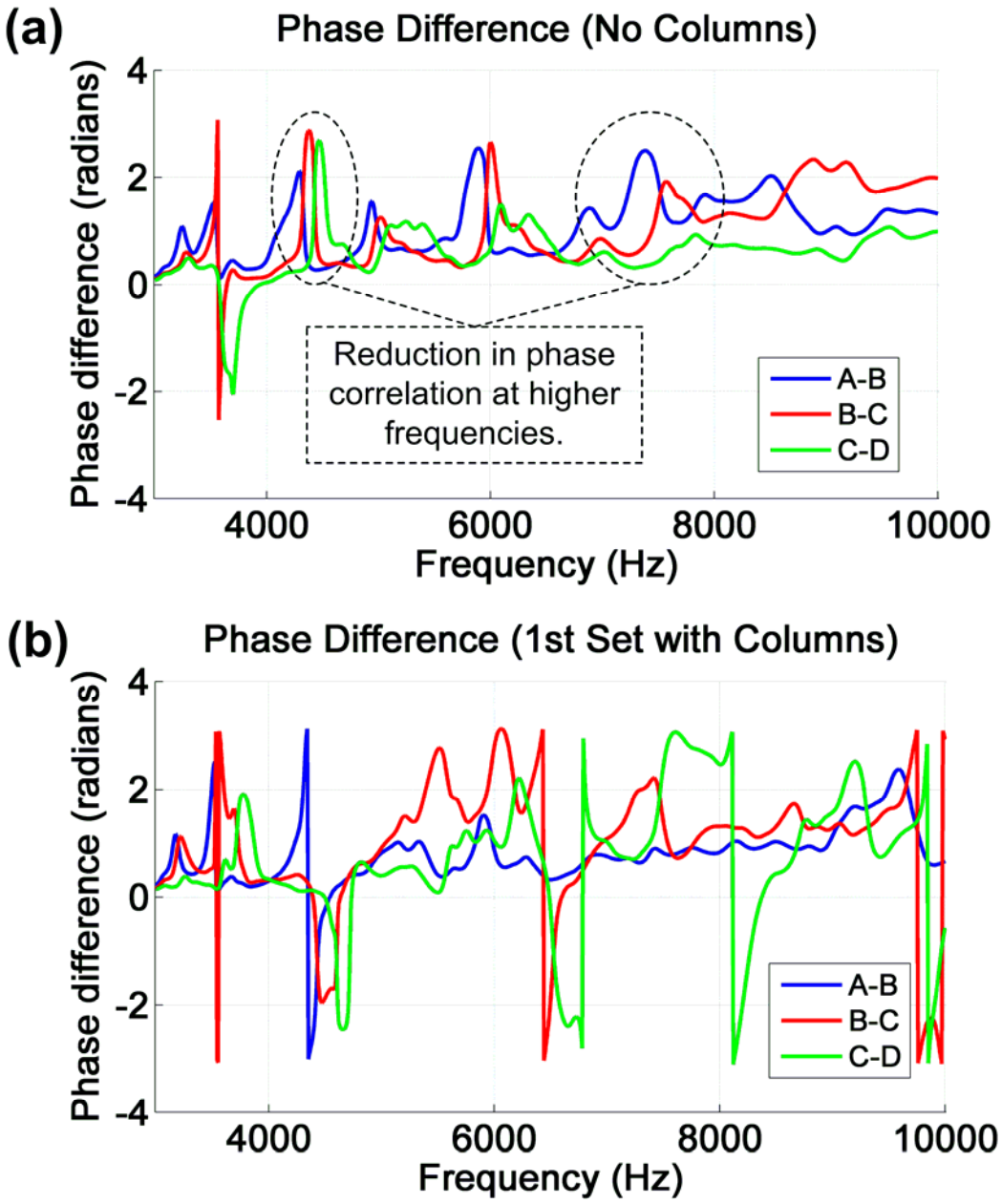

Figure 5.1: The phase differences for the 3 sensor-pairs from (a) measurements on concrete mortar without columns, and from (b) the first set of measurement on the concrete mortar with columns.

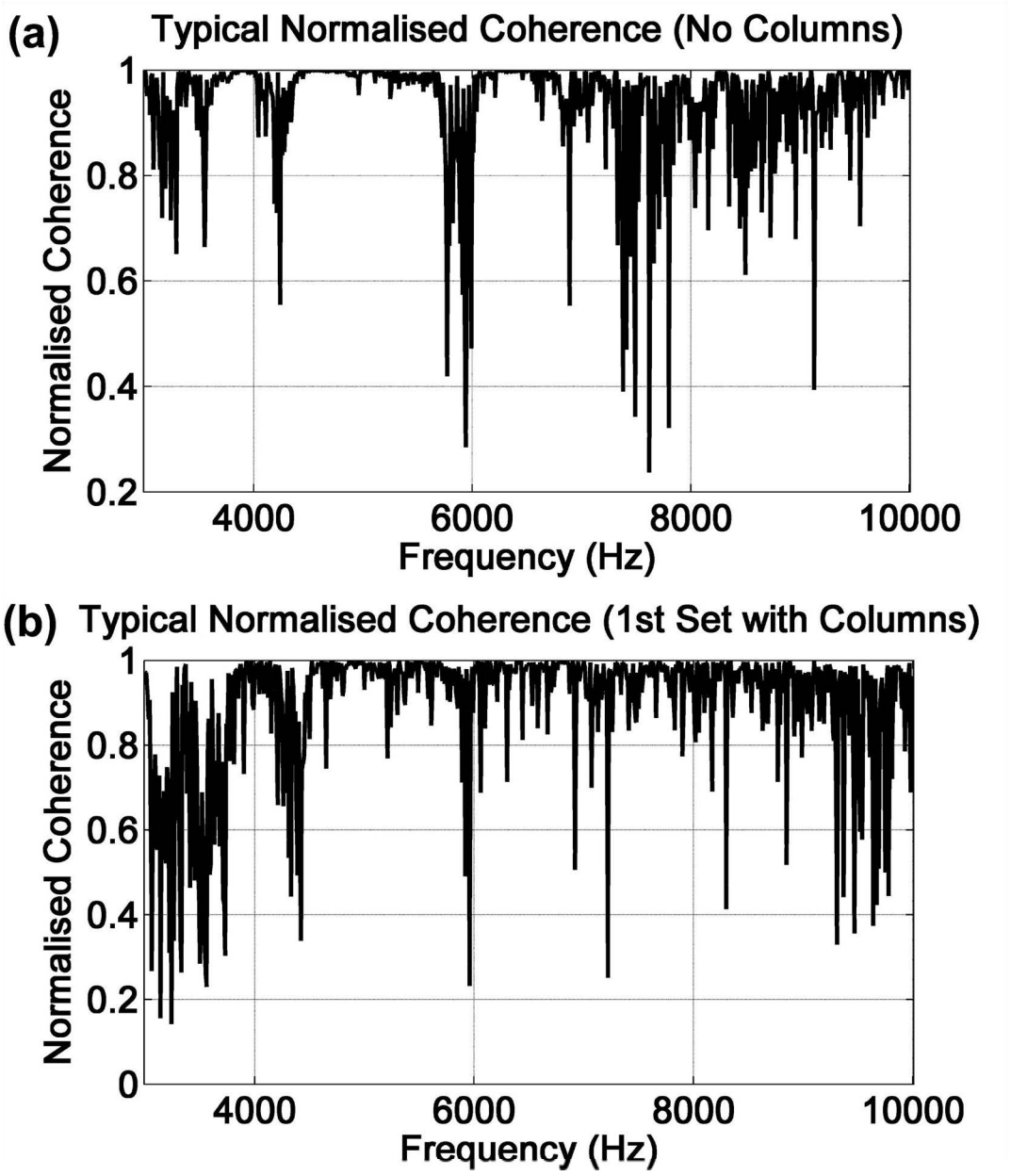

Figure 5.2: The normalised coherence between channels A and B from (a) measurements on concrete mortar without columns, and from (b) first set of measurement on the concrete mortar with columns.

The next step was to obtain the Rayleigh-wave phase velocity measurements. The effective frequency range, as predicted by equations 3.10 and 3.11, was from 6.7 kHz up to

the accelerometer's upper frequency limitation of 10 kHz. Since the constraints were only an approximation, a frequency range of between 6 to 10 kHz was chosen for processing. As there were only a very small number of frequencies that exceeded the threshold, this frequency range was divided into sub-bands of 400 Hz each. The velocities were calculated from the phase measurements using equation 4.7. Within each sub-band, the velocities that corresponded to the qualifying frequencies were averaged. In sub-bands that contained no qualifying frequencies, the average value from the higher sub-band was used. A low-pass interpolation filter was then applied to smooth and resample the data by a factor of 4, producing velocities that correspond to 100 Hz step increments. The results are shown in Figure 5.3. Figure 5.3(a) shows the result corresponding to the first set of measurements (based upon the sequence described in Figure 4.12) from 6 to 10 kHz. It can be observed from Figure 5.3(a) that the velocities at frequencies lower than 7 kHz had larger deviations from the expected Rayleigh-wave phase velocity for the material of concrete mortar and mild-steel column. This was likely to have been caused by interference from other wave modes at these lower frequencies. As such, the remaining data sets were processed using the range of 6.8 to 10 kHz. The results from all the 6 sets of measurements were merged to form a 2-D Rayleigh-wave phase velocity map as a function of frequency and lateral survey positions in Figure 5.3(b). Anomalies in the form of higher velocities were observed at positions 3, 8 and 13 where the columns were located.

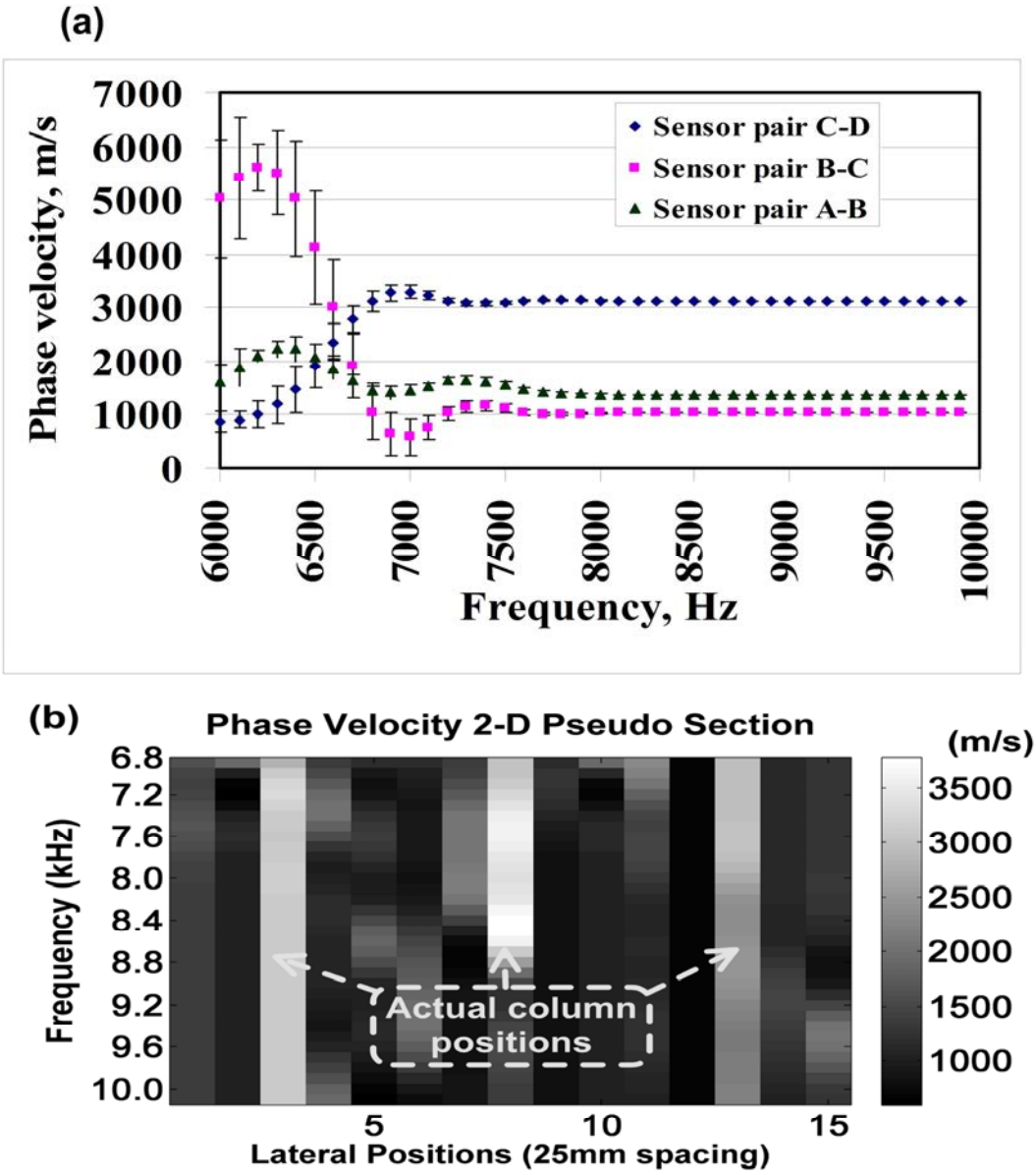

Figure 5.3: (a) The plot of phase velocity versus frequency and it standard deviation for the first set of measurements with columns and (b) the 2-D pseudo section across all the lateral survey positions.

The Rayleigh-wave phase velocities were converted into shear-wave velocities by a factor of 1.08 based upon Poisson's ratio 0.3 in equation 4.10. Where more discrete samples are available, either via the use of a wider frequency range or in cases where there are more frequencies that contain accurate phase measurements, the shear-wave velocity values can be interpolated to obtain a smoothed dataset. In this case, given the *a priori* knowledge that both the concrete mortar and the steel columns were relatively homogeneous with respect to frequency and also the sharp contact with larger contrast of density between concrete mortar and column, it was possible to average the shear-wave velocity measurements across the different frequencies, producing the result shown in Figure 5.4. When a small density contrast such as between clay and gravelly sand column, therefore it was not possible to average the velocity across frequencies as discussed in Chapter 7 and 8.

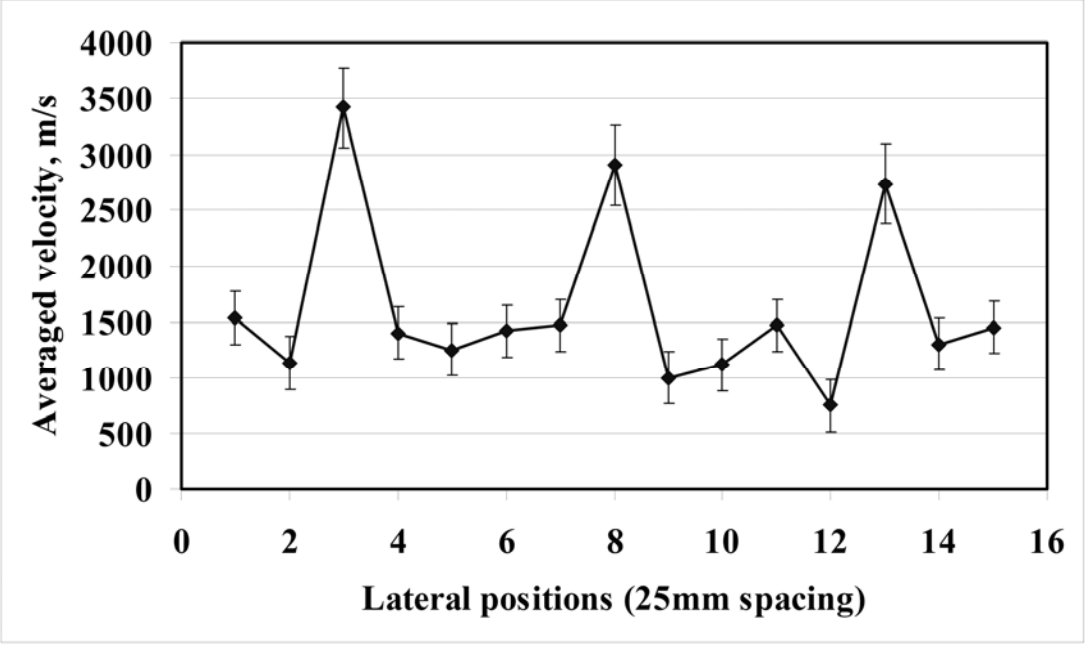

Figure 5.4: The average shear-wave across frequency for all the lateral survey positions.

For comparison, the Rayleigh-wave phase velocities in the three mild-steel columns, averaged along depth, were 3417, 2900 and 2733 m/s. The average Rayleigh wave velocity in the mild-steel column was 3017 m/s. The average Rayleigh-wave phase velocity in the concrete mortar was 1274 m/s. The expected phase velocity for the columns was 2970 and concrete mortar 1000 m/s (from literature). The error bar of stiffness in this experiment was approximately 12 % in the columns and 18 % for the concrete mortar.

5.3 Discussion

In this work, to develop a technique that is able to make measurements in lateral heterogenious material, the use of steel columns in concrete mortar provided the advantages that the effective geotechnical properties of the materials are well characterised. The use of these materials which have consistent properties and very significant differences in densities thus should be able to demonstrate the signal differences. In addition this approach introduces the constraints in the direct extrapolation of the results for site applications. Due to their vast differences in densities therefore, it was not possible to reflect the true densities between soft clay and columns that used in stablised soil. However this is important aspect in understanding the effect of changes in densities laterally in the process of development the seismic surface wave technique. The main difference is in the sharp variation of material density caused by the steel-to-concrete mortar interface. As the reflection coefficients at the boundary between two materials are proportional to the contrasts in density, the reflections are usually less severe in real sites

as the variation in density between stiffening rock columns and the surrounding soil is usually smaller (see Chapter 7 when testing conducted on natural soil). The gradient of density variation is also less sharp as the surrounding soil may mix into the rock column after compaction (in real stone column construction). This implies that the signal may also experience some level of refraction and, depending on the pattern of refraction, may reduce the energy near the surface for some frequency components.

From the perspective of the multi-channel surface wave analysis technique, the unique aspect of this target application is the pattern and proximity of lateral heterogeneity introduced by the columns. The energy introduced by the seismic source needs to contend with multiple changes in material density due to the arrangement and spacing of the columns, each introducing reflections and additional attenuation to the wave. Therefore, this may reduce the upper limit for the useful distance between the source and the furthest receiver, hence increasing the number of required array movements. The effect of reflections and attenuation on the source energy should also be taken into consideration in determining the optimal source-array configuration. It is also worth noting that measurements obtained for the column itself are more vulnerable to self-interference due to internal reflections; the width of the column has the same order of magnitude compared to the typical distance between two sensing geophones.

The interaction between the body waves and surface waves as a function of distance from the source and frequency are often difficult to predict in practice. The switch-over between the dominating waves is usually not instantaneous, and therefore mutual interference (self-noise) can occur over a range of distances from the source. With the use

of a stepped-frequency approach in this research, it can be observed from the result in Figure 5.1(a) that there exists a correlation of phase-difference between the sensor-pairs which becomes weaker at higher frequencies beginning with the sensor-pair furthest from the source. This might indicate a variation in the interaction between the different modes, but due to the weak signal coherence and the presence of relatively strong boundary reflections.

5.4 Limitation

The concrete mortar has a high phase velocity; as a result this created a limitation for seismic tests with respect to the seismic source-receivers array. The longest distance of a sensor from the seismic source demonstrated the most severe distortion and yield in the lack of signal coherence. Higher phase velocity in concrete mortar required a higher upper frequency limit up to 60 kHz. However, due to a restriction of the receiver sensor of 10 kHz, the test on concrete mortar cannot access the higher frequency behaviour. The strong seismic impedance due to the large difference in materials' densities (steel bar density 7850 kg/m³ and concrete mortar density 2080 kg/m³) in a lateral direction resulted in higher reflections, refractions and attenuations, thus weaker signal-to-noise ratio was observed in the phase response. However, this will be much less significant a problem with stone column, due to the small differences of densities between column material (crushed aggregate) and clay. Typical dry unit weight of column was 1835 kg/m^3 and soft clay 1427 kg/m^3 (Sonderamn and Wehr, 2004)

5.5 Conclusion

From the experience gained in this initial test using the concrete mortar was very useful for further development of surface wave test in the laboratory to investigate the quality of stone column. In the initial testing, the multi-channel surface wave analysis method was applied in a scenario with lateral heterogeneity caused by multiple stiffening columns. This technique used sensors and source in a linear array, where the seismic source was at one end of the array. The present of columns caused the strong level of self-interference, and therefore the furthest sensor suffering the weakest signal coherence. To overcome this problem, a stepped-frequency approach was adopted to increase the signal-to-noise ratio of the received signal.

The interaction between the body waves and surface waves was a function of distance from the source and the sensor constraint. The upper limit of frequency was beyond the receiver frequency range (less than 10 kHz). Further testing using natural soil was able to visualise full frequencies range and thus the interaction between the frequency and the array of source and sensors, namely the near-, far offset constraint and the spatial aliasing more understandable and is discussed in Chapter 7 and 8.

The 2-D Rayleigh-wave phase velocity map generated from the measurements showed prominent velocity anomalies at the survey positions that correspond to the columns. The surface-wave velocities corresponding to the mild steel columns and the concrete mortar were estimated from the measurements to be 2779 and 1173 m/s respectively. These

compared well with the expected velocities of 2970 and 1000 m/s, demonstrating a reasonable agreement between the measured and known stiffness profile of the materials. Therefore, this initial testing indicates that the equipment and system were suitable to use for seismic surface wave test in the laboratory on scale VSC. Further tests were conducted on the natural soil that better matches a real scenario and these presented in the following chapter (Chapters 6 and 7).

Chapter 6

DETAILED PROGRAMME OF WORK

6.1 Introduction

This chapter discusses experimental work as summarised in Section 4.2; pilot test and main test. The experimental programme involved was at first a pilot test using a small box, which contained kaolin clay as the clay test bed and installed with a single column. Meanwhile, a main test involved a larger size of container filled with Oxford clay bed test and a configuration of stone columns to simulate more realistic scenarios. These models are constructed with different purposes, however, directed to a key focus of this work was find an optimum receiver array deployment, which is able to maximize the rate of columns assessment on typical VSC improvement. In addition, this work ahead at assessing results in relation with the model properties and configuration.

6.2 Material and Properties of the Natural Clay

The reduced scale model of the stone column investigation focussed on the physical properties of the clay test bed and stone columns. Therefore, it was appropriate to use well defined materials. For this study a compacted higher moisture content of Oxford clay and kaolin were used to form the clay test bed with gravelly sand used to form the test column. The properties of the materials used are described in this chapter, which also contains descriptions of preliminary tests and the results of materials used throughout this work to ascertain the specific properties.

6.2.1 Clay Materials Used in Test Beds

Kaolin was initially used, mixed from dry processed powdered clay. This ensures a high degree of sample control and reduces variability throughout the test programme. Unfortunately due to the need for a relatively large test box for main programme of work, it was deemed more convenient to obtain an uniform sample of natural clay, in this case Oxford clay. Oxford clay here was used because of it relatively ease of sampling, occurring in significant quantity, whilst being relatively uniform across the sample taken. Oxford clay was obtained as a single batch from Hanson Bricks quarry in Peterborough, England. Oxford clay consists of marine sedimentary rock formation in aged of Jurassic and underlying much of southeast England, around Oxford, Peterborough and Weymouth.

In order to homogenize the clay all the samples were mixed before carrying out any tests. Thus any differences present in the samples were averaged out. The properties of the Oxford clay and kaolin used are given in Table 6.1.

Table 6.1: Summary of the index properties of Oxford clay, kaolin and gravelly sand.

Type of soil	Oxford clay	Kaolin	Gravelly sand
Plasticity test;			
Plastic limit	26.3 %	28.9 %	N/A
Liquid limit	47.4 %	59.3 %	
Plasticity index	21.1	30.4	
Compaction test;			
Optimum water content, OWC	23.5 %	28.0 %	9.5 %
Maximum dry density, MDD	1550 kg/m^3	1410 kg/m^3	1865 kg/m^3
Bulk density	1920 kg/m^3	1810 kg/m^3	2045 kg/m^3
Particle size (coarse fraction);			
Gravel 3.18 - 2.00 mm	No coarse fraction	No coarse fraction	34 %
Coarse sand 2.00 - 1.18 mm			54 %
Medium sand 1.18 - 0.60 mm			7 %
Fine sand < 0.60 mm			5 %
Specific gravity	2.60	2.65	2.70

6.2.2 Gravelly Sand

The material for constructing the stone column was obtained by sieving a fine quarry aggregate in the laboratory. The suitable grain sizes were based on the scaled-down prototype grain diameter (See Section 4.2.2). For this study, a prototype of bottom feed

technique of constructing stone columns was used with a typical grain size diameter of 10 to 40 mm. Therefore, the scaled-down material (gravelly sand) was used to represent the stone column and had a grain size diameter between 1.18 mm and 2.8 mm.

6.3 Physical Properties of the Model Stone Column

A suite of British Standard tests were carried out to determine the physical and mechanical properties of Oxford clay, kaolin and gravelly sand. This allowed comparison from similar test results with other researches to be made. The physical properties of the materials that were used throughout characterised:

i. the index properties of Oxford clay, kaolin and gravelly sand;

ii. Oxford clay, kaolin and gravelly sand compaction properties, and

iii. the relationship of the shear strength and clay moisture content using a quick undrained triaxial test on Oxford clay.

6.3.1 Plasticity Measurement

A liquid limit (LL) test was carried out using the cone penetrometer apparatus in accordance with Clause 4.3 of BS1377: Part 2: 1990 (BSI, 1990). A plastic limit (PL) test was carried out in accordance with Clause 5.0 of BS 1377:Part2:1990 (BSI, 1990). Oxford clay had a LL of 47.3 % and PL of 26.3 %, which are typical values for Oxford clay (Lee,

2001). Meanwhile, for kaolin LL is 59.2 % and PL 28.9 %, which are also typical values for kaolin (John, 2011).

6.3.2 Specific Gravity

Specific gravity tests were carried out using the small pyknometer method in accordance with Clause 8.3 of BS 1377: Part 2:1990 (BSI, 1990). Oven-dried soil passing through a 2 mm sieve was used for testing. The specific gravity of the Oxford clay ranged from 2.59 to 2.61 with an average of 2.60, kaolin 2.63 to 2.68 with an average of 2.65 and gravelly sand 2.69 to 2.73 with an average of 2.70. Again, these are typically what is expected for these soil types.

6.3.3 Particle Size Distribution

Particle size distribution was determined using the dry sieve analysis method in accordance with British Standard 1377 Part 2: 1990 (BSI, 1990). The gravelly sand consisted of 34 % gravel, 54 % for coarse sand between 1.18 mm and 2 mm and 12 % for medium to fine sand. The material is a uniformly graded gravelly sand (D_{50}=1700 μm, D_{10}= 1180 μm and D_{60}=1900 μm). The grading curves are shown in Figure 6.1.

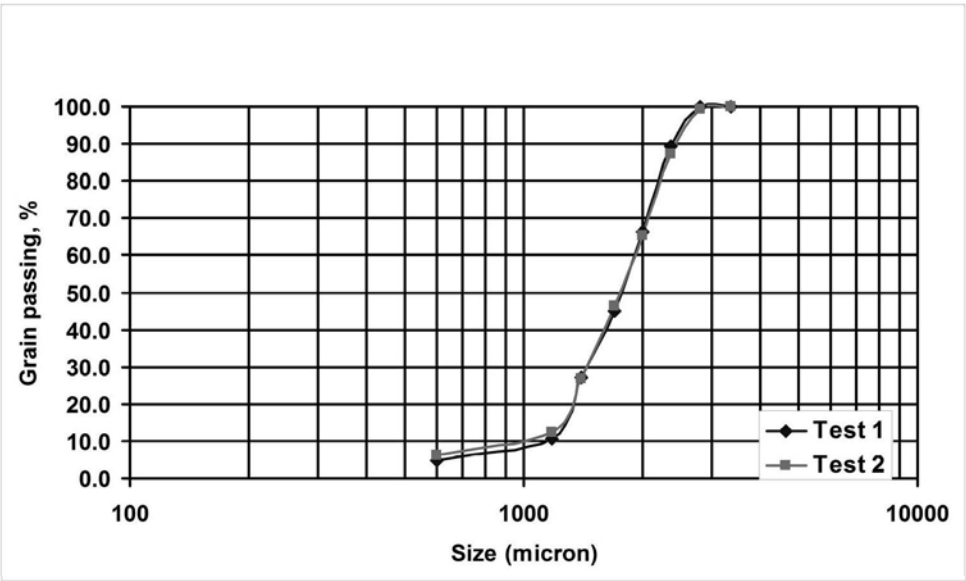

Figure 6.1: Particle size distribution of gravelly sand showing it to be uniformly graded (Uniformity coefficient of 1.76).

6.3.4 Compaction Test

The clay compaction tests were conducted using the Dietert method, where the samples were subjected to l0 blows at each end of sample tube. According to Head (1980), the compaction results obtained using the Dietert method are similar to these obtained using the BS 2.5 kg rammer method. Therefore, it deemed suitable for this test programme. Meanwhile, for gravelly sand, the compaction tests were carried out using the vibrating hammer method as described in BS 1377-4:1990 (BSI, 1990). A dry density-moisture content relationship for Oxford clay, kaolin and gravelly sand is shown in Figure 6.2. Oxford clay, kaolin and gravelly sand have maximum dry density of about 1550 kg/m^3,

1410 kg/m^3 and 1865 kg/m^3 at optimum water content of 23.5 %, 28.0 % and 9.5 % respectively.

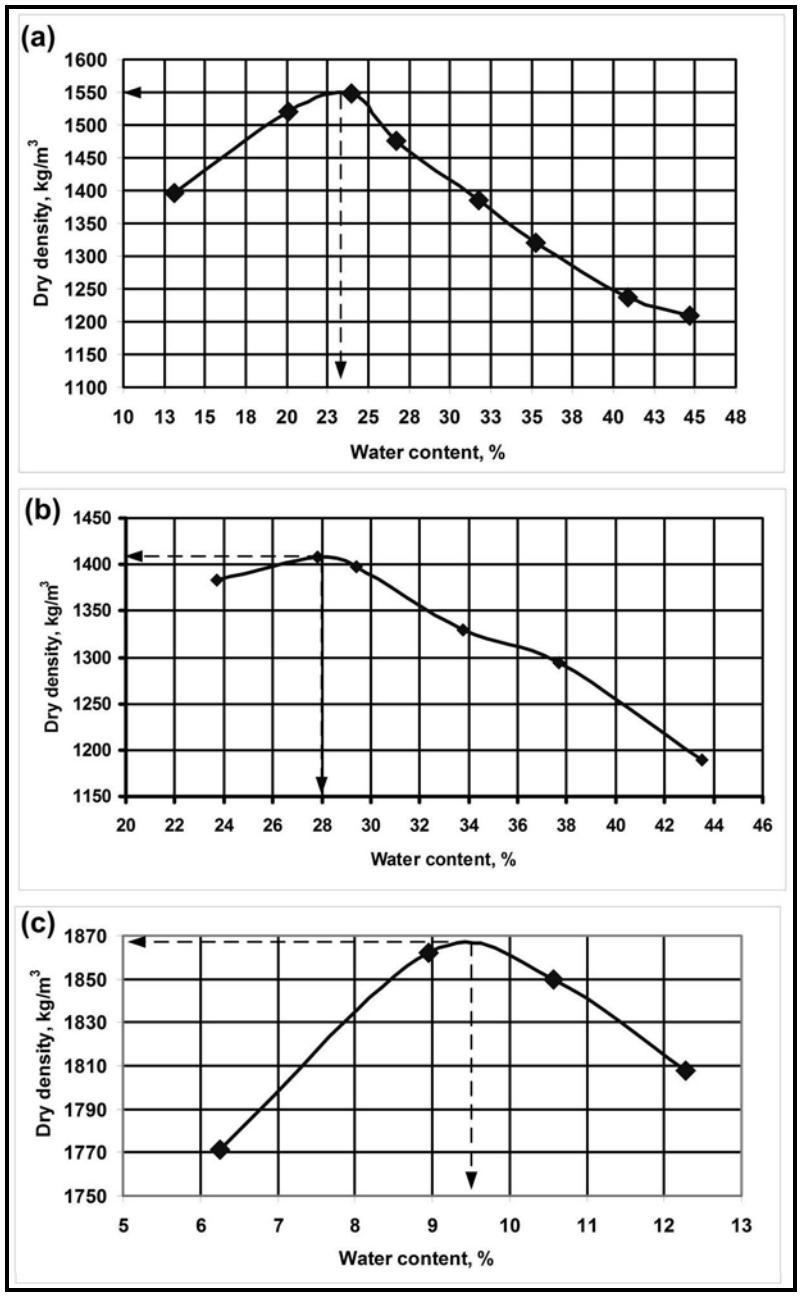

Figure 6.2: Compaction test for (a) Oxford clay, (b) kaolin and (c) gravelly sand.

6.3.5 Shear Strength and Moisture Content

Quick undrained triaxial tests were carried out to determine the shear strength for different water contents. To simulate very soft ground that has a shear strength below 20 kPa, a suitable moisture content has to be identified. Therefore, a series of quick undrained triaxial tests were performed at various water contents. Clay samples were prepared by compaction using the Dietert method. For these tests, confining pressures of 50 kPa, 100 kPa and 150 kPa were used. The consistency and accuracy of the results obtained were within the appropriate limits of the apparatus accuracy for example the pressure gauge was not sufficiently accurate for used in lower confining pressures. However for saturated clay, the undrained shear strength is independent of the total confining pressure (Terzaghi *et al.*, 1996), therefore the results are not affected by confining pressure. The tests were carried out in accordance with BS 1377: Part 8: 1990. Figure 6.3 shows the relationship between undrained shear strength and water content for Oxford clay. Kaolin clay is material used in the pilot test as clay test bed and most of data were collected based on literature study. For the undrained shear strength of the kaolin clay, the trial and error tests were carried out which indicated the water content that could give the shear strength below 20 kPa, which categories as very soft clay. Thus, a quick test using a few samples with different water content were tested, 37.5 % and 44.2 % gave 23.5 kPa and 17.9 kPa respectively. For this study Oxford clay and kaolin clay were prepared with average water content at 40.2 % and 45.2 % which both of clays gave shear strength of 16 kPa. All the quick undrained triaxial tests data are presented in Appendix A.

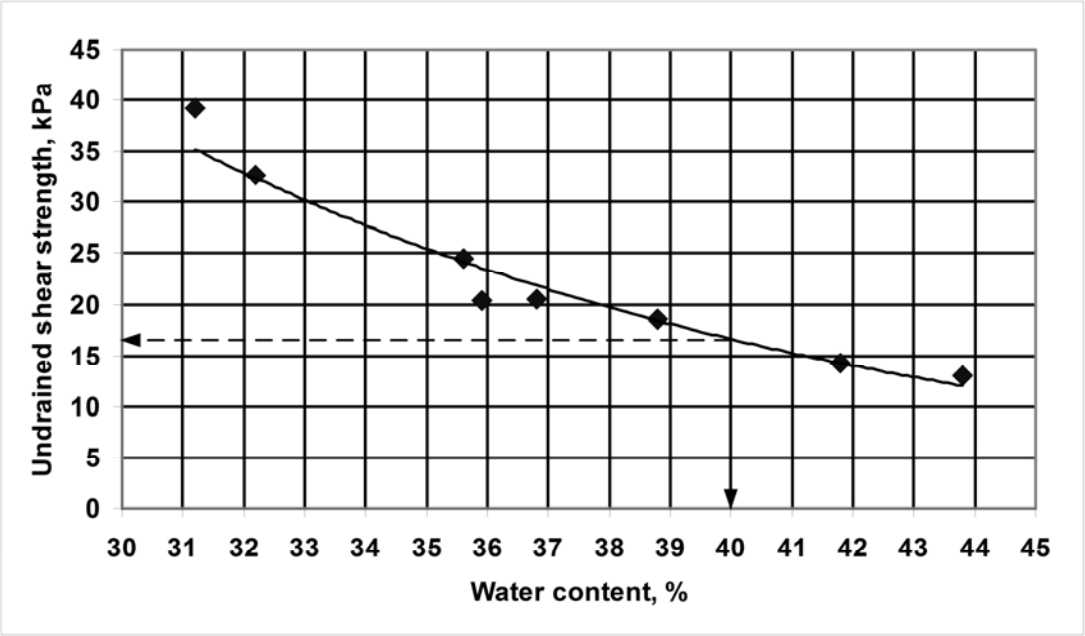

Figure 6.3: Correlation between undrained shear strength and moisture content for Oxford clay.

6.4 Pilot Test

The pilot test consisted of a kaolin clay with a single stone column. The aim was identify a suitable seismic source and array for testing in the natural clay model (see Section 4.2). Therefore, it is appropriate to use well defined materials. For this small pilot model the seismic surface wave test response using a small container size 600 mm x 300 mm x 300 mm in length, width and depth respectively was first evaluated. The outcome of the pilot tests was used to understand the response of wave propagation with a single column and be also to identify the phase velocity of the clay and column.

6.4.1 Preparation of the Kaolin Clay Test Bed

Kaolin index properties were discussed in Section 6.3. Dry kaolin at weight 60 kg was mixed using 28 kg water using a larger mixer for 30 minutes. The mixture was poured into a perspex frame in layers, and then compacted using a vibrator. Each layer consisted of 6 cm, and the achieved density was checked when final layer was reached by sampling using the thin wall tube. Three samples were taken and tested. The average water content was 45.2 %, the dry density achieved 1167 kg/m^3 and the undrained shear strength about 16 kPa. The upper layer of clay was covered by cling film to reduce evaporation.

6.4.2 Preparation of the Column

The second part of the tested model was constructed of kaolin clay with a single column. A cylindrical gravelly sand column measuring 150 mm in depth and 100 mm in diameter was constructed using a steel mould. The gravelly sand was mixed at 10 % water content and was compacted using a vibrating hammer in layers. The compaction technique was similar to that used in compaction tests conducted on the gravelly sand samples (see Section 6.3.4). The dry density of the column was 1853 kg/m^3, achieving 99 % of its maximum density. A hole was drilled in the kaolin clay, and the column was pushed into the pre-hole after breaking open the steel mould. The summary of the kaolin model is shown in Figure 6.4.

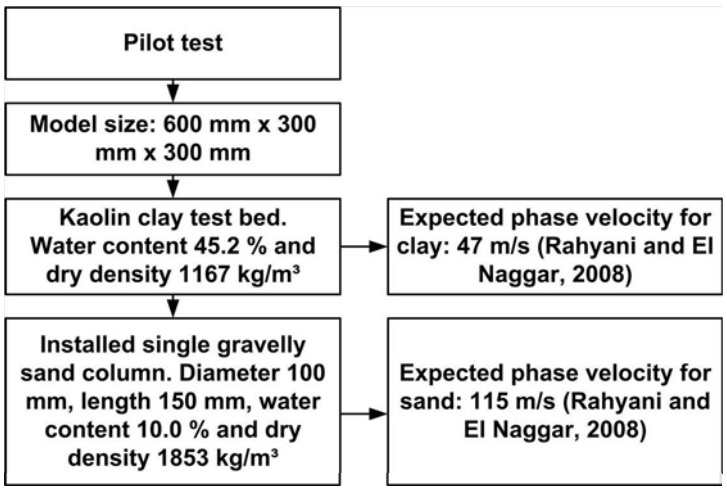

Figure 6.4: Summary of kaolin clay model.

6.4.3 Seismic Test

An illustration of seismic test laboratory setup without the column and with a single column are shown in Figure 6.5 and Figure 6.6 respectively. The expected phase velocity for soft clay and gravelly sand with poisson's ratio of 0.5 and 0.3 were approximately 48 m/s and 115 m/s respectively (Rahyani and El Naggar, 2008). The distance between the source and the first receiver, d, was tested by trial-error to obtain a suitable distance between the source and the first receiver and the receivers spacing, Δx. Values of d and Δx were subsequently chosen to achieve the larger frequency range with higher coherence values (> 0.9).

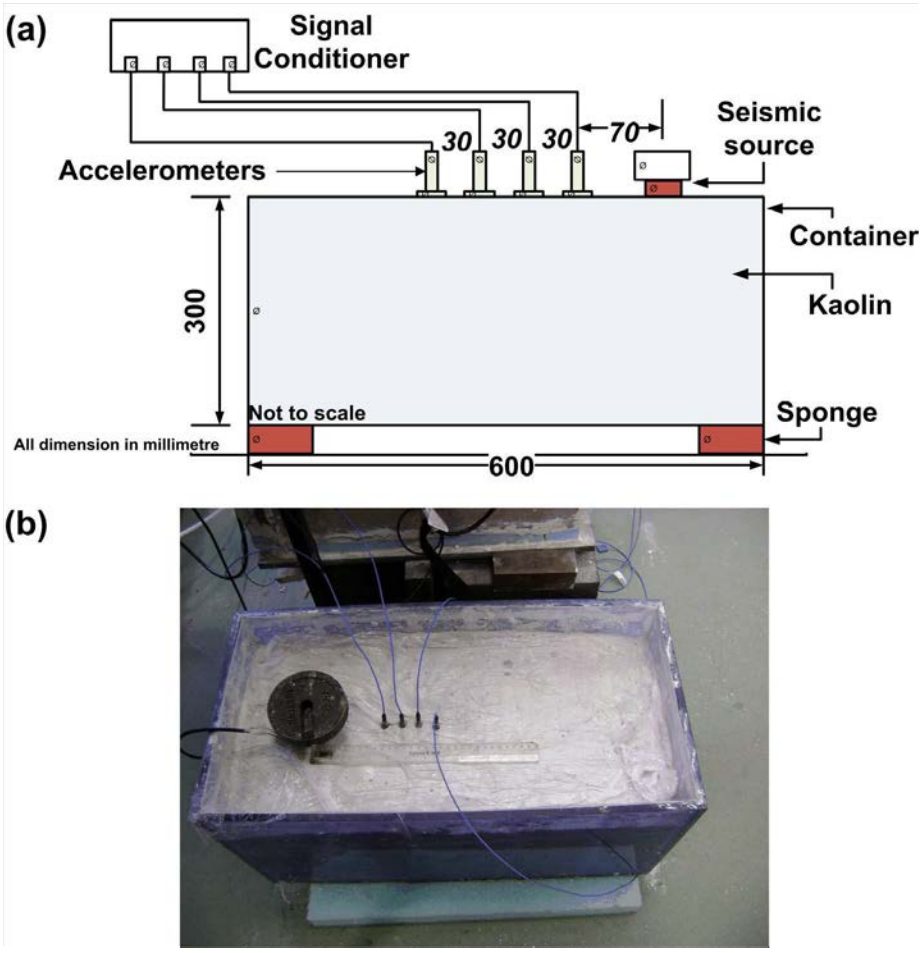

Figure 6.5: (a) Illustration of the laboratory-scaled model and equipment setup, and (b) photo of the kaolin model with seismic source located at the one end of the array.

For the homogeneous kaolin seismic test, the receivers consisted of a linear array of 4 piezoelectric accelerometers with the seismic source located at the one end of the array as shown in Figure 6.5. The distance of source-receivers deployed was limited by the quality of signal-to-noise ratio due to constraint of seismic source energy and size of model for the furthest receivers. As the laboratory model was scaled down, the frequency of the signal for the surface excitation was scaled up accordingly. Based on trial tests, the distances between the source and the first receiver, d, was set as 70 mm and receivers spacing, Δx,

between 25 and 30 mm. This array gave better vertical resolution with higher signal-to-noise ratio.

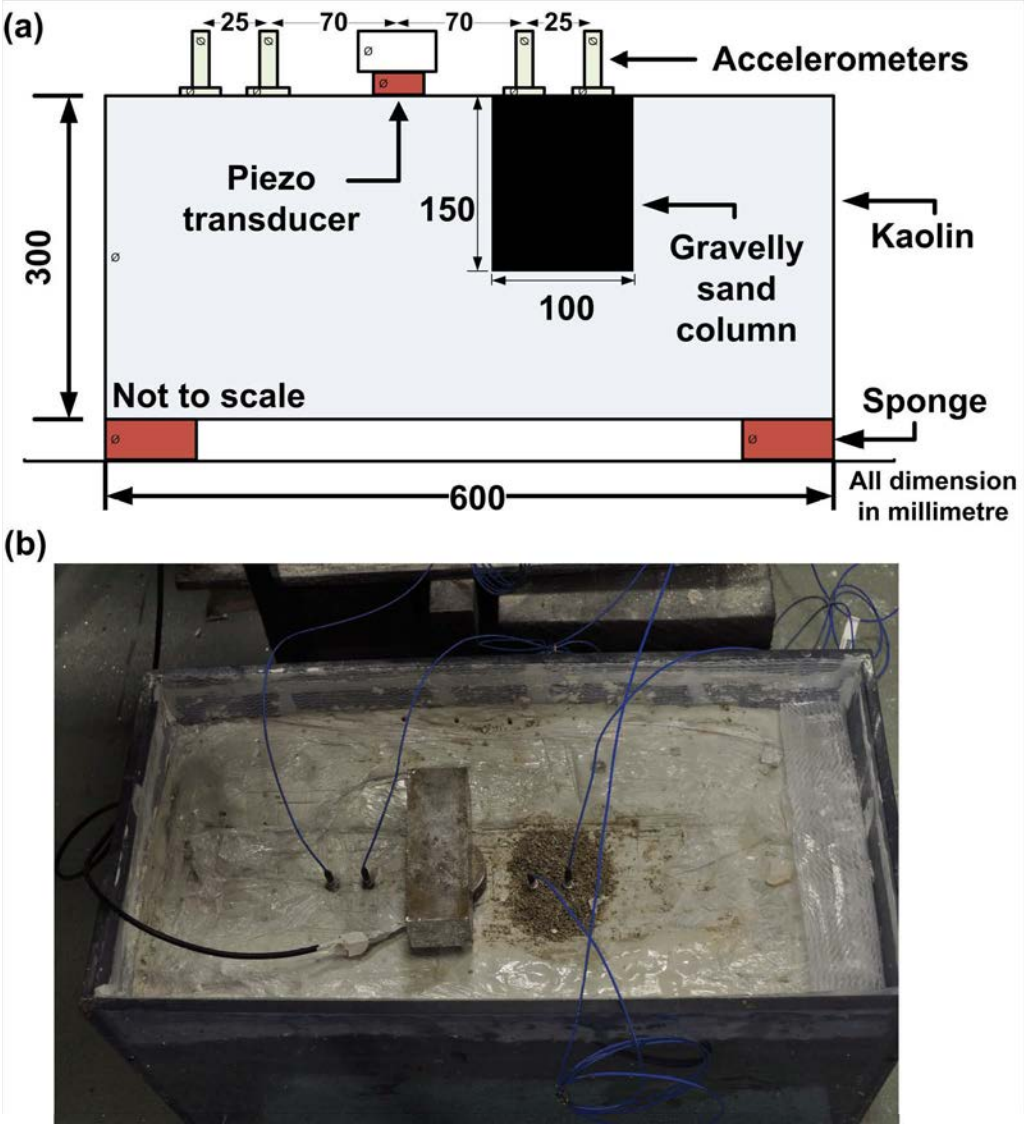

Figure 6.6: (a) Illustrated diagram of the set up of the laboratory scale model and (b) photograph of the kaolin model with a pair of sensing accelerometers located separately on kaolin and on the column(note the seismic source is located at centre of sensor-pair).

When the single column was installed, the source-receiver sensors was arranged with one of sensor-pair located on clay and other pair located on column, with the seismic source in the middle as shown in Figure 6.6. This source-receiver deployed was successful to achieved higher signal-to-noise ratio because both pairs of receivers are located closed to seismic source. The column acts as a wave barrier thus reduces the signal coherence for sensor pair on column compared with sensor pair on clay. The array set up in this experiment (see Figure 6.5 and 6.6) using Equation 3.10 and 3.11 is expected to have non-distortion frequency from 224 to 1410 Hz and 548 to 3450 Hz for clay and column respectively.

The piezo-ceramic transducer was used for generating the seismic source because it was suitable for generating higher frequency as discussed in Section 4.2.1. An audio power amplifier was used to drive the piezo-ceramic transducer with the excitation signals. The piezo-ceramic transducer was acoustically coupled to the surface using a weight padded with acoustic absorbers. The piezoelectric accelerometers were coupled to the soil surface with nails and the accelerometer was placed on top of a nail using bee's wax to ensure good coupling contact to soil surface as shown in Figure 6.7.

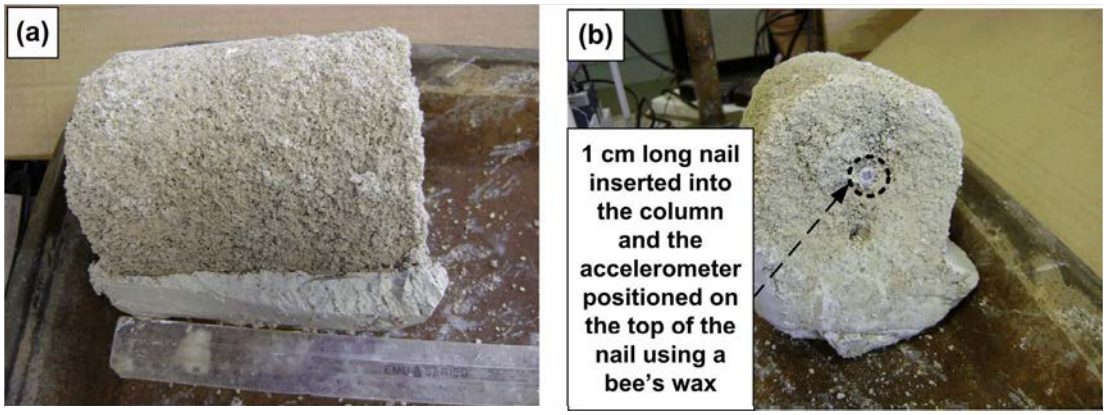

Figure 6.7: (a) Photograph of the column when removed from the kaolin test bed after completion of the tests, and (b) photograph of the nail on top of the column purposed to obtain good contact between sensor and test material.

6.5 Main Test

Following the initial tests (see Chapter 4) and the pilot tests (see Section 6.4), the main test arrangement was established, so enabling the main aim of the thesis to develop the most appropriate seismic surface wave method for attaining and utilizing the data to investigate vertical and lateral stiffness to be met. This ultimately will aid evaluation of the quality of VSC produced in the field. In addition, this main programme of work aided the understanding of the effect of lateral heterogeneous due to column inclusion in relation to the seismic surface wave result and the quality of stone column. Further details of the results and their discussion are presented in Chapters 7 and 8 respectively.

6.5.1 Configuration of the Stone Column

The dimension of the gravelly sand stone columns and their configuration followed the ratio of an actual ground improvement site (see Section 4.2.2). This led to the following stone column parameters being used for the main model tests.

i. Diameter of column was 41 mm,
ii. Length of column was 400 mm,
iii. The diameter of stone was 1.25 mm to 2.5 mm
iv. Column spacing was 130 mm centre to centre

The columns were installed in equilateral triangle array. This model of the stone column dimensions yielding an overall scaling of 15.

6.5.2 Preparation of the Oxford Clay Test Bed

The inner box dimensions were 1180 mm x 680 mm x 500 mm in length, width and depth respectively. An impermeable plastic sheet covered the inner layer of the box. Another thin layer of impermeable plastic was then placed together with styrofoam to avoid the water dissipating through the box. This plastic was also utilized for wrapping the top clay to minimize water evaporation as shown in Figure 6.8. The 50 mm thick styrofoam layer placed surrounding the box was also designed to reduce wave reflection. The laboratory temperature was kept controlled within an average of 21 ºC to reduce evaporation due to temperature changes. At the clay surface, cling film and an additional impermeable sheet

were used to maintain clay moisture throughout the main test programme. The plastic sheet was only removed during installation of the columns and subsequent seismic testing.

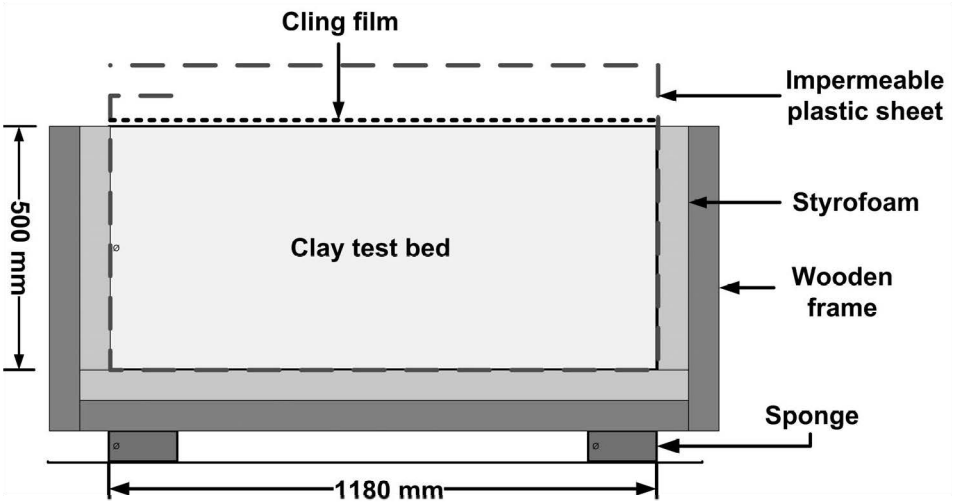

Figure 6.8: Wooden box lined with styrofoam and impermeable plastic sheet to reduce reflection of waves and water dissipation.

The index properties of the Oxford clay used for construction of the clay test bed of the main test is shown as in Table 6.1. The preparation of the Oxford clay test bed began with mixing in batches the dried clay with tap water using a larger mixer for 30 minutes to ensure Oxford clay was thoroughly mixed. For each batch an average of 100 kg of Oxford clay was mixed and poured into the container and compacted. A total of 700 kg of very soft Oxford clay was used to fill the container**.** The clay was compacted with a vibratory plate to achieve density at least 97 % or more of the respective water content and bulk density values determined during compaction tests (see Figure 6.2a). The box height of 500 mm required seven layers of clay to fill it to ensure a relatively uniform density profile with depth and lateral extend with the test bed. Before placing the next clay fill layer, the

surface of clay was grooved, in order to provide fine contact for the next layer and to avoid a plane of weakness between layers. The equivalent amount of clay was compacted in each layer, height of each layer was 71 mm, to give close uniform density throughout the height of the clay test bed. A density check was carried out for all the clay layer to identify achievable clay density. Table 6.2 shows the summary of the water content, density achieved for each layer of clay test bed, degree of compaction and degree of saturation. The clay mixtures had an average water content of 40.2 % and approximately gave 16 kPa undrained shear strength (using Figure 6.3) used to simulate the very soft ground condition. The range of initial water contents achieved was between 38.8 and 41.4 %, corresponding to undrained shear strength of between 18 to 15 kPa respectively (based on Figure 6.3). Thus, this was deemed very small for the purposes of the test programme being within expected experimental errors and the relative insensitivity of VSC to very small differences in undrained shear strength of the surrounding clay.

Table 6.2: Data for each layer of clay test bed.

Layer	Weight, g	Water content %	Dry density, kg/m³	Bulk density, kg/m³	Degree of compaction, %	Degree of saturation, Sr %
1	94.7	40.6	1224	1721	99	93.9
2	92.6	41.3	1191	1683	97	90.8
3	109.1	38.8	1250	1735	99	93.4
4	93.5	38.8	1241	1722	98	92.1
5	104.1	39.7	1222	1708	98	91.7
6	101.7	40.7	1228	1732	100	95.2
7	104.8	41.4	1185	1675	97	90.1
Average	100	40.2	1220	1711	98	92.4

The degree of saturation of the Oxford clay sample for the stone column model test was determined from the following equations (Head, 1980):

$$\rho = \frac{\rho_w (G_s + S_r e)}{1 + e} \quad \ldots\ldots\ldots\ldots \quad \text{Equation 6.1}$$

$$w = \frac{S_r e}{G_s} \quad \ldots\ldots\ldots\ldots\ldots\ldots \quad \text{Equation 6.2}$$

Where ρ is the clay bulk density (kg/m³), ρ_w is the water density taken as 1000 kg/m³, G_s is the specific gravity, S_r is the degree of clay saturation (%), e is the void ratio and w is the water content (%). The S_r value for each layer was calculated using Equation 6.1 and Equation 6.2. An average of S_r was 92.4 % where G_s of Oxford clay was 2.60**.** The degree of saturation of remoulded Oxford clay can be considered approximately fully saturated for the purposes of the tests reported herein as S_r value larger than 90 % (Lee, 2001).

To determine the homogeneity of the test clay test bed, water content as well as hand vane shear tests were carried out at different depths and locations throughout the test programme. For measuring the water content, the clay samples were taken while digging the columns holes. For each particular column, the water contents at different depths were determined. The hand vane shear test was carried out before digging the hole. The results showed that the water content and shear strength at different depths lay within the range of 38.9 to 41.0 % (taken from Table 6.3) and 12.1 to 17.2 kPa (taken from Table 6.4). The results presented in Table 6.3 and 6.4 demonstrate the Oxford clay test bed is relatively homogeneous. The test clay bed was prepared on 17 May 2010 and it showed consistent with time, throughout the test programme.

Table 6.3: The summary of water content tests at different depth, column locations throughout test programme (from 6 Jun 2010 to 10 November 2010).

Depth, mm	Column no., tested date and water content, %								
	1	2	3	4	5	6	7	8	Average
	06-Jul	29-Jul	29-Jul	10-Aug	10-Aug	12-Aug	12-Aug	10-Nov	
0-50	39.6	39.6	41.2	41.0	40.7	40.7	40.6	39.5	40.3
50-100	40.5	41.2	41.1	40.7	41.2	39.5	40.3	39.8	40.3
100-150	40.0	41.6	41.3	41.8	41.5	40.3	41.0	40.2	41.0
150-200	39.5	41.3	40.4	39.5	41.0	40.4	39.1	40.3	40.2
200-250	40.3	39.5	41.2	39.9	41.0	38.7	39.5	39.8	40.0
250-300	39.5	39.0	39.0	38.3	40.1	37.9	38.2	37.9	38.9
300-350	39.2	39.0	39.0	38.9	40.8	/	/	39.4	39.3
350-400	39.3	39.5	39.2	38.5	39.2	/	/	39.7	39.2

Note: / At point 6 and 7 the pre-column holes up to 300 mm depth.

Table 6.4: The summary of vane shear tests at different depth and column locations.

Depth, mm	Column no. and hand vane shear test, kPa							
	1	2	3	4	5	6	7	Average
0-100	12.0	12.5	11.8	13.0	14.0	13.2	13.6	12.1
100-150	13.0	15.2	13.2	13.8	15.0	14.0	14.3	13.8
150-200	15.5	17.5	17.5	16.2	15.3	16.0	15.6	16.8
200-250	17.0	18.0	16.5	17.0	15.3	17.0	17.5	17.2
250-300	17.0	17.5	14.0	16.8	16.5	15.5	17.3	16.2
300-350	15.8	16.2	14.5	15.5	16.0	13.5	16.7	15.5
350-400	15.5	15.3	14.0	14.5	15.8	14.0	15.2	14.9
400-450	14.5	15.8	14.0	14.5	14.7	14.2	13.0	14.8

6.5.3 Preparation of the Columns

A trial compaction test was carried out to examine column formation using a split plastic pipe. The split PVC pipe mould was tightened with a steel hose clamp. The gravelly sand was mixed at the optimum water content about 10 %. The gravelly sand was compacted by tamping a rod with a diameter of 30 mm and weight of 3566 g to achieve at least 98 % from maximum dry density of 1865 kg/ m^3 (see Figure 6.2c). The equipment for column preparation is shown in Figure 6.9. Six layers of gravelly sand was used to fill the column mould, where consistent weight at 180 g used for each layer to produce a consistent layer thickness after 40 times tamping with constant energy. The top surface of each layer required grooves to provide good interlayer contact. The compacted gravelly sand in the PVC pipe mould was kept in a freezer for 24 hours at –4 °C. This freezing technique was previously used very effectively by Sivakumar *et al.* (2004) in order to obtain reliable column densities.

To control the quality of the columns, each completed column was checked to have similar weights and bulk densities. The bulk density of the column was determined from measurements of the diameter and length of the column. The bulk and dry density for each column while still frozen is shown in Table 6.5. The dry densities of the columns ranged between 1861 and 1908 kg/m³ and gave an average of 1884 kg/m³. This small variation in density demonstrates the repeatability of the technique. Columns with reference number 8 and 9 were designed for defective non-compacted and larger diameter of columns respectively, hence differences in their densities. The frozen technique was subsequently

chosen as maintained the column diameter and column length throughout the installation the columns in the test box, whilst keeping densities effectively the same for each test.

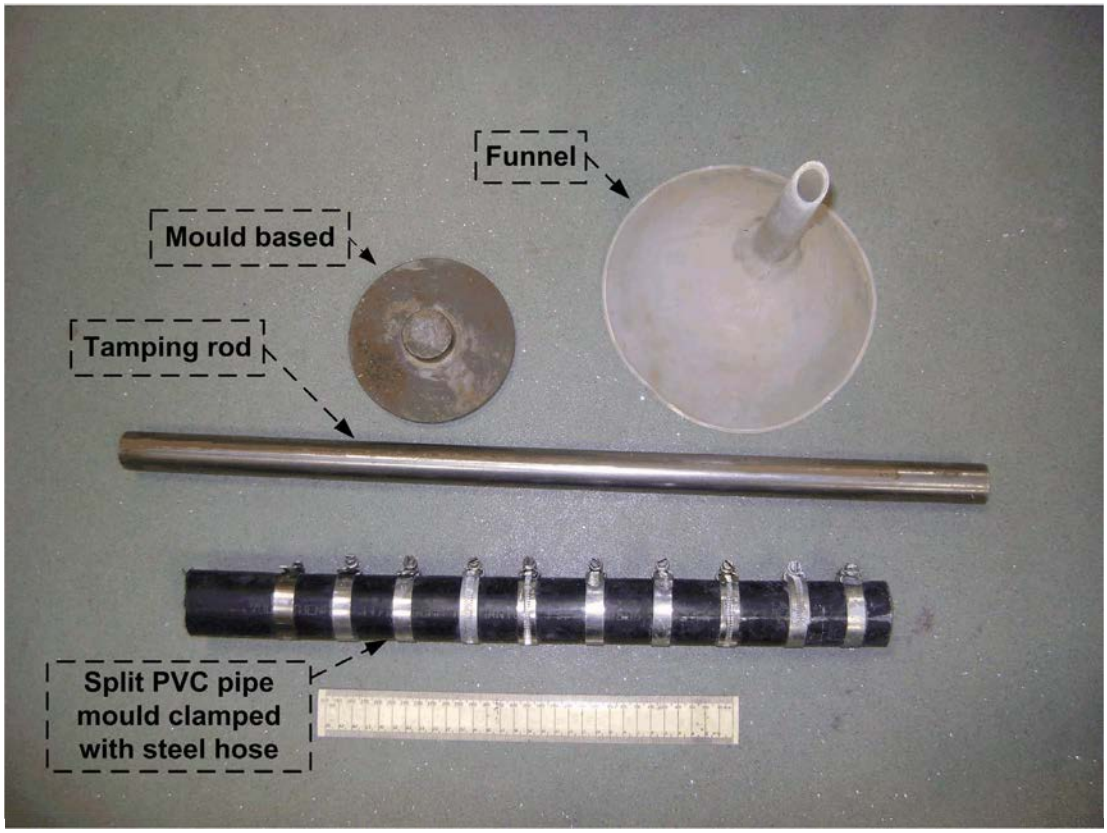

Figure 6.9: Equipment used to form columns.

For columns 8 and 9 a similar procedure was used as for good quality columns (no 1 to 7) using a pre-formed hole. For column 8 instead of a frozen column, wet gravelly sand at 9.9 % water content was used to fill the pre-hole using guided funnel. Very light tamping followed to ensure the pre-hole was filled with gravelly sand. The weight of gravelly sand used to fill the hole was measured as well as the size of the pre-hole. The dry density of the defective column was calculated at 1492 kg/m^3. Meanwhile, for the larger diameter column (no. 9), the-pre-hole at 105 mm diameter and 280 mm length was prepared. The

gravelly sand was mixed at 9.8 % water content and was compacted using a vibrating hammer in 6 layers. The dry density of the column was 1878 kg/m³, at about 100 % of its maximum density. The compacted column was stored in a freezer using the same procedure used for the other smaller well compacted columns.

Table 6.5: The summary of columns properties.

Column no.	1	2	3	4	5	6	7	8	9
Diameter, mm	41	41	41	41	41	41	41	41	105
Length, mm	400	390	410	395	400	393	405	400	280
Volume, mm³	528314	515106	541522	521710	528314	519069	534918	528314	2425500
Weight of column, g	1089.5	1068.1	1124.4	1082.6	1085.6	1081.5	1087.0	866.3	5000.3
Bulk density, kg/m³	2062	2073	2076	2075	2055	2084	2032	1640	2062
Water content, %	9.6	10.2	10.2	9.6	9.6	9.2	9.2	9.9	9.8
Dry density, kg/m³	1882	1882	1884	1893	1875	1908	1861	1492	1878

The construction of the stone column model in this study used a pre-drilled hole to create the uniform column model and to obtain adequate gravelly sand density (Sivakumar *et al.*,

2004). The plastic pipe tube has an external diameter of 41 mm with a trimmed sharp edge which was pushed vertically into the soft clay. In order to minimize disturbance to the surrounding clay during penetration of the tube, lubricating oil was smeared on the outside of the tube. The penetration was stopped at every 50 mm depth interval and the plastic pipe tube was rotated to weaken the bottom layer of clay. By capping the end of the pipe tube to provide a vacuum condition, the pipe was pulled out from the clay test bed gently. Clay trapped inside the pipe tube was sampled for the water content determination. The results showed that moisture content for each column presented in Table 6.3 generally ranged between 38.9 to 40.5 %. This confirmed that the clay was substantially homogeneous. The frozen sand column was then inserted into a predrilled empty borehole as shown in Figure 6.10. The column thawed within a short time after installation. The current methods were selected in order to ensure that uniform column density could be generated in a repeatable fashion.

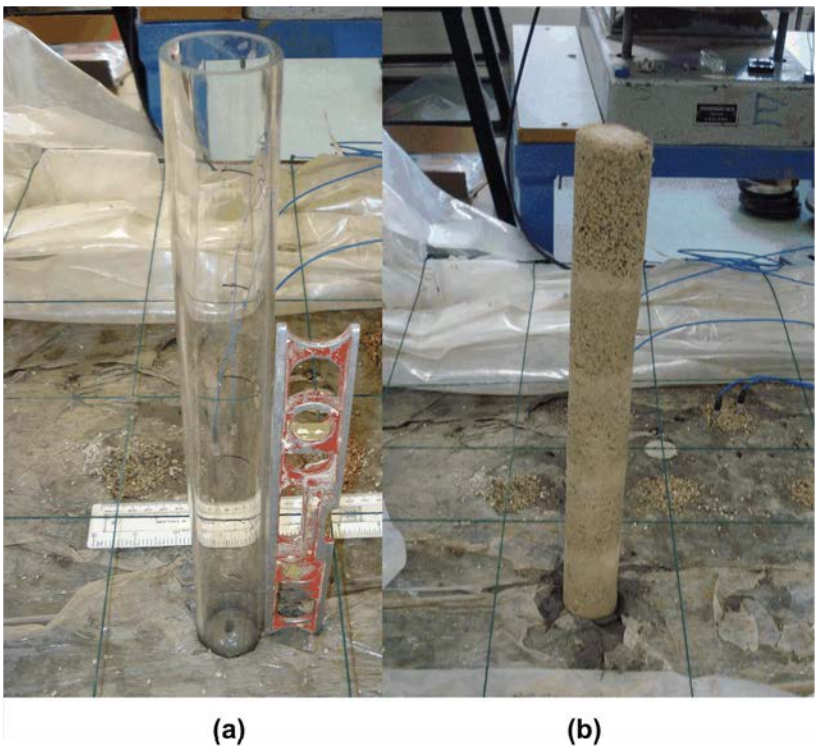

Figure 6.10: (a) Hollow pipe is embedded into the soft clay test bed in a vertical direction to prepare the pre-hole and (b) the subsequent installation of the frozen column.

6.5.4 Pattern and Sequence of a Stone Column

The model stone column was designed in equilateral triangle patterns, similar to prototype columns often formed in the field. The model stone column installation program was purposely designed to suit the study of lateral heterogeneities and quality of stone columns. The column installations were carried out periodically from 6 July until 24 November 2010. This longer period for column installations were due to fine tuning of the equipment and its system which are discussed in Section 7.3.1. The process of constructing a grid of columns led to clay bed disturbance which is involved pushing and extruding pipe into the clay bed for preparing the pre-holes. Therefore, to work with a

uniform level of disturbance, installation of the columns was always started from the centre of the grid and then progressed outwards in a symmetrical fashion. The area for column installations were limited to the centre of the container called the working zone and buffer zone around the container purposely to reduce the effect of wave reflection from the boundary. Figure 6.11 shows the area of the working zone and buffer zone within the container area. The column was installed in sequences, beginning with column 1 and followed consecutively by column numbers. There were 3 rows of columns in the final layout as shown in Figure 6.12.

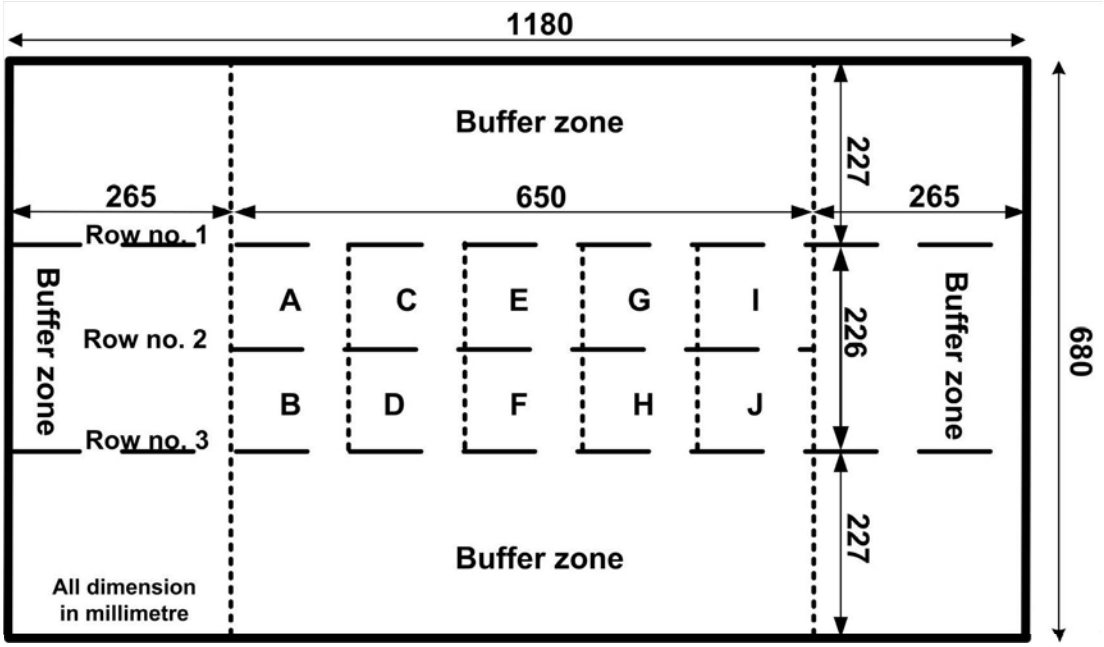

Figure 6.11: Illustration of the working zone and buffer zone within the container area.

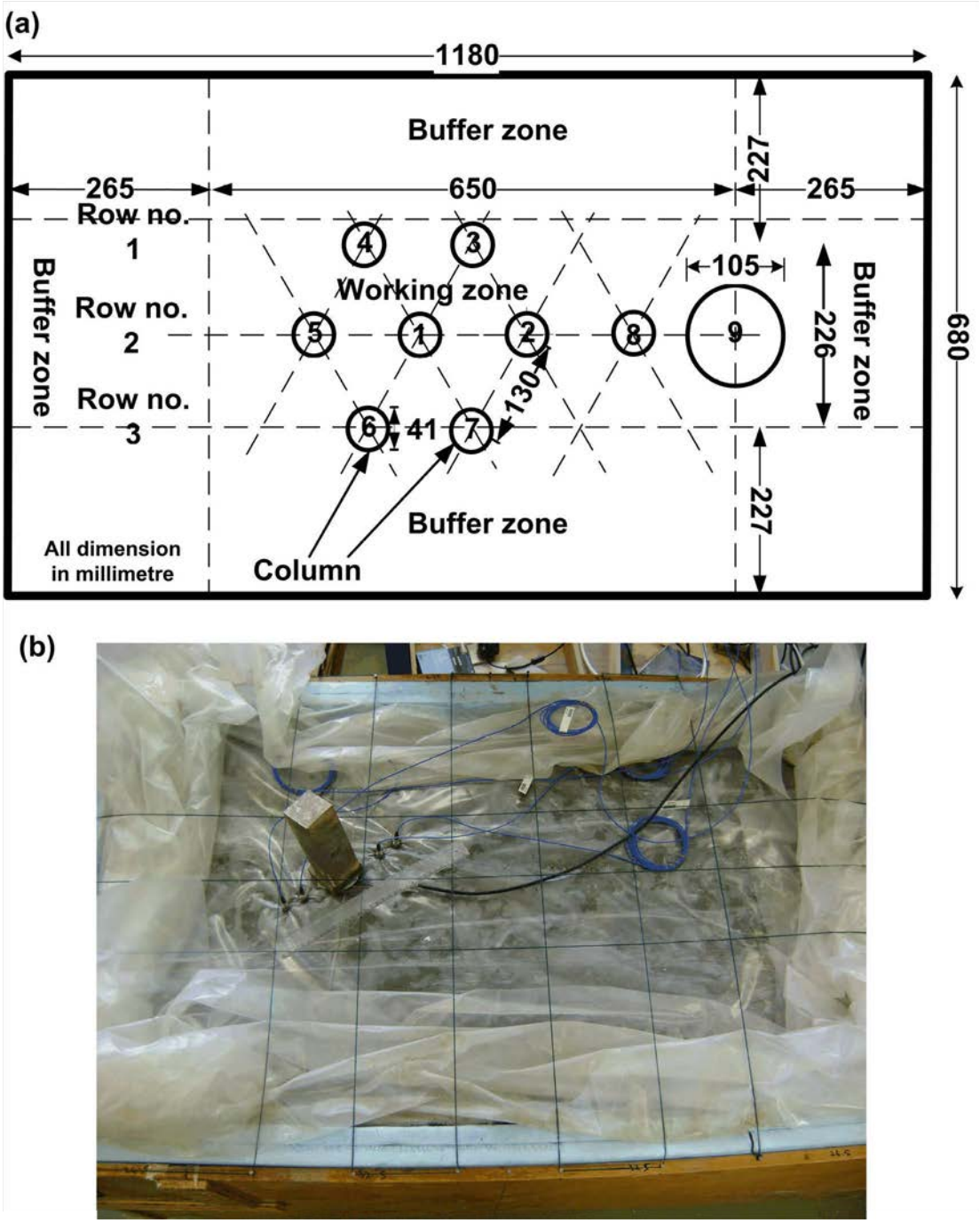

Figure 6.12: (a) Final layout of test programme where no. 1 to 7 were good quality columns, no. 8 defective column and no. 9 large diameter column, and (b) photograph of the Oxford clay model covered with cling film and plastic to avoid water desication.

6.5.5 Seismic Test

The experiment and seismic source-receiver approach developed from the concrete mortar and kaolin clay model was used during this programme of work (see Chapter 4 and Section 6.3). The configuration of the seismic test was based on the four of receiver sensors, namely A, B, C and D. There are two arrangements of seismic source and sensor-receivers, namely seismic source at the one end of the array and seismic source at the middle of the sensor-pairs. These two arrays are shown in Figure 6.13. The seismic wave tests were carried out on Oxford clay to establish the phase velocity of the homogeneous material prior to column installation. The tests covered the centre area of the box and avoided testing on the buffer zone. This buffer zone was created to minimize the effect of reflection from the wall.

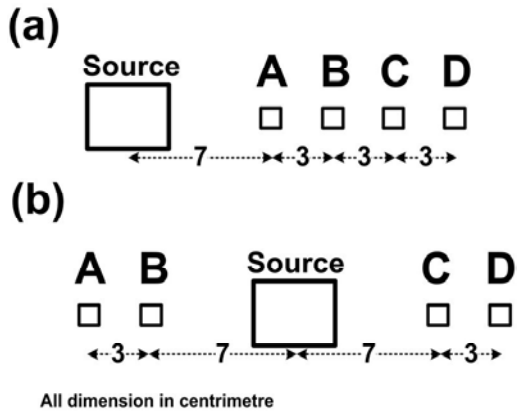

Figure 6.13: (a) The seismic source at the one end of the array receivers and (b) seismic source at the middle of the receiver sensor-pairs.

Sased on the outputs from the seismic tests on homogeneous Oxford clay, the seismic array was adjusted so as to maximize the output quality of the signal-to-noise ratio. There different lateral survey positions were selected; viz; sensor pairs on the clay area without columns, sensor pairs on the clay between columns and sensor pairs on the column. The seismic tests arrays were discussed in detail in Chapter 7. The homogeneity of the clay test bed (control test) and the lateral heterogeneities resulting from the column installation were compared and investigated through a siries of measurements where the excitation source and the sensing accelerometer were moved to different location.

The seismic control test was carried out initially before the columns were installed. The tests were confined to the working zone. The location of the seismic source was both at the one end of the array as well as the middle of the sensor-pairs. The distance, *d* of the first receiver from the source was always 7 cm, while sensors spacing was 3 cm (see Figure 6.13). The frequencies adopted for the seismic tests ranged from 50 Hz to 3000 Hz. The frequencies adopted were chosen so as to avoid the near-, far offset constraint and spatial aliasing as previously discussed in Section 3.4 of Chapter 3. Since these frequencies' constraints were only an approximation, thus larger range of frequency (50 Hz to 3000 Hz) was adopted deeming the data collection. The larger range was advantageous when selecting the useful wavelengths that fulfilled the frequency/wavelength criteria. The wavelengths were within the range of $d/2$ and $3d$, which corresponded to 3.5 cm and 21 cm for a *d* of 7 cm (using Equation 3.10 and 3.11). The processing of data when the coherence was set higher than 0.9, enable reliable phase differences to be obtained and a consequence the useful frequency was determined.

The excitation waveform consisted of a 1 second continuous wave shaded with a Tukey-window to reduce spectral side-lobes and increase the dynamic range of the narrow band of interest. The frequency of the sinusoidal wave was varied from 50 Hz up to 3000 Hz with a step-size of 10 Hz (step frequency approach). The repetitive measurements were obtained at each frequency step, in order to calculate the normalised coherence. Each measurement took 6 seconds and consumed 5.8 megabytes computer hard disk. Therefore, 5 repetitive measurements at each frequency step took about 30 seconds and used 29 megabytes computer hard disk. Accordingly, a single 10 Hz step size test in the range 50 Hz to 3000 Hz reach 2 hours and 45 minute and uses 8.6 gigabytes computer hard disk. Sometimes the frequency ranges, step size and number of repetitive measurements were changed minimise time consumption and allow for constraints of hard disk.

Minor differences in the final water content were observed after the mixing of the Oxford clay batches. The final water content observed in the total of 7 batches of mixed clay ranged between 38.8 % and 41.4 % (average 40.2 %). The author believes that such minor variability in final water content is inevitable, considering the size of each batch. Despite this range of water contents achieved, the corresponding variation in undrained shear strength was within considerably acceptable limits between 13 kPa and 17 kPa (average 15 kPa). It is also noteworthy that during the construction of the columns slight layering due to compaction was apparently observed. The upper layers showed evidence of particle grains being crushed due to the impact of the tamping rod. Despite this, the columns showed good overall consistencies in dry densities for columns 1 to 7 varying in the range 1861 to 1908 kg/m^3. As discussed further in Chapter 7, this had no significant effects on the seismic surface wave test observations.

The length of the piezoelectric accelerometer (receiver sensor) was 1 cm. and the centre to centre spacing between receivers was 3 cm. This sensor spacing had a significant impact as a consequence of the small scale of the seismic test. The measurement of the sensors spacing could also be considered as the edge to edge distances of receiver sensors instead of from centre to centre, (2 cm or 4 cm as the case may be - see Figure 6.12). However, any variation in centre to centre spacing was within a few millimetres which was insufficient to have any significant effect on the overall results that were dominated by the seismic characteristics of the clays tested. In addition, the use of a nail to position the sensor to the sample created heterogeneity in the material that may also influence the seismic velocity of the test material. It is worth noting that the sensors used in the field have a spike to position them to the ground. This, however, has minimum effect as it involves a larger volume of sample (with larger sensor spacing).

Chapter 7

SOIL MODEL TESTING

7.1 Introduction

In this chapter, the results of the experimental work detailed in Chapter 6 are presented, analysed and discussed. Kaolin clay, Oxford clay and gravelly sand column materials were used to validate the technique developed during the concrete mortar tests. This included development and calibration of the measurement system. The design of an optimal array that maximizes the rate of column assessment on a typical ground improvement site was also investigated. This chapter first details control test results of phase velocity measurement in a small physical model of homogeneous kaolin clay, then presents results from the larger model control test of homogeneous Oxford clay. The inclusion of a single cylindrical column in kaolin clay and multiple columns in Oxford clay are then presented.

7.2 Soil Clay Without Columns

7.2.1 Homogeneous Kaolin

The testing on the kaolin clay physical model was carried out using a linear array of accelerometers, which comprised of 4 sensing channels and a seismic source at one end of the array. The excitation was carried out with a frequency range of 100 to 3000 Hz, using a stepped-frequency approach with step-size of 50 Hz. A set of testing with total of 12 snapshots measurements were obtained at each frequency step for averaging and the calculation of the normalized coherence. The quality of signal in terms of the signal-to-noise ratio showed degradation when the frequency reached 2500 Hz as shown in Figure 7.1. For homogeneous material, the graph of frequency versus unwrapped phase difference for all sensor pairs should ideally show a linear function relationship. The corrupted unwrapped phase measurement shown in Figure 7.2 indicates that sensor-pair C-D was the most disturbed. Sensor pair C-D has the longest distance from the seismic source. The distortion in the phase response was most likely due to attenuation.

From the phase difference and distance between the sensors, phase velocity was calculated for each frequency. The graph of the frequency versus phase velocity is shown in Figure 7.3. This shows that for about 83 % of total data the threshold was above 0.9. Despite these data being above the 0.9 threshold, some of the data were extremely high (phase velocity more than 1000 m/s). Such data were deemed not acceptable and so not plotted due to being outside of frequency range to the geometry of array used (for example the sensor pair C-D frequency between 1400 and 1700 Hz). In general, the phase velocities

are consistent throughout the frequencies tested (Figure 7.3). However, the variation of phase velocity with wavelength shown in Figure 7.4, clearly indicates a deviation in the phase velocities for each of the sensor pairs. It can be observed that the velocities at frequencies lower than 350 Hz had larger deviations from the averaged phase velocity. It seem even though these data above threshold 0.9, the reliability of the phase velocities were also influenced by other factors. This phenomenon was likely due to interference from the body wave at lower frequencies as well as reflected wave front from the bottom of the container. It was reported by Zerwer *et al.*, (2002) who explained the deviated phase velocities were caused by the unformed Rayleigh wave for wavelengths larger than half of it medium depth. It worth noting that container depth was 30 cm. Further discussion was presented in Section 7.2.2. The C-D sensor-pair shows larger phase velocities deviation compared with the rest. This could be due to insufficient energy and exacerbated by interfering reflected wave from the boundary of the container as C-D was the furthest from the source. The phase velocities across the frequencies were non-dispersive and thus suggested that the kaolin clay is reasonably homogeneous.

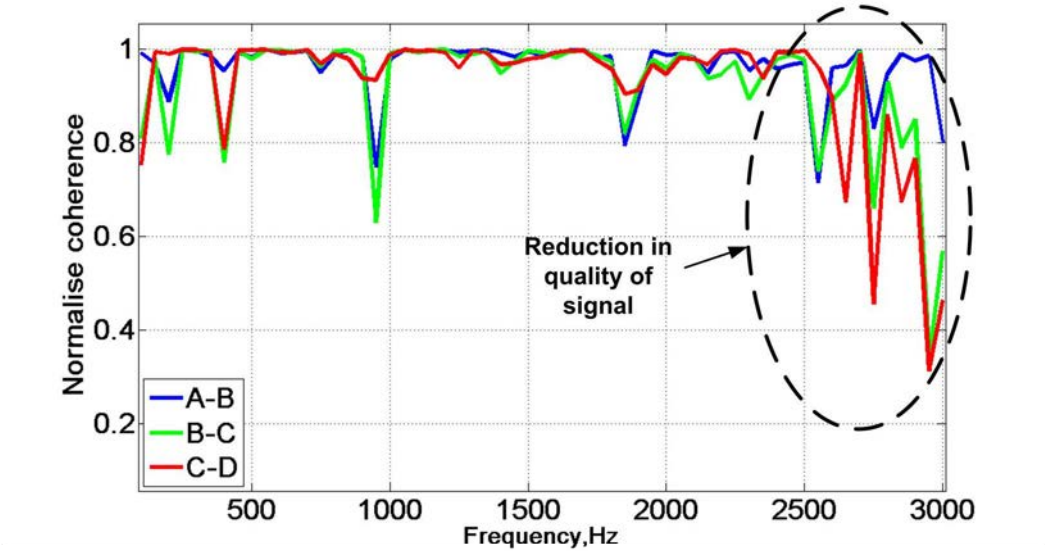

Figure 7.1: The normalized coherence for the 3 sensor-pairs located on the kaolin clay.

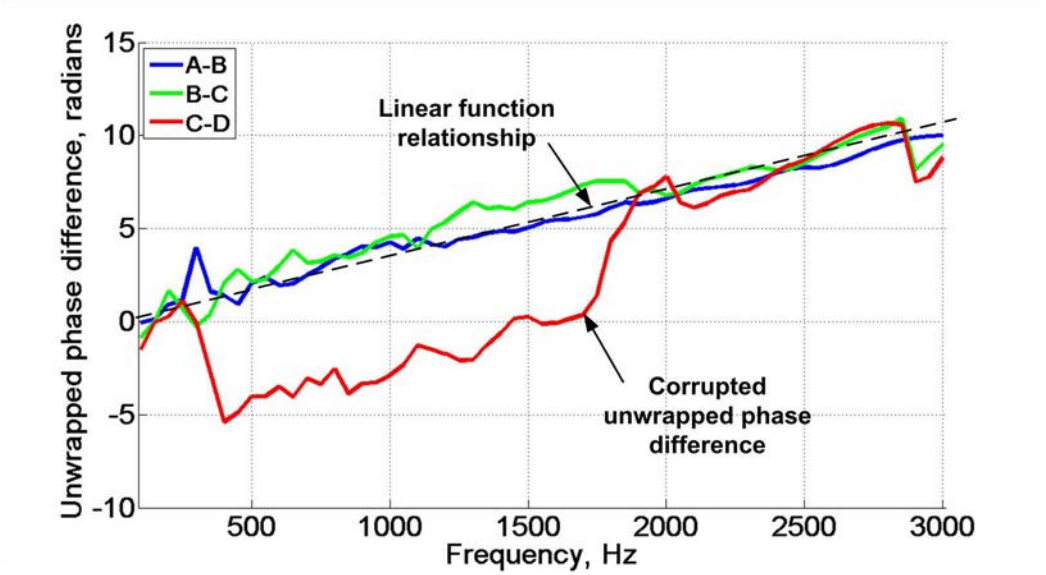

Figure 7.2: The unwrapped phase differences showing linear function for A-B and B-C sensor-pairs, but not in the case of C-D.

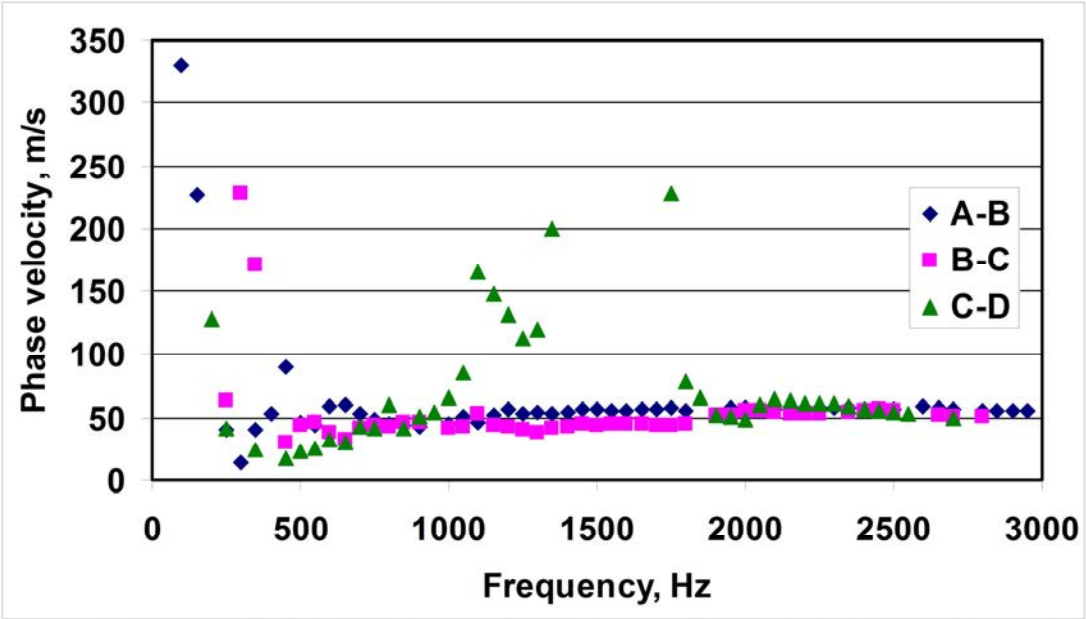

Figure 7.3: Dispersive curve for the kaolin clay.

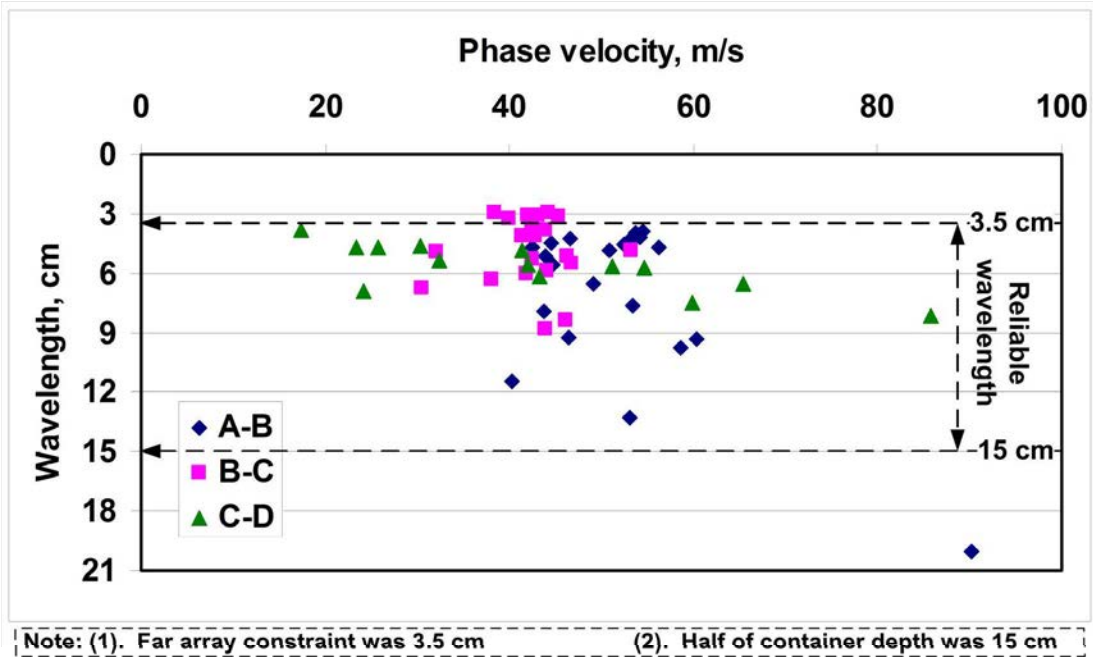

Figure 7.4: Variation of phase velocity with wavelength showing highly deviated phase velocities for sensor pair C-D which is the furthest away from the seismic source.

A weighed-mean phase velocity and non-weighted average are calculated from coherence threshold of 0.7, 0.9 and 0.95 is shown in Table 7.1. This corresponds to expected undisturbed frequencies for A-B, B-C and C-D that were from 350 to 1400 Hz, 350 to 1000 Hz, and 350 to 750 Hz, respectively. The useful frequency ranges were based on the calculation using Equation 3.11 (see Section 3.4) and maximum wavelength was half of container depth. It worth noting that the assumption of phase velocity of soft clay was 50 m/s. These results indicate that the weighted-mean had less variation throughout the threshold compared with the non-weighted average. The average weighed-mean phase velocity for sensor pair A-B was found to be 51.3 m/s.

Table 7.1: Summary of average phase velocity calculated using different threshold.

Sensor-pair	Threshold: 0.7		Threshold: 0.9		Threshold: 0.95	
	Mean for coherence > 0.7, m/s	Weighted-mean, m/s	Mean for coherence > 0.9, m/s	Weighted-mean, m/s	Mean for coherence > 0.95, m/s	Weighted-mean, m/s
A-B	51.7	51.3	52.0	51.3	52.0	51.3
B-C	50.9	53.4	52.0	53.4	52.0	53.4
C-D	28.1	28.7	29.9	28.7	29.9	28.7

The initial water content of kaolin clay was 45.2 % with a shear strength 16 kPa. The shear strength was used to estimate shear wave velocity via empirical conversion, $c_u = 0.0424 v_s^{1.462}$, as established by Mattsson *et al.* (2005). The correlation was based on

stabilised Uppsala clay with cement. The conversion shear wave velocity to phase velocity or vice versa was using Equation 4.10, ($v_s = 1.047 \cdot v_r$ or $v_r = 0.955 \cdot v_s$), where the assumption of Poisson's ratio for clay was 0.5. The converted phase velocity from shear strength was 55 m/s. According to Chan (2006) and Asaka and Abe (2011) relationship between shear strength and soil wave velocity is dependent on the base clay mineralogy and soil type. However Atkinson (2007) demonstrated the relationship of undrained shear strength is a function of liquidity index, with increasing liquidity index resulting in decreasing of the undrained shear strength. The stabilisation process is affected by the response of minerals and as well as the void ratio of inter-particle. However void ratio more significantly influencing the shear strength rather than mineralogy and soil types (Mitchell and Soga, 2005). Thus although caution should be employed when using such correlations, the use of Mattsson *et al*. (2005), provide a method to assess relative changes. Confidence can be gain by the good agreement between estimated and measured phase velocities. Moreover, the values of G_{max} achieve compare favourably with other soil of similar nature (e.g. see Shibuya and Tanaka, 1996).

Using kaolin at water content 50 % mixed with 3 % cement, Chan (2006) tested using bender element. There are various techniques to analyse the clay velocity in the bender element as discussed in Chan (2006) which demonstrate the techniques involved time domain and frequency domain. Using frequency domain which using cross spectrum was minimised the error due to visual time picking in time domain. The cross-spectrum method showed the phase velocity was 51 m/s for frequencies between 1 kHz and 3 kHz which used similar processing technique and the frequencies ranges. Meanwhile, Rahyani and El Naggar, (2007) using mixture of sodium bentonite powder and glycerine to

simulate soft clay tested using hammer test and gave phase velocity of 48 m/s. The experimental result of average phase velocity in kaolin clay obtained from weighted-mean from sensor pair A-B was 51.3 m/s, demonstrating close agreement to empirical conversion values by Mattsson *et al.* (2005) and phase velocity obtained by Chan (2006) and Rahyani and El Naggar (2007). Result from sensor pair A-B was chose due to the higher signal-to-noise ratio compared with others sensor pairs (B-C and C-D). The correlation introduced by Mattsson *et al.* (2005) showed it can be applied in kaolin clay.

This control testing on kaolin clay demonstrated that the measurement system can give reliable results. The analysis using weighted-means gives consistent results throughout the selected coherence threshold compared to the non-weighted approach. The test indicates that phase velocities at low frequencies (below 350 Hz) deviated from the expected phase velocity. These low frequency distortions were caused by the small physical size of the clay container, in which severe noise from the boundary and bottom reflections occurred .

7.2.2 Homogeneous Oxford Clay

A second, larger, also control experimental clay model was built using Oxford clay. A total of 25 tests covering the clay area were conducted using an array consisting of an accelerometer, which comprised of 4 sensing channels and a seismic source set in front of the array, together with a relocating the seismic source set at the middle of the array. The test array arrangements and locations on the clay model are shown in Figure 7.5. Where the seismic source is at one end of the array, 4 receiver sensors created 3 sensor-pairs at

equal distance, namely as A-B, B-C and C-D, which was similar to that used in tests on kaolin. In cases where the seismic source is located at the middle of the array, there were 2 sensor-pairs, namely A-B and C-D. The seismic source at the middle was adopted to obtain higher signal-to-noise ratio results. The measurements were carried out with a frequency range of 50 Hz to 3000 Hz, using a stepped-frequency approach with a step-size of 25 Hz. Reducing the step size as compared to kaolin was deliberate in order to obtain as much data as possible, thus reducing gaps in the stiffness profile results. At each frequency step, 5 repetitive measurements were obtained for averaging and the calculation of the normalized coherence.

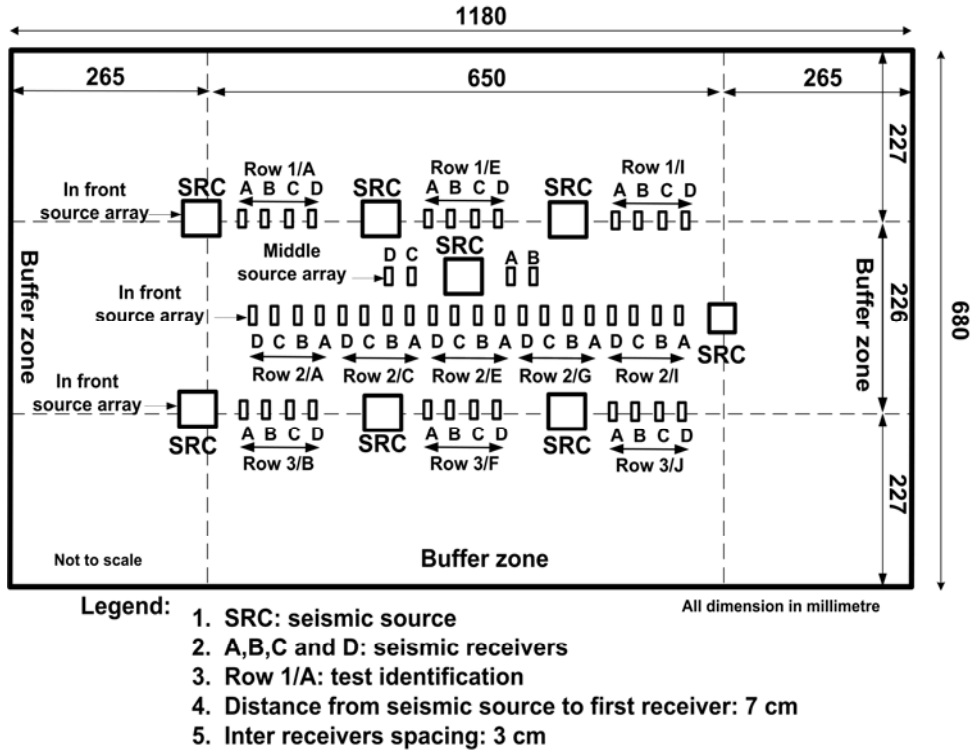

Figure 7.5: Layout of tests throughout the box.

The signal quality in terms of the signal-to-noise ratio was shown in the normalized coherence plot. A larger distance to the seismic source caused a reduction in coherence as shown by sensor-pair C-D. The plot of normalized coherence for different arrays, for cases where the source was located in the front and in the middle of the arrays is shown in Figure 7.6. The plot in Figure 7.6 shows a better signal quality between frequencies 250 and 1500 Hz. For the sensor-pair located nearer to the seismic source, there are a higher number of measurements that exceed the coherence threshold compared to the sensor pair located far from the seismic source, see Figure 7.6 (a). Signals with small wavelengths attenuated relatively quicker than signals with larger wavelengths, thus reducing the signal quality at higher frequencies. For sensor-pairs that were located at a similar distance from the seismic source, a fairly similar normalized coherence relationship, as a function of frequency, was observed, as demonstrated in Figure 7.6 (b). Both Figure 7.6(a) and (b) demonstrate the effect of the near offset constraint for the lower frequency (below 200 Hz) and the far offset constraint (above 1500 Hz) had lower coherence values (see Section 3.4 Equation 3.10 and 3.11).

In general both unwrapped phase difference shown in Figure 7.7 and 7.8 were a linear function. The linear plots show a larger deviation beyond the frequency of 2500 Hz due to a reduction of signal quality. The unwrapped phase difference between the receivers shows that the measurements were corrupted especially above a frequency of 1500 Hz and sensor-pair C-D most deviated from the linear line as shown in Figure 7.7. Meanwhile, in Figure 7.8 where the source was located at the middle of the array, there is a better correlation of unwrapped phase difference between sensor-pairs. Both unwrapped phase differences show an uneven graph at lower frequencies due to the reduction of measured

signal quality, as these frequencies correspond to wavelengths that exceed the distance constraints of the sensors with respect to the source.

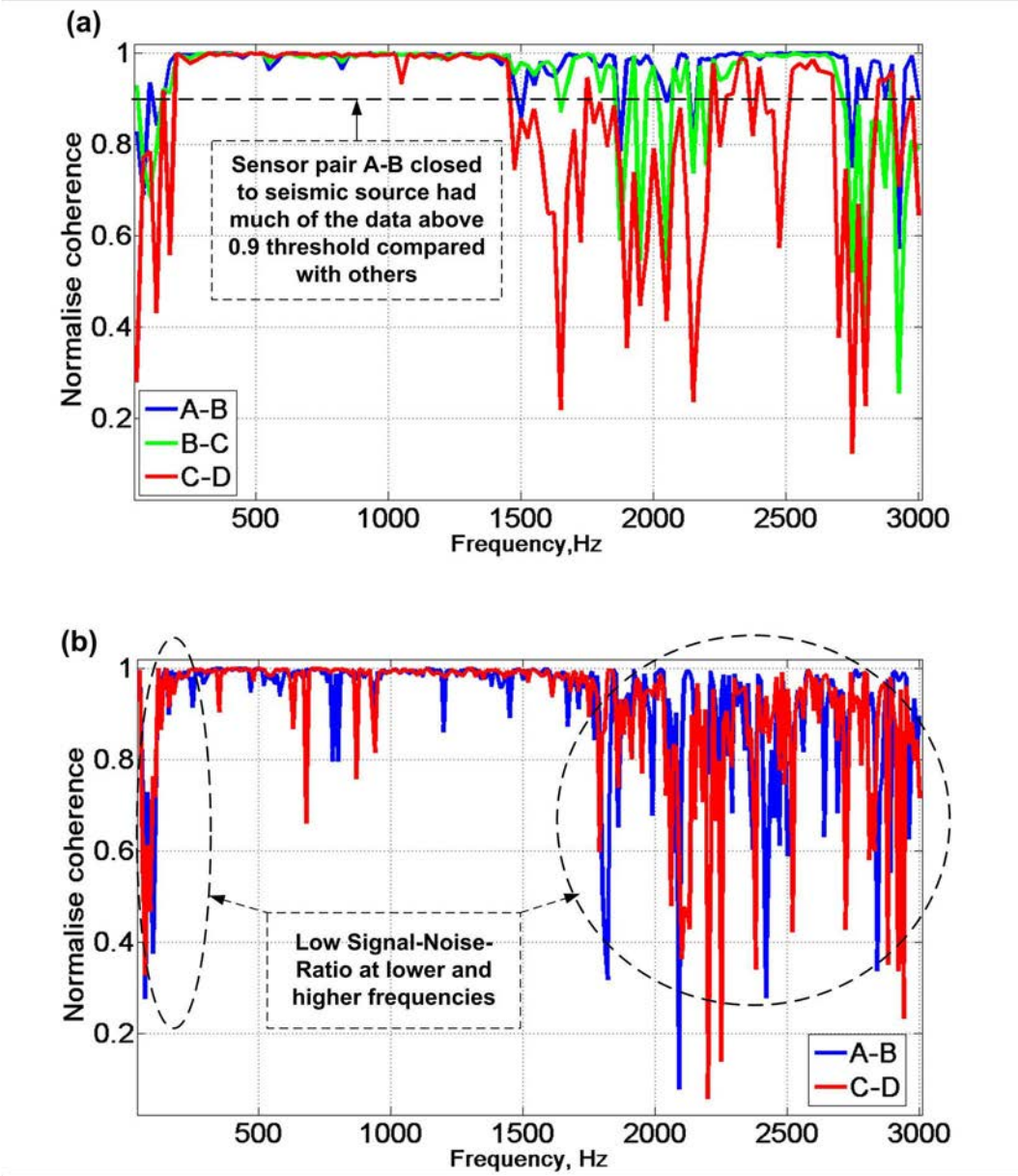

Figure 7.6: Typical coherence in seismic wave testing on soft clay model without column (a) in front of linear array of seismic source and (b) in the centre of the linear array of seismic source.

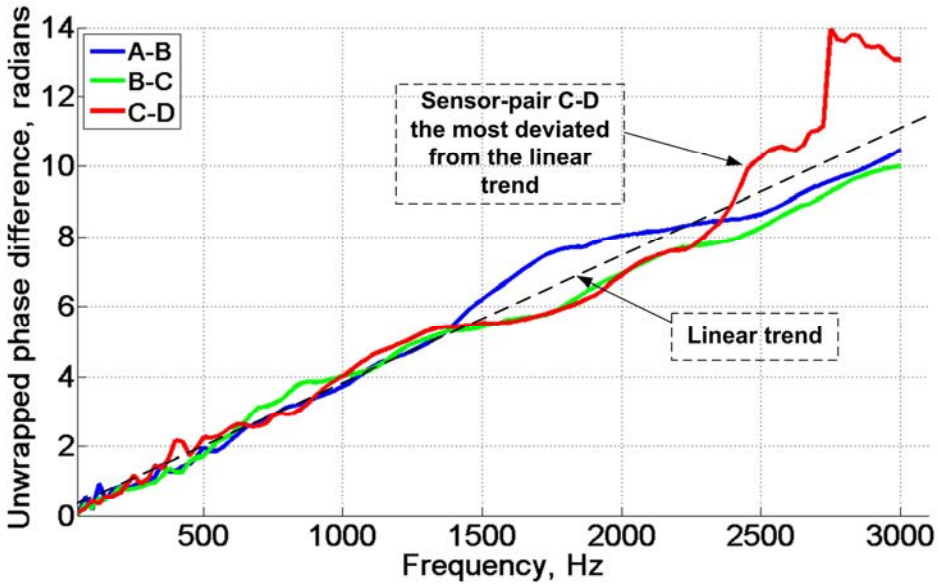

Figure 7.7: Linear function graph for the unwrapped phase difference using in front of the linear array of seismic source when the A-B sensor pair is the nearest to seismic source and C-D the furthest away.

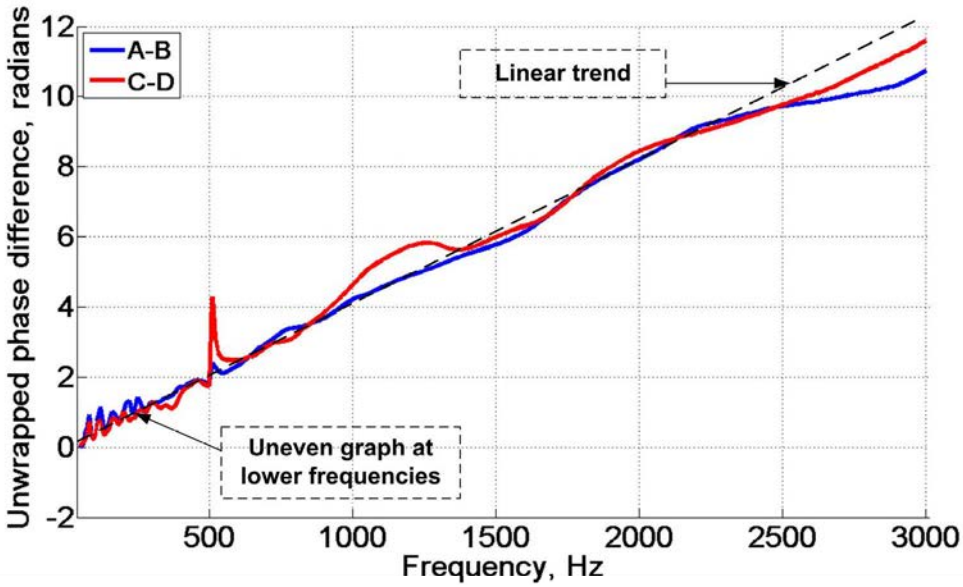

Figure 7.8: The unwrapped phase differences at the centre of seismic source linear array where A-B and C-D sensor-pairs are equidistant from seismic source.

Figure 7.9 shows a typical phase dispersion plot for one set of test without considering coherence threshold (plotted all the data) indicating that the phase velocities are relatively consistent at frequencies between 250 and 2600 Hz. Unusual clay phase velocities were observed for frequencies below 100 Hz, which was likely caused by the body waves. The plots of phase dispersion, for all data (without considering threshold) from the 21 sets of tests in where the seismic source was located on one end of the array, and the 4 sets of tests where the seismic source was located in the middle of the array, show a similar trend of consistency (see Figure 7.10 and 7.11). About 75 % and 84 % of data from Figure 7.10 and 7.11 respectively were above the coherence threshold 0.9. The plots of mean and standard deviation reveal that the phase velocities are highly deviated at the lower and higher frequencies, which showed by the lower coherence values (see Figure 7.6). Despite lower coherence value at lower and higher frequencies, this does not invalidate the phase velocities obtained. From observation, phase velocities were reliable (closed to mean value of phase velocity) when data fulfil the frequency or wavelength requirements, even though data had lower coherence threshold 0.9. The phase velocities deviation was not caused by the change of clay properties, but caused by the frequencies/wavelength constraint that influences the near and far-offset distance of the source from the receivers, as well as some reflected waves from the boundary of the clay container. The small standard deviation observed for cases where the seismic source was in the middle of the array (see Figure 7.11) demonstrates that this is an optimal arrangement for array deployment to carry out the seismic surface wave test.

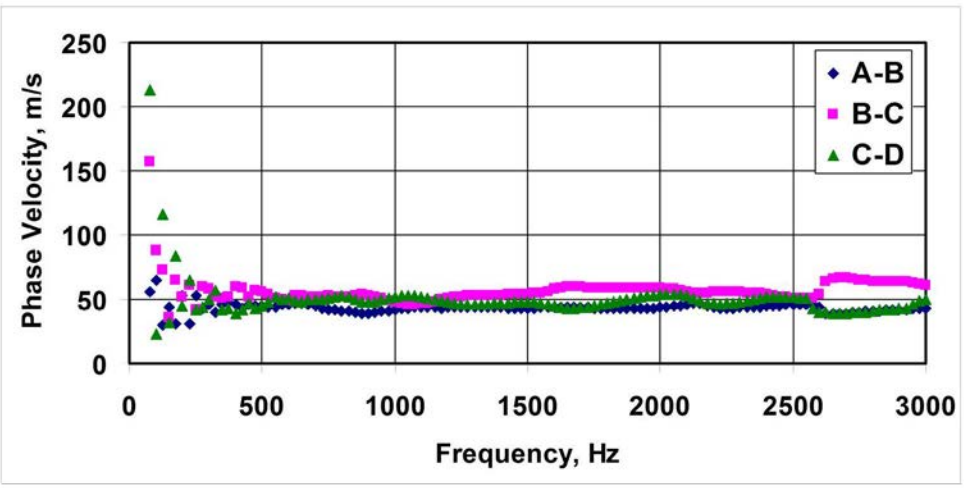

Figure 7.9: Example of graph showing variation of phase velocities across the frequencies from one set of test (ID Row 2/C) from frequency 75 to 3000 Hz.

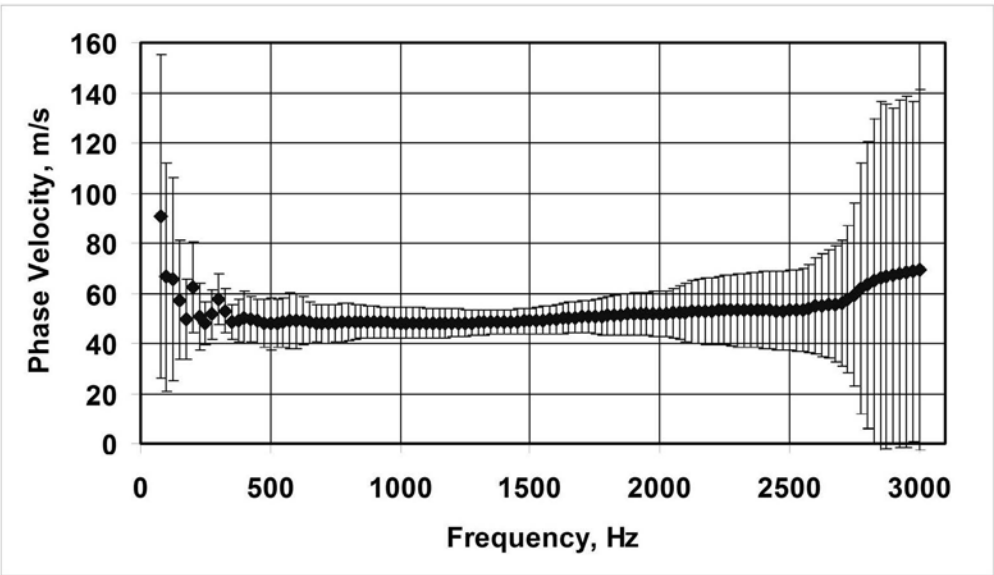

Figure 7.10: Variation of average phase velocities and standard deviation across the frequencies for the 21 sets of tests where the seismic source was located in front of the linear sensors.

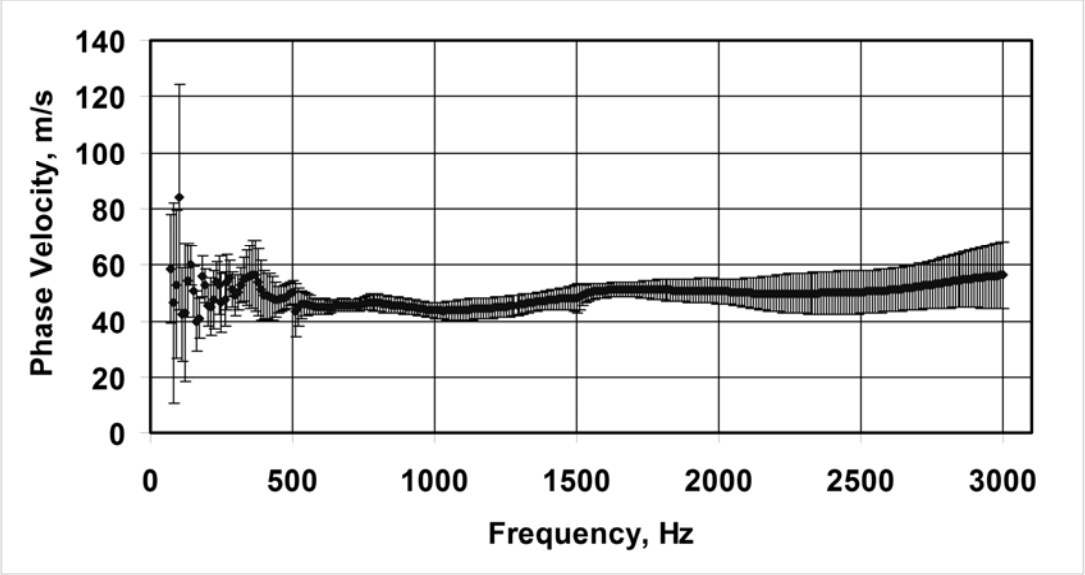

Figure 7.11: Variation of average phase velocities and standard deviation across the frequencies from a sets of 4 tests where the seismic source was located at centre of the array of linear sensors.

In the case where the seismic source was at the one end of the array, the source was 7 cm from the first receiver while the sensors were 3 cm apart. This corresponds to expected undisturbed frequencies for A-B, B-C and C-D that were from 190 to 1200 Hz, 133 to 923 Hz, and 103 to 750 Hz, respectively (based on expected phase velocity on clay was 40 m/s). Meanwhile, for the source set in the middle of array, the expected useful frequencies for pair-sensors A-B and C-D were from 190 to 1200 Hz. The useful frequency range was based on the calculation using equation 3.10 and 3.11. A weighed-mean phase velocity and non-weighted average were calculated from a coherence threshold of 0.9, as well as without limiting the coherence. Table 7.2 shows a comparison of the phase velocities calculated using a coherence larger than 0.9 and without using coherence for the seismic source in the front of the array. Meanwhile, Table 7.3 shows the phase velocities calculated using a coherence larger than 0.9 and without using coherence for the seismic

source in the middle of array. In general the results showed the standard deviation were smaller when the seismic source placed at middle of the array compared to the seismic source in the front of the array. Figure 7.12 shows the distribution of weighted-mean phase velocities throughout the clay model.

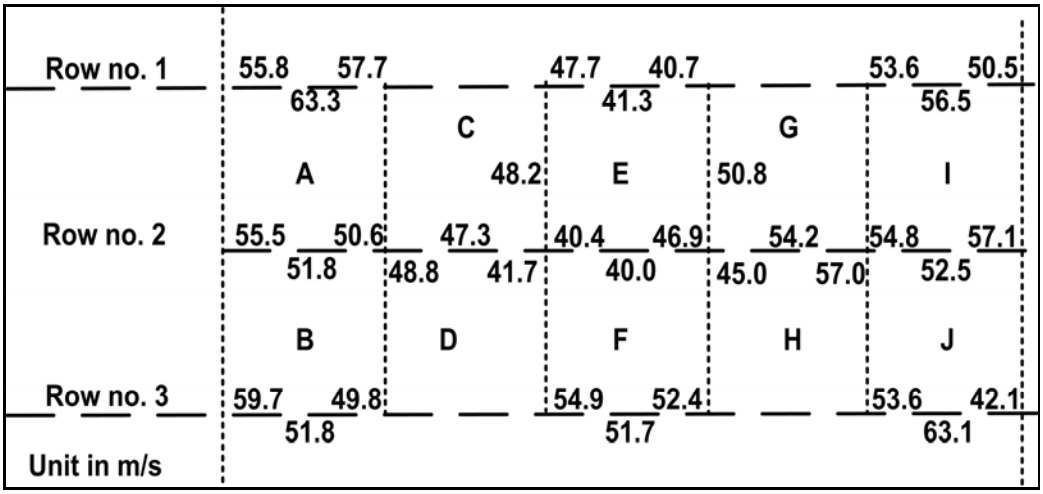

Figure 7.12: Distribution of the phase velocity analysis via weighted-mean throughout the Oxford clay container .

Table 7.2: Summary of average phase velocities for seismic source located in the front of array.

Test identification	Coherence > 0.9 and 190-1200 Hz, A-B	All data from 190 – 1200 Hz, A-B	Coherence > 0.9 and 133-923 Hz, B-C	All data from 190 – 1200 Hz, B-C	Coherence > 0.9 and 103-750 Hz, C-D	All data from 190 – 1200 Hz, C-D
Row1/A	56.5 ± 5.0	56.5 ± 5.0	57.4 ± 8.3	56.7 ± 7.0	54.5 ± 12.3	53.9 ± 8.9
Row1/E	50.0 ± 4.7	50.0 ± 4.6	41.3 ± 9.3	40.8 ± 5.7	45.8 ± 10.1	42.2 ± 7.7
Row1/I	47.9 ± 8.2	45.8± 8.3	51.6 ± 9.9	55.6 ± 12.9	51.4 ± 11.9	51.2 ± 9.9
Row2/I	54.9 ± 7.2	54.7 ± 5.5	52.1 ± 9.6	51.7 ± 7.3	51.1 ± 12.0	52.0 ± 8.5
Row2/G	55.3 ± 10.8	55.2 ± 10.8	48.1 ± 12.6	49.2 ± 10.9	45.8 ± 9.6	46.3 ± 7.7
Row2/E	47.5 ± 4.8	47.5 ± 4.8	41.7 ± 8.4	40.1 ± 5.0	41.1 ± 12.4	39.2 ± 5.0
Row2/C	41.4 ± 4.3	41.4 ± 4.2	49.5 ± 5.2	48.3 ± 4.6	47.9 ± 11.5	47.5 ± 4.3
Row2/A	49.5 ± 5.3	49.7 ± 5.5	54.3 ± 10.7	53.8 ± 10.0	56.9 ± 12.2	57.8 ± 11.6
Row3/B	46.8 ± 6.4	47.5 ± 6.6	46.1 ± 6.1	46.8 ± 4.7	49.5 ± 5.6	49.8 ± 4.7
Row3/F	52.8 ± 3.5	53.0 ± 3.6	53.5 ± 6.8	51.7 ± 5.4	51.4 ± 13.2	50.7 ± 7.9
Row3/J	50.9 ± 3.1	50.9 ± 3.1	50.8 ± 7.3	49.6 ± 6.2	47.0 ± 5.8	47.0 ± 4.4
Average	50.1 ± 8.0	50.0 ± 7.8	49.3 ± 8.5	49.1 ± 9.2	48.7 ± 12.1	48.7 ± 9.5

Table 7.3: Summary of average phase velocities for seismic source located at the centre of array.

Test identification	Coherence > 0.9 and 190-1200 Hz, A-B	All data from 190 – 1200 Hz, A-B	Coherence > 0.9 and 190-1200 Hz, C-D	All data from 190 – 1200 Hz, C-D
13	47.0 ± 4.1	46.9 ± 4.0	44.0 ± 3.9	44.1 ± 3.9
14	45.2 ± 3.1	45.3 ± 3.1	45.2 ± 6.1	45.3 ± 6.0
15	48.4 ± 6.5	48.4 ± 6.5	46.1 ± 5.1	45.9 ± 5.1
18	46.5 ± 5.8	46.4 ± 5.7	53.3 ± 7.5	53.1 ± 7.4
Average	46.8 ± 5.2	46.7 ± 5.1	47.2 ± 6.8	47.1 ± 6.7

The average phase velocities fulfilled the criteria of the frequencies and wavelengths. The phase velocities were analysed using different techniques, i.e. the weighed-mean, non-

weighted average with coherence threshold of 0.9 and without limiting the coherence. Figure 7.13 compares these three techniques of calculation for 15 sets of tests identified as Row 2/A to Row 2/I. These tests were located at the middle of the box (see Figure 7.5). Though different analysing techniques were adopted, they all gave reasonably similar phase velocity results as shown in Figure 7.13. The averaged phase velocity for coherence threshold of 0.9 was 48.4 ± 8.5 m/s. However, when the coherence threshold was not limited, the phase velocity was 48.3 ± 7.7 m/s. The weighted-mean phase velocities show that a range from 40.0 to 63.3 m/s with an average of 50.3 ± 6.4 m/s (see Figure 7.13). All sensor pairs gave reasonable phase velocity results as shown in Table 7.2, Table 7.3 and Figure 7.13.

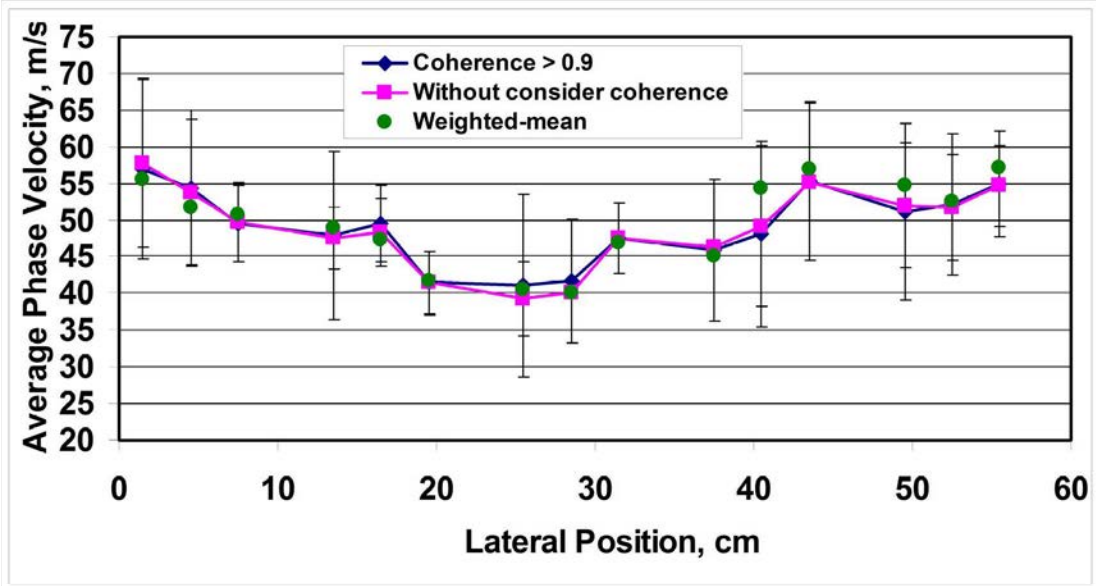

Figure 7.13: The distribution of mean phase velocities and standard deviations along row no. 2 (15 set tests) for three different types of manipulated calculations.

The tests carried out with the seismic source at one end of the array and at the middle of array indicated that the homogeneous clay gave reliable phase velocities for all sensor pairs. However the difference between the standard deviations (see Figure 7.10 and 7.11) for the above two arrays was comparatively small. Nevertheless, the arrangement of the seismic source in the middle of the array demonstrated an even smaller standard deviation suggesting that this array is an optimal arrangement for deployment to carry out the seismic surface wave test.

Figure 7.14 is a plot of all data obtained from 21 sets of tests with no constraint on the coherence threshold. This plot is important to evaluate the reliability of phase velocity data, which should ideally be constant across a wide range of wavelengths for the homogeneous clay. The reliability of data needs to be checked not only on the basis of coherence threshold but also on the constancy of phase velocity with changes in wavelengths. The variation of average phase velocity versus wavelength indicates a range of phase velocities between wavelengths 2 and 37 cm. However, phase velocities were reasonably constant for wavelengths between 3.5 and 21 cm. The biggest deviations from this constancy in phase velocity occurrs for wavelengths below 3.5 cm and above 21 cm. It seem these deviations in the phase velocities are most likely due to the wavelengths constraint associated with the distance of source from the first receiver, d (See Figure 6.13). To avoid far-offset constraint, the wavelengths should be larger than 3.5 cm (using Equation 3.11), and to avoid near-offset constraint, the wavelengths should be below than 21 cm (using Equation 3.10).

Rayleigh waves are another phenomenon reported by Zerwer *et al.*, (2002), who studied the propagation of a wave on the surface of a homogeneous medium. These waves had constant velocity when the wavelength was shorter than half the depth of the medium. It is worth noting that the model container used in this research study has a depth of 50 cm. From equation 4.8, and for a constant *k* equal to one, that the maximum wavelength was 50 cm. Therefore, for wavelengths less than 25 cm (half of maximum wavelength) the phase velocity must be constant. Further discussion on this is presented in Chapter 8.

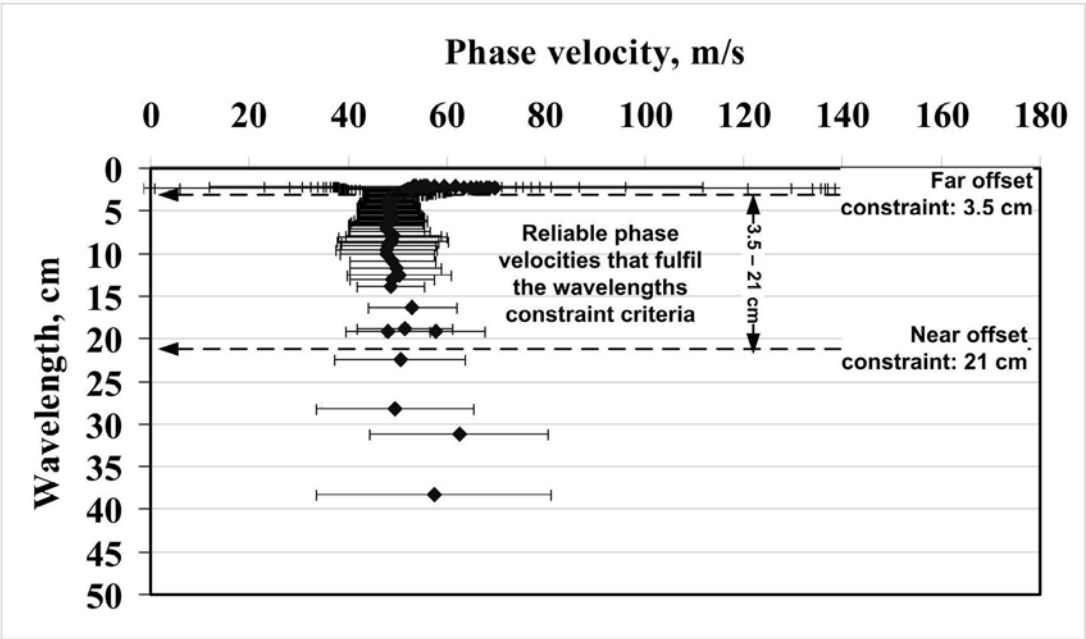

Figure 7.14: Relatively consistent of the mean phase velocities and it standard deviations throughout the wavelengths 3.5 to 21 cm.

This homogeneous soft clay is considered to have a constant phase velocity across the depth due to its relatively uniform density profile both laterlly and vertically (with depth). The test bed was as described in Section 6.5.2 A constant phase velocity was observed for

wavelengths from 3.5 to 15 cm. There were minor deviations from this constancy over the wavelengths 15 to 21 cm. Thus these phase velocities are considerd reliable. The phase velocities were converted into shear wave velocities using Equation 4.10 ($v_s = 1.047 \cdot v_r$) based upon a Poisson's ratio of 0.5 for the clay. The shear wave velocities were then converted into shear modulus using the measured average bulk density for Oxford clay of 1711 kg/m³ and the Equation 4.11 ($G_{\max} = \rho \cdot v_s^2$). The average shear wave velocity and shear modulus obtained using the weighted-mean phase velocity (50.3 m/s) were 53 m/s and 4.7 MPa respectively. Figure 7.15 presents the evaluated shear modulus variation with wavelength. It shows a relatively small increase of shear modulus with increasing wavelength.

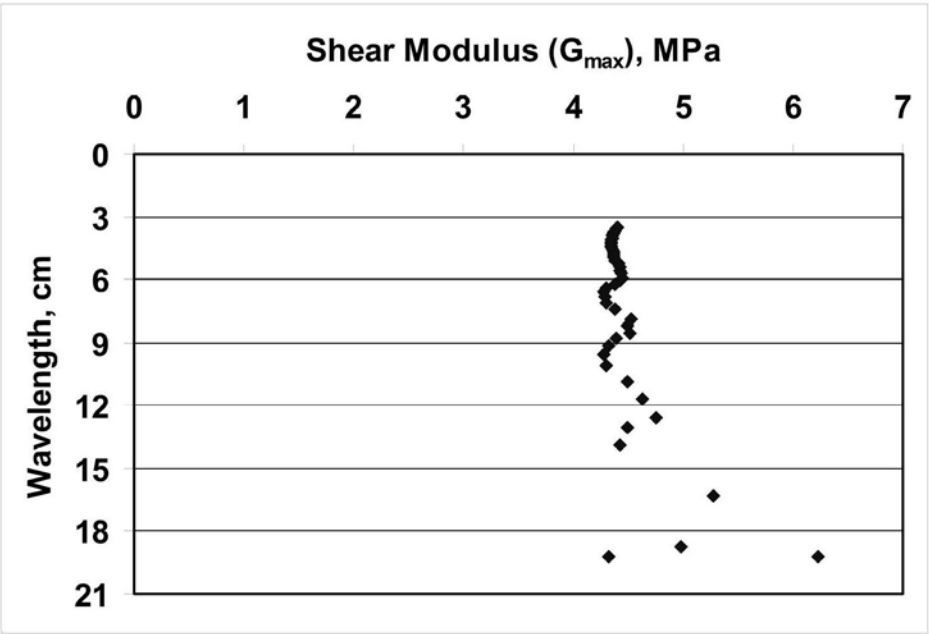

Figure 7.15: Plot of shear modulus, G_{max}, of clay versus wavelength.

The average water content of Oxford clay was 40.2 % which is equivalent to a shear strength of 16 kPa. This correlates with the graph of water content versus shear strength

reported in Chapter 6 (see Figure 6.3). The shear strength was used to estimate phase velocity via the empirical conversion of $c_u = 0.0424 v_s^{1.462}$, based on stabilised Uppsala clay with cement as established by Mattsson *et al.* (2005) (see discussion in Section 7.2.1). The converted phase velocity from shear strength was 55 m/s. Meanwhile, the phase velocity of kaolin determined by Chan (2006) was 51 m/s and Rahyani and El Naggar (2007) was 48 m/s. The average phase velocity in Oxford clay, calculated using weighted-mean was 50.3 m/s, which agrees closely with the phase velocity values cited by Mattsson *et al*. (2005), Chan (2006) and Rahyani and El Naggar (2007).

7.2.3 Discussion

The phase velocities measured in kaolin and Oxford clay were 51.3 m/s and 50.3 m/s respectively. The result demonstrates that weighted-mean velocities are closer to the expected phase velocity value in the soft clay reported by Rahyani and El Naggar (2008) and Chan. (2006) in both models of homogeneous kaolin and Oxford clay. The weighted velocities gave consistent performance over a range of thresholds (0.7, 0.9 and 0.95) in kaolin. This phenomenon was reported in Madun *et al.* (2010b). However, without restricted on the coherence threshold, phase velocities indicated reliability via the frequency / wavelength constraints associated with the near and far array offset constraint (see Figure 7.14). The quality of measurement at low frequencies was influenced by the size of the physical clay model. The larger physical model provided an increase in useful frequencies, which had reliable phase velocity when wavelength half of the model depth.

The higher coherence values and less deviation from the average value were also indicator of the quality of measurement.

The control tests demonstrated that the arrangement of sensors and source also played a role in the quality of measurements, as well as the reliability of the results. A seismic source located in the middle of an array resulted in smaller deviation from the average due to both sensor-pairs receiving equal and relatively higher amount of energy when compared with the source placed on one end of the sensor array.

7.3 Soft Clay with Column

7.3.1 Homogeneous Kaolin with a Single Column

The tests were carried out in an optimal arrangement where the source was at the centre of array. The test array arrangement was described in Chapter 6. The source to first receiver separation was 7 cm, and the sensors were 2.5 cm apart (see Chapter 6, Figure 6.6). The measurements were carried out with the frequency range of 400 Hz to 1400 Hz, using a stepped-frequency approach with a step-size of 50 Hz. The selection of the frequency range referred to the control test results in kaolin. At each frequency step, 5 repetitive measurements were obtained for averaging and the calculation of the normalized coherence.

Figure 7.16 shows a plot of frequency and phase velocity for coherence above 0.9. By comparing the plot for both sensor-pairs, it was possible to differentiate both materials in

terms of the variation in phase velocity. The global average of phase velocities between the frequency range of 400 Hz to 1400 Hz for a sensor-pair placed directly on top of a column was 118.6 m/s, while for the sensor-pair placed on kaolin (with column installed nearby) was 58.6 m/s. The sensor-pair on homogeneous clay gave constant phase velocity for all frequencies.. However, the sensor-pair on the column showed a trend of increasing phase velocities with increasing frequencies.

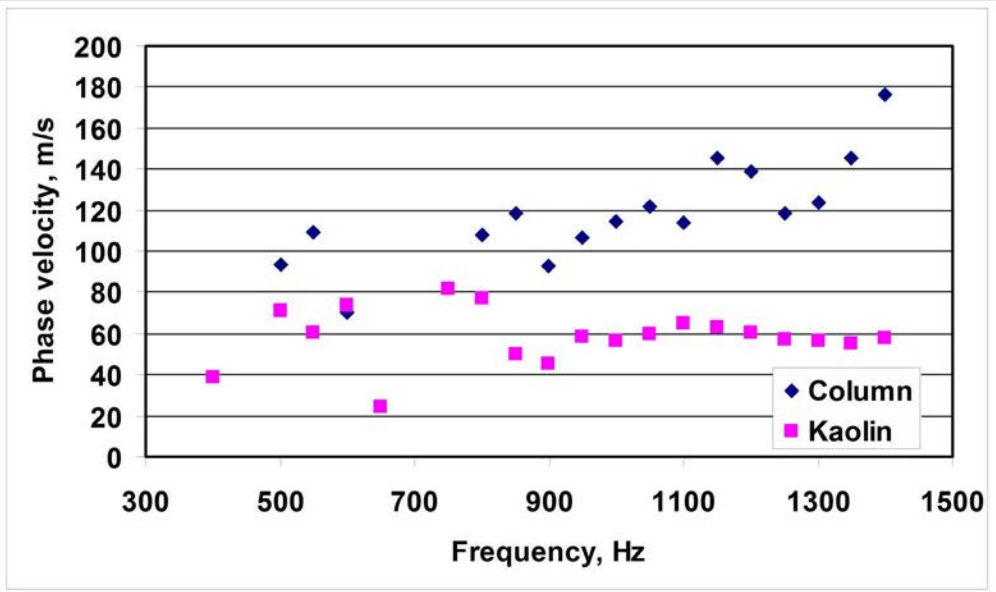

Figure 7.16: Dispersion curve for kaolin clay and 10 cm diameter of column.

In Figure 7.17 (a), by plotting the phase velocity as a function of wavelength, it can be observed that the maximum phase velocity measured was represented the column phase velocity. The reliable phase velocities between wavelength 3.5 and 15 cm, which fulfilled the far-offset constraints with half of distance from source to the nearest receiver, *d*, (see Equation 3.11) and wavelength less than half of model depth. It is worth noting that the distance from source to the nearest receiver (*d*) was 7 cm and the model container depth was 30 cm. The average phase velocity of the column at 120 m/s is represented by the

wavelengths below 12.5 cm, closer to the expected phase velocity value in the sand with 115 m/s reported by Rahyani and El Naggar (2007). Figure 7.17 (b) illustrates the effective region measurement of one Rayleigh wavelength (12.5 cm wavelength) sampling volume with assumption elliptical shape particle movement within the medium of propagation. The sizes of the semi major and semi minor axis of the ellipse within the column was 12.5 cm and 10 cm respectively (see later discussion in Section 7.4 and Figure 7.40). The size of ellipse became smaller with the decreasing wavelengths. It is worth noting that the diameter of column was 10 cm.

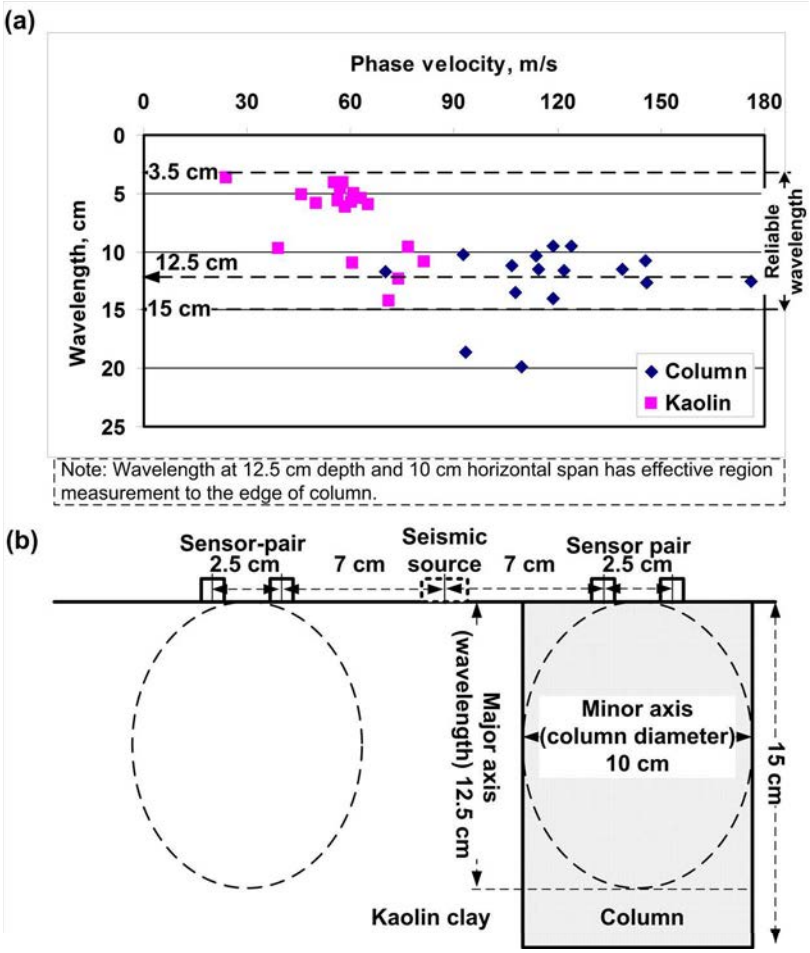

Figure 7.17: Distribution of phase velocities in the column and kaolin clay (a) demonstrates that wavelength of 12.5 cm and below gave higher velocity on column and (b) illustration of the elliptical shape of the sampling volume in column and kaolin clay.

Using the approach of sampling volume in ellipse shape was able to explain the changes of phase velocities with frequencies / wavelengths. Further discussion about the elliptical shape assumption is given in Chapter 8. The scattered phase velocities in column were also observed in similar diameter of column in Oxford clay model (see Section 7.3.2.4). Meanwhile, slightly increased velocities in clay at low frequencies were most likely due to interference of the reflected wave from the container boundary. The kaolin phase

velocities obtained in control test and when the column presented were 51.3 m/s and 58.6 m/s respectively. These differences were likely to be due to the column inclusion, which was a cause of a noisy seismic environment and also changed the soil properties. These tests results are in good agreement, thus an essential indicator that the testing equipment and system were able to perform measurement reliably.

It was very clear in theory that phase velocity is a function of wavelength / frequency. If the properties of medium changed vertically, therefore phase velocity should be also changed with wavelength / frequency. The test hypothesis in this study was the phase velocity of material is subject to the location of the measurement is carried out. From the homogeneous kaolin test bed with homogeneous single column showed the phase velocities of column change throughout the wavelengths / frequencies, which were difficult to understand and interpret. Due to this problem in earlier stages fine-tuning of the equipment and its system was necessary. After further tests were carried out using larger box with Oxford clay test bed with series of columns installation (Section 7.3.2), the relationship phase velocities with wavelengths / frequencies enable clarity to be gained. The phase velocities showed decreasing trend with increasing wavelengths observed either when tested in single column or when testing a few columns. Thus, the suggested hypothesis was the sampling volume based on the ellipse shape with function of the wavelength / frequency could be used to explain the phenomenon. This is discussed further in Section 7.4 and Chapter 8.

7.3.2 Oxford clay with Multi Columns

The optimal seismic source-sensors array was deployed to give better resolution for the evaluation of stone columns. A total of 7 compacted columns were installed at reduced scale factor of 15 from typical stone column geometry. Additional 2 columns consist of the defective and larger diameter to study the effect of material density and column diameter (see Section 7.3.2.3 and 7.3.2.4 below). The source was placed at the middle of the array to capture data with maximum signal-to-noise ratio. There were four types of measurement arrangements; sensor-pairs within the clay area (between columns), sensor-pairs on top of the columns, sensor-pair on the defective column and sensor-pair on the larger column diameter.

7.3.2.1 Sensor-Pairs Located on Clay

A total of 10 sets of tests were carried out on the clay area using a linear array, in which measurement was performed using 4 sensing channels and a seismic source in the middle of the array. The arrangement is shown in Figure 7.18. The source-receiver separation was 7 cm and the inter-sensor spacing was 3 cm. The excitation frequency range was from 100 Hz to 1200 Hz, applied using a stepped-frequency approach with a step-size of 10 Hz. At each frequency step, 5 repetitive measurements were obtained for averaging and the calculation of the normalized coherence. This small step-size was purposely chosen to obtain higher number of data and thus small gaps in stiffness profile. However a drawback was taken longer time and used larger volume of computer hard disk. Each measurement

consumed 5.8 megabytes computer and for whole series of test (100 Hz to 1200 Hz) using 3.2 gigabytes hard disk.

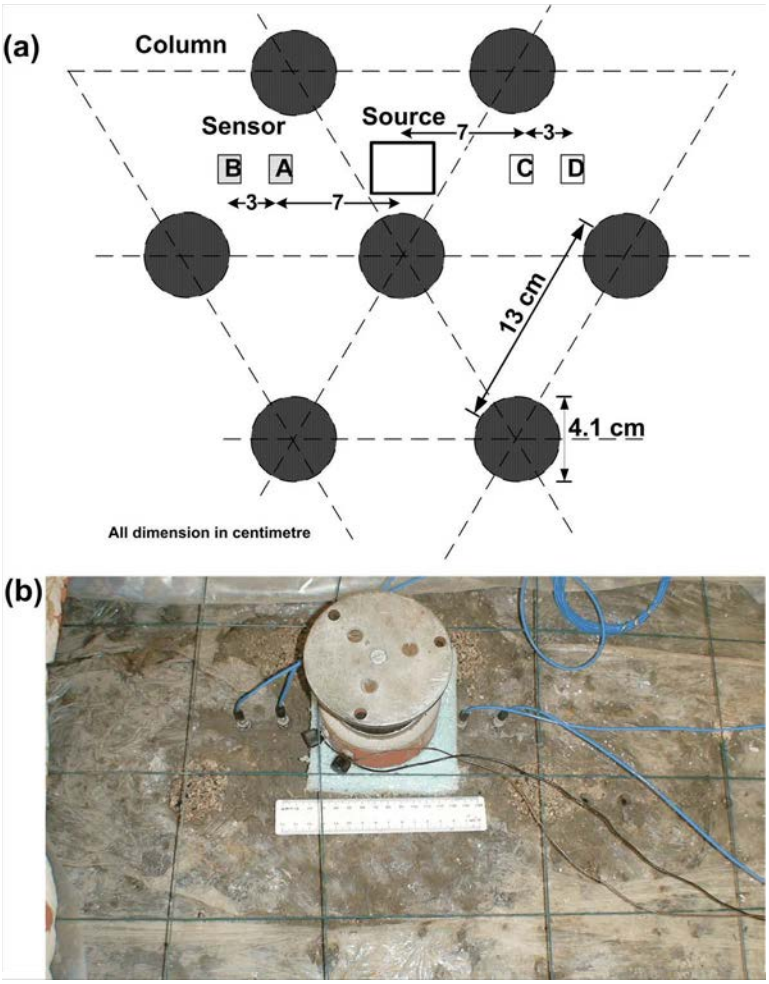

Figure 7.18: (a) Illustration of the arrays for both sensor-pairs located on clay, and (b) photo of the sensor pairs on top of Oxford clay where the seismic source was located in the middle.

The plot of one set of test normalized coherence in Figure 7.19 shows a higher signal quality between frequencies 250 and 800 Hz. In general, the normalized coherence is significantly reduced when compared with the results obtained from the control test (the

clay model without columns, see Figure 7.6), with higher signal quality extended to 1500 Hz. This is caused by the presence of columns nearby, which introduced additional reflections due to the contrast of material density between clay and column. A similarity, between the results from the models with and without column, were observed at frequencies below 200 Hz, where the Rayleigh-waves were dominated by body wave and boundary reflections from a longer wavelength. In Figure 7.20, it can be seen that the unwrapped phase velocities exhibited a non-linear relationship at frequency regions that correspond to very low normalised coherence. The upper frequency limit was 1200 Hz for this measurement as this was the estimated as the wavelength that satisfies the far offset requirement

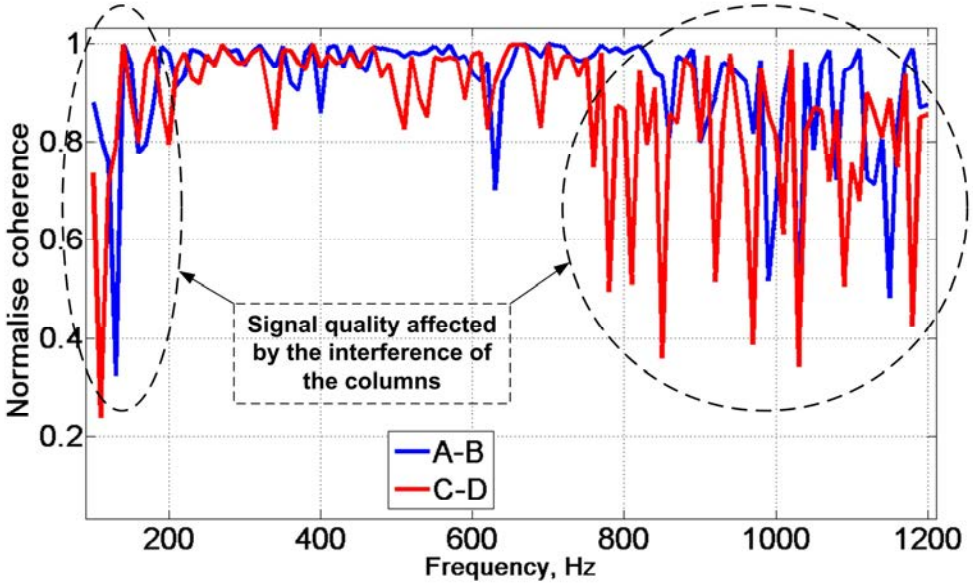

Figure 7.19: The typical plot of normalized coherence showing a higher signal quality in the frequency range of 250 and 800 Hz.

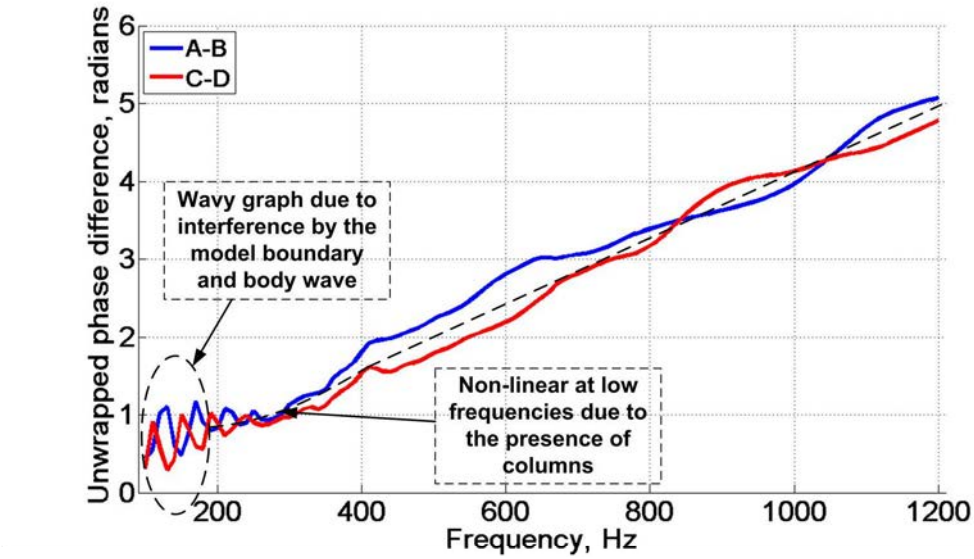

Figure 7.20: Typical seismic wave tests which sensor-pairs located on soft clay shows unwrapped phase difference.

The typical plot one set test of the phase dispersion relationship in Figure 7.21 demonstrates that the velocities at frequencies lower than 500 Hz had larger deviations from the expected phase velocity within clay. At lower frequencies, and hence longer wavelength, the propagating Rayleigh wave with elliptical particle movement will begin to encapsulate the nearby gravelly sand column. When the wavelength of the Rayleigh wave approaches the distance between the sensors and the nearby columns, some of this energy would be reflected, while some was refracted into the column. Due to the relatively small bulk density contrast between clay and column (1711 kg/m^3 and 2045 kg/m^3), it was reasonable to expect that most of the Rayleigh wave energy would travel across into, and through, the column. As a result of this phenomenon at lower frequencies and larger wavelengths, the measured phase velocity was affected by the properties of both the clay and the nearby columns. An average of the phase velocities and standard deviations of all

10 sets of tests in Figure 7.22 shows clearly that the measured phase velocities of lower frequencies were influenced by the nearby columns.

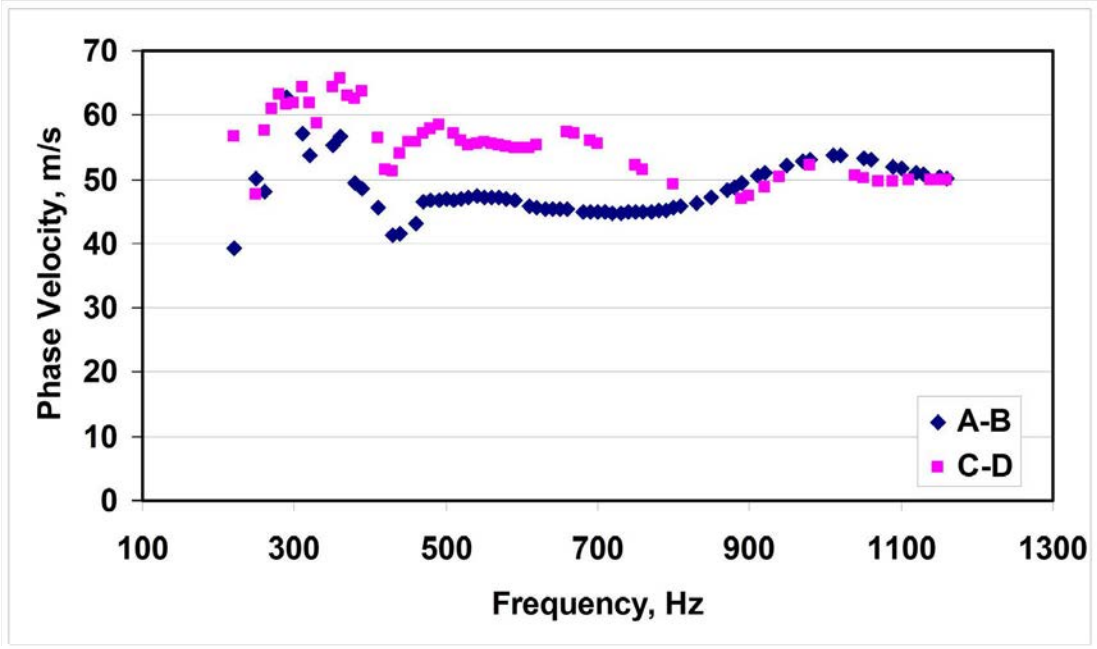

Figure 7.21: Typical dispersion curve for both sensor-pairs located on clay.

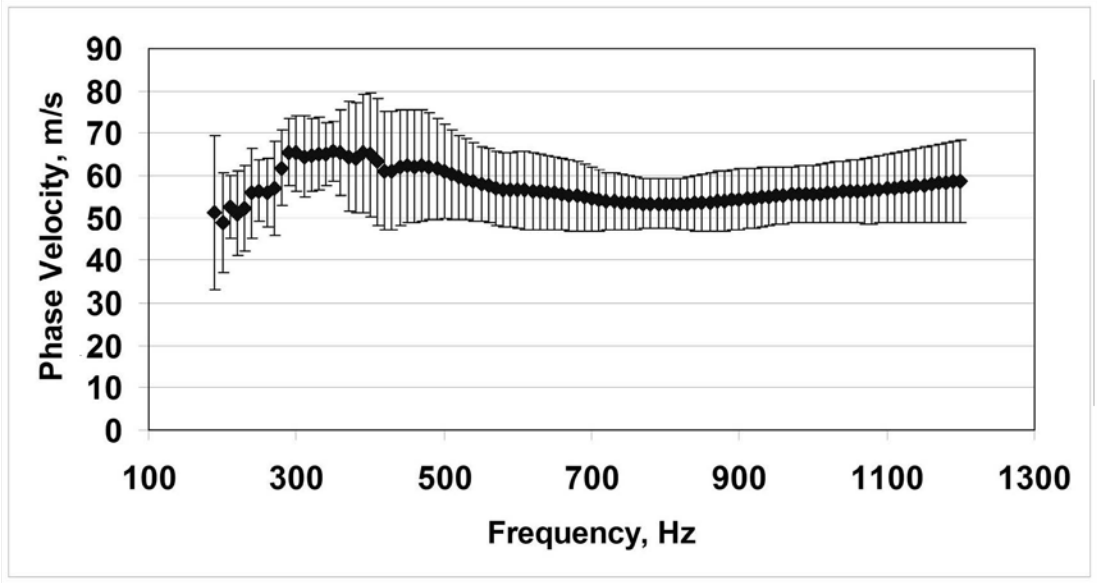

Figure 7.22: Dispersion curve average from 10 **sets of** tests.

The dispersion curve in Figure 7.23 displayed 3 distinct groups of wavelengths that have similar phase velocities, seemingly indicating 3 different horizontal layers of clay with distinct properties. However, given the knowledge that this clay was essentially homogeneous vertically and heterogeneous laterally, it can be concluded that this phenomenon was caused by the nearby columns. The larger wavelength encroaching the area of nearby columns, as a result, influences the measured phase velocities. Wavelengths between 16 and 21 cm show a higher phase velocity, indicating that at these wavelengths there were the highest portion of nearby columns being detected by the sensor-pairs located on the clay. The phase velocities above the wavelengths of 21 cm are influenced by the body wave, called near-offset constraint.

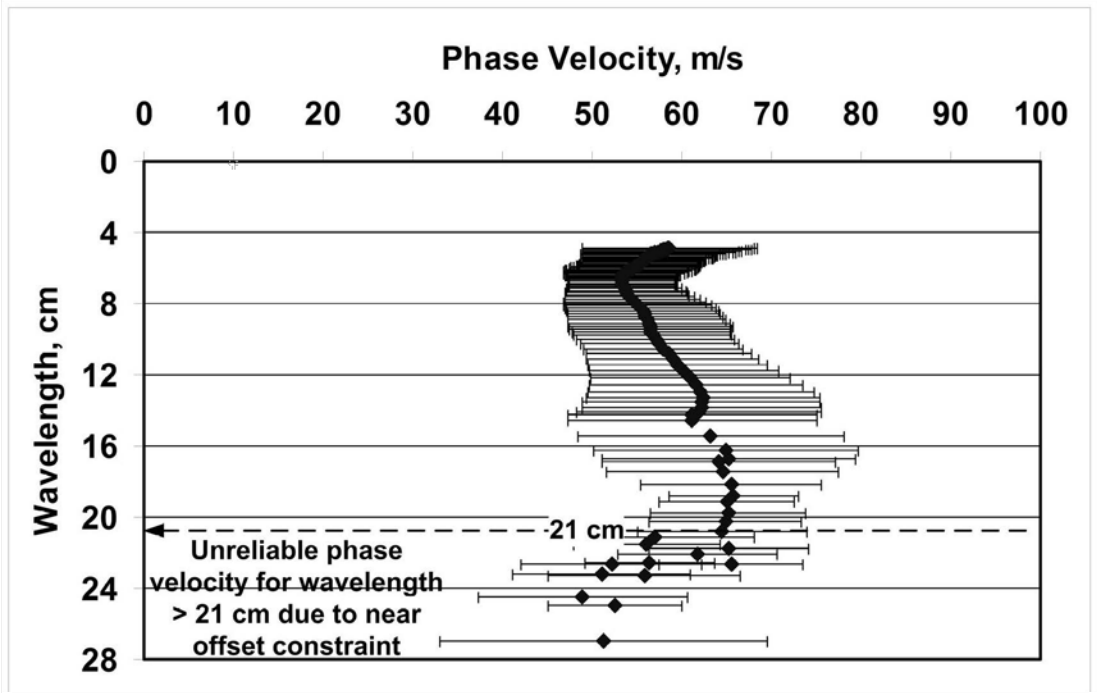

Figure 7.23: Plot of phase velocities versus wavelength.

7.3.2.2 Sensor-Pairs Located on the Columns

A total of 5 sets of tests were conducted directly on two columns, using a seismic source arranged at an angle of 60º to both the sensor-pairs array as shown in Figure 7.24. The source-receiver separation was 7 cm and the inter-sensor distance was 3 cm. The measurements were carried out across the frequency range of 200 Hz to 2500 Hz using a stepped-frequency approach with a step-size of 10 Hz. At each frequency step, 5 repetitive measurements were obtained for averaging and the calculation of the normalized coherence. Each test between 200 and 2500 Hz used 13.4 gigabytes computer hard disk.

The plot of typical single set of test normalized coherence in Figure 7.25 shows a reduction of signal quality across the whole frequency range. This phenomenon was likely to have been caused by reflection and refraction due to the presence of the columns, thus reducing the signal quality. This observation of normalized coherence was in contrast with the result obtained without columns (see Section 7.2.2), where there was higher coherence at lower frequencies below 1500 Hz. The non-linear function exhibited by the unwrapped phase differences, observed for both sensor-pairs, shows that the measurements detected lateral heterogeneous soil properties as demonstrated in Figure 7.26 (typical result from single set of test).

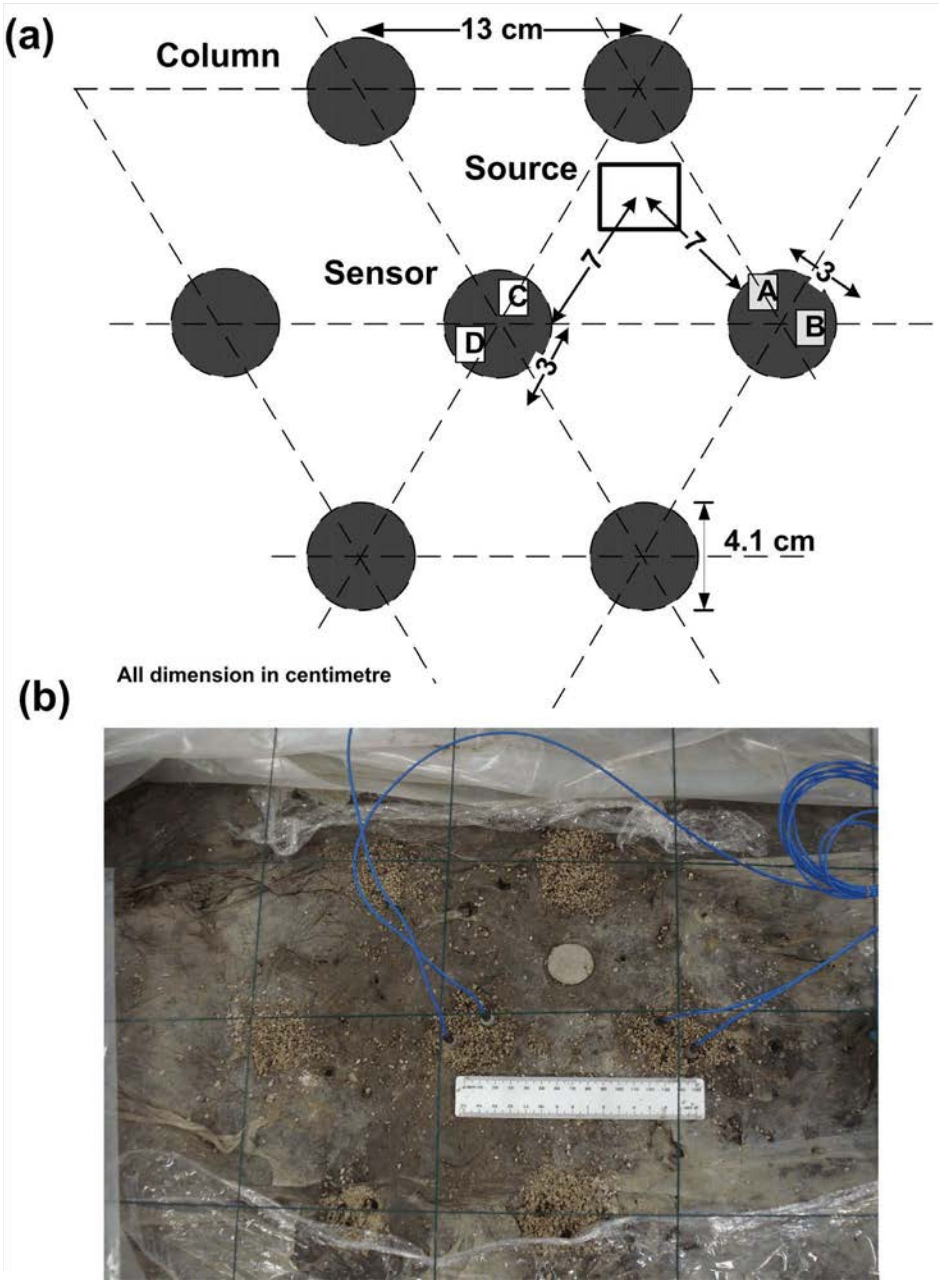

Figure 7.24: Illustration of test array for both sensor-pairs on columns and (b) photo of the stone columns with sensing accelerometers on top.

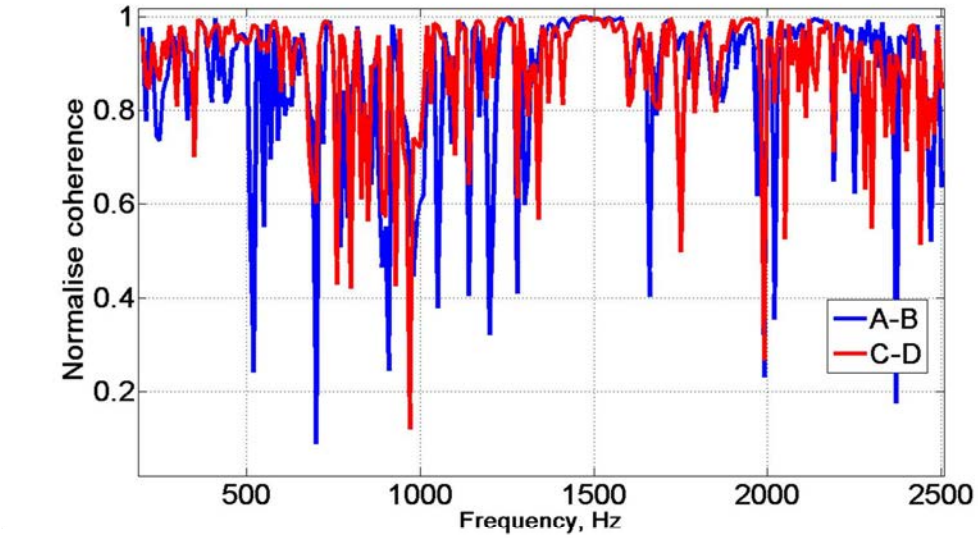

Figure 7.25: The typical plot of normalized coherence shows a reduction of signal quality for whole range of the frequencies which are influenced by columns.

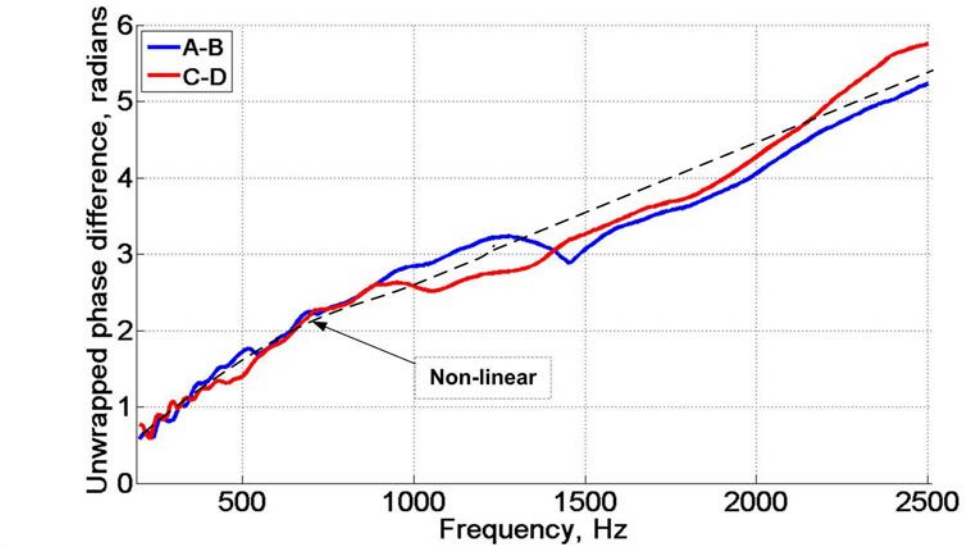

Figure 7.26: The non-linear function unwrapped phase differences for both sensor-pairs located on columns.

Figure 7.27 shows a typical plot of the phase dispersion relationship for a single set of tests where the data was obtained for a coherence larger than 0.9. About 67 % of data were above the coherence threshold 0.9. Meanwhile, Figure 7.28 shows all the average phase velocities obtained from 5 sets of repeated tests throughout the measured frequency range without consideration being given to the coherence threshold. Both plots show a similar trend, even though some of data had lower coherence values. It seems that the phase velocity was highly affected by the frequency and wavelength criterion. Generally the phase velocity gradually increased with frequency and stabilized when the frequencies beyond 2000 Hz. At low frequencies, in which the wavelengths exceed the diameter of the column, the waves measured by the sensors are propagating through both the column and clay. Below 500 Hz shows phase velocities significantly deviated due to the near-offset constraint and reflection from boundary.

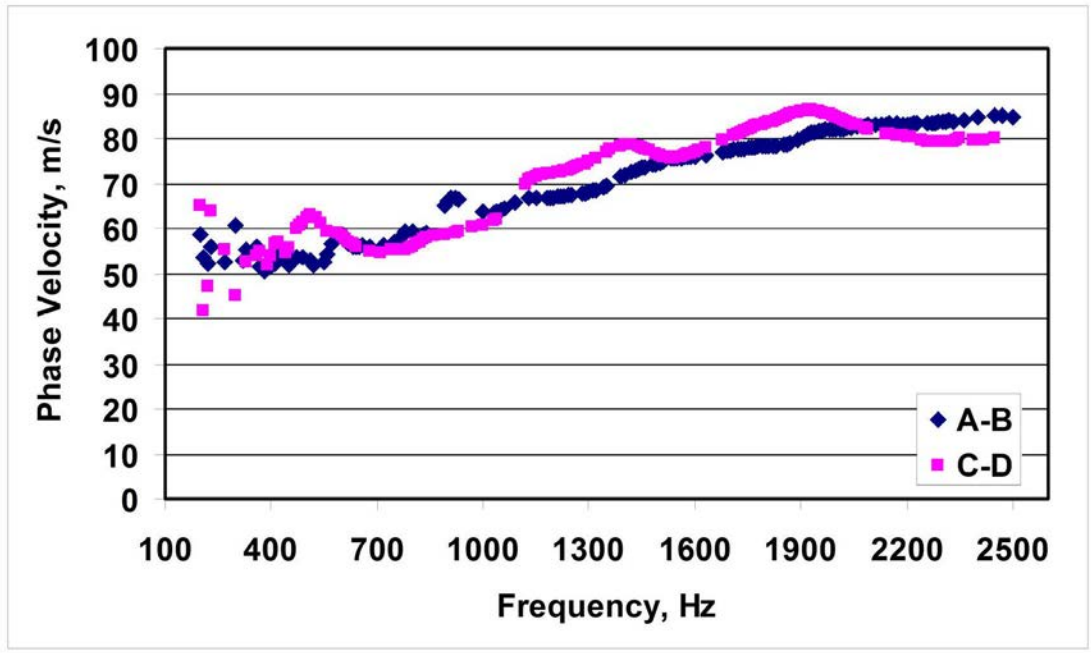

Figure 7.27: Typical dispersive curve for single test when the coherence is larger than 0.9.

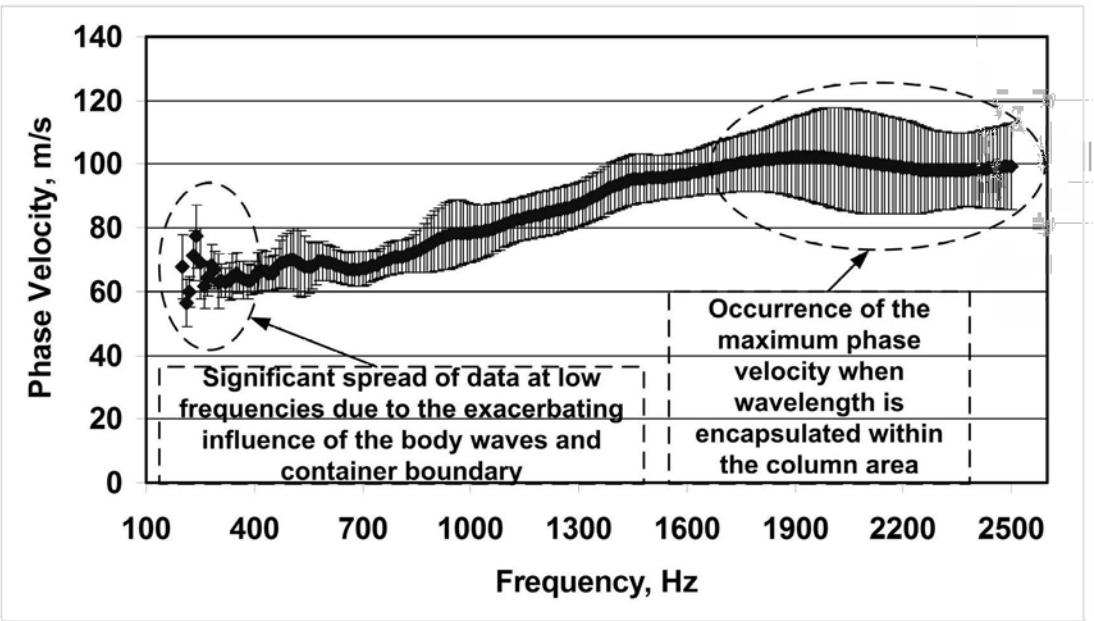

Figure 7.28: Dispersion curve obtained from 5 sets of tests of both sensor-pairs.

Figure 7.29 shows the entire plot of average phase velocity versus wavelength for 5 sets of tests regardless of the coherence threshold value. The maximum phase velocity was 102 m/s occurring at about 5 cm wavelength. The phase velocity decreased dramatically between the wavelengths of 5 and 10 cm, and then gradually decreased after 10 cm. From the dispersive curve, the phase velocities can be associated with the volume ratio between the column and the size of one Rayleigh wavelength with an elliptical shape (see later discussion in Chapter 8). When the wavelength decreased, the proportion of the wavelength in clay was reduced, thus the phase velocity gradually increased toward the phase velocity in the column. It is worth noting that the diameter of the installed columns was 4.1 cm. The peak phase velocity (102 m/s) of the Rayleigh waves at a wavelength of 5 cm was most likely a consequence of the sampling around the column area. The phase

velocities between the wavelengths of 3.5 and 21 cm fulfil the wavelength criterion i.e. the near- and far-offset constraint and spatial aliasing. Layering in column did not appear to have an effect on the dispersive curve due to the similar densities of the gravelly sand layers.

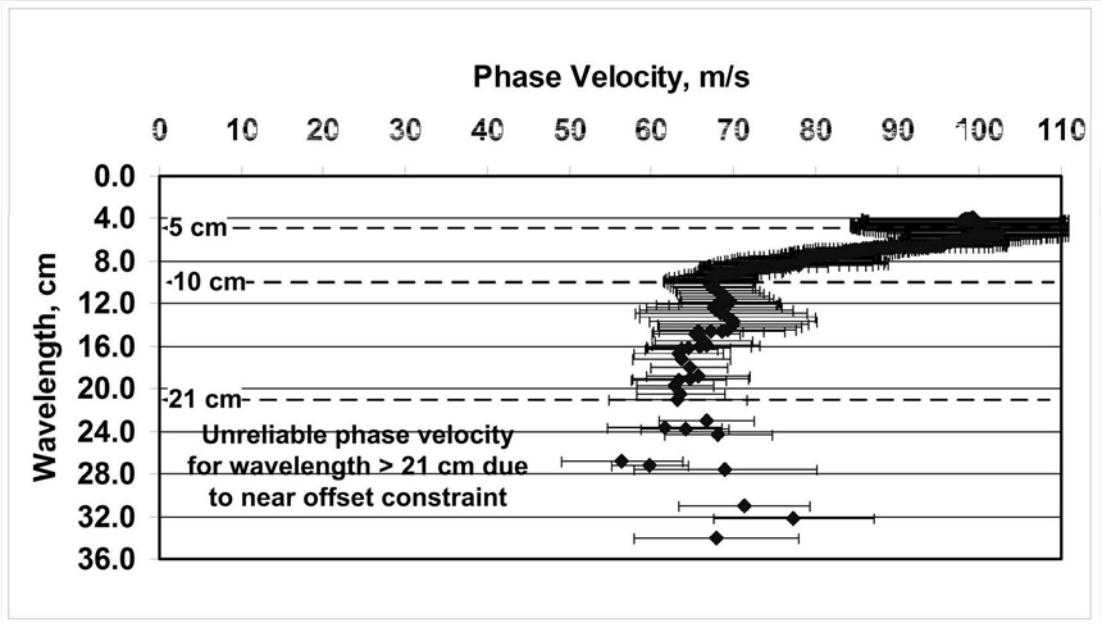

Figure 7.29: The plot of average phase velocity versus wavelength.

7.3.2.3 Sensor-Pairs Located on Defective Column

Additional column was installed as part of understanding the wave behaviour propagation. This time a simulated defective column was used. The defective column was constructed by not properly compacting gravelly sand (see Chapter 6). Figure 7.30 shows the results from a total of 4 sets of tests with both the defective column and compacted column, using sensor-pairs and source arranged in a triangular pattern. The source-receiver separation was 7 cm and inter-sensor spacing was 3 cm. The measurements were carried out across

the frequency range of 200 Hz to 2500 Hz, using stepped-frequency approach with a step-size of 10 Hz. At each frequency step, 5 repeat measurements were made for averaging and to calculate of the normalized coherence.

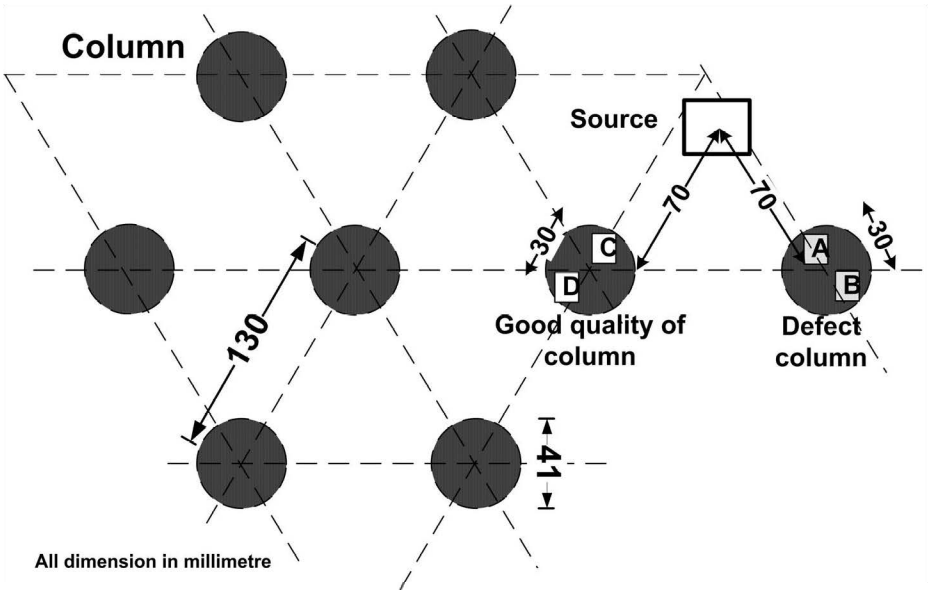

Figure 7.30: Test array for sensor-pairs on defective column and compacted column.

The plot of normalized coherence in Figure 7.31 shows a reduction of signal quality for the whole frequency range. In general, the normalized coherence shows both sensor-pairs had lower signal quality across the frequencies. About 57 % of data from defective column were above coherence threshold 0.9, meanwhile 75 % data from compacted column. This phenomenon was a result of the loose material (higher void ratio). The difference in bulk density between clay and column exacerbated the wave propagation passing the defective column and compacted column. The unwrapped phase differences are shown in Figure 7.32. The phenomenon observed in unwrapped phase difference for A-B (defective column) was in linear line until 1700 Hz, meanwhile for sensor C-D (compacted column) non linear.

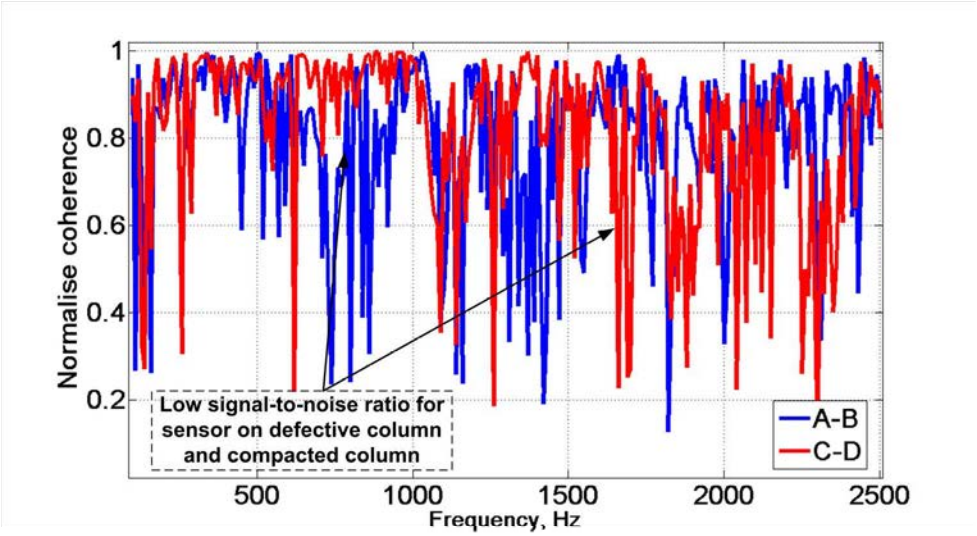

Figure 7.31: The normalised coherence over the whole range of tested frequencies, showing a reduction of signal quality in the defective column (A-B) compared with that of the good quality column (C-D).

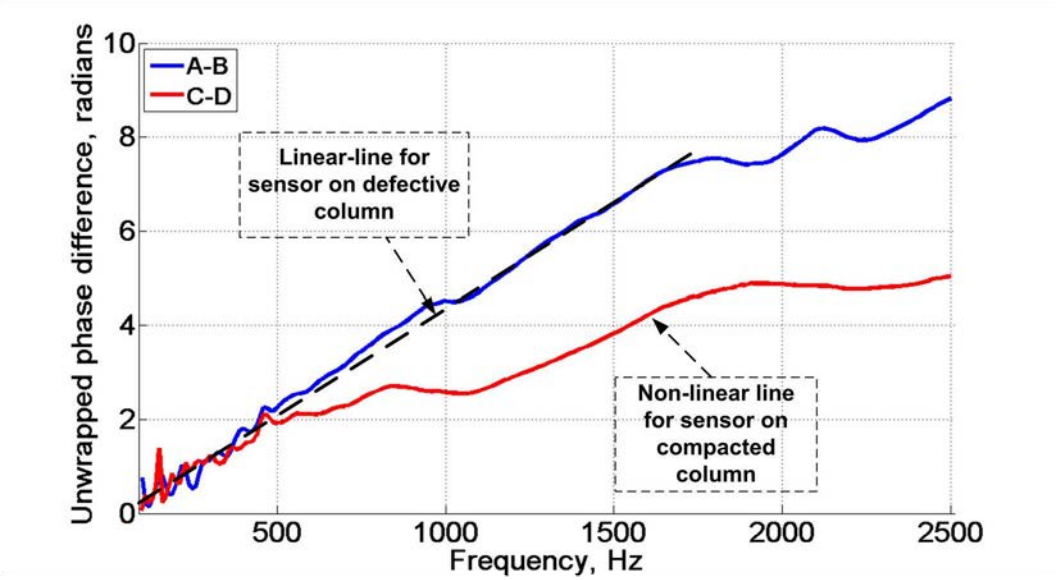

Figure 7.32: Observations of the linear function (up to a frequency of 1700 Hz) phase difference from the sensor pairs on the defective column (A-B) and the non linear function on the compacted column (C-D).

Figure 7.33 shows a plot of the average phase velocities data across all frequencies without limiting the coherence threshold. At low frequencies, in which the wavelengths exceeded the diameter of the column, the waves measured by the sensors are propagating through both the column and clay. From the dispersive curve, the phase velocities can be differentiated between the defective column (dry density 1492 kg/m^3) and the good quality column (bulk density 1884 kg/m^3). When the frequency is increased, the proportion of wavelength in the clay (bulk density 1220 kg/m^3) was reduced, thus the phase velocity gradually increased toward the phase velocity in the column. Figure 7.34 shows the plot of average phase velocities with wavelength and the reliable phase velocities were between 3.5 cm and 21 cm wavelengths. Despite only 57 % of data is above coherence threshold 0.9 on the defective column, the phase velocities showed reliable results fulfilling the criteria of near-, far-offset constraint and spatial aliasing requirement. The average phase velocity of the defective column was lower than that of the compacted column. Thus the comparison between them clearly demonstrates the ability of the surface wave to identify the defective column.

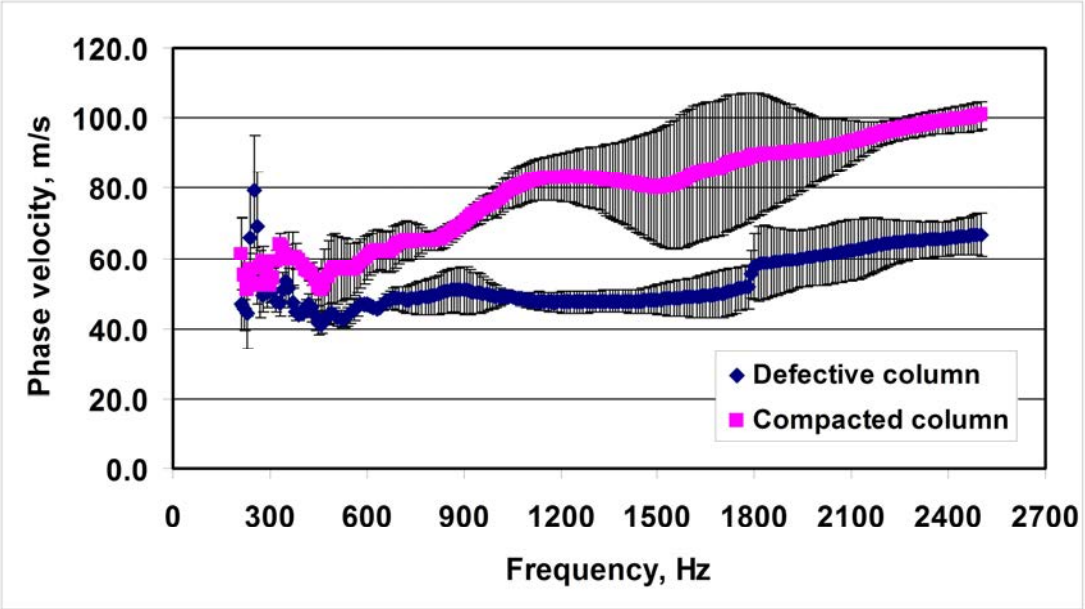

Figure 7.33: Phase velocity changes on the defective and compacted column over the range of frequencies used in the testing.

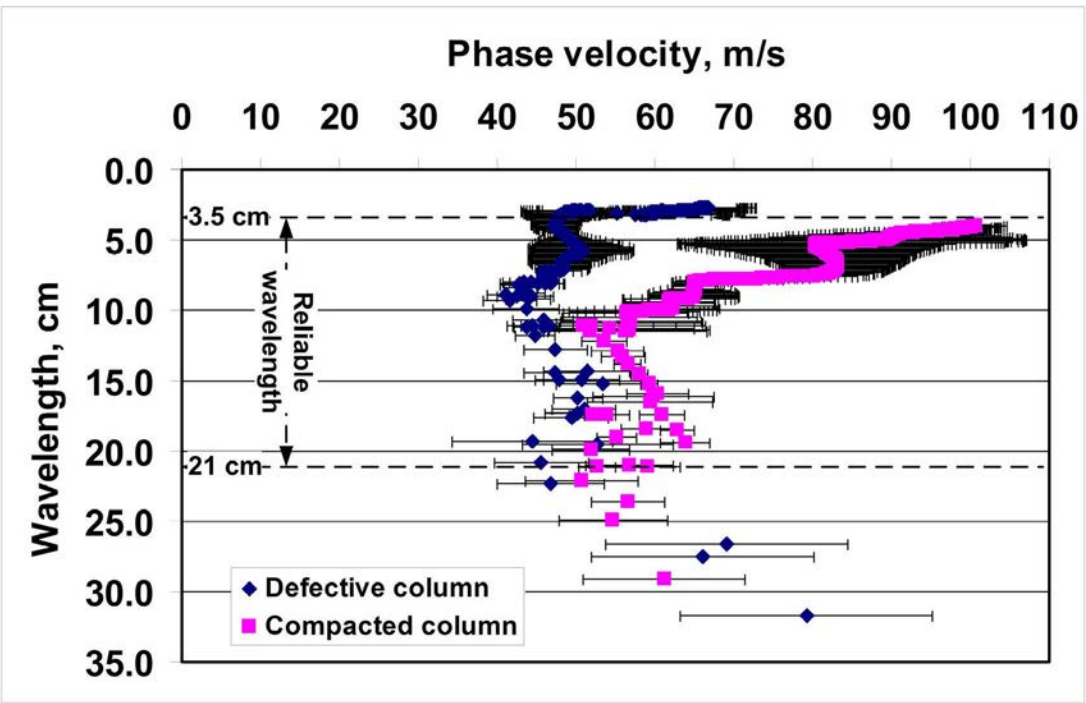

Figure 7.34: The plot of average phase velocity versus wavelength.

7.3.2.4 Sensor-Pairs Located on Larger Diameter of Column

The test covering the larger column and clay using the sensor-pairs array arranged in linear is shown in Figure 7.35. The source-receiver separation was 7 cm and inter-sensor spacing was 3 cm. The measurements were carried out across the frequency range of 200 Hz to 3000 Hz, using a stepped-frequency approach with a step-size of 20 Hz. At each frequency step, 5 repetitive measurements were obtained for averaging and the calculation of the normalized coherence.

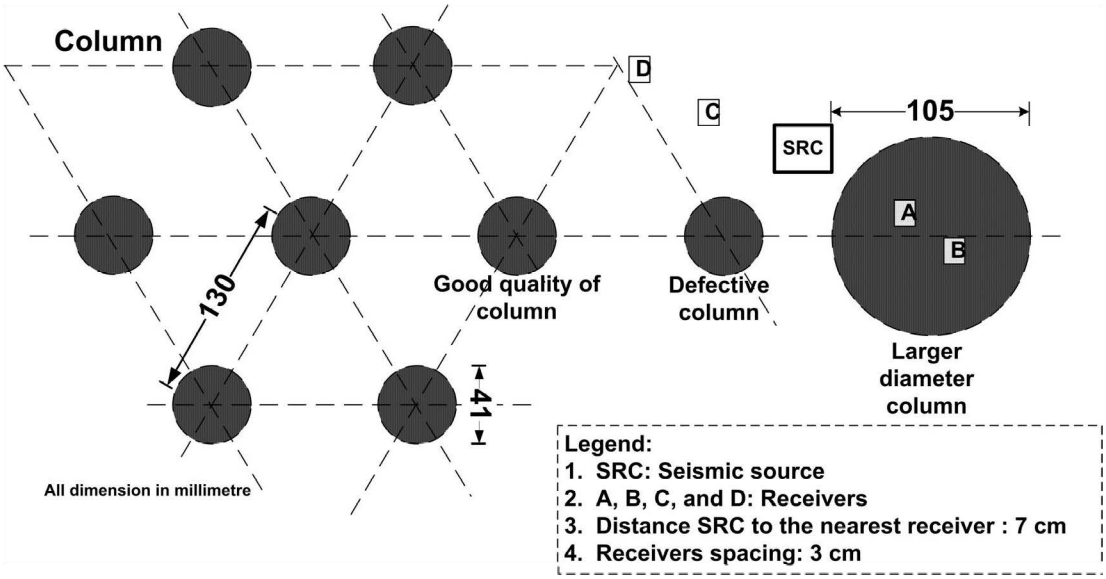

Figure 7.35: Test array for sensor-pairs on column and clay.

The plot of normalized coherence in Figure 7.36 shows a reduction of signal quality for the A-B (larger column) at low frequency range. In general, the normalized coherence shows significantly better signal quality for higher frequencies compared with lower frequencies for sensor-pair A-B (on larger column). Meanwhile, the sensor-pair C-D (on clay) gave a better quality signal for frequencies below 1400 Hz. This phenomenon in column and clay

was likely due to a different frequency criterion between these materials. While the unwrapped phase differences for A-B (on larger column) was non linear, that for sensor pair C-D (on clay) was linear as shown in Figure 7.37.

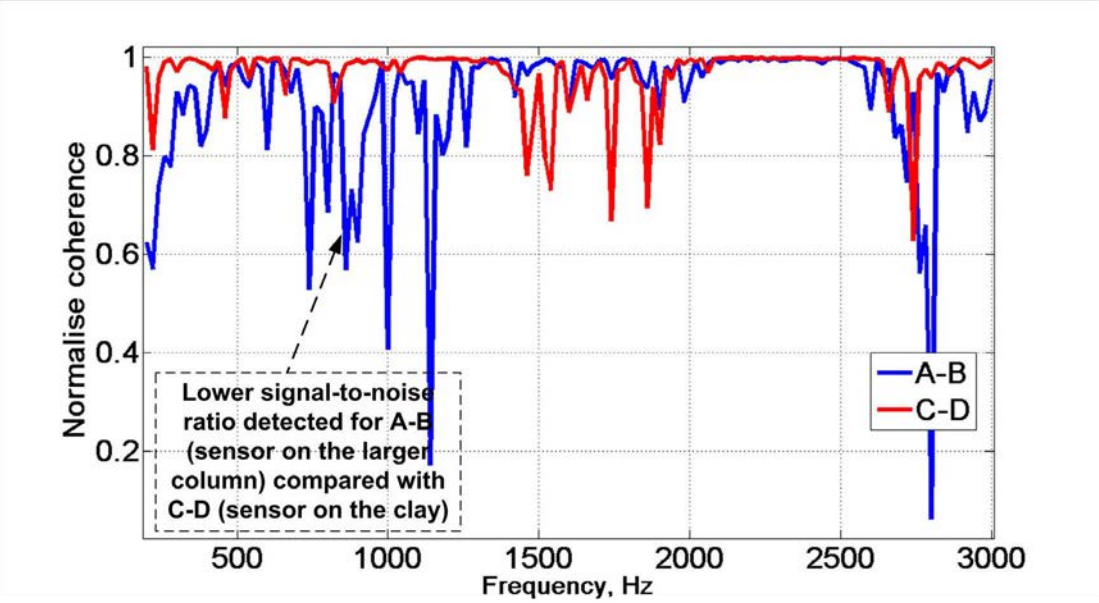

Figure 7.36: The normalised coherence for the whole range of test frequencies, showing a reduction of signal quality in the column area compared with the non column area.

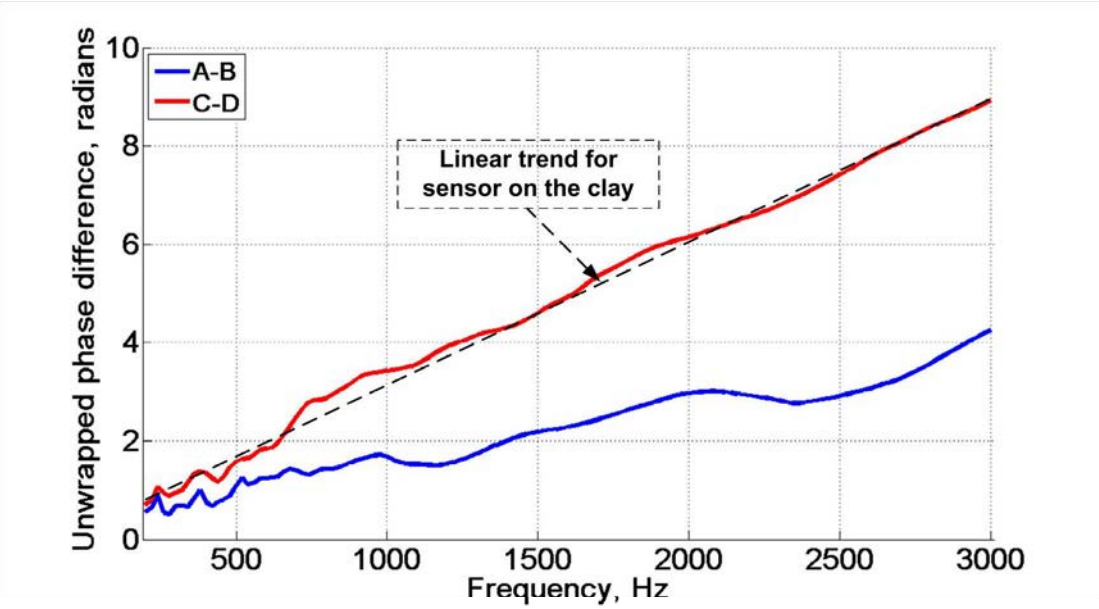

Figure 7.37: Observations of the sensor pairs on larger column (A-B) with non-linear function unwrapped phase differences, and on the clay (C-D) with linear function.

Figure 7.38 shows the results from a total of 5 sets of tests with both the sensor pair on the larger column and on the clay. The phase velocities increased with frequencies in the case of the column whereas in the case of the clay, the phase velocities were constant with the different frequencies. The higher phase velocity occurred when the frequency reached a value of 1200 Hz and until 3000 Hz, where the wavelengths corresponded to a value smaller than the column diameter (10.5 cm). The phase velocities became different at frequencies below 500 Hz for the sensor pair on the larger column diameter. It demonstrated a similar trend to the other tests due to near-array offset criterion and the interference of the reflected wave from the container boundaries.

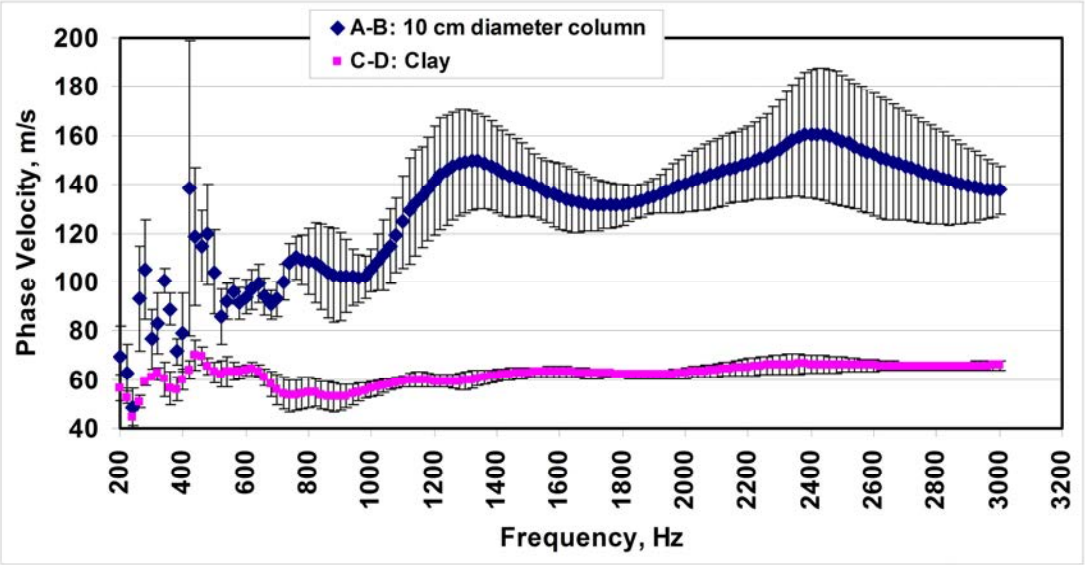

Figure 7.38: Variation of the phase velocity with frequency for larger column and clay.

Figure 7.39 shows the variation of phase velocity with wavelength when the sensor is placed on the larger column and on the clay. The reliable phase velocities were between wavelengths 3.5 cm and 21 cm which satisfied the near-, far-offset criteria and spatial aliasing requirement. The higher phase velocity occurred when the wavelength was smaller than 13 cm. The phase velocity decreased gradually after the wavelengths became larger than 13 cm. This was probably caused by the ratio of wavelength to the diameter of the column. It is noteworthy that the diameter of the installed columns was 10.5 cm. The increasing Rayleigh wavelength could be related with a ratio between the effective volume of wavelength and that of the column which is reduced after encroaching the clay area. Hence the decrease in the phase velocities. The small Rayleigh wavelength below 13 cm was likely to have resulted from the sampling within the column area, which therefore gave a higher phase velocity. The variations of phase velocities of column been seen is due to the effect of wave reflection within the column as observed by Nasseri-Moghadam (2006), who studied the energy of the waves when travelling through the void. An average

phase velocity for the column represented by a wavelength smaller than 13 cm is about 138 m/s.

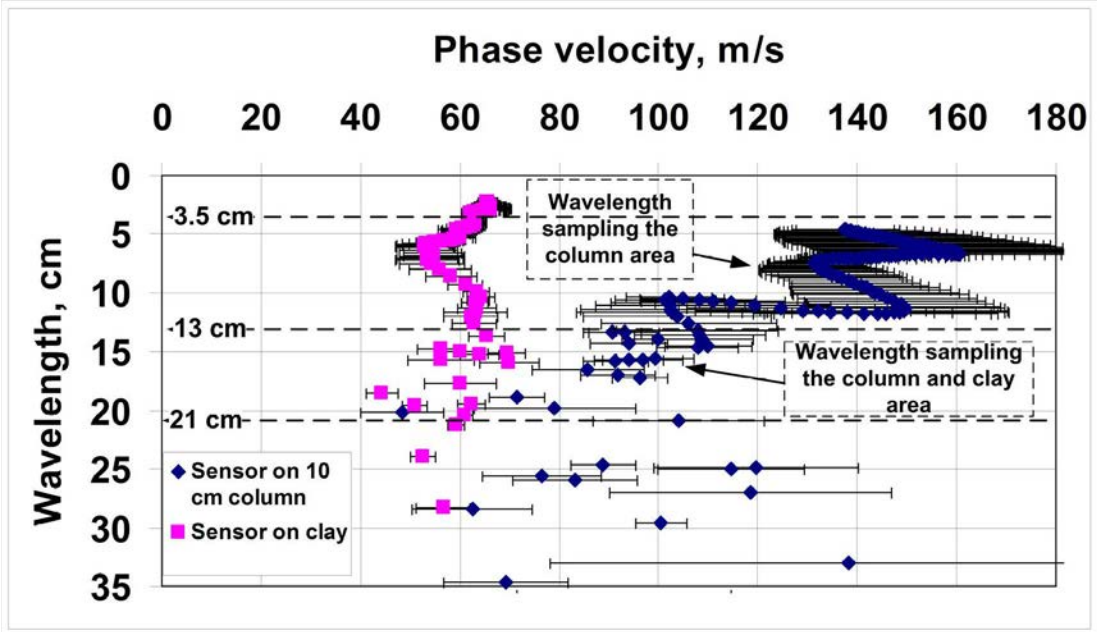

Figure 7.39: The plot of dispersive curve for 10.5 cm diameter column and clay.

7.4 Discussion

In this research, the use of the gravelly sand column in the Oxford clay and kaolin clay medium provided the advantages to access the geotechnical properties of the individual materials as well as global properties of the materials. The elliptical particle movement of Rayleigh wave contributed to the variation of the measured velocity with wavelength with changes in wavelength. The larger size of wavelength increased the area traversed by the propagating elliptical particle movement across the column-clay boundary. Since the reflection coefficients at the boundary between clay-column are proportional to the density

contrast, the most likely reflections are relatively less severe as the density variation is smaller. The signal experienced a relatively small level of interference from refraction and reflection, and consequently a portion of the wave travelled in both materials.

The results demonstrated that there was an apparent relationship between wavelength and the lateral, or horizontal span of the effective measurement region. The shape and size of this effective measurement region in medium had lateral and vertical dimension that could be used to identify the sampling volume of the wavelength. Thus far, this observation has received little treatment in the literature on the analysis of surface waves. The measured phase velocities were influenced by the volume traversed by the propagating Rayleigh wave with an elliptical particle movement, which in turn is a function of its wavelength. As a result, the measured phase velocities are directly influenced by the energy propagated through the elliptical particle motion. This is important as it suggests that the wavelength not only related to an effective depth (major axis), but may also be related to the lateral span (minor axis) and is therefore jointly associated to an effective volume.

A simplified shape and size of elliptical Rayleigh wavelength is used to approximate the effective measurement volume. By relating the wavelengths beyond which the phase velocities exhibit a downward trend, ellipses with semi major axes of 5 cm and 13 cm, and semi minor axes of 4.1 cm and 10.5 cm can be approximated for the 4.1 cm and 10.5 cm diameter columns respectively. As shown in Figure 7.40, almost 100% of the elliptical effective region falls within the column. As the wavelength increases further, this effective region will grow as its axes grows associated with wavelengths. The growth of this effective region will present the largest change in averaged phase velocity at the stage

where the ellipse begins to encroach into the surrounding clay, but as it grows further, the change in ratio of column to clay included within the effective region stabilises. This can thus explain the downward trend in phase velocities just beyond 5 cm and 13 cm, and then stabilising with further increase in wavelength. Similarly, for the measurement on clay as shown in Figure 7.41, a growing effective region will begin to include nearby columns, leading to an increase in phase velocity as the wavelength increases. Based on the dimension ratio, the volume of the effective region in relation to the volume of column inclusion was calculated and is presented in Section 8.3.2.

In the case of the Oxford clay model, when the size of the wavelengths was smaller than the diameter of column and the waves were mainly within the column, the phase velocity of the column can be reliably determined. A similar case was observed for the 10.5 cm diameter column, where the wavelengths corresponding to wavelengths below 13 cm are mainly within the diameter of the column. The larger deviation of the measured phase velocities occurred when there was an exacerbated reflection of waves inside the column and also could be caused by the changes of the bulk density at the column boundaries. The average phase velocity of the column was 138 m/s.

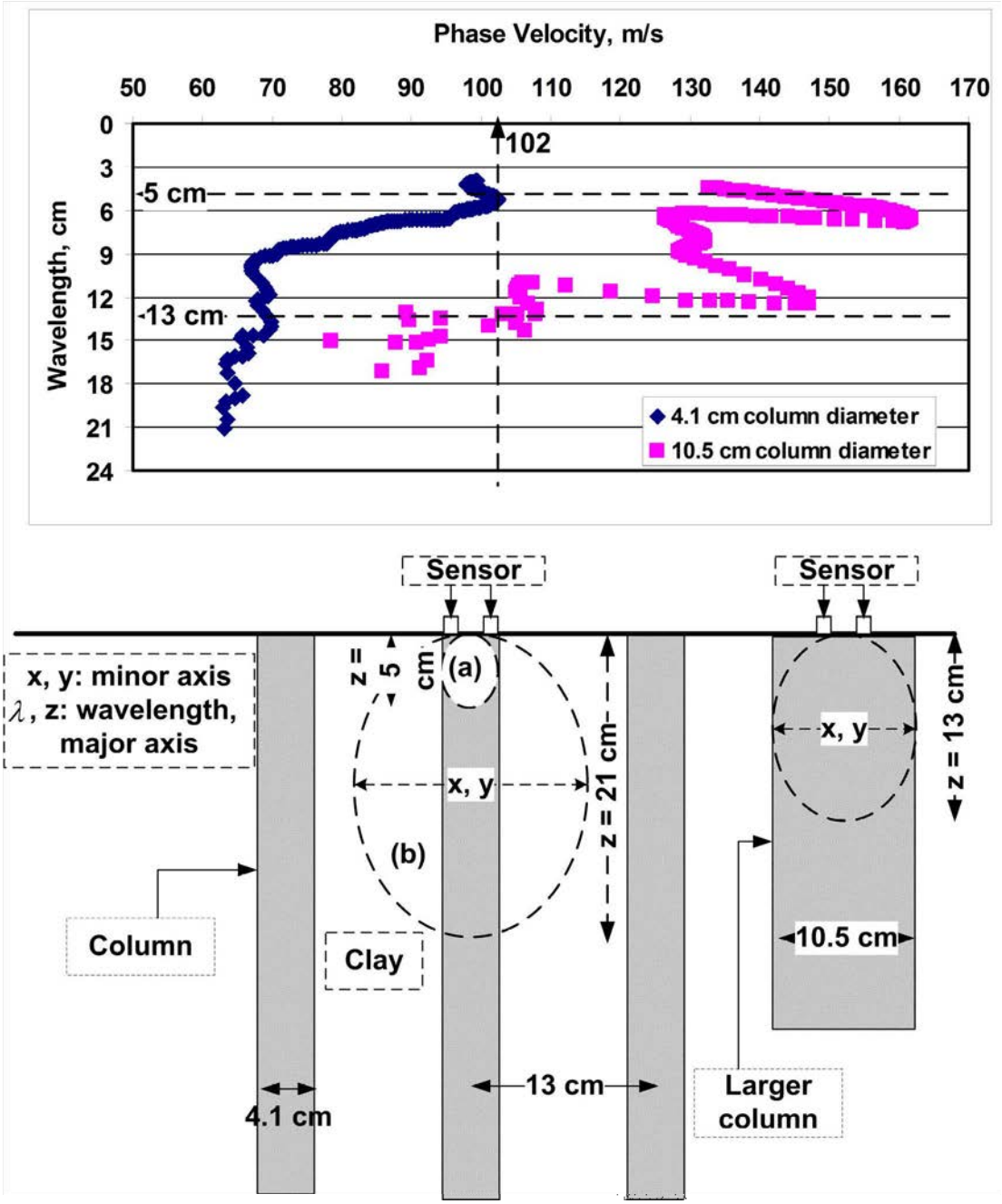

Figure 7.40: Illustrations of the effective region measurement in the elliptical shape where the vertical major axis (z) equivalents with one wavelength on the column.

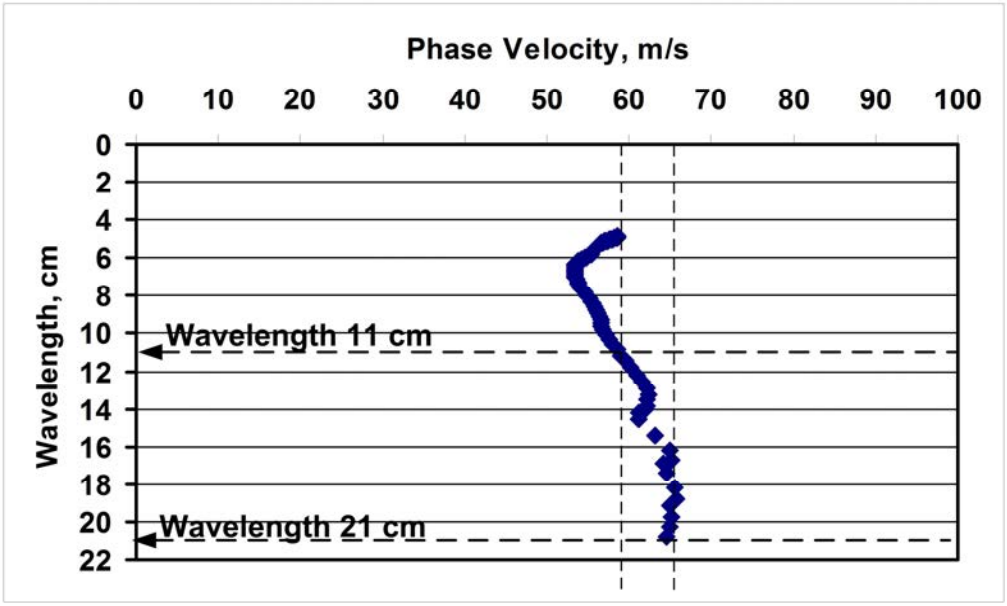

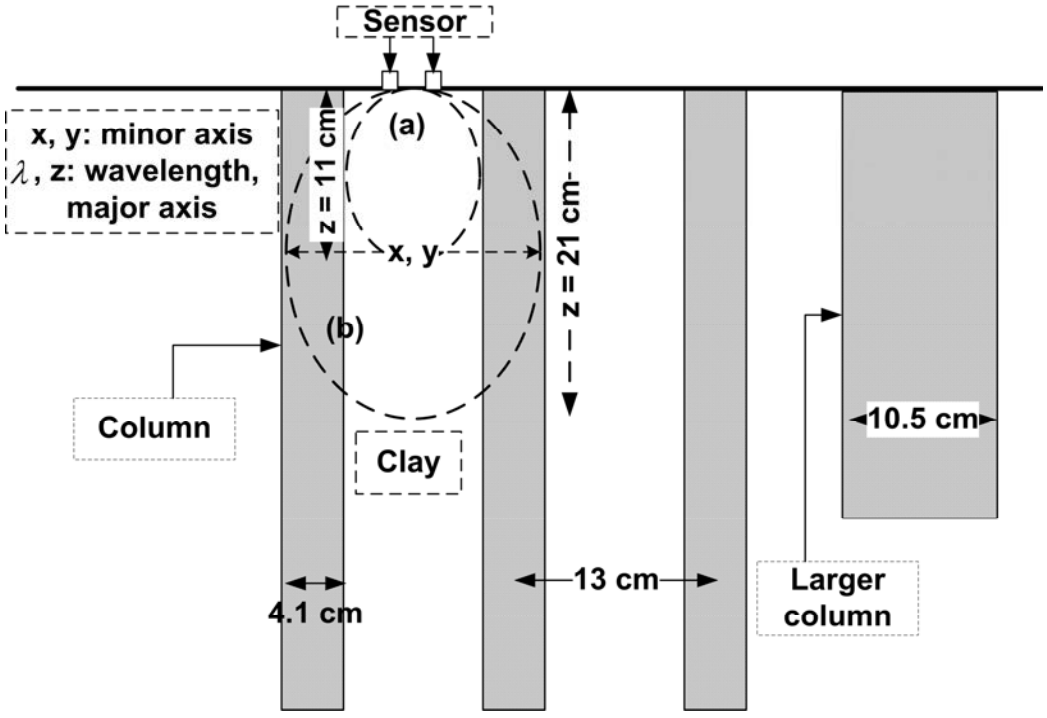

Figure 7.41: Elliptical shaped region of effective measurement. Vertical major axis (z) is equivalent to one wave length on the clay between two columns.

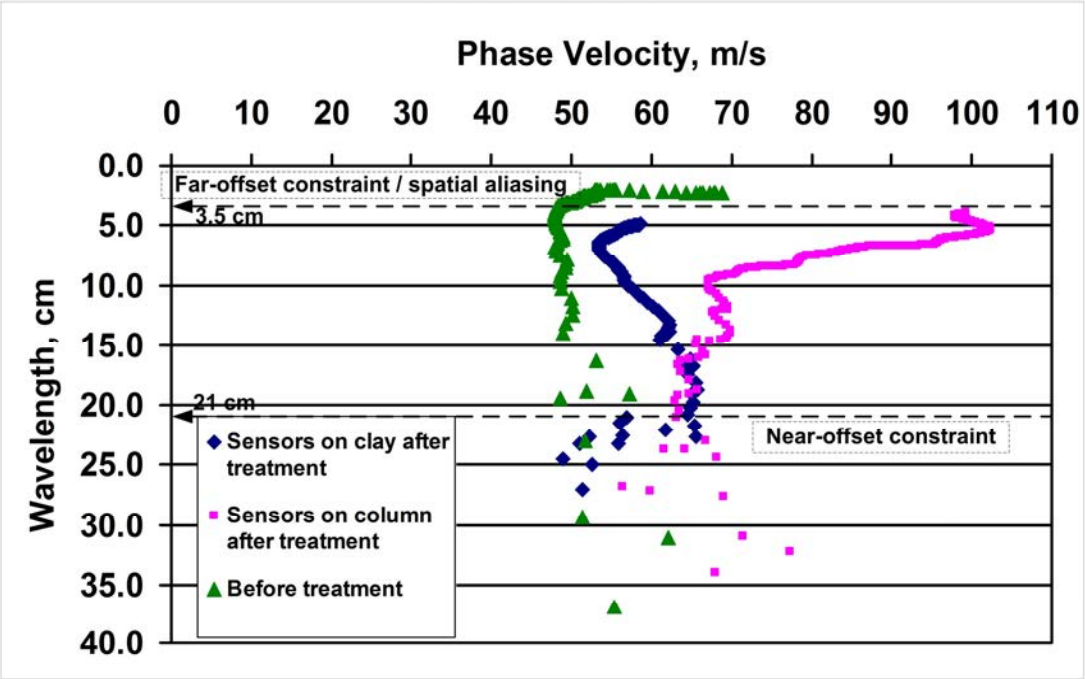

Figure 7.42: The graph of dispersion in difference stage of improvement and sensor locations.

Figure 7.42 shows all the phase velocities without limiting their wavelengths and coherence constraints in Oxford clay. In general, the phase velocity was increased after column installation. Location of receiver sensors is crucial to describe the improvement from the column installation. Receiver sensors on the column gave higher phase velocities when compared with the sensors on the clay. The dispersion curves after stone column treatment were related with the sampling volume of a particular wavelength in relation to the volume of column inclusion. It is also interesting to note that with increasing wavelengths, the phase velocity measured on the clay and on the column, post treatment, approaches a similar value, supporting the premise that the measured phase velocities with larger wavelengths are affected by its encroachment across the clay-column boundaries.

The highly deviated phase velocities observed at shorter wavelengths due to far-offset constraint, were a consequence of higher frequencies attenuated much quicker. As well as for larger wavelengths, a Rayleigh wave yet to form caused non-uniform phase velocity beyond the half depth of the soil container. The larger Rayleigh wave was also corrupted by the body wave, i.e. near-offset constraint.

Average phase velocities of Oxford clay before column installation was 50.3 m/s. The importance of the wavelength in the phase velocities' profiles obtained from a surface wave test, after treatment, was highlighted. It was observed that at larger wavelengths, the measured phase velocities on clay will be affected by the surrounding column. This underlined the importance of wavelength selection and sensor separation in the interpretation of the measured profiles. Similar results were reported by Madhyannapu *et al.* (2010) in studying deep soil mixing in the field. The global phase velocities (averaged) after column installation across all wavelengths for sensors placed on Oxford clay and columns were 57.3 m/s and 86.2 m/s respectively. As a result a global improvement between 1.14 and 1.7 was recorded.

The control seismic tests on kaolin and Oxford clay are an essential indicator that the testing equipment and system was able to carry out relaible measurement. The tests with the seismic source in the middle of the array, demonstrated that it was the optimal arrangement for array deployment to carry out the seismic surface wave test. The phase velocity deviation observed was caused by the frequencies / wavelengths constraint that influences the near- and far-offset distance of the source from the receivers, as well as some interference caused by the reflected waves from the boundary of the soil container.

The phase velocities in soft clay and gravelly sand column showed good agreement even when tested in different sizes of soil models. Hence, within reason boundary effects had limited impact.

The phase velocity dependent on wavelength is called dispersive. The phase velocity is not only related to an effective depth but also have a lateral span and this therefore is associated with the effective volume. The effective volume is based on the assumption that the area traversed by a propagating elliptical particle movement of the Rayleigh wave. This in turn is a function of its wavelength / frequency. The dispersion curves obtained from the measurement on the clay, between the columns, on the column, on the defective column and on the larger column explained the effect of the effective volume when the soil properties changed laterally. Further discussion about the effective volume of wavelength is presented in Chapter 8.

Chapter 8

DISCUSSION

8.1 After Treatment

The inclusion of vertical columns introduced lateral heterogeneities to the soil, which reduced the wave energy propagated laterally. The interaction between the column and the Rayleigh wave resulted in the energy being reflected, diffracted and transmitted and thus created a seismically noisy environment. The optimized data acquisitions were when the seismic source was placed centrally such that it was surrounded by receiver sensors, providing higher signal-to-noise ratio. Phase velocities were related to the signal coherence, and therefore their reliabilities were proportional to the signal-to-noise ratio. Despite there being no column, the distance of the receiver sensors caused a reduced attenuation of the seismic wave energy, as the signal to noise ratio was reduced as discussed previously in Chapter 7 (see Figure 7.6) Even in the absence of columns, the wave energy experiences attenuation as a function of distance from the source, hence as

expected the phase velocities would have a larger standard deviation further from the source.

Graphical error bars have been included in the Figures 7.11, 7.14, 7.23, 7.29, 7.34 and 7.39 to represent the uncertainty in the data. These error bars have been plotted for standard deviation in more than 4 data sets, and sometimes up to 21. This error in all the figures demonstrates a reasonable statistical fit of the data and their pattern of variation of phase velocity versus wavelength. The implication of this individual figure and the research cases are further outlined in Table 8.1.

The measured phase velocities, as shown in Chapter 7 Section 7.3.2 demonstrated that there was an apparent relationship between wavelength and the lateral or horizontal, span of the effective measurement region. The shape and size of the effective region of measurement in the medium in both lateral and vertical dimensions could be used to identify the sampling volume of the wavelength. As discussed in Abbiss (1983) and Graff (1991), Rayleigh wave energy extends to approximately one wavelength depth, as 95% of energy density is propagated within the one wavelength, with the remainder propagating within 1 to 2 wavelengths. The amplitude of measurable energy decreases exponentially beyond one wavelength. It is also worth noting that the particle motion is elliptical in the case of a uniform medium (Xia *et al.*, 2004), but can be more complicated for laterally heterogeneous structures.

Table 8.1: The implication and relevance of the error bar on the research findings

Research case	Reference in the thesis	Margin of experimental error	Noteworthy features	Field relevance	Implication of error bar
Oxford clay without column (Measurement on the clay)	Figure 7.11 (seismic source was at centre of array) Figure 7.14 (seismic source was at one end of receivers)	Average error at ±9 % (seismic source at centre of array) Average error at ±16 % (seismic source at one end of receivers)	Zone of reliable wavelengths (3.5 and 21 cm) showed repeatable results	Distance between seismic source and first receiver controls the reliable wavelengths.	Seismic source at the centre of array gave smaller error compared with the source at one end of receivers Upper and lower bound of the error bar contains the reliable wavelengths that produced the same pattern of variation of the mean.
Oxford clay with column (Measurement on the clay surrounded by the columns)	Figure 7.23 (Seismic source was at the middle of array)	Average error at ±16 % for measurement on the clay	Zone of reliable wavelengths (3.5 and 21 cm) showed repeatable results	Distance between seismic source and first receiver controls the reliable wavelengths.	Upper and lower bound of the error bar contains the reliable wavelengths that produced the same pattern of variation of the mean.
Oxford clay with column (Measurement on the column surrounded by the clay)	Figure 7.29 (Seismic source was at the middle of array)	Average error at ±10 % for measurement on the column	Zone of reliable wavelengths (3.5 and 21 cm) showed repeatable results	Distance between seismic source and first receiver controls the reliable wavelengths. Seismic source was at the middle of array.	Upper and lower bound of the error bar contains the reliable wavelengths that produced the same pattern of variation of the mean.
Oxford clay with column (Measurement on the defective column surrounded by the clay)	Figure 7.34 (Seismic source was at the middle of array)	Average error at ±10 % for measurement on the defective column	Zone of reliable wavelengths (3.5 and 21 cm) showed repeatable results	Distance between seismic source and first receiver controls the reliable wavelengths. Seismic source was at the middle of array.	Upper and lower bound of the error bar contains the reliable wavelengths that produced the same pattern of variation of the mean.
Oxford clay with larger column diameter (Measurement on the larger column diameter surrounded by the clay)	Figure 7.39 (Seismic source was at the middle of array)	Average error at ±12 % for measurement on the larger diameter column	Zone of reliable wavelengths (3.5 and 21 cm) showed repeatable results	Distance between seismic source and first receiver controls the reliable wavelengths. Seismic source at the middle of array.	Upper and lower bound of the error bar contains the reliable wavelengths that produced the same pattern of variation of the mean.

Particles motion in Rayleigh waves when moving in elliptical trajectories have semi major axis perpendicular to the surface of the ground and semi minor axis parallel to the direction of wave propagation. However, the semi major axis of the ellipse does not necessarily align vertically as illustrated in Figure 7.40 and 7.41 (see Chapter 7). It can be tilted in another direction particularly when the medium properties are changed, but generally the vertical component of motion is larger than the horizontal component (Greenhalgh, 2010). The measured phase velocities were influenced by the shape and size of the effective region measurement by the propagating Rayleigh wave with elliptical particle movement, which in turn is a function of its wavelength. This is important as it suggests that the wavelength not only relates to an effective depth, but may also have a lateral span and is therefore associated to an effective volume.

Figure 8.1 shows five dispersion graphs; one before treatment and four after treatment. The knowledge that this soil is relatively homogeneous before treatment is shown by a non-dispersion graph as shown in Figure 8.1(a). Dispersive graphs after treatment show the influenced of wavelength in vertical and horizontal span where sampling volume is encroaching the area of nearby materials (see Figure 7.40 and 7.41 in Chapter 7), as a result influences the measured phase velocities. The observations from the sensor on the column showed the interaction of wave with this single column and the surrounding clay. Meanwhile the observations made with the sensor on the clay is influenced by the adjacent columns. Figure 8.1(b) shows the dispersion curves resulting from the lateral soil property changes following the installation of the column. However in the case of the defective (uncompacted) column, where the bulk density (1640 kg/m^3) was slightly lower

than surrounding clay (1711 kg/m^3) ,the dispersive curve does not show any significant increase of phase velocity with decreasing wavelengths (see Figure 8.1(c)). Thus, the measurements conducted on columns were able to demonstrate the quality of columns. It worth noting that the dry densities of defective column was 1492 kg/m^3 and clay 1220 kg/m^3, which showed the effect of the density to the phase velocity.

In general, the phase velocities increased when wavelengths decreased for measurements on top of the 10.5 cm diameter column as shown in Figure 8.1(c). The similarity in the phase velocity at 102 m/s was observed when the wavelengths were 1.2 times the column diameters at 4.1 cm and 10.5 cm, as shown via the wavelengths 5 cm and 13 cm in Figure 8.1(b) and Figure 8.1(c) respectively. The wavelengths at 5 cm and 13 cm for the two different columns were likely to have effective sampling volumes within the edge of columns (discussed later in Figure 8.4 in this section).

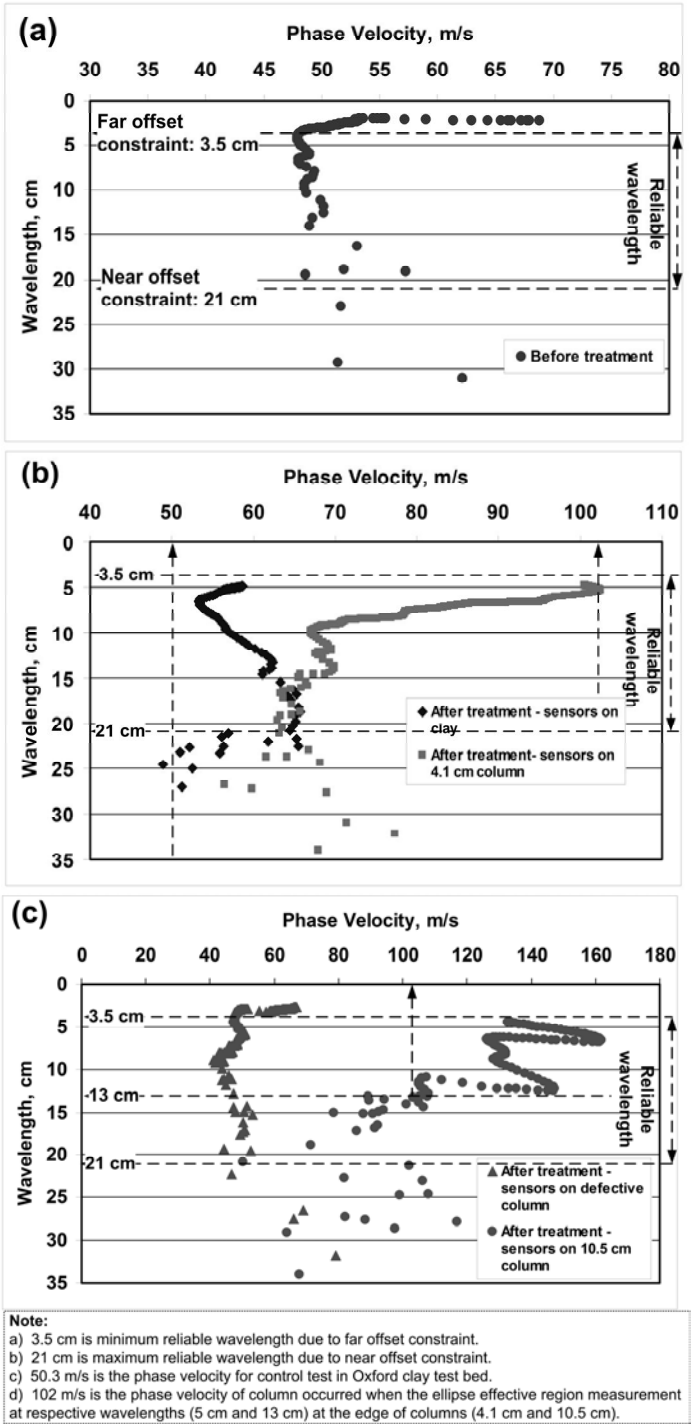

Figure 8.1: Dispersive curves for; (a) prior to column installation, (b) after installing column and with sensors on the clay and column, (c) after installation of columns with sensors on defective column and larger diameter column.

The variable phase velocity measurements for wavelengths smaller than 13 cm within the 10.5 cm diameter of column seem to be caused by the self-interference due to internal reflections caused by the heterogeneous transition of acoustic impedance at the column-soil boundary as well as differences in densities and void ratios between the middle and the edge of the column. The factor that may have exacerbated the soil-column boundary effect was that the diameter of the pre-hole may have been slightly larger than the diameter of the installed column. As a result, the column material might have filled that gap and reduce slightly the column density at the edges compared to the density at the middle of the column. Meanwhile, three main events would have occurred when Rayleigh wave in the soil approached the stone column; (1) part of the energy was reflected, (2) part of the energy was refracted around the column, and (3) part of the energy continued along its direct path within the column. Thus, the measurement of the phase velocity within the columns with cylindrical geometries was inevitably noisy.

The scattered phase velocities in the column were not seen in the 4.1 cm diameter column due to insufficient wavelength data below 5 cm wavelength (see Figure 8.1b sensors on column). The phase velocity of the gravelly sand column was in the range of 102 m/s to 162 m/s and averaged 138 m/s. Measurements in the pilot test also showed that the phase velocity of gravelly sand column was 120 m/s (see Section 7.3.1). The nearest comparable material was sand with a reported phase velocity of 115 m/s (Rahyani and El Naggar, 2008). The measured and expected gravelly sand column phase velocities showed good agreement noting that the value reported by (Rahyani and El Naggar, 2008) was for sand of a lower density than those tested in the present study.

The trade-off in carrying out the tests on the vibro-stone column area was an upper and lower constraints on the usable frequencies/wavelengths due to spatial aliasing, near-, and far offset constraint as the spacing between receivers are limited by the column width and columns spacing. In order to avoid spatial aliasing for 3 cm receiver spacing, the reliable wavelengths were constrained to larger than 3 cm (see Chapter 3, Section 3.4, Equation 3.12). Based on the near offset constraint (see Section 3.4, Equation 3.10), the distance between source and first sensor (*d*) tests was set 7 cm, therefore the reliable wavelengths were for wavelengths smaller than 3 times *d* (smaller than 21 cm). Meanwhile, the lower bound reliable wavelength was larger than half of *d* (larger than 3.5 cm) (see Section 3.4, Equation 3.11). The phase velocities were unreliable for wavelength sizes larger than 21 cm and also beyond half of the soil depth (25 cm), which was related to the contamination by body wave and as such the Rayleigh wave had not formed completely as shown in Figure 8.1 (see discussion in Chapter 7).

In the majority of geophysics applications, the heterogeneous boundaries of the medium are not known *a priori*. A key distinction in this application is that the locations of the stone columns are generally known to some degree, and can therefore be individually assessed without the influences from non-column material. Given the knowledge of the column location, it is possible to plan the survey to meet specific requirements. On a typical site with a dense arrangement of vibro-stone columns, the wave reflections, refractions and attenuations caused by the boundaries of material density and the close proximities of the columns all play a role in introducing constraints to the source-array configuration. The measurements using the receiver-pairs technique are such that their

locations were different while the seismic source remained unchanged at the centre of the array. Therefore, these tests achieved the objective (3) of this study, which is to establish the optimal surface wave testing array for evaluating the individual columns as well as non-column material.

The simplified shape and size of the effective region measurement of elliptical particle motion is used to approximate the effective volume of measurement. From the test results of the two test column diameters, the ellipse's semi major axes, i.e. wavelengths were 5 cm and 13 cm and semi minor of 4.1 cm and 10.5 cm respectively, gave 100 % sampling measurements within the columns. Both wavelengths indicated similar phase velocities at 102 m/s (see Figure 8.1a and 8.1b). Therefore, the ellipse describes the vertical major axis, which was about 1.2 times the horizontal minor axis.

The volume of the effective region for each wavelength in relation to the volume of the column inclusion was calculated. The vertical major axis was found to be about 1.2 times the horizontal minor axis, the volumes of column within the volumes enclosed by 3-dimensional ellipses that correspond to one Rayleigh wavelength were calculated. Table 8.2, Table 8.3 and Table 8.4 summarizes the relationship of phase velocity, wavelength, volume of the effective region measurement of one Rayleigh wavelength and volume of column within the effective region measurement for sensor-pairs on the 4.1 cm and 10.5 cm diameter columns, as well as on clay (between the two columns) respectively. With these data, the shear wave velocities were calculated from the proportion of column and clay as a function of wavelength using Equation 4.11 and thus the shear modulus was obtained (see Table 8.3).

Table 8.2: Relationship of phase velocities with wavelength and column volume when sensor-pairs on 4.1 cm diameter column.

Phase velocity, m/s	Wavelength (vertical major axis), cm	Effective region measurement, cm^3	Volume of the column in the effective region of measurement, cm^3	Percentage of the column volume in the effective region of measurement, %	Shear wave velocity, m/s	Shear modulus, MPa
102	5	41.90	59.32	100%	110	24.8
98	6	72.41	66.57	92%	106	22.5
85	7	114.99	84.47	73%	91	16.2
77	8	171.64	97.04	57%	82	12.8
70	9	244.39	112.36	46%	74	10.3
67	10	335.24	124.93	37%	71	9.2
68	11	446.20	137.50	31%	72	9.4
69	12	579.29	150.07	26%	73	9.5
69	13	736.52	162.64	22%	73	9.4
69	14	919.89	175.22	19%	73	9.4
66	15	1131.43	187.79	17%	69	8.5
65	16	1373.14	200.36	15%	68	8.2
64	17	1647.02	212.93	13%	67	7.9
63	20	2681.90	251.43	9%	66	7.6
63	21	3104.64	264.00	9%	66	7.6
*50	N/A	N/A	N/A	0%	53	4.7

Note: * phase velocity measured before columns installation

Figure 8.2 shows the relationship of shear modulus before and after treatment for reliable wavelengths (between 3.5 cm and 21 cm). These shear modulus profiles were related to the graph in Figure 8.1 (phase velocity profiles). Figure 8.2(a) shows the shear modulus profile before the column installation (control test), which is relatively homogeneous clay. Figure 8.2(b) shows the shear modulus profiles after the 4.1 cm diameter column installation with different sensors location measurement (on clay and on column) and

Figure 8.2(c) on a defective column and a larger diameter of column (10.5 cm). The shear modulus was calculated based on the proportion of bulk density and Poisson's ratio of clay and column. The proportion of density and Poisson's ratio were calculated based on the percentage of column volume, such that a 100 % column volume would imply that the bulk density and Poisson's ratio would be 100% that of the column material (based upon a Poisson's ratio of 0.3 for column and 0.5 for clay). The columns exhibit stiffness that was more than 5 times greater than the soil stiffness before treatment. Stiffness profile for the 10.5 cm diameter column shows larger differences in shear modulus at wavelengths smaller than 13 cm which could be due to the measurements severely influenced by the internal wave reflection and also could be the differences in densities between the edge and the centre region of the column.

Table 8.3: Relationship of phase velocities with wavelength and column volume when sensor-pairs on 10.5 cm diameter column.

Phase velocity, m/s	Wavelength (vertical major axis), cm	Effective region measurement, cm^3	Volume of the column in the effective region of measurement, cm^3	Percentage of the column volume in the effective region of measurement, %	Shear wave velocity, m/s	Shear modulus, MPa
135	10	335.2	785.7	100%	146	43.5
142	11	446.2	864.3	100%	153	48.1
105	12	579.3	942.9	100%	113	26.3
107	13	736.5	731.0	99%	116	27.3
100	14	919.9	873.7	95%	108	23.6
95	15	1131.4	1047.6	93%	102	21.2
90	16	1373.1	1190.1	87%	97	18.8
86	17	1647.0	1297.2	79%	93	16.9
*50	N/A	N/A	N/A	0%	53	4.7

Note: * phase velocity measured before columns installation

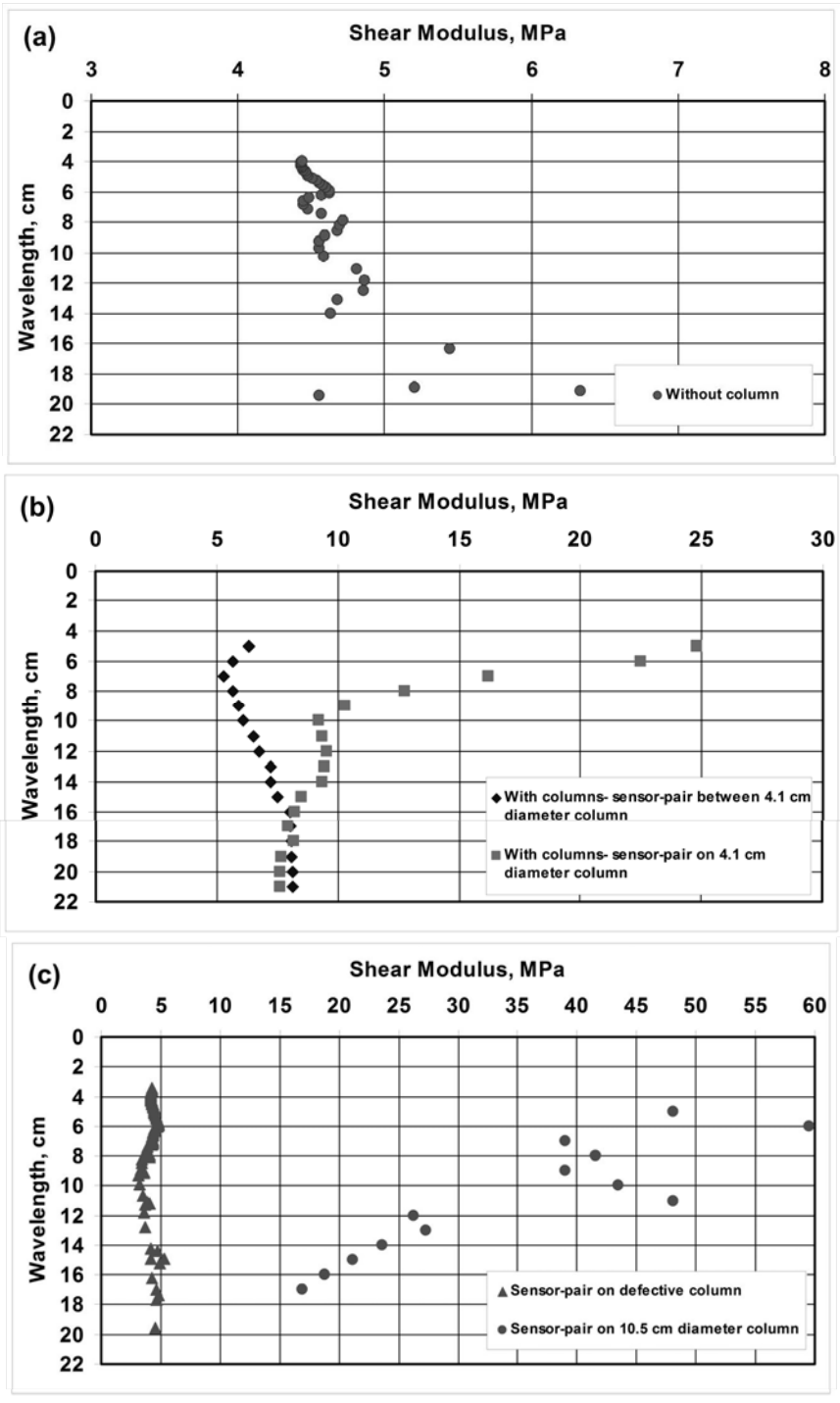

Figure 8.2: Stiffness profiles; (a) prior to column installation, (b) after installing 4.1cm diameter column, (c) after installation of defective column and 10.5 cm diameter column.

Table 8.4: Relationship of phase velocities with wavelength and column volume when sensor-pairs on clay between two columns.

Phase velocity, m/s	Wavelength (vertical major axis), cm	Effective region measurement, cm^3	Volume of the column in the effective region of measurement, cm^3	Percentage of the column volume in the effective region of measurement, %	Shear wave velocity, m/s	Shear modulus, MPa
*50	N/A	N/A	0.00	0.0%	53	4.7
58	5	41.90	0.00	0.0%	61	6.3
55	6	72.41	0.00	0.0%	58	5.7
53	7	114.99	0.00	0.0%	56	5.3
55	8	171.64	0.00	0.0%	58	5.7
56	9	244.39	0.00	0.0%	59	5.9
57	10	335.24	0.00	0.0%	60	6.1
59	11	446.20	0.08	0.0%	62	6.5
60	12	579.29	0.75	0.1%	63	6.8
62	13	736.52	4.00	0.5%	65	7.2
62	14	919.89	14.33	1.6%	65	7.2
63	15	1131.43	27.58	2.4%	66	7.5
65	16	1373.14	55.22	4.0%	68	8.0
65	17	1647.02	83.13	5.0%	68	8.0
65	18	1955.11	126.01	6.4%	68	8.1
65	19	2299.40	182.22	7.9%	68	8.1
65	20	2681.90	242.55	9.0%	68	8.1
65	21	3104.64	325.18	10.5%	68	8.1

Note: * phase velocity measured before columns installation

At larger wavelengths, the ratio of column volume to clay volume is smaller for sensor-pairs on a column, and the inverse applies to sensor-pairs on clay (between the two columns) due to the horizontal span of the effective region of measurement as shown in Figure 8.3. At a wavelength of 16 cm, which is equivalent to *4D* (the ratio of wavelength and 4.1 cm diameter column), the combination of both materials gave similar shear

modulus at 8 MPa at both sensor-pairs (on clay and on column). It worth noting that the failure mechanisms of single stone columns in the upper soil layer are generally caused through excessive bulging, which generally occurs at a depth of 2 to 3 column diameters (Barksdale and Bachus, 1983). Thus, a depth of *4D* can be considered to be below this critical failure mechanism zone.

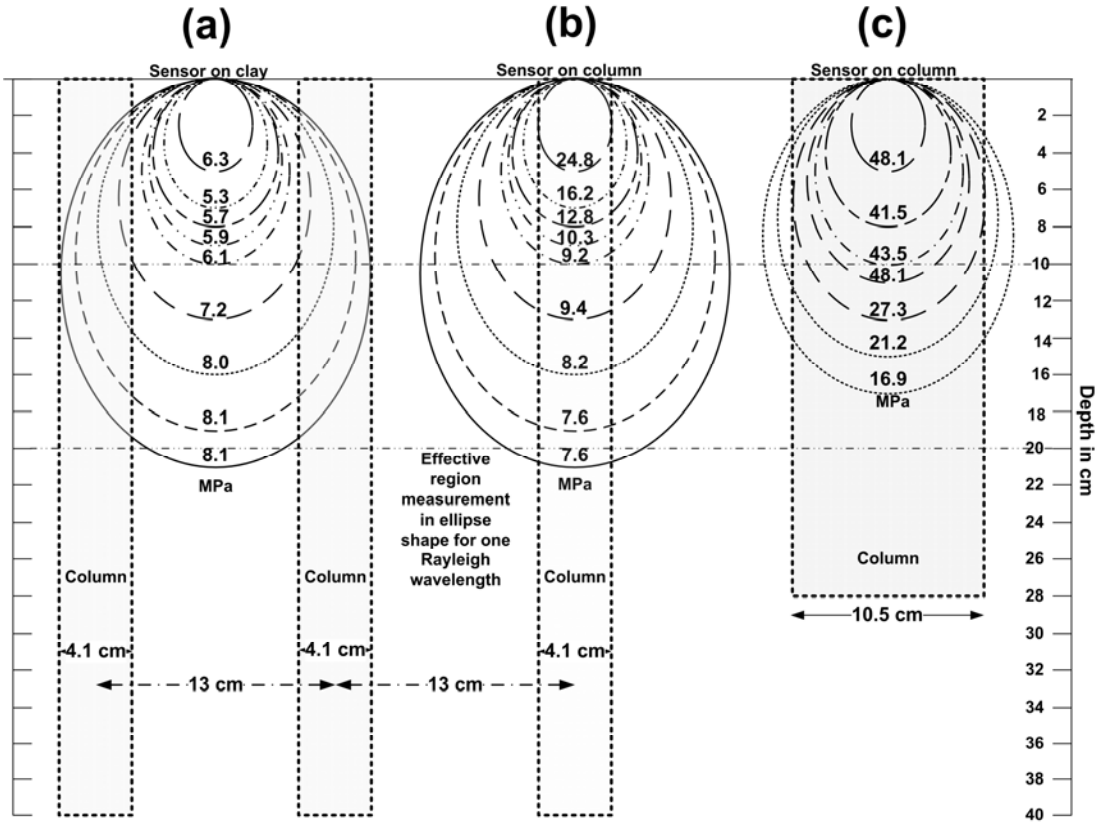

Figure 8.3: Effective region of Rayleigh wavelength measurement within an ellipse with a major axis, about 1.2 times the minor axis depending on the shear modulus for the respective sensor locations; (a) on the clay, with shear modulus increasing with increasing wavelength, (b) on the 4.1 cm. diameter column , with shear modulus decreasing with increasing wavelength, (c) on the 10.5 cm. diameter column, with shear modulus decreasing with increasing wavelength.

Figure 8.3 illustrated that the simplified effective region of measurement has an ellipse with a major axis that is about 1.2 times the length of the minor axis perpendicular to the ground surface. On the basis of the results presented in Figure 8.4, the two column diameters (4.1 cm and 10.5 cm) gave similar shear modulii at wavelengths of 5 cm and 13 cm respectively. As the effective region of measurement represented by these wavelengths encapsulate a similar ratio of column to clay, they provided the basis for hypothesising that the dimension of an effective region of measurement can be approximated by an ellipsoid with both a major and a minor axis that are associated with the wavelength and columns diameter respectively.

The control test result (without columns), indicated that the soil to be relatively homogeneous (see Figure 8.2a). However when measurements were carried out using sensors on clay that was surrounded by columns, the shear modulus varied with wavelengths (see Figure 8.3a). The change of shear modulus with wavelengths also occurred for measurements performed on the columns (see Figure 8.3b and 8.3c). Given that the column was relatively homogeneous in the depth (vertical) direction, these stiffness profiles point to the influence of both vertical and horizontal span of measurement. The sudden increase of shear modulus from 27.3 MPa to 48.3 MPa (see Figure 8.3c) was due to the measurements at corresponding wavelengths being severely influenced by the internal wave reflection and the differences in densities and void ratios between the edge and the centre region of the column.

Menzies (2001) reported that the ellipse major axis is about 1.5 times the minor axis without giving detail on the condition of the medium in which the wave propagated, and

Greenhalgh (2010) explained that the ellipse could be tilted due to the variation of medium properties. As illustrated in Figure 8.4 different ellipses (with major to minor axis ratios of 1.2,1.5 and 2 and major axis orientations of vertical and 45º from horizontal) were analysed. These were used to identify the sensitivity of the ellipses' shape to the calculated result. This Figure 8.3 further illustrates the examples of the effective region of measurement shapes for the major axes (wavelength) at 5 cm and different minor axes within the column diameter 4.1 cm. Using these parameters, Figure 8.5 shows the non linear correlation of phase velocities with a percentage of the column encapsulated by the effective region of measurements in the different orientations of vertical and tilted ellipses at different major axes.

In general the graph in Figure 8.5 shows only a small sensitivity to the change of shapes for the effective region of measurement. All the ellipse shapes considered produced a similar phase velocities for cases with less than 50 % of the column volume being encapsulated by the effective region of measurement. However, the phase velocities diverged when the column volume is more than 50 % in the effective region of measurement. The measured results were sensitive to the changes in the shapes of the effective region of measurements when the volume being encapsulated contained more than 50 % of column.

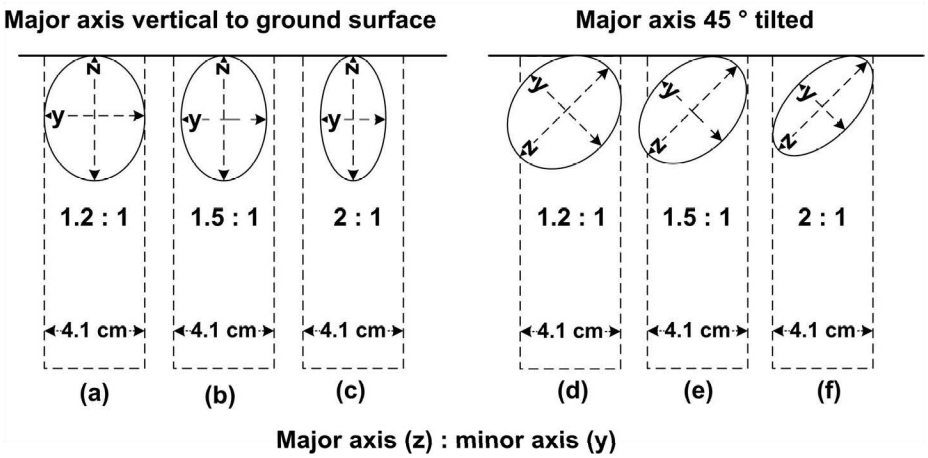

Figure 8.4: Effective elliptical shaped region of measurement for different ratios of major axis (z) to minor axis (y) and axis orientation: (a), (b) and (c) - major axis (z) is vertical (normal to horizontal ground surface); (d), (e) and (f) - major axis (z) is inclined at 45º to horizontal.

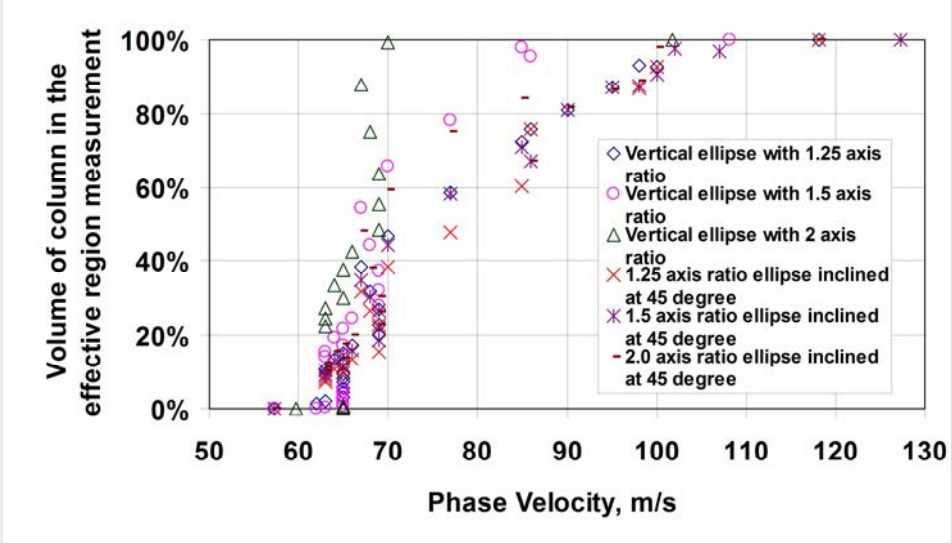

Figure 8.5: Phase velocity changes with the volume of column being increased to accommodate increasing regions of effective measurement.

The relationship between the phase velocity and the volume of column in the effective region for each wavelength was important for analysing and interpreting the result from the quality assessment of stone columns. The phase velocity could be estimated via knowledge of the volume of the column in the effective region, if the expected velocity (i.e. corresponding to the required geotechnical benchmark after installation) of each individual material is known. The volume of column in the effective region can be estimated based on the ellipse shape of wavelengths within the column (see Figure 8.3). In the stone column work, the defective stone columns are not known *a priori*. In order to identify any defective columns within the construction site, the comparison between the dispersive curve obtained from a known, good quality column, and the unknown quality column will facilitate the detection of defective columns. Thus, this provides a useful methodology to assess the quality of stone columns in a non-destructive and non-invasive way.

Analysing data using the receiver pair offers higher signal-to-noise ratio. Therefore, as the receiver pair can be easily relocated, the spatial variation in phase velocity could be identified, thus the study achieved the objective (4) to identify a suitable data-processing technique in order to investigate the variation of lateral and vertical shear wave velocity. Using the elliptical shape and size at respective wavelengths to approximate an effective volume of measurement, demonstrates the achievement of objective (5) namely to understand the effect of lateral heterogeneity caused by column inclusion in relation to the seismic surface wave result and the quality of the vibro-stone column.

Zerwer *et al*. (2003) used finite element modelling (FEM) for detection and understanding the Rayleigh wave propagation when passing through anomalies. Calibration of FEM results can be used to improve the data. The FEM was also used in other geophysical testing such as for simulating GPR wave propagation in complex subsurface (Cassidy and Millington 2009). Therefore the finite element modelling is recommended for future study in order to understand the Rayleigh wave behaviour when travel through the stone column, thus increased the level of confident on the geophysical results.

8.2 Significance to Field Applications

In general, the trend of the decreasing stiffness with wavelength observed in the laboratory model studies presented in this thesis are in agreement with such observations made in the field. The field stone column gives a higher stiffness for shallow layers after treatment. This observed stiffness decreases and finally gives a comparable stiffness level to that before the installation of the column (Cuellar and Valerio, 1997; Moxhay *et al.*, 2001; Moxhay *et al.*, 2008). Moxhay *et al.* (2001) explained this long period of time taken to notice an increase in soil stiffness at deeper layer to be a consequence of the need to allow pore water pressure in clay and column to equilibrate. Meanwhile, the laboratory studies indicate that the locations of measurements are also a contributory factor that influences the trend of stiffness profiles. Therefore, the interpretations of stone columns stiffness profiles need to consider both factors, i.e. time and location of measurements.

Test carried out on defective columns demonstrated that the surface wave technique can differentiate the material densities, thus the quality of the construction process. The defective column can be located by comparing it with the stiffness profile of a known good quality stone column (for example the tested trial stone column). If there is a 'suspicious' or non conforming stiffness profile, it can be used as a basis for further quality testing such as a field load test.

Another important finding in this study was that the Rayleigh wave phase velocity is not only dependent on the depth but also on the horizontal spans of the soil properties. Hence, the depth and horizontal spans can be used to identify the sampling volume. The sampling volume is based on the elliptical particle movement. This in turn is a function of its wavelength (the assumed ratio between depth and horizontal span was 1.2:1 as discussed in Section 8.3.2). As a result, the dispersive curve can be estimated via the relationship between the properties of the soil encapsulated within the sampling volume for each wavelength. All the elliptical shaped sampling volumes shown in Figure 8.6 (except the case where vertical major axis is 2 times the minor axis) are likely to be suitable for estimating the volume of column in the effective region of one wavelength. These are based upon the similarity in the dispersive curve shape measurements made on top of the column. Further studies are needed to investigate the sensitivity of these elliptical shapes in other mediums such as the case of layered mediums. This, however was beyond the scope of the current research.

The interpretation of the surface wave study relies on the inversion of the dispersion curve to model the soil stiffness profiles. In practice of the quality control of VSCs, the material

within the column is constructed to be homogeneous throughout its depth (similar density) but the soil between the columns is likely to be layered (different densities). This laboratory study showed that the phase velocity is influenced by the vertical and horizontal spans, and the inversion becomes much more complicated and this observation has received little attention in the past literature. However, the understanding of the relationship between the wavelength and the effective region measurement (the sampling volume) is important to plot a graphical representation of the dispersion curve. This delineates the variation of the column quality and defines the soil boundaries. As a result, the seismic surface wave can potentially provide a powerful tool to assess the quality of stone columns in a non-destructive and non-invasive way.

The scale of the VSC model in the laboratory was 1:15. If further studies are carried out at a full scale, the stiffness profile at depths between 0.5 and 3.2 m may be observed using a similar testing array. This depth is sufficient to investigate the critical depth of the stone column, (up to 3 times the stone column diameter), which is about 1.8 m in depth if the full scale stone column diameter is set at 0.6 m (Barksdale and Bachus, 1983). On top of this, the distance of the source to the first receiver (d) could be increased to maximise the reliable wavelengths/depth. To reduce the time required for testing and to increase the spatial resolution, the number of the sensor pairs can be increased whilst keeping the seismic source at the centre of the array. As a result, from the spatial stiffness profiles for each sensor pair it should be possible to identify any anomalies (changes in density) below the ground surface of the stone column site, down to a depth of at least 3.2 m depth.

The practical implication of the research was able to evaluate interaction between the individual column and it surrounding soil. This was important for evaluating the quality of vibro-stone columns works and its effect on the surrounding soil. The geometry and size of stone column do not affect the result and interpretations, however the distance between seismic source and first receiver, and distance between receiver pair affect the depth of reliable data obtained. The important information of the column or soil property was for the region from ground surface to depth of between 3 and 4 column diameter. Therefore the distance of the seismic source to first receiver should more than one column diameter. For instance, if the column diameter is 1 metre, thus the minimum distance of the seismic source to first receiver is also 1 metre. It is thus suggested to increase numbers of sensor pairs and place surrounding seismic source (in circle). This technique will reduce survey time and any spatial soil property changes will be easily detected. However, this will increase the cost of the equipment.

8.3 Limitation

The arrangement of the equipments (the seismic source and the receivers) and the materials phase velocities are factors that bounding the required frequency range in the seismic surface test. In Chapter 5, the concrete mortar test required larger frequency range beyond 10 kHz of the seismic source and the receivers due to bigger phase velocity of concrete mortar (1000 m/s) and steel bar (7850 m/s). This requirement was not fulfil due to constraint of the receivers frequency range. When tested on the natural soil (see Chapter 7), i.e. Oxford clay (50 m/s) and gravelly sand (138 m/s), the required frequency

range was sufficient. However a number of limitations still remained when testing in the laboratory scale, due to the reliable stiffness profile restricted by the soil depth, i.e. shallower than the half of soil depth is reliable stiffness.

On the other hand a full scale field seismic surface wave test was conducted with the constrained depth due to the soil container depth being eliminated. However, the limitation arising from the arrangement of the equipment (the distance of seismic source to the first receiver, d, and the inter receivers spacing, Δx) still existed. The benefit from a larger d is the acquisition of information from a deeper layer. However, the larger d causes a lower signal-to-noise ratio and less information for the shallow layer. The close proximities of the columns caused insufficient wave energy to be propagated to a larger distance because of the reflection and the refraction of wave caused by the columns, and thus only a small amount of energy being propagated through the columns. Therefore, the maximum d recommended is similar to the distance of the inter columns spacing to avoid the seismic source located behind the column, and the columns are deemed to behave as a wave barrier. Meanwhile, the Δx is limited to the distance of the column diameter. These array distances are sufficient to monitor beyond the critical depth for the vibro-stone column of 3 x column diameters.

The stiffness profile interpretation was based on the wavelength is equivalent to the depth for vertically homogeneous soil using a constant of 1. If the soil densities changed with depth, the wavelength might not be equal to the depth. Therefore, the relationship of the wavelength and the depth should be first established in the beginning of a seismic surface test before the installation of the columns.

Chapter 9

CONCLUSIONS

9.1 Introduction

In this thesis research into the seismic surface wave technique has been illustrated using different sizes of model and material properties. The testing programme developed and discussed in this thesis has enabled, through laboratory testing, a range of stone columns configurations to be examined and so have met the aim of the study is to develop the most appropriate seismic surface wave method for attaining and utilizing data in order to investigate vertical and lateral stiffness and thus being able to evaluate the quality of ground improvement achieved when using stone column methods.

The objectives (see Chapter 1) were to:

(1) identify suitable seismic surface wave equipment for laboratory scale,

(2) develop a system for seismic surface wave testing in the laboratory,

(3) establish the most optimal surface wave testing array for data acquisition to evaluate the individual columns and non-column material,

(4) identify a suitable data-processing technique in order to investigate the spatial and profiles of the phase velocity (shear modulus) in the vibro-stone column ground improvement, and,

(5) understand the effect of lateral heterogeneity due to column inclusion in relation to the seismic surface wave result and the quality of the vibro-stone column.

All testing was conducted in the laboratory as no significant detailed previous work on seismic response of stone columns had been undertaken outside a few relatively simple field observations. It was clear from the literature review that a detailed programme of work was needed, based in the laboratory, to ensure a detailed assessment of soil and surface characteristics could take place. In all, three stages of testing where undertaken in the laboratory: (1) Preliminary tests using concrete mortar; (2) a sand column in kaolin and (3) sand columns in Oxford clay. While the equipment and system reliability performance were established and checked using the concrete mortar and kaolin material, the larger Oxford clay model allowed a detailed investigation into seismic surface wave tests on stone columns configuration. Based on the results and experience gathered from the laboratory work, this chapter summarizes the main findings and gives recommendations for future studies. The main findings are subdivided into key conclusions to highlight the most important outcomes of the research, and then the most important practical implications of the research are listed. This work focused on laboratory scale models so providing essential parameter and boundary control, not present in most field tests. From

this work ways to adapt approaches developed for full scale field and ultimately quality assurance testing can be developed. This is discussed later in Section 9.3.

9.2 Main Outcomes

9.2.1 Key conclusions

One of the key outcomes from this research was the development of robust testing equipment with an associated system methodically verified to give reliable and representative measurements, with careful investigations being made to assess the repeatability of observations. The prime indicators established from this work were;

(a) the phase velocities from the surface wave tests demonstrated a strong correcspondance with the physical tests, i.e. hand vane shear test, water content. Furthermore, these did concur very well with previous pertinent literature, and

(b) the phase velocities in the soft clay and the gravelly sand column showed good agreement even over the widely different scales of the soil models. These findings demonstrate that the objectives of this study were achieved, viz:

(1) to identify a suitable seismic surface wave equipment for laboratory scale tests, and

(2) to develop a system for seismic surface wave testing in the laboratory.

The optimal arrangement of the array deployed to carry out the seismic surface wave tests on columns was systematically shown to be that with the seismic source at the centre of the array. This was confirmed by the smaller deviation in the phase velocities, which was a consequence of both sensor-pairs receiving equal and relatively higher amount of energy.

The larger phase velocity deviation resulted from the frequency/wavelength constraint, which was related to the near and far offset constraint distances of the source to the receivers. In addition, Rayleigh waves were formed having consistent velocities when the wavelengths were shorter than half the soil depth. Hence, this research objective (3) was achieved. It established the most optimal surface wave testing array for data acquisition in order to evaluate the differences in the cases of individual column and non-column material.

The measurement positions were shown to influence the stiffness profile in the stone column. Thus, the data processing technique using each of the receiver pair was appropriate for surface wave velocity analysis. Thus it enabled the investigation of the effect of small variation in spatial soil properties to be carried out. This was made apparent when the defective column was tested with differences in stiffness profiles between the compacted and non-compacted columns. In this instance, there were differences of minor significance, which were, however, consistent with the differences in results from the other physical tests. Thus, surface wave techniques proved able to be used to locate defective columns. In addition, the stiffness profiles obtained from measurements made on the clay (i.e. between two columns), were different from that obtained when measurements were carried out on the column. These findings also demonstrate that the positioning of the sensor with respect to the survey target is important when interpreting surface seismic data. This is particularly true for the case of a soil that is known to be laterally heterogeneous. In this case this was laterally variability through the inclusion of vibro-stone columns. This created a discrete vertical heterogeneity within the soil mass. The increasing volume of the column in which the elliptical Rayleigh wave is

contained with respect to its wavelength was able to provide a plausible explaination to how increases in the phase velocity and shear modulus could be assessed. For example, measurements by the sensors confirmed that in the case where the sensors were on the column, at low frequency waves with wavelengths that were larger than the diameter of the column, propagated through both the column and clay. However, when the frequency of the source increased, the proportion of the wavelength in the clay was reduced, thus the phase velocity gradually increased toward the phase velocity found for the column. Therefore, the spatial phase velocity changes could be identified, hence demonstrating how objective (4) was achieved. Thus, this work has shown how to identify a suitable data-processing technique in order to investigate both the spatial and vertical profiles of the phase velocity (shear modulus) in vibro-stone column ground improvement.

From the work reported in this thesis a relationship between the percentage of column volume and the phase velocity in the stone column has been established (see Section 8.3.2). This study suggests that the Rayleigh wave phase velocity is not only dependent on the vertical spans, but also the horizontal spans of the soil properties. The shape and size of the effective region of measurement in the medium in both lateral and vertical dimensions could be used to identify the sampling volume of the wavelength. The sampling volume is based on the elliptical particle movement, which in turn is a function of its wavelength. The volume of the column within the sampling volume at a respective wavelength was the key factor influencing the stiffness profile in the stone column. In this study, the wavelength is related to the depth using a constant of 1 in Equation 4.23, where wavelength is equivalent to depth for vertically homogeneous soil.

The results from the complete test programme showed that in the characterization of lateral non-homogeneities, the phase velocity versus wavelength relationship varies for stone columns of different diameters. This pointed to the potential for estimating the phase velocity and shear modulus of an effective region that spans both the lateral and depth axes. The use of the elliptical shapes in relating (1) the dispersive curve, (2) the sampling volume of the wavelengths and (3) the location of measurements was consistent with the results obtained and presented in Chapter 7 and discussed in Chapter 8. Using the elliptical shape and size at respective wavelengths to measure the effective volume measurement allowed objective (5) to be achieved, namely to understand the effect of lateral heterogeneity due to column inclusion in relation to the seismic surface wave result and the quality of the vibro-stone column.

The trade-off in conducting tests on a vibro-stone column area, was that the upper and lower constraints on the usable frequencies / wavelengths due to spatial aliasing as well as due to near-, and far offset constraints was that the spacing between the receivers are limited by the column width and columns spacing. For the laboratory seismic surface wave array set-up, the distance between the source and the first sensor (d) and sensors spacing (Δx) were 7 cm and 3 cm respectively. This array gave reliable wavelengths between 3.5 cm and 21 cm, which derived from half of d and three times d, respectively. Unreliable phase velocities also were likely to occur for wavelengths larger than half of soil depth due to the Rayleigh wave had not formed completely. The size of models in the future development of seismic test arrays, the distance (d) and the depth of model are crucial for the determination of the reliable wavelength range and consequently a likewise reliable depth of phase velocity/stiffness. For any further studies at a full scale, the

stiffness profile at depths between 0.5 and 3.2 m may be observed using a similar testing array (laboratory scale down was 1:15). This depth is sufficient to investigate beyond the critical depth for stone columns, up to 3 times of the stone column diameter, which corresponds to 1.8 m in depth if the full scale stone column diameter is set at 0.6 m (Barksdale and Bachus, 1983). In addition, the distance of the source to the first receiver (*d*) could be increased in the field to maximise the reliable wavelengths/depth. This positive outcome should be explored in the future.

9.2.2 Subsidiary Findings

The other finding in the thesis concerned the interference of surface waves with body waves (near offset constraint effect) and the attenuation of the surface wave (far offset constraint effect). These were identified via the anomalies in the phase-response of the coherence plot and unwrapped phase difference. A weaker signal quality at higher frequencies was due to a quicker attenuation of the shorter wavelength as well as the presence of a relatively strong boundary reflection, thus reducing the signal quality at higher frequencies and deviation of associated phase velocities. The furthest sensor location from the source received insufficient energy and was exacerbated by the interfering reflected wave from the boundary of the container. When Rayleigh wave propagation approached the stone column; some of energy was reflected, some of the energy was refracted around the column, and thus less energy continued along its direct path causing insufficient energy for sensors. Thus, the step frequency method was the most suitable technique to increase the signal-to-noise ratio.

The phase velocities are consistent for homogeneous soil when they fulfil the frequency/wavelength constraint (near and far array constraint). With an inclusion of columns, the phase velocities dispersed with frequency/wavelength. The larger wavelength encroached the area of the nearby columns, as a result the volume measurements (vertical and horizontal span) between the wavelength and column influences the measured phase velocities.

The quality of the measurements at low frequencies was influenced by the size of the physical soil model. The larger physical model provided an increase in useful frequencies, which had higher coherence values and deviated less from the average value as shown in the kaolin and Oxford clay test models. This phenomenon related to the condition in which the Rayleigh wave formed completely, i.e. when the wavelength was shorter than half of the model depth.

The experiments on concrete mortar identified higher reflection coefficients at the boundary between the concrete mortar-steel bar, which were proportional to the contrasts in density. The reflections were severe, as the variation in density was large, with a bulk density of 2080 kg/m^3 for concrete mortar and a density of 7850 kg/m^3 for the steel bars. The larger wavelength increased the area traversed by the propagating elliptical wave across the concrete mortar-steel boundary. The low signal to noise ratio was the effect from this signal which had a high refraction and reflection . However, the tests on soil indicated a significantly less severe problem related to wave reflections and refractions as

the differences in material density was not large, with a bulk density of 1711 kg/m^3 for the clay and 2045 kg/m^3 for the column.

Therefore, the aim of the study to develop the most appropriate seismic surface wave method for attaining and utilizing data in order to investigate vertical and lateral stiffness, and thus to evaluate the quality of ground improvement using a physical model of stone columns was achieved. This now allows fuller development of field and full-scale assessment approaches using seismic surveys to be developed. However, there are a number of practical implications that must be considered before any such approach is developed:

[1] Defective columns can be detected via conducting comparative stiffness profiles between the good quality column and unknown column quality, thus it is possible to predict the quality of any unknown column.

[2] The relationship of phase velocities, wavelength and percentage volume of column within the elliptical wave are useful for estimating the stiffness profile.

[3] The seismic source should always be in the middle of the array to provide an optimal arrangement for array deployment in order to carry out the seismic surface wave test on stone columns effectively.

9.3 Recommendations for Future Studies

[1] For any further testing of a similar nature to be carried out, the following suggestions could be adopted:

- The maximum information on the soil properties is limited to half of the model depth. To investigate the whole length of a column, this boundary restriction must be eliminated via increasing the clay bed size and maintaining the column scaling factor.
- Conduct the test using multi-component (triaxial) sensors. This would give X-Y, X-Z and Y-Z plots which ought to trace out an ellipse for the Rayleigh wave portion (Greenhalgh, 2010).
- Conduct the seismic test using bender elements to validate the seismic surface wave results.
- Load should be applied to investigate the influence of the adjacent columns, which leads to an increase of the soil shear strength due to the stone column drainage effect.
- To conduct the seismic test on columns with different stiffness such as, admixture columns. These will then investigate the materials effect or to apply same in other ground improvement works.

[2] Field measurements are ultimately required to validate the measurement technique established in the laboratory.

[3] The column-clay stiffness profile established from the seismic test should be validated via computer modelling.

[4] The developed seismic surface wave equipment and system for the quality control tests in the stone column could be expanded and used in different types of ground improvement or for forensic geotechnical investigation.

REFERENCES

Abbiss C.P (2001). Deformation of landfill from measurements of shear wave velocity and damping. **Geotechnique**, 51(6): 483-492.

Abbiss C.P. (1983) Calculation of elasticities and settlements for long periods of time and high strains from seismic measurements. **Géotechnique**, 33(4): 397-405.

Abbiss, C.P. (1981) Shear wave measurements of the elasticity of the ground. **Géotechnique**, 31(1): 91-104.

Abdrabbo, F.M. and Gaaver, K.E. (2002) "Interpretation of plate loading tests on granular soils." In **4th International Conference on Ground Improvement Techniques, Kuala Lumpur, Malaysia, 26-28 March 2002**. pp 171-178.

Abu-Hassanein, Z.S., Benson, C.H. and Blotz, L.R. (1996) Electrical resistivity of compacted clay. **Journal of Geotechnical Engineering**, ASCE, 122(5):397-406.

Adam, D., Brandl, H. and Kopf, F. et al. (2007) Heavy tamping integrated dynamic compaction control. **Ground Improvement**, 11 (4): 237–243.

Addo, K.O. and Robertson, P.K. (1992) Shear-wave velocity measurement of soils using Rayleigh waves. **Canadian Geotechnical Journal,** 29(4): 558-568.

Al-Hunaidi M.O. (1993) Insight on the SASW non-destructive testing method. **Canadian Geotechnical Journal**, 20: 940–950.

Arulanandan, K and Muraleetharan, K (1988) Level ground soil-liquefaction analysis using in-situ properties. **Journal Geotechnical Engineering ASCE**, 114(7): 753-770

Asaka, Y and Abe, T. (2011) Non-destructive technique for assessing cement-treated ground. **Ground Improvement**, 164 (G13): 179–187.

ASM International. (1993) **ASM Metals Reference Book**, 3rd edition. Bauccio, M.L. (ed.). USA: ASM International.

Atkinson, J. (2007) **The mechanics of soils and foundations**. 2nd edition. Oxon: Taylor and Francis.

Ballard, R.F. and Mclean, F.G. (1975) "Seismic field methods for in-situ moduli." In **Proceeding Conference on in situ Measurement of Soil Properties. Special Conference Geotechnical Engineering Division ASCE, 1975, Raleigh, North Carolina**, 1: 121-150.

Barksdale, R.D and Bachus, R.C. (1983) Design and construction of stone columns, Vol.1. Report No. FHWA/RD-83/026, NTIS, Virginia, USA.

Bowles, J.W. (1996) **Foundation analysis and design**. 5th edition. New York: McGraw-Hill.

BSI (1990) **Methods of Test for Soils for Civil Engineering Purposes BS1377**. London: British Standards Institution.

BSI (2005) **Group treatment by deep vibration. EN 14731: Execution of special geotechnical works**. London: British Standards Institution.

Butcher, A.P. and Powell J.J.M. (1995) "Practical considerations for field geophysical techniques used to assess ground stiffness." In Craig, C. (ed) **Advances in site investigation practice**. London: Thomas Telford. pp. 701-714.

Cascante, G., Najjaran, H. and Crespi, P. (2008) Novel methodology for nondestructive evaluation of brick walls: fuzzy logic analysis of masw tests. **Journal of Infrastructure Systems**, 14(2): 117–128.

Cassidy, N.J. (2007) "Frequency-dependent attenuation and velocity characteristics of magnetically lossy materials." In **IEEE Proceedings of the 4th International Workshop on Advanced Ground Penetrating Radar, Naples**, pp. 142–146.

Cassidy, N.J. and Millington, T.M. (2009) The application of finite-difference time-domain modelling for the assessment of GPR in magnetically lossy materials. **Journal of Applied Geophysics,** 67 (2009): 296-308.

Chan C.M. (2006) **A laboratory investigation of shear wave velocity in stabilized soft soils**. PhD thesis, University of Sheffield.

Charles, J.A. (2002) Ground improvement: the interaction of engineering science and experience-based technology. **Géotechnique**, 52 (7): 527-532.

Charles, J.A. and Watts, K.S. (2002) **Treated ground engineering properties and performance**. London: Construction Industry Research and Information Association, ClRlA C572.

Chu, J. and Yan, S.W. (2005) "Implementation Application of the vacuum preloading method in soil improvement projects." In **Ground Improvement: case histories**. Elsevier Geo-engineering book series vol 3, pp. 91-117.

Clayton, C.R.I. (2011) Stiffness at small strain: research and practice. **Géotechnique**, 61 (1): 5-37.

Clayton, C.R.I., Gordon, M.A., and Matthews, M.C. (1994) "Measurements of stiffness of soils and weak rocks using small strain laboratory testing and geophysics." In: Craig, C. (ed.) **Proceedings of an International Symposium on Pre-failure Deformation Characteristics of Geomaterials**. Rotterdam, Balkema. pp. 229-234.

Clayton, C.R.I., Matthews, M.C. and Simons, N.E. (1995) **Site Investigation**. 2nd edition. London: Blackwell Science Ltd.

Clayton, C.R.I., Theron, M. and Best, A.I. (2004) The measurement of vertical shear-wave velocity using side-mounted bender elements in the triaxial apparatus. **Géotechnique,** 54 (7): 495–498.

Cosenza, P., Marmet, E., Rejiba F., Cui, Y.J., Tabbagh, A. and Charlery, Y. (2006) Correlations between geotechnical and electrical data: A case study at Garchy in France. **Journal of Applied Geophysics**, 60 (2006): 165–178.

Crice, D. (2005) MASW: the wave of the future**. Journal of Environmental and Engineering Geophysics**, 10(2): 77–79.

Crocco, L., Prisco, G., Soldovieri, F. and Cassidy, N.J. (2009) Early-stage leaking pipes GPR monitoring via microwave tomographic inversion. **Journal of Applied Geophysics,** 67: 270–277.

Cuellar, V. and Valerio, J. (1997) "Use of the SASW method to evaluate soil improvement techniques." In **14th International conference, Hamburg**: Balkema, pp. 461-464.

Cuellar, V. (1997) "Geotechnical applications of the spectral analysis of surface waves." In: McCann, D.M., Eddleston, M., Fenning, P.J. and Reeves, G.M. (ed) **Modern Geophysics in Engineering Geology, Geological Society Engineering Geology Special Publication No. 12**, pp. 53-62.

Daniels, D.J., Gunton, D.J., Scott, H.F. (1988) Introduction to subsurface radar. **IEEE Proceedings,** 135: 278 320.

Das, B.M. (2007) **Principle of Foundation Enginnering, 7th edition**. Stamford: Cengage Learning.

Fam, M. and Santamarina, J.C. (1997) A study of consolidation using mechanical and electromagnetic waves. **Géotechnique**, 47(2): 203-219.

Forbriger, T. (2003) Inversion of shallow-seismic wavefields: II. Inferring subsurface properties from wavefield transforms. **Geophysical Journal International**, 153(3): 735–752.

Foti, S. and Butcher, A.P. (2004) "General report: Geophysical method applied to geotechnical engineering." In: da Fonseca, A.V. and Mayne, P.W. (ed) **Proceeding ISC-2 on Geotechnical and Geophysical Site Characterisation, Vol 1,** Rotterdam: Millpress, pp. 409-418.

Ganji, V., Gucunski, N., and Maher, A. (1997) Detection of underground obstacles by sasw method- numerical aspects. **Journal of Geotechnical and Geoenvironmental Engineering**, ASCE, 123(3): 212-219.

Garcia-Bengochea, I., Lovell, C. and Altschaeffl (1979) Pore Distribution and permeability of silty clay. **Journal of Geotechnical Engineering, ASCE**, 105 (7): 839-856.

Giao P.H., Chung S.G., Kim D.Y., and Tanaka, H. (2003) Electric imaging and laboratory testing for geotechnical investigation of Pusan clay deposits. **Journal of Applied Geophysics,** 52 (2003): 157-175.

Gordon, M.A., Clayton, C.R.I., Thomas, T.C. and Matthews, M.C. (1996) "The selection in interpretation of seismic geophysical methods for site investigation." In: Craig, C. (ed) **Advances in site investigation practice**. London: Thomas Telford. pp. 727-738.

Graff, K. (1991) **Wave motion in elastic solids**, New York: Dover publications Inc.

Greenhalgh, S. (2010) Personal communication.

Greenwood, D.A. (1970) Mechanical improvement of soils below ground surface. Proceeding of the Ground Engineering Conference, Institution of Civil Engineers, June 11-12.

Guetif, Z., Bouassida, M. and Debats, J.M. (2007) Improved soft clay characteristics due to stone column installation. **Computers and Geotechnics**, 34: 104–111.

Haegeman, W And Baertsoen, A. (2007) Evaluation of a preloading consolidation: a case Study. **Ground Improvement,** 6 (4): 169–173.

Haskell, N.A. (1953) The dispersion of subsurface waves on multilayered media. **Bull. Seismological Soc. America**, 43(1), 17-34.

Head, K.H. (1980) **Manual of soil laboratory testing. Volume l: Soil classification and compaction tests**. London: Pentech Press.

Heisey, J.S., Stokoe, K.H., and Meyer, A.H. (1982) "Moduli of pavement systems from spectral analysis of surface waves." In **Strength and deformation characteristics of pavements. Transportation Research Record 852**, Transportation Research Board, National Research Council, Washington, D.C., pp. 22–31.

Heukolom W. and Foster C.R. (1962) Dynamic testing of pavements. **Trans. ASCE,** 127: 425-456.

Hooker, P (2002) Measure for measure. Article featured in ground engineering magazine, Oct. 2002.

Hosoya, Y., Ogino, T., Nasu, T., Kohata, Y., Hibi, Y. and Makihara, Y. (1996). "Japanese Geotechnical Society Technical Report- An evaluation of strength of soils improved by DMM." In **Proceedings of the 2nd. International Conference on Ground Improvement Geosystems, Tokyo, Japan**, Vol. 2, pp. 919-924.

Hu, W. (1995) **Physical modelling of group behaviour of stone column foundations**. PhD thesis, University of Glasgow.

Ifeachor E.C. and Jervis B.W. (1993) **Digital signal processing: a practical approach**. Addison: Wesley Publishing, 184-191.

Jefferson, I., O'Hara-Dhand, K.A. and Serridge, C.J. (2008) "Assessment of the ground improvement of problematical soils." In **Proc. of 3rd Int. Conf. on Site Characterization. Taipei, Taiwan April 2008**, Expanded Abstracts.

John, U.E. (2011) **Chemical performance of cement stabilised contaminated clay**. PhD thesis, University of Birmingham.

Jones, R. (1958) In-situ measurements of the dynamic properties of soil by vibration methods. **Géotechnique**, 8(1): 1–21.

Keller, G. and Frischknecht, F. (1966) **Electrical methods in geophysical propecting**. New York: Pergamon Press.

Khan, Z., Majid, A., Cascante, G., Hutchinson, D.J. and Pezeshkpour, P. (2006) Characterization of a cemented sand with the pulse-velocity method. **Canadian Geotechnical Journal**, 43(3): 294-309.

Kim, D.S. and Park, H.C. (1999) Evaluation of ground densification using spectral analysis of surface waves (SASW) and resonant column (RC) tests. **Canadian Geotechnical Journal**, 36: 291-299.

Kirsch, F. (2009) Geotechnics of Soft Soils: Focus on Ground Improvement. In Karstunen, M and Leoni, M. (eds) **Proceedings of the 2nd International Workshop on Geotechnics of Soft Soils, Glasgow, Scotland, 3 - 5 September 2008**. London: Taylor & Francis, pp 241–247.

Kitazume, M. (2005) "State of Practice Reports: Field and laboratory investigations, properties of binders and stabilised soils." In **Proceedings of the International Conference on Deep Mixing Best Practice and Recent Advances, Stockholm, Sweden**, Vol. 2, pp. 660-684.

Landon, M.M., DeGroot, D.J., and Sheahan, T.C. (2007) Sample quality assessment using shear wave velocity for a marine clay. **Journal of Geotechnical and Geoenvironmental Engineering, ASCE**, 133(4): 424-432.

Lankston, R.W. (1990) "High-resolution refraction seismic data acquisition and interpretation." In Ward, S.H. (ed) **Investigations in Geophysics no. 5, Volume 1: Review and Tutorial**. Oklahoma: Society of Exploration Geophysicists. pp. 1-30.

Lee, L. (2001) **Soil-pile interaction of bored and case in-situ piles**. PhD Thesis, University of Birmingham.

Long, M. and Donohue, S. (2007) In situ shear wave velocity from multichannel analysis of surface waves (MASW) tests at eight Norwegian research sites. **Canadian Geotechnical Journal**, 44: 533–544.

Luke, B. (1999) Site investigations function better with seismic waves. **IEEE Potentials**, 18(1), Feb.-March 1999: 33-35.

Luna, R. and Jadi, H. (2000) "Determination of dynamic soil properties using geophysical methods." In **Proceedings of the First International Conference on the Application of Geophysical and NDT Methodologies to Transportation Facilities and Infrastructure, St. Louis, December 2000,** pp. 1-15.

Madhyannapu, R. S., Puppala, A.J., Nazarian, S. and Yuan, D. (2010) Quality assessment and quality control of deep soil mixing construction for stabilizing expansive subsoils. **Journal of Geotechnical and Geoenvironmental Engineering**, 136(1): 119–128.

Madun, A., Jefferson, I., Chapman, D.N., Culshaw, M.G., Foo K.Y. and Atkins, P.R. (2010a) Evaluation of the multi-channel surface wave analysis approach for the monitoring of multiple soil-stiffening columns. **Near Surface Geophysics**, 8(6): 611-621.

Madun, A., Jefferson, I., Foo K.Y., Chapman, D.N., Culshaw, M.G. and Atkins, P.R. Characterization and quality control of stone columns using surface waves testing. **Canadian Geotechnical Journal** (under review).

Madun, A., Jefferson, I., Foo, K.Y., Atkins, P.R., Chapman, D.N. and Culshaw, M. (2010b) "Robust weighted-mean approach for the evaluation of ground improvement columns using surface wave analysis." In **16th European Meeting of Environmental and Engineering Geophysics, Zurich, 6 - 8 September 2010** (in CD-ROM, ISBN 978-90-73781-88-7 EAGE 2010).

Massarsch K.R. (2005) "Deformation properties of stabilized soil columns." In **Proceedings International Conference on Deep Mixing, Stockhom, 23 - 25 May 2005**.

Matthews M.C., Hope V.S. and Clayton C.R.I. (1995) The geotechnical value of ground stiffness determined using seismic methods. **Geological Society, London, Engineering Geology Special Publications**, 12: 113-123.

Matthews, M.C. Hope, Y.S. and Clayton, C.R.I. (1996) The use of surface waves in the determination of ground stiffness profiles. **Proceedings of the Institution of Civil Engineers Geotechnical Engineering**, 119: 84-95.

Matthews, M.C., Clayton, C.R.I. and Own, Y. (2000) The use of field geophysical techniques to determine geotechnical stiffness parameters. **Proceedings of the Institution of Civil Engineers Geotechnical Engineering**, 143: 31-42.

Mattsson, H., Larsson, R., Holm, G., Dannewitz, N. and Eriksson, H. (2005) "Down-hole technique improves quality control on dry mix columns." In **Proceedings of the International Conference on Deep Mixing Best Practice and Recent Advances,**

Stockholm, Sweden, Vol. 1, pp. 581-592.

McCabe, B.A., Nimmons, G.J. and Egan, D. (2009) A review of field performance of stone columns in soft soils. **Proceedings of Institution of Civil Engineers, Geotechnical Engineering**, 162(6): 323-334.

McDowell, P.W., Barker, R.D. and Butcher, A.P., et al. (2002) **Geophysics in engineering investigations**. London: Construction Industry Research and Information Association, ClRlA C562.

McKelvey, D., Sivakumar, V., Bell, A. and Graham, J. (2004) Modelling vibrated stone columns in soft clay. **Proceedings of the Institution of Civil Engineers Geotechnical Engineering**, 157(3): 137–149.

Menzies B.K. (2001) "Near-surface site characterisation by ground stiffness profiling using surface wave geophysics." In **Instrumentation in Geotechnical Engineering** (eds K.R. Saxena and V.M. Sharma), H.C.Verma Commemorative Volume, 43-71. Oxford & IBH Publishing Co. Pvt. Ltd., New Delhi, Calcultta.

Menzies, B. and Matthews, M. (1996) "The continuous surface-wave system: A modern technique for site investigation." In **Special lecture: Indian Geotechnical Conference Madras, December 11-14th 1996.**

Mitchell, J.M. and Jardine, F.M. (2002) **A guide to ground treatment**. London: Construction Industry Research and Information Association, ClRlA C573.

Mitchell, J.K. and Soga, K (2005) **Fundamentals of soil behaviour, 3rd edition**. New Jersey: John Wiley & Sons.

Moxhay, A.L., Tinsley, R.D. and Sutton J.A. (2001) Monitoring of soil stiffness during ground improvement using seismic surface waves. **Ground Engineering Magazine,** January: 34-37.

Moxhay, A.L., Tinsley, R.D., Redgers, J.D. and Gravell, D.C. (2008) The prediction of ground settlement from continuous surface wave data. **Ground Engineering Magazine**, July: 34-38.

Nasseri-Moghaddam, A. (2006) **Study of the effect of lateral inhomogeneties on the propagation of Rayleigh waves in an elastic medium**. PhD thesis, University of Waterloo.

Nasseri-Moghaddam, A., Cascante, G. and Hutchinson, J. (2005) A new quantitative procedure to determine the location and embedment depth of a void using surface waves. **Journal Environment and Engineering Geophysics**, 10(1): 29-37.

Nasseri-Moghaddam, A., Cascante, G., Phillips, C. et al. (2007) Effects of underground cavities on Rayleigh waves—Field and numerical experiments. **Soil Dynamics and Earthquake Engineering,** 27 (2007): 300–313.

Omar, M.N., Abbiss, C.P., Taha, M.R. and Mohd Nayan, K.A. (2010) "Prediction of long-term settlement of soft clay using the continuous surface wave method and damping measurement." In **8th International Conference in Geotechnical and Transportation Geotropika 2010, Sabah 1-3 December 2010.**

Park, C.B., Miller, R.D. and Xia, J. (2007) Multichannel Analysis Of Surface Waves (MASW)-Active And Passive Methods. **The Leading Edge**, January 2007, 60-64.

Park, C.B., Xia, J. and Miller, R.D. (1998) "Surface waves as a tool to image near-surface anomaly." In **68th Ann. Internat. Mtg., Soc. Expl. Geophys.**, Expanded Abstracts, pp. 874–877.

Park, C.B., Miller, R.D., and Xia, J. (1999) Multichannel analysis of surface waves. **Geophysics,** 64(3): 800-808.

Park, C.B., Miller, R.D., Ryden, N., Xia, J., and Ivanov, J., (2005) Combined use of active and passive surface waves. **Journal of Engineering and Environmental Geophysics**, 10 (3): 323-334.

Phillips, C., Cascante, G. and Hutchinson, D.J. (2004) Evaluation of horizontal homogeneity of geomaterials with the distance analysis of surface waves. **Canadian Geotechnical Journal**, 41(2004): 212–226.

Priebe, H.J. (1995) The design of vibro replacement. **Ground Engineering,** 28(10): 31–37.

Raju, V.R. (2002) "Vibro replacement for high earth embankments and bridge abutment slopes in Putrajaya, Malaysia." In **4th International Conference on Ground Improvement Techniques, Malaysia, 26 – 28 March 2002**, pp. 607–614.

Raju, V.R. and Hoffmann, G. (1996) "Treatment of tin mine tailings in Kuala Lumpur using vibro replacement." In **Proc. 12th Southeast Asian Geotechnical Conference, Kuala Lumpur, Malaysia**.

Raju, V.R. and Sondermann, W. (2005) "Ground improvement using deep vibro techniques." In **Ground Improvement: case histories**. Elsevier Geo-engineering book series vol 3, pp 601-638.

Raju, V.R. and Yandamuri, H.K. (2010) Ground improvement for infrastructure projects in Malaysia. **Proceedings of the Institution of Civil Engineers Ground Improvement**, 163 (GI4): 251–263.

Raju, V.R., Wegner, R. and Hari Krishna, Y. (2004) "Ground improvement using vibro replacement in Asia 1994 to 2004 - A 10 year review." In **5th International Conference on Ground Improvement Techniques, Kuala Lumpur, March 2004**.

Rayhani, M.H.T. and El Naggar, M.H. (2007) Centrifuge modeling of seismic response of layered soft clay. **Bulletin of Earthquake Engineering**, 5: 571–589.

Rayhani, M.H.T. and El Naggar, M.H. (2008) Numerical modeling of seismic response of rigid foundation on soft soil. **International Journal of Geomechanics**, 8(6): 336–346.

Redges, J.D., Moxhay, A.L., Ghataora, G.S. and Jefferson, I. (2008) "Case histories of settlement performance comparisons on ground improvements using stiffness, seismic waves and traditional methods." In **Proc. 6th International Conference on Case Histories in Geotechnical Engineering, Arlington, VA, 11-16 August 2008,** Expanded Abstracts.

Reynolds, J.M. (1997) **An introduction to applied and environmental geophysics**. John Wiley & Sons.

Rhazi, J., Hassaim, M., Ballivy, G. and Hunaidi, O. (2002) Effects of concrete non-homogeneity on Rayleigh waves dispersion. Magazine of Concrete Research, 2002, 54, No. 3, June, 193–201.

Richart, F.E., Wood, R.D., Hall, J.R. (1970) **Vibration of soils and foundations**. New Jersey: Prentice-Hall.

Roy, D.R.N. (2010) **Continuous surface wave testing of vibro-stonecolumn ground improvement**. MSc thesis, University of Birmingham.

Serridge, C.J. (2005) Achieving sustainability in vibro-stonecolumn techniques. **Proceedings of the Institution of Civil Engineers – Engineering Sustainability**, 158(4): 211–222.

Serridge, C.J. and Synac, O. (2007) Ground improvement solutions for motorway widening schemes and new highway embankment construction over soft ground. **Ground Improvement**, 11(4): 219-228.

Sheriff, R.E. and Geldart, L.P. (1982) **Exploration seismology, volume 1**. Cambridge University Press.

Sheriff, R.E. and Geldart, L.P. (1995) **Exploration seismology**. 2nd edition. New York: Cambridge University Press.

Shibuya, S. and Tanaka, H. (1996) Estimate of elastic shear modulus in Holocene soil deposits. **Soil Fdns**, 36(4): 45-55.

Shibuya, S., Mitachi, T. and Yamashita, S. et al. (1995) "Recent Japanese practice for investigation elastic stiffness of ground." In Craig, C. **Advances in site investigation practice**. London: Thomas Telford. pp. 875-886.

Shrivastava A.K. (2007) Assessment of ground improvement work using radioisotope cone penetrometers. **Ground Improvement**, 11 (3): 101–110.

Silva, S.D. (2005) "Implementation and performance of sone columns at Penny's Bay reclaimation in Hong Kong." In **Ground Improvement: case histories**. Elsevier Geo-engineering book series vol 3. pp 639-664.

Sivakumar, V., McKelvey, J., Graham, J. and Hughes, D. (2004) Triaxial tests on model sand columns in clay. **Canadian Geotechnical Journal,** 41: 299-312.

Socco, L.V. and Strobbia, C. (2004) Surface wave method for near-surface characterization: a tutorial. **Near Surface Geophysics**, 2004, 165-185.

Sondermann, W. and Wehr, J. (2004) "Deep Vibro techniques," In: Moseley, M.P. and K. Kirsch, K. (eds) **Ground Improvement, 2nd Edition.** Spon Press. pp. 57-92.

Staab, D.A., Edil, T.B. and Alumbaugh, D.L. (2004) "Non-Destructive Evaluation of Cement-Mixed Soils". In **Drilled Shafts, Micropiling, Deep Mixing, Remedial and Specialty Foundation Systems, Geotechnical Special Publication No. 124**, ASCE. Orlando, Florida: Geo-Support 2004. pp. 838-848.

Steeples, D.W., and Miller, R.D. (1990) "Seismic reflection methods applied to engineering, environmental, and groundwater problems:" In Ward, S.H. (ed) **Investigations in Geophysics no. 5, Volume 1: Review and Tutorial**. Oklahoma: Society of Exploration Geophysicists. pp. 1-30.

Stokoe, K.H., Wright, G.W., III, Bay, J.A., and Roesset, J.M. (1994) "Characterisation of geotechnical sites by SASW method." In Woods, R.D. (ed) **Geophysical Characterisation of Sites**. New York: Oxford Publishers.

Stroud, M.A. (1989) The standard penetration test – its application and interpretation. **Proc. ICE Conf. on Penetration Testing in the UK, Birmingham**. London: Thomas Telford.

Sutton, J.A. and Snelling, K. (1998) "Assessment of ground improvement using the continuous surface wave method." In **4th meeting of the environmental and engineering geophysical society, Barcelona, 14-17th September 1998.**

Tallavo F., Cascante G. and Pandey M. (2009) Experimental and numerical analysis of MASW tests for detection of buried timber trestles. **Soil Dynamics and Earthquake Engineering,** 29: 91-102.

Tamura, M., Hibino, S. and Fuji l, M. et al. (2002) "Applicability of resistivity method for the quality evaluation of mechanical deep-mixing of soil stabilization method." In **Proceedings 4th International Conference on Ground Improvement Techniques, Kuala Lumpur,** pp. 707-714.

Tavenas, F., Mieussens, C. and Bourges, F. (1979) Lateral displacements in clay foundations under embankments. **Canadian Geotechnical Journal**, 16(3): 523-550.

Terashi, M. and Juran, I. (2000) "Ground improvement – state of the art." In **An International Conference on Geotechnical & Geological Engineering. Melbourne, Australia, 19-24 November 2000.**

Terzaghi, K., Peck, R.B. and Mesri, G. (1996) **Soil Mechanics in Engineering Practice**. 3rd. edition. New York: John Wiley & sons, Inc.

Thevanayagam, S. (1993) Electrical response of two-phase soil: theory and applications. **Journal Geotechnical Engineering ASCE**, 119 (8): 1250-1275.

Thomas, A.M. (2010) **Measurement of electromagnetic signal velocities in saturated fine-grained soils**. PhD thesis, University of Birmingham.

Thomson W.T. (1950) Transmission of elastic waves through a stratified solid medium. **Journal Applied Physics**, 21: 89-93.

Van Impe, W.F. and Madhav, M.R. (1992) Analysis and settlement of dilating stone column reinforced soil. **Austrian Geotechnical Journal**, Feb.-March, Vol. 137: 114-121.

Xia, J., Chen C., Li, P.H. and Lewis, M.J. (2004) Delineation of a collapse feature in a noisy environment using a multichannel surface wave technique. **Géotechnique**, 54(1): 17-27.

Xia, J., Miller, R.D. , Park, C.B. et al (2002) Comparing shear wave velocity profiles inverted from multichannel surface wave with borehole measurements. **Soil Dynamics and Earthquake Engineering**, 22: 181-190.

Xu, C. and Butt, S.D. (2006) Evaluation of MASW techniques to image steeply dipping cavities in laterally inhomogeneous terrain. **Journal of Applied Geophysics**, 59: 106–116.

Yuan, D., Nazarian, S., Madhyannapu, R.S., Puppala, A.J. (2008) "Soil velocity profiles from in-situ seismic tests at deep-mixing sites." In Alshawabkeh, A.N., Reddy, K.R. and Khire, M.V. (eds.) **GeoCongress 2008: Characterization, Monitoring, and Modeling of GeoSystems, New Orleans, Louisiana, 9-12 March 2008**: ASCE. pp. 388-395.

Zerwer, A., Polak, M.A. and Santamarina, J.C. (2000) Wave propagation in thin Plexiglas plates: implications for Rayleigh waves. **NDT&E International**, 33(2000): 33-41.

Zerwer, A., Polak, M.A. and Santamarina, J.C. (2002). Effect of surface cracks on rayleigh wave propagation: an experimental study. **Journal Structural Engineering**, 128(2): 240-248.

Zywicki, D.J. (1999) **Advanced signal processing methods applied to engineering analysis of seismic surface waves**. PhD thesis, Georgia Institute of Technology.

APPENDICES

Appendix A

i. Detail results of geotechnical testing

A(1) Data of sieve analysis

A(1a) Data of sieve analysis for sand use to construct concrete mortar

Seive, micron	Test 1			Test 2			Test 3		
	Retain	Passing	passing	Retain	Passing	passing	Retain	Passing	passing
	(g)	(g)	%	(g)	(g)	%	(g)	(g)	%
10000	0.0	997.4	100.0	0.0	998.0	100.0	0.0	598.7	100.0
6300	3.2	994.2	99.7	9.9	988.1	99.0	2.4	596.2	99.6
3350	75.4	918.8	92.1	60.9	927.2	92.9	40.5	555.8	92.8
2000	53.6	865.2	86.7	49.6	877.6	87.9	31.0	524.7	87.6
600	140.9	724.2	72.6	145.3	732.2	73.4	81.8	442.9	74.0
425	184.2	540.1	54.2	171.4	560.9	56.2	92.0	350.9	58.6
300	273.6	266.5	26.7	304.9	255.9	25.6	166.3	184.6	30.8
212	164.6	101.8	10.2	162.5	93.5	9.4	111.3	73.3	12.2
150	57.5	44.3	4.4	54.3	39.1	3.9	38.6	34.7	5.8
63	33.2	11.1	1.1	29.9	9.2	0.9	25.0	9.7	1.6
Pan	11.1	0	0	9.2	0	0	9.7	0	0
Total weight, g	997.35			997.98			598.67		

A(1b) Data of sieve analysis for gravelly sand to construct column

Sieve (micron)	Test1			Test2		
	Retain weight (g)	Passing weight (g)	Passing (%)	Retain weight (g)	Passing weight (g)	Passing (%)
3350	0	497.42	100.0	0	594.42	100.0
2800	0.65	496.77	99.9	3.71	590.71	99.4
2360	52.76	444.01	89.3	71.86	518.85	87.3
2000	114.85	329.16	66.2	131.18	387.67	65.2
1700	104.49	224.67	45.2	112.09	275.58	46.4
1400	90.36	134.31	27.0	116.09	159.49	26.8
1180	80.71	53.6	10.8	86.68	72.81	12.2
600	29.97	23.63	4.8	35.67	37.14	6.2
Pan	23.63		0	37.14		0.0
	497.42			594.42		

A(2) Data of compaction test

A(2a) Data of compaction test in Oxford clay (Dietert method)

Measurement no.	(1)			(2)			(3)		
Weight of wet soil, g	107.45			117.9			119.95		
Diameter of wet soil, mm	38.13			38.47			38.01		
Length of wet soil, mm	59.5			55.47			55.03		
Volume, m^3	67969.6801			64501.1099			62468.3308		
Wet density, ρ kg/m^3	1580.8519			1827.8755			1920.1730		
Container no.	1	2	3	1	2	3	L8	L17	9E
Wet soil & container, g	29.75	28.63	33.5	117.9	30.6	35.4	33.1	33.05	35.96
Dry soil & container, g	26.93	25.93	30.23	98.12	26.36	30.35	27.49	27.36	29.56
Container, g	5.48	5.5	5.34	0	5.48	5.33	3.8	3.81	3.33
Dry soil, g	21.45	20.43	24.89	98.12	20.88	25.02	23.69	23.55	26.23
Moisture loss, g	2.82	2.7	3.27	19.78	4.24	5.05	5.61	5.69	6.4
Moisture content, %	13.15	13.22	13.14	20.16	20.31	20.18	23.68	24.16	24.40
Average moisture, %	13.17			20.22			24.08		
Dry density ρd Mg/m^3	1396.9215			1520.4870			1547.5208		
Spesific gravity, Gs	2.6			2.6			2.6		
w=Sr.e/Gs (Sr.e)	0.34			0.53			0.63		
P=Pw (Gs+ Sr.e)/1+e (void ratio)	0.86			0.71			0.68		
Degree of saturation, Sr	39.7			74.0			92.1		

Measurement no.	(4)			(5)			(6)		
Weight of wet soil, g	108.53			166.11			159.52		
Diameter of wet soil, mm	37.85			37.71			37.86		
Length of wet soil, mm	51.47			81.39			79.15		
Volume, m^3	57936.2772			90938.7044			89140.8535		
Wet density, ρ kg/m^3	1873.2650			1826.6150			1789.5274		
Container no.	A3	9	E	A3	17	11	E	6	M2
Wet soil & container, g	23	24.47	23.83	34.27	31.15	31.56	32.3	31.69	32.16
Dry soil & container, g	18.97	20.02	19.51	26.97	24.57	24.71	24.87	24.39	24.66
Container, g	4.03	3.33	3.47	4.02	4.05	3.2	3.96	3.85	3.42
Dry soil, g	14.94	16.69	16.04	22.95	20.52	21.51	20.91	20.54	21.24
Moisture loss, g	4.03	4.45	4.32	7.3	6.58	6.85	7.43	7.3	7.5
Moisture content, %	26.97	26.66	26.93	31.81	32.07	31.85	35.53	35.54	35.31
Average moisture, %	26.86			31.91			35.46		
Dry density ρd Mg/m^3	1476.6788			1384.7776			1321.0602		
Spesific gravity, Gs	2.6			2.6			2.6		
w=Sr.e/Gs (Sr.e)	0.70			0.83			0.92		
P=Pw (Gs+ Sr.e)/1+e (void ratio)	0.76			0.88			0.97		
Degree of saturation, Sr	91.8			94.5			95.2		

Measurement no.	(7)			(8)		
Weight of wet soil, g	149.8			146.76		
Diameter of wet soil, mm	37.64			37.07		
Length of wet soil, mm	77.04			77.52		
Volume, m^3	85759.0878			83699.6391		
Wet density, ρ kg/m^3	1746.7537			1753.4126		
Container no.	B4	A7	C7	B4	A7	C7
Wet soil & container, g	25.52	25.93	25.98	24.89	18.3	22.99
Dry soil & container, g	19.01	19.29	19.57	18.24	13.72	17.08
Container, g	3.2	3.21	3.94	3.48	3.93	3.32
Dry soil, g	15.81	16.08	15.63	14.76	9.79	13.76
Moisture loss, g	6.51	6.64	6.41	6.65	4.58	5.91
Moisture content, %	41.18	41.29	41.01	45.05	46.78	42.95
Average moisture, %	41.2			44.9		
Dry density ρd Mg/m^3	1237.4256			1209.8419		
Spesific gravity, Gs	2.6			2.6		
w=Sr.e/Gs (Sr.e)	1.07			1.17		
P=Pw (Gs+ Sr.e)/1+e (void ratio)	1.10			1.15		
Degree of saturation, Sr	97.2			101.7		

A(2b) Data of compaction test in kaolin (Dietert method)

BS 1377:1990	Location:					
No of layers: 1	Soil description: Clay					
Blow per layer 10 each side	Sample type: English-china clay					
Compacted by: machine	Sample preparation: Mixing by hand					
Sample preparation						
Measurement no.	(1)	(3)	(3)	(4)	(5)	(6)
Sample weight, g	100	100	100	100	100	100
Water, g	25	28	30	35	40	45
Weight of wet soil, g	121.35	126.59	127.73	130.8	131.47	136.55
Diameter of wet soil, mm	37.97	38.23	37.88	37.76	37.11	37.82
Length of wet soil, mm	62.6	61.23	62.61	65.66	68.22	71.2
Volume, m3	70912	70313	70588	73558	73817	80018
Wet density, ρ kg/m3	1711	1800	1810	1778	1781	1706
Water content						
Container no.	1	2	3	4	5	6
Wet soil, g	130.67	150.26	137.19	157.96	141.02	160.22
Dry soil, g	107.42	122.72	108.15	124.93	105.03	118.8
Weight of container, g	9.32	23.67	9.46	27.16	9.55	23.67
Water loss, g	23.25	27.54	29.04	33.03	35.99	41.42
Weight of dry soil, g	98.1	99.05	98.69	97.77	95.48	95.13
Water content, %	23.7	27.8	29.4	33.8	37.7	43.5
Dry density ρd Mg/m3	1383	1409	1398	1329	1293	1189
Spesific gravity, Gs	2.65	2.65	2.65	2.65	2.65	2.65

w=Sr.e/Gs (Sr.e)	0.63	0.74	0.78	0.90	1.00	1.15
P=Pw (Gs+ Sr.e)/1+e (void ratio)	0.92	0.88	0.90	0.99	1.05	1.23
Degree of saturation, Sr (%)	68.6	83.6	87.1	90.1	95.2	93.9

A(2c) Data of compaction test in gravelly sand (vibrating method)

BS 1377:1990	Location:
No of layers: 3	Soil description:
Blow per layer 1 minute	Sample type: Sand
Compacted by: hand	Sample preparation: Mixing by hand

Density : Volume of cylinder (V) (dia: 15.271cm, length: 11.675cm) :

2139 cm3

Measurement no.	1	2
Cylinder & soil, A g	9872	10187
Cylinder, B g	5846.5	5846.5
Wet soil, A - B g	4025.5	4340.5
Volume, m3	2139	2139
Wet density, ρ Mg/m^3	1882	2029

Moisture content

Container no.	1	2	3	4	5	6
Wet soil & container, g	130.7	136.1	140.5	74.19	79.42	81.38
Dry soil & container, g	124.61	128.64	133.54	68.54	73.20	75.61
Container, g	26.23	9.61	23.68	5.44	5.44	9.59
Dry soil, g	98.38	119	109.9	63.1	67.76	66.02
Moisture loss, g	6.06	7.48	6.92	5.65	6.22	5.77
Moisture content, %	6.16	6.28	6.30	8.95	9.18	8.74
Average moisture, %	6.25			9.0		
Dry density ρd Mg/m^3	1771			1862		

Measurement no.	3	4
Cylinder & soil, A g	10222	10188
Cylinder, B g	5846.5	5846.5
Wet soil, A - B g	4375.5	4341.5
Volume, m3	2139	2139
Wet density, ρ Mg/m^3	2045	2029

Moisture content

Container no.	7	8	9	10	11	12
Wet soil & container, g	75.27	81.73	84.88	76.66	84.08	72.57
Dry soil & container, g	68.74	74.68	77.37	69.39	75.61	65.20

Container, g	5.57	9.51	6.1	8.34	8.43	5.34
Dry soil, g	63.17	65.17	71.27	61.05	67.18	59.86
Moisture loss, g	6.53	7.05	7.51	7.27	8.47	7.37
Moisture content, %	10.34	10.82	10.54	11.91	12.61	12.31
Average moisture, %	10.6			12.3		
Dry density ρd Mg/m^3	1850			1808		

Remarks: CBR mould, 3 layers at 5cm each layer before compaction using vibrating hammer for 1 minute.

A(2d) Data of trial compaction test in Oxford clay (vibrating method)

Trial No	Trial 1								
Weight of wet soil, g	142.77			138.61			129.94		
Diameter of wet soil, mm	37.82			38.09			37.94		
Length of wet soil, mm	69.57			67.05			63.31		
Volume, mm^3	78186.1			76433.8			71603.1		
Wet density, ρ kg/m^3	1826.0			1813.5			1814.7		
Average wet density, ρ kg/m^3	1818.1								
Container no.	A	H7	A7	A3	7	D31	F	17	9E
Wet soil & container, g	24.97	20.4	19.97	27.79	25.91	29.86	35.06	25.28	24.4
Dry soil & container, g	20.34	16.69	16.47	22.1	20.54	23.53	27.48	20.28	19.39
Container, g	5.36	4.75	5.27	4.05	3.36	3.21	3.24	4.07	3.39
Dry soil, g	14.98	11.94	11.2	18.05	17.18	20.32	24.24	16.21	16
Moisture loss, g	4.63	3.71	3.5	5.69	5.37	6.33	7.58	5	5.01
Moisture content, %	30.91	31.07	31.25	31.52	31.26	31.15	31.27	30.85	31.31
Average moisture, %	31.1			31.3			31.1		
Average moisture, %	31.2								
Dry density, ρd Mg/m^3	1393.1			1381.0			1383.8		
Average dry density, ρd Mg/m^3	1386.0								

Remarks: Sample preparation by vibrating hammer for 30 second on 60mm thicknesss of loose soil layer on 400mm diameter cylinder mould.

Trial No	Trial 2								
Weight of wet soil, g	150.35			151.44			150.72		
Diameter of wet soil, mm	38.08			37.8			37.51		
Length of wet soil, mm	73.46			75.73			76.27		
Volume, mm^3	83696.9			85019.0			84581.8		
Wet density, ρ kg/m^3	1796.4			1781.2			1781.9		
Average wet density, ρ kg/m^3	1786.5								
Container no.	L12	E	E2	B4	H7	A7	A3	PL1	PL2

Wet soil & container, g	22.87	37.44	27.61	27.01	33.56	31.33	31.2	27.28	23.81
Dry soil & container, g	17.86	28.43	21.17	21.3	25.99	24.48	23.83	21.14	18.36
Container, g	4	3.25	3.23	5.35	4.75	5.25	3.35	4.05	3.22
Dry soil, g	13.86	25.18	17.94	15.95	21.24	19.23	20.48	17.09	15.14
Moisture loss, g	5.01	9.01	6.44	5.71	7.57	6.85	7.37	6.14	5.45
Moisture content, %	36.15	35.78	35.90	35.80	35.64	35.62	35.99	35.93	36.00
Average moisture, %	35.9			35.7			36.0		
Average moisture, %	35.9								
Dry density, ρd Mg/m^3	1321.4			1312.8			1310.5		
Average dry density, ρd Mg/m^3	1314.9								

Remarks: Sample preparation by vibrating hammer for 15 second on 60mm thicknesss of loose soil layer on 400mm diameter cylinder mould.

A(2e) Plot trial compaction using vibrating hammer and dietert compaction in Oxford clay.

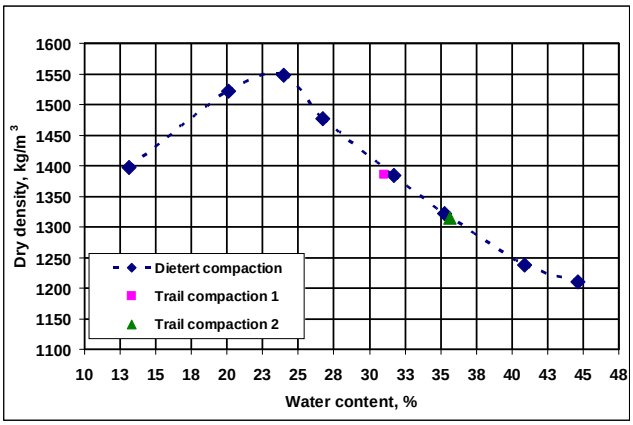

A(3) Data of specific gravity test

A(3a) Data of specific gravity test on Oxford clay

Bottle no	A	B	C
Bottle + stopper, m1	30.9	31.36	29.53
Bottle + stopper + soil, m2	35.46	37.54	35.7
Bottle + stopper + soil + liquid, m3	87.23	89.17	84.75
Bottle + stopper + liquid, m4	84.43	85.38	80.94
Gs=GL(m2-m1)/[(m4-m1)-(m3-m2)]	2.59	2.59	2.61
Average	2.60		

A(3b) Data of specific gravity test on kaolin

Bottle no	1	2	3
Bottle + stopper, m1	30.74	30.29	30.33
Bottle + stopper + soil, m2	36.25	35.05	35.12
Bottle + stopper + soil + liquid, m3	86.14	86.77	82.75
Bottle + stopper + liquid, m4	82.69	83.81	79.79
Gs=GL(m2-m1)/[(m4-m1)-(m3-m2)]	2.67	2.64	2.62
Average	2.65		

A(3c) Data of specific gravity test on gravelly sand

Bottle no	B	1145	94	44
Bottle + stopper, m1	31.36	36.27	17.81	20.89
Bottle + stopper + soil, m2	38.11	42.47	21.22	25.63
Bottle + stopper + soil + liquid, m3	89.66	137.38	44.11	48.86
Bottle + stopper + liquid, m4	85.38	133.48	41.97	45.88
Gs=GL(m2-m1)/[(m4-m1)-(m3-m2)]	2.73	2.70	2.69	2.69
Average	2.70			

Remarks: Liquid using de-ionised water

A(4) Data of quick undrained triaxial test in Oxford clay

Summary of water content versus undrained shear strength test

Test no.	Water content, %	Undrained shear strength, kPa
1	31.2	39.2
2	32.2	32.7
3	35.6	24.5
4	35.9	20.4
5	36.8	20.5
6	41.8	14.2
7	38.8	18.5
8	43.8	13.0

A(4a) Data of quick undrained triaxial in Oxford clay test 1 at average water content, 31.2 %

Sample 1 = 50kPa			Moisture content			
Weight	g	142.77	Tin no	A	H7	A7
Length of sample	mm	69.57	Wet weight, g	24.97	20.4	19.97
Diameter of sample	mm	37.96	Dry weight, g	20.34	16.69	16.47
Area of sample	mm^2	1132.18	Tin empty, g	5.36	4.75	5.27

Horizontal stress		kPa	50	Dry soil, g		14.98	11.94	11.2
Force gauge correction factor		kN/division	0.0004	Weight of water, g		4.63	3.71	3.5
Corrected compression gauge reading		mm	0.01mm	Moisture content %		30.91	31.07	31.25
Shear strength		kPa	38.66	Average		31.1		
Compression gauge reading (div)	Force gauge reading (div)	Corrected compression gauge reading (mm)	Corrected force gauge reading (div)	Axial strain	Corrected area (mm2)	Force (kN)	Deviator stress (kN/m2)	Vertical stress (kN/m2)
0	0	0	0	0.000	1132.18	0	0.00	50.00
50	33	0.5	33	0.007	1140.38	0.0132	11.58	61.58
100	35	1	35	0.014	1148.69	0.014	12.19	62.19
150	44	1.5	44	0.022	1157.13	0.0176	15.21	65.21
200	58	2	58	0.029	1165.69	0.0232	19.90	69.90
250	110	2.5	110	0.036	1174.38	0.044	37.47	87.47
300	132	3	132	0.043	1183.20	0.0528	44.62	94.62
350	145	3.5	145	0.050	1192.16	0.058	48.65	98.65
400	156	4	156	0.057	1201.25	0.0624	51.95	101.95
450	166	4.5	166	0.065	1210.48	0.0664	54.85	104.85
500	174	5	174	0.072	1219.85	0.0696	57.06	107.06
550	182	5.5	182	0.079	1229.37	0.0728	59.22	109.22
600	190	6	190	0.086	1239.04	0.076	61.34	111.34
650	196	6.5	196	0.093	1248.86	0.0784	62.78	112.78
700	203	7	203	0.101	1258.84	0.0812	64.50	114.50
750	208	7.5	208	0.108	1268.98	0.0832	65.56	115.56
800	215	8	215	0.115	1279.29	0.086	67.22	117.22
850	220	8.5	220	0.122	1289.76	0.088	68.23	118.23
900	228	9	228	0.129	1300.41	0.0912	70.13	120.13
950	232	9.5	232	0.137	1311.23	0.0928	70.77	120.77
1000	237	10	237	0.144	1322.24	0.0948	71.70	121.70
1050	243	10.5	243	0.151	1333.43	0.0972	72.89	122.89
1100	246	11	246	0.158	1344.81	0.0984	73.17	123.17
1150	252	11.5	252	0.165	1356.39	0.1008	74.31	124.31
1200	257	12	257	0.172	1368.17	0.1028	75.14	125.14
1250	261	12.5	261	0.180	1380.16	0.1044	75.64	125.64
1300	266	13	266	0.187	1392.36	0.1064	76.42	126.42
1350	270	13.5	270	0.194	1404.78	0.108	76.88	126.88
1400	274	14	274	0.201	1417.42	0.1096	77.32	127.32
1450	279	14.5	279	0.208	1430.28	0.1116	78.03	128.03
1500	284	15	284	0.216	1443.39	0.1136	78.70	128.70
1550	286	15.5	286	0.223	1456.74	0.1144	78.53	128.53
1600	289	16	289	0.230	1470.33	0.1156	78.62	128.62
1650	294	16.5	294	0.237	1484.19	0.1176	79.24	129.24
1700	296	17	296	0.244	1498.30	0.1184	79.02	129.02
1750	300	17.5	300	0.252	1512.69	0.12	79.33	129.33
1800	301	18	301	0.259	1527.36	0.1204	78.83	128.83
1850	301	18.5	301	0.266	1542.31	0.1204	78.06	128.06

1900	302	19	302	0.273	1557.56	0.1208	77.56	127.56
1950	302	19.5	302	0.280	1573.11	0.1208	76.79	126.79
2000	302	20	302	0.287	1588.98	0.1208	76.02	126.02

Sample 2 = 100kPa				Moisture content				
Weight		g	137.61	Tin no		A3	7	D31
Length of sample		mm	67.05	Wet weight, g		27.79	25.91	29.86
Diameter of sample		mm	37.96	Dry weight, g		22.1	20.54	23.53
Area of sample		mm^2	1132.18	Tin empty, g		4.05	3.36	3.21
Horizontal stress		kPa	50	Dry soil, g		18.05	17.18	20.32
Force gauge correction factor		kN/division	0.0004	Weight of water, g		5.69	5.37	6.33
Corrected compression gauge reading		mm	0.01mm	Moisture content %		31.52	31.26	31.15
Shear strength		kPa	36.96	Average		31.3		
Compression gauge reading (div)	Force gauge reading (div)	Corrected compression gauge reading (mm)	Corrected force gauge reading (div)	Axial strain	Corrected area (mm2)	Force (kN)	Deviator stress (kN/m2)	Vertical stress (kN/m2)
0	0	0	0	0.000	1132.18	0	0.00	100.00
50	35	0.5	35	0.007	1140.69	0.014	12.27	112.27
100	47	1	47	0.015	1149.32	0.0188	16.36	116.36
150	92	1.5	92	0.022	1158.09	0.0368	31.78	131.78
200	103	2	103	0.030	1166.99	0.0412	35.30	135.30
250	128	2.5	128	0.037	1176.03	0.0512	43.54	143.54
300	147	3	147	0.045	1185.21	0.0588	49.61	149.61
350	157	3.5	157	0.052	1194.53	0.0628	52.57	152.57
400	167	4	167	0.060	1204.01	0.0668	55.48	155.48
450	175	4.5	175	0.067	1213.63	0.07	57.68	157.68
500	184	5	184	0.075	1223.41	0.0736	60.16	160.16
550	191	5.5	191	0.082	1233.35	0.0764	61.95	161.95
600	201	6	201	0.089	1243.45	0.0804	64.66	164.66
650	209	6.5	209	0.097	1253.72	0.0836	66.68	166.68
700	218	7	218	0.104	1264.16	0.0872	68.98	168.98
750	225	7.5	225	0.112	1274.77	0.09	70.60	170.60
800	231	8	231	0.119	1285.57	0.0924	71.87	171.87
850	235	8.5	235	0.127	1296.54	0.094	72.50	172.50
900	239	9	239	0.134	1307.71	0.0956	73.10	173.10
950	241	9.5	241	0.142	1319.07	0.0964	73.08	173.08
1000	243	10	243	0.149	1330.63	0.0972	73.05	173.05
1050	246	10.5	246	0.157	1342.40	0.0984	73.30	173.30
1100	249	11	249	0.164	1354.37	0.0996	73.54	173.54
1150	251	11.5	251	0.172	1366.56	0.1004	73.47	173.47
1200	255	12	255	0.179	1378.98	0.102	73.97	173.97
1250	257	12.5	257	0.186	1391.62	0.1028	73.87	173.87
1300	259	13	259	0.194	1404.49	0.1036	73.76	173.76
1350	262	13.5	262	0.201	1417.60	0.1048	73.93	173.93
1400	264	14	264	0.209	1430.96	0.1056	73.80	173.80
1450	265	14.5	265	0.216	1444.58	0.106	73.38	173.38

1500	266	15	266	0.224	1458.46	0.1064	72.95	172.95
1550	267	15.5	267	0.231	1472.60	0.1068	72.52	172.52
1600	268	16	268	0.239	1487.03	0.1072	72.09	172.09
1650	269	16.5	269	0.246	1501.73	0.1076	71.65	171.65
1700	270	17	270	0.254	1516.74	0.108	71.21	171.21
1750	272	17.5	272	0.261	1532.04	0.1088	71.02	171.02
1800	272	18	272	0.268	1547.66	0.1088	70.30	170.30
1850	272	18.5	272	0.276	1563.60	0.1088	69.58	169.58
1900	273	19	273	0.283	1579.87	0.1092	69.12	169.12
1950	273	19.5	273	0.291	1596.48	0.1092	68.40	168.40
2000	273	20	273	0.298	1613.45	0.1092	67.68	167.68

Sample 3 = 150kPa				Tin no		F	17	9E
Weight		g	129.94	Wet weight, g		35.06	25.28	24.4
Length of sample		mm	63.31	Dry weight, g		27.48	20.28	19.39
Diameter of sample		mm	37.96	Tin empty, g		3.24	4.07	3.39
Area of sample		mm^2	1132.18	Dry soil, g		24.24	16.21	16
Horizontal stress		kPa	50	Weight of water, g		7.58	5	5.01
Force gauge correction factor		kN/division	0.0004	Moisture content %		31.27	30.85	31.31
Corrected compression gauge reading		mm	0.01mm	Average		31.1		
Shear strength		kPa	41.97					
Compression gauge reading (div)	Force gauge reading (div)	Corrected compression gauge reading (mm)	Corrected force gauge reading (div)	Axial strain	Corrected area (mm2)	Force (kN)	Deviator stress (kN/m2)	Vertical stress (kN/m2)
0	0	0	0	0.000	1132.18	0	0.00	150.00
50	35	0.5	35	0.008	1141.19	0.014	12.27	162.27
100	46	1	46	0.016	1150.35	0.0184	16.00	166.00
150	95	1.5	95	0.024	1159.66	0.038	32.77	182.77
200	126	2	126	0.032	1169.11	0.0504	43.11	193.11
250	142	2.5	142	0.039	1178.73	0.0568	48.19	198.19
300	154	3	154	0.047	1188.50	0.0616	51.83	201.83
350	165	3.5	165	0.055	1198.43	0.066	55.07	205.07
400	176	4	176	0.063	1208.54	0.0704	58.25	208.25
450	187	4.5	187	0.071	1218.81	0.0748	61.37	211.37
500	196	5	196	0.079	1229.26	0.0784	63.78	213.78
550	205	5.5	205	0.087	1239.89	0.082	66.13	216.13
600	214	6	214	0.095	1250.71	0.0856	68.44	218.44
650	222	6.5	222	0.103	1261.72	0.0888	70.38	220.38
700	230	7	230	0.111	1272.92	0.092	72.27	222.27
750	237	7.5	237	0.118	1284.33	0.0948	73.81	223.81
800	245	8	245	0.126	1295.94	0.098	75.62	225.62
850	251	8.5	251	0.134	1307.76	0.1004	76.77	226.77
900	258	9	258	0.142	1319.80	0.1032	78.19	228.19
950	265	9.5	265	0.150	1332.06	0.106	79.58	229.58
1000	271	10	271	0.158	1344.56	0.1084	80.62	230.62
1050	277	10.5	277	0.166	1357.29	0.1108	81.63	231.63
1100	282	11	282	0.174	1370.26	0.1128	82.32	232.32

1150	288	11.5	288	0.182	1383.48	0.1152	83.27	233.27
1200	291	12	291	0.190	1396.97	0.1164	83.32	233.32
1250	295	12.5	295	0.197	1410.71	0.118	83.65	233.65
1300	299	13	299	0.205	1424.73	0.1196	83.95	233.95
1350	303	13.5	303	0.213	1439.03	0.1212	84.22	234.22
1400	306	14	306	0.221	1453.63	0.1224	84.20	234.20
1450	310	14.5	310	0.229	1468.52	0.124	84.44	234.44
1500	314	15	314	0.237	1483.72	0.1256	84.65	234.65
1550	317	15.5	317	0.245	1499.23	0.1268	84.58	234.58
1600	321	16	321	0.253	1515.08	0.1284	84.75	234.75
1650	326	16.5	326	0.261	1531.26	0.1304	85.16	235.16
1700	331	17	331	0.269	1547.79	0.1324	85.54	235.54
1750	333	17.5	333	0.276	1564.69	0.1332	85.13	235.13
1800	335	18	335	0.284	1581.95	0.134	84.71	234.71
1850	338	18.5	338	0.292	1599.61	0.1352	84.52	234.52
1900	340	19	340	0.300	1617.66	0.136	84.07	234.07
Average water content sample 1, 2 and 3, %				**Average shear strength sample 1, 2 and 3, kPa**				
31.2				**39.2**				

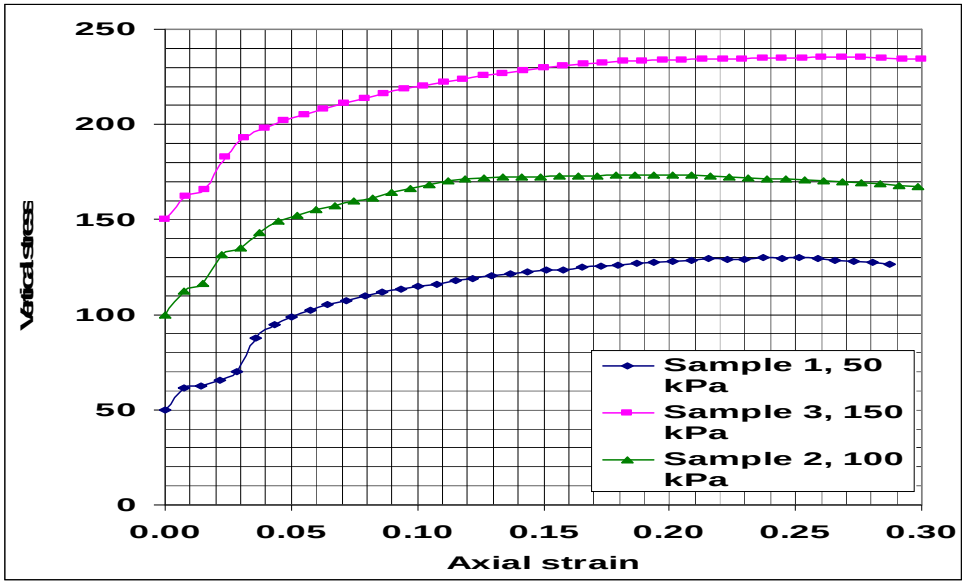

A(4b) Data of quick undrained triaxial in Oxford clay test 2 at average water content 32.8 %

Sample 1 = 50kPa			Moisture content			
Weight	g	158.37	Tin no	A28		
Length of sample	mm	76.14	Wet weight, g	161.24		
Diameter of sample	mm	37.96	Dry weight, g	123.27		
Area of sample	mm^2	1132.18	Tin empty, g	3.21		
Horizontal stress	kPa	50	Dry soil, g	120.06		

Force gauge correction factor		kN/division	0.0004	Weight of water, g		37.97		
Corrected compression gauge reading		mm	0.01	Moisture content %		31.63		
Shear strength		kPa	33.77					
Compression gauge reading (div)	Force gauge reading (div)	Corrected compression gauge reading (mm)	Corrected force gauge reading (div)	Axial strain	Corrected area (mm2)	Force (kN)	Deviator stress (kN/m2)	Vertical stress (kN/m2)
0	0	0	0	0.000	1132.18	0	0.00	50.00
50	61	0.5	61	0.007	1139.66	0.0244	21.41	71.41
100	81	1	81	0.013	1147.25	0.0324	28.24	78.24
150	94	1.5	94	0.020	1154.93	0.0376	32.56	82.56
200	104	2	104	0.026	1162.72	0.0416	35.78	85.78
250	118	2.5	118	0.033	1170.62	0.0472	40.32	90.32
300	126	3	126	0.039	1178.62	0.0504	42.76	92.76
350	134	3.5	134	0.046	1186.73	0.0536	45.17	95.17
400	141	4	141	0.053	1194.96	0.0564	47.20	97.20
450	149	4.5	149	0.059	1203.30	0.0596	49.53	99.53
500	155	5	155	0.066	1211.75	0.062	51.17	101.17
550	160	5.5	160	0.072	1220.33	0.064	52.44	102.44
600	167	6	167	0.079	1229.03	0.0668	54.35	104.35
650	172	6.5	172	0.085	1237.85	0.0688	55.58	105.58
700	177	7	177	0.092	1246.81	0.0708	56.79	106.79
750	182	7.5	182	0.099	1255.89	0.0728	57.97	107.97
800	187	8	187	0.105	1265.10	0.0748	59.13	109.13
850	192	8.5	192	0.112	1274.46	0.0768	60.26	110.26
900	197	9	197	0.118	1283.95	0.0788	61.37	111.37
950	201	9.5	201	0.125	1293.58	0.0804	62.15	112.15
1000	205	10	205	0.131	1303.36	0.082	62.91	112.91
1050	208	10.5	208	0.138	1313.29	0.0832	63.35	113.35
1100	212	11	212	0.144	1323.37	0.0848	64.08	114.08
1150	215	11.5	215	0.151	1333.60	0.086	64.49	114.49
1200	219	12	219	0.158	1344.00	0.0876	65.18	115.18
1250	223	12.5	223	0.164	1354.56	0.0892	65.85	115.85
1300	226	13	226	0.171	1365.29	0.0904	66.21	116.21
1350	229	13.5	229	0.177	1376.18	0.0916	66.56	116.56
1400	232	14	232	0.184	1387.26	0.0928	66.89	116.89
1450	234	14.5	234	0.190	1398.51	0.0936	66.93	116.93
1500	237	15	237	0.197	1409.95	0.0948	67.24	117.24
1550	240	15.5	240	0.204	1421.57	0.096	67.53	117.53
1600	243	16	243	0.210	1433.39	0.0972	67.81	117.81
1650	245	16.5	245	0.217	1445.41	0.098	67.80	117.80
1700	247	17	247	0.223	1457.63	0.0988	67.78	117.78
1750	249	17.5	249	0.230	1470.06	0.0996	67.75	117.75
1800	251	18	251	0.236	1482.70	0.1004	67.71	117.71
1850	253	18.5	253	0.243	1495.56	0.1012	67.67	117.67
1900	255	19	255	0.250	1508.65	0.102	67.61	117.61
1950	258	19.5	258	0.256	1521.97	0.1032	67.81	117.81
2000	261	20	261	0.263	1535.52	0.1044	67.99	117.99

Sample 2 = 100kPa				Moisture content				
Weight		g	157.86	Tin no		B7		
Length of sample		mm	76.14	Wet weight, g		161.49		
Diameter of sample		mm	37.96	Dry weight, g		122.81		
Area of sample		mm^2	1132.18	Tin empty, g		4.02		
Horizontal stress		kPa	100	Dry soil, g		118.79		
Force gauge correction factor		kN/division	0.0004	Weight of water, g		38.68		
Corrected compression gauge reading		mm	0.01mm	Moisture content %		32.56		
Shear strength		kPa	30.25					
Compression gauge reading (div)	Force gauge reading (div)	Corrected compression gauge reading (mm)	Corrected force gauge reading (div)	Axial strain	Corrected area (mm2)	Force (kN)	Deviator stress (kN/m2)	Vertical stress (kN/m2)
0	0	0	0	0.000	1132.18	0	0.00	100.00
50	26	0.5	26	0.007	1139.66	0.0104	9.13	109.13
100	45	1	45	0.013	1147.25	0.018	15.69	115.69
150	60	1.5	60	0.020	1154.93	0.024	20.78	120.78
200	71	2	71	0.026	1162.72	0.0284	24.43	124.43
250	79	2.5	79	0.033	1170.62	0.0316	26.99	126.99
300	86	3	86	0.039	1178.62	0.0344	29.19	129.19
350	95	3.5	95	0.046	1186.73	0.038	32.02	132.02
400	101	4	101	0.053	1194.96	0.0404	33.81	133.81
450	109	4.5	109	0.059	1203.30	0.0436	36.23	136.23
500	115	5	115	0.066	1211.75	0.046	37.96	137.96
550	122	5.5	122	0.072	1220.33	0.0488	39.99	139.99
600	128	6	128	0.079	1229.03	0.0512	41.66	141.66
650	134	6.5	134	0.085	1237.85	0.0536	43.30	143.30
700	140	7	140	0.092	1246.81	0.056	44.91	144.91
750	146	7.5	146	0.099	1255.89	0.0584	46.50	146.50
800	151	8	151	0.105	1265.10	0.0604	47.74	147.74
850	156	8.5	156	0.112	1274.46	0.0624	48.96	148.96
900	162	9	162	0.118	1283.95	0.0648	50.47	150.47
950	166	9.5	166	0.125	1293.58	0.0664	51.33	151.33
1000	171	10	171	0.131	1303.36	0.0684	52.48	152.48
1050	176	10.5	176	0.138	1313.29	0.0704	53.61	153.61
1100	180	11	180	0.144	1323.37	0.072	54.41	154.41
1150	183	11.5	183	0.151	1333.60	0.0732	54.89	154.89
1200	187	12	187	0.158	1344.00	0.0748	55.65	155.65
1250	191	12.5	191	0.164	1354.56	0.0764	56.40	156.40
1300	196	13	196	0.171	1365.29	0.0784	57.42	157.42
1350	200	13.5	200	0.177	1376.18	0.08	58.13	158.13
1400	204	14	204	0.184	1387.26	0.0816	58.82	158.82
1450	207	14.5	207	0.190	1398.51	0.0828	59.21	159.21
1500	210	15	210	0.197	1409.95	0.084	59.58	159.58
1550	215	15.5	215	0.204	1421.57	0.086	60.50	160.50
1600	218	16	218	0.210	1433.39	0.0872	60.83	160.83

1650	221	16.5	221	0.217	1445.41	0.0884	61.16	161.16
1700	224	17	224	0.223	1457.63	0.0896	61.47	161.47
1750	227	17.5	227	0.230	1470.06	0.0908	61.77	161.77
1800	232	18	232	0.236	1482.70	0.0928	62.59	162.59
1850	239	18.5	239	0.243	1495.56	0.0956	63.92	163.92
1900	242	19	242	0.250	1508.65	0.0968	64.16	164.16
1950	245	19.5	245	0.256	1521.97	0.098	64.39	164.39
2000	248	20	248	0.263	1535.52	0.0992	64.60	164.60

Sample 3 = 150kPa				Tin no		B7		
Weight		g	157.11	Wet weight, g		160.67		
Length of sample		mm	76.14	Dry weight, g		122.2		
Diameter of sample		mm	37.96	Tin empty, g		3.9		
Area of sample		mm^2	1132.18	Dry soil, g		118.3		
Horizontal stress		kPa	150	Weight of water, g		38.47		
Force gauge correction factor		kN/division	0.0004	Moisture content %		32.52		
Corrected compression gauge reading		mm	0.01mm					
Shear strength		kPa	34.05					
Compression gauge reading (div)	Force gauge reading (div)	Corrected compression gauge reading (mm)	Corrected force gauge reading (div)	Axial strain	Corrected area (mm2)	Force (kN)	Deviator stress (kN/m2)	Vertical stress (kN/m2)
0	0	0	0	0.000	1132.18	0	0.00	150.00
50	30	0.5	30	0.007	1139.66	0.012	10.53	160.53
100	32	1	32	0.013	1147.25	0.0128	11.16	161.16
150	55	1.5	55	0.020	1154.93	0.022	19.05	169.05
200	74	2	74	0.026	1162.72	0.0296	25.46	175.46
250	88	2.5	88	0.033	1170.62	0.0352	30.07	180.07
300	101	3	101	0.039	1178.62	0.0404	34.28	184.28
350	112	3.5	112	0.046	1186.73	0.0448	37.75	187.75
400	124	4	124	0.053	1194.96	0.0496	41.51	191.51
450	133	4.5	133	0.059	1203.30	0.0532	44.21	194.21
500	142	5	142	0.066	1211.75	0.0568	46.87	196.87
550	151	5.5	151	0.072	1220.33	0.0604	49.49	199.49
600	158	6	158	0.079	1229.03	0.0632	51.42	201.42
650	164	6.5	164	0.085	1237.85	0.0656	52.99	202.99
700	171	7	171	0.092	1246.81	0.0684	54.86	204.86
750	177	7.5	177	0.099	1255.89	0.0708	56.37	206.37
800	183	8	183	0.105	1265.10	0.0732	57.86	207.86
850	189	8.5	189	0.112	1274.46	0.0756	59.32	209.32
900	194	9	194	0.118	1283.95	0.0776	60.44	210.44
950	199	9.5	199	0.125	1293.58	0.0796	61.53	211.53
1000	205	10	205	0.131	1303.36	0.082	62.91	212.91
1050	210	10.5	210	0.138	1313.29	0.084	63.96	213.96
1100	213	11	213	0.144	1323.37	0.0852	64.38	214.38
1150	218	11.5	218	0.151	1333.60	0.0872	65.39	215.39
1200	221	12	221	0.158	1344.00	0.0884	65.77	215.77

1250	224	12.5	224	0.164	1354.56	0.0896	66.15	216.15
1300	228	13	228	0.171	1365.29	0.0912	66.80	216.80
1350	231	13.5	231	0.177	1376.18	0.0924	67.14	217.14
1400	234	14	234	0.184	1387.26	0.0936	67.47	217.47
1450	237	14.5	237	0.190	1398.51	0.0948	67.79	217.79
1500	239	15	239	0.197	1409.95	0.0956	67.80	217.80
1550	242	15.5	242	0.204	1421.57	0.0968	68.09	218.09
1600	244	16	244	0.210	1433.39	0.0976	68.09	218.09
1650	247	16.5	247	0.217	1445.41	0.0988	68.35	218.35
1700	249	17	249	0.223	1457.63	0.0996	68.33	218.33
1750	252	17.5	252	0.230	1470.06	0.1008	68.57	218.57
1800	254	18	254	0.236	1482.70	0.1016	68.52	218.52
1850	256	18.5	256	0.243	1495.56	0.1024	68.47	218.47
1900	258	19	258	0.250	1508.65	0.1032	68.41	218.41
1950	260	19.5	260	0.256	1521.97	0.104	68.33	218.33
2000	262	20	262	0.263	1535.52	0.1048	68.25	218.25
Average water content sample 1, 2 and 3, %				**Average shear strength sample 1, 2 and 3, kPa**				
32.2				**32.7**				

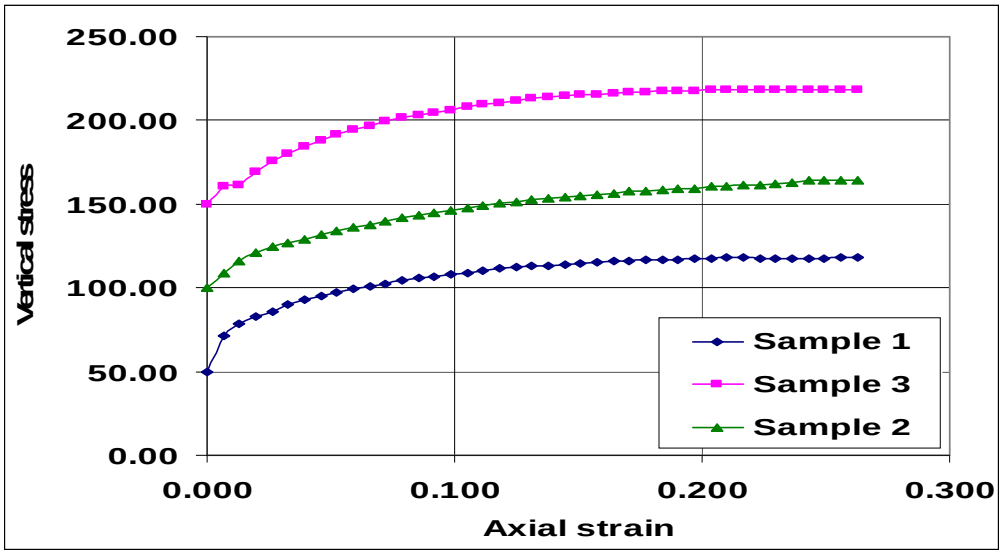

A(4c) Data of quick undrained triaxial in Oxford clay test 3 at average water content 35.7 %

Sample 1 = 50kPa			Moisture content			
Weight	g	152.74	Tin no	F		
Length of sample	mm	76.14	Wet weight, g	157.56		
Diameter of sample	mm	37.96	Dry weight, g	117.64		
Area of sample	mm^2	1132.18	Tin empty, g	5.38		
Horizontal stress	kPa	50	Dry soil, g	112.26		
Force gauge	kN/division	0.0004	Weight of water,	39.92		

correction factor				g				
Corrected compression gauge reading		mm	0.01mm	Moisture content %		35.56		
Shear strength		kPa	25.75					
Comression gauge reading (div)	Force gauge reading (div)	Corrected compression gauge reading (mm)	Corrected force gauge reading (div)	Axial strain	Corrected area (mm2)	Force (kN)	Deviator stress (kN/m2)	Vertical stress (kN/m2)
0	0	0	0	0.000	1132.18	0	0.00	50.00
50	62	0.5	62	0.007	1139.66	0.0248	21.76	71.76
100	82	1	82	0.013	1147.25	0.0328	28.59	78.59
150	92	1.5	92	0.020	1154.93	0.0368	31.86	81.86
200	99	2	99	0.026	1162.72	0.0396	34.06	84.06
250	103	2.5	103	0.033	1170.62	0.0412	35.20	85.20
300	108	3	108	0.039	1178.62	0.0432	36.65	86.65
350	112	3.5	112	0.046	1186.73	0.0448	37.75	87.75
400	116	4	116	0.053	1194.96	0.0464	38.83	88.83
450	120	4.5	120	0.059	1203.30	0.048	39.89	89.89
500	127	5	127	0.066	1211.75	0.0508	41.92	91.92
550	133	5.5	133	0.072	1220.33	0.0532	43.59	93.59
600	136	6	136	0.079	1229.03	0.0544	44.26	94.26
650	140	6.5	140	0.085	1237.85	0.056	45.24	95.24
700	143	7	143	0.092	1246.81	0.0572	45.88	95.88
750	146	7.5	146	0.099	1255.89	0.0584	46.50	96.50
800	150	8	150	0.105	1265.10	0.06	47.43	97.43
850	153	8.5	153	0.112	1274.46	0.0612	48.02	98.02
900	156	9	156	0.118	1283.95	0.0624	48.60	98.60
950	159	9.5	159	0.125	1293.58	0.0636	49.17	99.17
1000	162	10	162	0.131	1303.36	0.0648	49.72	99.72
1050	164	10.5	164	0.138	1313.29	0.0656	49.95	99.95
1100	166	11	166	0.144	1323.37	0.0664	50.18	100.18
1150	169	11.5	169	0.151	1333.60	0.0676	50.69	100.69
1200	170	12	170	0.158	1344.00	0.068	50.60	100.60
1250	171	12.5	171	0.164	1354.56	0.0684	50.50	100.50
1300	175	13	175	0.171	1365.29	0.07	51.27	101.27
1350	176	13.5	176	0.177	1376.18	0.0704	51.16	101.16
1400	178	14	178	0.184	1387.26	0.0712	51.32	101.32
1450	179	14.5	179	0.190	1398.51	0.0716	51.20	101.20
1500	181	15	181	0.197	1409.95	0.0724	51.35	101.35
1550	183	15.5	183	0.204	1421.57	0.0732	51.49	101.49
1600	185	16	185	0.210	1433.39	0.074	51.63	101.63
1650	187	16.5	187	0.217	1445.41	0.0748	51.75	101.75
1700	188	17	188	0.223	1457.63	0.0752	51.59	101.59
1750	190	17.5	190	0.230	1470.06	0.076	51.70	101.70
1800	192	18	192	0.236	1482.70	0.0768	51.80	101.80
1850	194	18.5	194	0.243	1495.56	0.0776	51.89	101.89
1900	197	19	197	0.250	1508.65	0.0788	52.23	102.23
1950	198	19.5	198	0.256	1521.97	0.0792	52.04	102.04
2000	200	20	200	0.263	1535.52	0.08	52.10	102.10

Sample 2 = 100kPa				Moisture content				
Weight		g	129.34	Tin no		F		
Length of sample		mm	64.46	Wet weight, g		157.56		
Diameter of sample		mm	37.96	Dry weight, g		117.64		
Area of sample		mm^2	1132.18	Tin empty, g		5.38		
Horizontal stress		kPa	50	Dry soil, g		112.26		
Force gauge correction factor		kN/division	0.0004	Weight of water, g		39.92		
Corrected compression gauge reading		mm	0.01mm	Moisture content %		35.56		
Shear strength		kPa	22.85					
Compression gauge reading (div)	Force gauge reading (div)	Corrected compression gauge reading (mm)	Corrected force gauge reading (div)	Axial strain	Corrected area (mm2)	Force (kN)	Deviator stress (kN/m2)	Vertical stress (kN/m2)
0	0	0	0	0.000	1132.18	0	0.00	100.00
50	26	0.5	26	0.008	1141.03	0.0104	9.11	109.11
100	54	1	54	0.016	1150.02	0.0216	18.78	118.78
150	66	1.5	66	0.023	1159.15	0.0264	22.78	122.78
200	76	2	76	0.031	1168.43	0.0304	26.02	126.02
250	81	2.5	81	0.039	1177.86	0.0324	27.51	127.51
300	86	3	86	0.047	1187.44	0.0344	28.97	128.97
350	91	3.5	91	0.054	1197.18	0.0364	30.40	130.40
400	96	4	96	0.062	1207.08	0.0384	31.81	131.81
450	101	4.5	101	0.070	1217.15	0.0404	33.19	133.19
500	106	5	106	0.078	1227.39	0.0424	34.54	134.54
550	111	5.5	111	0.085	1237.79	0.0444	35.87	135.87
600	115	6	115	0.093	1248.38	0.046	36.85	136.85
650	119	6.5	119	0.101	1259.15	0.0476	37.80	137.80
700	123	7	123	0.109	1270.11	0.0492	38.74	138.74
750	127	7.5	127	0.116	1281.26	0.0508	39.65	139.65
800	131	8	131	0.124	1292.60	0.0524	40.54	140.54
850	135	8.5	135	0.132	1304.15	0.054	41.41	141.41
900	138	9	138	0.140	1315.91	0.0552	41.95	141.95
950	141	9.5	141	0.147	1327.88	0.0564	42.47	142.47
1000	144	10	144	0.155	1340.07	0.0576	42.98	142.98
1050	148	10.5	148	0.163	1352.49	0.0592	43.77	143.77
1100	150	11	150	0.171	1365.14	0.06	43.95	143.95
1150	154	11.5	154	0.178	1378.03	0.0616	44.70	144.70
1200	157	12	157	0.186	1391.16	0.0628	45.14	145.14
1250	160	12.5	160	0.194	1404.55	0.064	45.57	145.57
1300	162	13	162	0.202	1418.20	0.0648	45.69	145.69
1350	164	13.5	164	0.209	1432.11	0.0656	45.81	145.81
1400	166	14	166	0.217	1446.30	0.0664	45.91	145.91
1450	168	14.5	168	0.225	1460.78	0.0672	46.00	146.00
1500	171	15	171	0.233	1475.54	0.0684	46.36	146.36
1550	174	15.5	174	0.240	1490.61	0.0696	46.69	146.69
1600	179	16	179	0.248	1505.99	0.0716	47.54	147.54
1650	184	16.5	184	0.256	1521.69	0.0736	48.37	148.37

1700	189	17	189	0.264	1537.72	0.0756	49.16	149.16
1750	191	17.5	191	0.271	1554.10	0.0764	49.16	149.16
1800	193	18	193	0.279	1570.82	0.0772	49.15	149.15
1850	195	18.5	195	0.287	1587.91	0.078	49.12	149.12
1900	196	19	196	0.295	1605.37	0.0784	48.84	148.84
1950	196	19.5	196	0.303	1623.23	0.0784	48.30	148.30
2000	196	20	196	0.310	1641.48	0.0784	47.76	147.76

Sample 3 = 150kPa				Tin no		A3		
Weight		g	151.36	Wet weight, g		154.3		
Length of sample		mm	76.14	Dry weight, g		114.58		
Diameter of sample		mm	37.96	Tin empty, g		3.23		
Area of sample		mm^2	1132.18	Dry soil, g		111.35		
Horizontal stress		kPa	50	Weight of water, g		39.72		
Force gauge correction factor		kN/division	0.0004	Moisture content %		35.67		
Corrected compression gauge reading		mm	0.01					
Shear strength		kPa	24.90					
Compression gauge reading (div)	Force gauge reading (div)	Corrected compression gauge reading (mm)	Corrected force gauge reading (div)	Axial strain	Corrected area (mm2)	Force (kN)	Deviator stress (kN/m2)	Vertical stress (kN/m2)
0	0	0	0	0.000	1132.18	0	0.00	150.00
50	42	0.5	42	0.007	1139.66	0.0168	14.74	164.74
100	60	1	60	0.013	1147.25	0.024	20.92	170.92
150	78	1.5	78	0.020	1154.93	0.0312	27.01	177.01
200	87	2	87	0.026	1162.72	0.0348	29.93	179.93
250	94	2.5	94	0.033	1170.62	0.0376	32.12	182.12
300	100	3	100	0.039	1178.62	0.04	33.94	183.94
350	106	3.5	106	0.046	1186.73	0.0424	35.73	185.73
400	112	4	112	0.053	1194.96	0.0448	37.49	187.49
450	116	4.5	116	0.059	1203.30	0.0464	38.56	188.56
500	120	5	120	0.066	1211.75	0.048	39.61	189.61
550	123	5.5	123	0.072	1220.33	0.0492	40.32	190.32
600	127	6	127	0.079	1229.03	0.0508	41.33	191.33
650	130	6.5	130	0.085	1237.85	0.052	42.01	192.01
700	134	7	134	0.092	1246.81	0.0536	42.99	192.99
750	138	7.5	138	0.099	1255.89	0.0552	43.95	193.95
800	142	8	142	0.105	1265.10	0.0568	44.90	194.90
850	145	8.5	145	0.112	1274.46	0.058	45.51	195.51
900	148	9	148	0.118	1283.95	0.0592	46.11	196.11
950	150	9.5	150	0.125	1293.58	0.06	46.38	196.38
1000	153	10	153	0.131	1303.36	0.0612	46.96	196.96
1050	156	10.5	156	0.138	1313.29	0.0624	47.51	197.51
1100	160	11	160	0.144	1323.37	0.064	48.36	198.36
1150	163	11.5	163	0.151	1333.60	0.0652	48.89	198.89
1200	165	12	165	0.158	1344.00	0.066	49.11	199.11

1250	167	12.5	167	0.164	1354.56	0.0668	49.31	199.31
1300	170	13	170	0.171	1365.29	0.068	49.81	199.81
1350	172	13.5	172	0.177	1376.18	0.0688	49.99	199.99
1400	174	14	174	0.184	1387.26	0.0696	50.17	200.17
1450	175	14.5	175	0.190	1398.51	0.07	50.05	200.05
1500	176	15	176	0.197	1409.95	0.0704	49.93	199.93
1550	177	15.5	177	0.204	1421.57	0.0708	49.80	199.80
1600	178	16	178	0.210	1433.39	0.0712	49.67	199.67
1650	179	16.5	179	0.217	1445.41	0.0716	49.54	199.54
1700	180	17	180	0.223	1457.63	0.072	49.40	199.40
1750	181	17.5	181	0.230	1470.06	0.0724	49.25	199.25
1800	182	18	182	0.236	1482.70	0.0728	49.10	199.10
1850	182	18.5	182	0.243	1495.56	0.0728	48.68	198.68
1900	182	19	182	0.250	1508.65	0.0728	48.26	198.26
1950	182	19.5	182	0.256	1521.97	0.0728	47.83	197.83
2000	182	20	182	0.263	1535.52	0.0728	47.41	197.41
Average water content sample 1, 2 and 3, %				**Average shear strength sample 1, 2 and 3, kPa**				
35.6				**24.5**				

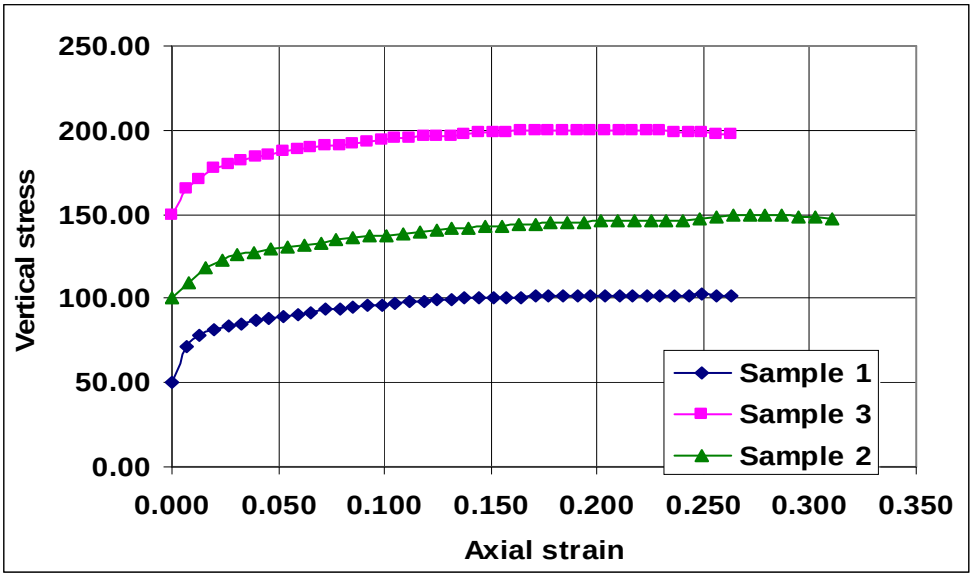

A(4d) Data of quick undrained triaxial in Oxford clay test 4 at average water content 35.9 %

Sample 1 = 50kPa			Moisture content			
Weight	g	150.35	Tin no	L12	E	E2
Length of sample	mm	76.14	Wet weight, g	22.87	37.44	27.61
Diameter of sample	mm	37.96	Dry weight, g	17.86	28.43	21.17
Area of sample	mm^2	1132.18	Tin empty, g	4	3.25	3.23
Horizontal stress	kPa	50	Dry soil, g	13.86	25.18	17.94

Force gauge correction factor		kN/division	0.0004	Weight of water, g		5.01	9.01	6.44
Corrected compression gauge reading		mm	0.01	Moisture content %		36.15	35.78	35.90
Shear strength		kPa	22.41	Average		35.9		
Comression gauge reading (div)	Force gauge reading (div)	Corrected compression gauge reading (mm)	Corrected force gauge reading (div)	Axial strain	Corrected area (mm2)	Force (kN)	Deviator stress (kN/m2)	Vertical stress (kN/m2)
0	0	0	0	0.000	1132.18	0	0.00	50.00
50	62	0.5	62	0.007	1139.66	0.0248	21.76	71.76
100	78	1	78	0.013	1147.25	0.0312	27.20	77.20
150	85	1.5	85	0.020	1154.93	0.034	29.44	79.44
200	92	2	92	0.026	1162.72	0.0368	31.65	81.65
250	96	2.5	96	0.033	1170.62	0.0384	32.80	82.80
300	100	3	100	0.039	1178.62	0.04	33.94	83.94
350	105	3.5	105	0.046	1186.73	0.042	35.39	85.39
400	109	4	109	0.053	1194.96	0.0436	36.49	86.49
450	111	4.5	111	0.059	1203.30	0.0444	36.90	86.90
500	116	5	116	0.066	1211.75	0.0464	38.29	88.29
550	119	5.5	119	0.072	1220.33	0.0476	39.01	89.01
600	123	6	123	0.079	1229.03	0.0492	40.03	90.03
650	125	6.5	125	0.085	1237.85	0.05	40.39	90.39
700	128	7	128	0.092	1246.81	0.0512	41.06	91.06
750	130	7.5	130	0.099	1255.89	0.052	41.40	91.40
800	132	8	132	0.105	1265.10	0.0528	41.74	91.74
850	135	8.5	135	0.112	1274.46	0.054	42.37	92.37
900	137	9	137	0.118	1283.95	0.0548	42.68	92.68
950	139	9.5	139	0.125	1293.58	0.0556	42.98	92.98
1000	140	10	140	0.131	1303.36	0.056	42.97	92.97
1050	141	10.5	141	0.138	1313.29	0.0564	42.95	92.95
1100	144	11	144	0.144	1323.37	0.0576	43.53	93.53
1150	145	11.5	145	0.151	1333.60	0.058	43.49	93.49
1200	148	12	148	0.158	1344.00	0.0592	44.05	94.05
1250	150	12.5	150	0.164	1354.56	0.06	44.29	94.29
1300	152	13	152	0.171	1365.29	0.0608	44.53	94.53
1350	153	13.5	153	0.177	1376.18	0.0612	44.47	94.47
1400	155	14	155	0.184	1387.26	0.062	44.69	94.69
1450	157	14.5	157	0.190	1398.51	0.0628	44.90	94.90
1500	158	15	158	0.197	1409.95	0.0632	44.82	94.82
1550	160	15.5	160	0.204	1421.57	0.064	45.02	95.02
1600	161	16	161	0.210	1433.39	0.0644	44.93	94.93
1650	163	16.5	163	0.217	1445.41	0.0652	45.11	95.11
1700	164	17	164	0.223	1457.63	0.0656	45.00	95.00
1750	165	17.5	165	0.230	1470.06	0.066	44.90	94.90
1800	165	18	165	0.236	1482.70	0.066	44.51	94.51
1850	166	18.5	166	0.243	1495.56	0.0664	44.40	94.40
1900	167	19	167	0.250	1508.65	0.0668	44.28	94.28
1950	168	19.5	168	0.256	1521.97	0.0672	44.15	94.15
2000	169	20	169	0.263	1535.52	0.0676	44.02	94.02

Sample 2 = 100kPa				Moisture content				
Weight		g	151.44	Tin no		B4	H7	A7
Length of sample		mm	76.14	Wet weight, g		27.01	33.56	31.33
Diameter of sample		mm	37.96	Dry weight, g		21.3	25.99	24.48
Area of sample		mm^2	1132.18	Tin empty, g		5.35	4.75	5.25
Horizontal stress		kPa	50	Dry soil, g		15.95	21.24	19.23
Force gauge correction factor		kN/division	0.0004	Weight of water, g		5.71	7.57	6.85
Corrected compression gauge reading		mm	0.01	Moisture content %		35.80	35.64	35.62
Shear strength		kPa	20.82	Average		35.7		
Compression gauge reading (div)	Force gauge reading (div)	Corrected compression gauge reading (mm)	Corrected force gauge reading (div)	Axial strain	Corrected area (mm2)	Force (kN)	Deviator stress (kN/m2)	Vertical stress (kN/m2)
0	0	0	0	0.000	1132.18	0	0.00	100.00
50	25	0.5	25	0.007	1139.66	0.01	8.77	108.77
100	48	1	48	0.013	1147.25	0.0192	16.74	116.74
150	68	1.5	68	0.020	1154.93	0.0272	23.55	123.55
200	76	2	76	0.026	1162.72	0.0304	26.15	126.15
250	81	2.5	81	0.033	1170.62	0.0324	27.68	127.68
300	85	3	85	0.039	1178.62	0.034	28.85	128.85
350	88	3.5	88	0.046	1186.73	0.0352	29.66	129.66
400	92	4	92	0.053	1194.96	0.0368	30.80	130.80
450	95	4.5	95	0.059	1203.30	0.038	31.58	131.58
500	99	5	99	0.066	1211.75	0.0396	32.68	132.68
550	103	5.5	103	0.072	1220.33	0.0412	33.76	133.76
600	107	6	107	0.079	1229.03	0.0428	34.82	134.82
650	110	6.5	110	0.085	1237.85	0.044	35.55	135.55
700	113	7	113	0.092	1246.81	0.0452	36.25	136.25
750	116	7.5	116	0.099	1255.89	0.0464	36.95	136.95
800	119	8	119	0.105	1265.10	0.0476	37.63	137.63
850	121	8.5	121	0.112	1274.46	0.0484	37.98	137.98
900	123	9	123	0.118	1283.95	0.0492	38.32	138.32
950	125	9.5	125	0.125	1293.58	0.05	38.65	138.65
1000	127	10	127	0.131	1303.36	0.0508	38.98	138.98
1050	130	10.5	130	0.138	1313.29	0.052	39.60	139.60
1100	133	11	133	0.144	1323.37	0.0532	40.20	140.20
1150	135	11.5	135	0.151	1333.60	0.054	40.49	140.49
1200	138	12	138	0.158	1344.00	0.0552	41.07	141.07
1250	140	12.5	140	0.164	1354.56	0.056	41.34	141.34
1300	141	13	141	0.171	1365.29	0.0564	41.31	141.31
1350	142	13.5	142	0.177	1376.18	0.0568	41.27	141.27
1400	143	14	143	0.184	1387.26	0.0572	41.23	141.23
1450	144	14.5	144	0.190	1398.51	0.0576	41.19	141.19
1500	146	15	146	0.197	1409.95	0.0584	41.42	141.42
1550	148	15.5	148	0.204	1421.57	0.0592	41.64	141.64
1600	150	16	150	0.210	1433.39	0.06	41.86	141.86

1650	152	16.5	152	0.217	1445.41	0.0608	42.06	142.06
1700	153	17	153	0.223	1457.63	0.0612	41.99	141.99
1750	155	17.5	155	0.230	1470.06	0.062	42.18	142.18
1800	156	18	156	0.236	1482.70	0.0624	42.09	142.09
1850	158	18.5	158	0.243	1495.56	0.0632	42.26	142.26
1900	160	19	160	0.250	1508.65	0.064	42.42	142.42
1950	161	19.5	161	0.256	1521.97	0.0644	42.31	142.31
2000	163	20	163	0.263	1535.52	0.0652	42.46	142.46
2050	164	20.5	164	0.269	1549.32	0.0656	42.34	142.34
2100	165	21	165	0.276	1563.37	0.066	42.22	142.22

Sample 3 = 150kPa				Tin no		A3	PL1	PL2
Weight		g	150.72	Wet weight, g		31.2	27.28	23.81
Length of sample		mm	76.27	Dry weight, g		23.83	21.14	18.36
Diameter of sample		mm	37.51	Tin empty, g		3.35	4.05	3.22
Area of sample		mm^2	1105.50	Dry soil, g		20.48	17.09	15.14
Horizontal stress		kPa	50	Weight of water, g		7.37	6.14	5.45
Force gauge correction factor		kN/division	0.0004	Moisture content %		35.99	35.93	36.00
Corrected compression gauge reading		mm	0.01	Average		36.0		
Shear strength		kPa	17.87					
Compression gauge reading (div)	Force gauge reading (div)	Corrected compression gauge reading (mm)	Corrected force gauge reading (div)	Axial strain	Corrected area (mm2)	Force (kN)	Deviator stress (kN/m2)	Vertical stress (kN/m2)
0	0	0	0	0.000	1132.18	0	0.00	150.00
50	18	0.5	18	0.007	1139.66	0.0072	6.32	156.32
100	22	1	22	0.013	1147.25	0.0088	7.67	157.67
150	45	1.5	45	0.020	1154.93	0.018	15.59	165.59
200	57	2	57	0.026	1162.72	0.0228	19.61	169.61
250	64	2.5	64	0.033	1170.62	0.0256	21.87	171.87
300	68	3	68	0.039	1178.62	0.0272	23.08	173.08
350	72	3.5	72	0.046	1186.73	0.0288	24.27	174.27
400	76	4	76	0.053	1194.96	0.0304	25.44	175.44
450	78	4.5	78	0.059	1203.30	0.0312	25.93	175.93
500	82	5	82	0.066	1211.75	0.0328	27.07	177.07
550	85	5.5	85	0.072	1220.33	0.034	27.86	177.86
600	88	6	88	0.079	1229.03	0.0352	28.64	178.64
650	90	6.5	90	0.085	1237.85	0.036	29.08	179.08
700	91	7	91	0.092	1246.81	0.0364	29.19	179.19
750	93	7.5	93	0.099	1255.89	0.0372	29.62	179.62
800	95	8	95	0.105	1265.10	0.038	30.04	180.04
850	97	8.5	97	0.112	1274.46	0.0388	30.44	180.44
900	100	9	100	0.118	1283.95	0.04	31.15	181.15
950	103	9.5	103	0.125	1293.58	0.0412	31.85	181.85
1000	106	10	106	0.131	1303.36	0.0424	32.53	182.53
1050	108	10.5	108	0.138	1313.29	0.0432	32.89	182.89
1100	110	11	110	0.144	1323.37	0.044	33.25	183.25

1150	112	11.5	112	0.151	1333.60	0.0448	33.59	183.59
1200	114	12	114	0.158	1344.00	0.0456	33.93	183.93
1250	116	12.5	116	0.164	1354.56	0.0464	34.25	184.25
1300	118	13	118	0.171	1365.29	0.0472	34.57	184.57
1350	120	13.5	120	0.177	1376.18	0.048	34.88	184.88
1400	122	14	122	0.184	1387.26	0.0488	35.18	185.18
1450	124	14.5	124	0.190	1398.51	0.0496	35.47	185.47
1500	126	15	126	0.197	1409.95	0.0504	35.75	185.75
1550	127	15.5	127	0.204	1421.57	0.0508	35.74	185.74
1600	129	16	129	0.210	1433.39	0.0516	36.00	186.00
1650	130	16.5	130	0.217	1445.41	0.052	35.98	185.98
1700	130	17	130	0.223	1457.63	0.052	35.67	185.67
1750	130	17.5	130	0.230	1470.06	0.052	35.37	185.37
1800	130	18	130	0.236	1482.70	0.052	35.07	185.07
1850	129	18.5	129	0.243	1495.56	0.0516	34.50	184.50
1900	129	19	129	0.250	1508.65	0.0516	34.20	184.20
1950	130	19.5	130	0.256	1521.97	0.052	34.17	184.17
2000	132	20	132	0.263	1535.52	0.0528	34.39	184.39
2050	133	20.5	133	0.269	1549.32	0.0532	34.34	184.34
2100	133	21	133	0.276	1563.37	0.0532	34.03	184.03
Average water content sample 1, 2 and 3, %				**Average shear strength sample 1, 2 and 3, kPa**				
35.9				**20.4**				

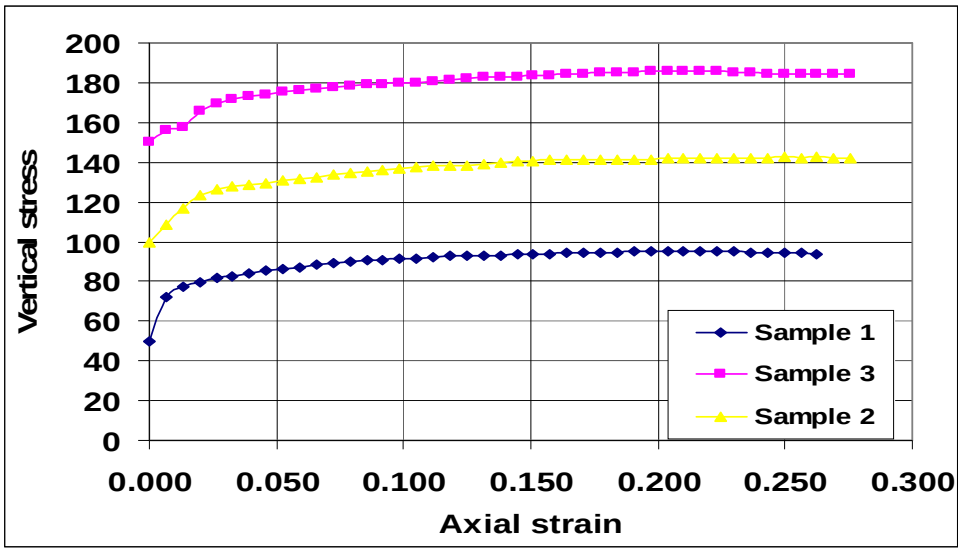

A(4e) Data of quick undrained triaxial in Oxford clay test 5 at average water content 36.6 %

Sample 1 = 50kPa			Moisture content			
Weight	g	154.59	Tin no	A28		
Length of sample	mm	76.14	Wet weight, g	156.44		

Diameter of sample		mm	37.96	Dry weight, g		115.22		
Area of sample		mm^2	1132.18	Tin empty, g		3.42		
Horizontal stress		kPa	50	Dry soil, g		111.8		
Force gauge correction factor		kN/division	0.0004	Weight of water, g		41.22		
Corrected compression gauge reading		mm	0.01	Moisture content %		36.87		
Shear strength		kPa	22.37					
Compression gauge reading (div)	Force gauge reading (div)	Corrected compression gauge reading (mm)	Corrected force gauge reading (div)	Axial strain	Corrected area (mm2)	Force (kN)	Deviator stress (kN/m2)	Vertical stress (kN/m2)
0	0	0	0	0.000	1132.18	0	0.00	50.00
50	30	0.5	30	0.007	1139.66	0.012	10.53	60.53
100	75	1	75	0.013	1147.25	0.03	26.15	76.15
150	83	1.5	83	0.020	1154.93	0.0332	28.75	78.75
200	92	2	92	0.026	1162.72	0.0368	31.65	81.65
250	99	2.5	99	0.033	1170.62	0.0396	33.83	83.83
300	107	3	107	0.039	1178.62	0.0428	36.31	86.31
350	111	3.5	111	0.046	1186.73	0.0444	37.41	87.41
400	114	4	114	0.053	1194.96	0.0456	38.16	88.16
450	117	4.5	117	0.059	1203.30	0.0468	38.89	88.89
500	122	5	122	0.066	1211.75	0.0488	40.27	90.27
550	125	5.5	125	0.072	1220.33	0.05	40.97	90.97
600	128	6	128	0.079	1229.03	0.0512	41.66	91.66
650	130	6.5	130	0.085	1237.85	0.052	42.01	92.01
700	132	7	132	0.092	1246.81	0.0528	42.35	92.35
750	135	7.5	135	0.099	1255.89	0.054	43.00	93.00
800	137	8	137	0.105	1265.10	0.0548	43.32	93.32
850	139	8.5	139	0.112	1274.46	0.0556	43.63	93.63
900	141	9	141	0.118	1283.95	0.0564	43.93	93.93
950	143	9.5	143	0.125	1293.58	0.0572	44.22	94.22
1000	145	10	145	0.131	1303.36	0.058	44.50	94.50
1050	147	10.5	147	0.138	1313.29	0.0588	44.77	94.77
1100	148	11	148	0.144	1323.37	0.0592	44.73	94.73
1150	149	11.5	149	0.151	1333.60	0.0596	44.69	94.69
1200	150	12	150	0.158	1344.00	0.06	44.64	94.64
1250	152	12.5	152	0.164	1354.56	0.0608	44.89	94.89
1300	152	13	152	0.171	1365.29	0.0608	44.53	94.53
1350	153	13.5	153	0.177	1376.18	0.0612	44.47	94.47
1400	154	14	154	0.184	1387.26	0.0616	44.40	94.40
1450	155	14.5	155	0.190	1398.51	0.062	44.33	94.33
1500	157	15	157	0.197	1409.95	0.0628	44.54	94.54
1550	159	15.5	159	0.204	1421.57	0.0636	44.74	94.74
1600	160	16	160	0.210	1433.39	0.064	44.65	94.65
1650	161	16.5	161	0.217	1445.41	0.0644	44.55	94.55
1700	162	17	162	0.223	1457.63	0.0648	44.46	94.46
1750	162	17.5	162	0.230	1470.06	0.0648	44.08	94.08
1800	162	18	162	0.236	1482.70	0.0648	43.70	93.70
1850	163	18.5	163	0.243	1495.56	0.0652	43.60	93.60

1900	165	19	165	0.250	1508.65	0.066	43.75	93.75
1950	166	19.5	166	0.256	1521.97	0.0664	43.63	93.63
2000	167	20	167	0.263	1535.52	0.0668	43.50	93.50

Sample 2 = 100kPa								
Weight		g	153.34	Tin no		11		
Length of sample		mm	76.14	Wet weight, g		156.03		
Diameter of sample		mm	37.96	Dry weight, g		115.05		
Area of sample		mm^2	1132.18	Tin empty, g		3.38		
Horizontal stress		kPa	50	Dry soil, g		111.67		
Force gauge correction factor		kN/division	0.0004	Weight of water, g		40.98		
Corrected compression gauge reading		mm	0.01	Moisture content %		36.70		
Shear strength		kPa	20.40					
Compression gauge reading (div)	Force gauge reading (div)	Corrected compression gauge reading (mm)	Corrected force gauge reading (div)	Axial strain	Corrected area (mm2)	Force (kN)	Deviator stress (kN/m2)	Vertical stress (kN/m2)
0	0	0	0	0.000	1132.18	0	0.00	100.00
50	46	0.5	46	0.007	1139.66	0.0184	16.15	116.15
100	63	1	63	0.013	1147.25	0.0252	21.97	121.97
150	71	1.5	71	0.020	1154.93	0.0284	24.59	124.59
200	77	2	77	0.026	1162.72	0.0308	26.49	126.49
250	82	2.5	82	0.033	1170.62	0.0328	28.02	128.02
300	86	3	86	0.039	1178.62	0.0344	29.19	129.19
350	90	3.5	90	0.046	1186.73	0.036	30.34	130.34
400	95	4	95	0.053	1194.96	0.038	31.80	131.80
450	98	4.5	98	0.059	1203.30	0.0392	32.58	132.58
500	101	5	101	0.066	1211.75	0.0404	33.34	133.34
550	105	5.5	105	0.072	1220.33	0.042	34.42	134.42
600	108	6	108	0.079	1229.03	0.0432	35.15	135.15
650	112	6.5	112	0.085	1237.85	0.0448	36.19	136.19
700	115	7	115	0.092	1246.81	0.046	36.89	136.89
750	118	7.5	118	0.099	1255.89	0.0472	37.58	137.58
800	121	8	121	0.105	1265.10	0.0484	38.26	138.26
850	124	8.5	124	0.112	1274.46	0.0496	38.92	138.92
900	126	9	126	0.118	1283.95	0.0504	39.25	139.25
950	128	9.5	128	0.125	1293.58	0.0512	39.58	139.58
1000	130	10	130	0.131	1303.36	0.052	39.90	139.90
1050	132	10.5	132	0.138	1313.29	0.0528	40.20	140.20
1100	135	11	135	0.144	1323.37	0.054	40.80	140.80
1150	137	11.5	137	0.151	1333.60	0.0548	41.09	141.09
1200	138	12	138	0.158	1344.00	0.0552	41.07	141.07
1250	139	12.5	139	0.164	1354.56	0.0556	41.05	141.05
1300	140	13	140	0.171	1365.29	0.056	41.02	141.02
1350	141	13.5	141	0.177	1376.18	0.0564	40.98	140.98
1400	142	14	142	0.184	1387.26	0.0568	40.94	140.94
1450	143	14.5	143	0.190	1398.51	0.0572	40.90	140.90

1500	144	15	144	0.197	1409.95	0.0576	40.85	140.85
1550	145	15.5	145	0.204	1421.57	0.058	40.80	140.80
1600	146	16	146	0.210	1433.39	0.0584	40.74	140.74
1650	147	16.5	147	0.217	1445.41	0.0588	40.68	140.68
1700	148	17	148	0.223	1457.63	0.0592	40.61	140.61
1750	149	17.5	149	0.230	1470.06	0.0596	40.54	140.54
1800	150	18	150	0.236	1482.70	0.06	40.47	140.47
1850	151	18.5	151	0.243	1495.56	0.0604	40.39	140.39
1900	151	19	151	0.250	1508.65	0.0604	40.04	140.04
1950	152	19.5	152	0.256	1521.97	0.0608	39.95	139.95
2000	153	20	153	0.263	1535.52	0.0612	39.86	139.86

Sample 3 = 150kPa				Tin no		E2		
Weight		g	153.83	Wet weight, g		156.27		
Length of sample		mm	76.45	Dry weight, g		115.16		
Diameter of sample		mm	38.39	Tin empty, g		3.23		
Area of sample		mm^2	1157.98	Dry soil, g		111.93		
Horizontal stress		kPa	50	Weight of water, g		41.11		
Force gauge correction factor		kN/division	0.0004	Moisture content %		36.73		
Corrected compression gauge reading		mm	0.01					
Shear strength		kPa	18.71					
Compression gauge reading (div)	Force gauge reading (div)	Corrected compression gauge reading (mm)	Corrected force gauge reading (div)	Axial strain	Corrected area (mm2)	Force (kN)	Deviator stress (kN/m2)	Vertical stress (kN/m2)
0	0	0	0	0.000	1132.18	0	0.00	150.00
50	31	0.5	31	0.007	1139.66	0.0124	10.88	160.88
100	47	1	47	0.013	1147.25	0.0188	16.39	166.39
150	56	1.5	56	0.020	1154.93	0.0224	19.40	169.40
200	62	2	62	0.026	1162.72	0.0248	21.33	171.33
250	66	2.5	66	0.033	1170.62	0.0264	22.55	172.55
300	71	3	71	0.039	1178.62	0.0284	24.10	174.10
350	75	3.5	75	0.046	1186.73	0.03	25.28	175.28
400	80	4	80	0.053	1194.96	0.032	26.78	176.78
450	83	4.5	83	0.059	1203.30	0.0332	27.59	177.59
500	87	5	87	0.066	1211.75	0.0348	28.72	178.72
550	91	5.5	91	0.072	1220.33	0.0364	29.83	179.83
600	94	6	94	0.079	1229.03	0.0376	30.59	180.59
650	97	6.5	97	0.085	1237.85	0.0388	31.34	181.34
700	101	7	101	0.092	1246.81	0.0404	32.40	182.40
750	104	7.5	104	0.099	1255.89	0.0416	33.12	183.12
800	107	8	107	0.105	1265.10	0.0428	33.83	183.83
850	109	8.5	109	0.112	1274.46	0.0436	34.21	184.21
900	111	9	111	0.118	1283.95	0.0444	34.58	184.58
950	113	9.5	113	0.125	1293.58	0.0452	34.94	184.94
1000	115	10	115	0.131	1303.36	0.046	35.29	185.29

1050	117	10.5	117	0.138	1313.29	0.0468	35.64	185.64
1100	118	11	118	0.144	1323.37	0.0472	35.67	185.67
1150	120	11.5	120	0.151	1333.60	0.048	35.99	185.99
1200	122	12	122	0.158	1344.00	0.0488	36.31	186.31
1250	123	12.5	123	0.164	1354.56	0.0492	36.32	186.32
1300	125	13	125	0.171	1365.29	0.05	36.62	186.62
1350	127	13.5	127	0.177	1376.18	0.0508	36.91	186.91
1400	128	14	128	0.184	1387.26	0.0512	36.91	186.91
1450	129	14.5	129	0.190	1398.51	0.0516	36.90	186.90
1500	130	15	130	0.197	1409.95	0.052	36.88	186.88
1550	133	15.5	133	0.204	1421.57	0.0532	37.42	187.42
1600	136	16	136	0.210	1433.39	0.0544	37.95	187.95
1650	138	16.5	138	0.217	1445.41	0.0552	38.19	188.19
1700	139	17	139	0.223	1457.63	0.0556	38.14	188.14
1750	140	17.5	140	0.230	1470.06	0.056	38.09	188.09
1800	140	18	140	0.236	1482.70	0.056	37.77	187.77
1850	140	18.5	140	0.243	1495.56	0.056	37.44	187.44
1900	141	19	141	0.250	1508.65	0.0564	37.38	187.38
1950	142	19.5	142	0.256	1521.97	0.0568	37.32	187.32
2000	143	20	143	0.263	1535.52	0.0572	37.25	187.25
Average water content sample 1, 2 and 3, %				**Average shear strength sample 1, 2 and 3, kPa**				
36.8				**20.5**				

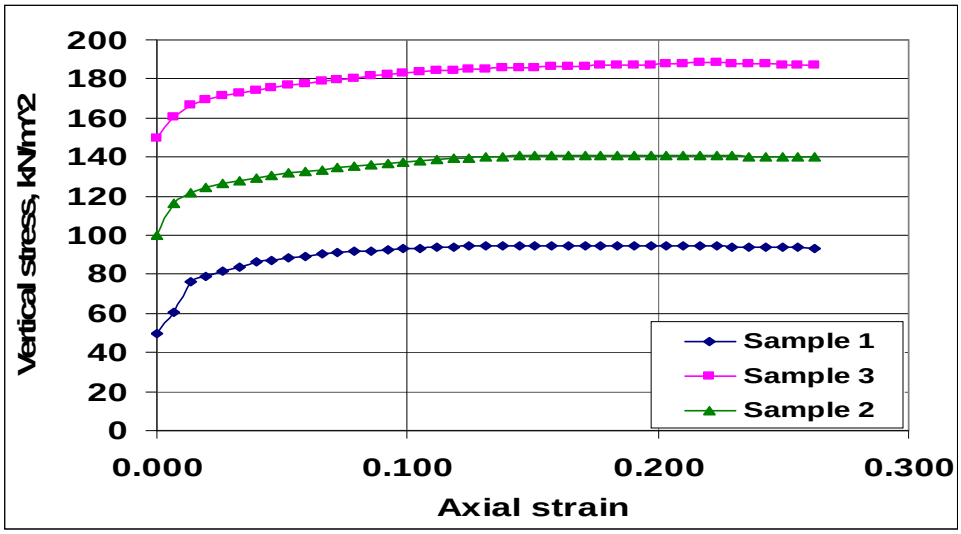

A(4f) Data of quick undrained triaxial in Oxford clay test 6 at average water content 38.8 %

Sample 1 = 50kPa						
Weight	g	148.99	Tin no	F	2	D31
Length of sample	mm	76.14	Wet weight, g	35.49	31.33	31.92

Diameter of sample		mm	37.96	Dry weight, g		26.46	23.63	23.88
Area of sample		mm^2	1132.18	Tin empty, g		3.32	4.07	3.38
Horizontal stress		kPa	50	Dry soil, g		23.14	19.56	20.5
Force gauge correction factor		kN/division	0.0004	Weight of water, g		9.03	7.7	8.04
Corrected compression gauge reading		mm	0.01mm	Moisture content %		39.02	39.37	39.22
Shear strength		kPa	19.42	Average		39.2		
Compression gauge reading (div)	Force gauge reading (div)	Corrected compression gauge reading (mm)	Corrected force gauge reading (div)	Axial strain	Corrected area (mm2)	Force (kN)	Deviator stress (kN/m2)	Vertical stress (kN/m2)
0	0	0	0	0.000	1132.18	0	0.00	50.00
50	58	0.5	58	0.007	1139.66	0.0232	20.36	70.36
100	69	1	69	0.013	1147.25	0.0276	24.06	74.06
150	73	1.5	73	0.020	1154.93	0.0292	25.28	75.28
200	79	2	79	0.026	1162.72	0.0316	27.18	77.18
250	82	2.5	82	0.033	1170.62	0.0328	28.02	78.02
300	85	3	85	0.039	1178.62	0.034	28.85	78.85
350	88	3.5	88	0.046	1186.73	0.0352	29.66	79.66
400	94	4	94	0.053	1194.96	0.0376	31.47	81.47
450	97	4.5	97	0.059	1203.30	0.0388	32.24	82.24
500	99	5	99	0.066	1211.75	0.0396	32.68	82.68
550	101	5.5	101	0.072	1220.33	0.0404	33.11	83.11
600	103	6	103	0.079	1229.03	0.0412	33.52	83.52
650	105	6.5	105	0.085	1237.85	0.042	33.93	83.93
700	107	7	107	0.092	1246.81	0.0428	34.33	84.33
750	109	7.5	109	0.099	1255.89	0.0436	34.72	84.72
800	111	8	111	0.105	1265.10	0.0444	35.10	85.10
850	113	8.5	113	0.112	1274.46	0.0452	35.47	85.47
900	115	9	115	0.118	1283.95	0.046	35.83	85.83
950	116	9.5	116	0.125	1293.58	0.0464	35.87	85.87
1000	118	10	118	0.131	1303.36	0.0472	36.21	86.21
1050	119	10.5	119	0.138	1313.29	0.0476	36.24	86.24
1100	122	11	122	0.144	1323.37	0.0488	36.88	86.88
1150	125	11.5	125	0.151	1333.60	0.05	37.49	87.49
1200	126	12	126	0.158	1344.00	0.0504	37.50	87.50
1250	128	12.5	128	0.164	1354.56	0.0512	37.80	87.80
1300	130	13	130	0.171	1365.29	0.052	38.09	88.09
1350	132	13.5	132	0.177	1376.18	0.0528	38.37	88.37
1400	133	14	133	0.184	1387.26	0.0532	38.35	88.35
1450	135	14.5	135	0.190	1398.51	0.054	38.61	88.61
1500	136	15	136	0.197	1409.95	0.0544	38.58	88.58
1550	138	15.5	138	0.204	1421.57	0.0552	38.83	88.83
1600	140	16	140	0.210	1433.39	0.056	39.07	89.07
1650	141	16.5	141	0.217	1445.41	0.0564	39.02	89.02
1700	142	17	142	0.223	1457.63	0.0568	38.97	88.97
1750	143	17.5	143	0.230	1470.06	0.0572	38.91	88.91
1800	144	18	144	0.236	1482.70	0.0576	38.85	88.85
1850	145	18.5	145	0.243	1495.56	0.058	38.78	88.78

1900	146	19	146	0.250	1508.65	0.0584	38.71	88.71
1950	148	19.5	148	0.256	1521.97	0.0592	38.90	88.90
2000	149	20	149	0.263	1535.52	0.0596	38.81	88.81
2050	151	20.5	151	0.269	1549.32	0.0604	38.98	88.98
2100	152	21	152	0.276	1563.37	0.0608	38.89	88.89

Sample 2 = 100kPa			Moisture content			
Weight	g	149.8	Tin no	B4	A7	C7
Length of sample	mm	76.14	Wet weight, g	41.25	36.09	35.33
Diameter of sample	mm	37.96	Dry weight, g	31.09	27.42	26.96
Area of sample	mm^2	1132.18	Tin empty, g	4.77	5.28	5.37
Horizontal stress	kPa	100	Dry soil, g	26.32	22.14	21.59
Force gauge correction factor	kN/division	0.0004	Weight of water, g	10.16	8.67	8.37
Corrected compression gauge reading	mm	0.01mm	Moisture content %	38.60	39.16	38.77
Shear strength	kPa	19.56	Average	38.8		

Compression gauge reading (div)	Force gauge reading (div)	Corrected compression gauge reading (mm)	Corrected force gauge reading (div)	Axial strain	Corrected area (mm2)	Force (kN)	Deviator stress (kN/m2)	Vertical stress (kN/m2)
0	0	0	0	0.000	1132.18	0	0.00	100.00
50	40	0.5	40	0.007	1139.66	0.016	14.04	114.04
100	55	1	55	0.013	1147.25	0.022	19.18	119.18
150	63	1.5	63	0.020	1154.93	0.0252	21.82	121.82
200	68	2	68	0.026	1162.72	0.0272	23.39	123.39
250	74	2.5	74	0.033	1170.62	0.0296	25.29	125.29
300	78	3	78	0.039	1178.62	0.0312	26.47	126.47
350	82	3.5	82	0.046	1186.73	0.0328	27.64	127.64
400	86	4	86	0.053	1194.96	0.0344	28.79	128.79
450	90	4.5	90	0.059	1203.30	0.036	29.92	129.92
500	94	5	94	0.066	1211.75	0.0376	31.03	131.03
550	96	5.5	96	0.072	1220.33	0.0384	31.47	131.47
600	99	6	99	0.079	1229.03	0.0396	32.22	132.22
650	103	6.5	103	0.085	1237.85	0.0412	33.28	133.28
700	105	7	105	0.092	1246.81	0.042	33.69	133.69
750	110	7.5	110	0.099	1255.89	0.044	35.03	135.03
800	112	8	112	0.105	1265.10	0.0448	35.41	135.41
850	114	8.5	114	0.112	1274.46	0.0456	35.78	135.78
900	118	9	118	0.118	1283.95	0.0472	36.76	136.76
950	120	9.5	120	0.125	1293.58	0.048	37.11	137.11
1000	124	10	124	0.131	1303.36	0.0496	38.06	138.06
1050	125	10.5	125	0.138	1313.29	0.05	38.07	138.07
1100	126	11	126	0.144	1323.37	0.0504	38.08	138.08
1150	128	11.5	128	0.151	1333.60	0.0512	38.39	138.39
1200	129	12	129	0.158	1344.00	0.0516	38.39	138.39
1250	130	12.5	130	0.164	1354.56	0.052	38.39	138.39
1300	132	13	132	0.171	1365.29	0.0528	38.67	138.67

1350	133	13.5	133	0.177	1376.18	0.0532	38.66	138.66
1400	133	14	133	0.184	1387.26	0.0532	38.35	138.35
1450	135	14.5	135	0.190	1398.51	0.054	38.61	138.61
1500	136	15	136	0.197	1409.95	0.0544	38.58	138.58
1550	139	15.5	139	0.204	1421.57	0.0556	39.11	139.11
1600	141	16	141	0.210	1433.39	0.0564	39.35	139.35
1650	144	16.5	144	0.217	1445.41	0.0576	39.85	139.85
1700	146	17	146	0.223	1457.63	0.0584	40.07	140.07
1750	148	17.5	148	0.230	1470.06	0.0592	40.27	140.27
1800	148	18	148	0.236	1482.70	0.0592	39.93	139.93
1850	150	18.5	150	0.243	1495.56	0.06	40.12	140.12
1900	150	19	150	0.250	1508.65	0.06	39.77	139.77
1950	151	19.5	151	0.256	1521.97	0.0604	39.69	139.69
2000	152	20	152	0.263	1535.52	0.0608	39.60	139.60
2050	154	20.5	154	0.269	1549.32	0.0616	39.76	139.76

Sample 3 = 150kPa				Tin no		A3	PL1	PL2
Weight		g	148.83	Wet weight, g		27.16	33.2	27.83
Length of sample		mm	76.14	Dry weight, g		20.51	24.84	21.05
Diameter of sample		mm	37.96	Tin empty, g		3.23	3.22	3.33
Area of sample		mm^2	1132.18	Dry soil, g		17.28	21.62	17.72
Horizontal stress		kPa	150	Weight of water, g		6.65	8.36	6.78
Force gauge correction factor		kN/division	0.0004	Moisture content %		38.48	38.67	38.26
Corrected compression gauge reading		mm	0.01mm	Average		38.5		
Shear strength		kPa	16.47					
Compression gauge reading (div)	Force gauge reading (div)	Corrected compression gauge reading (mm)	Corrected force gauge reading (div)	Axial strain	Corrected area (mm2)	Force (kN)	Deviator stress (kN/m2)	Vertical stress (kN/m2)
0	0	0	0	0.000	1132.18	0	0.00	150.00
50	34	0.5	34	0.007	1139.66	0.0136	11.93	161.93
100	40	1	40	0.013	1147.25	0.016	13.95	163.95
150	45	1.5	45	0.020	1154.93	0.018	15.59	165.59
200	50	2	50	0.026	1162.72	0.02	17.20	167.20
250	58	2.5	58	0.033	1170.62	0.0232	19.82	169.82
300	64	3	64	0.039	1178.62	0.0256	21.72	171.72
350	68	3.5	68	0.046	1186.73	0.0272	22.92	172.92
400	71	4	71	0.053	1194.96	0.0284	23.77	173.77
450	74	4.5	74	0.059	1203.30	0.0296	24.60	174.60
500	78	5	78	0.066	1211.75	0.0312	25.75	175.75
550	81	5.5	81	0.072	1220.33	0.0324	26.55	176.55
600	83	6	83	0.079	1229.03	0.0332	27.01	177.01
650	85	6.5	85	0.085	1237.85	0.034	27.47	177.47
700	87	7	87	0.092	1246.81	0.0348	27.91	177.91
750	90	7.5	90	0.099	1255.89	0.036	28.66	178.66
800	92	8	92	0.105	1265.10	0.0368	29.09	179.09

850	95	8.5	95	0.112	1274.46	0.038	29.82	179.82
900	96	9	96	0.118	1283.95	0.0384	29.91	179.91
950	99	9.5	99	0.125	1293.58	0.0396	30.61	180.61
1000	100	10	100	0.131	1303.36	0.04	30.69	180.69
1050	102	10.5	102	0.138	1313.29	0.0408	31.07	181.07
1100	104	11	104	0.144	1323.37	0.0416	31.43	181.43
1150	106	11.5	106	0.151	1333.60	0.0424	31.79	181.79
1200	107	12	107	0.158	1344.00	0.0428	31.85	181.85
1250	109	12.5	109	0.164	1354.56	0.0436	32.19	182.19
1300	110	13	110	0.171	1365.29	0.044	32.23	182.23
1350	111	13.5	111	0.177	1376.18	0.0444	32.26	182.26
1400	112	14	112	0.184	1387.26	0.0448	32.29	182.29
1450	115	14.5	115	0.190	1398.51	0.046	32.89	182.89
1500	116	15	116	0.197	1409.95	0.0464	32.91	182.91
1550	118	15.5	118	0.204	1421.57	0.0472	33.20	183.20
1600	119	16	119	0.210	1433.39	0.0476	33.21	183.21
1650	119	16.5	119	0.217	1445.41	0.0476	32.93	182.93
1700	121	17	121	0.223	1457.63	0.0484	33.20	183.20
1750	123	17.5	123	0.230	1470.06	0.0492	33.47	183.47
1800	125	18	125	0.236	1482.70	0.05	33.72	183.72
1850	126	18.5	126	0.243	1495.56	0.0504	33.70	183.70
1900	128	19	128	0.250	1508.65	0.0512	33.94	183.94
1950	129	19.5	129	0.256	1521.97	0.0516	33.90	183.90
2000	130	20	130	0.263	1535.52	0.052	33.86	183.86
2050	131	20.5	131	0.269	1549.32	0.0524	33.82	183.82
2100	132	21	132	0.276	1563.37	0.0528	33.77	183.77
2150	134	21.5	134	0.282	1577.68	0.0536	33.97	183.97
2200	135	22	135	0.289	1592.25	0.054	33.91	183.91
Average water content sample 1, 2 and 3, %				**Average shear strength sample 1, 2 and 3, kPa**				
38.8				**18.5**				

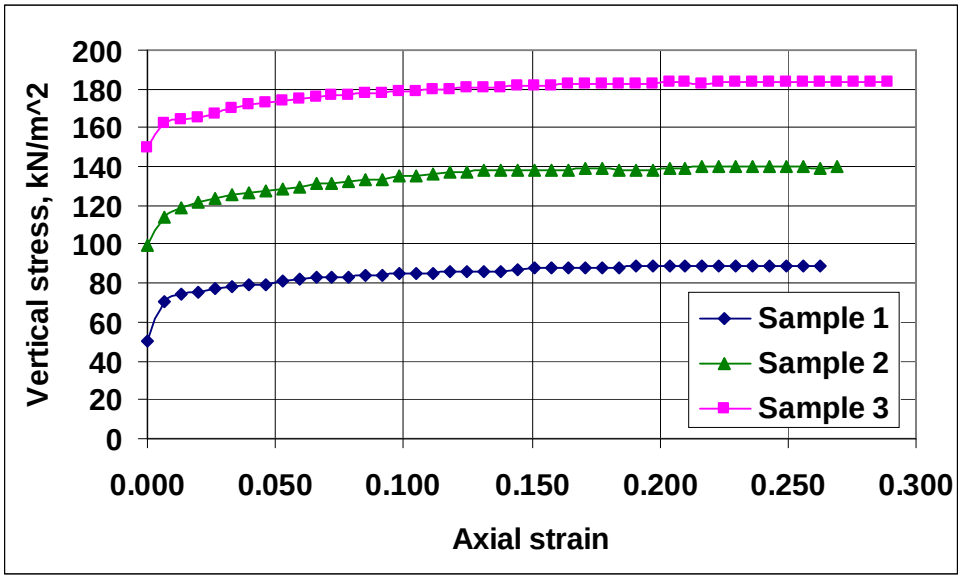

A(4g) Data of quick undrained triaxial in Oxford clay test 7 at average water content 41.8 %

Sample 1 = 50kPa				Moisture content				
Weight		g	150.98	Tin no		F	2	D31
Length of sample		mm	76.14	Wet weight, g		24.49	26.04	27.58
Diameter of sample		mm	37.96	Dry weight, g		18.25	19.42	20.5
Area of sample		mm^2	1132.18	Tin empty, g		4.06	3.48	4.03
Horizontal stress		kPa	50	Dry soil, g		14.19	15.94	16.47
Force gauge correction factor		kN/division	0.0004	Weight of water, g		6.24	6.62	7.08
Corrected compression gauge reading		mm	0.01	Moisture content %		43.97	41.53	42.99
Shear strength		kPa	15.34	Average		42.8		
Compression gauge reading (div)	Force gauge reading (div)	Corrected compression gauge reading (mm)	Corrected force gauge reading (div)	Axial strain	Corrected area (mm2)	Force (kN)	Deviator stress (kN/m2)	Vertical stress (kN/m2)
0	0	0	0	0.000	1132.18	0.000	0.00	50.00
50	56	0.5	56	0.007	1139.66	0.022	19.65	69.65
100	62	1	62	0.013	1147.25	0.025	21.62	71.62
150	69	1.5	69	0.020	1154.93	0.028	23.90	73.90
200	73	2	73	0.026	1162.72	0.029	25.11	75.11
250	77	2.5	77	0.033	1170.62	0.031	26.31	76.31
300	79	3	79	0.039	1178.62	0.032	26.81	76.81
350	80	3.5	80	0.046	1186.73	0.032	26.96	76.96
400	82	4	82	0.053	1194.96	0.033	27.45	77.45
450	84	4.5	84	0.059	1203.30	0.034	27.92	77.92
500	86	5	86	0.066	1211.75	0.034	28.39	78.39
550	88	5.5	88	0.072	1220.33	0.035	28.84	78.84
600	90	6	90	0.079	1229.03	0.036	29.29	79.29
650	92	6.5	92	0.085	1237.85	0.037	29.73	79.73
700	94	7	94	0.092	1246.81	0.038	30.16	80.16
750	95	7.5	95	0.099	1255.89	0.038	30.26	80.26
800	97	8	97	0.105	1265.10	0.039	30.67	80.67
850	98	8.5	98	0.112	1274.46	0.039	30.76	80.76
900	99	9	99	0.118	1283.95	0.040	30.84	80.84
950	100	9.5	100	0.125	1293.58	0.040	30.92	80.92
1000	101	10	101	0.131	1303.36	0.040	31.00	81.00
1050	103	10.5	103	0.138	1313.29	0.041	31.37	81.37
1100	104	11	104	0.144	1323.37	0.042	31.43	81.43
1150	105	11.5	105	0.151	1333.60	0.042	31.49	81.49
1200	106	12	106	0.158	1344.00	0.042	31.55	81.55
1250	106	12.5	106	0.164	1354.56	0.042	31.30	81.30
1300	107	13	107	0.171	1365.29	0.043	31.35	81.35
1350	107	13.5	107	0.177	1376.18	0.043	31.10	81.10
1400	107	14	107	0.184	1387.26	0.043	30.85	80.85

1450	107	14.5	107	0.190	1398.51	0.043	30.60	80.60
1500	108	15	108	0.197	1409.95	0.043	30.64	80.64
1550	109	15.5	109	0.204	1421.57	0.044	30.67	80.67
1600	111	16	111	0.210	1433.39	0.044	30.98	80.98
1650	111	16.5	111	0.217	1445.41	0.044	30.72	80.72
1700	112	17	112	0.223	1457.63	0.045	30.73	80.73
1750	113	17.5	113	0.230	1470.06	0.045	30.75	80.75
1800	114	18	114	0.236	1482.70	0.046	30.75	80.75
1850	115	18.5	115	0.243	1495.56	0.046	30.76	80.76
1900	116	19	116	0.250	1508.65	0.046	30.76	80.76
1950	118	19.5	118	0.256	1521.97	0.047	31.01	81.01
2000	120	20	120	0.263	1535.52	0.048	31.26	81.26

Sample 2 = 100kPa			Moisture content			
Weight	g	149.96	Tin no	B4	A7	C7
Length of sample	mm	76.14	Wet weight, g	25.52	25.93	25.98
Diameter of sample	mm	37.96	Dry weight, g	19.01	19.29	19.57
Area of sample	mm^2	1132.18	Tin empty, g	3.2	3.21	3.94
Horizontal stress	kPa	50	Dry soil, g	15.81	16.08	15.63
Force gauge correction factor	kN/division	0.0004	Weight of water, g	6.51	6.64	6.41
Corrected compression gauge reading	mm	0.01	Moisture content %	41.18	41.29	41.01
Shear strength	kPa	12.80	Average	41.2		

Compression gauge reading (div)	Force gauge reading (div)	Corrected compression gauge reading (mm)	Corrected force gauge reading (div)	Axial strain	Corrected area (mm2)	Force (kN)	Deviator stress (kN/m2)	Vertical stress (kN/m2)
0	0	0	0	0.000	1132.18	0.000	0.00	100.00
50	23	0.5	23	0.007	1139.66	0.009	8.07	108.07
100	41	1	41	0.013	1147.25	0.016	14.30	114.30
150	49	1.5	49	0.020	1154.93	0.020	16.97	116.97
200	54	2	54	0.026	1162.72	0.022	18.58	118.58
250	57	2.5	57	0.033	1170.62	0.023	19.48	119.48
300	60	3	60	0.039	1178.62	0.024	20.36	120.36
350	62	3.5	62	0.046	1186.73	0.025	20.90	120.90
400	65	4	65	0.053	1194.96	0.026	21.76	121.76
450	67	4.5	67	0.059	1203.30	0.027	22.27	122.27
500	70	5	70	0.066	1211.75	0.028	23.11	123.11
550	72	5.5	72	0.072	1220.33	0.029	23.60	123.60
600	74	6	74	0.079	1229.03	0.030	24.08	124.08
650	75	6.5	75	0.085	1237.85	0.030	24.24	124.24
700	76	7	76	0.092	1246.81	0.030	24.38	124.38
750	77	7.5	77	0.099	1255.89	0.031	24.52	124.52
800	78	8	78	0.105	1265.10	0.031	24.66	124.66
850	80	8.5	80	0.112	1274.46	0.032	25.11	125.11
900	81	9	81	0.118	1283.95	0.032	25.23	125.23
950	82	9.5	82	0.125	1293.58	0.033	25.36	125.36

1000	83	10	83	0.131	1303.36	0.033	25.47	125.47
1050	84	10.5	84	0.138	1313.29	0.034	25.58	125.58
1100	85	11	85	0.144	1323.37	0.034	25.69	125.69
1150	86	11.5	86	0.151	1333.60	0.034	25.79	125.79
1200	87	12	87	0.158	1344.00	0.035	25.89	125.89
1250	88	12.5	88	0.164	1354.56	0.035	25.99	125.99
1300	88	13	88	0.171	1365.29	0.035	25.78	125.78
1350	88	13.5	88	0.177	1376.18	0.035	25.58	125.58
1400	88	14	88	0.184	1387.26	0.035	25.37	125.37
1450	89	14.5	89	0.190	1398.51	0.036	25.46	125.46
1500	90	15	90	0.197	1409.95	0.036	25.53	125.53
1550	91	15.5	91	0.204	1421.57	0.036	25.61	125.61
1600	92	16	92	0.210	1433.39	0.037	25.67	125.67
1650	93	16.5	93	0.217	1445.41	0.037	25.74	125.74
1700	94	17	94	0.223	1457.63	0.038	25.80	125.80
1750	95	17.5	95	0.230	1470.06	0.038	25.85	125.85
1800	96	18	96	0.236	1482.70	0.038	25.90	125.90
1850	97	18.5	97	0.243	1495.56	0.039	25.94	125.94
1900	98	19	98	0.250	1508.65	0.039	25.98	125.98
1950	100	19.5	100	0.256	1521.97	0.040	26.28	126.28
2000	103	20	103	0.263	1535.52	0.041	26.83	126.83
2050	105	20.5	105	0.269	1549.32	0.042	27.11	127.11
2100	105	21	105	0.276	1563.37	0.042	26.87	126.87

Sample 3 = 150kPa			Tin no		A3	PL1	PL2
Weight	g	151.91	Wet weight, g		24.48	19.54	18.54
Length of sample	mm	76.14	Dry weight, g		18.25	14.8	14.04
Diameter of sample	mm	37.96	Tin empty, g		3.21	3.34	3.17
Area of sample	mm^2	1132.18	Dry soil, g		15.04	11.46	10.87
Horizontal stress	kPa	50	Weight of water, g		6.23	4.74	4.5
Force gauge correction factor	kN/division	0.0004	Moisture content %		41.42	41.36	41.40
Corrected compression gauge reading	mm	0.01	Average		41.4		
Shear strength	kPa	14.35					

Compression gauge reading (div)	Force gauge reading (div)	Corrected compression gauge reading (mm)	Corrected force gauge reading (div)	Axial strain	Corrected area (mm2)	Force (kN)	Deviator stress (kN/m2)	Vertical stress (kN/m2)
0	0	0	0	0.000	1132.18	0.000	0.00	150.00
50	24	0.5	24	0.007	1139.66	0.010	8.42	158.42
100	45	1	45	0.013	1147.25	0.018	15.69	165.69
150	50	1.5	50	0.020	1154.93	0.020	17.32	167.32
200	56	2	56	0.026	1162.72	0.022	19.27	169.27
250	59	2.5	59	0.033	1170.62	0.024	20.16	170.16
300	62	3	62	0.039	1178.62	0.025	21.04	171.04
350	65	3.5	65	0.046	1186.73	0.026	21.91	171.91
400	67	4	67	0.053	1194.96	0.027	22.43	172.43

450	69	4.5	69	0.059	1203.30	0.028	22.94	172.94
500	72	5	72	0.066	1211.75	0.029	23.77	173.77
550	74	5.5	74	0.072	1220.33	0.030	24.26	174.26
600	75	6	75	0.079	1229.03	0.030	24.41	174.41
650	77	6.5	77	0.085	1237.85	0.031	24.88	174.88
700	79	7	79	0.092	1246.81	0.032	25.34	175.34
750	80	7.5	80	0.099	1255.89	0.032	25.48	175.48
800	81	8	81	0.105	1265.10	0.032	25.61	175.61
850	83	8.5	83	0.112	1274.46	0.033	26.05	176.05
900	84	9	84	0.118	1283.95	0.034	26.17	176.17
950	86	9.5	86	0.125	1293.58	0.034	26.59	176.59
1000	88	10	88	0.131	1303.36	0.035	27.01	177.01
1050	90	10.5	90	0.138	1313.29	0.036	27.41	177.41
1100	92	11	92	0.144	1323.37	0.037	27.81	177.81
1150	94	11.5	94	0.151	1333.60	0.038	28.19	178.19
1200	95	12	95	0.158	1344.00	0.038	28.27	178.27
1250	96	12.5	96	0.164	1354.56	0.038	28.35	178.35
1300	97	13	97	0.171	1365.29	0.039	28.42	178.42
1350	98	13.5	98	0.177	1376.18	0.039	28.48	178.48
1400	99	14	99	0.184	1387.26	0.040	28.55	178.55
1450	100	14.5	100	0.190	1398.51	0.040	28.60	178.60
1500	101	15	101	0.197	1409.95	0.040	28.65	178.65
1550	102	15.5	102	0.204	1421.57	0.041	28.70	178.70
1600	104	16	104	0.210	1433.39	0.042	29.02	179.02
1650	106	16.5	106	0.217	1445.41	0.042	29.33	179.33
1700	107	17	107	0.223	1457.63	0.043	29.36	179.36
1750	108	17.5	108	0.230	1470.06	0.043	29.39	179.39
1800	110	18	110	0.236	1482.70	0.044	29.68	179.68
1850	111	18.5	111	0.243	1495.56	0.044	29.69	179.69
1900	112	19	112	0.250	1508.65	0.045	29.70	179.70
1950	113	19.5	113	0.256	1521.97	0.045	29.70	179.70
2000	115	20	115	0.263	1535.52	0.046	29.96	179.96
Average water content sample 1, 2 and 3, %				**Average shear strength sample 1, 2 and 3, kPa**				
41.8				**14.2**				

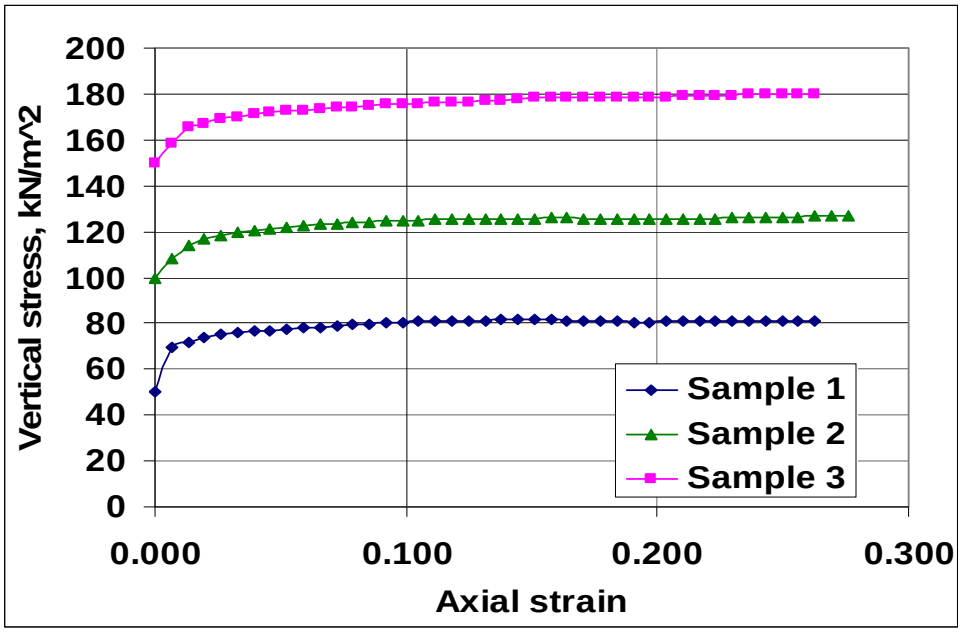

A(4h) Data of quick undrained triaxial in Oxford clay test 8 at average water content 43.8 %

Sample 1 = 50kPa								
Weight		g	147.83	Tin no		F	2	D31
Length of sample		mm	76.14	Wet weight, g		19.97	28.27	29.8
Diameter of sample		mm	37.96	Dry weight, g		15.11	20.74	21.95
Area of sample		mm^2	1132.18	Tin empty, g		4.06	3.48	4.03
Horizontal stress		kPa	50	Dry soil, g		11.05	17.26	17.92
Force gauge correction factor		kN/division	0.0004	Weight of water, g		4.86	7.53	7.85
Corrected compression gauge reading		mm	0.01	Moisture content %		43.98	43.63	43.81
Shear strength		kPa	15.90	Average		43.8		
Compression gauge reading (div)	Force gauge reading (div)	Corrected compression gauge reading (mm)	Corrected force gauge reading (div)	Axial strain	Corrected area (mm2)	Force (kN)	Deviator stress (kN/m2)	Vertical stress (kN/m2)
0	0	0	0	0.000	1132.18	0	0.00	50.00
50	42	0.5	42	0.007	1139.66	0.0168	14.74	64.74
100	50	1	50	0.013	1147.25	0.02	17.43	67.43
150	62	1.5	62	0.020	1154.93	0.0248	21.47	71.47
200	70	2	70	0.026	1162.72	0.028	24.08	74.08
250	74	2.5	74	0.033	1170.62	0.0296	25.29	75.29
300	77	3	77	0.039	1178.62	0.0308	26.13	76.13
350	79	3.5	79	0.046	1186.73	0.0316	26.63	76.63
400	83	4	83	0.053	1194.96	0.0332	27.78	77.78
450	85	4.5	85	0.059	1203.30	0.034	28.26	78.26
500	88	5	88	0.066	1211.75	0.0352	29.05	79.05

550	89	5.5	89	0.072	1220.33	0.0356	29.17	79.17
600	91	6	91	0.079	1229.03	0.0364	29.62	79.62
650	93	6.5	93	0.085	1237.85	0.0372	30.05	80.05
700	95	7	95	0.092	1246.81	0.038	30.48	80.48
750	96	7.5	96	0.099	1255.89	0.0384	30.58	80.58
800	98	8	98	0.105	1265.10	0.0392	30.99	80.99
850	99	8.5	99	0.112	1274.46	0.0396	31.07	81.07
900	100	9	100	0.118	1283.95	0.04	31.15	81.15
950	101	9.5	101	0.125	1293.58	0.0404	31.23	81.23
1000	101	10	101	0.131	1303.36	0.0404	31.00	81.00
1050	101	10.5	101	0.138	1313.29	0.0404	30.76	80.76
1100	102	11	102	0.144	1323.37	0.0408	30.83	80.83
1150	102	11.5	102	0.151	1333.60	0.0408	30.59	80.59
1200	104	12	104	0.158	1344.00	0.0416	30.95	80.95
1250	105	12.5	105	0.164	1354.56	0.042	31.01	81.01
1300	107	13	107	0.171	1365.29	0.0428	31.35	81.35
1350	108	13.5	108	0.177	1376.18	0.0432	31.39	81.39
1400	110	14	110	0.184	1387.26	0.044	31.72	81.72
1450	110	14.5	110	0.190	1398.51	0.044	31.46	81.46
1500	112	15	112	0.197	1409.95	0.0448	31.77	81.77
1550	113	15.5	113	0.204	1421.57	0.0452	31.80	81.80
1600	115	16	115	0.210	1433.39	0.046	32.09	82.09
1650	115	16.5	115	0.217	1445.41	0.046	31.82	81.82
1700	117	17	117	0.223	1457.63	0.0468	32.11	82.11
1750	118	17.5	118	0.230	1470.06	0.0472	32.11	82.11
1800	119	18	119	0.236	1482.70	0.0476	32.10	82.10
1850	120	18.5	120	0.243	1495.56	0.048	32.09	82.09
1900	120	19	120	0.250	1508.65	0.048	31.82	81.82
1950	123	19.5	123	0.256	1521.97	0.0492	32.33	82.33
2000	126	20	126	0.263	1535.52	0.0504	32.82	82.82

Sample 2 = 100kPa								
Weight		g	146.76	Tin no		B4	A7	C7
Length of sample		mm	76.14	Wet weight, g		24.89	18.3	22.99
Diameter of sample		mm	37.96	Dry weight, g		18.24	13.72	17.08
Area of sample		mm^2	1132.18	Tin empty, g		3.48	3.93	3.32
Horizontal stress		kPa	50	Dry soil, g		14.76	9.79	13.76
Force gauge correction factor		kN/division	0.0004	Weight of water, g		6.65	4.58	5.91
Corrected compression gauge reading		mm	0.01	Moisture content %		45.05	46.78	42.95
Shear strength		kPa	12.38	Average		44.9		
Compression gauge reading (div)	Force gauge readin g (div)	Corrected compressio n gauge reading (mm)	Corrected force gauge reading (div)	Axial strain	Correcte d area (mm2)	Force (kN)	Devi ator stress (kN/ m2)	Vertical stress (kN/m2)
0	0	0	0	0.000	1132.18	0	0.00	100.00

50	28	0.5	28	0.007	1139.66	0.0112	9.83	109.83
100	37	1	37	0.013	1147.25	0.0148	12.90	112.90
150	40	1.5	40	0.020	1154.93	0.016	13.85	113.85
200	43	2	43	0.026	1162.72	0.0172	14.79	114.79
250	45	2.5	45	0.033	1170.62	0.018	15.38	115.38
300	48	3	48	0.039	1178.62	0.0192	16.29	116.29
350	51	3.5	51	0.046	1186.73	0.0204	17.19	117.19
400	54	4	54	0.053	1194.96	0.0216	18.08	118.08
450	55	4.5	55	0.059	1203.30	0.022	18.28	118.28
500	57	5	57	0.066	1211.75	0.0228	18.82	118.82
550	59	5.5	59	0.072	1220.33	0.0236	19.34	119.34
600	61	6	61	0.079	1229.03	0.0244	19.85	119.85
650	63	6.5	63	0.085	1237.85	0.0252	20.36	120.36
700	66	7	66	0.092	1246.81	0.0264	21.17	121.17
750	68	7.5	68	0.099	1255.89	0.0272	21.66	121.66
800	70	8	70	0.105	1265.10	0.028	22.13	122.13
850	71	8.5	71	0.112	1274.46	0.0284	22.28	122.28
900	71	9	71	0.118	1283.95	0.0284	22.12	122.12
950	72	9.5	72	0.125	1293.58	0.0288	22.26	122.26
1000	73	10	73	0.131	1303.36	0.0292	22.40	122.40
1050	75	10.5	75	0.138	1313.29	0.03	22.84	122.84
1100	76	11	76	0.144	1323.37	0.0304	22.97	122.97
1150	78	11.5	78	0.151	1333.60	0.0312	23.40	123.40
1200	79	12	79	0.158	1344.00	0.0316	23.51	123.51
1250	80	12.5	80	0.164	1354.56	0.032	23.62	123.62
1300	81	13	81	0.171	1365.29	0.0324	23.73	123.73
1350	83	13.5	83	0.177	1376.18	0.0332	24.12	124.12
1400	85	14	85	0.184	1387.26	0.034	24.51	124.51
1450	86	14.5	86	0.190	1398.51	0.0344	24.60	124.60
1500	87	15	87	0.197	1409.95	0.0348	24.68	124.68
1550	88	15.5	88	0.204	1421.57	0.0352	24.76	124.76
1600	89	16	89	0.210	1433.39	0.0356	24.84	124.84
1650	90	16.5	90	0.217	1445.41	0.036	24.91	124.91
1700	92	17	92	0.223	1457.63	0.0368	25.25	125.25
1750	93	17.5	93	0.230	1470.06	0.0372	25.31	125.31
1800	95	18	95	0.236	1482.70	0.038	25.63	125.63
1850	96	18.5	96	0.243	1495.56	0.0384	25.68	125.68
1900	97	19	97	0.250	1508.65	0.0388	25.72	125.72
1950	98	19.5	98	0.256	1521.97	0.0392	25.76	125.76
2000	100	20	100	0.263	1535.52	0.04	26.05	126.05
2050	102	20.5	102	0.269	1549.32	0.0408	26.33	126.33
2100	105	21	105	0.276	1563.37	0.042	26.87	126.87
2150	106	21.5	106	0.282	1577.68	0.0424	26.87	126.87
2200	107	22	107	0.289	1592.25	0.0428	26.88	126.88

Sample 3 = 150kPa			Tin no	A3	PL1	PL2
Weight	g	146.04	Wet weight, g	26.51	29.33	28.56
Length of sample	mm	76.14	Dry weight, g	19.42	21.71	20.95

Diameter of sample		mm	37.96	Tin empty, g		3.16	3.33	3.2
Area of sample		mm^2	1132.18	Dry soil, g		16.26	18.38	17.75
Horizontal stress		kPa	50	Weight of water, g		7.09	7.62	7.61
Force gauge correction factor		kN/division	0.0004	Moisture content %		43.60	41.46	42.87
Corrected compression gauge reading		mm	0.01mm	Average		42.6		
Shear strength		kPa	10.69					
Compression gauge reading (div)	Force gauge reading (div)	Corrected compression gauge reading (mm)	Corrected force gauge reading (div)	Axial strain	Corrected area (mm2)	Force (kN)	Deviator stress (kN/m2)	Vertical stress (kN/m2)
0	0	0	0	0.000	1132.18	0	0.00	150.00
50	17	0.5	17	0.007	1139.66	0.0068	5.97	155.97
100	20	1	20	0.013	1147.25	0.008	6.97	156.97
150	25	1.5	25	0.020	1154.93	0.01	8.66	158.66
200	28	2	28	0.026	1162.72	0.0112	9.63	159.63
250	31	2.5	31	0.033	1170.62	0.0124	10.59	160.59
300	34	3	34	0.039	1178.62	0.0136	11.54	161.54
350	38	3.5	38	0.046	1186.73	0.0152	12.81	162.81
400	40	4	40	0.053	1194.96	0.016	13.39	163.39
450	43	4.5	43	0.059	1203.30	0.0172	14.29	164.29
500	46	5	46	0.066	1211.75	0.0184	15.18	165.18
550	48	5.5	48	0.072	1220.33	0.0192	15.73	165.73
600	50	6	50	0.079	1229.03	0.02	16.27	166.27
650	51	6.5	51	0.085	1237.85	0.0204	16.48	166.48
700	52	7	52	0.092	1246.81	0.0208	16.68	166.68
750	54	7.5	54	0.099	1255.89	0.0216	17.20	167.20
800	55	8	55	0.105	1265.10	0.022	17.39	167.39
850	56	8.5	56	0.112	1274.46	0.0224	17.58	167.58
900	58	9	58	0.118	1283.95	0.0232	18.07	168.07
950	59	9.5	59	0.125	1293.58	0.0236	18.24	168.24
1000	61	10	61	0.131	1303.36	0.0244	18.72	168.72
1050	62	10.5	62	0.138	1313.29	0.0248	18.88	168.88
1100	64	11	64	0.144	1323.37	0.0256	19.34	169.34
1150	65	11.5	65	0.151	1333.60	0.026	19.50	169.50
1200	67	12	67	0.158	1344.00	0.0268	19.94	169.94
1250	67	12.5	67	0.164	1354.56	0.0268	19.79	169.79
1300	69	13	69	0.171	1365.29	0.0276	20.22	170.22
1350	70	13.5	70	0.177	1376.18	0.028	20.35	170.35
1400	72	14	72	0.184	1387.26	0.0288	20.76	170.76
1450	73	14.5	73	0.190	1398.51	0.0292	20.88	170.88
1500	75	15	75	0.197	1409.95	0.03	21.28	171.28
1550	76	15.5	76	0.204	1421.57	0.0304	21.38	171.38
1600	78	16	78	0.210	1433.39	0.0312	21.77	171.77
1650	79	16.5	79	0.217	1445.41	0.0316	21.86	171.86
1700	80	17	80	0.223	1457.63	0.032	21.95	171.95
1750	81	17.5	81	0.230	1470.06	0.0324	22.04	172.04
1800	83	18	83	0.236	1482.70	0.0332	22.39	172.39
1850	85	18.5	85	0.243	1495.56	0.034	22.73	172.73

1900	87	19	87	0.250	1508.65	0.0348	23.07	173.07
1950	90	19.5	90	0.256	1521.97	0.036	23.65	173.65
2000	93	20	93	0.263	1535.52	0.0372	24.23	174.23
2050	96	20.5	96	0.269	1549.32	0.0384	24.79	174.79
2100	99	21	99	0.276	1563.37	0.0396	25.33	175.33
2150	100	21.5	100	0.282	1577.68	0.04	25.35	175.35
2200	102	22	102	0.289	1592.25	0.0408	25.62	175.62
Average water content sample 1, 2 and 3, %				**Average shear strength sample 1, 2 and 3, kPa**				
43.8				**13.0**				

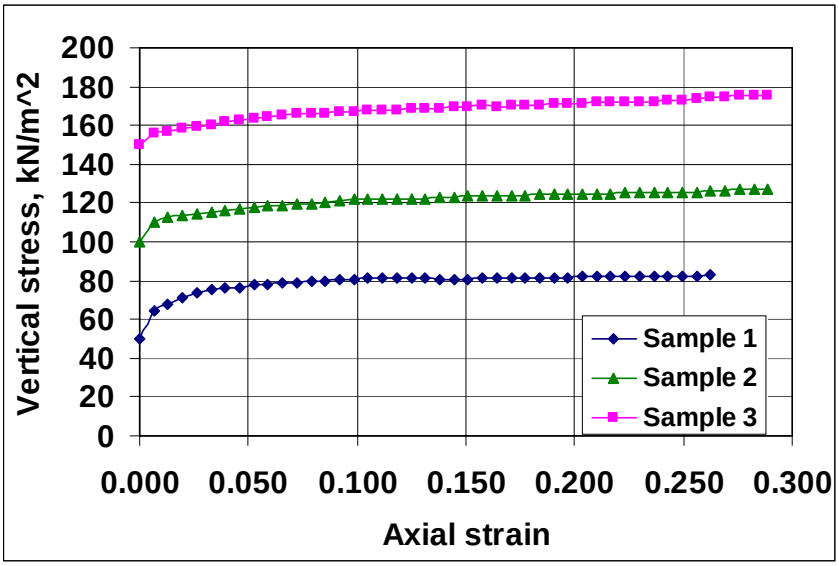

A(5) Data of quick undrained triaxial of kaolin

Summary of water content versus undrained shear strength test

Test no.	Average water content, %	Undrained shear strength, kPa
1	37.5	23.2
2	44.2	17.9
3	45.2	15.9

A(5a) Data of quick undrained triaxial in kaolin test 1 at average water content 37.5 %

Sample 1 = 50kPa			Moisture content			
Weight	g	154.1	Tin no	B4		

Length of sample		mm	76.14	Wet weight, g		157.9		
Diameter of sample		mm	37.96	Dry weight, g		116.36		
Area of sample		mm^2	1132.18	Tin empty, g		5.8		
Horizontal stress		kPa	100	Dry soil, g		110.56		
Force gauge correction factor		kN/division	0.0004	Weight of water, g		41.54		
Corrected compression gauge reading		mm	0.01mm	Moisture content %		37.57		
Shear strength		kPa	21.67					
Compression gauge reading (div)	Force gauge reading (div)	Corrected compression gauge reading (mm)	Corrected force gauge reading (div)	Axial strain	Corrected area (mm2)	Force (kN)	Deviator stress (kN/m2)	Vertical stress (kN/m2)
0	0	0	0	0.000	1132.18	0	0.00	50.00
50	38	0.5	38	0.007	1139.66	0.0152	13.34	63.34
100	49	1	49	0.013	1147.25	0.0196	17.08	67.08
150	55	1.5	55	0.020	1154.93	0.022	19.05	69.05
200	61	2	61	0.026	1162.72	0.0244	20.99	70.99
250	67	2.5	67	0.033	1170.62	0.0268	22.89	72.89
300	72	3	72	0.039	1178.62	0.0288	24.44	74.44
350	78	3.5	78	0.046	1186.73	0.0312	26.29	76.29
400	83	4	83	0.053	1194.96	0.0332	27.78	77.78
450	89	4.5	89	0.059	1203.30	0.0356	29.59	79.59
500	94	5	94	0.066	1211.75	0.0376	31.03	81.03
550	98	5.5	98	0.072	1220.33	0.0392	32.12	82.12
600	103	6	103	0.079	1229.03	0.0412	33.52	83.52
650	107	6.5	107	0.085	1237.85	0.0428	34.58	84.58
700	110	7	110	0.092	1246.81	0.044	35.29	85.29
750	112	7.5	112	0.099	1255.89	0.0448	35.67	85.67
800	115	8	115	0.105	1265.10	0.046	36.36	86.36
850	119	8.5	119	0.112	1274.46	0.0476	37.35	87.35
900	122	9	122	0.118	1283.95	0.0488	38.01	88.01
950	125	9.5	127	0.125	1293.58	0.0508	39.27	89.27
1000	127	10	129	0.131	1303.36	0.0516	39.59	89.59
1050	129	10.5	132	0.138	1313.29	0.0528	40.20	90.20
1100	132	11	134	0.144	1323.37	0.0536	40.50	90.50
1150	134	11.5	135	0.151	1333.60	0.054	40.49	90.49
1200	135	12	138	0.158	1344.00	0.0552	41.07	91.07
1250	138	12.5	140	0.164	1354.56	0.056	41.34	91.34
1300	140	13	143	0.171	1365.29	0.0572	41.90	91.90
1350	143	13.5	147	0.177	1376.18	0.0588	42.73	92.73
1400	147	14	149	0.184	1387.26	0.0596	42.96	92.96
1450	149	14.5	150	0.190	1398.51	0.06	42.90	92.90
1500	150	15	151	0.197	1409.95	0.0604	42.84	92.84
1550	151	15.5	154	0.204	1421.57	0.0616	43.33	93.33
1600	154	16	158	0.210	1433.39	0.0632	44.09	94.09
1650	158	16.5	161	0.217	1445.41	0.0644	44.55	94.55
1700	161	17	163	0.223	1457.63	0.0652	44.73	94.73
1750	163	17.5	165	0.230	1470.06	0.066	44.90	94.90

1800	165	18	166	0.236	1482.70	0.0664	44.78	94.78
1850	166	18.5	168	0.243	1495.56	0.0672	44.93	94.93
1900	168	19	168	0.250	1508.65	0.0672	44.54	94.54
1950	169	19.5	169	0.256	1521.97	0.0676	44.42	94.42
2000	170	20	170	0.263	1535.52	0.068	44.28	94.28
2050	172	20.5	172	0.269	1549.32	0.0688	44.41	94.41
2100	174	21	174	0.276	1563.37	0.0696	44.52	94.52

Sample 2 = 100kPa				Tin no		B3		
Weight		g	153.12	Wet weight, g		159.2		
Length of sample		mm	76.14	Dry weight, g		117.48		
Diameter of sample		mm	37.96	Tin empty, g		6.5		
Area of sample		mm^2	1132.18	Dry soil, g		110.98		
Horizontal stress		kPa	150	Weight of water, g		41.72		
Force gauge correction factor		kN/division	0.0004	Moisture content %		37.59		
Corrected compression gauge reading		mm	0.01mm					
Shear strength		kPa	23.50					
Compression gauge reading (div)	Force gauge reading (div)	Corrected compression gauge reading (mm)	Corrected force gauge reading (div)	Axial strain	Corrected area (mm2)	Force (kN)	Deviator stress (kN/m2)	Vertical stress (kN/m2)
0	0	0	0	0.000	1132.18	0	0.00	100.00
50	24	0.5	24	0.007	1139.66	0.0096	8.42	108.42
100	50	1	50	0.013	1147.25	0.02	17.43	117.43
150	61	1.5	61	0.020	1154.93	0.0244	21.13	121.13
200	69	2	69	0.026	1162.72	0.0276	23.74	123.74
250	73	2.5	73	0.033	1170.62	0.0292	24.94	124.94
300	78	3	78	0.039	1178.62	0.0312	26.47	126.47
350	83	3.5	83	0.046	1186.73	0.0332	27.98	127.98
400	87	4	87	0.053	1194.96	0.0348	29.12	129.12
450	91	4.5	91	0.059	1203.30	0.0364	30.25	130.25
500	96	5	96	0.066	1211.75	0.0384	31.69	131.69
550	100	5.5	100	0.072	1220.33	0.04	32.78	132.78
600	104	6	104	0.079	1229.03	0.0416	33.85	133.85
650	107	6.5	107	0.085	1237.85	0.0428	34.58	134.58
700	110	7	110	0.092	1246.81	0.044	35.29	135.29
750	114	7.5	114	0.099	1255.89	0.0456	36.31	136.31
800	122	8	122	0.105	1265.10	0.0488	38.57	138.57
850	128	8.5	128	0.112	1274.46	0.0512	40.17	140.17
900	134	9	134	0.118	1283.95	0.0536	41.75	141.75
950	136	9.5	136	0.125	1293.58	0.0544	42.05	142.05
1000	138	10	138	0.131	1303.36	0.0552	42.35	142.35
1050	140	10.5	140	0.138	1313.29	0.056	42.64	142.64
1100	144	11	144	0.144	1323.37	0.0576	43.53	143.53
1150	147	11.5	147	0.151	1333.60	0.0588	44.09	144.09
1200	151	12	151	0.158	1344.00	0.0604	44.94	144.94
1250	153	12.5	153	0.164	1354.56	0.0612	45.18	145.18

1300	156	13	156	0.171	1365.29	0.0624	45.70	145.70
1350	158	13.5	158	0.177	1376.18	0.0632	45.92	145.92
1400	161	14	161	0.184	1387.26	0.0644	46.42	146.42
1450	165	14.5	165	0.190	1398.51	0.066	47.19	147.19
1500	167	15	167	0.197	1409.95	0.0668	47.38	147.38
1550	167	15.5	167	0.204	1421.57	0.0668	46.99	146.99
1600	172	16	172	0.210	1433.39	0.0688	48.00	148.00
1650	175	16.5	175	0.217	1445.41	0.07	48.43	148.43
1700	177	17	177	0.223	1457.63	0.0708	48.57	148.57
1750	179	17.5	179	0.230	1470.06	0.0716	48.71	148.71
1800	182	18	182	0.236	1482.70	0.0728	49.10	149.10
1850	184	18.5	184	0.243	1495.56	0.0736	49.21	149.21
1900	186	19	186	0.250	1508.65	0.0744	49.32	149.32
1950	188	19.5	188	0.256	1521.97	0.0752	49.41	149.41
2000	190	20	190	0.263	1535.52	0.076	49.49	149.49
2050	192	20.5	192	0.269	1549.32	0.0768	49.57	149.57
2100	194	21	194	0.276	1563.37	0.0776	49.64	149.64

Sample 3 = 150kPa				Tin no		C3		
Weight		g	153.8	Wet weight, g		170.3		
Length of sample		mm	76.14	Dry weight, g		128.75		
Diameter of sample		mm	37.96	Tin empty, g		17.6		
Area of sample		mm^2	1132.18	Dry soil, g		111.15		
Horizontal stress		kPa	150	Weight of water, g		41.55		
Force gauge correction factor		kN/division	0.0004	Moisture content %		37.38		
Corrected compression gauge reading		mm	0.01mm					
Shear strength		kPa	24.48					
Compression gauge reading (div)	Force gauge reading (div)	Corrected compression gauge reading (mm)	Corrected force gauge reading (div)	Axial strain	Corrected area (mm2)	Force (kN)	Deviator stress (kN/m2)	Vertical stress (kN/m2)
0	0	0	0	0.000	1132.18	0	0.00	150.00
50	18	0.5	18	0.007	1139.66	0.0072	6.32	156.32
100	22	1	22	0.013	1147.25	0.0088	7.67	157.67
150	26	1.5	26	0.020	1154.93	0.0104	9.00	159.00
200	31	2	31	0.026	1162.72	0.0124	10.66	160.66
250	37	2.5	37	0.033	1170.62	0.0148	12.64	162.64
300	45	3	45	0.039	1178.62	0.018	15.27	165.27
350	54	3.5	54	0.046	1186.73	0.0216	18.20	168.20
400	66	4	66	0.053	1194.96	0.0264	22.09	172.09
450	72	4.5	72	0.059	1203.30	0.0288	23.93	173.93
500	81	5	81	0.066	1211.75	0.0324	26.74	176.74
550	88	5.5	88	0.072	1220.33	0.0352	28.84	178.84
600	95	6	95	0.079	1229.03	0.038	30.92	180.92
650	104	6.5	104	0.085	1237.85	0.0416	33.61	183.61
700	113	7	113	0.092	1246.81	0.0452	36.25	186.25

750	119	7.5	119	0.099	1255.89	0.0476	37.90	187.90
800	124	8	124	0.105	1265.10	0.0496	39.21	189.21
850	128	8.5	128	0.112	1274.46	0.0512	40.17	190.17
900	133	9	133	0.118	1283.95	0.0532	41.43	191.43
950	138	9.5	138	0.125	1293.58	0.0552	42.67	192.67
1000	143	10	143	0.131	1303.36	0.0572	43.89	193.89
1050	146	10.5	146	0.138	1313.29	0.0584	44.47	194.47
1100	150	11	150	0.144	1323.37	0.06	45.34	195.34
1150	153	11.5	153	0.151	1333.60	0.0612	45.89	195.89
1200	156	12	156	0.158	1344.00	0.0624	46.43	196.43
1250	160	12.5	160	0.164	1354.56	0.064	47.25	197.25
1300	163	13	163	0.171	1365.29	0.0652	47.76	197.76
1350	165	13.5	165	0.177	1376.18	0.066	47.96	197.96
1400	168	14	168	0.184	1387.26	0.0672	48.44	198.44
1450	171	14.5	171	0.190	1398.51	0.0684	48.91	198.91
1500	173	15	173	0.197	1409.95	0.0692	49.08	199.08
1550	174	15.5	174	0.204	1421.57	0.0696	48.96	198.96
1600	175	16	175	0.210	1433.39	0.07	48.84	198.84
1650	177	16.5	177	0.217	1445.41	0.0708	48.98	198.98
1700	179	17	179	0.223	1457.63	0.0716	49.12	199.12
1750	181	17.5	181	0.230	1470.06	0.0724	49.25	199.25
1800	182	18	182	0.236	1482.70	0.0728	49.10	199.10
1850	184	18.5	184	0.243	1495.56	0.0736	49.21	199.21
1900	186	19	186	0.250	1508.65	0.0744	49.32	199.32
1950	187	19.5	187	0.256	1521.97	0.0748	49.15	199.15
2000	189	20	189	0.263	1535.52	0.0756	49.23	199.23
Average water content sample 1, 2 and 3, %				**Average shear strength sample 1, 2 and 3, kPa**				
37.5				**23.2**				

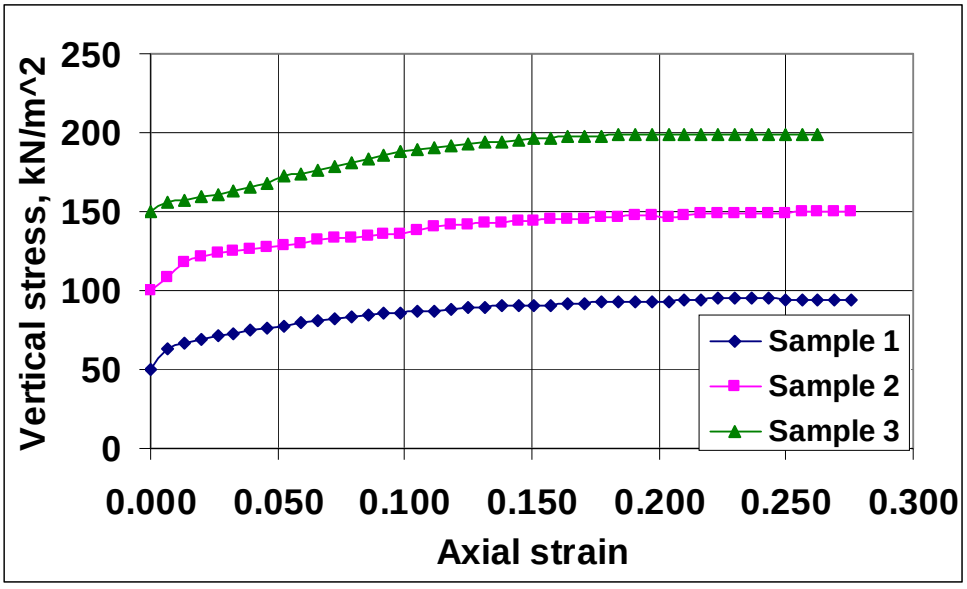

A(5b) Data of quick undrained triaxial in kaolin test 2 at average water content 44.2 %.

Sample 1= 50kPa				Moisture content				
Weight		g	145.05	Tin no		B1		
Length of sample		mm	76.14	Wet weight, g		57.5		
Diameter of sample		mm	37.96	Dry weight, g		41.51		
Area of sample		mm^2	1132.18	Tin empty, g		5.33		
Horizontal stress		kPa	100	Dry soil, g		36.18		
Force gauge correction factor		kN/division	0.0004	Weight of water, g		15.99		
Corrected compression gauge reading		mm	0.01	Moisture content %		44.20		
Shear strength		kPa	18.01					
Compression gauge reading (div)	Force gauge reading (div)	Corrected compression gauge reading (mm)	Corrected force gauge reading (div)	Axial strain	Corrected area (mm2)	Force (kN)	Deviator stress (kN/m2)	Vertical stress (kN/m2)
0	0	0	0	0.000	1132.18	0	0.00	50.00
50	25	0.5	25	0.007	1139.66	0.01	8.77	58.77
100	35	1	35	0.013	1147.25	0.014	12.20	62.20
150	41	1.5	41	0.020	1154.93	0.016	14.20	64.20
200	46	2	46	0.026	1162.72	0.018	15.82	65.82
250	50	2.5	50	0.033	1170.62	0.02	17.09	67.09
300	55	3	55	0.039	1178.62	0.022	18.67	68.67
350	61	3.5	61	0.046	1186.73	0.024	20.56	70.56
400	67	4	67	0.053	1194.96	0.027	22.43	72.43
450	70	4.5	70	0.059	1203.30	0.028	23.27	73.27
500	75	5	75	0.066	1211.75	0.03	24.76	74.76
550	77	5.5	77	0.072	1220.33	0.031	25.24	75.24
600	81	6	81	0.079	1229.03	0.032	26.36	76.36
650	85	6.5	85	0.085	1237.85	0.034	27.47	77.47
700	88	7	88	0.092	1246.81	0.035	28.23	78.23
750	91	7.5	91	0.099	1255.89	0.036	28.98	78.98
800	95	8	95	0.105	1265.10	0.038	30.04	80.04
850	97	8.5	97	0.112	1274.46	0.039	30.44	80.44
900	98	9	98	0.118	1283.95	0.039	30.53	80.53
950	101	9.5	101	0.125	1293.58	0.04	31.23	81.23
1000	105	10	105	0.131	1303.36	0.042	32.22	82.22
1050	108	10.5	108	0.138	1313.29	0.043	32.89	82.89
1100	110	11	110	0.144	1323.37	0.044	33.25	83.25
1150	113	11.5	113	0.151	1333.60	0.045	33.89	83.89
1200	115	12	115	0.158	1344.00	0.046	34.23	84.23
1250	118	12.5	118	0.164	1354.56	0.047	34.85	84.85
1300	120	13	120	0.171	1365.29	0.048	35.16	85.16
1350	122	13.5	122	0.177	1376.18	0.049	35.46	85.46
1400	124	14	124	0.184	1387.26	0.05	35.75	85.75
1450	125	14.5	125	0.190	1398.51	0.05	35.75	85.75
1500	126	15	126	0.197	1409.95	0.05	35.75	85.75

1550	128	15.5	128	0.204	1421.57	0.051	36.02	86.02
1600	129	16	129	0.210	1433.39	0.052	36.00	86.00
1650	130	16.5	130	0.217	1445.41	0.052	35.98	85.98
1700	130	17	130	0.223	1457.63	0.052	35.67	85.67
1750	132	17.5	132	0.230	1470.06	0.053	35.92	85.92
1800	132	18	132	0.236	1482.70	0.053	35.61	85.61
1850	133	18.5	133	0.243	1495.56	0.053	35.57	85.57
1900	134	19	134	0.250	1508.65	0.054	35.53	85.53
1950	134	19.5	134	0.256	1521.97	0.054	35.22	85.22
2000	135	20	135	0.263	1535.52	0.054	35.17	85.17
2050	135	20.5	135	0.269	1549.32	0.054	34.85	84.85
2100	136	21	136	0.276	1563.37	0.054	34.80	84.80

Sample 2 = 100kPa				Moisture content				
Weight		g	146.76	Tin no		B4		
Length of sample		mm	76.14	Wet weight, g		87.03		
Diameter of sample		mm	37.96	Dry weight, g		62.04		
Area of sample		mm^2	1132.18	Tin empty, g		5.43		
Horizontal stress		kPa	100	Dry soil, g		56.61		
Force gauge correction factor		kN/division	0.0004	Weight of water, g		24.99		
Corrected compression gauge reading		mm	0.01mm	Moisture content %		44.14		
Shear strength		kPa	17.02	Average				
Compression gauge reading (div) 1.5	Force gauge reading (div) 7	Corrected compression gauge reading (mm)	Corrected force gauge reading (div)	Axial strain	Corrected area (mm2)	Force (kN)	Deviator stress (kN/m2)	Vertical stress (kN/m2)
0	0	0	0	0.000	1132.18	0	0.00	100.00
50	36	0.5	36	0.007	1139.66	0.014	12.64	112.64
100	56	1	56	0.013	1147.25	0.022	19.52	119.52
150	58	1.5	58	0.020	1154.93	0.023	20.09	120.09
200	60	2	60	0.026	1162.72	0.024	20.64	120.64
250	63	2.5	63	0.033	1170.62	0.025	21.53	121.53
300	64	3	64	0.039	1178.62	0.026	21.72	121.72
350	67	3.5	67	0.046	1186.73	0.027	22.58	122.58
400	69	4	69	0.053	1194.96	0.028	23.10	123.10
450	71	4.5	71	0.059	1203.30	0.028	23.60	123.60
500	73	5	73	0.066	1211.75	0.029	24.10	124.10
550	76	5.5	76	0.072	1220.33	0.03	24.91	124.91
600	79	6	79	0.079	1229.03	0.032	25.71	125.71
650	82	6.5	82	0.085	1237.85	0.033	26.50	126.50
700	85	7	85	0.092	1246.81	0.034	27.27	127.27
750	88	7.5	88	0.099	1255.89	0.035	28.03	128.03
800	90	8	90	0.105	1265.10	0.036	28.46	128.46
850	92	8.5	92	0.112	1274.46	0.037	28.88	128.88
900	94	9	94	0.118	1283.95	0.038	29.28	129.28
950	96	9.5	96	0.125	1293.58	0.038	29.69	129.69
1000	98	10	98	0.131	1303.36	0.039	30.08	130.08

1050	100	10.5	100	0.138	1313.29	0.04	30.46	130.46
1100	103	11	103	0.144	1323.37	0.041	31.13	131.13
1150	106	11.5	106	0.151	1333.60	0.042	31.79	131.79
1200	109	12	109	0.158	1344.00	0.044	32.44	132.44
1250	111	12.5	111	0.164	1354.56	0.044	32.78	132.78
1300	113	13	113	0.171	1365.29	0.045	33.11	133.11
1350	114	13.5	114	0.177	1376.18	0.046	33.14	133.14
1400	115	14	115	0.184	1387.26	0.046	33.16	133.16
1450	117	14.5	117	0.190	1398.51	0.047	33.46	133.46
1500	119	15	119	0.197	1409.95	0.048	33.76	133.76
1550	121	15.5	121	0.204	1421.57	0.048	34.05	134.05
1600	123	16	123	0.210	1433.39	0.049	34.32	134.32
1650	125	16.5	125	0.217	1445.41	0.05	34.59	134.59
1700	125	17	125	0.223	1457.63	0.05	34.30	134.30
1750	126	17.5	126	0.230	1470.06	0.05	34.28	134.28
1800	127	18	127	0.236	1482.70	0.051	34.26	134.26
1850	128	18.5	128	0.243	1495.56	0.051	34.23	134.23
1900	129	19	129	0.250	1508.65	0.052	34.20	134.20
1950	130	19.5	130	0.256	1521.97	0.052	34.17	134.17
2000	131	20	131	0.263	1535.52	0.052	34.13	134.13

Sample 3 = 150kPa				Tin no		A3		
Weight		g	144.84	Wet weight, g		163.7		
Length of sample		mm	76.14	Dry weight, g		115		
Diameter of sample		mm	37.96	Tin empty, g		4.76		
Area of sample		mm^2	1132.18	Dry soil, g		110.2		
Horizontal stress		kPa	150	Weight of water, g		48.72		
Force gauge correction factor		kN/division	0.0004	Moisture content %		44.19		
Corrected compression gauge reading		mm	0.01mm	Average				
Shear strength		kPa	18.71					
Compression gauge reading (div)	Force gauge reading (div)	Corrected compression gauge reading (mm)	Corrected force gauge reading (div)	Axial strain	Corrected area (mm2)	Force (kN)	Deviator stress (kN/m2)	Vertical stress (kN/m2)
0	0	0	0	0.000	1132.18	0	0.00	150.00
50	38	0.5	38	0.007	1139.66	0.015	13.34	163.34
100	45	1	45	0.013	1147.25	0.018	15.69	165.69
150	50	1.5	50	0.020	1154.93	0.02	17.32	167.32
200	54	2	54	0.026	1162.72	0.022	18.58	168.58
250	58	2.5	58	0.033	1170.62	0.023	19.82	169.82
300	60	3	60	0.039	1178.62	0.024	20.36	170.36
350	64	3.5	64	0.046	1186.73	0.026	21.57	171.57
400	67	4	67	0.053	1194.96	0.027	22.43	172.43
450	71	4.5	71	0.059	1203.30	0.028	23.60	173.60
500	75	5	75	0.066	1211.75	0.03	24.76	174.76
550	79	5.5	79	0.072	1220.33	0.032	25.89	175.89
600	83	6	83	0.079	1229.03	0.033	27.01	177.01

650	85	6.5	85	0.085	1237.85	0.034	27.47	177.47
700	89	7	89	0.092	1246.81	0.036	28.55	178.55
750	92	7.5	92	0.099	1255.89	0.037	29.30	179.30
800	95	8	95	0.105	1265.10	0.038	30.04	180.04
850	98	8.5	98	0.112	1274.46	0.039	30.76	180.76
900	101	9	101	0.118	1283.95	0.04	31.47	181.47
950	103	9.5	103	0.125	1293.58	0.041	31.85	181.85
1000	106	10	106	0.131	1303.36	0.042	32.53	182.53
1050	110	10.5	110	0.138	1313.29	0.044	33.50	183.50
1100	113	11	113	0.144	1323.37	0.045	34.16	184.16
1150	115	11.5	115	0.151	1333.60	0.046	34.49	184.49
1200	116	12	116	0.158	1344.00	0.046	34.52	184.52
1250	118	12.5	118	0.164	1354.56	0.047	34.85	184.85
1300	120	13	120	0.171	1365.29	0.048	35.16	185.16
1350	123	13.5	123	0.177	1376.18	0.049	35.75	185.75
1400	125	14	125	0.184	1387.26	0.05	36.04	186.04
1450	128	14.5	128	0.190	1398.51	0.051	36.61	186.61
1500	131	15	131	0.197	1409.95	0.052	37.16	187.16
1550	133	15.5	133	0.204	1421.57	0.053	37.42	187.42
1600	134	16	134	0.210	1433.39	0.054	37.39	187.39
1650	137	16.5	137	0.217	1445.41	0.055	37.91	187.91
1700	139	17	139	0.223	1457.63	0.056	38.14	188.14
1750	140	17.5	140	0.230	1470.06	0.056	38.09	188.09
1800	142	18	142	0.236	1482.70	0.057	38.31	188.31
1850	144	18.5	144	0.243	1495.56	0.058	38.51	188.51
1900	146	19	146	0.250	1508.65	0.058	38.71	188.71
1950	148	19.5	148	0.256	1521.97	0.059	38.90	188.90
2000	150	20	150	0.263	1535.52	0.06	39.07	189.07
2050	153	20.5	153	0.269	1549.32	0.061	39.50	189.50
2100	155	21	155	0.276	1563.37	0.062	39.66	189.66
2150	156	21.5	156	0.282	1577.68	0.062	39.55	189.55
Average water content sample 1, 2 and 3, %				**Average shear strength sample 1, 2 and 3, kPa**				
44.2				**17.9**				

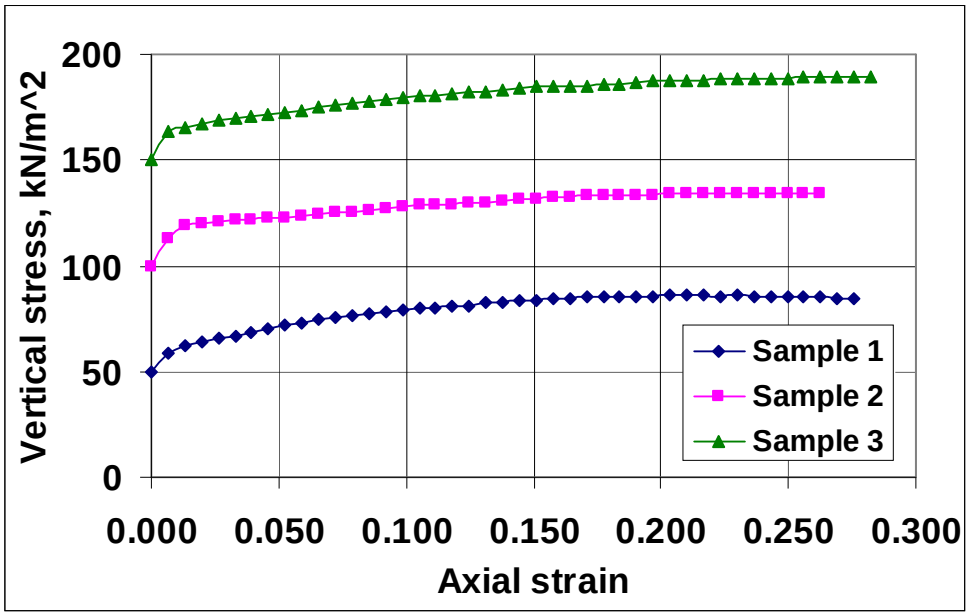

A(5c) Data of quick undrained triaxial in kaolin test 3 at average water content 45.2 %

Sample 1= 50kPa				Moisture content				
Weight		g	141.44	Tin no		B1		
Length of sample		mm	76.14	Wet weight, g		84.6		
Diameter of sample		mm	37.96	Dry weight, g		59.92		
Area of sample		mm^2	1132.18	Tin empty, g		5.33		
Horizontal stress		kPa	100	Dry soil, g		54.59		
Force gauge correction factor		kN/division	0.0004	Weight of water, g		24.68		
Corrected compression gauge reading		mm	0.01	Moisture content %		45.21		
Shear strength		kPa	15.62					
Compression gauge reading (div)	Force gauge reading (div)	Corrected compression gauge reading (mm)	Corrected force gauge reading (div)	Axial strain	Corrected area (mm2)	Force (kN)	Deviator stress (kN/m2)	Vertical stress (kN/m2)
0	0	0	0	0.000	1132.18	0	0.00	50.00
50	27	0.5	27	0.007	1139.66	0.011	9.48	59.48
100	35	1	35	0.013	1147.25	0.014	12.20	62.20
150	37	1.5	37	0.020	1154.93	0.015	12.81	62.81
200	40	2	40	0.026	1162.72	0.016	13.76	63.76
250	43	2.5	43	0.033	1170.62	0.017	14.69	64.69
300	47	3	47	0.039	1178.62	0.019	15.95	65.95
350	51	3.5	51	0.046	1186.73	0.02	17.19	67.19
400	54	4	54	0.053	1194.96	0.022	18.08	68.08
450	57	4.5	57	0.059	1203.30	0.023	18.95	68.95

500	61	5	61	0.066	1211.75	0.024	20.14	70.14
550	65	5.5	65	0.072	1220.33	0.026	21.31	71.31
600	67	6	67	0.079	1229.03	0.027	21.81	71.81
650	69	6.5	69	0.085	1237.85	0.028	22.30	72.30
700	71	7	71	0.092	1246.81	0.028	22.78	72.78
750	74	7.5	74	0.099	1255.89	0.03	23.57	73.57
800	77	8	77	0.105	1265.10	0.031	24.35	74.35
850	79	8.5	79	0.112	1274.46	0.032	24.79	74.79
900	81	9	81	0.118	1283.95	0.032	25.23	75.23
950	83	9.5	83	0.125	1293.58	0.033	25.67	75.67
1000	85	10	85	0.131	1303.36	0.034	26.09	76.09
1050	87	10.5	87	0.138	1313.29	0.035	26.50	76.50
1100	90	11	90	0.144	1323.37	0.036	27.20	77.20
1150	93	11.5	93	0.151	1333.60	0.037	27.89	77.89
1200	95	12	95	0.158	1344.00	0.038	28.27	78.27
1250	97	12.5	97	0.164	1354.56	0.039	28.64	78.64
1300	100	13	100	0.171	1365.29	0.04	29.30	79.30
1350	102	13.5	102	0.177	1376.18	0.041	29.65	79.65
1400	104	14	104	0.184	1387.26	0.042	29.99	79.99
1450	107	14.5	107	0.190	1398.51	0.043	30.60	80.60
1500	109	15	109	0.197	1409.95	0.044	30.92	80.92
1550	111	15.5	111	0.204	1421.57	0.044	31.23	81.23
1600	113	16	113	0.210	1433.39	0.045	31.53	81.53
1650	115	16.5	115	0.217	1445.41	0.046	31.82	81.82
1700	118	17	118	0.223	1457.63	0.047	32.38	82.38
1750	119	17.5	119	0.230	1470.06	0.048	32.38	82.38
1800	120	18	120	0.236	1482.70	0.048	32.37	82.37
1850	122	18.5	122	0.243	1495.56	0.049	32.63	82.63
1900	123	19	123	0.250	1508.65	0.049	32.61	82.61
1950	123	19.5	123	0.256	1521.97	0.049	32.33	82.33
2000	124	20	124	0.263	1535.52	0.05	32.30	82.30
2050	124	20.5	124	0.269	1549.32	0.05	32.01	82.01
2100	125	21	125	0.276	1563.37	0.05	31.98	81.98

Sample 2 = 100kPa			Moisture content			
Weight	g	146.76	Tin no	E4		
Length of sample	mm	76.14	Wet weight, g	75.13		
Diameter of sample	mm	37.96	Dry weight, g	53.54		
Area of sample	mm^2	1132.18	Tin empty, g	5.48		
Horizontal stress	kPa	100	Dry soil, g	48.06		
Force gauge correction factor	kN/division	0.0004	Weight of water, g	21.59		
Corrected compression gauge reading	mm	0.01mm	Moisture content %	44.92		
Shear strength	kPa	15.76	Average			

Compression gauge reading (div) 1.5	Force gauge reading (div) 7	Corrected compression gauge reading (mm)	Corrected force gauge reading (div)	Axial strain	Corrected area (mm2)	Force (kN)	Deviator stress (kN/m2)	Vertical stress (kN/m2)
0	0	0	0	0.000	1132.18	0	0.00	100.00
50	38	0.5	38	0.007	1139.66	0.015	13.34	113.34
100	44	1	44	0.013	1147.25	0.018	15.34	115.34
150	47	1.5	47	0.020	1154.93	0.019	16.28	116.28
200	51	2	51	0.026	1162.72	0.02	17.55	117.55
250	54	2.5	54	0.033	1170.62	0.022	18.45	118.45
300	56	3	56	0.039	1178.62	0.022	19.01	119.01
350	59	3.5	59	0.046	1186.73	0.024	19.89	119.89
400	62	4	62	0.053	1194.96	0.025	20.75	120.75
450	64	4.5	64	0.059	1203.30	0.026	21.27	121.27
500	67	5	67	0.066	1211.75	0.027	22.12	122.12
550	70	5.5	70	0.072	1220.33	0.028	22.94	122.94
600	72	6	72	0.079	1229.03	0.029	23.43	123.43
650	75	6.5	75	0.085	1237.85	0.03	24.24	124.24
700	77	7	77	0.092	1246.81	0.031	24.70	124.70
750	80	7.5	80	0.099	1255.89	0.032	25.48	125.48
800	82	8	82	0.105	1265.10	0.033	25.93	125.93
850	85	8.5	85	0.112	1274.46	0.034	26.68	126.68
900	86	9	86	0.118	1283.95	0.034	26.79	126.79
950	88	9.5	88	0.125	1293.58	0.035	27.21	127.21
1000	90	10	90	0.131	1303.36	0.036	27.62	127.62
1050	92	10.5	92	0.138	1313.29	0.037	28.02	128.02
1100	95	11	95	0.144	1323.37	0.038	28.71	128.71
1150	97	11.5	97	0.151	1333.60	0.039	29.09	129.09
1200	99	12	99	0.158	1344.00	0.04	29.46	129.46
1250	102	12.5	102	0.164	1354.56	0.041	30.12	130.12
1300	104	13	104	0.171	1365.29	0.042	30.47	130.47
1350	105	13.5	105	0.177	1376.18	0.042	30.52	130.52
1400	107	14	107	0.184	1387.26	0.043	30.85	130.85
1450	109	14.5	109	0.190	1398.51	0.044	31.18	131.18
1500	110	15	110	0.197	1409.95	0.044	31.21	131.21
1550	112	15.5	112	0.204	1421.57	0.045	31.51	131.51
1600	113	16	113	0.210	1433.39	0.045	31.53	131.53
1650	115	16.5	115	0.217	1445.41	0.046	31.82	131.82
1700	118	17	118	0.223	1457.63	0.047	32.38	132.38
1750	119	17.5	119	0.230	1470.06	0.048	32.38	132.38
1800	121	18	121	0.236	1482.70	0.048	32.64	132.64
1850	122	18.5	122	0.243	1495.56	0.049	32.63	132.63
1900	123	19	123	0.250	1508.65	0.049	32.61	132.61
1950	123	19.5	123	0.256	1521.97	0.049	32.33	132.33
2000	123	20	123	0.263	1535.52	0.049	32.04	132.04

Sample 3 = 150kPa				Tin no	E3		

Weight		g	144.84	Wet weight, g		105.7		
Length of sample		mm	76.14	Dry weight, g		74.02		
Diameter of sample		mm	37.96	Tin empty, g		4.58		
Area of sample		mm^2	1132.18	Dry soil, g		69.44		
Horizontal stress		kPa	150	Weight of water, g		31.65		
Force gauge correction factor		kN/division	0.0004	Moisture content %		45.58		
Corrected compression gauge reading		mm	0.01mm	Average				
Shear strength		kPa	16.46					
Compression gauge reading (div)	Force gauge reading (div)	Corrected compression gauge reading (mm)	Corrected force gauge reading (div)	Axial strain	Corrected area (mm2)	Force (kN)	Deviator stress (kN/m2)	Vertical stress (kN/m2)
0	0	0	0	0.000	1132.18	0	0.00	150.00
50	39	0.5	39	0.007	1139.66	0.016	13.69	163.69
100	43	1	43	0.013	1147.25	0.017	14.99	164.99
150	45	1.5	45	0.020	1154.93	0.018	15.59	165.59
200	48	2	48	0.026	1162.72	0.019	16.51	166.51
250	52	2.5	52	0.033	1170.62	0.021	17.77	167.77
300	56	3	56	0.039	1178.62	0.022	19.01	169.01
350	59	3.5	59	0.046	1186.73	0.024	19.89	169.89
400	62	4	62	0.053	1194.96	0.025	20.75	170.75
450	65	4.5	65	0.059	1203.30	0.026	21.61	171.61
500	69	5	69	0.066	1211.75	0.028	22.78	172.78
550	72	5.5	72	0.072	1220.33	0.029	23.60	173.60
600	75	6	75	0.079	1229.03	0.03	24.41	174.41
650	78	6.5	78	0.085	1237.85	0.031	25.20	175.20
700	80	7	80	0.092	1246.81	0.032	25.67	175.67
750	82	7.5	82	0.099	1255.89	0.033	26.12	176.12
800	84	8	84	0.105	1265.10	0.034	26.56	176.56
850	87	8.5	87	0.112	1274.46	0.035	27.31	177.31
900	88	9	88	0.118	1283.95	0.035	27.42	177.42
950	91	9.5	91	0.125	1293.58	0.036	28.14	178.14
1000	93	10	93	0.131	1303.36	0.037	28.54	178.54
1050	95	10.5	95	0.138	1313.29	0.038	28.94	178.94
1100	98	11	98	0.144	1323.37	0.039	29.62	179.62
1150	100	11.5	100	0.151	1333.60	0.04	29.99	179.99
1200	102	12	102	0.158	1344.00	0.041	30.36	180.36
1250	105	12.5	105	0.164	1354.56	0.042	31.01	181.01
1300	107	13	107	0.171	1365.29	0.043	31.35	181.35
1350	109	13.5	109	0.177	1376.18	0.044	31.68	181.68
1400	110	14	110	0.184	1387.26	0.044	31.72	181.72
1450	112	14.5	112	0.190	1398.51	0.045	32.03	182.03
1500	114	15	114	0.197	1409.95	0.046	32.34	182.34
1550	117	15.5	117	0.204	1421.57	0.047	32.92	182.92

1600	119	16	119	0.210	1433.39	0.048	33.21	183.21
1650	121	16.5	121	0.217	1445.41	0.048	33.49	183.49
1700	123	17	123	0.223	1457.63	0.049	33.75	183.75
1750	125	17.5	125	0.230	1470.06	0.05	34.01	184.01
1800	128	18	128	0.236	1482.70	0.051	34.53	184.53
1850	131	18.5	131	0.243	1495.56	0.052	35.04	185.04
1900	134	19	134	0.250	1508.65	0.054	35.53	185.53
1950	137	19.5	137	0.256	1521.97	0.055	36.01	186.01
2000	140	20	140	0.263	1535.52	0.056	36.47	186.47
2050	142	20.5	142	0.269	1549.32	0.057	36.66	186.66
2100	143	21	143	0.276	1563.37	0.057	36.59	186.59
2150	143	21.5	143	0.282	1577.68	0.057	36.26	186.26

Average water content sample 1, 2 and 3, %	Average shear strength sample 1, 2 and 3, kPa
45.2	15.9
Remarks: Sample preparation by dietert compaction, rate of compression 1.2mm/minute.	

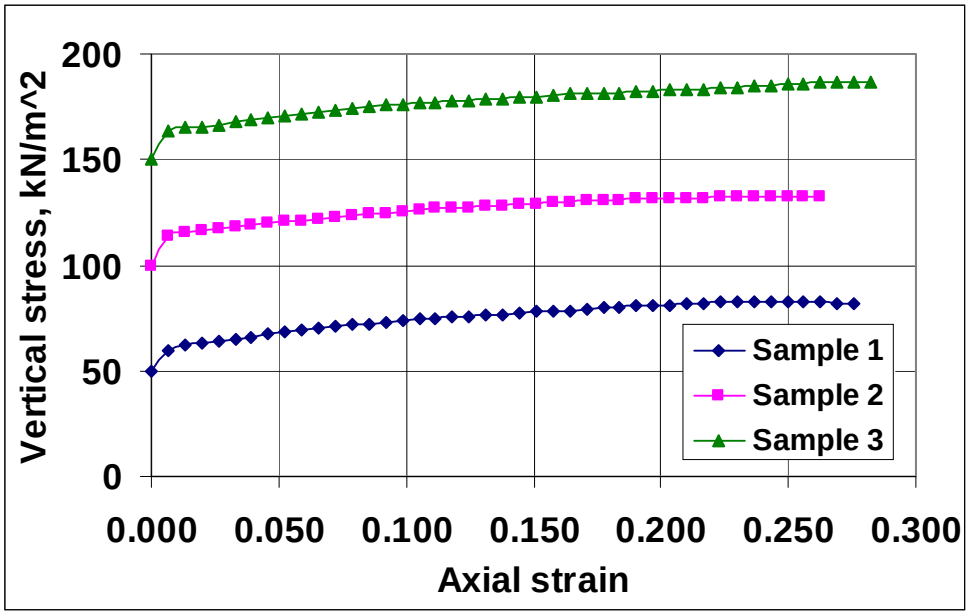

ii. Detail results of seismic surface wave testing

A(6) Data of seismic test result in homogeneous kaolin (see Section 7.2.1)

Seismic test carried out using kaolin clay before columns installation which the seismic source at one end of the array.
Test ID: 15Mar10_01
Date of test: 15 March 2010
Test frequency range / interval: 100 to 3000 Hz / 50 Hz
Remarks: Phase velocities without limiting with coherence.

Frequency, Hz	A-B, m/s	B-C, m/s	C-D, m/s	Frequency, Hz	A-B, m/s	B-C, m/s	C-D, m/s
99.9	330.7	22.7	12.9	1549.9	55.1	45.2	2626.4
149.9	226.5	1070.9	981.4	1599.9	55.2	45.2	4207.9
199.9	40.3	22.7	128.5	1649.9	56.8	44.5	2068.7
249.9	40.5	63.7	41.5	1699.8	57.0	43.8	868.5
299.8	14.3	227.6	773.1	1750.2	57.3	43.8	227.4
350.2	40.2	170.7	24.2	1800.2	55.6	45.1	78.9
400.2	53.0	37.3	14.0	1850.1	54.5	46.4	65.6
450.1	90.2	30.6	17.3	1900.1	56.7	51.7	52.4
500.1	46.4	43.9	23.5	1950.1	57.5	52.0	51.1
550.1	43.8	46.2	25.8	2000.0	57.2	55.5	48.5
600.1	58.6	38.0	32.4	2050.0	56.2	56.0	60.5
650.0	60.4	32.0	30.3	2100.0	56.1	54.0	64.6
700.0	53.4	41.9	43.2	2150.0	56.7	53.1	63.9
750.0	49.1	44.0	42.1	2199.9	57.3	53.0	61.4
799.9	44.8	42.6	59.9	2249.9	58.0	52.8	60.9
849.9	43.9	46.8	41.4	2299.9	58.1	52.5	61.2
899.9	42.5	46.3	51.2	2349.9	57.5	53.8	59.1
949.9	44.9	42.2	54.7	2399.8	56.6	55.7	56.1
999.8	44.5	41.4	65.4	2450.2	56.3	56.3	55.0
1050.2	50.9	42.8	85.7	2500.2	56.9	55.5	54.4
1100.2	46.5	53.2	165.6	2550.1	58.3	54.0	52.9
1150.1	52.5	43.8	147.8	2600.1	58.4	52.9	51.4
1200.1	56.2	42.4	131.7	2650.1	57.7	52.0	50.4
1250.1	53.2	40.0	113.4	2700.0	56.9	51.1	49.4
1300.0	54.2	38.4	120.1	2750.0	55.9	50.7	49.2
1350.0	53.7	42.0	200.1	2800.0	55.4	50.5	49.6
1400.0	54.5	43.1	437.5	2850.0	55.2	49.3	50.7
1450.0	56.7	45.3	1505.5	2899.9	55.4	67.4	73.0
1499.9	56.2	44.3	1050.4	2949.9	55.8	62.9	71.7
				2999.9	56.5	59.5	64.4

Seismic test carried out using kaolin clay before columns installation which the seismic source at one end of the array.
Test ID: 15Mar10_01
Date of test: 15 March 2010
Test frequency range / interval: 100 to 3000 Hz / 50 Hz

Remarks: Phase velocities with limiting with coherence larger than 0.9

Frequency, Hz	A-B, m/s	Frequency, Hz	B-C, m/s	Frequency, Hz	C-D, m/s
99.9	330.7	149.9	1070.9	149.9	981.4
149.9	226.5	249.9	63.7	199.9	128.5
249.9	40.5	299.8	227.6	249.9	41.5
299.8	14.3	350.2	170.7	299.8	773.1
350.2	40.2	450.1	30.6	350.2	24.2
400.2	53.0	500.1	43.9	450.1	17.3
450.1	90.2	550.1	46.2	500.1	23.5
500.1	46.4	600.1	38.0	550.1	25.8
550.1	43.8	650.0	32.0	600.1	32.4
600.1	58.6	700.0	41.9	650.0	30.3
650.0	60.4	750.0	44.0	700.0	43.2
700.0	53.4	799.9	42.6	750.0	42.1
750.0	49.1	849.9	46.8	799.9	59.9
799.9	44.8	899.9	46.3	849.9	41.4
849.9	43.9	999.8	41.4	899.9	51.2
899.9	42.5	1050.2	42.8	949.9	54.7
999.8	44.5	1100.2	53.2	999.8	65.4
1050.2	50.9	1150.1	43.8	1050.2	85.7
1100.2	46.5	1200.1	42.4	1100.2	165.6
1150.1	52.5	1250.1	40.0	1150.1	147.8
1200.1	56.2	1300.0	38.4	1200.1	131.7
1250.1	53.2	1350.0	42.0	1250.1	113.4
1300.0	54.2	1400.0	43.1	1300.0	120.1
1350.0	53.7	1450.0	45.3	1350.0	200.1
1400.0	54.5	1499.9	44.3	1400.0	437.5
1450.0	56.7	1549.9	45.2	1450.0	1505.5
1499.9	56.2	1599.9	45.2	1499.9	1050.4
1549.9	55.1	1649.9	44.5	1549.9	2626.4
1599.9	55.2	1699.8	43.8	1599.9	4207.9
1649.9	56.8	1750.2	43.8	1649.9	2068.7
1699.8	57.0	1800.2	45.1	1699.8	868.5
1750.2	57.3	1900.1	51.7	1750.2	227.4
1800.2	55.6	1950.1	52.0	1800.2	78.9
1950.1	57.5	2000.0	55.5	1850.1	65.6
2000.0	57.2	2050.0	56.0	1900.1	52.4
2050.0	56.2	2100.0	54.0	1950.1	51.1
2100.0	56.1	2150.0	53.1	2000.0	48.5
2150.0	56.7	2199.9	53.0	2050.0	60.5
2199.9	57.3	2249.9	52.8	2100.0	64.6
2249.9	58.0	2349.9	53.8	2150.0	63.9
2299.9	58.1	2399.8	55.7	2199.9	61.4
2349.9	57.5	2450.2	56.3	2249.9	60.9
2399.8	56.6	2500.2	55.5	2299.9	61.2
2450.2	56.3	2650.1	52.0	2349.9	59.1
2500.2	56.9	2700.0	51.1	2399.8	56.1
2600.1	58.4	2800.0	50.5	2450.2	55.0

2650.1	57.7		2500.2	54.4
2700.0	56.9		2550.1	52.9
2800.0	55.4		2700.0	49.4
2850.0	55.2			
2899.9	55.4			
2949.9	55.8			

A(7) Data of seismic test result in homogeneous Oxford-clay (see Section 7.2.2)

A(7a) Data of seismic test result in homogeneous Oxford-clay for Test ID: 08Jun10_03 (Test 22), 09Jun10_01 (Test 43), and 09Jun10_02 (Test 24)
Date of test: 8 to 9 Jun 2010

Seismic test carried out using Oxford-clay before columns installation which the seismic source at one end of the array.
Test frequency range / interval: 75 to 3000 Hz / 25 Hz

Frequency, Hz	Test (22) Row3/J, m/s			Test (23) Row3/F, m/s			Test (24) Row3/B, m/s		
	A-B	B-C	C-D	A-B	B-C	C-D	A-B	B-C	C-D
75.1	25.0	41.3	68.9	31.5	80.5	138.2	29.5	75.2	92.2
99.9	102.7	95.2	44.3	105.0	57.6	31.2	50.3	32.1	57.0
125.1	25.2	45.7	70.6	37.1	36.1	55.6	56.4	52.4	47.9
149.9	59.2	61.3	50.5	54.2	73.5	87.9	52.5	50.7	57.9
175.1	43.2	52.8	59.0	52.1	44.3	48.2	46.1	50.2	64.5
199.9	44.6	44.6	57.2	47.2	53.6	63.5	48.0	52.5	60.7
225.1	52.1	55.4	46.5	51.9	48.2	60.7	54.3	50.4	56.7
249.9	53.4	59.2	39.8	52.7	39.6	35.3	51.2	46.4	47.4
275.0	55.0	61.1	55.5	60.3	67.3	67.0	64.7	56.3	52.6
299.8	56.1	60.9	53.4	59.3	59.0	50.5	59.3	54.4	52.2
325.0	53.8	63.7	41.9	48.6	59.2	58.3	51.5	51.3	65.4
350.2	44.4	57.3	47.9	51.7	48.5	57.0	62.3	49.7	48.6
375.0	54.7	51.6	43.0	52.7	45.0	46.2	61.7	45.1	47.9
400.2	58.5	59.3	34.7	54.4	47.7	31.9	61.3	52.6	41.5
425.0	56.1	63.0	37.9	60.4	51.7	35.2	57.3	54.2	40.5
450.1	56.4	54.0	49.1	57.0	49.5	37.4	52.2	51.4	43.4
474.9	53.0	53.7	45.8	55.0	48.6	35.8	49.3	46.3	45.5
500.1	48.3	54.9	41.9	52.4	50.9	34.0	48.0	42.4	46.0
524.9	53.4	51.7	44.3	54.6	61.8	57.3	40.8	39.8	44.7
550.1	55.7	48.1	45.6	59.4	59.6	53.9	40.5	36.3	48.5
574.9	54.2	48.6	45.1	61.5	60.8	53.0	38.8	37.0	48.5
600.1	51.6	48.2	44.4	60.1	58.6	51.6	36.5	38.4	53.5
624.8	49.9	46.6	44.8	56.2	55.7	52.0	41.4	36.1	56.0

650.0	48.4	45.0	46.7	50.4	56.7	53.9	43.6	37.0	53.3
674.8	48.9	43.2	49.9	48.6	56.2	54.4	43.7	39.4	49.5
700.0	50.1	42.1	51.0	50.3	53.2	52.6	43.7	42.2	47.3
725.2	48.6	43.2	51.2	51.9	51.3	50.5	44.1	43.9	48.0
750.0	48.9	43.9	48.9	52.3	50.7	49.3	44.2	45.8	49.4
775.1	48.5	44.1	49.6	51.5	51.2	49.3	44.6	47.2	51.9
799.9	48.3	43.1	51.6	50.6	50.8	50.4	44.9	48.2	54.1
825.1	49.1	42.2	52.6	50.4	49.5	52.9	45.0	49.3	54.2
849.9	50.0	42.0	52.1	50.8	48.1	55.7	44.6	50.5	53.1
875.1	50.1	42.7	50.9	51.4	47.0	57.7	44.5	50.8	52.2
899.9	50.0	44.0	49.3	51.8	46.4	57.9	44.5	50.3	51.7
925.1	50.1	45.2	48.0	51.7	46.3	57.2	44.7	49.7	51.0
949.9	50.4	45.9	47.4	51.4	46.7	55.6	44.9	48.8	50.3
975.0	50.7	46.3	47.1	51.0	47.5	53.7	45.2	47.9	49.9
999.8	50.7	46.9	46.9	51.0	48.0	52.5	45.5	47.2	49.4
1025.0	50.2	47.6	46.6	51.7	48.1	52.0	45.7	47.2	48.2
1050.2	49.8	48.4	46.1	52.4	48.3	51.6	45.6	47.6	47.0
1075.0	49.4	49.1	45.7	52.5	49.2	50.7	45.3	47.8	46.3
1100.2	49.0	49.5	45.4	52.1	50.3	49.3	45.0	47.8	46.3
1125.0	48.8	49.5	45.5	51.3	51.3	48.0	44.8	47.7	46.6
1150.1	48.9	49.2	45.6	50.6	52.0	47.3	44.6	47.7	47.0
1174.9	49.2	48.6	45.8	50.1	52.3	47.1	44.5	47.8	47.1
1200.1	49.5	48.1	46.0	49.8	52.1	47.2	44.1	47.9	46.9
1224.9	49.8	47.8	46.2	49.7	51.6	47.5	43.7	47.9	46.4
1250.1	49.9	47.8	46.3	49.7	51.1	48.1	43.4	47.6	46.3
1274.9	49.9	48.0	46.3	49.8	50.6	48.5	43.4	47.3	46.4
1300.0	49.8	48.3	46.4	50.0	50.1	49.0	43.8	47.1	46.5
1324.8	49.7	48.5	46.7	49.9	49.8	49.4	44.2	47.0	46.5
1350.0	49.4	48.8	47.2	49.8	49.7	49.6	44.4	47.1	46.8
1374.8	48.9	49.1	47.9	49.7	49.6	49.7	44.5	47.4	47.3
1400.0	47.9	49.7	48.7	49.6	49.5	49.7	44.5	47.8	47.8
1425.2	47.1	50.4	49.5	49.5	49.4	49.9	44.5	48.2	48.2
1450.0	46.4	51.2	50.0	49.5	49.3	50.2	44.6	48.5	48.5
1475.1	45.8	51.9	50.6	49.5	49.3	50.6	44.7	48.8	48.7
1499.9	45.6	52.2	51.2	49.5	49.3	50.9	44.7	49.0	48.6
1525.1	45.3	52.8	52.2	49.5	49.4	51.1	44.6	49.2	48.4
1549.9	45.0	53.2	53.0	49.5	49.6	51.2	44.6	49.4	48.3
1575.1	44.7	53.3	53.7	49.4	50.0	51.1	44.7	49.6	48.2
1599.9	44.5	53.7	54.4	49.4	50.3	51.0	44.8	49.8	48.1
1625.1	44.3	54.2	54.9	49.4	50.5	50.9	44.9	50.0	48.1
1649.9	44.0	54.8	55.3	49.4	50.7	50.8	45.0	50.2	47.9

1675.0	43.8	55.5	55.6	49.5	50.8	50.8	45.1	50.5	47.4
1699.8	43.6	56.1	56.0	49.7	50.7	50.7	45.1	50.9	46.9
1725.0	43.6	56.5	56.2	49.8	50.6	50.7	45.0	51.2	46.3
1750.2	43.7	56.6	56.5	50.0	50.4	50.7	45.0	51.5	45.5
1775.0	43.9	56.5	56.7	50.2	50.1	50.7	45.0	51.6	45.5
1800.2	44.3	56.1	56.8	50.4	49.8	50.8	44.9	51.6	46.0
1825.0	44.7	55.7	57.0	50.6	49.4	50.9	44.9	51.6	48.1
1850.1	45.2	55.3	56.9	50.8	49.1	50.9	44.8	51.5	53.0
1874.9	45.7	54.9	56.9	51.0	48.9	50.9	44.8	51.5	56.9
1900.1	45.8	54.8	56.8	51.1	48.7	50.8	44.8	51.4	57.4
1924.9	45.9	54.6	56.4	51.4	48.6	50.6	44.8	51.4	57.6
1950.1	46.3	54.5	55.7	51.6	48.6	50.5	44.9	51.4	57.4
1974.9	46.6	54.4	55.1	51.7	48.7	50.5	45.0	51.3	57.0
2000.0	46.9	54.4	54.8	51.8	48.8	50.5	45.1	51.2	57.2
2024.8	47.3	54.3	54.1	51.9	49.0	50.6	45.3	51.0	58.4
2050.0	47.7	54.2	53.8	51.9	49.2	50.6	45.4	50.9	58.8
2074.8	48.1	54.1	53.5	52.0	49.3	50.7	45.6	50.7	60.3
2100.0	48.6	54.0	53.6	52.0	49.4	50.8	45.7	50.6	62.3
2125.2	49.1	53.9	53.7	52.1	49.6	51.0	45.8	50.4	64.4
2150.0	49.5	53.9	54.0	52.2	49.7	51.2	45.9	50.2	65.4
2175.1	49.9	54.0	54.0	52.3	49.8	51.5	46.0	50.1	65.7
2199.9	50.2	54.2	54.5	52.4	49.9	51.8	46.0	50.0	67.4
2225.1	50.5	54.4	55.0	52.6	50.1	52.2	46.2	49.8	68.4
2249.9	50.8	54.8	55.0	52.7	50.2	52.6	46.3	49.7	66.4
2275.1	51.2	55.3	54.5	52.8	50.3	53.3	46.4	49.5	64.8
2299.9	51.5	55.7	53.9	52.9	50.3	54.1	46.5	49.5	62.3
2325.1	51.9	56.2	53.3	53.1	50.4	54.3	46.6	49.4	60.7
2349.9	52.4	56.5	52.8	53.3	50.5	54.6	46.6	49.5	59.1
2375.0	52.8	56.9	51.6	53.6	50.6	54.8	46.6	49.5	58.7
2399.8	53.2	57.1	50.3	53.8	50.7	55.0	46.6	49.7	57.7
2425.0	53.6	57.2	48.6	54.1	50.8	54.3	46.5	49.9	57.2
2450.2	54.0	57.1	46.7	54.4	51.0	54.2	46.5	50.1	56.6
2475.0	54.3	57.1	46.1	54.8	51.0	55.7	46.4	50.4	56.4
2500.2	54.5	57.1	46.0	55.1	51.3	56.7	46.4	50.6	55.9
2524.9	54.6	56.9	45.6	55.6	51.5	58.0	46.3	51.0	55.8
2550.1	54.6	56.6	45.7	56.1	51.8	58.3	46.3	51.1	55.8
2574.9	54.5	56.4	46.0	56.5	52.1	63.2	46.2	51.3	54.8
2600.1	54.4	56.3	46.7	56.9	52.5	97.6	46.2	51.5	54.9
2624.9	54.2	56.2	47.3	57.4	52.8	93.6	46.3	51.6	54.4
2650.1	54.1	56.1	47.1	58.0	52.8	90.4	46.3	51.9	54.3
2674.9	54.0	56.5	46.0	58.6	52.9	81.8	46.3	52.0	54.1

2700.0	54.0	56.3	46.2	59.4	52.8	65.2	46.3	52.0	53.4
2724.8	54.0	56.1	45.9	60.2	52.7	68.7	46.3	52.3	53.7
2750.0	54.1	55.9	37.1	61.3	52.3	83.4	46.4	52.2	53.7
2774.8	54.1	55.7	38.3	62.6	51.8	58.4	46.5	52.1	54.8
2800.0	54.2	55.6	38.8	64.0	51.4	57.6	46.5	52.1	55.6
2825.2	54.3	55.5	38.6	65.6	50.9	59.3	46.5	52.2	55.6
2850.0	54.4	55.4	39.0	67.3	50.2	60.6	46.5	52.3	56.4
2875.1	54.4	55.5	40.2	69.0	49.8	57.6	46.6	52.1	57.1
2899.9	54.4	55.6	40.7	70.1	49.5	60.0	46.6	52.0	57.6
2925.1	54.4	55.8	41.0	71.2	49.0	59.2	46.5	52.2	57.9
2949.9	54.3	55.9	42.0	71.7	48.8	56.3	46.5	52.6	58.2
2975.1	54.1	56.2	42.9	71.4	48.8	57.5	46.5	52.3	60.4
2999.9	53.9	56.6	43.2	69.4	49.0	61.8	46.3	52.5	60.3

A(7b) Data of seismic test result in homogeneous Oxford-clay for Test ID: 10Jun10_01 (Test 28), 14Jun10_03 (Test 35), and 16Jun10_02 (Test 41).

Seismic test carried out using Oxford-clay before columns installation which the seismic source at one end of the array.
Date of test: 10 to 16 Jun 2010
Test frequency range / interval: 75 to 3000 Hz / 25 Hz

Frequency, Hz	Test (28) Row1/A, m/s			Test (35) Row1/E, m/s			Test (41) Row1/I, m/s		
	A-B	B-C	C-D	A-B	B-C	C-D	A-B	B-C	C-D
75.1	29.3	31.2	44.0	37.4	127.6	137.0	58.7	76.5	114.9
99.9	82.6	95.7	106.8	128.9	187.1	290.7	61.1	74.5	97.7
125.1	56.1	57.0	39.8	17.9	27.9	110.0	52.8	29.8	16.2
149.9	61.3	40.4	27.4	73.6	78.5	61.3	37.5	66.6	109.4
175.1	50.3	42.0	50.4	45.9	40.2	57.7	50.3	47.8	25.2
199.9	55.4	67.6	73.9	56.2	62.4	62.4	44.3	56.4	77.9
225.1	51.9	78.1	92.3	34.5	42.3	75.2	36.7	45.3	52.7
249.9	46.0	60.0	68.7	53.5	48.1	35.2	55.8	39.5	39.4
275.0	54.2	56.3	62.8	59.8	41.4	48.7	56.3	54.5	48.3
299.8	50.6	62.8	56.6	58.2	55.3	47.1	61.8	64.5	48.6
325.0	52.1	58.0	52.1	50.7	41.6	62.2	50.4	53.6	54.7
350.2	60.7	63.0	55.8	48.5	42.6	40.7	52.8	50.1	36.8
375.0	59.6	62.5	64.9	52.7	40.0	39.9	63.7	47.2	37.7
400.2	64.3	56.5	58.9	51.2	39.7	46.1	57.7	67.0	36.7
425.0	66.5	65.2	45.8	44.6	43.5	37.1	53.7	55.6	42.3
450.1	54.9	69.6	45.0	48.1	40.4	36.5	49.1	59.7	35.0
474.9	60.1	65.9	38.1	53.0	38.7	35.5	51.8	54.8	36.7

500.1	66.4	66.9	41.2	55.1	34.6	38.9	48.6	48.8	40.7
524.9	66.3	59.2	47.1	53.9	32.2	42.7	48.5	39.7	45.5
550.1	67.3	60.8	52.1	54.6	30.6	44.7	52.7	32.9	52.0
574.9	63.5	64.0	52.8	53.4	31.0	45.0	52.3	27.4	72.1
600.1	60.2	62.4	53.7	50.3	32.8	43.7	64.9	29.1	49.2
624.8	56.7	60.0	55.2	44.4	35.5	42.5	36.3	57.6	54.5
650.0	52.4	57.3	55.1	44.5	34.9	42.4	39.0	46.3	60.2
674.8	53.0	52.4	54.5	45.9	36.0	40.4	39.5	43.2	64.0
700.0	56.9	49.2	52.8	44.6	37.2	39.6	39.6	43.8	65.9
725.2	61.8	47.8	51.8	44.4	38.3	39.8	46.1	40.3	61.3
750.0	61.3	48.4	52.3	45.3	38.6	40.4	49.6	39.8	54.3
775.1	57.8	50.6	53.0	46.3	38.6	40.3	49.3	58.5	37.6
799.9	54.8	51.8	53.7	46.5	39.3	39.5	44.0	55.4	44.9
825.1	54.1	51.2	54.3	46.7	39.8	39.2	46.5	53.7	57.4
849.9	55.4	50.9	54.1	47.8	40.6	38.6	45.6	54.3	58.6
875.1	55.6	51.4	54.2	48.9	41.6	38.2	43.9	57.3	57.6
899.9	54.6	52.6	54.1	49.1	42.7	37.7	42.4	60.1	58.2
925.1	52.8	53.9	53.4	49.0	43.6	37.5	40.9	62.1	59.1
949.9	51.5	54.9	52.5	49.4	44.0	37.4	39.2	64.2	58.0
975.0	51.2	54.4	52.4	49.9	44.0	37.5	37.5	67.5	56.4
999.8	51.7	53.0	52.7	50.3	43.8	37.8	36.0	71.1	55.2
1025.0	52.5	51.6	52.9	50.6	43.7	38.0	35.0	73.8	54.2
1050.2	53.1	50.8	52.3	51.2	43.4	38.2	34.7	73.9	53.7
1075.0	53.5	50.6	51.1	52.0	42.8	38.8	35.3	71.8	52.7
1100.2	53.8	50.6	49.7	52.7	42.2	39.6	36.4	71.0	49.9
1125.0	54.3	50.7	48.3	53.2	41.9	40.4	37.6	72.7	46.6
1150.1	55.2	50.6	47.2	53.5	41.7	40.9	39.1	72.7	45.0
1174.9	55.8	50.5	46.2	53.6	41.6	41.1	40.3	72.1	44.7
1200.1	55.7	50.7	45.5	53.4	41.6	41.2	41.5	71.4	44.5
1224.9	55.3	50.7	45.3	53.0	41.6	41.2	42.7	68.4	45.3
1250.1	55.3	50.4	45.4	52.6	41.6	41.1	43.3	65.7	46.4
1274.9	55.7	49.5	45.8	52.3	41.7	41.1	43.9	61.8	48.9
1300.0	56.3	49.0	45.7	52.1	41.7	41.1	44.6	57.4	52.5
1324.8	56.8	48.8	45.5	52.0	41.6	41.2	45.5	54.0	55.9
1350.0	56.8	48.7	45.1	52.0	41.7	41.3	46.7	51.1	58.5
1374.8	56.4	48.9	44.8	52.0	41.7	41.4	48.3	49.3	60.0
1400.0	56.0	49.3	44.4	52.1	41.6	41.6	49.5	48.0	60.4
1425.2	55.6	49.7	44.0	52.2	41.6	41.9	51.3	47.6	59.0
1450.0	55.5	49.8	43.9	52.3	41.7	42.0	53.1	47.2	57.8
1475.1	55.6	49.7	43.8	52.4	41.9	42.1	54.9	46.9	56.5
1499.9	55.9	49.5	43.9	52.4	42.1	42.2	56.3	47.0	54.7

1525.1	56.1	49.4	43.9	52.5	42.4	42.2	58.0	47.6	53.7
1549.9	56.4	49.5	44.1	52.6	42.8	42.1	59.0	48.0	53.0
1575.1	56.5	49.6	44.3	52.7	43.1	41.9	59.5	48.5	52.5
1599.9	56.6	49.8	44.6	52.7	43.4	41.6	59.5	49.2	51.9
1625.1	56.7	49.8	45.0	52.8	43.7	41.5	59.2	50.0	51.4
1649.9	57.0	49.8	45.4	52.8	44.0	41.6	58.9	51.0	51.0
1675.0	57.2	49.7	45.8	52.7	44.3	41.9	58.5	52.3	50.9
1699.8	57.4	49.6	46.2	52.6	44.5	42.3	57.9	53.8	50.5
1725.0	57.6	49.6	46.5	52.6	44.8	43.0	57.3	55.6	49.5
1750.2	57.7	49.5	46.7	52.6	45.1	43.9	56.9	56.8	49.1
1775.0	57.8	49.5	46.9	52.6	45.3	45.0	56.4	58.1	48.7
1800.2	58.0	49.5	47.0	52.7	45.5	45.8	56.2	60.5	47.2
1825.0	58.3	49.5	47.0	52.8	45.6	46.1	56.6	62.1	45.7
1850.1	58.6	49.4	47.0	53.0	45.7	46.1	57.0	62.5	45.1
1874.9	58.9	49.4	46.9	53.2	45.6	46.1	57.3	62.8	44.7
1900.1	59.1	49.4	46.7	53.5	45.5	46.0	57.4	67.7	42.3
1924.9	59.4	49.4	46.5	53.8	45.3	46.1	57.8	69.9	40.9
1950.1	59.7	49.5	46.2	54.0	45.2	46.0	58.0	68.9	40.7
1974.9	60.0	49.7	45.9	54.2	45.1	45.8	58.1	75.6	38.4
2000.0	60.2	49.8	45.7	54.4	45.1	45.7	58.3	71.6	39.0
2024.8	60.3	50.0	45.5	54.6	45.0	45.6	58.6	59.1	43.7
2050.0	60.4	50.1	45.2	54.7	45.0	45.5	58.2	51.0	49.8
2074.8	60.5	50.3	44.8	54.8	45.0	45.5	58.0	48.6	52.8
2100.0	60.6	50.4	44.6	54.9	45.0	45.4	58.1	50.3	51.0
2125.2	60.6	50.5	44.3	54.9	45.0	45.4	57.9	50.2	51.8
2150.0	60.6	50.5	44.1	54.9	45.1	45.4	57.5	50.9	52.2
2175.1	60.7	50.4	44.1	55.0	45.1	45.6	57.2	50.9	53.0
2199.9	60.8	50.4	43.9	54.9	45.1	45.8	57.6	51.2	53.2
2225.1	60.9	50.4	43.7	54.8	45.0	46.1	57.7	51.9	53.0
2249.9	61.1	50.4	43.6	54.7	45.0	46.4	57.8	52.7	52.5
2275.1	61.3	50.4	43.4	54.6	44.9	46.6	57.8	52.8	53.2
2299.9	61.6	50.4	43.2	54.6	44.9	46.8	58.0	53.3	53.0
2325.1	61.8	50.3	43.0	54.5	45.0	47.0	58.4	54.4	52.0
2349.9	62.1	50.2	42.9	54.5	45.0	47.1	58.8	54.8	52.1
2375.0	62.3	50.1	42.8	54.5	45.1	47.1	59.2	54.8	53.2
2399.8	62.6	49.9	42.8	54.5	45.2	47.1	59.3	55.3	52.8
2425.0	62.8	49.8	42.7	54.6	45.3	47.2	59.3	55.8	52.9
2450.2	63.1	49.5	42.6	54.6	45.4	47.2	59.4	55.6	54.3
2475.0	63.3	49.0	42.7	54.7	45.4	47.3	59.7	55.6	55.2
2500.2	63.5	47.9	43.3	54.9	45.4	47.4	59.9	55.9	55.8
2524.9	63.7	44.5	46.3	55.0	45.4	47.8	60.1	56.0	56.9

2550.1	63.9	39.9	52.3	55.1	45.4	48.0	60.3	56.2	58.0
2574.9	64.1	38.7	54.2	55.2	45.3	48.1	60.6	56.3	58.1
2600.1	64.3	38.3	54.8	55.3	47.7	45.9	60.7	56.6	58.1
2624.9	64.4	38.3	54.9	55.4	61.8	37.8	60.9	56.5	59.0
2650.1	64.4	38.3	54.8	55.5	61.3	38.0	61.0	57.1	58.2
2674.9	64.4	38.1	55.2	55.5	60.7	38.4	61.4	57.4	58.2
2700.0	64.5	37.8	56.8	55.6	60.5	38.6	63.4	59.0	55.7
2724.8	64.8	37.6	58.5	55.7	60.7	38.6	65.4	61.5	52.6
2750.0	65.1	37.0	63.0	55.7	61.7	38.5	67.3	63.0	50.4
2774.8	65.3	36.3	68.5	55.9	62.4	38.4	67.2	65.6	48.9
2800.0	65.3	35.8	70.4	56.1	63.4	38.1	67.7	67.8	47.6
2825.2	64.7	35.5	70.6	56.3	64.5	37.7	68.1	70.0	46.8
2850.0	64.1	35.3	70.1	56.5	66.5	37.1	68.6	70.5	46.5
2875.1	63.6	35.3	69.6	56.8	67.5	36.9	70.2	69.1	46.8
2899.9	63.3	36.0	66.2	57.0	69.6	36.0	69.1	68.2	47.3
2925.1	62.8	36.9	63.0	57.2	71.7	35.5	68.1	68.9	48.4
2949.9	62.5	36.8	63.0	57.3	74.1	34.6	68.0	69.2	48.8
2975.1	62.3	37.2	62.1	57.5	77.0	34.2	68.8	67.8	49.2
2999.9	62.0	37.2	62.1	57.6	85.8	32.8	67.9	67.7	49.3

A(7c) Data of seismic test result in homogeneous Oxford-clay for Test ID: 19Jun10_11 (Test 42), 19Jun10_12 (Test 43), and 20Jun10_13 (Test 44)
Date of test: 20 Jun 2010

Seismic test carried out using Oxford-clay before columns installation which the seismic source at one end of the array.
Test frequency range / interval: 75 to 3000 Hz / 25 Hz
Remarks: -

Frequency, Hz	Test (42) Row2/I, m/s			Test (43) Row2/I, m/s			Test (44) Row2/I, m/s		
	A-B	B-C	C-D	A-B	B-C	C-D	A-B	B-C	C-D
75.1	29.7	45.6	42.7	39.8	34.2	40.0	32.9	49.8	51.1
99.9	45.6	30.1	19.1	40.9	26.3	18.3	40.4	25.9	22.5
125.1	51.5	39.2	47.9	54.3	38.8	45.1	47.6	41.0	57.1
149.9	40.1	52.6	78.4	40.0	55.1	83.8	42.2	59.4	90.0
175.1	38.4	50.4	71.4	37.9	51.2	69.7	41.6	52.8	67.8
199.9	64.3	79.9	75.5	63.9	80.3	74.6	68.8	79.9	72.4
225.1	47.1	50.2	61.4	46.9	50.4	62.8	47.3	52.7	67.7
249.9	46.9	54.2	62.6	46.7	55.4	62.5	48.0	57.5	63.4
275.0	59.0	53.5	35.6	57.6	55.6	38.7	60.2	50.8	38.7
299.8	63.9	69.7	71.8	62.8	67.5	73.0	65.9	69.1	72.0

325.0	55.9	57.6	62.8	54.8	56.4	65.1	59.5	59.7	67.5
350.2	52.5	50.8	51.1	52.5	49.4	52.6	57.1	53.7	55.7
375.0	58.6	49.8	35.1	61.8	48.0	35.6	62.6	46.2	46.5
400.2	63.4	67.0	43.8	65.9	66.2	45.3	68.4	68.0	43.3
425.0	57.5	61.8	42.3	59.6	61.8	44.3	64.3	63.9	46.6
450.1	52.4	57.7	41.9	52.7	58.4	44.0	57.7	64.1	46.0
474.9	55.2	50.2	38.3	55.7	51.2	38.9	56.8	56.2	44.1
500.1	57.4	50.6	35.6	62.3	51.8	34.7	60.7	53.0	41.6
524.9	59.3	53.0	33.2	64.2	55.9	33.5	63.2	55.4	37.4
550.1	61.0	46.3	41.9	64.0	48.7	43.8	64.2	52.7	43.3
574.9	61.0	40.7	47.5	64.5	43.3	46.3	63.7	47.9	51.4
600.1	61.4	37.3	48.8	65.3	42.8	43.7	63.6	44.1	54.3
624.8	52.9	49.7	47.2	54.1	51.3	47.9	54.8	56.6	53.7
650.0	50.8	48.3	50.3	51.6	49.7	51.3	52.3	55.0	58.3
674.8	50.3	46.6	51.7	51.0	47.5	52.6	52.7	52.8	57.1
700.0	50.1	46.1	51.3	50.8	46.9	51.8	53.1	52.7	54.5
725.2	49.9	46.4	50.4	50.4	47.3	50.3	53.1	52.8	52.6
750.0	49.8	46.1	51.6	50.2	46.9	51.3	53.5	51.5	53.0
775.1	50.2	45.8	54.2	50.7	46.4	54.1	54.3	49.9	55.5
799.9	50.6	45.4	55.6	51.2	46.0	55.3	54.8	49.3	56.3
825.1	50.6	45.8	54.7	51.4	46.6	54.5	54.7	50.0	54.9
849.9	50.1	47.0	53.7	51.1	48.0	53.8	54.5	50.9	54.7
875.1	49.5	47.7	53.7	50.6	48.8	53.9	54.2	51.5	55.8
899.9	49.0	47.8	53.8	50.3	48.9	54.1	54.1	52.0	56.2
925.1	48.7	47.6	53.5	50.1	48.8	53.8	54.0	52.5	56.0
949.9	48.6	47.2	53.2	50.1	48.5	53.5	54.0	52.6	55.7
975.0	48.7	46.6	53.0	50.2	48.0	53.4	54.0	52.3	55.9
999.8	48.8	46.1	52.8	50.2	47.4	53.4	53.9	51.9	56.1
1025.0	49.1	45.7	52.4	50.5	46.8	53.1	53.8	51.5	55.9
1050.2	49.4	45.8	51.7	50.8	46.8	52.5	53.7	51.4	55.5
1075.0	49.6	46.1	51.2	51.1	47.0	52.1	53.6	51.4	55.7
1100.2	49.8	46.3	50.8	51.6	47.1	51.9	53.7	51.3	56.2
1125.0	50.0	46.5	50.3	52.0	47.1	51.5	54.0	51.3	56.3
1150.1	50.0	46.8	50.0	52.1	47.2	51.3	54.4	51.3	56.2
1174.9	50.0	47.1	50.0	52.1	47.4	51.3	54.7	51.4	56.1
1200.1	50.0	47.2	50.0	52.1	47.6	51.3	55.0	51.4	56.2
1224.9	50.1	47.2	50.2	52.2	47.5	51.4	55.3	51.3	56.4
1250.1	50.3	47.0	50.4	52.2	47.4	51.5	55.8	51.0	56.5
1274.9	50.4	46.9	50.8	52.2	47.4	51.6	56.1	50.9	56.6
1300.0	50.6	46.9	51.3	52.3	47.5	51.7	56.3	50.8	56.7
1324.8	50.8	46.9	51.5	52.4	47.6	51.5	56.5	50.7	56.9

1350.0	51.1	47.0	51.4	52.7	47.8	51.3	56.7	50.7	57.0
1374.8	51.5	47.2	51.0	52.9	48.0	51.0	57.1	50.8	56.8
1400.0	51.9	47.6	50.6	53.2	48.3	50.8	57.6	50.8	56.4
1425.2	52.4	48.1	50.2	53.5	48.6	50.7	58.1	50.8	56.1
1450.0	52.8	48.6	50.0	53.7	48.9	50.6	58.7	50.7	55.9
1475.1	53.2	49.4	50.0	54.0	49.4	50.6	59.2	50.8	55.8
1499.9	53.5	50.2	50.2	54.2	49.9	50.7	59.8	51.1	55.8
1525.1	53.7	50.9	50.6	54.3	50.5	50.9	60.4	51.6	55.5
1549.9	53.7	51.6	51.4	54.3	51.2	51.3	61.0	52.3	55.2
1575.1	53.6	52.2	52.5	54.3	51.8	52.1	61.6	53.1	55.3
1599.9	53.3	52.6	53.8	54.3	52.3	53.3	62.2	53.9	55.8
1625.1	53.0	52.8	55.4	54.2	52.7	54.7	62.7	54.8	56.5
1649.9	52.5	53.0	57.0	54.2	53.0	56.4	63.2	55.5	57.1
1675.0	51.8	53.0	58.5	54.1	53.2	58.3	63.9	56.2	57.9
1699.8	51.0	53.0	59.9	54.0	53.2	60.3	64.4	56.8	58.6
1725.0	50.0	53.0	61.0	53.9	53.2	62.1	64.8	57.4	59.3
1750.2	49.0	52.7	62.0	53.9	53.0	63.7	65.1	58.0	60.0
1775.0	48.2	52.5	62.7	53.8	52.8	65.1	65.4	58.5	60.6
1800.2	47.5	52.2	63.3	53.8	52.5	65.8	65.7	59.0	61.1
1825.0	46.9	51.9	63.9	53.9	52.2	66.4	66.1	59.4	61.8
1850.1	46.4	51.5	64.1	53.8	51.8	67.6	66.2	59.8	62.6
1874.9	46.0	51.3	63.9	53.8	51.4	67.4	66.5	60.1	63.4
1900.1	45.7	51.0	63.5	53.8	51.1	67.0	67.0	60.2	64.7
1924.9	45.4	50.9	62.6	53.8	50.9	66.4	67.6	60.3	66.2
1950.1	45.2	50.9	61.7	53.7	51.0	65.4	68.4	60.4	68.0
1974.9	45.0	51.0	60.2	53.6	51.1	63.5	69.9	60.2	70.0
2000.0	44.9	51.2	59.5	53.4	51.2	61.7	72.5	60.0	71.9
2024.8	44.7	51.4	59.0	53.3	51.5	60.4	77.6	59.7	74.2
2050.0	44.5	51.6	58.5	53.3	51.7	59.7	87.5	59.2	75.7
2074.8	44.0	51.9	58.9	53.3	51.9	59.3	100.3	58.6	76.3
2100.0	43.4	52.0	59.2	53.2	52.1	59.3	111.8	57.8	76.1
2125.2	43.4	51.5	59.9	53.2	52.1	59.4	119.7	57.4	75.5
2150.0	44.5	50.3	60.8	53.3	52.2	59.7	124.4	56.9	74.0
2175.1	46.0	49.4	61.7	53.2	52.2	60.1	129.6	56.5	72.2
2199.9	46.9	49.2	62.3	53.5	52.2	60.4	134.1	56.0	69.7
2225.1	47.4	49.3	63.1	53.4	52.2	60.9	137.4	55.8	66.3
2249.9	47.7	49.5	63.5	53.3	52.2	61.2	140.6	55.6	64.0
2275.1	47.9	49.4	64.6	53.4	52.2	61.7	145.2	55.4	63.2
2299.9	48.1	49.4	65.5	53.2	52.1	62.4	147.8	55.4	62.4
2325.1	48.3	49.2	66.9	53.2	52.0	63.1	150.2	55.4	62.2
2349.9	48.4	48.9	68.0	53.1	51.9	63.5	152.4	55.2	62.7

2375.0	48.5	48.6	68.3	52.9	51.6	64.3	153.6	55.0	63.3
2399.8	48.6	48.2	67.9	52.6	51.3	64.3	155.2	54.9	64.3
2425.0	48.6	48.0	61.3	52.5	50.8	63.5	156.3	54.8	65.1
2450.2	48.6	47.8	54.6	52.4	50.2	61.7	157.6	54.6	66.1
2475.0	48.4	48.0	52.9	51.7	50.0	60.0	158.8	54.3	67.0
2500.2	48.2	48.2	54.2	50.9	50.1	59.5	160.9	53.9	67.9
2524.9	47.9	48.7	54.6	50.5	49.9	59.5	162.5	53.8	68.1
2550.1	47.4	49.3	56.8	49.6	50.2	59.8	165.3	53.5	68.7
2574.9	46.9	50.4	59.8	48.9	50.6	60.3	170.8	52.9	71.1
2600.1	46.2	51.8	60.5	47.5	51.5	61.5	178.8	52.1	74.2
2624.9	45.7	53.0	62.2	46.5	52.5	62.4	188.7	73.1	52.8
2650.1	44.9	55.0	62.5	45.7	53.3	63.1	201.3	72.2	54.3
2674.9	44.3	57.0	63.5	44.9	54.2	64.4	215.4	71.6	52.6
2700.0	43.6	59.6	62.6	44.2	55.2	65.7	231.4	70.8	52.6
2724.8	43.1	61.1	63.3	43.5	56.1	66.5	243.7	68.8	68.2
2750.0	42.5	63.5	61.6	43.0	57.0	67.4	251.9	71.7	65.2
2774.8	42.0	65.6	60.5	42.7	57.8	69.1	254.8	76.8	64.9
2800.0	41.7	66.9	61.2	42.4	58.8	70.1	253.1	93.5	61.1
2825.2	41.4	68.0	60.3	42.4	59.5	72.1	248.7	96.5	58.0
2850.0	41.2	70.0	61.0	42.4	60.4	74.6	249.5	98.1	60.0
2875.1	41.2	70.9	65.2	42.4	61.0	77.9	238.4	97.2	62.4
2899.9	41.4	71.7	66.9	42.6	62.0	79.9	232.8	97.4	62.9
2925.1	41.6	72.7	67.3	42.7	63.1	82.4	225.5	97.5	63.9
2949.9	41.9	73.7	67.5	43.1	65.7	81.9	219.2	97.7	64.8
2975.1	42.2	74.0	69.1	43.4	70.3	78.0	211.4	97.2	66.7
2999.9	42.6	74.3	69.1	43.8	77.7	71.8	203.8	97.9	67.6

A(7d) Data of seismic test result in homogeneous Oxford-clay for test ID: 20Jun10_21 (Test 45), 20Jun10_22 (Test 46), and 20Jun10_23 (Test 47)

Seismic test carried out using Oxford-clay before columns installation which the seismic source at one end of the array.
Date of test: 20 Jun 2010
Test frequency range / interval: 75 to 3000 Hz / 25 Hz
Remarks: -

	Test (45) Row2/G			**Test (46) Row2/G**			**Test (47) Row2/G**		
Frequency	A-B	B-C	C-D	A-B	B-C	C-D	A-B	B-C	C-D
75.1	27.9	65.5	79.4	28.2	68.9	87.7	26.3	66.4	84.4
99.9	72.9	55.5	45.3	80.5	64.9	56.8	74.3	60.9	49.8
125.1	58.0	107.6	117.0	59.8	108.7	118.8	56.3	106.2	115.0

149.9	46.3	39.1	28.9	45.0	38.2	28.6	46.6	38.9	27.3
175.1	33.8	37.7	58.6	33.0	39.0	60.0	33.7	37.9	58.9
199.9	50.3	81.0	64.9	50.4	80.1	64.4	49.3	80.8	65.7
225.1	51.9	51.3	35.9	50.7	50.4	36.0	50.3	50.6	36.5
249.9	41.3	57.2	42.8	41.6	59.1	42.7	41.4	57.3	42.2
275.0	56.9	68.4	35.7	57.0	70.6	35.8	56.9	70.8	37.1
299.8	53.6	65.0	53.7	53.7	67.8	54.4	53.5	67.0	55.0
325.0	53.9	66.6	43.4	54.2	69.4	44.9	52.5	68.7	46.3
350.2	45.2	50.3	40.9	44.8	53.5	41.6	44.8	51.1	42.4
375.0	56.6	57.5	32.4	55.7	61.0	33.0	55.5	60.8	34.2
400.2	60.1	56.1	33.2	59.4	59.3	34.2	59.1	60.4	35.2
425.0	63.9	49.1	36.2	63.5	51.9	37.1	61.8	53.6	40.7
450.1	63.5	43.2	37.4	63.6	46.1	37.7	62.9	47.0	38.9
474.9	73.3	38.3	35.4	71.7	39.9	36.9	71.7	44.1	35.3
500.1	77.8	35.9	37.2	76.9	36.1	38.9	74.3	46.3	33.7
524.9	72.9	34.2	43.1	73.7	34.6	44.3	68.4	44.8	38.5
550.1	73.7	31.2	49.8	73.2	31.6	52.0	68.4	38.6	44.9
574.9	76.0	29.1	58.8	78.0	28.8	60.1	75.2	33.2	51.2
600.1	71.1	28.9	64.2	78.0	27.9	66.9	73.2	32.6	55.3
624.8	95.4	73.0	42.5	59.0	46.6	44.9	52.4	38.5	49.6
650.0	71.4	58.9	40.1	55.0	44.9	49.8	48.2	41.7	49.2
674.8	62.3	47.7	45.8	57.6	40.7	52.8	46.6	45.1	47.1
700.0	61.8	40.1	50.6	60.8	37.7	54.0	45.7	48.0	46.3
725.2	59.5	37.7	52.7	58.8	38.1	53.0	43.7	51.0	47.8
750.0	55.6	38.8	51.8	56.1	39.8	51.9	41.2	56.9	50.5
775.1	53.1	40.4	51.4	56.3	39.8	53.2	39.5	63.2	53.6
799.9	52.3	40.2	51.9	56.6	39.4	53.9	41.8	60.0	57.3
825.1	51.1	40.7	50.2	54.7	41.0	51.5	61.2	41.8	59.6
849.9	48.4	43.6	46.5	51.9	44.1	48.5	68.6	39.1	60.3
875.1	46.3	46.7	43.7	50.1	46.0	47.6	65.2	40.0	60.5
899.9	45.9	47.8	43.0	49.6	46.6	47.6	63.2	39.9	60.4
925.1	45.5	48.6	42.7	49.0	47.5	46.7	59.2	41.2	57.5
949.9	44.9	50.0	42.0	48.1	49.4	45.3	55.7	43.6	53.3
975.0	44.6	51.1	41.4	47.4	50.8	44.3	53.6	45.8	50.2
999.8	44.5	51.3	41.4	47.0	51.1	44.4	52.3	47.1	48.9
1025.0	44.6	50.8	41.9	46.8	51.0	44.5	51.1	48.2	48.2
1050.2	44.5	50.5	42.3	46.3	51.3	44.3	49.7	49.5	47.0
1075.0	44.3	50.6	42.4	46.0	51.7	44.0	48.4	51.2	45.7
1100.2	44.4	50.4	42.7	45.9	51.6	44.2	47.7	53.2	45.0
1125.0	44.7	49.7	43.3	46.1	51.1	44.7	47.3	53.7	45.3
1150.1	45.1	49.0	44.0	46.3	50.6	45.5	47.0	53.9	45.4

1174.9	45.2	48.5	44.6	46.4	50.4	46.1	46.8	54.1	45.4
1200.1	45.3	48.2	45.2	46.5	50.3	46.6	46.7	54.4	45.6
1224.9	45.5	47.7	45.8	46.7	49.9	47.1	46.6	54.4	45.8
1250.1	45.7	47.3	46.1	46.8	49.6	47.6	46.7	54.3	46.2
1274.9	45.8	46.8	46.4	46.9	49.2	48.0	46.7	54.1	46.4
1300.0	46.0	46.5	46.8	47.0	48.9	48.3	46.8	53.8	46.7
1324.8	46.1	46.4	47.3	47.1	48.5	48.7	47.1	53.2	47.0
1350.0	46.1	46.4	47.8	47.1	48.2	49.0	47.4	52.6	47.4
1374.8	46.1	46.4	48.3	47.1	48.0	49.5	47.6	52.1	47.8
1400.0	46.0	46.5	49.1	46.9	47.9	50.0	47.7	51.6	48.3
1425.2	45.9	46.5	50.1	46.8	47.8	50.6	47.8	51.3	48.7
1450.0	45.6	46.2	51.4	46.6	47.7	51.2	47.8	51.0	49.1
1475.1	45.3	46.0	53.3	46.4	47.6	52.1	47.7	50.7	49.6
1499.9	44.8	45.6	55.5	46.1	47.4	53.0	47.5	50.5	50.1
1525.1	44.2	45.1	58.5	45.7	47.2	54.4	47.2	50.4	50.7
1549.9	43.6	44.9	61.1	45.3	47.0	55.7	46.9	50.4	51.3
1575.1	42.9	45.1	63.2	44.9	46.6	57.1	46.5	50.2	51.9
1599.9	42.2	45.7	64.4	44.5	46.3	58.7	46.2	50.1	52.6
1625.1	41.3	46.8	64.9	44.2	46.0	60.0	45.8	49.9	53.2
1649.9	40.3	48.7	63.8	44.0	45.8	60.7	45.6	49.7	53.7
1675.0	38.9	51.7	61.7	44.1	45.5	61.0	45.4	49.5	53.9
1699.8	37.7	55.1	56.2	44.4	45.1	61.0	45.4	49.3	54.1
1725.0	36.5	58.9	49.7	45.7	44.0	60.8	45.6	49.0	54.4
1750.2	28.7	62.2	44.7	48.6	41.8	60.5	46.1	48.4	54.5
1775.0	26.7	63.8	43.8	53.5	38.9	60.0	47.0	47.3	54.6
1800.2	26.8	64.5	44.0	57.7	37.1	59.5	48.9	45.5	54.7
1825.0	27.0	65.1	43.7	60.0	36.3	59.2	52.5	42.5	55.1
1850.1	27.3	65.0	43.7	61.4	36.0	59.1	56.3	40.5	55.0
1874.9	27.5	64.0	44.0	62.5	35.7	59.3	58.7	39.5	55.0
1900.1	27.8	62.6	44.5	63.2	35.6	59.8	60.1	39.2	54.7
1924.9	28.1	60.8	45.2	63.7	35.5	59.8	60.9	39.2	54.1
1950.1	28.4	58.9	46.1	64.2	35.3	60.2	61.2	39.7	53.3
1974.9	28.7	57.3	46.9	64.5	34.9	61.2	61.5	40.4	52.1
2000.0	29.1	55.9	47.2	64.9	34.0	64.6	61.6	41.8	50.5
2024.8	29.5	55.0	47.4	65.2	32.1	72.6	61.6	43.6	48.3
2050.0	29.8	54.5	47.2	65.5	30.6	80.4	61.7	46.0	46.0
2074.8	30.2	54.1	46.0	65.7	30.0	83.7	61.7	47.8	44.7
2100.0	30.4	54.1	41.2	65.8	29.9	85.5	61.7	49.2	44.0
2125.2	30.7	54.1	37.6	65.7	29.9	84.9	61.7	50.1	43.7
2150.0	30.9	54.1	36.3	65.6	30.0	83.5	61.8	50.8	44.0
2175.1	31.0	54.3	36.1	65.3	30.1	83.5	61.8	51.5	43.8

2199.9	31.2	54.6	35.6	64.7	30.2	78.3	61.9	51.9	44.1
2225.1	31.3	54.7	35.5	64.3	30.3	78.9	62.0	52.2	44.0
2249.9	31.4	54.9	35.9	63.9	30.4	78.2	62.1	52.4	43.8
2275.1	31.6	54.9	33.3	63.6	30.5	69.1	62.1	52.6	44.7
2299.9	31.7	54.6	27.4	63.3	30.5	65.2	62.2	52.7	44.1
2325.1	31.8	54.5	28.0	63.0	30.6	58.2	62.2	52.8	44.1
2349.9	32.0	54.4	28.5	62.8	30.7	54.2	62.3	53.0	43.5
2375.0	32.1	54.3	28.8	62.6	30.8	52.8	62.4	53.0	43.7
2399.8	32.2	54.3	28.7	62.2	30.9	52.4	62.6	53.0	43.5
2425.0	32.3	54.1	28.9	61.8	31.0	50.6	62.7	53.1	44.8
2450.2	32.4	54.0	29.2	61.5	31.1	50.4	62.9	53.2	44.1
2475.0	32.5	54.0	29.3	60.9	31.3	52.3	63.0	53.3	44.9
2500.2	32.6	53.9	29.6	60.2	31.4	52.4	63.1	53.4	45.4
2524.9	32.6	54.1	29.5	59.4	31.6	50.7	63.2	53.6	45.1
2550.1	32.5	54.5	29.5	58.3	32.0	49.6	63.2	53.8	45.5
2574.9	32.5	54.6	29.9	57.4	32.2	50.8	63.3	53.6	46.5
2600.1	32.4	54.7	30.0	56.4	32.4	49.3	63.2	53.3	46.6
2624.9	32.3	54.9	30.1	55.5	32.6	49.3	62.7	52.6	47.5
2650.1	32.2	55.1	30.4	54.9	32.9	49.1	60.4	51.9	48.6
2674.9	32.2	55.0	30.6	54.3	33.0	49.2	51.1	50.6	48.7
2700.0	32.1	54.9	31.0	54.0	33.0	49.2	48.3	49.8	43.2
2724.8	32.0	54.6	31.5	53.8	33.0	49.7	47.8	48.9	41.3
2750.0	32.0	54.2	32.0	53.5	33.0	50.8	47.9	48.4	41.8
2774.8	32.0	53.7	32.7	53.3	32.8	51.4	48.0	48.1	43.2
2800.0	32.1	53.2	33.7	53.3	32.6	51.7	48.2	47.8	43.2
2825.2	32.2	52.5	35.4	53.2	32.5	55.3	48.3	47.8	43.7
2850.0	32.3	52.0	37.6	53.2	32.3	56.3	48.4	47.7	44.2
2875.1	32.6	51.5	40.6	53.3	32.1	81.1	48.6	47.7	45.0
2899.9	32.8	51.1	42.1	53.4	32.0	84.8	48.7	47.6	45.8
2925.1	33.1	50.8	43.7	53.4	32.0	83.6	48.9	47.8	46.5
2949.9	33.4	50.2	44.5	53.4	32.0	86.2	49.0	47.7	48.5
2975.1	33.8	49.9	45.2	53.4	32.1	91.0	49.1	47.8	49.4
2999.9	34.4	49.4	46.1	53.5	32.3	91.4	49.4	47.9	50.3

A(7e) Data of seismic test result in homogeneous Oxford-clay for test ID: 20Jun10_31 (Test 48), 21Jun10_32 (Test 49), and 21Jun10_33 (Test 50)

Seismic test carried out using Oxford-clay before columns installation which the seismic source at one end of the array.
Date of test: 20 to 21 Jun 2010
Test frequency range / interval: 75 to 3000 Hz / 25 Hz

Remarks: -

Frequency, Hz	Test (48) Row2/E, m/s			Test (49) Row2/E, m/s			Test (50) Row2/E, m/s		
	A-B	B-C	C-D	A-B	B-C	C-D	A-B	B-C	C-D
75.1	49.5	120.8	182.3	46.0	108.6	155.1	50.8	106.6	166.9
99.9	72.7	84.2	92.6	76.0	86.2	91.2	73.1	84.6	86.7
125.1	42.4	18.7	15.5	40.8	16.1	19.5	47.5	21.7	16.5
149.9	35.9	63.2	91.4	38.3	70.7	100.2	38.6	72.6	104.2
175.1	55.3	60.4	19.4	60.0	66.9	16.1	60.6	63.4	15.3
199.9	40.5	38.1	55.1	37.9	41.2	63.9	37.9	41.9	65.1
225.1	34.6	40.1	36.3	37.6	44.0	39.2	38.6	44.8	37.9
249.9	47.1	44.9	26.1	50.9	39.6	31.6	51.4	39.6	31.5
275.0	44.2	46.5	39.4	46.7	54.1	45.1	46.6	55.6	46.1
299.8	41.1	49.1	37.4	48.8	56.8	42.1	48.5	57.1	42.2
325.0	40.9	40.2	35.1	43.2	47.5	42.3	43.3	48.1	42.2
350.2	40.0	41.6	29.4	44.2	50.5	33.8	44.3	50.2	33.9
375.0	47.2	36.4	31.5	49.3	46.6	39.5	49.5	46.1	39.1
400.2	43.3	36.6	32.4	46.8	47.6	39.7	47.2	46.7	39.7
425.0	45.1	31.7	35.5	48.5	42.5	39.9	48.7	42.0	39.6
450.1	45.0	31.6	33.0	52.5	41.6	36.2	52.3	41.6	35.9
474.9	40.7	33.1	31.3	52.6	42.7	35.4	52.4	42.5	35.3
500.1	37.8	33.4	35.9	49.0	41.1	41.5	48.4	40.9	41.5
524.9	38.3	31.9	37.2	46.8	39.7	41.4	46.1	39.7	41.4
550.1	39.0	31.9	36.2	47.2	38.8	39.8	46.7	38.7	40.0
574.9	39.7	31.7	35.8	46.8	39.6	39.1	46.2	39.4	39.6
600.1	39.8	31.3	38.0	46.2	38.2	42.7	45.7	37.9	43.7
624.8	39.1	33.0	38.5	43.3	39.6	45.0	44.4	37.9	45.5
650.0	40.4	33.1	37.9	45.6	39.5	41.9	45.3	38.2	44.3
674.8	41.6	33.4	36.8	47.4	39.5	40.4	46.1	38.4	43.8
700.0	42.4	33.8	36.2	47.9	39.7	41.6	46.9	38.6	44.0
725.2	43.7	33.7	35.8	49.0	39.2	42.5	47.7	39.1	43.6
750.0	44.8	33.8	35.5	50.6	38.7	42.0	48.9	39.2	43.1
775.1	45.2	34.1	35.6	51.6	38.9	41.4	50.2	39.0	43.2
799.9	45.7	34.1	36.1	51.6	39.5	42.0	51.0	39.1	43.5
825.1	46.2	34.2	36.4	52.1	39.9	42.7	51.9	39.3	43.7
849.9	46.5	34.7	36.1	52.7	40.2	42.1	52.4	39.8	43.2
875.1	46.3	35.2	35.5	52.8	40.7	40.9	52.6	40.5	42.2
899.9	46.3	35.4	35.0	52.8	41.1	39.9	52.9	41.0	41.1
925.1	46.5	35.4	34.8	53.1	41.4	39.3	53.4	41.3	40.2
949.9	46.8	35.3	34.9	53.5	41.6	38.9	53.9	41.6	39.5
975.0	46.7	35.6	35.0	53.5	41.9	38.8	54.2	41.7	39.3

999.8	46.6	35.9	35.1	53.4	42.1	38.9	54.4	41.8	39.4
1025.0	46.4	36.1	35.2	53.3	42.2	39.0	54.5	42.0	39.5
1050.2	46.1	36.3	35.4	53.1	42.4	38.9	54.4	42.2	39.5
1075.0	45.8	36.3	35.7	52.8	42.7	38.8	54.1	42.4	39.5
1100.2	45.5	36.2	36.1	52.5	42.9	38.7	53.8	42.6	39.7
1125.0	45.3	36.2	36.3	52.3	43.1	38.7	53.6	42.8	39.7
1150.1	45.0	36.2	36.5	52.3	43.0	38.8	53.4	42.9	39.7
1174.9	44.8	36.4	36.6	52.6	42.8	39.0	53.4	42.9	39.8
1200.1	44.7	36.5	36.7	52.8	42.5	39.4	53.3	42.9	40.2
1224.9	44.8	36.6	36.8	52.9	42.2	39.8	53.3	42.7	40.6
1250.1	45.1	36.7	36.8	52.8	42.1	40.2	53.3	42.6	41.0
1274.9	45.5	36.9	36.7	52.6	42.1	40.5	53.2	42.5	41.4
1300.0	45.8	37.1	36.7	52.4	42.3	40.5	52.9	42.6	41.6
1324.8	46.3	37.3	36.6	52.2	42.5	40.5	52.7	42.7	41.7
1350.0	46.7	37.5	36.6	52.0	42.8	40.5	52.4	42.9	41.7
1374.8	47.2	37.7	36.5	51.8	43.1	40.3	52.2	43.1	41.6
1400.0	47.7	37.9	36.5	51.8	43.5	40.1	52.1	43.4	41.5
1425.2	48.1	38.1	36.4	51.9	43.8	40.0	52.1	43.7	41.2
1450.0	48.5	38.3	36.3	51.9	44.1	40.0	52.1	44.1	41.0
1475.1	49.0	38.3	36.3	52.1	44.4	40.1	52.1	44.5	40.8
1499.9	49.4	38.4	36.3	52.3	44.7	40.3	52.2	44.8	40.8
1525.1	49.8	38.4	36.5	52.5	44.9	40.6	52.3	45.1	40.8
1549.9	50.2	38.5	36.6	52.9	45.1	40.8	52.6	45.4	41.0
1575.1	50.5	38.5	36.8	53.2	45.3	41.1	53.0	45.6	41.3
1599.9	50.8	38.4	37.2	53.6	45.4	41.4	53.4	45.7	41.7
1625.1	51.0	38.3	37.4	54.1	45.4	41.7	53.9	45.9	42.2
1649.9	51.2	38.2	37.7	54.5	45.4	41.9	54.4	46.0	42.6
1675.0	51.3	38.1	38.1	54.9	45.4	41.9	54.9	46.1	42.8
1699.8	51.4	37.9	38.7	55.2	45.3	41.8	55.4	46.2	43.0
1725.0	51.5	37.8	39.2	55.4	45.3	41.6	55.9	46.2	43.3
1750.2	51.5	37.8	39.7	55.7	45.2	41.2	56.3	46.1	43.3
1775.0	51.5	37.9	40.1	55.9	45.0	40.8	56.8	45.9	43.2
1800.2	51.4	38.1	40.6	56.2	44.8	40.7	57.1	45.7	42.8
1825.0	51.3	38.3	41.1	56.4	44.6	40.9	57.5	45.4	42.6
1850.1	51.1	38.7	41.6	56.6	44.4	41.4	57.7	45.1	42.7
1874.9	50.9	39.0	41.8	56.8	44.2	42.3	57.9	44.7	43.1
1900.1	50.6	39.4	41.7	57.0	44.0	43.3	58.1	44.4	43.6
1924.9	50.4	39.8	41.4	57.2	43.9	44.2	58.2	44.1	44.2
1950.1	50.1	40.2	40.0	57.4	43.8	45.1	58.4	44.0	44.9
1974.9	49.9	40.7	37.4	57.7	43.7	46.0	58.5	43.9	45.2
2000.0	49.7	41.1	35.6	58.0	43.6	46.7	58.7	44.0	45.8

2024.8	49.7	41.6	35.0	58.3	43.6	47.0	58.8	44.1	46.1
2050.0	49.6	42.1	35.1	58.7	43.6	46.9	59.0	44.3	46.2
2074.8	49.5	42.4	35.5	58.8	43.7	46.8	59.1	44.5	46.4
2100.0	49.4	42.6	36.0	58.6	43.9	46.6	59.1	44.7	46.7
2125.2	49.2	42.8	36.5	58.2	44.1	46.5	58.8	45.0	46.9
2150.0	49.2	42.8	37.1	57.8	44.3	46.4	58.4	45.4	47.7
2175.1	49.2	42.7	37.7	57.4	44.5	46.2	57.4	45.8	47.7
2199.9	49.3	42.3	38.6	57.1	44.8	46.1	55.9	46.3	48.1
2225.1	49.5	41.7	39.5	56.9	44.9	46.0	53.8	46.6	48.5
2249.9	49.8	41.1	40.6	56.9	45.1	45.8	52.0	47.0	48.4
2275.1	50.2	40.6	41.6	57.0	45.2	45.5	50.9	47.4	48.4
2299.9	50.6	40.2	42.8	57.1	45.3	45.0	50.3	47.7	47.7
2325.1	51.1	40.0	54.0	57.2	45.3	44.8	50.4	47.9	46.0
2349.9	51.7	40.0	59.3	57.4	45.4	44.7	50.9	48.0	45.2
2375.0	52.2	40.0	64.3	57.6	45.5	44.5	51.4	48.1	44.5
2399.8	52.8	40.0	64.5	57.7	45.6	44.6	51.9	48.4	44.2
2425.0	53.3	40.2	65.6	58.0	45.6	44.7	52.5	48.1	44.1
2450.2	53.9	40.5	68.5	58.2	45.6	44.7	53.1	48.0	44.3
2475.0	54.4	40.8	68.9	58.4	45.7	44.9	53.7	47.7	44.8
2500.2	54.9	41.0	71.5	58.6	45.8	44.7	54.3	47.4	45.2
2524.9	55.3	41.3	73.5	58.8	45.9	44.6	55.0	47.1	46.1
2550.1	55.7	41.7	75.1	59.0	46.1	44.0	55.7	46.7	46.9
2574.9	56.1	42.0	77.2	59.2	46.3	43.5	56.3	46.7	46.7
2600.1	56.4	42.2	78.3	59.3	46.7	42.6	56.8	46.8	46.7
2624.9	56.5	42.4	79.2	59.5	47.0	42.3	57.3	46.8	46.2
2650.1	56.8	42.6	82.1	59.6	47.3	41.4	57.9	46.9	44.8
2674.9	56.9	42.1	86.9	59.8	47.8	41.1	58.4	47.0	42.7
2700.0	57.0	39.8	100.6	59.9	48.3	40.7	58.9	47.3	41.5
2724.8	57.0	38.0	161.7	60.1	48.7	40.6	59.4	47.4	41.1
2750.0	57.1	37.5	248.3	60.1	49.2	40.5	59.9	47.7	40.7
2774.8	57.0	37.4	386.9	60.2	49.8	40.5	60.4	47.8	40.7
2800.0	57.0	37.6	455.9	60.3	50.2	40.9	60.9	48.1	40.6
2825.2	57.0	37.9	524.5	60.4	51.0	41.0	61.4	48.3	41.3
2850.0	57.0	38.2	572.1	60.5	51.8	41.5	61.9	48.5	40.9
2875.1	57.0	38.5	564.6	60.6	53.1	41.3	62.4	48.8	41.2
2899.9	56.9	39.1	548.5	60.6	55.2	42.0	62.8	49.0	41.6
2925.1	57.0	39.7	570.3	60.7	59.3	43.6	63.2	49.5	41.4
2949.9	56.6	40.3	579.6	60.8	62.8	44.7	63.6	49.6	41.3
2975.1	56.5	40.9	562.3	60.8	67.3	44.0	63.9	49.5	41.6
2999.9	55.5	42.2	599.5	60.9	69.0	43.8	64.2	49.5	41.7

A(7f) Data of seismic test result in homogeneous Oxford-clay for test ID: 21Jun10_41(Test 51), 21Jun10_42 (Test 52), and 21Jun10_43 (Test 53)

Seismic test carried out using Oxford-clay before columns installation which the seismic source at one end of the array.
Date of test: 21 Jun 2010
Test frequency range / interval: 75 to 3000 Hz / 25 Hz
Remarks: -

Frequency, Hz	Test (51) Row2/C, m/s			Test (52) Row2/C, m/s			Test (53) Row2/C, m/s		
	A-B	B-C	C-D	A-B	B-C	C-D	A-B	B-C	C-D
75.1	74.0	306.8	280.5	67.8	184.8	265.6	55.8	156.7	213.4
99.9	69.6	114.4	26.8	70.2	97.0	25.5	65.2	88.4	23.1
125.1	30.9	77.2	131.6	30.5	74.3	122.6	30.1	73.3	116.1
149.9	47.0	38.5	32.5	46.2	37.9	32.4	44.2	36.0	31.9
175.1	30.1	63.0	85.8	30.5	63.0	84.3	31.2	64.8	84.1
199.9	51.3	51.1	45.4	52.3	52.6	45.3	52.8	51.8	45.1
225.1	28.8	54.3	63.9	29.1	56.3	64.0	30.8	61.5	65.0
249.9	51.9	44.3	39.8	53.8	44.3	39.3	53.4	42.4	41.6
275.0	39.4	52.9	43.1	41.2	55.7	43.9	42.9	59.8	44.3
299.8	41.7	52.7	46.3	43.4	54.7	47.5	45.9	58.3	49.9
325.0	37.6	47.5	52.0	39.0	48.7	53.5	40.4	52.5	57.5
350.2	40.8	45.7	43.5	43.1	48.5	41.4	46.1	51.0	41.6
375.0	41.8	43.1	44.8	44.1	46.5	43.3	47.6	51.9	43.3
400.2	40.7	47.3	40.3	42.6	52.6	38.4	46.4	59.5	38.9
425.0	39.6	47.9	41.2	41.3	51.7	40.4	43.2	59.5	42.1
450.1	40.8	42.9	48.2	43.1	46.8	45.9	46.3	52.4	47.2
474.9	40.1	46.0	44.8	42.2	50.8	42.4	45.3	56.8	43.4
500.1	40.4	45.0	45.0	42.4	49.1	44.0	44.9	56.1	44.5
524.9	39.1	44.9	47.8	41.2	48.3	47.6	44.0	53.8	48.3
550.1	38.9	44.7	49.5	41.2	47.1	50.4	44.1	51.2	51.8
574.9	39.7	43.9	48.3	42.2	46.3	49.5	45.9	49.6	50.0
600.1	39.1	44.8	47.9	41.9	46.6	50.6	45.7	49.4	50.8
624.8	42.0	44.7	47.0	44.5	52.7	45.4	47.0	53.5	49.3
650.0	39.8	45.0	45.1	43.6	49.7	45.8	46.6	53.0	48.2
674.8	37.7	44.6	45.9	42.1	48.7	47.3	45.5	52.0	49.7
700.0	35.7	44.5	46.1	41.0	48.2	48.0	44.5	52.2	50.2
725.2	34.5	44.4	46.3	40.3	47.6	48.9	42.9	52.4	50.4
750.0	33.9	44.2	46.8	40.2	47.1	49.6	42.0	52.7	50.9
775.1	33.8	43.8	47.1	40.1	46.6	50.7	41.8	52.5	51.8
799.9	34.0	43.1	47.2	39.5	46.6	50.9	41.5	52.0	52.7

825.1	34.5	42.7	47.3	38.9	47.3	49.9	40.7	52.1	52.4
849.9	34.9	43.2	46.8	38.4	48.4	48.2	39.8	52.9	50.5
875.1	35.4	43.9	45.4	38.3	49.2	47.0	39.3	53.7	48.5
899.9	36.1	44.1	44.4	38.6	49.0	46.8	39.4	53.5	47.7
925.1	36.8	43.4	44.3	39.2	47.8	47.4	40.1	52.2	48.5
949.9	37.5	42.5	44.6	39.8	46.4	48.1	40.7	50.6	49.8
975.0	37.9	41.9	44.9	40.4	45.3	48.6	41.2	49.3	50.9
999.8	38.4	41.5	45.4	41.1	44.3	49.1	42.0	48.2	52.0
1025.0	38.9	41.1	45.8	41.7	43.7	49.4	42.9	47.0	52.7
1050.2	39.1	41.1	45.8	42.0	43.7	49.2	43.4	46.3	52.9
1075.0	39.1	41.4	45.6	42.2	44.0	48.8	43.5	46.4	52.7
1100.2	39.3	41.8	45.3	42.5	44.4	48.2	43.6	46.7	52.1
1125.0	39.6	42.0	45.0	42.7	44.9	47.4	43.6	47.3	51.2
1150.1	39.7	42.4	44.6	43.0	45.5	46.6	43.5	48.3	50.2
1174.9	39.8	42.7	44.3	43.2	46.2	45.8	43.5	49.5	49.1
1200.1	39.7	43.0	44.1	43.5	46.9	45.1	43.7	50.7	48.0
1224.9	39.6	43.2	44.3	43.7	47.5	44.6	44.0	51.6	47.0
1250.1	39.4	43.3	44.8	43.7	48.0	44.5	44.2	52.3	46.3
1274.9	39.0	43.5	45.3	43.4	48.4	44.6	44.4	52.7	46.0
1300.0	38.7	43.5	46.0	43.1	48.7	44.9	44.4	52.9	45.9
1324.8	38.3	43.3	46.7	42.7	48.9	45.3	44.3	53.0	46.0
1350.0	38.0	43.2	47.3	42.4	49.1	45.8	44.1	53.1	46.3
1374.8	37.6	43.1	47.7	41.9	49.2	46.2	43.9	53.2	46.6
1400.0	37.2	43.0	47.6	41.5	49.3	46.7	43.7	53.3	47.0
1425.2	36.8	43.1	47.2	41.0	49.4	47.2	43.5	53.5	47.3
1450.0	36.6	43.3	46.7	40.6	49.3	47.5	43.4	53.7	47.6
1475.1	36.4	43.6	46.0	40.3	49.2	47.8	43.3	53.9	47.8
1499.9	36.3	44.0	45.5	39.9	49.2	48.0	43.4	54.2	47.9
1525.1	36.5	44.2	45.1	39.9	48.9	48.0	43.5	54.6	47.8
1549.9	36.7	44.4	45.0	40.1	48.5	48.0	43.6	55.3	47.3
1575.1	37.0	44.7	45.1	40.4	48.3	47.8	43.8	56.5	46.4
1599.9	37.4	44.9	45.4	40.7	48.4	47.5	43.9	57.9	45.2
1625.1	37.6	45.4	45.8	41.0	48.9	46.9	44.0	59.1	44.1
1649.9	37.6	46.1	46.1	41.2	49.6	46.4	44.0	59.8	43.4
1675.0	37.5	47.1	46.3	41.3	50.4	46.0	43.9	59.9	43.3
1699.8	37.4	48.3	46.5	41.3	51.2	45.9	43.8	59.7	43.7
1725.0	37.3	49.3	46.7	41.3	51.9	46.2	43.6	59.5	44.3
1750.2	37.2	50.1	46.9	41.1	52.6	46.7	43.4	59.2	45.2
1775.0	37.1	50.5	46.7	41.0	53.0	47.2	43.2	59.0	46.2
1800.2	37.0	50.8	45.9	40.7	53.5	48.0	43.0	58.9	47.2
1825.0	37.0	51.0	44.7	40.4	54.2	48.8	42.9	58.8	48.2

1850.1	37.0	51.0	42.9	40.1	54.8	49.6	42.7	58.8	49.2
1874.9	36.9	50.8	42.2	39.8	55.4	50.4	42.7	58.9	50.2
1900.1	37.1	50.5	41.4	39.5	55.8	51.2	42.7	58.9	51.1
1924.9	37.2	50.2	41.4	39.3	56.2	51.8	42.8	58.9	52.0
1950.1	37.5	49.7	41.4	39.1	56.2	52.4	43.0	58.9	52.7
1974.9	37.7	49.4	41.6	39.1	56.0	52.7	43.2	58.9	53.4
2000.0	38.1	48.8	41.8	39.2	55.6	52.3	43.5	58.6	53.8
2024.8	38.5	48.2	41.8	39.5	54.8	51.3	43.9	58.3	54.0
2050.0	39.0	47.5	42.0	39.9	53.8	49.7	44.5	57.7	54.0
2074.8	39.5	46.9	42.1	40.5	52.5	48.3	45.2	56.9	53.6
2100.0	40.1	46.1	42.7	41.3	51.1	47.3	46.0	56.0	52.5
2125.2	40.6	45.4	43.5	42.1	49.9	47.0	46.6	55.3	50.6
2150.0	41.1	44.7	44.4	42.7	48.9	47.2	46.8	54.9	48.9
2175.1	41.4	44.3	45.7	43.3	48.2	47.5	44.6	55.4	47.2
2199.9	41.7	44.0	50.5	43.7	47.6	47.9	43.7	55.6	46.6
2225.1	41.8	43.8	56.1	44.0	47.2	48.3	43.4	55.7	46.5
2249.9	41.9	44.0	58.3	44.2	46.8	48.9	43.3	55.8	46.5
2275.1	41.9	44.4	58.3	44.4	46.6	49.1	43.4	55.9	47.3
2299.9	41.9	45.1	59.6	44.5	46.2	49.6	43.6	55.8	47.8
2325.1	41.8	46.0	58.0	44.4	46.1	50.1	43.8	55.5	49.3
2349.9	41.7	47.3	58.6	44.5	45.9	50.3	44.0	55.2	50.1
2375.0	41.5	49.2	43.8	44.4	45.9	50.2	44.4	54.6	51.1
2399.8	41.4	51.2	39.6	44.1	46.2	49.7	44.8	53.7	51.9
2425.0	41.3	53.6	39.0	43.9	47.1	48.3	45.1	52.9	52.4
2450.2	41.3	55.8	38.6	43.6	48.2	46.2	45.4	52.2	52.0
2475.0	41.6	57.5	38.1	43.2	49.8	43.9	45.7	51.5	51.8
2500.2	41.8	59.1	38.1	42.8	52.1	42.1	46.0	51.0	52.1
2524.9	42.2	60.5	37.9	42.5	54.6	40.4	46.1	50.6	51.4
2550.1	42.9	61.5	37.9	42.3	56.4	39.5	46.2	50.6	50.6
2574.9	43.8	62.5	37.7	42.1	58.3	38.9	46.3	50.6	42.6
2600.1	44.8	63.5	38.0	42.0	59.8	38.7	44.2	53.6	39.6
2624.9	46.1	64.4	38.2	42.2	60.7	38.6	39.1	64.0	39.7
2650.1	47.7	65.0	38.8	42.3	61.5	38.6	38.5	66.4	39.3
2674.9	49.5	65.9	39.1	42.6	61.7	38.8	38.6	66.9	39.3
2700.0	51.4	67.1	39.4	43.0	61.8	38.8	39.0	66.5	39.3
2724.8	53.9	68.9	39.5	43.3	62.5	39.2	39.6	65.9	39.7
2750.0	56.2	71.1	39.4	43.6	62.5	40.0	40.1	65.3	40.2
2774.8	59.7	72.3	39.7	43.9	63.0	40.6	40.6	64.8	40.5
2800.0	63.2	72.2	39.9	44.1	63.2	42.0	41.0	64.5	40.7
2825.2	67.5	72.2	40.0	44.6	63.4	43.3	41.4	64.4	41.8
2850.0	73.1	71.5	40.3	45.4	62.7	45.0	41.8	64.3	41.9

2875.1	80.8	71.4	40.4	46.3	64.9	45.2	42.0	64.0	42.3
2899.9	90.3	71.4	40.7	47.5	71.0	42.9	42.2	63.9	42.7
2925.1	98.9	71.5	41.0	48.8	83.3	39.6	42.5	63.6	43.1
2949.9	104.9	71.6	41.3	51.0	82.0	39.4	42.7	63.3	45.9
2975.1	109.7	71.8	41.5	52.4	78.8	40.1	42.8	62.2	49.2
2999.9	113.6	72.1	42.0	54.0	76.8	40.3	42.9	61.1	49.7

A(7g) Data of seismic test result in homogeneous Oxford-clay for test ID: 22Jun10_51 (Test 54), 22Jun10_52 (Test 55), and 23Jun10_53 (Test 56)
Date of test: 22 to 23 Jun 2010

Seismic test carried out using Oxford-clay before columns installation which the seismic source at one end of the array.
Test frequency range / interval: 75 to 3000 Hz / 25 Hz
Remarks: -

Frequency, Hz	Test (54) Row2/A, m/s			Test (55) Row2/A, m/s			Test (56) Row2/A, m/s		
	A-B	B-C	C-D	A-B	B-C	C-D	A-B	B-C	C-D
75.1	60.4	156.5	171.1	62.7	92.0	142.8	88.6	70.7	139.7
99.9	53.0	15.9	11.9	26.7	16.6	22.4	149.9	15.5	15.4
125.1	81.8	123.8	161.8	82.2	136.1	190.1	65.4	110.3	140.2
149.9	37.1	80.1	118.1	35.2	76.1	115.7	34.1	68.6	99.1
175.1	69.1	42.6	31.2	67.7	43.2	29.1	64.3	42.0	32.1
199.9	58.6	99.7	113.7	55.5	96.2	111.0	57.2	94.4	104.8
225.1	36.8	51.4	77.7	37.0	50.2	75.7	37.8	48.8	74.7
249.9	52.0	49.2	49.7	50.6	50.0	50.8	53.7	49.9	50.4
275.0	59.1	49.9	34.6	58.8	52.6	34.8	60.8	50.7	36.3
299.8	57.1	83.9	64.5	55.3	83.0	64.8	59.4	83.5	64.4
325.0	47.1	56.9	69.4	46.7	56.6	67.6	48.0	58.6	70.4
350.2	52.6	53.6	52.6	52.0	53.2	53.0	53.7	54.2	56.1
375.0	50.7	54.6	54.1	51.2	54.4	54.6	53.7	56.2	56.5
400.2	52.6	58.4	44.0	52.4	59.5	45.3	55.3	62.0	46.9
425.0	49.9	55.6	50.5	49.9	56.4	51.8	51.6	59.3	54.5
450.1	52.7	49.5	59.8	53.1	50.7	61.5	54.9	53.4	62.7
474.9	50.3	52.2	52.2	51.1	54.1	52.6	54.0	55.4	54.5
500.1	49.3	51.7	50.4	49.9	52.6	50.7	51.8	56.0	52.2
524.9	52.8	46.6	48.9	53.6	48.8	46.8	56.0	51.5	49.0
550.1	50.8	48.0	46.4	51.4	52.3	44.4	54.6	53.2	46.6
574.9	47.6	51.0	46.7	47.8	55.5	46.5	51.1	56.9	47.4
600.1	46.8	51.1	49.5	47.3	54.1	49.6	49.4	57.1	50.1
624.8	49.3	41.0	53.3	48.4	52.5	53.2	56.8	33.6	62.6

650.0	48.1	41.2	56.3	48.0	51.2	54.0	55.3	31.5	81.0
674.8	47.5	41.6	61.0	47.2	53.4	53.2	49.8	34.3	77.9
700.0	48.4	40.6	63.0	47.8	52.6	54.2	40.7	40.9	76.0
725.2	45.8	42.4	61.9	48.9	50.6	54.8	32.2	56.4	74.6
750.0	42.4	46.1	61.6	49.4	50.2	53.9	30.8	64.7	71.3
775.1	40.7	49.3	62.6	49.5	50.6	54.0	31.9	66.0	69.3
799.9	40.6	50.1	64.0	49.5	50.4	56.8	35.4	62.2	69.1
825.1	40.2	51.8	60.0	49.5	49.9	58.4	40.1	59.4	64.4
849.9	40.1	55.2	52.6	49.3	49.9	58.0	44.2	58.9	58.4
875.1	41.6	57.2	47.7	49.0	50.2	57.4	47.4	58.9	55.2
899.9	45.6	54.3	47.6	48.6	50.5	57.0	49.8	58.0	54.7
925.1	50.1	50.2	50.5	48.5	50.7	56.4	51.5	56.8	55.3
949.9	52.0	47.7	53.2	48.6	50.7	55.5	52.4	55.9	55.4
975.0	52.9	46.3	54.6	49.1	50.5	54.9	53.0	55.2	55.3
999.8	53.4	45.5	55.5	49.6	50.2	54.7	53.5	54.5	55.5
1025.0	53.4	45.3	56.2	49.9	50.2	54.7	53.8	54.2	55.9
1050.2	52.8	45.7	56.3	50.1	50.6	54.3	53.9	54.4	56.0
1075.0	52.2	46.6	55.9	50.4	50.8	53.6	54.0	54.8	55.9
1100.2	51.3	48.0	55.4	50.6	51.3	53.1	54.1	55.1	56.0
1125.0	50.2	49.7	54.8	50.4	52.1	52.7	53.8	55.7	56.0
1150.1	49.3	51.3	54.1	50.1	52.9	52.4	53.4	56.5	55.8
1174.9	48.6	52.4	53.3	50.0	53.5	52.0	53.1	57.1	55.6
1200.1	48.0	53.2	53.1	49.8	53.9	51.9	52.8	57.5	55.6
1224.9	47.2	54.2	53.0	49.5	54.3	52.0	52.4	57.9	55.7
1250.1	46.9	55.1	52.6	49.4	54.6	52.0	52.0	58.5	55.5
1274.9	46.9	55.5	52.1	49.5	54.8	51.8	51.8	58.8	55.2
1300.0	47.1	55.2	51.7	49.7	54.8	51.5	51.7	59.1	54.8
1324.8	47.4	54.5	51.7	50.0	54.6	51.3	51.7	59.1	54.5
1350.0	47.9	53.7	52.0	50.4	54.3	51.2	51.8	59.0	54.3
1374.8	48.5	52.9	52.2	50.7	53.9	51.2	52.0	58.7	54.2
1400.0	49.1	52.1	52.4	51.0	53.5	51.3	52.4	58.2	54.1
1425.2	49.6	51.5	52.7	51.3	53.2	51.5	52.7	57.7	54.2
1450.0	50.1	51.0	52.9	51.5	52.8	51.7	53.1	57.2	54.3
1475.1	50.4	50.6	52.9	51.7	52.6	52.0	53.4	56.8	54.5
1499.9	50.6	50.4	52.7	51.7	52.3	52.2	53.8	56.3	54.6
1525.1	50.8	50.3	52.6	51.7	52.1	52.5	54.0	55.9	54.8
1549.9	51.0	50.2	52.6	51.7	51.9	52.9	54.2	55.6	55.1
1575.1	51.3	50.3	52.7	51.7	51.8	53.3	54.4	55.3	55.5
1599.9	51.6	50.5	53.0	51.7	51.7	53.9	54.6	55.1	56.0
1625.1	51.8	50.7	53.2	51.8	51.5	54.4	54.7	54.9	56.5
1649.9	52.0	50.9	53.6	51.9	51.4	54.9	54.7	54.8	57.2

1675.0	52.2	51.1	54.1	52.1	51.3	55.6	54.8	54.8	57.9
1699.8	52.4	51.3	54.9	52.2	51.2	56.6	54.9	54.9	58.7
1725.0	52.6	51.4	55.8	52.3	51.1	57.5	55.1	54.9	59.4
1750.2	52.7	51.5	56.6	52.4	51.0	58.3	55.3	54.9	59.8
1775.0	52.8	51.5	57.3	52.6	50.9	58.9	55.5	54.8	60.0
1800.2	52.9	51.4	57.9	52.8	50.8	59.5	55.6	54.8	60.2
1825.0	53.0	51.3	58.5	53.0	50.7	59.9	55.7	54.7	60.4
1850.1	53.1	51.2	58.8	53.3	50.6	60.1	55.8	54.7	60.6
1874.9	53.2	51.1	59.0	53.5	50.5	60.2	55.9	54.6	60.7
1900.1	53.3	51.1	59.3	53.8	50.5	60.4	56.0	54.6	60.8
1924.9	53.4	51.2	59.1	54.1	50.7	60.3	56.2	54.7	60.7
1950.1	53.6	51.3	58.8	54.3	51.0	60.0	56.3	54.7	60.5
1974.9	53.7	51.4	58.1	54.5	51.3	59.4	56.4	54.9	60.3
2000.0	54.0	51.5	57.5	54.8	51.8	58.6	56.5	55.1	59.9
2024.8	54.1	51.7	56.9	55.0	52.4	57.8	56.6	55.2	59.5
2050.0	54.3	51.9	56.5	55.1	53.1	57.0	56.8	55.4	59.0
2074.8	54.4	52.1	56.4	55.3	53.7	56.5	57.0	55.6	58.5
2100.0	54.6	52.3	56.2	55.6	54.4	56.2	57.1	55.9	58.1
2125.2	54.8	52.4	56.0	55.9	54.8	56.2	57.3	56.2	57.7
2150.0	54.9	52.6	55.9	56.3	55.2	56.2	57.5	56.5	57.4
2175.1	55.1	52.9	55.8	56.8	55.4	56.5	57.7	56.9	57.2
2199.9	55.2	53.1	55.8	57.4	55.5	56.9	57.9	57.3	57.0
2225.1	55.3	53.3	55.8	57.8	55.7	57.3	58.1	57.8	56.9
2249.9	55.5	53.6	55.6	58.3	55.8	57.8	58.4	58.4	56.8
2275.1	55.7	53.8	55.1	58.6	56.0	58.1	58.7	59.0	56.8
2299.9	55.9	54.0	54.1	58.8	56.2	58.3	59.0	59.6	57.3
2325.1	56.1	54.1	52.6	59.0	56.4	58.2	59.3	60.2	58.1
2349.9	56.3	54.1	50.6	59.0	56.7	58.3	59.6	60.7	59.3
2375.0	56.5	54.0	49.3	59.1	57.0	57.6	59.9	61.1	60.8
2399.8	56.6	53.7	48.8	59.0	57.3	56.2	60.1	61.5	62.3
2425.0	56.8	53.0	49.0	58.9	57.6	51.1	60.3	61.8	62.6
2450.2	57.0	52.1	49.8	58.8	57.7	47.5	60.4	61.9	63.1
2475.0	57.1	50.9	51.3	58.6	57.7	47.1	60.5	62.1	57.5
2500.2	57.0	49.8	53.6	58.3	57.6	47.5	60.5	61.9	48.4
2524.9	57.0	49.3	55.8	58.0	56.4	49.1	60.4	61.8	48.2
2550.1	56.8	49.2	57.9	57.5	54.2	52.0	60.3	61.4	49.3
2574.9	56.5	49.5	59.9	57.0	51.7	55.9	60.1	60.7	50.8
2600.1	56.2	50.0	62.1	56.3	50.6	59.0	59.8	59.7	52.6
2624.9	55.9	50.8	64.0	55.7	50.4	61.0	59.5	58.6	54.5
2650.1	55.5	51.6	66.1	55.0	50.9	62.4	59.1	57.4	56.9
2674.9	55.1	52.5	67.4	54.3	51.6	63.5	58.7	56.7	59.1

2700.0	54.8	53.4	68.5	53.7	52.4	64.4	58.3	56.4	60.9
2724.8	54.6	54.3	69.2	53.1	53.4	65.3	57.9	56.5	62.5
2750.0	54.3	55.3	69.9	52.6	54.5	66.0	57.5	56.8	63.7
2774.8	54.1	56.2	70.4	52.2	55.5	66.7	57.2	57.3	64.6
2800.0	54.0	57.2	70.7	52.0	56.4	67.5	56.9	57.8	65.5
2825.2	53.9	58.0	71.2	51.8	57.4	68.3	56.7	58.4	66.2
2850.0	53.8	58.9	71.6	51.8	58.3	69.0	56.5	59.0	66.8
2875.1	53.8	59.7	72.1	51.7	59.2	69.9	56.3	59.6	67.5
2899.9	53.8	60.5	72.9	51.8	60.0	70.8	56.3	60.3	68.2
2925.1	53.8	61.5	74.2	51.8	60.8	71.9	56.2	60.9	69.2
2949.9	53.8	62.4	76.2	52.0	61.5	73.2	56.1	61.5	70.3
2975.1	53.9	63.4	78.9	52.1	62.2	74.9	56.1	62.1	71.6
2999.9	54.0	64.3	81.7	52.3	62.9	76.9	56.2	62.7	73.1

A(7h) Data of seismic test result in homogeneous Oxford-clay for test ID: 02Jun10_01 (Test 13), 02Jun10_02 (Test 14), 03Jun10_01 (Test 15), and 07Jun10_01 (Test 18)

Seismic test carried out using Oxford-clay before columns installation which the seismic source at the centred of array.
Date of test: 2 to 7 Jun 2010
Test frequency range / interval: 50 to 3000 Hz / 10 Hz
Remarks: -

Frequency, Hz	Test 13, m/s		Test 14, m/s		Test 15, m/s		Test 18, m/s	
	A-B	C-D	A-B	C-D	A-B	C-D	A-B	C-D
70.2	50.1	55.2	26.9	51.4	54.8	83.2	87.9	59.9
80.1	22.3	14.4	16.3	20.6	101.3	59.8	96.4	40.8
90.0	57.1	102.5	59.5	69.1	43.1	16.5	27.4	49.4
99.9	76.8	86.5	69.1	69.9	48.2	133.9	36.4	151.9
109.9	39.0	36.5	26.9	29.1	38.3	75.4	34.3	59.9
120.2	23.9	20.8	20.0	30.4	70.4	44.9	87.8	46.2
130.1	48.2	72.8	43.8	71.9	50.7	49.6	63.0	36.7
140.0	61.2	72.9	50.7	65.0	52.7	59.5	60.0	57.6
149.9	57.8	53.5	40.5	56.4	56.7	40.1	39.5	60.0
159.8	39.4	25.8	29.9	37.1	58.1	33.5	43.8	51.9
170.1	38.2	32.6	33.9	39.0	45.3	50.9	37.3	50.6
180.1	52.6	68.8	46.1	53.4	55.3	64.4	53.2	54.5
190.0	48.3	59.4	42.0	49.8	57.8	55.1	56.5	52.5
199.9	40.8	38.5	40.7	37.2	53.4	50.0	50.9	54.8

210.2	43.1	31.9	31.3	45.2	59.1	46.4	45.4	58.4
220.1	57.1	39.8	31.5	55.1	58.3	39.5	44.0	56.7
230.0	61.2	47.4	45.5	54.0	58.2	49.7	50.8	65.8
239.9	58.8	41.9	41.5	55.0	53.8	49.8	49.0	73.1
249.9	43.2	36.6	33.4	47.1	47.3	53.7	42.9	67.2
260.2	41.8	41.6	39.5	45.6	47.0	56.2	42.9	67.5
270.1	49.1	49.8	51.3	48.6	48.3	63.1	46.3	74.1
280.0	54.9	50.4	49.5	53.6	50.3	62.5	53.5	67.1
289.9	50.6	45.0	45.1	47.7	46.7	55.6	56.9	61.8
299.8	46.1	40.7	43.9	43.8	52.6	48.7	56.3	62.0
310.1	47.1	41.0	46.0	47.5	56.9	47.7	57.7	57.9
320.1	51.5	44.1	47.7	52.5	56.7	50.0	62.8	57.7
330.0	53.7	43.7	47.9	56.3	57.0	49.3	67.0	62.4
339.9	53.7	40.7	46.4	54.8	61.8	50.5	68.9	66.4
350.2	52.0	38.2	47.2	54.4	70.6	52.1	64.4	67.4
360.1	52.3	37.4	47.9	60.4	76.2	52.0	58.0	68.7
370.0	51.3	37.3	47.7	64.3	73.1	53.0	51.1	72.3
379.9	48.0	37.2	46.0	61.2	66.0	53.6	45.7	73.1
389.9	44.4	38.1	43.9	55.0	58.7	53.6	44.3	71.0
400.2	41.0	41.1	44.0	49.8	51.6	52.6	48.2	67.5
410.1	39.1	44.2	45.1	47.4	45.9	52.2	53.1	65.0
420.0	38.6	44.8	44.9	46.6	42.5	53.2	56.1	63.3
429.9	38.2	44.3	44.5	46.7	41.9	52.2	57.4	59.6
439.8	38.7	44.7	44.5	46.2	43.5	51.2	56.6	54.8
450.1	39.9	45.6	44.8	45.3	47.0	52.8	53.4	52.1
460.1	40.6	45.8	45.7	45.6	51.5	53.8	50.0	51.0
470.0	40.7	45.8	47.2	47.7	54.6	53.1	47.5	50.4
479.9	40.9	47.3	48.8	50.6	54.6	52.3	46.0	50.6
490.2	41.9	51.1	50.1	53.0	52.6	52.1	45.2	51.8
500.1	42.9	55.3	50.6	53.9	50.2	51.2	44.8	53.1
510.0	47.3	50.6	40.0	22.4	46.1	47.9	42.4	54.1
519.9	47.3	49.9	43.2	31.5	44.6	46.8	43.3	54.9
529.9	46.4	48.9	46.3	37.2	43.6	45.8	44.8	54.8
540.2	45.1	48.2	48.3	39.9	42.9	44.8	46.2	53.9
550.1	43.9	47.3	49.0	41.5	42.6	44.0	47.1	52.6
560.0	43.0	46.4	49.3	42.4	42.9	43.4	47.0	51.5

569.9	42.3	45.7	49.2	43.2	43.6	43.0	45.9	50.3
579.8	42.1	45.8	49.0	44.2	44.5	42.7	44.2	49.3
590.1	42.4	46.4	48.8	45.2	45.4	42.5	42.3	48.6
600.1	43.0	47.1	48.5	45.9	46.0	42.3	41.0	47.9
610.0	43.8	47.5	48.2	46.4	46.2	42.1	40.4	47.3
619.9	44.3	47.2	47.9	46.6	46.0	42.0	40.7	46.9
630.2	44.6	46.7	47.2	46.7	45.4	42.2	41.6	46.9
640.1	44.9	46.5	46.4	46.5	44.7	42.7	42.6	47.4
650.0	45.1	46.4	46.2	47.5	44.0	43.6	43.4	48.4
659.9	45.2	46.4	45.7	47.5	43.6	44.6	43.6	49.4
669.9	45.4	46.5	45.2	47.1	43.4	45.3	43.5	50.1
680.2	45.4	46.9	45.0	46.6	43.6	45.6	43.2	50.2
690.1	45.5	47.2	44.8	46.2	43.9	45.7	42.9	50.0
700.0	45.6	47.4	44.6	46.0	44.3	45.4	42.7	49.7
709.9	45.8	47.5	44.4	45.8	44.6	45.2	42.7	49.5
719.8	45.6	48.2	44.1	45.9	44.7	45.0	42.9	49.5
730.1	46.9	47.5	43.9	46.3	44.6	44.9	43.3	49.7
740.1	48.0	47.1	43.6	46.7	44.4	45.1	43.9	50.1
750.0	49.0	46.8	43.3	47.1	44.2	45.5	44.5	50.5
759.9	49.6	46.5	43.2	47.5	44.0	45.7	45.1	51.0
770.2	50.1	46.2	43.2	47.8	43.8	45.9	45.4	51.5
780.1	50.2	45.9	43.5	48.1	43.8	45.8	45.5	51.8
790.0	50.3	45.6	43.8	48.1	43.8	45.4	45.3	52.0
799.9	50.3	45.3	44.3	47.7	43.8	45.0	44.9	51.9
809.9	50.1	45.0	44.7	47.2	43.7	44.7	44.6	51.9
820.2	50.0	44.8	45.0	46.6	43.7	44.4	44.3	51.8
830.1	49.8	44.6	45.3	46.1	43.5	44.4	43.9	51.6
840.0	49.7	44.5	45.4	45.8	43.4	44.4	43.5	51.4
849.9	49.6	44.2	45.5	45.6	43.3	44.4	43.3	51.1
859.8	49.6	44.0	45.7	45.4	43.4	44.3	43.2	50.9
870.1	49.5	43.6	45.9	45.1	43.5	44.2	43.2	50.6
880.1	49.4	43.3	46.0	44.9	43.7	44.0	43.3	50.3
890.0	49.2	42.9	46.1	44.6	43.9	43.9	43.3	49.9
899.9	49.0	42.6	46.1	44.3	44.2	43.8	43.3	49.6
910.2	48.8	42.3	46.1	43.9	44.4	43.8	43.1	49.3
920.1	48.6	42.2	46.0	43.6	44.5	43.8	42.9	49.0

930.0	48.4	42.1	45.9	43.2	44.6	43.7	42.8	48.8
939.9	48.2	42.1	45.7	42.9	44.7	43.5	42.7	48.4
949.9	48.0	42.1	45.4	42.5	44.7	43.1	42.7	48.3
960.2	47.9	42.0	45.2	42.2	44.8	42.7	42.8	48.2
970.1	47.7	41.8	45.0	41.8	44.9	42.3	43.0	48.1
980.0	47.5	41.6	44.8	41.4	45.0	41.9	43.1	47.9
989.9	47.4	41.3	44.8	41.1	45.2	41.7	43.3	47.7
999.8	47.2	41.1	44.7	40.7	45.6	41.4	43.4	47.4
1010.1	47.1	40.9	44.8	40.4	46.1	41.2	43.6	47.2
1020.1	46.9	40.8	44.8	40.1	46.6	41.1	43.7	47.0
1030.0	46.8	40.7	44.9	39.8	47.1	40.9	43.8	46.8
1039.9	46.6	40.7	45.2	39.4	47.7	40.8	43.9	46.6
1050.2	46.5	40.7	45.3	39.3	48.1	40.6	44.0	46.4
1060.1	46.4	40.8	45.4	39.2	48.4	40.5	44.1	46.4
1070.0	46.4	40.9	45.5	39.1	48.7	40.5	44.2	46.3
1079.9	46.3	41.1	45.5	39.0	48.9	40.4	44.3	46.4
1089.9	46.3	41.2	45.6	39.0	49.2	40.3	44.4	46.4
1100.2	46.4	41.4	45.6	39.0	49.4	40.3	44.4	46.5
1110.1	46.4	41.6	45.7	39.0	49.7	40.3	44.5	46.6
1120.0	46.5	41.8	45.7	39.0	49.8	40.4	44.5	46.8
1129.9	46.6	42.0	45.7	39.0	49.9	40.4	44.4	46.9
1139.8	46.7	42.3	45.8	39.1	50.0	40.4	44.4	47.1
1150.1	46.8	42.5	45.8	39.1	49.9	40.4	44.4	47.2
1160.0	46.9	42.8	45.8	39.2	49.8	40.4	44.3	47.4
1170.0	47.0	43.1	45.9	39.2	49.6	40.4	44.3	47.6
1179.9	47.1	43.3	46.0	39.3	49.4	40.3	44.3	47.8
1190.2	47.3	43.5	46.1	39.4	49.3	40.3	44.4	48.0
1200.1	47.4	43.6	46.2	39.4	49.3	40.2	44.5	48.1
1210.0	47.5	43.7	46.3	39.6	49.2	40.2	44.6	48.2
1219.9	47.7	43.7	46.5	39.8	49.3	40.2	44.8	48.3
1229.9	47.8	43.7	46.6	39.9	49.3	40.1	44.9	48.4
1240.2	47.9	43.7	46.7	40.2	49.4	40.1	45.0	48.5
1250.1	48.1	43.6	46.8	40.4	49.5	40.1	45.2	48.6
1260.0	48.2	43.6	46.9	40.8	49.6	40.1	45.4	48.7
1269.9	48.3	43.7	47.0	41.1	49.7	40.0	45.6	48.8
1279.8	48.4	43.7	47.1	41.5	49.8	40.0	45.8	48.9

1290.1	48.5	43.7	47.2	42.0	49.9	40.1	46.0	48.9
1300.0	48.7	43.8	47.2	42.5	50.0	40.2	46.2	49.0
1310.0	48.8	43.8	47.3	43.0	50.1	40.3	46.4	49.0
1319.9	49.0	43.8	47.4	43.5	50.2	40.5	46.6	49.1
1330.2	49.1	43.9	47.4	44.1	50.3	40.7	46.8	49.1
1340.1	49.3	43.9	47.4	44.7	50.4	40.9	47.1	49.2
1350.0	49.4	43.8	47.5	45.1	50.6	41.1	47.3	49.2
1359.9	49.6	43.8	47.6	45.5	50.8	41.3	47.5	49.3
1369.9	49.8	43.9	47.6	45.9	51.0	41.4	47.6	49.4
1380.2	50.0	43.9	47.7	46.2	51.3	41.6	47.8	49.5
1390.1	50.2	43.8	47.8	46.4	51.5	41.8	48.0	49.6
1400.0	50.4	43.8	47.9	46.6	51.7	41.8	48.1	49.7
1409.9	50.6	43.7	48.0	46.7	51.9	42.0	48.3	49.8
1419.8	50.8	43.5	48.2	46.8	52.2	42.1	48.4	49.9
1430.1	51.0	43.3	48.3	46.9	52.5	42.4	48.5	50.0
1440.0	51.2	42.9	48.4	47.0	52.7	42.7	48.7	50.1
1450.0	51.4	42.6	48.5	47.1	52.9	43.0	48.8	50.2
1459.9	51.7	42.1	48.6	47.1	53.2	43.4	49.0	50.3
1470.2	52.0	41.6	48.7	47.1	53.4	43.8	49.1	50.5
1480.1	52.2	41.0	48.8	47.2	53.7	44.2	49.3	50.6
1490.0	52.5	39.3	48.9	47.2	53.9	44.7	49.5	50.7
1499.9	52.6	37.3	49.0	47.2	54.3	45.2	49.6	50.9
1509.9	52.8	39.3	49.0	47.2	54.6	45.8	49.8	51.0
1520.2	52.8	42.8	49.1	47.3	54.8	46.3	50.0	51.2
1530.1	52.9	45.4	49.2	47.3	55.1	47.0	50.2	51.3
1540.0	52.9	46.9	49.2	47.3	55.3	47.6	50.4	51.4
1549.9	52.8	47.6	49.2	47.4	55.5	48.1	50.6	51.6
1559.8	52.7	48.1	49.3	47.5	55.7	48.7	50.7	51.7
1570.1	52.6	48.2	49.3	47.5	55.8	49.3	50.9	51.9
1580.0	52.5	48.4	49.3	47.6	55.8	49.8	51.1	52.0
1590.0	52.4	48.5	49.2	47.7	55.8	50.2	51.2	52.2
1599.9	52.2	48.6	49.2	47.8	55.8	50.7	51.3	52.3
1610.2	52.1	48.7	49.1	48.0	55.8	51.0	51.5	52.4
1620.1	52.0	48.9	49.0	48.0	55.8	51.3	51.6	52.5
1630.0	51.9	48.9	48.8	48.1	55.7	51.6	51.7	52.5
1639.9	51.9	49.0	48.7	48.1	55.7	51.9	51.7	52.6

1649.9	51.8	49.1	48.5	48.1	55.5	52.1	51.8	52.7
1660.2	51.8	49.1	48.4	48.1	55.4	52.3	51.9	52.8
1670.1	51.7	49.2	48.2	48.1	55.2	52.6	52.0	52.9
1680.0	51.7	49.2	48.0	48.0	55.1	53.0	52.0	52.9
1689.9	51.7	49.3	47.8	47.9	55.0	53.3	52.1	53.0
1699.8	51.7	49.5	47.6	47.8	54.8	53.7	52.1	53.0
1710.1	51.6	49.6	47.4	47.6	54.7	53.9	52.1	53.1
1720.0	51.6	49.6	47.2	47.4	54.5	54.2	52.1	53.1
1730.0	51.6	49.8	47.1	47.3	54.4	54.5	52.0	53.2
1739.9	51.5	49.8	46.9	47.1	54.3	54.8	52.0	53.2
1750.2	51.5	49.9	46.8	46.9	54.2	55.2	52.0	53.3
1760.1	51.5	49.9	46.6	46.7	54.1	55.6	51.9	53.3
1770.0	51.4	49.9	46.5	46.5	53.9	55.9	51.9	53.3
1779.9	51.4	50.0	46.4	46.3	53.9	56.2	51.9	53.2
1789.9	51.4	50.0	46.4	46.1	53.9	56.4	51.9	53.2
1800.2	51.4	50.0	46.3	46.0	53.8	56.6	51.9	53.1
1810.1	51.3	50.0	46.2	45.7	53.8	56.7	51.9	53.0
1820.0	51.3	50.1	46.2	45.6	53.8	56.8	51.9	52.8
1829.9	51.3	50.1	46.1	45.4	53.9	56.9	51.9	52.7
1839.8	51.3	50.1	46.1	45.3	54.0	56.9	52.0	52.5
1850.1	51.3	50.0	46.0	45.1	54.1	56.8	52.0	52.3
1860.0	51.4	50.0	46.0	45.0	54.2	56.8	52.0	52.0
1870.0	51.4	50.0	46.0	45.0	54.4	56.8	52.1	51.8
1879.9	51.5	50.0	46.0	44.9	54.6	56.8	52.1	51.5
1890.2	51.5	50.0	46.0	44.9	54.7	56.9	52.2	51.3
1900.1	51.6	50.0	45.9	44.8	54.9	57.0	52.3	51.0
1910.0	51.7	49.9	45.9	44.8	55.0	57.1	52.4	50.7
1919.9	51.9	49.9	45.9	44.8	55.1	57.1	52.4	50.4
1929.9	52.0	49.8	45.9	44.7	55.3	57.1	52.5	50.1
1940.2	52.1	49.8	45.9	44.7	55.4	56.9	52.6	49.9
1950.1	52.2	49.7	46.0	44.6	55.5	56.8	52.7	49.5
1960.0	52.3	49.7	46.0	44.6	55.6	56.7	52.8	49.1
1969.9	52.5	49.7	46.0	44.6	55.7	56.5	52.9	48.7
1979.8	52.6	49.7	46.0	44.6	55.8	56.3	53.0	48.3
1990.1	52.7	49.7	46.0	44.7	55.8	56.1	53.0	47.8
2000.0	52.8	49.8	46.0	44.7	55.9	55.9	53.1	47.4

2010.0	52.9	49.8	46.0	44.7	55.9	55.8	53.2	46.9
2019.9	53.0	49.8	46.0	44.7	55.9	55.6	53.2	46.4
2030.2	53.1	49.8	46.0	44.8	55.9	55.4	53.3	46.0
2040.1	53.2	49.8	46.0	44.8	55.9	55.2	53.4	45.5
2050.0	53.3	49.7	46.0	44.9	55.9	55.1	53.5	45.0
2059.9	53.4	49.7	45.9	45.0	55.9	54.9	53.5	44.4
2069.9	53.5	49.7	45.9	45.0	55.8	54.9	53.6	43.9
2080.2	53.6	49.6	45.9	45.1	55.7	54.7	53.7	43.3
2090.1	53.6	49.5	45.8	45.2	55.6	54.7	53.8	42.7
2100.0	53.7	49.5	45.8	45.3	55.6	54.7	53.9	42.2
2109.9	53.8	49.4	45.7	45.4	55.5	54.7	54.0	41.6
2119.8	53.9	49.3	45.7	45.5	55.3	54.7	54.1	41.1
2130.1	54.0	49.3	45.6	45.6	55.3	54.9	54.3	40.6
2140.0	54.1	49.2	45.6	45.7	55.2	55.0	54.4	40.1
2150.0	54.2	49.2	45.5	45.8	55.1	55.1	54.5	39.7
2159.9	54.3	49.1	45.5	45.9	55.0	55.2	54.7	39.3
2170.2	54.4	49.1	45.4	46.0	54.9	55.3	54.9	38.8
2180.1	54.5	49.0	45.4	46.1	54.8	55.4	55.0	38.5
2190.0	54.6	49.0	45.4	46.2	54.7	55.7	55.1	38.2
2199.9	54.7	49.0	45.5	46.3	54.6	55.8	55.1	37.9
2209.9	54.8	48.9	45.5	46.4	54.6	56.0	55.2	37.6
2220.2	54.9	48.9	45.6	46.4	54.5	56.2	55.3	37.3
2230.1	54.9	48.9	45.7	46.5	54.5	56.4	55.3	37.1
2240.0	55.0	48.8	45.8	46.6	54.4	56.5	55.4	36.9
2249.9	55.1	48.8	45.9	46.7	54.4	56.6	55.4	36.7
2259.8	55.1	48.8	46.1	46.8	54.3	56.7	55.5	36.5
2270.1	55.2	48.7	46.2	46.9	54.3	56.7	55.5	36.3
2280.0	55.2	48.7	46.3	46.9	54.3	56.7	55.5	36.1
2290.0	55.3	48.7	46.4	47.0	54.3	56.7	55.5	35.8
2299.9	55.3	48.6	46.5	47.1	54.3	56.6	55.5	35.6
2310.2	55.4	48.6	46.6	47.2	54.3	56.6	55.6	35.4
2320.1	55.5	48.6	46.7	47.3	54.3	56.5	55.6	35.2
2330.0	55.6	48.6	46.8	47.3	54.3	56.5	55.6	35.0
2339.9	55.6	48.6	46.9	47.4	54.3	56.5	55.6	34.8
2349.9	55.7	48.6	47.0	47.5	54.3	56.4	55.6	34.6
2360.2	55.8	48.6	47.1	47.5	54.4	56.4	55.7	34.4

2370.1	55.9	48.7	47.1	47.6	54.5	56.3	55.7	34.3
2380.0	56.1	48.7	47.2	47.6	54.5	56.2	55.8	34.2
2389.9	56.2	48.8	47.3	47.7	54.6	56.1	55.8	34.1
2399.8	56.3	48.9	47.4	47.8	54.6	56.1	55.8	34.0
2410.1	56.4	48.9	47.5	47.8	54.6	56.0	55.8	34.0
2420.0	56.4	49.0	47.6	47.9	54.7	55.9	55.8	33.9
2430.0	56.5	49.1	47.7	47.9	54.7	55.8	55.8	33.9
2439.9	56.5	49.2	47.8	48.0	54.7	55.7	55.9	33.8
2450.2	56.5	49.3	47.9	48.0	54.7	55.7	55.9	33.8
2460.1	56.5	49.5	48.0	48.1	54.8	55.6	55.9	33.8
2470.0	56.5	49.6	48.1	48.1	54.8	55.6	55.9	33.8
2479.9	56.5	49.7	48.2	48.2	54.8	55.7	56.0	33.8
2489.9	56.5	49.9	48.3	48.2	54.8	55.6	56.0	33.8
2500.2	56.5	50.0	48.5	48.3	54.9	55.6	56.0	33.8
2510.1	56.5	50.2	48.6	48.3	54.8	55.5	56.1	33.8
2520.0	56.5	50.3	48.7	48.4	54.9	55.5	56.1	33.8
2529.9	56.5	50.5	48.8	48.4	55.0	55.5	56.2	33.9
2539.8	56.5	50.6	49.0	48.5	54.9	55.4	56.2	33.9
2550.1	56.5	50.7	49.1	48.5	54.9	55.5	56.2	34.0
2560.0	56.6	50.9	49.3	48.6	55.1	55.5	56.3	34.0
2570.0	56.7	51.0	49.4	48.6	55.1	55.6	56.3	34.0
2579.9	56.7	51.2	49.6	48.7	55.1	55.7	56.3	34.0
2590.2	56.8	51.4	49.7	48.7	55.2	55.9	56.4	34.0
2600.1	56.9	51.5	49.8	48.8	55.3	56.1	56.3	34.0
2610.0	56.9	51.7	50.0	48.9	55.4	56.3	56.3	34.1
2619.9	57.0	51.9	50.1	48.9	55.5	56.6	56.3	34.1
2629.9	57.1	52.1	50.2	49.0	55.6	56.9	56.3	34.2
2640.2	57.1	52.3	50.3	49.0	55.6	57.2	56.3	34.2
2650.1	57.1	52.5	50.4	49.1	55.8	57.5	56.3	34.3
2660.0	57.2	52.7	50.6	49.1	56.0	57.9	56.2	34.3
2669.9	57.3	52.9	50.7	49.1	56.0	58.4	56.3	34.4
2679.8	57.4	53.1	50.8	49.1	56.3	58.7	56.3	34.4
2690.1	57.5	53.3	50.9	49.1	56.3	59.2	56.3	34.4
2700.0	57.6	53.5	51.0	49.1	56.5	59.7	56.3	34.5
2710.0	57.7	53.7	51.1	49.1	56.8	60.2	56.3	34.5
2719.9	57.9	53.9	51.2	49.1	57.0	60.6	56.3	34.6

2730.2	58.0	54.1	51.3	49.1	57.1	61.2	56.3	34.6
2740.1	58.2	54.3	51.4	49.1	57.3	61.6	56.4	34.6
2750.0	58.3	54.5	51.5	49.1	57.5	62.1	56.4	34.7
2759.9	58.5	54.7	51.6	49.0	57.8	62.6	56.5	34.7
2769.9	58.7	54.8	51.7	49.0	58.1	63.0	56.6	34.7
2780.2	58.9	55.0	51.8	49.0	58.3	63.7	56.6	34.8
2790.1	59.1	55.2	51.9	49.0	58.6	64.0	56.7	34.8
2800.0	59.3	55.3	52.1	49.0	59.0	64.4	56.7	34.8
2809.9	59.5	55.4	52.2	49.0	59.2	64.8	56.7	34.8
2819.8	59.8	55.6	52.3	49.0	59.6	65.3	56.6	34.8
2830.1	60.0	55.7	52.4	49.1	60.0	66.0	56.5	34.8
2840.0	60.2	55.9	52.5	49.0	60.2	66.2	56.5	34.8
2850.0	60.5	56.0	52.6	49.0	60.4	66.6	56.4	34.9
2859.9	60.7	56.1	52.7	49.0	60.7	67.1	56.3	34.9
2870.2	61.0	56.2	52.7	49.0	61.0	67.8	56.1	34.9
2880.1	61.3	56.4	52.8	49.0	61.1	68.3	56.0	34.9
2890.0	61.5	56.4	52.9	49.0	61.4	68.7	55.8	34.9
2899.9	61.7	56.5	52.9	49.0	61.7	69.2	55.6	34.9
2909.9	62.0	56.6	53.0	49.0	61.8	69.7	55.4	34.9
2920.2	62.3	56.6	52.9	49.0	61.9	70.7	55.3	34.9
2930.1	62.5	56.7	52.9	49.0	62.2	71.1	55.1	34.9
2940.0	62.7	56.8	52.9	49.0	62.3	71.5	55.1	34.9
2949.9	63.0	56.9	52.9	49.0	62.5	72.0	55.0	34.8
2959.8	63.2	57.0	52.9	48.9	62.6	72.4	55.0	34.8
2970.1	63.5	57.0	52.8	48.9	62.9	73.3	55.0	34.8
2980.0	63.7	57.1	52.8	48.8	62.9	73.9	55.0	34.8
2990.0	64.0	57.1	52.7	48.8	63.2	74.3	55.0	34.8
2999.9	64.2	57.2	52.7	48.8	63.3	74.8	55.1	34.8

A(8) Data of seismic test result in kaolin with a Single Column (see Section 7.3.1)

Seismic test carried out using Oxford-clay after columns installation which sensor-pairs on clay test bed (sensor pair A-B and C-D).
Test ID: 01Apr10_04 (Test 154), 01Apr10_05 (Test 155), and 01Apr10_06 (Test 170)
Date of test: 10 to 31 August 2010
Test frequency range / interval: 190 to 1200 Hz / 10 Hz
Remarks: Sensor pairs located on top of kaolin and 10 cm diameter of column

01Apr10_04			01Apr10_05			01Apr10_06		
Frequency	A-B	C-D	Frequency	A-B	C-D	Frequency	A-B	C-D
799.9	75.0	53.5	400.2	116.3	39.0	500.1	115.7	71.2
849.9	118.7	50.1	450.1	367.6	91.9	550.1	106.1	60.5
899.9	82.7	45.7	500.1	71.0	89.6	600.1	76.1	72.3
949.9	93.9	64.4	550.1	112.7	61.5	650.0	80.6	23.4
999.8	106.5	56.0	600.1	64.4	75.5	700.0	502.7	70.6
1050.2	93.1	58.5	650.0	116.2	24.7	750.0	159.5	83.6
1100.2	114.3	59.9	700.0	222.4	66.5	799.9	123.3	96.8
1150.1	117.5	57.2	750.0	156.5	79.2	849.9	84.8	56.5
1200.1	103.1	59.3	799.9	92.0	80.3	899.9	84.5	55.7
1250.1	108.2	55.5	849.9	79.7	52.9	949.9	119.4	55.9
1300.0	102.9	53.7	899.9	102.7	59.6	999.8	118.1	55.6
1350.0	108.9	54.4	949.9	111.0	55.4	1050.2	137.9	56.8
1400.0	106.7	55.8	999.8	122.7	56.1	1100.2	119.3	66.4
			1050.2	134.5	55.3	1150.1	133.8	69.9
			1100.2	107.1	65.9	1200.1	165.3	69.3
			1150.1	154.2	69.0	1250.1	132.6	62.8
			1200.1	138.7	64.4	1300.0	125.3	58.8
			1250.1	115.1	59.8	1350.0	145.3	56.2
			1300.0	143.4	55.1	1400.0	133.3	61.8
			1350.0	223.9	56.0			
			1400.0	219.0	59.4			

A(9) Data of seismic test result in Oxford clay with stone column configuration (see Section 7.3.1)

A(9a) Data of seismic test result in Oxford clay with column configuration which sensor-pairs located on clay for test ID: 10Aug10_02 (Test 154), 11Aug10_01 (Test 155), 11Aug10_02 (Test 156), 31Aug10_01 (Test 169) and 31Aug10_02 (Test 170) (see Section 7.3.2.1).

Seismic test carried out using Oxford-clay after columns installation which sensor-pairs on clay test bed (sensor pair A-B and C-D).
Date of test: 10 to 31 August 2010
Test frequency range / interval: 190 to 1200 Hz / 10 Hz
Remarks: Both sensor pairs located on top of clay

Frequency, Hz	Test 154, m/s		Test 155, m/s		Test 156, m/s		Test 169, m/s		Test 170, m/s	
	A-B	C-D	A-B	C-D	A-B	C-D	A-B	C-D	A-B	C-D
190.0	45.3	35.0	43.0	54.3	42.8	54.7	47.8	35.1	47.2	34.4
199.9	45.3	42.0	50.4	29.5	49.3	29.9	38.7	49.7	38.0	45.6
210.2	36.7	54.3	48.3	56.5	47.6	56.0	53.8	57.5	55.9	68.1
220.1	40.3	50.8	39.1	56.6	39.2	56.6	61.6	49.6	62.0	49.9

230.0	49.9	47.0	43.0	50.5	43.6	50.5	56.9	46.6	57.2	43.3
239.9	50.4	45.6	55.9	48.3	55.0	48.9	56.4	51.8	57.5	48.7
249.9	44.9	52.4	51.4	47.4	50.2	47.6	58.7	50.4	61.2	60.5
260.2	52.1	56.5	48.9	57.1	48.0	57.6	54.3	53.7	55.5	64.5
270.1	54.3	58.0	59.8	61.0	58.0	61.0	53.5	51.8	54.0	56.2
280.0	55.2	57.9	61.9	63.6	59.6	63.2	60.2	58.6	61.5	63.5
289.9	53.6	56.5	65.6	61.2	62.7	61.6	66.4	63.6	69.3	70.9
299.8	50.1	58.4	63.0	61.6	59.9	61.8	64.8	74.2	66.8	85.8
310.1	49.2	57.6	60.3	64.6	57.2	64.4	60.1	81.6	61.5	93.6
320.1	48.9	55.9	57.2	62.1	53.9	61.8	65.8	75.1	67.8	87.8
330.0	49.6	56.7	54.7	59.0	51.2	58.8	69.0	68.9	72.3	79.7
339.9	50.2	59.8	56.4	58.5	52.4	58.4	69.1	68.1	73.6	75.5
350.2	49.8	59.2	60.6	64.4	55.4	64.4	76.1	68.7	82.1	73.1
360.1	46.3	55.9	63.4	66.1	56.7	65.8	84.5	68.2	93.8	69.8
370.0	45.1	53.9	59.1	63.7	52.4	63.0	88.0	68.2	104.1	72.6
379.9	44.8	53.2	55.8	63.4	49.4	62.6	87.8	69.4	101.4	76.8
389.9	43.6	51.6	55.0	64.8	48.5	63.8	87.7	74.0	99.9	87.5
400.2	41.6	49.1	54.1	63.4	47.6	61.7	87.8	78.1	99.9	85.6
410.1	40.3	48.1	52.0	58.6	45.7	56.5	86.5	77.6	101.1	77.3
420.0	40.5	49.6	48.3	53.3	42.8	51.5	87.5	74.5	94.2	61.4
429.9	41.2	52.0	46.0	52.7	41.4	51.3	90.3	72.6	93.0	57.0
439.8	41.9	53.3	45.8	55.6	41.6	54.0	90.3	72.6	93.7	58.8
450.1	42.1	53.4	46.4	57.6	42.5	55.7	88.1	72.5	93.3	62.1
460.1	42.3	52.9	46.9	57.9	43.2	55.8	86.2	73.4	92.6	64.2
470.0	42.5	53.3	47.3	58.0	46.4	57.1	85.1	76.2	91.7	65.5
479.9	42.6	53.5	47.5	58.7	46.6	57.8	83.0	77.8	89.6	66.2
490.2	42.5	53.0	47.7	59.4	46.8	58.5	80.0	76.5	86.7	66.9
500.1	42.3	52.6	47.7	58.9	46.9	58.1	76.7	74.0	83.4	66.9
510.0	42.3	52.6	47.3	57.7	46.8	57.1	73.3	72.4	79.9	67.0
519.9	42.5	52.8	47.3	56.5	46.9	56.0	69.9	72.1	76.2	67.5
529.9	42.5	52.5	47.7	56.0	47.3	55.3	66.7	72.0	72.8	68.5
540.2	42.5	52.0	48.0	56.1	47.4	55.4	64.3	70.6	70.0	69.0
550.1	42.1	51.7	48.1	56.4	47.3	55.7	62.5	67.9	67.7	68.5
560.0	41.6	51.7	48.1	56.2	47.2	55.6	61.6	64.8	66.0	67.8
569.9	41.1	51.8	48.1	55.8	47.2	55.3	60.8	62.4	65.1	67.8
579.8	40.7	51.8	47.9	55.7	47.0	55.1	60.3	60.2	64.8	68.2

590.1	40.4	51.7	47.4	55.7	46.7	54.9	60.8	58.5	65.1	67.9
600.1	40.3	51.6	46.7	55.7	46.2	54.8	61.7	58.0	65.6	66.9
610.0	40.3	51.5	46.1	56.0	45.8	54.9	62.5	57.9	66.2	65.9
619.9	40.2	50.9	45.8	56.4	45.5	55.3	63.1	57.9	66.6	65.1
630.2	40.2	50.2	45.7	57.1	45.4	55.9	63.5	57.8	67.0	64.6
640.1	40.3	49.5	45.5	57.9	45.4	56.5	63.6	57.5	67.5	64.3
650.0	40.6	48.8	45.3	58.2	45.5	57.1	63.6	57.3	67.8	64.0
659.9	41.2	48.4	45.0	58.1	45.3	57.4	63.1	57.3	67.7	63.8
669.9	42.0	47.3	44.7	58.0	45.1	57.2	62.8	57.4	67.0	63.3
680.2	42.4	46.9	44.6	57.5	45.0	56.7	62.1	57.7	66.2	63.2
690.1	42.7	46.8	44.6	56.9	45.0	56.1	61.2	58.1	65.3	62.9
700.0	43.1	46.9	44.6	56.3	45.0	55.7	60.4	58.6	64.3	62.7
709.9	43.6	47.0	44.5	55.3	44.9	54.9	59.5	59.0	63.2	62.5
719.8	43.9	46.9	44.4	54.4	44.8	54.2	58.4	59.3	62.0	62.4
730.1	44.1	46.8	44.3	53.7	44.7	53.6	57.4	59.5	61.0	62.4
740.1	44.2	46.9	44.3	53.0	44.9	53.0	56.6	59.6	60.3	62.5
750.0	44.2	47.0	44.5	52.2	45.0	52.2	56.1	59.4	59.8	62.7
759.9	44.2	47.3	44.8	51.4	44.9	51.4	55.8	59.0	59.6	62.8
770.2	44.2	47.6	45.2	50.8	45.0	50.8	55.7	59.0	59.5	63.0
780.1	44.2	47.9	45.7	50.2	45.1	50.1	55.6	59.1	59.3	63.2
790.0	44.3	47.8	46.0	49.6	45.3	49.6	55.5	59.1	59.2	63.4
799.9	44.5	47.6	45.9	49.1	45.5	49.1	55.4	59.2	59.0	63.8
809.9	44.7	47.2	45.9	48.7	45.8	48.6	55.4	59.1	58.9	64.3
820.2	44.9	46.7	46.3	48.3	46.1	48.3	55.4	58.8	58.9	65.1
830.1	45.1	46.1	46.8	48.0	46.4	47.9	55.5	58.5	59.1	66.0
840.0	45.3	45.4	47.3	47.8	46.8	47.5	55.7	58.0	59.3	67.1
849.9	45.5	44.8	47.9	47.8	47.2	47.2	56.0	57.6	59.6	68.7
859.8	45.8	44.3	48.6	47.9	47.7	46.9	56.3	57.2	60.2	69.9
870.1	46.1	44.0	49.4	48.2	48.3	46.8	56.6	57.0	60.7	71.0
880.1	46.4	43.7	50.1	48.6	48.8	46.8	56.9	57.0	61.0	71.9
890.0	46.6	43.5	50.6	49.2	49.4	47.0	57.2	57.2	61.4	72.6
899.9	46.8	43.4	51.0	49.7	50.0	47.4	57.5	57.5	61.8	73.0
910.2	47.0	43.4	51.3	50.1	50.6	48.0	57.8	58.1	62.1	73.3
920.1	47.2	43.5	51.6	50.4	51.0	48.7	58.0	58.6	62.2	73.4
930.0	47.4	43.7	51.8	50.7	51.3	49.5	58.0	59.3	62.3	73.3
939.9	47.6	43.9	52.1	50.9	51.7	50.3	58.0	60.0	62.1	73.1

949.9	47.7	44.1	52.4	50.9	52.1	51.0	58.0	60.5	62.0	72.9
960.2	47.8	44.5	52.7	50.9	52.5	51.7	57.9	60.8	61.8	72.8
970.1	47.8	44.8	52.9	50.7	52.8	52.0	57.7	60.9	61.6	72.8
980.0	47.8	45.1	53.1	50.4	53.1	52.1	57.6	60.9	61.4	72.8
989.9	47.7	45.4	53.2	50.0	53.3	52.1	57.5	60.8	61.2	72.9
999.8	47.6	45.7	53.3	49.6	53.5	51.9	57.4	60.6	61.1	73.0
1010.1	47.3	45.8	53.2	49.2	53.7	51.6	57.4	60.5	61.1	73.1
1020.1	47.0	45.9	53.0	48.9	53.8	51.3	57.6	60.4	61.1	73.1
1030.0	46.6	46.0	52.8	48.7	53.7	51.0	57.8	60.3	61.2	72.9
1039.9	46.3	46.1	52.6	48.6	53.6	50.6	57.9	60.3	61.2	72.6
1050.2	45.9	46.2	52.4	48.6	53.3	50.2	58.2	60.4	61.2	72.5
1060.1	45.6	46.4	52.1	48.5	53.0	49.9	58.5	60.4	61.3	72.5
1070.0	45.2	46.6	51.8	48.5	52.7	49.8	58.8	60.5	61.6	72.3
1079.9	44.8	46.8	51.5	48.7	52.3	49.7	59.1	60.6	61.8	72.1
1089.9	44.5	47.0	51.1	49.0	52.0	49.7	59.6	60.7	62.1	71.9
1100.2	44.2	47.2	50.8	49.3	51.7	49.7	60.3	60.8	62.4	71.6
1110.1	43.9	47.4	50.4	49.5	51.4	49.8	61.0	60.9	62.7	71.3
1120.0	43.8	47.5	50.0	49.7	51.1	49.9	61.9	61.0	63.1	70.9
1129.9	43.8	47.5	49.7	50.0	50.8	49.9	63.0	60.8	63.5	70.5
1139.8	43.8	47.5	49.5	50.3	50.5	49.9	64.0	60.4	64.0	70.0
1150.1	43.9	47.5	49.4	50.4	50.3	49.9	64.9	60.3	64.4	69.7
1160.0	44.0	47.5	49.3	50.5	50.1	50.0	65.8	60.1	64.8	69.4
1170.0	44.2	47.4	49.3	50.5	49.9	50.1	67.1	59.8	65.2	69.2
1179.9	44.3	47.4	49.4	50.5	49.8	50.1	68.1	59.7	65.6	69.0
1190.2	44.5	47.3	49.6	50.6	49.7	50.2	68.9	59.6	66.0	68.9
1200.1	44.6	47.4	49.7	50.7	49.6	50.2	69.5	59.4	66.3	68.7

A(9b) Data of seismic test result in Oxford clay with column configuration which sensor-pairs located on clay for test ID: 31Aug10_03 (Test 171), 31Aug10_04 (Test 172), 31Aug10_05 (Test 173), 01Sep10_01 (Test 174) and 01Sep10_02 (Test 175) (see Section 7.3.2.1).

Seismic test carried out using Oxford-clay after columns installation which sensor-pairs on clay test bed (sensor pair A-B and C-D).
Date of test: 31 August to 1 September 2010
Test frequency range / interval: 190 to 1200 Hz / 10 Hz
Remarks: Both sensor pairs located on top of clay

Frequency, Hz	Test 171, m/s		Test 172, m/s		Test 173, m/s		Test 174, m/s		Test 175, m/s	
	A-B	C-D	A-B	C-D	A-B	C-D	A-B	C-D	A-B	C-D
190.0	46.3	31.5	47.9	106.7	59.8	91.7	55.9	45.8	51.9	48.5
199.9	41.2	40.1	52.1	73.8	61.1	68.0	60.5	54.3	60.7	48.9
210.2	53.7	61.6	54.0	42.5	50.3	40.7	51.3	52.0	61.9	47.4
220.1	56.8	44.7	54.8	29.1	51.5	38.6	53.1	55.1	63.9	67.7
230.0	48.7	34.4	52.9	79.6	51.8	74.3	50.9	51.3	53.9	56.9
239.9	49.8	36.1	62.2	86.5	60.4	76.1	60.1	55.7	57.9	53.1
249.9	50.3	60.2	62.1	69.9	55.2	66.9	56.5	59.2	68.5	54.2
260.2	48.1	67.7	49.4	68.6	46.9	71.2	47.0	50.0	70.6	53.4
270.1	45.2	55.8	43.4	83.1	49.7	81.0	47.4	38.6	70.4	57.2
280.0	54.7	48.5	57.5	80.6	58.8	77.4	57.0	48.9	80.3	67.6
289.9	61.9	44.4	74.2	74.1	65.7	72.3	66.1	69.8	79.6	71.6
299.8	63.9	45.2	75.3	63.7	66.1	63.2	67.9	75.4	69.6	69.4
310.1	64.5	53.5	69.0	60.4	65.8	60.9	66.3	67.8	67.5	64.4
320.1	69.2	60.4	66.3	60.4	69.4	61.8	69.2	62.9	74.4	66.7
330.0	68.6	66.1	68.2	60.2	69.5	62.8	70.1	64.7	82.4	71.0
339.9	63.5	67.7	70.6	62.6	66.9	64.2	68.4	67.3	79.5	67.7
350.2	63.7	66.9	69.5	63.8	63.8	64.6	66.6	66.3	74.3	61.5
360.1	65.0	67.6	63.3	64.2	61.6	64.7	64.2	60.2	72.5	56.3
370.0	65.3	68.6	57.3	64.6	61.0	64.4	61.9	53.9	69.0	54.3
379.9	70.1	66.5	57.2	62.1	63.8	61.8	63.3	53.8	65.6	53.8
389.9	75.5	64.6	61.8	59.6	68.3	59.0	68.2	58.0	62.5	51.0
400.2	75.2	64.5	65.3	58.8	68.4	59.3	71.0	61.5	57.9	47.4
410.1	73.6	66.6	64.9	59.0	64.6	61.1	69.9	61.1	54.4	45.9
420.0	75.0	68.1	62.3	60.2	60.3	62.6	68.1	59.7	54.0	48.9
429.9	76.4	67.8	60.9	63.0	58.1	65.1	64.3	60.6	54.9	54.6
439.8	75.6	67.7	61.7	65.8	56.0	67.2	62.1	60.7	55.1	58.0
450.1	75.0	67.8	62.8	67.8	53.7	69.4	60.7	61.5	54.5	57.7
460.1	74.8	67.6	63.0	69.6	51.3	71.4	58.5	61.5	53.7	56.5
470.0	73.9	67.2	62.6	70.6	49.5	72.2	56.3	61.2	53.4	56.8
479.9	71.8	66.6	62.0	71.1	49.0	72.3	55.0	60.5	52.6	57.8
490.2	69.1	65.9	62.1	71.2	49.2	72.3	54.2	60.0	50.9	59.4
500.1	66.9	65.4	62.5	70.8	49.8	72.5	53.9	59.4	49.3	60.8
510.0	65.8	64.9	61.8	70.5	49.8	72.9	53.4	58.2	48.5	61.4

519.9	65.2	64.4	60.9	70.4	49.2	73.0	52.4	57.2	48.4	61.5
529.9	63.9	64.5	60.7	70.0	48.6	72.5	51.1	56.9	48.9	61.7
540.2	61.7	64.4	60.6	69.4	48.4	72.2	50.0	56.8	49.4	62.2
550.1	59.9	63.0	59.9	69.3	48.2	73.0	49.3	56.0	49.7	63.2
560.0	58.7	61.6	58.8	69.9	47.9	74.2	48.8	54.8	50.2	64.5
569.9	58.0	60.5	57.8	70.0	47.6	74.8	48.5	54.0	50.6	65.0
579.8	57.3	59.9	56.9	69.2	47.3	75.2	48.2	53.6	50.9	64.7
590.1	56.8	59.6	56.2	68.5	47.3	76.1	48.3	53.2	51.1	64.4
600.1	56.4	59.2	55.9	69.7	47.5	77.2	48.8	52.6	51.1	64.4
610.0	55.9	58.8	55.5	70.8	47.8	77.4	49.4	52.0	51.1	64.3
619.9	55.4	58.5	54.9	70.6	48.1	76.5	50.2	51.6	51.0	63.6
630.2	54.8	58.3	54.4	69.3	48.4	74.9	50.8	51.3	50.6	62.6
640.1	54.4	58.4	53.9	67.8	48.6	73.6	51.1	50.8	50.0	62.0
650.0	54.2	58.6	53.3	66.6	48.8	72.7	51.2	50.2	49.2	62.8
659.9	54.1	58.9	52.8	66.0	49.0	72.0	51.3	49.6	48.1	63.9
669.9	54.1	59.2	52.3	65.6	49.2	71.3	51.3	49.0	47.1	64.3
680.2	54.2	59.3	51.8	65.2	49.3	70.4	51.3	48.6	46.5	63.6
690.1	54.3	59.2	51.6	64.6	49.3	69.2	51.2	48.2	46.1	62.6
700.0	54.4	59.2	51.7	63.7	49.2	67.8	51.1	47.9	46.0	61.6
709.9	54.5	59.3	52.0	62.5	49.1	66.5	51.0	47.7	46.1	61.0
719.8	54.5	59.6	52.8	61.3	49.2	65.3	50.9	47.5	46.3	60.5
730.1	54.6	59.5	53.6	62.9	49.4	64.3	50.9	47.4	46.7	60.0
740.1	54.7	59.2	53.7	64.0	49.7	63.5	50.9	47.4	47.1	59.7
750.0	55.1	58.8	53.6	63.1	50.0	62.6	51.0	47.4	47.7	59.4
759.9	55.4	58.3	53.4	61.7	50.4	62.0	51.2	47.3	48.7	59.2
770.2	55.6	57.8	53.0	60.3	50.7	61.8	51.5	47.1	49.9	59.2
780.1	55.7	57.4	52.6	59.5	50.9	62.0	51.8	46.9	51.3	59.3
790.0	55.7	57.0	52.1	58.9	51.1	62.3	52.1	46.7	52.8	59.4
799.9	55.6	56.7	51.6	58.5	51.2	62.8	52.3	46.6	54.4	59.1
809.9	55.3	56.3	51.0	58.1	51.3	63.3	52.5	46.4	56.2	58.4
820.2	54.8	55.9	50.7	57.5	51.5	63.9	52.6	46.3	58.0	57.3
830.1	54.5	55.6	50.6	57.0	51.9	64.4	52.9	46.1	59.4	56.2
840.0	54.6	55.4	50.3	56.7	52.3	64.8	53.2	45.8	60.4	55.3
849.9	54.7	55.2	50.2	56.7	52.8	65.0	53.6	45.6	60.9	54.5
859.8	54.7	54.9	50.1	56.8	53.3	65.0	54.0	45.3	61.3	53.8
870.1	54.6	54.5	50.0	57.0	53.9	64.8	54.2	45.2	61.6	53.4

880.1	54.6	54.1	50.0	57.3	54.4	64.5	54.3	45.0	61.8	53.1
890.0	54.6	53.8	50.1	57.6	54.9	64.2	54.4	44.9	62.0	52.8
899.9	54.8	53.8	50.2	58.0	55.4	63.9	54.5	44.8	62.0	52.4
910.2	55.0	53.9	50.4	58.2	55.8	63.5	54.7	44.7	61.7	52.0
920.1	55.3	54.0	50.7	58.4	56.2	63.1	54.8	44.6	61.2	51.7
930.0	55.7	54.2	50.9	58.8	56.5	62.8	55.1	44.6	60.7	51.5
939.9	56.1	54.2	51.2	59.1	56.9	62.6	55.4	44.6	60.2	51.2
949.9	56.5	54.2	51.2	59.7	57.2	62.6	55.8	44.6	59.8	50.9
960.2	56.9	54.2	51.3	60.2	57.4	62.7	56.3	44.7	59.2	50.8
970.1	57.3	54.2	51.4	60.8	57.7	62.9	56.8	44.7	58.6	50.8
980.0	57.8	54.2	51.5	61.4	57.9	63.1	57.2	44.7	58.0	50.8
989.9	58.2	54.2	51.5	61.9	58.2	63.4	57.7	44.7	57.5	50.8
999.8	58.7	54.2	51.6	62.6	58.7	63.7	58.2	44.6	57.0	50.9
1010.1	59.2	54.3	51.7	63.1	59.3	64.0	58.7	44.6	56.6	51.2
1020.1	59.8	54.4	51.7	63.8	60.0	64.3	59.3	44.5	56.4	51.5
1030.0	60.4	54.5	51.9	64.3	60.9	64.9	60.2	44.6	56.2	51.8
1039.9	61.0	54.6	52.0	64.9	61.3	65.4	61.1	44.8	56.1	52.1
1050.2	61.7	54.7	52.1	65.5	61.6	65.6	61.6	45.2	56.1	52.4
1060.1	62.3	54.8	52.2	66.0	61.8	65.7	61.0	45.1	56.1	52.8
1070.0	63.0	54.9	52.3	66.6	62.2	65.6	60.7	44.8	56.2	53.2
1079.9	63.8	55.1	52.4	67.2	62.6	65.5	61.1	44.6	56.3	53.6
1089.9	64.5	55.3	52.4	67.9	63.2	65.4	61.7	44.6	56.4	54.1
1100.2	65.3	55.5	52.4	68.4	63.9	65.3	62.5	44.6	56.5	54.7
1110.1	66.0	55.7	52.5	68.9	64.6	65.2	63.4	44.5	56.6	55.3
1120.0	66.7	55.8	52.4	69.4	65.4	65.0	64.4	44.4	56.7	55.8
1129.9	67.2	55.9	52.4	69.8	66.2	64.8	65.4	44.3	56.8	56.3
1139.8	67.8	56.0	52.6	70.1	66.9	64.6	66.5	44.1	56.9	56.6
1150.1	68.2	56.1	52.8	70.6	67.5	64.5	67.6	43.9	57.2	56.7
1160.0	68.5	56.3	52.8	71.1	68.0	64.4	68.6	43.8	57.5	57.0
1170.0	68.7	56.6	52.8	71.7	68.5	64.3	69.5	43.6	57.8	57.3
1179.9	69.0	56.8	52.8	72.2	68.9	64.2	70.2	43.4	57.8	57.6
1190.2	69.3	57.0	52.7	72.5	69.2	64.1	70.9	43.3	57.9	57.7
1200.1	69.7	57.1	52.6	72.8	69.5	64.1	71.5	43.2	58.0	57.7

A(10) Data of seismic test result in Oxford clay with column configuration which sensor-pairs located on column for test ID: 13Aug10_02 (Test 159), 16Aug10_01 (Test 160), 16Aug10_02 (Test 161), 17Aug10_01 (Test 162) and 18Aug10_02 (Test 164) (see Section 7.3.2.2).

Seismic test carried out using Oxford-clay after columns installation which sensor-pairs on a compacted 4.1 diameter columns (sensor pair A-B and C-D).
Date of test: 13 to 17 August November 2010
Test frequency range / interval: 200 to 2500 Hz / 10 Hz
Remarks: Both sensor pairs located on top of column

Frequency, Hz	Test 159, m/s		test 160, m/s		test 161, m/s		test 162, m/s		test 164, m/s	
	A-B	B-C	A-B	B-C	A-B	B-C	A-B	B-C	A-B	B-C
199.9	64.5	49.0	70.2	78.2	71.7	75.3	66.3	78.2	52.8	73.4
210.2	62.2	52.9	64.1	49.9	67.9	51.9	63.8	54.9	48.2	48.5
220.1	59.5	66.6	62.5	56.4	66.1	57.3	62.3	60.8	53.4	53.6
230.0	69.8	75.2	67.1	76.7	71.4	77.1	66.7	82.4	53.2	74.3
239.9	75.7	63.3	86.5	75.4	90.4	78.2	86.1	83.0	60.5	74.4
249.9	63.1	53.0	83.0	62.4	85.2	65.2	84.2	68.8	63.8	61.4
260.2	56.2	55.4	69.6	57.0	73.1	57.3	71.7	61.2	57.4	57.1
270.1	57.8	61.8	63.1	66.4	66.3	68.4	64.4	72.1	53.7	67.3
280.0	65.1	60.4	66.6	69.9	68.8	74.3	65.4	77.5	57.8	76.1
289.9	67.2	52.5	71.2	63.0	72.8	66.8	69.8	69.4	65.1	69.8
299.8	67.9	52.4	73.0	53.9	75.1	55.7	71.7	58.0	65.4	59.0
310.1	61.3	60.5	70.8	57.4	72.5	58.2	69.4	60.9	62.9	61.5
320.1	58.2	59.6	63.6	63.7	64.3	65.4	61.1	69.8	54.7	68.6
330.0	61.9	56.5	66.3	63.0	67.2	65.6	63.1	71.0	51.1	67.3
339.9	61.4	56.9	74.3	59.9	74.9	62.3	72.4	67.8	56.2	61.3
350.2	57.2	60.5	73.9	61.6	74.1	63.3	73.6	67.8	64.4	60.9
360.1	54.2	61.7	67.2	64.7	67.3	66.2	68.2	70.6	60.4	65.8
370.0	53.5	59.5	61.7	66.1	62.3	68.6	62.8	73.0	59.0	70.5
379.9	54.9	57.7	60.7	64.2	61.8	67.2	61.1	71.4	62.5	71.5
389.9	56.1	59.1	62.0	62.4	62.7	65.2	61.7	68.9	68.3	69.8
400.2	56.1	60.9	62.0	64.8	62.4	68.1	60.7	71.6	69.9	69.6
410.1	55.6	60.7	62.5	68.0	63.3	72.3	60.6	76.5	68.7	70.4
420.0	54.7	59.8	64.6	68.2	66.5	72.6	63.4	77.4	68.9	70.8
429.9	53.9	60.3	65.1	66.4	67.4	70.3	65.1	75.5	69.4	70.8
439.8	54.5	62.5	62.9	65.5	65.0	68.8	62.7	74.0	67.8	71.0
450.1	55.8	64.9	62.3	66.7	64.0	69.7	61.2	74.4	65.8	72.4
460.1	56.3	66.0	63.5	69.4	64.6	72.4	62.0	76.7	66.3	75.9
470.0	55.8	66.0	64.1	71.9	65.2	75.0	62.7	79.4	67.3	79.5
479.9	55.2	66.4	64.1	73.0	65.4	76.0	62.9	80.9	67.7	81.2
490.2	54.8	67.3	64.4	73.6	65.0	76.9	63.2	81.4	67.6	81.9
500.1	54.7	67.7	64.4	74.7	64.0	78.4	63.5	82.3	66.9	82.9
510.0	54.9	66.7	63.5	75.7	62.2	80.1	62.8	83.7	65.8	84.1
519.9	55.7	65.2	62.2	75.6	60.1	80.8	61.1	84.0	64.3	83.9
529.9	57.6	63.7	61.5	74.8	58.8	80.2	59.8	83.1	62.9	82.7
540.2	60.2	62.6	61.8	73.4	58.6	78.9	59.6	81.5	62.5	80.3

550.1	61.3	62.3	63.0	72.0	59.7	77.4	60.4	79.7	62.4	78.4
560.0	61.2	62.1	65.1	71.3	62.0	76.5	61.9	78.4	63.1	77.9
569.9	61.4	61.7	67.9	71.3	64.9	76.3	64.0	77.6	64.7	78.4
579.8	61.1	61.7	70.6	71.2	66.5	76.0	66.2	76.7	66.4	78.8
590.1	60.7	62.0	71.6	70.7	66.1	75.4	68.1	75.8	66.9	78.8
600.1	60.2	62.4	70.5	69.9	65.5	74.9	67.8	74.8	68.3	78.2
610.0	60.1	62.7	69.1	69.1	64.7	74.5	67.0	74.2	70.6	77.2
619.9	60.5	62.7	67.9	68.5	63.8	73.9	66.3	73.4	71.1	76.6
630.2	60.9	62.4	67.2	67.8	63.4	73.1	65.8	72.3	71.1	76.6
640.1	60.8	62.0	67.0	67.2	63.5	72.0	65.5	71.2	70.9	76.8
650.0	59.9	61.4	67.3	66.8	64.1	70.7	65.5	70.1	70.8	76.7
659.9	58.9	60.7	67.6	66.5	64.7	69.8	65.8	69.4	71.5	76.7
669.9	58.2	60.3	67.5	66.3	64.8	69.6	66.2	68.7	72.4	76.6
680.2	57.9	60.1	67.3	65.9	65.0	69.5	66.4	68.8	73.0	76.5
690.1	58.1	60.0	66.8	65.6	65.3	69.4	66.5	69.4	73.1	76.2
700.0	58.9	59.6	66.8	65.5	65.5	69.4	66.8	70.1	73.2	76.0
709.9	60.2	59.3	67.0	65.5	65.7	69.4	67.3	70.8	73.3	75.9
719.8	61.4	59.8	67.4	65.6	66.2	69.5	67.6	71.7	73.2	75.9
730.1	61.5	60.5	67.6	66.1	67.0	69.7	67.9	72.8	72.6	75.7
740.1	61.7	61.3	68.1	66.5	67.9	70.0	68.7	73.4	71.9	74.0
750.0	62.0	62.0	68.5	66.5	69.1	70.3	69.8	74.0	72.8	74.5
759.9	62.2	62.6	69.0	66.3	70.3	70.2	71.0	74.4	73.3	76.5
770.2	62.7	63.1	70.1	66.2	70.8	70.5	72.2	74.4	73.0	78.6
780.1	63.1	63.4	71.2	66.4	70.9	70.9	73.6	74.3	72.1	80.4
790.0	63.4	63.9	71.4	66.8	70.6	71.1	74.0	74.0	70.7	81.5
799.9	63.8	64.5	71.1	67.3	70.3	71.3	73.9	74.0	70.3	81.6
809.9	64.1	64.8	70.8	67.9	70.0	71.7	73.7	74.6	70.1	81.6
820.2	64.2	64.9	70.6	68.5	69.9	72.8	73.6	75.7	69.9	82.0
830.1	64.6	64.7	70.6	69.0	69.8	74.4	73.6	77.2	69.7	82.3
840.0	64.8	64.5	70.8	69.5	69.7	76.6	73.6	78.6	69.7	82.9
849.9	64.6	64.5	71.5	69.8	69.7	79.2	73.6	79.8	69.7	83.8
859.8	64.4	64.3	72.7	69.9	69.8	82.4	73.3	80.4	69.7	84.3
870.1	64.4	64.3	74.5	70.0	70.0	85.9	73.0	81.5	69.8	84.3
880.1	64.3	64.3	76.4	70.1	70.7	89.0	72.9	83.1	69.8	83.9
890.0	64.4	64.5	78.1	70.2	71.4	91.4	73.1	85.1	69.8	83.4
899.9	64.5	65.3	79.4	70.3	72.3	92.6	73.4	87.2	69.9	83.0
910.2	64.5	66.1	80.1	70.6	73.3	93.2	73.9	89.7	69.7	82.7
920.1	64.5	66.7	80.1	70.8	74.3	93.8	74.7	92.1	69.3	82.2
930.0	64.3	67.2	79.9	71.2	75.3	93.9	75.8	94.6	69.4	81.6
939.9	64.3	67.6	79.8	71.5	76.0	93.6	76.7	97.0	69.8	81.3
949.9	64.4	68.2	79.5	71.9	76.4	92.9	77.3	99.0	70.6	81.1
960.2	64.7	69.0	78.6	72.1	76.5	91.6	77.6	99.7	71.4	81.2
970.1	65.0	69.9	78.0	72.2	76.5	90.3	78.1	99.8	72.1	81.7
980.0	65.4	70.8	77.5	72.4	76.3	89.1	78.3	99.7	72.7	82.1
989.9	65.8	71.9	77.0	72.6	76.0	88.1	78.4	99.3	73.0	82.4
999.8	66.3	73.0	76.6	72.9	75.8	87.5	78.2	98.9	73.0	82.6
1010.1	66.9	74.4	76.4	73.4	75.6	87.1	78.2	98.0	72.9	82.7
1020.1	67.4	75.6	76.2	73.7	75.7	86.8	78.1	97.5	72.6	82.6
1030.0	68.0	76.7	76.1	74.1	75.9	86.7	78.1	97.3	72.4	82.4
1039.9	68.4	77.8	76.4	74.6	76.2	86.7	78.2	97.3	72.4	82.5
1050.2	68.8	78.7	76.8	75.3	76.8	86.8	78.3	97.1	72.5	82.9

1060.1	69.0	79.4	77.2	75.9	77.4	87.1	78.5	96.8	72.7	83.3
1070.0	69.1	79.8	77.8	77.0	78.0	87.5	78.7	96.3	73.3	83.9
1079.9	69.3	80.2	78.4	78.2	78.7	87.9	79.0	95.6	73.9	84.6
1089.9	69.4	80.4	78.8	79.5	79.1	88.0	79.2	95.1	74.5	85.3
1100.2	69.6	80.7	79.3	81.2	79.4	88.4	79.6	94.8	75.2	86.3
1110.1	69.6	80.8	79.6	82.6	79.7	88.6	80.1	94.3	75.8	87.2
1120.0	69.8	80.9	79.9	83.8	79.8	88.8	80.6	94.0	76.5	88.2
1129.9	69.9	81.0	80.0	84.8	79.9	89.0	81.0	93.8	77.1	89.2
1139.8	70.0	81.0	80.1	85.5	80.0	89.2	81.3	93.7	77.7	90.0
1150.1	70.4	81.2	80.3	85.8	80.2	89.5	81.5	93.8	78.5	90.6
1160.0	70.6	81.5	80.3	86.1	80.3	89.8	81.6	93.6	78.9	91.1
1170.0	70.8	81.9	80.3	86.4	80.5	90.1	81.7	93.5	79.2	91.9
1179.9	70.9	82.2	80.2	86.5	80.7	90.5	81.6	93.4	79.6	92.8
1190.2	71.1	82.5	80.3	86.7	80.9	91.0	81.8	93.4	80.2	93.7
1200.1	71.3	82.8	80.3	86.8	81.0	91.4	81.8	93.4	80.7	94.3
1210.0	71.6	83.2	80.4	87.0	81.1	91.9	82.0	93.5	81.3	94.7
1219.9	71.8	83.7	80.5	87.2	81.1	92.3	82.0	93.6	81.9	94.9
1229.9	72.1	84.2	80.6	87.3	81.2	92.8	82.1	93.9	82.5	95.0
1240.2	72.6	84.7	80.9	87.6	81.3	93.4	82.3	94.2	83.1	95.1
1250.1	73.1	85.3	81.0	88.0	81.5	94.0	82.3	94.6	83.7	95.0
1260.0	73.6	85.8	81.1	88.2	81.6	94.4	82.3	94.9	84.0	95.1
1269.9	74.1	86.5	81.1	88.6	81.8	95.0	82.4	95.0	84.2	95.3
1279.8	74.7	87.0	81.2	88.9	82.1	95.5	82.5	95.2	84.4	95.6
1290.1	75.4	87.5	81.5	89.3	82.4	96.1	82.7	95.6	84.6	96.1
1300.0	76.2	87.9	81.8	89.7	82.8	96.7	83.0	95.9	84.7	96.6
1310.0	77.0	88.4	82.0	90.3	83.2	97.4	83.4	96.3	84.8	97.2
1319.9	77.9	88.7	82.2	90.8	83.6	98.2	83.8	96.7	84.8	98.0
1330.2	79.1	88.9	82.6	91.4	84.1	99.2	84.4	97.3	85.0	99.0
1340.1	79.9	89.0	83.0	91.9	84.7	100.0	85.0	97.9	85.2	99.8
1350.0	80.8	89.1	83.5	92.5	85.3	100.9	85.6	98.7	85.4	100.7
1359.9	81.7	89.0	84.0	93.1	85.9	101.7	86.3	99.6	85.8	101.6
1369.9	82.6	88.8	84.6	93.5	86.5	102.6	86.9	100.6	86.2	102.5
1380.2	83.9	88.4	85.2	93.9	87.3	103.5	87.7	101.7	86.6	103.4
1390.1	85.0	88.0	85.7	94.1	87.8	104.4	88.5	102.4	87.1	104.0
1400.0	86.0	87.6	86.2	94.2	88.4	105.2	89.1	103.0	87.6	104.5
1409.9	87.4	87.2	86.7	94.3	88.8	105.9	89.8	103.6	88.1	104.9
1419.8	89.1	86.8	87.2	94.3	89.1	106.4	90.2	104.2	88.5	105.3
1430.1	91.1	86.6	87.6	94.1	89.6	107.0	90.5	104.8	89.1	105.5
1440.0	92.6	86.3	87.8	93.8	89.9	107.3	90.8	105.3	89.4	105.4
1450.0	94.7	86.2	88.1	93.5	90.2	107.6	91.1	105.6	89.8	105.3
1459.9	95.2	86.2	88.1	93.1	90.5	108.0	91.3	105.7	90.4	105.0
1470.2	94.2	86.4	88.6	92.7	90.9	108.1	91.7	105.9	91.8	105.0
1480.1	93.5	86.5	88.9	92.3	91.3	107.9	92.0	105.8	92.9	104.9
1490.0	92.9	86.5	89.2	91.8	91.6	107.7	92.1	105.7	93.8	104.8
1499.9	92.3	86.6	89.7	91.5	91.9	107.4	92.2	105.4	94.8	104.7
1509.9	91.9	86.8	90.1	91.1	92.2	107.0	92.4	105.2	95.8	104.6
1520.2	91.7	86.9	90.6	90.9	92.6	106.7	92.8	105.0	96.8	104.6
1530.1	91.3	86.9	90.6	90.8	92.9	106.4	93.0	104.8	97.7	104.5
1540.0	91.0	87.1	90.7	90.9	93.2	106.2	93.3	105.0	98.5	104.5
1549.9	90.6	87.1	90.8	91.0	93.4	106.0	93.5	105.0	99.3	104.5
1559.8	90.2	87.2	90.9	91.1	93.6	105.9	93.8	105.0	100.0	104.5

1570.1	90.1	87.3	91.0	91.4	93.9	105.9	94.0	104.9	100.7	104.7
1580.0	89.9	87.4	91.2	91.7	94.1	106.0	94.2	104.9	101.2	104.7
1590.0	89.9	87.4	91.2	92.0	94.3	106.1	94.3	105.1	101.8	104.7
1599.9	90.0	87.5	91.2	92.4	94.5	106.4	94.5	105.2	102.2	104.9
1610.2	90.2	87.6	91.3	92.8	94.9	106.9	94.9	105.5	102.6	105.1
1620.1	90.3	87.6	91.3	93.2	95.5	107.5	95.0	105.8	102.9	105.4
1630.0	90.4	87.7	91.5	93.6	95.6	108.1	95.0	106.3	102.8	105.8
1639.9	90.7	87.7	91.5	94.1	95.7	108.7	95.1	106.8	102.6	106.0
1649.9	90.8	87.7	91.7	94.5	95.8	109.4	95.1	107.5	102.3	106.1
1660.2	91.1	87.7	92.0	94.9	96.0	110.1	95.2	108.2	102.1	106.2
1670.1	91.2	87.8	92.1	95.3	96.2	110.8	95.2	109.0	101.9	106.6
1680.0	91.3	87.9	92.3	95.6	96.3	111.5	95.2	109.5	101.8	107.0
1689.9	91.3	88.1	92.6	96.1	96.4	112.2	95.2	110.1	101.5	107.2
1699.8	91.4	88.5	92.7	96.5	96.7	112.8	95.3	110.6	101.1	107.5
1710.1	91.6	88.7	93.0	96.9	96.9	113.4	95.5	111.0	100.9	107.7
1720.0	91.7	88.9	93.2	97.3	97.1	113.9	95.6	111.4	100.5	107.9
1730.0	91.9	89.1	93.2	97.6	97.2	114.4	95.8	111.9	100.2	108.1
1739.9	92.1	89.3	93.3	97.9	97.5	115.0	95.9	112.7	99.7	108.2
1750.2	92.5	89.5	93.5	98.4	97.8	115.8	96.0	113.4	99.4	108.1
1760.1	92.7	89.9	93.5	98.7	98.0	116.3	96.0	114.0	98.9	108.0
1770.0	93.0	90.2	93.6	99.1	98.3	116.8	96.1	114.5	98.2	107.8
1779.9	93.3	90.4	93.8	99.5	98.5	117.4	96.2	115.0	97.6	107.7
1789.9	93.5	90.6	93.8	99.8	98.7	118.0	96.1	115.3	97.0	107.6
1800.2	93.7	90.8	94.1	100.1	99.0	118.9	96.3	115.8	96.3	107.5
1810.1	93.7	90.9	94.1	100.4	99.0	119.6	96.4	116.4	95.5	107.5
1820.0	93.8	90.9	93.9	100.6	99.0	120.2	96.5	117.0	94.9	107.6
1829.9	93.8	90.9	93.9	101.0	99.0	120.9	96.6	117.5	94.4	107.7
1839.8	93.8	90.8	94.1	101.3	99.0	121.5	96.7	118.1	93.7	108.1
1850.1	93.8	90.7	94.4	101.7	99.0	122.2	97.0	118.8	93.0	108.4
1860.0	93.8	90.7	94.6	102.2	99.0	122.8	97.0	119.5	92.2	108.8
1870.0	93.7	90.6	94.6	102.5	98.8	123.3	97.2	120.0	91.1	109.0
1879.9	93.5	90.5	94.8	102.8	98.7	123.8	97.5	120.2	89.7	109.3
1890.2	93.7	90.3	95.5	103.1	98.8	124.4	97.9	120.5	88.0	109.8
1900.1	93.8	90.1	96.0	103.3	98.9	125.0	98.1	120.6	86.6	110.3
1910.0	93.7	90.0	96.6	103.5	99.0	125.5	98.2	120.6	85.2	110.6
1919.9	93.7	89.9	97.0	103.5	99.1	126.0	98.3	120.9	83.5	111.0
1929.9	93.7	89.8	97.5	103.6	99.4	126.5	98.5	121.1	82.5	111.4
1940.2	93.8	89.4	97.8	103.5	99.6	126.9	98.8	121.4	81.3	111.7
1950.1	93.7	89.2	98.0	103.3	99.7	127.3	99.1	121.6	80.2	111.9
1960.0	93.7	89.0	98.2	103.0	99.9	127.6	99.3	121.9	79.0	111.9
1969.9	93.5	88.8	98.2	102.7	100.0	127.8	99.7	122.2	77.9	112.1
1979.8	93.4	88.7	98.3	102.3	100.1	128.1	100.1	122.3	76.9	112.0
1990.1	93.2	88.4	98.4	102.0	100.2	128.3	100.5	122.4	76.0	112.1
2000.0	92.9	88.2	98.4	101.8	100.3	128.4	100.7	122.1	75.2	112.0
2010.0	92.7	87.9	98.4	101.4	100.4	128.4	100.8	122.0	74.5	111.8
2019.9	92.5	87.7	98.5	101.0	100.6	128.3	100.9	121.9	73.9	111.6
2030.2	92.1	87.4	98.8	100.5	101.0	128.3	101.3	121.7	73.2	111.2
2040.1	91.9	87.3	99.0	100.2	101.2	128.2	101.5	121.4	72.6	110.8
2050.0	91.8	87.1	99.2	99.8	101.3	128.1	101.6	120.9	72.1	110.4
2059.9	91.6	87.0	99.3	99.5	101.4	128.0	101.7	120.5	71.9	110.1
2069.9	91.4	86.9	99.3	99.0	101.5	127.9	101.9	120.2	71.4	109.7

2080.2	91.2	86.7	99.4	98.7	101.7	127.7	102.0	119.8	70.9	109.3
2090.1	91.0	86.6	99.5	98.5	101.8	127.4	102.1	119.4	70.8	108.9
2100.0	90.8	86.5	99.6	98.3	101.9	127.1	102.3	119.2	70.8	108.5
2109.9	90.6	86.3	99.6	98.0	101.9	126.9	102.4	118.8	70.5	108.0
2119.8	90.6	86.3	99.7	97.7	101.9	126.6	102.5	118.3	70.5	107.6
2130.1	90.4	86.0	99.8	97.6	102.1	126.2	102.7	118.0	70.6	107.2
2140.0	90.3	85.8	99.8	97.3	102.2	125.8	102.9	117.7	70.9	106.7
2150.0	90.2	85.6	100.0	97.2	102.3	125.4	103.0	117.4	71.3	106.2
2159.9	90.0	85.3	100.0	97.0	102.3	125.0	103.1	117.1	71.3	105.8
2170.2	89.8	85.1	100.0	96.8	102.4	124.5	103.2	116.8	71.1	105.2
2180.1	89.7	84.8	99.9	96.7	102.5	124.0	103.2	116.7	71.5	104.7
2190.0	89.5	84.4	99.8	96.7	102.5	123.6	103.1	116.6	71.9	104.0
2199.9	89.5	84.2	99.8	96.6	102.5	123.1	103.0	116.4	72.1	103.4
2209.9	89.5	83.9	99.8	96.5	102.6	122.6	102.9	116.2	72.2	102.9
2220.2	89.6	83.6	99.9	96.2	102.6	122.2	102.9	115.9	72.7	102.0
2230.1	89.7	83.3	100.0	96.0	102.6	121.7	102.8	115.4	73.4	100.9
2240.0	89.6	83.1	99.9	95.7	102.7	121.2	102.7	114.7	74.0	100.2
2249.9	89.6	83.0	99.7	95.4	102.7	120.8	102.7	114.1	74.9	99.3
2259.8	89.6	82.9	99.9	95.3	102.7	120.4	102.7	113.6	75.9	98.5
2270.1	89.5	82.6	100.1	95.1	102.7	120.1	102.7	113.4	77.2	97.5
2280.0	89.5	82.4	100.2	95.0	102.8	119.9	102.6	113.2	78.4	96.1
2290.0	89.4	82.3	100.4	95.0	102.8	119.6	102.5	113.1	79.7	95.0
2299.9	89.5	82.2	100.6	95.0	102.8	119.3	102.5	113.0	80.8	94.1
2310.2	89.5	81.9	100.7	95.0	102.8	119.0	102.6	113.2	81.9	93.0
2320.1	89.5	81.8	100.7	95.0	102.9	118.7	102.7	113.3	83.2	92.1
2330.0	89.4	81.7	100.6	95.3	102.9	118.6	102.6	113.2	84.5	90.6
2339.9	89.4	81.5	100.7	95.6	102.9	118.4	102.6	113.2	85.7	89.5
2349.9	89.5	81.4	100.8	95.8	102.8	118.2	102.3	113.2	87.6	88.6
2360.2	89.5	81.2	101.0	96.1	102.8	118.0	102.3	113.3	89.2	87.7
2370.1	89.6	81.1	101.1	95.8	102.7	117.8	102.4	113.4	91.0	86.3
2380.0	89.8	80.8	101.3	95.6	102.6	117.7	102.5	113.7	92.7	85.3
2389.9	89.9	80.6	101.4	95.5	102.6	117.6	102.7	114.0	94.3	84.5
2399.8	90.0	80.6	101.6	95.3	102.6	117.5	102.5	114.2	95.7	83.6
2410.1	90.1	80.6	101.8	95.3	102.7	117.4	102.7	114.4	96.9	82.4
2420.0	90.0	80.8	102.0	95.4	102.8	117.3	102.7	114.7	98.3	81.4
2430.0	90.0	80.9	102.1	95.5	102.8	117.3	102.8	115.0	99.5	80.5
2439.9	90.0	81.0	102.2	95.7	102.7	117.2	102.9	115.4	100.7	79.5
2450.2	90.1	81.1	102.2	95.8	102.6	117.0	103.0	115.7	101.7	78.7
2460.1	90.1	81.3	102.2	95.9	102.5	116.8	103.2	115.9	103.1	78.1
2470.0	89.8	81.4	102.1	95.8	102.5	116.7	103.2	116.3	104.9	77.7
2479.9	89.9	81.6	102.1	95.7	102.4	116.4	103.3	116.5	106.4	77.0
2489.9	90.0	81.8	102.0	95.7	102.3	116.2	103.3	116.7	108.0	76.1
2500.2	90.2	81.9	101.8	95.8	102.3	115.8	103.4	116.9	109.7	75.6

A(11a) Data of seismic test result in Oxford clay with column configuration which sensor-pairs located on defective column for test ID: 17Nov10_01, 17Nov10_01, 17Nov10_02 and 15Nov10_01 (see Section 7.3.2.3).

Seismic test carried out using Oxford-clay after columns installation which sensor-pairs on a defective column (sensor pair A-B).
Date of test: 15 November to 17 November 2010
Test frequency range / interval: 210 to 2500 Hz / 10 Hz
Remarks: These tests carried out in parallel with compacted column.

Frequency, Hz / File name	Defect column					
	17Nov 10_03	17Nov 10_01	17Nov 10_02	15Nov 10_01	Average, m/s	Wavelength, cm
210.2	42.5	49.4	55.0	40.2	46.8	22.3
220.1	34.2	32.8	44.3	30.8	35.5	16.1
230.0	51.3	33.3	54.6	38.6	44.5	19.3
239.9	73.4	50.8	81.7	58.1	66.0	27.5
249.9	80.5	66.5	101.4	68.6	79.3	31.7
260.2	66.6	61.1	91.4	57.4	69.1	26.6
270.1	53.9	46.1	65.8	45.2	52.7	19.5
280.0	51.8	49.3	53.7	42.9	49.4	17.6
289.9	51.1	51.9	53.6	44.3	50.2	17.3
299.8	50.6	52.7	55.1	45.7	51.0	17.0
310.1	48.7	52.2	53.4	46.7	50.3	16.2
320.1	47.4	46.6	52.0	45.1	47.8	14.9
330.0	48.1	44.0	52.8	44.6	47.4	14.4
339.9	52.7	46.6	56.6	46.9	50.7	14.9
350.2	55.5	48.1	60.5	49.2	53.3	15.2
360.1	52.8	46.6	58.4	47.6	51.3	14.3
370.0	48.2	44.5	52.7	44.1	47.4	12.8
379.9	44.7	44.3	48.2	42.0	44.8	11.8
389.9	44.0	43.5	45.9	41.8	43.8	11.2
400.2	45.2	43.5	45.9	43.0	44.4	11.1
410.1	46.4	43.9	48.4	44.8	45.9	11.2
420.0	46.9	43.2	50.5	46.2	46.7	11.1
429.9	46.2	41.1	50.6	45.3	45.8	10.7
439.8	44.5	38.8	48.9	42.5	43.7	9.9
450.1	43.1	37.9	45.6	40.0	41.7	9.3
460.1	43.5	39.4	42.2	38.9	41.0	8.9
470.0	44.8	42.5	43.5	39.1	42.5	9.0
479.9	45.5	45.1	45.5	39.6	43.9	9.2
490.2	45.2	45.4	46.5	40.2	44.3	9.0
500.1	44.2	44.2	46.2	40.5	43.8	8.8
510.0	43.7	42.8	45.5	40.2	43.0	8.4
519.9	43.8	41.7	45.1	39.8	42.6	8.2
529.9	44.6	41.4	45.1	40.1	42.8	8.1
540.2	45.8	41.8	45.2	40.5	43.3	8.0
550.1	47.0	43.4	45.5	40.9	44.2	8.0
560.0	48.0	45.5	45.7	41.5	45.2	8.1
569.9	48.5	47.0	46.3	42.7	46.1	8.1
579.8	48.2	47.6	46.9	44.3	46.8	8.1
590.1	47.4	47.6	47.2	45.5	46.9	7.9
600.1	46.6	47.1	46.9	46.1	46.7	7.8
610.0	45.9	46.4	46.6	46.2	46.3	7.6

619.9	45.2	45.6	46.2	46.2	45.8	7.4
630.2	44.9	45.4	46.0	46.5	45.7	7.3
640.1	44.9	46.3	45.9	47.2	46.1	7.2
650.0	45.1	48.0	46.0	48.1	46.8	7.2
659.9	45.3	49.5	46.1	49.0	47.5	7.2
669.9	45.5	50.6	46.3	49.9	48.1	7.2
680.2	45.3	51.3	46.3	50.5	48.4	7.1
690.1	45.1	51.5	46.3	50.9	48.4	7.0
700.0	45.0	51.4	46.2	51.1	48.4	6.9
709.9	44.7	51.2	45.9	51.3	48.3	6.8
719.8	44.5	51.0	45.7	51.6	48.2	6.7
730.1	44.4	50.9	45.4	52.0	48.2	6.6
740.1	44.3	51.0	45.2	52.4	48.2	6.5
750.0	44.3	51.5	45.1	52.9	48.4	6.5
759.9	44.2	52.1	45.0	53.0	48.6	6.4
770.2	44.2	52.5	45.0	53.1	48.7	6.3
780.1	44.4	52.8	44.9	53.3	48.9	6.3
790.0	44.6	53.1	44.7	53.5	49.0	6.2
799.9	44.7	53.4	44.6	53.7	49.1	6.1
809.9	45.0	53.9	44.5	53.9	49.3	6.1
820.2	45.2	54.6	44.5	54.0	49.6	6.0
830.1	45.5	55.5	44.5	54.2	49.9	6.0
840.0	45.9	56.5	44.6	54.2	50.3	6.0
849.9	46.2	57.4	44.8	54.0	50.6	6.0
859.8	46.5	58.0	44.8	53.7	50.7	5.9
870.1	46.7	58.4	44.9	53.1	50.8	5.8
880.1	46.8	58.8	44.9	52.8	50.8	5.8
890.0	46.7	59.2	44.8	52.5	50.8	5.7
899.9	46.7	59.5	44.6	52.3	50.8	5.6
910.2	46.6	59.5	44.5	52.1	50.7	5.6
920.1	46.5	58.5	44.5	52.2	50.4	5.5
930.0	46.5	57.0	44.4	52.5	50.1	5.4
939.9	46.4	56.5	44.4	52.8	50.0	5.3
949.9	46.4	56.0	44.4	52.8	49.9	5.3
960.2	46.5	55.3	44.8	52.3	49.7	5.2
970.1	46.6	54.5	45.2	51.6	49.5	5.1
980.0	46.8	53.9	45.4	50.7	49.2	5.0
989.9	47.1	53.4	45.6	50.0	49.0	5.0
999.8	47.4	52.8	45.9	49.6	48.9	4.9
1010.1	47.7	52.3	46.5	49.2	48.9	4.8
1020.1	47.9	51.8	47.0	48.9	48.9	4.8
1030.0	48.0	51.5	47.5	48.6	48.9	4.7
1039.9	48.2	51.2	47.8	48.2	48.8	4.7
1050.2	48.4	50.9	48.0	47.5	48.7	4.6
1060.1	48.6	50.6	48.3	46.9	48.6	4.6
1070.0	48.8	50.3	48.5	46.3	48.5	4.5
1079.9	48.9	50.0	48.6	45.7	48.3	4.5
1089.9	49.1	49.6	48.6	45.2	48.1	4.4
1100.2	49.3	49.3	48.5	44.9	48.0	4.4
1110.1	49.4	49.0	48.4	44.6	47.8	4.3

1120.0	49.4	48.7	48.3	44.3	47.7	4.3
1129.9	50.1	48.5	48.1	44.2	47.7	4.2
1139.8	49.8	48.4	48.0	44.0	47.6	4.2
1150.1	49.8	48.5	48.0	44.0	47.6	4.1
1160.0	49.7	48.5	48.0	43.7	47.5	4.1
1170.0	49.7	48.5	47.9	43.5	47.4	4.1
1179.9	49.8	48.4	47.9	43.5	47.4	4.0
1190.2	50.0	48.4	47.8	43.4	47.4	4.0
1200.1	50.2	48.3	47.7	43.4	47.4	3.9
1210.0	50.4	48.3	47.6	43.4	47.4	3.9
1219.9	50.6	48.3	47.4	43.5	47.5	3.9
1229.9	50.8	48.2	47.3	43.4	47.4	3.9
1240.2	50.9	48.1	47.2	43.5	47.5	3.8
1250.1	51.0	48.0	47.1	43.7	47.4	3.8
1260.0	51.1	47.8	47.0	43.7	47.4	3.8
1269.9	51.2	47.7	46.9	43.9	47.4	3.7
1279.8	51.3	47.6	46.8	44.2	47.5	3.7
1290.1	51.4	47.5	46.8	44.6	47.6	3.7
1300.0	51.5	47.3	46.8	44.8	47.6	3.7
1310.0	51.7	47.2	46.8	45.0	47.7	3.6
1319.9	51.8	47.1	46.8	45.0	47.7	3.6
1330.2	51.9	47.0	46.8	45.1	47.7	3.6
1340.1	52.0	47.0	46.8	45.2	47.7	3.6
1350.0	52.0	46.9	46.8	45.3	47.7	3.5
1359.9	52.1	46.7	46.8	45.3	47.7	3.5
1369.9	52.1	46.5	46.7	45.5	47.7	3.5
1380.2	52.2	46.3	46.6	45.8	47.7	3.5
1390.1	52.2	46.2	46.6	45.8	47.7	3.4
1400.0	52.2	46.0	46.7	45.6	47.6	3.4
1409.9	52.2	46.0	46.8	45.6	47.6	3.4
1419.8	52.3	45.9	46.9	45.5	47.6	3.4
1430.1	52.4	45.8	47.0	45.6	47.7	3.3
1440.0	52.6	45.7	47.1	45.6	47.7	3.3
1450.0	52.8	45.5	47.3	45.6	47.8	3.3
1459.9	53.0	45.5	47.4	45.7	47.9	3.3
1470.2	53.3	45.4	47.4	45.9	48.0	3.3
1480.1	53.5	45.3	47.4	46.0	48.1	3.2
1490.0	53.9	45.2	47.3	46.1	48.1	3.2
1499.9	54.2	45.1	47.3	46.1	48.2	3.2
1509.9	54.5	44.9	47.3	46.1	48.2	3.2
1520.2	54.9	44.9	47.2	46.2	48.3	3.2
1530.1	55.3	44.9	47.2	46.3	48.4	3.2
1540.0	55.5	44.7	47.1	46.4	48.4	3.1
1549.9	55.7	44.6	47.1	46.4	48.5	3.1
1559.8	55.8	44.6	47.1	46.5	48.5	3.1
1570.1	56.1	44.6	47.0	46.6	48.6	3.1
1580.0	56.2	44.6	47.0	46.7	48.6	3.1
1590.0	56.4	44.5	46.9	46.7	48.6	3.1
1599.9	56.6	44.5	46.9	46.7	48.7	3.0
1610.2	56.9	44.6	46.9	46.8	48.8	3.0

1620.1	57.2	44.5	46.9	46.8	48.9	3.0
1630.0	57.6	44.4	46.9	46.9	48.9	3.0
1639.9	57.9	44.3	46.9	47.0	49.0	3.0
1649.9	58.2	44.3	46.9	47.1	49.1	3.0
1660.2	58.5	44.4	47.1	47.3	49.3	3.0
1670.1	58.8	44.3	47.2	47.4	49.4	3.0
1680.0	59.0	44.2	47.3	47.5	49.5	2.9
1689.9	59.2	44.1	47.4	47.6	49.6	2.9
1699.8	59.5	44.2	47.6	47.7	49.8	2.9
1710.1	59.8	44.6	47.8	47.9	50.0	2.9
1720.0	60.0	45.1	48.0	48.2	50.3	2.9
1730.0	60.0	45.5	48.1	48.4	50.5	2.9
1739.9	60.2	46.0	48.3	48.7	50.8	2.9
1750.2	60.4	46.9	48.5	48.9	51.2	2.9
1760.1	60.5	47.2	48.6	49.1	51.4	2.9
1770.0	60.7	47.4	48.8	49.3	51.6	2.9
1779.9	61.0	47.7	49.0	49.5	51.8	2.9
1789.9	61.2	61.0	49.2	49.6	55.3	3.1
1800.2	61.6	69.3	49.5	49.7	57.5	3.2
1810.1	61.9	71.8	49.7	49.7	58.3	3.2
1820.0	62.1	72.2	50.1	49.9	58.6	3.2
1829.9	62.3	72.4	50.5	49.9	58.7	3.2
1839.8	62.5	71.8	50.9	49.9	58.8	3.2
1850.1	62.6	71.0	51.3	50.0	58.7	3.2
1860.0	62.7	71.0	51.7	50.1	58.9	3.2
1870.0	62.8	70.8	52.2	50.3	59.0	3.2
1879.9	62.8	70.7	52.5	50.4	59.1	3.1
1890.2	63.0	70.5	52.9	50.6	59.2	3.1
1900.1	63.1	70.5	53.1	50.8	59.4	3.1
1910.0	63.1	70.4	53.3	51.0	59.4	3.1
1919.9	63.1	69.9	53.5	51.3	59.5	3.1
1929.9	63.1	69.7	53.8	51.7	59.6	3.1
1940.2	63.2	69.6	54.1	52.1	59.7	3.1
1950.1	63.4	69.9	54.2	52.3	60.0	3.1
1960.0	63.5	70.1	54.4	52.4	60.1	3.1
1969.9	63.7	70.3	54.5	52.4	60.2	3.1
1979.8	63.9	70.4	54.5	52.5	60.3	3.0
1990.1	64.1	70.5	54.4	52.8	60.4	3.0
2000.0	64.4	70.8	54.4	53.1	60.6	3.0
2010.0	64.7	70.9	54.3	53.2	60.8	3.0
2019.9	65.0	71.1	54.1	53.4	60.9	3.0
2030.2	65.3	71.1	54.1	53.7	61.1	3.0
2040.1	65.7	71.3	54.0	53.9	61.2	3.0
2050.0	66.3	71.3	53.9	54.3	61.4	3.0
2059.9	66.9	71.2	53.8	54.5	61.6	3.0
2069.9	67.7	71.0	53.7	54.8	61.8	3.0
2080.2	68.4	70.7	53.5	55.2	62.0	3.0
2090.1	69.0	70.6	53.4	55.5	62.1	3.0
2100.0	69.3	70.4	53.4	55.8	62.2	3.0
2109.9	69.7	70.2	53.5	56.2	62.4	3.0

2119.8	69.9	70.1	53.7	56.5	62.6	3.0
2130.1	70.1	70.0	54.0	57.0	62.8	2.9
2140.0	70.4	70.0	54.4	57.2	63.0	2.9
2150.0	70.5	70.0	54.8	57.5	63.2	2.9
2159.9	70.6	70.0	55.3	57.8	63.4	2.9
2170.2	70.7	70.0	55.8	58.1	63.7	2.9
2180.1	70.7	70.0	56.3	58.3	63.8	2.9
2190.0	70.6	70.2	56.8	58.4	64.0	2.9
2199.9	70.4	70.2	57.2	58.6	64.1	2.9
2209.9	70.4	70.3	57.6	58.8	64.3	2.9
2220.2	70.2	70.3	58.0	59.3	64.4	2.9
2230.1	70.0	70.3	58.3	59.5	64.5	2.9
2240.0	69.9	70.3	58.6	59.7	64.6	2.9
2249.9	69.7	70.3	58.8	60.0	64.7	2.9
2259.8	69.6	70.3	59.0	60.4	64.8	2.9
2270.1	69.4	70.3	59.1	60.9	64.9	2.9
2280.0	69.3	70.4	59.2	61.2	65.0	2.9
2290.0	69.3	70.4	59.2	61.5	65.1	2.8
2299.9	69.2	70.4	59.2	61.7	65.1	2.8
2310.2	68.9	70.3	59.2	62.1	65.2	2.8
2320.1	68.8	70.4	59.2	62.4	65.2	2.8
2330.0	68.6	70.5	59.3	62.8	65.3	2.8
2339.9	68.5	70.7	59.3	63.0	65.4	2.8
2349.9	68.3	70.9	59.3	63.5	65.5	2.8
2360.2	68.0	70.8	59.3	63.7	65.4	2.8
2370.1	67.8	70.6	59.3	64.2	65.5	2.8
2380.0	67.7	70.5	59.2	64.5	65.5	2.8
2389.9	67.6	70.6	59.2	64.9	65.6	2.7
2399.8	67.6	70.9	59.2	65.4	65.8	2.7
2410.1	67.3	71.0	59.1	66.1	65.9	2.7
2420.0	67.2	71.1	59.0	66.8	66.0	2.7
2430.0	67.1	71.0	58.9	67.5	66.1	2.7
2439.9	66.9	71.0	58.9	68.2	66.2	2.7
2450.2	66.6	70.8	58.9	68.9	66.3	2.7
2460.1	66.4	70.9	58.8	69.5	66.4	2.7
2470.0	66.3	71.0	58.8	70.2	66.6	2.7
2479.9	66.1	71.2	58.8	70.7	66.7	2.7
2489.9	65.9	71.1	58.8	71.2	66.8	2.7
2500.2	65.7	71.0	58.8	72.0	66.9	2.7

A(11b) Data of seismic test result in Oxford clay with column configuration which sensor-pairs located on defective column for test ID: 17Nov10_01, 17Nov10_01, 17Nov10_02 and 15Nov10_011 (see Section 7.3.2.3).

Seismic test carried out using Oxford-clay after columns installation which sensor-pairs on a compacted column (sensor pair C-D).
Date of test: 15 November to 17 November 2010
Test frequency range / interval: 210 to 2500 Hz / 10 Hz
Remarks: These tests carried out in parallel with defective column.

Frequency, Hz / File name	Compacted column					
	17Nov 10_03	17Nov 10_01	17Nov 10_02	15Nov 10_01	Average, m/s	Wavelength, cm
210.2	69.4	46.2	64.9	64.3	61.2	29.1
220.1	53.3	64.8	49.6	51.2	54.7	24.9
230.0	44.3	60.3	46.6	51.9	50.8	22.1
239.9	54.0	52.0	58.0	62.5	56.6	23.6
249.9	53.6	55.4	51.0	50.6	52.7	21.1
260.2	50.1	56.9	54.7	45.8	51.9	19.9
270.1	49.8	55.0	61.6	60.6	56.8	21.0
280.0	55.3	56.0	62.9	62.6	59.2	21.1
289.9	54.1	58.8	54.7	53.1	55.2	19.0
299.8	50.6	56.5	50.2	51.1	52.1	17.4
310.1	54.3	50.6	53.6	57.5	54.0	17.4
320.1	60.3	54.1	60.1	61.5	59.0	18.4
330.0	65.5	59.2	65.7	65.1	63.9	19.4
339.9	65.4	60.0	63.3	62.8	62.9	18.5
350.2	60.7	64.2	61.6	57.2	60.9	17.4
360.1	54.4	69.7	61.4	52.1	59.4	16.5
370.0	54.5	69.3	62.5	52.7	59.8	16.1
379.9	58.2	64.9	62.1	56.3	60.4	15.9
389.9	58.7	59.8	60.5	58.2	59.3	15.2
400.2	57.6	57.1	59.6	57.8	58.0	14.5
410.1	56.5	55.3	58.9	55.4	56.5	13.8
420.0	57.4	53.7	59.1	53.6	56.0	13.3
429.9	57.8	53.0	58.4	51.9	55.3	12.9
439.8	54.7	54.1	56.1	49.5	53.6	12.2
450.1	48.7	58.4	53.6	46.4	51.7	11.5
460.1	45.3	63.2	51.9	43.3	50.9	11.1
470.0	46.5	66.9	52.0	42.4	52.0	11.1
479.9	49.4	69.7	52.7	45.6	54.4	11.3
490.2	52.6	71.5	52.7	48.4	56.3	11.5
500.1	54.2	71.7	52.4	49.0	56.8	11.4
510.0	54.8	70.8	52.7	48.4	56.7	11.1
519.9	55.3	69.8	54.1	47.7	56.7	10.9
529.9	55.3	69.0	56.1	47.5	57.0	10.8
540.2	54.8	67.9	57.2	47.3	56.8	10.5
550.1	54.3	66.6	57.1	47.5	56.4	10.2
560.0	54.7	66.5	56.9	48.4	56.6	10.1
569.9	55.8	67.4	57.1	49.8	57.5	10.1
579.8	56.8	68.3	57.6	51.1	58.5	10.1
590.1	57.7	68.9	58.5	52.1	59.3	10.0
600.1	58.8	69.0	59.9	53.0	60.2	10.0
610.0	60.1	69.1	61.2	54.0	61.1	10.0
619.9	61.0	69.3	62.4	54.6	61.8	10.0
630.2	61.6	69.5	63.1	55.0	62.3	9.9
640.1	61.9	68.9	63.4	54.8	62.2	9.7
650.0	62.1	67.9	63.3	54.2	61.9	9.5
659.9	62.1	67.5	63.5	53.7	61.7	9.4

669.9	62.1	68.2	63.9	53.6	62.0	9.2
680.2	62.3	69.9	63.7	54.2	62.5	9.2
690.1	62.8	71.0	63.7	55.7	63.3	9.2
700.0	63.5	71.9	63.8	57.6	64.2	9.2
709.9	64.1	72.6	63.8	58.8	64.8	9.1
719.8	64.3	72.7	63.9	58.9	64.9	9.0
730.1	64.2	72.3	64.2	58.6	64.8	8.9
740.1	63.9	72.0	64.6	58.7	64.8	8.8
750.0	63.7	71.6	65.4	59.1	64.9	8.7
759.9	63.5	70.8	65.9	60.2	65.1	8.6
770.2	63.5	69.4	66.4	61.1	65.1	8.5
780.1	63.5	68.2	66.8	61.7	65.1	8.3
790.0	63.6	67.3	67.3	61.9	65.0	8.2
799.9	63.5	66.8	67.7	61.9	65.0	8.1
809.9	63.5	66.7	68.2	61.9	65.1	8.0
820.2	63.6	67.0	68.6	62.0	65.3	8.0
830.1	63.9	67.5	69.0	62.4	65.7	7.9
840.0	64.3	68.3	69.5	63.0	66.3	7.9
849.9	65.0	68.9	69.9	63.6	66.9	7.9
859.8	65.9	69.3	70.3	64.4	67.5	7.8
870.1	66.9	69.6	70.8	65.1	68.1	7.8
880.1	67.9	69.8	71.3	65.8	68.7	7.8
890.0	68.9	70.0	71.8	66.5	69.3	7.8
899.9	70.1	70.4	72.6	67.0	70.0	7.8
910.2	71.3	71.0	73.6	67.4	70.8	7.8
920.1	72.5	71.5	74.8	67.8	71.7	7.8
930.0	73.6	71.9	75.6	68.3	72.3	7.8
939.9	74.6	72.3	76.2	68.6	72.9	7.8
949.9	75.6	72.8	76.7	69.0	73.5	7.7
960.2	76.6	73.3	77.2	69.5	74.1	7.7
970.1	77.2	73.5	77.7	70.6	74.7	7.7
980.0	78.1	73.5	78.2	71.4	75.3	7.7
989.9	79.3	72.9	78.8	72.0	75.7	7.7
999.8	80.5	71.9	79.4	72.8	76.2	7.6
1010.1	81.4	72.1	80.2	74.1	76.9	7.6
1020.1	82.5	72.9	80.8	75.3	77.9	7.6
1030.0	83.4	73.2	81.3	76.3	78.5	7.6
1039.9	84.3	73.3	81.9	77.0	79.1	7.6
1050.2	85.4	73.3	82.5	77.6	79.7	7.6
1060.1	86.2	73.4	83.0	78.2	80.2	7.6
1070.0	86.7	73.7	83.6	78.8	80.7	7.5
1079.9	87.0	74.0	84.1	79.3	81.1	7.5
1089.9	87.2	74.2	84.6	79.8	81.5	7.5
1100.2	87.4	74.4	85.2	80.4	81.8	7.4
1110.1	87.4	74.4	85.7	80.9	82.1	7.4
1120.0	87.3	74.3	86.2	81.3	82.3	7.3
1129.9	87.2	74.2	87.2	81.7	82.6	7.3
1139.8	87.0	74.2	87.4	82.1	82.7	7.3
1150.1	86.9	74.1	87.9	82.4	82.8	7.2
1160.0	86.6	74.0	88.2	82.6	82.9	7.1

1170.0	86.3	73.8	88.6	83.0	82.9	7.1
1179.9	86.0	73.7	88.9	83.3	83.0	7.0
1190.2	85.9	73.5	89.1	83.7	83.1	7.0
1200.1	85.7	73.4	89.3	84.1	83.1	6.9
1210.0	85.6	73.2	89.4	84.5	83.2	6.9
1219.9	85.5	73.0	89.5	84.9	83.2	6.8
1229.9	85.3	72.7	89.6	85.2	83.2	6.8
1240.2	85.3	72.2	89.7	85.7	83.2	6.7
1250.1	85.3	71.7	89.8	86.0	83.2	6.7
1260.0	85.2	71.3	89.9	86.2	83.2	6.6
1269.9	85.0	70.9	90.1	86.4	83.1	6.5
1279.8	84.9	70.6	90.2	86.5	83.0	6.5
1290.1	84.8	70.4	90.3	86.6	83.0	6.4
1300.0	84.7	70.3	90.5	86.6	83.0	6.4
1310.0	84.5	69.9	90.6	86.6	82.9	6.3
1319.9	84.3	69.3	90.7	86.6	82.7	6.3
1330.2	84.3	68.3	90.9	86.6	82.5	6.2
1340.1	84.0	67.6	91.1	86.7	82.4	6.1
1350.0	83.9	67.1	91.3	86.7	82.2	6.1
1359.9	83.6	66.6	91.4	86.8	82.1	6.0
1369.9	83.4	66.1	91.5	86.9	82.0	6.0
1380.2	83.3	65.7	91.6	87.1	81.9	5.9
1390.1	83.2	65.1	91.7	87.3	81.8	5.9
1400.0	83.0	64.3	91.9	87.6	81.7	5.8
1409.9	82.9	63.5	91.9	87.8	81.5	5.8
1419.8	82.8	62.4	92.1	88.0	81.3	5.7
1430.1	82.7	61.6	92.2	88.3	81.2	5.7
1440.0	82.5	61.0	92.3	88.6	81.1	5.6
1450.0	82.3	60.3	92.3	88.9	81.0	5.6
1459.9	82.1	59.4	92.3	89.2	80.7	5.5
1470.2	81.9	58.8	92.2	89.6	80.6	5.5
1480.1	81.7	58.1	92.1	90.0	80.5	5.4
1490.0	81.5	57.3	92.0	90.5	80.3	5.4
1499.9	81.3	56.8	91.9	91.1	80.3	5.4
1509.9	81.0	56.3	91.9	91.9	80.3	5.3
1520.2	80.8	56.0	91.9	92.9	80.4	5.3
1530.1	80.6	55.7	91.9	94.0	80.5	5.3
1540.0	80.3	55.6	91.9	95.3	80.8	5.2
1549.9	80.0	55.7	91.9	96.6	81.1	5.2
1559.8	79.8	55.9	91.9	97.9	81.4	5.2
1570.1	79.6	56.4	91.9	99.6	81.9	5.2
1580.0	79.3	56.8	91.8	101.2	82.3	5.2
1590.0	79.0	57.6	91.7	102.8	82.8	5.2
1599.9	78.6	58.6	91.5	104.2	83.2	5.2
1610.2	78.5	59.7	91.4	105.5	83.8	5.2
1620.1	78.3	60.6	91.2	106.4	84.1	5.2
1630.0	78.0	61.3	91.0	107.3	84.4	5.2
1639.9	77.9	62.0	90.9	108.1	84.7	5.2
1649.9	77.7	62.6	90.8	108.7	84.9	5.1
1660.2	77.8	63.1	90.9	109.0	85.2	5.1

1670.1	77.9	63.6	90.7	109.1	85.3	5.1
1680.0	77.8	64.0	90.5	109.4	85.4	5.1
1689.9	77.9	64.4	90.5	109.5	85.6	5.1
1699.8	78.0	64.7	91.6	109.6	86.0	5.1
1710.1	78.1	65.1	94.1	109.8	86.8	5.1
1720.0	78.1	65.6	95.4	109.8	87.2	5.1
1730.0	78.2	66.2	96.0	109.8	87.6	5.1
1739.9	78.4	66.8	95.9	109.7	87.7	5.0
1750.2	78.6	67.4	96.3	109.7	88.0	5.0
1760.1	78.7	68.0	96.7	109.7	88.2	5.0
1770.0	78.7	68.6	96.8	109.6	88.4	5.0
1779.9	78.8	69.2	97.1	109.6	88.7	5.0
1789.9	78.9	69.8	97.7	109.6	89.0	5.0
1800.2	79.3	70.5	98.2	109.5	89.4	5.0
1810.1	79.4	71.2	98.4	109.4	89.6	4.9
1820.0	79.6	71.8	98.1	109.2	89.7	4.9
1829.9	79.8	72.4	97.9	109.0	89.8	4.9
1839.8	79.8	73.0	97.7	108.7	89.8	4.9
1850.1	80.1	73.6	97.5	108.4	89.9	4.9
1860.0	80.1	74.3	97.2	107.9	89.9	4.8
1870.0	80.3	75.0	96.9	107.5	89.9	4.8
1879.9	80.5	75.8	96.7	107.2	90.0	4.8
1890.2	80.8	76.4	96.5	106.9	90.2	4.8
1900.1	81.0	77.1	96.3	106.6	90.2	4.7
1910.0	81.2	77.7	95.9	106.3	90.3	4.7
1919.9	81.6	78.4	95.5	105.9	90.3	4.7
1929.9	81.9	79.1	95.2	105.4	90.4	4.7
1940.2	82.4	79.8	94.9	105.0	90.5	4.7
1950.1	82.8	80.5	94.5	104.4	90.6	4.6
1960.0	83.2	81.1	94.2	104.0	90.6	4.6
1969.9	83.8	81.7	93.8	103.7	90.7	4.6
1979.8	84.3	82.2	93.5	103.3	90.8	4.6
1990.1	84.6	82.7	93.3	103.1	90.9	4.6
2000.0	85.1	83.2	93.0	102.8	91.0	4.6
2010.0	85.7	83.6	92.9	102.7	91.2	4.5
2019.9	86.3	84.0	92.8	102.6	91.4	4.5
2030.2	86.9	84.3	92.7	102.5	91.6	4.5
2040.1	87.3	84.7	92.6	102.4	91.8	4.5
2050.0	87.9	85.1	92.7	102.3	92.0	4.5
2059.9	88.3	85.6	93.0	102.2	92.3	4.5
2069.9	88.7	86.1	93.1	102.0	92.5	4.5
2080.2	89.2	86.8	93.3	101.9	92.8	4.5
2090.1	89.5	87.3	93.4	101.7	93.0	4.4
2100.0	90.0	87.9	93.4	101.6	93.2	4.4
2109.9	90.5	88.5	93.5	101.4	93.5	4.4
2119.8	91.0	89.2	93.5	101.2	93.7	4.4
2130.1	91.5	89.9	93.6	101.0	94.0	4.4
2140.0	92.0	90.5	93.5	100.9	94.2	4.4
2150.0	92.6	91.0	93.5	100.8	94.5	4.4
2159.9	93.2	91.7	93.4	100.7	94.8	4.4

2170.2	94.0	92.2	93.4	100.6	95.1	4.4
2180.1	94.6	92.9	93.3	100.6	95.4	4.4
2190.0	95.2	93.5	93.2	100.5	95.6	4.4
2199.9	95.7	94.0	93.2	100.4	95.9	4.4
2209.9	96.1	94.5	93.2	100.4	96.0	4.3
2220.2	96.6	95.0	93.2	100.5	96.3	4.3
2230.1	97.0	95.4	93.2	100.5	96.5	4.3
2240.0	97.4	95.9	93.2	100.5	96.7	4.3
2249.9	97.8	96.3	93.2	100.5	96.9	4.3
2259.8	98.1	96.7	93.2	100.4	97.1	4.3
2270.1	98.4	97.1	93.3	100.4	97.3	4.3
2280.0	98.7	97.5	93.3	100.4	97.5	4.3
2290.0	99.0	97.8	93.3	100.4	97.6	4.3
2299.9	99.3	98.0	93.3	100.5	97.8	4.3
2310.2	99.7	98.3	93.5	100.5	98.0	4.2
2320.1	100.0	98.6	93.6	100.5	98.2	4.2
2330.0	100.3	98.9	93.7	100.4	98.3	4.2
2339.9	100.7	99.2	93.8	100.5	98.5	4.2
2349.9	100.9	99.5	93.9	100.5	98.7	4.2
2360.2	101.1	99.7	94.0	100.6	98.8	4.2
2370.1	101.3	99.7	94.1	100.7	98.9	4.2
2380.0	101.6	99.7	94.1	100.8	99.1	4.2
2389.9	101.8	99.8	94.1	100.8	99.1	4.1
2399.8	102.0	100.0	94.1	100.9	99.2	4.1
2410.1	102.1	100.2	94.2	101.1	99.4	4.1
2420.0	102.2	100.4	94.1	101.3	99.5	4.1
2430.0	102.2	100.7	94.1	101.4	99.6	4.1
2439.9	102.1	100.9	94.1	101.5	99.7	4.1
2450.2	102.2	101.2	94.1	101.7	99.8	4.1
2460.1	102.3	101.3	94.2	101.8	99.9	4.1
2470.0	102.5	101.5	94.3	102.1	100.1	4.1
2479.9	102.7	101.7	94.4	102.3	100.3	4.0
2489.9	102.8	101.9	94.6	102.5	100.4	4.0
2500.2	103.1	102.2	94.8	102.6	100.7	4.0

A(12) Data of seismic test result in Oxford clay with column configuration which sensor-pairs on a 10.5 cm diameter column and Oxford-clay for test ID: 21Dec_04 (see Section 7.3.2.4).

Seismic test carried out after columns installation which
Date of test: 22Dec_03, 22 Dec_04, 22Dec_05, 22Dec_06 and 23Dec_01
Test frequency range / interval: 200 to 3000 Hz / 20 Hz

Data for 10.5 cm column;

Frequency	**22-Dec-04**	**22-Dec-05**	**22-Dec-06**	**22-Dec-03**	**23-Dec-01**	Average	StdDev	Wavelength
199.9	67.9	60.0	69.3	90.1	58.8	69.2	12.6	34.6
220.1	64.1	59.6	64.5	79.0	45.1	62.5	12.1	28.4
239.9	50.1	47.8	49.4	58.8	35.7	48.4	8.3	20.2

260.2	91.7	82.8	89.7	129.0	71.8	93.0	21.6	35.7
280.0	100.9	92.9	101.5	140.6	90.3	105.2	20.4	37.6
299.8	82.0	76.9	83.3	84.8	55.7	76.5	12.0	25.5
320.1	88.4	81.8	87.4	95.5	62.6	83.1	12.5	26.0
339.9	97.5	96.2	104.5	107.4	97.2	100.6	5.1	29.6
360.1	81.9	82.2	90.7	93.4	96.1	88.9	6.5	24.7
379.9	71.4	68.0	72.7	65.7	80.0	71.6	5.5	18.8
400.2	99.0	82.1	83.9	54.4	76.3	79.1	16.2	19.8
420.0	116.8	108.9	120.8	245.3	100.0	138.4	60.3	32.9
439.8	108.1	103.3	112.5	168.7	99.9	118.5	28.5	26.9
460.1	106.2	102.5	112.2	140.0	112.4	114.7	14.8	24.9
479.9	102.0	101.8	112.5	148.7	132.9	119.6	20.6	24.9
500.1	85.8	90.5	100.3	117.9	125.6	104.0	17.2	20.8
519.9	78.5	78.1	81.5	85.5	105.1	85.7	11.2	16.5
540.2	91.2	89.7	94.7	81.6	102.1	91.9	7.5	17.0
560.0	92.2	94.1	97.5	91.9	105.2	96.2	5.5	17.2
579.8	87.7	87.5	90.9	88.0	102.7	91.4	6.5	15.8
600.1	90.7	89.1	92.0	92.0	106.1	94.0	6.9	15.7
619.9	92.5	90.1	94.0	97.4	110.6	96.9	8.1	15.6
640.1	94.1	91.9	98.7	99.5	112.0	99.2	7.8	15.5
659.9	89.6	86.9	94.1	92.9	107.1	94.1	7.8	14.3
680.2	89.3	86.6	92.6	85.1	99.7	90.7	5.8	13.3
700.0	94.2	92.1	98.1	81.5	99.4	93.1	7.1	13.3
719.8	101.1	99.9	107.0	87.8	104.1	100.0	7.3	13.9
740.1	106.4	108.9	118.5	95.8	109.8	107.9	8.1	14.6
759.9	105.0	111.1	122.3	99.0	112.6	110.0	8.7	14.5
780.1	103.2	110.5	122.9	96.1	111.8	108.9	10.1	14.0
799.9	105.2	113.1	126.4	89.5	107.6	108.4	13.3	13.5
820.2	107.8	115.7	128.5	84.9	102.2	107.8	16.2	13.1
840.0	108.0	115.7	127.5	81.1	98.2	106.1	17.6	12.6
859.8	106.8	113.4	124.1	74.0	100.6	103.8	18.8	12.1
880.1	105.8	111.1	121.3	70.4	104.2	102.6	19.2	11.7
899.9	105.1	109.8	119.4	71.8	106.0	102.4	18.0	11.4
920.1	105.2	108.6	116.9	77.2	103.9	102.4	14.9	11.1
939.9	105.5	107.4	114.4	83.7	99.2	102.0	11.6	10.9
960.2	105.9	106.4	111.7	86.0	96.9	101.4	10.1	10.6
980.0	107.4	106.6	110.2	89.9	96.0	102.0	8.6	10.4
999.8	112.1	108.9	111.7	96.8	94.3	104.8	8.6	10.5
1020.1	118.7	113.8	116.6	99.3	92.6	108.2	11.6	10.6
1039.9	124.8	118.2	121.1	98.2	92.7	111.0	14.5	10.7
1060.1	129.5	121.4	124.1	104.0	93.5	114.5	15.2	10.8
1079.9	132.9	123.7	125.5	121.7	93.0	119.4	15.3	11.1
1100.2	135.4	125.7	126.7	142.7	93.3	124.8	18.9	11.3
1120.0	138.6	128.5	128.3	154.6	95.4	129.1	21.6	11.5
1139.8	142.2	132.8	131.6	156.7	97.7	132.2	21.7	11.6
1160.0	145.1	137.6	135.5	155.1	100.3	134.7	20.7	11.6
1179.9	147.0	142.2	140.1	158.4	102.1	138.0	21.2	11.7
1200.1	147.2	146.2	145.3	164.5	104.1	141.4	22.3	11.8
1219.9	147.1	149.8	151.5	166.9	105.7	144.2	22.9	11.8
1240.2	145.6	151.5	155.9	167.7	108.2	145.8	22.5	11.8

1260.0	144.1	153.5	160.1	168.3	110.8	147.4	22.3	11.7
1279.8	142.3	154.9	163.8	168.5	113.9	148.7	21.9	11.6
1300.0	140.2	155.0	165.5	168.7	117.6	149.4	21.0	11.5
1319.9	137.9	153.6	166.0	169.5	121.3	149.7	20.1	11.3
1340.1	135.6	151.3	165.2	170.4	124.8	149.5	19.3	11.2
1359.9	133.7	149.2	163.1	171.0	126.8	148.8	18.8	10.9
1380.2	132.2	147.3	160.7	170.2	127.2	147.5	18.3	10.7
1400.0	130.8	145.3	158.8	168.9	126.5	146.0	18.0	10.4
1419.8	129.4	143.4	157.4	167.1	126.3	144.7	17.6	10.2
1440.0	128.7	142.1	156.1	165.2	126.3	143.7	16.9	10.0
1459.9	128.3	141.1	154.6	163.2	126.5	142.7	16.1	9.8
1480.1	128.8	140.7	153.4	160.2	126.0	141.8	14.9	9.6
1499.9	129.2	140.4	152.3	156.6	125.0	140.7	13.8	9.4
1520.2	129.7	140.0	151.5	153.0	123.0	139.5	13.2	9.2
1540.0	130.2	139.7	150.7	149.6	120.6	138.2	12.9	9.0
1559.8	130.8	139.4	150.0	146.5	117.9	136.9	12.9	8.8
1580.0	131.5	139.4	149.6	143.8	115.5	136.0	13.2	8.6
1599.9	132.0	139.1	149.0	141.5	113.6	135.0	13.4	8.4
1620.1	132.1	138.6	148.2	139.4	112.4	134.1	13.4	8.3
1639.9	132.1	137.6	147.0	137.4	112.3	133.3	12.9	8.1
1660.2	131.9	137.1	146.0	135.8	112.3	132.6	12.5	8.0
1680.0	131.7	137.0	145.0	133.9	113.5	132.2	11.6	7.9
1699.8	131.3	136.8	144.0	132.3	114.7	131.8	10.8	7.8
1720.0	130.8	136.9	143.2	131.4	115.1	131.5	10.4	7.6
1739.9	130.3	137.0	142.5	130.4	117.1	131.5	9.5	7.6
1760.1	129.8	137.3	142.4	130.1	117.6	131.4	9.4	7.5
1779.9	129.1	137.4	141.9	129.6	118.8	131.3	8.9	7.4
1800.2	128.4	137.7	141.7	129.4	120.4	131.5	8.4	7.3
1820.0	128.5	138.2	141.5	129.3	123.1	132.1	7.5	7.3
1839.8	128.1	138.7	141.6	129.0	125.9	132.7	7.0	7.2
1860.0	127.8	139.5	142.0	129.0	128.9	133.4	6.7	7.2
1879.9	127.2	140.3	142.4	128.9	132.3	134.2	6.8	7.1
1900.1	126.8	141.2	143.0	129.1	135.7	135.2	7.2	7.1
1919.9	126.4	142.4	143.8	129.0	139.8	136.3	8.0	7.1
1940.2	126.3	143.2	144.7	129.0	143.6	137.4	9.0	7.1
1960.0	126.3	144.0	145.6	128.9	147.0	138.4	9.9	7.1
1979.8	126.3	144.7	146.5	128.8	149.8	139.2	10.9	7.0
2000.0	126.9	145.4	147.5	128.9	152.6	140.3	11.6	7.0
2019.9	127.5	146.3	148.5	128.9	154.9	141.2	12.3	7.0
2040.1	128.4	147.2	149.5	128.9	156.8	142.1	12.9	7.0
2059.9	129.0	148.2	150.7	128.7	158.2	143.0	13.4	6.9
2080.2	130.2	149.4	151.6	128.3	159.6	143.8	13.9	6.9
2100.0	131.6	150.6	152.6	128.1	160.6	144.7	14.1	6.9
2119.8	133.3	152.1	153.5	127.7	161.0	145.5	14.3	6.9
2140.0	135.5	153.6	154.4	127.2	161.2	146.4	14.3	6.8
2159.9	137.3	154.9	155.3	126.6	161.1	147.0	14.5	6.8
2180.1	139.6	156.3	156.3	125.7	161.1	147.8	14.8	6.8
2199.9	141.7	157.9	157.3	125.0	160.9	148.6	15.2	6.8
2220.2	144.0	160.0	158.5	124.0	160.9	149.5	15.8	6.7
2240.0	146.3	162.2	159.9	123.2	161.1	150.5	16.6	6.7

2259.8	148.0	164.9	161.4	122.2	161.0	151.5	17.6	6.7
2280.0	150.8	168.0	163.7	121.4	160.8	152.9	18.7	6.7
2299.9	153.5	171.7	166.0	120.5	160.7	154.5	20.1	6.7
2320.1	156.6	175.3	168.9	119.8	160.6	156.3	21.6	6.7
2339.9	159.1	178.7	172.1	119.4	160.6	158.0	23.0	6.8
2360.2	160.6	180.8	175.1	118.7	160.6	159.2	24.3	6.7
2380.0	161.2	183.1	178.2	118.2	160.6	160.3	25.6	6.7
2399.8	161.2	183.4	180.1	117.5	160.8	160.6	26.3	6.7
2420.0	161.5	182.8	181.5	116.4	160.8	160.6	26.9	6.6
2439.9	161.5	181.9	182.3	115.5	160.5	160.3	27.2	6.6
2460.1	161.8	180.0	181.9	114.3	160.0	159.6	27.2	6.5
2479.9	161.8	178.7	181.4	113.5	159.4	159.0	27.2	6.4
2500.2	161.5	176.5	179.9	112.6	158.7	157.8	26.9	6.3
2520.0	161.2	174.3	178.3	112.1	157.9	156.8	26.4	6.2
2539.8	160.6	171.8	176.5	111.5	157.2	155.5	25.9	6.1
2560.0	160.4	170.0	174.7	110.5	156.3	154.4	25.6	6.0
2579.9	160.2	168.3	173.1	109.5	155.6	153.3	25.4	5.9
2600.1	159.7	166.7	171.5	108.4	155.0	152.3	25.3	5.9
2619.9	158.7	164.9	169.4	107.7	154.6	151.0	24.9	5.8
2640.2	157.8	163.2	167.8	107.1	154.2	150.0	24.6	5.7
2660.0	157.5	161.7	166.0	107.4	153.4	149.2	23.8	5.6
2679.8	156.8	160.4	164.2	108.0	152.7	148.4	23.0	5.5
2700.0	155.7	159.7	162.8	108.3	151.6	147.6	22.4	5.5
2719.9	154.3	158.7	161.1	108.6	150.4	146.6	21.7	5.4
2740.1	152.5	158.2	160.2	108.4	149.1	145.7	21.3	5.3
2759.9	150.9	157.1	158.9	108.6	147.8	144.7	20.7	5.2
2780.2	149.3	156.5	157.9	108.5	147.3	143.9	20.3	5.2
2800.0	147.7	155.8	156.9	109.2	146.9	143.3	19.6	5.1
2819.8	145.5	154.5	155.8	109.7	146.5	142.4	18.9	5.1
2840.0	143.6	153.0	154.9	109.7	146.5	141.5	18.4	5.0
2859.9	141.9	151.2	153.8	110.8	146.2	140.8	17.4	4.9
2880.1	140.5	149.6	152.6	111.8	146.1	140.1	16.4	4.9
2899.9	139.1	148.3	151.7	113.1	145.5	139.5	15.5	4.8
2920.2	137.7	146.8	150.5	114.3	145.1	138.9	14.5	4.8
2940.0	136.4	145.2	149.3	116.2	145.0	138.4	13.3	4.7
2959.8	135.0	143.7	148.4	118.4	144.8	138.0	12.0	4.7
2980.0	133.9	142.5	147.7	120.3	144.2	137.7	11.0	4.6
2999.9	132.7	141.3	146.7	122.8	144.4	137.6	9.8	4.6

Data for sensor pair on clay;

Frequency	22-Dec-04	22-Dec-05	22-Dec-06	22-Dec-03	23-Dec-01	Average	StdDev	Wavelength
199.9	53.7	52.0	52.6	62.2	62.6	56.6	5.3	28.3
220.1	51.8	50.4	51.0	56.7	53.3	52.7	2.5	23.9
239.9	42.2	42.0	42.2	46.8	48.6	44.4	3.1	18.5
260.2	52.5	51.5	51.9	52.2	46.7	51.0	2.4	19.6
280.0	59.5	57.9	59.1	57.6	62.1	59.3	1.8	21.2

299.8	60.0	60.7	61.5	63.4	59.7	61.0	1.5	20.4
320.1	60.6	59.8	60.6	65.1	65.7	62.3	2.8	19.5
339.9	55.2	55.6	56.8	60.6	72.3	60.1	7.1	17.7
360.1	51.3	51.9	52.8	57.8	67.4	56.2	6.8	15.6
379.9	52.0	53.1	53.8	62.9	58.7	56.1	4.6	14.8
400.2	55.8	57.5	57.3	65.8	63.5	60.0	4.4	15.0
420.0	63.5	64.7	64.3	68.9	58.3	64.0	3.8	15.2
439.8	70.9	71.9	71.6	75.5	59.6	69.9	6.0	15.9
460.1	67.7	69.4	69.4	75.6	65.5	69.5	3.7	15.1
479.9	61.7	63.8	64.6	71.2	65.4	65.3	3.5	13.6
500.1	59.4	61.2	61.8	70.6	61.7	62.9	4.4	12.6
519.9	59.8	61.9	62.0	71.2	56.2	62.2	5.5	12.0
540.2	61.6	64.5	64.8	71.5	53.8	63.3	6.4	11.7
560.0	61.1	63.8	64.2	69.1	58.9	63.4	3.8	11.3
579.8	59.7	63.0	63.8	66.8	62.0	63.1	2.6	10.9
600.1	61.4	64.8	66.1	65.2	61.4	63.8	2.2	10.6
619.9	62.7	66.2	67.2	65.0	60.4	64.3	2.7	10.4
640.1	61.1	64.2	65.3	66.2	60.1	63.4	2.7	9.9
659.9	58.0	60.9	61.7	66.6	58.3	61.1	3.5	9.3
680.2	55.2	58.0	58.8	66.3	53.0	58.3	5.0	8.6
700.0	53.0	55.7	56.4	65.9	49.0	56.0	6.2	8.0
719.8	51.1	53.6	54.4	65.0	47.6	54.3	6.5	7.5
740.1	50.1	52.8	53.6	63.8	46.8	53.4	6.4	7.2
759.9	50.5	53.5	54.5	62.8	45.9	53.4	6.2	7.0
780.1	51.7	54.9	56.3	62.9	45.5	54.3	6.4	7.0
799.9	52.4	55.5	57.0	63.0	46.4	54.9	6.1	6.9
820.2	52.5	55.1	56.5	62.1	46.5	54.5	5.7	6.6
840.0	52.4	54.4	55.8	60.9	45.0	53.7	5.8	6.4
859.8	52.4	54.0	55.2	60.1	43.9	53.1	5.9	6.2
880.1	52.3	53.4	54.5	60.2	43.9	52.9	5.9	6.0
899.9	52.0	52.8	53.7	60.5	45.1	52.8	5.5	5.9
920.1	52.0	52.5	53.3	60.8	47.5	53.2	4.8	5.8
939.9	52.5	52.9	53.6	60.9	49.6	53.9	4.2	5.7
960.2	53.4	53.6	54.5	60.9	51.5	54.8	3.6	5.7
980.0	54.2	54.4	55.2	60.9	52.9	55.5	3.1	5.7
999.8	54.9	55.0	55.8	61.4	53.6	56.1	3.0	5.6
1020.1	55.7	55.6	56.6	61.9	54.1	56.8	3.0	5.6
1039.9	56.5	56.1	57.0	62.2	55.1	57.4	2.8	5.5
1060.1	57.2	56.7	57.6	62.4	56.5	58.1	2.4	5.5
1079.9	57.8	57.2	57.9	62.5	58.2	58.7	2.1	5.4
1100.2	58.0	57.4	58.1	62.6	60.0	59.2	2.1	5.4
1120.0	58.0	57.4	58.1	62.7	63.2	59.9	2.8	5.3
1139.8	57.9	57.4	58.0	62.8	64.2	60.0	3.2	5.3
1160.0	57.7	57.3	57.9	63.0	63.7	59.9	3.1	5.2
1179.9	57.6	57.3	57.9	63.4	62.3	59.7	2.9	5.1
1200.1	57.6	57.6	58.0	63.6	60.6	59.5	2.6	5.0
1219.9	57.8	58.0	58.4	63.6	59.2	59.4	2.4	4.9
1240.2	58.3	58.4	58.7	63.9	57.5	59.3	2.6	4.8
1260.0	58.5	58.8	59.1	64.1	55.8	59.3	3.0	4.7
1279.8	58.7	59.4	59.6	64.3	54.3	59.2	3.6	4.6

1300.0	59.0	60.0	60.3	64.3	53.9	59.5	3.7	4.6
1319.9	59.4	60.7	61.2	64.1	54.3	59.9	3.6	4.5
1340.1	59.9	61.5	62.1	63.6	55.3	60.5	3.2	4.5
1359.9	60.4	62.2	62.9	62.9	56.2	60.9	2.8	4.5
1380.2	60.8	62.9	63.6	62.3	57.1	61.3	2.6	4.4
1400.0	61.1	63.3	64.1	61.9	57.8	61.6	2.5	4.4
1419.8	61.4	63.7	64.5	61.7	58.3	61.9	2.4	4.4
1440.0	61.7	64.1	64.9	61.8	58.9	62.3	2.3	4.3
1459.9	61.7	64.3	65.2	62.2	59.4	62.6	2.3	4.3
1480.1	61.6	64.3	65.3	62.7	59.9	62.8	2.2	4.2
1499.9	61.4	64.2	65.3	63.4	60.2	62.9	2.1	4.2
1520.2	61.2	64.1	65.2	64.0	60.4	63.0	2.1	4.1
1540.0	61.0	63.9	65.1	64.6	60.4	63.0	2.1	4.1
1559.8	61.1	63.8	64.9	64.9	60.4	63.0	2.2	4.0
1580.0	61.2	63.8	64.8	65.2	60.3	63.1	2.2	4.0
1599.9	61.2	63.9	64.7	65.3	60.3	63.1	2.2	3.9
1620.1	61.0	63.8	64.6	65.3	60.4	63.0	2.2	3.9
1639.9	60.7	63.6	64.5	65.2	60.5	62.9	2.2	3.8
1660.2	60.3	63.2	64.4	65.1	60.9	62.8	2.1	3.8
1680.0	60.0	62.8	64.2	65.0	61.2	62.6	2.1	3.7
1699.8	59.8	62.5	63.9	64.8	61.6	62.5	2.0	3.7
1720.0	59.8	62.3	63.5	64.7	62.0	62.5	1.9	3.6
1739.9	59.8	62.2	63.2	64.5	62.3	62.4	1.7	3.6
1760.1	59.8	62.1	62.9	64.3	62.6	62.3	1.6	3.5
1779.9	59.8	62.0	62.7	64.0	62.8	62.3	1.6	3.5
1800.2	59.7	61.8	62.5	63.7	63.2	62.2	1.5	3.5
1820.0	59.7	61.6	62.4	63.4	63.4	62.1	1.6	3.4
1839.8	59.7	61.5	62.4	63.1	63.6	62.0	1.6	3.4
1860.0	59.7	61.3	62.3	62.7	63.9	62.0	1.6	3.3
1879.9	59.8	61.2	62.2	62.4	64.1	62.0	1.6	3.3
1900.1	60.0	61.2	62.2	62.1	64.4	61.9	1.6	3.3
1919.9	60.2	61.3	62.1	61.8	64.7	62.0	1.7	3.2
1940.2	60.4	61.4	62.1	61.6	65.2	62.1	1.8	3.2
1960.0	60.7	61.5	62.2	61.5	65.6	62.3	1.9	3.2
1979.8	61.0	61.7	62.2	61.5	66.1	62.5	2.1	3.2
2000.0	61.3	61.9	62.2	61.6	66.6	62.7	2.2	3.1
2019.9	61.5	62.1	62.3	61.8	67.1	63.0	2.3	3.1
2040.1	61.7	62.2	62.5	61.9	67.5	63.2	2.4	3.1
2059.9	61.9	62.4	62.6	62.2	67.9	63.4	2.5	3.1
2080.2	62.1	62.5	62.8	62.4	68.4	63.6	2.7	3.1
2100.0	62.3	62.7	63.0	62.6	68.8	63.9	2.8	3.0
2119.8	62.4	62.8	63.2	62.9	69.3	64.1	2.9	3.0
2140.0	62.6	63.0	63.4	63.0	69.8	64.4	3.0	3.0
2159.9	62.8	63.2	63.6	63.2	70.3	64.6	3.2	3.0
2180.1	63.0	63.4	63.8	63.3	70.8	64.9	3.3	3.0
2199.9	63.2	63.7	64.1	63.4	71.3	65.1	3.5	3.0
2220.2	63.3	63.9	64.3	63.4	71.8	65.3	3.6	2.9
2240.0	63.5	64.1	64.6	63.4	72.2	65.6	3.8	2.9
2259.8	63.6	64.3	64.8	63.5	72.6	65.8	3.9	2.9
2280.0	63.7	64.5	65.0	63.5	72.9	65.9	4.0	2.9

2299.9	63.8	64.7	65.3	63.6	73.2	66.1	4.0	2.9
2320.1	63.8	64.8	65.5	63.6	73.3	66.2	4.1	2.9
2339.9	63.9	65.0	65.6	63.6	73.4	66.3	4.0	2.8
2360.2	63.9	65.1	65.8	63.5	73.3	66.3	4.0	2.8
2380.0	63.9	65.1	65.9	63.5	73.1	66.3	3.9	2.8
2399.8	63.9	65.2	66.0	63.4	72.9	66.3	3.8	2.8
2420.0	63.8	65.2	66.1	63.4	72.6	66.2	3.7	2.7
2439.9	63.8	65.2	66.2	63.6	72.3	66.2	3.6	2.7
2460.1	63.7	65.2	66.2	63.8	72.0	66.2	3.4	2.7
2479.9	63.6	65.2	66.2	64.0	71.7	66.1	3.3	2.7
2500.2	63.6	65.2	66.2	64.2	71.3	66.1	3.1	2.6
2520.0	63.5	65.2	66.2	64.4	70.9	66.0	2.9	2.6
2539.8	63.4	65.1	66.1	64.6	70.5	66.0	2.7	2.6
2560.0	63.3	65.1	66.1	64.8	70.1	65.9	2.6	2.6
2579.9	63.2	65.1	66.1	65.0	69.8	65.8	2.4	2.6
2600.1	63.1	65.0	66.1	65.2	69.4	65.7	2.3	2.5
2619.9	63.0	65.0	66.0	65.4	69.1	65.7	2.2	2.5
2640.2	63.0	64.9	66.0	65.7	68.7	65.7	2.1	2.5
2660.0	63.0	64.9	66.0	65.9	68.4	65.6	1.9	2.5
2679.8	63.1	64.8	66.0	65.9	67.9	65.5	1.8	2.4
2700.0	63.1	64.7	66.0	65.9	67.5	65.4	1.6	2.4
2719.9	63.0	64.6	66.0	66.1	67.1	65.4	1.6	2.4
2740.1	63.0	64.5	65.9	66.3	66.8	65.3	1.5	2.4
2759.9	63.0	64.5	65.9	66.5	66.5	65.3	1.5	2.4
2780.2	62.9	64.5	65.9	66.8	66.2	65.3	1.6	2.3
2800.0	62.9	64.6	65.9	67.0	66.0	65.3	1.6	2.3
2819.8	63.0	64.6	66.0	67.3	65.9	65.3	1.6	2.3
2840.0	63.0	64.7	66.0	67.5	65.8	65.4	1.7	2.3
2859.9	63.1	64.8	66.0	67.8	65.7	65.5	1.7	2.3
2880.1	63.2	64.8	66.1	68.0	65.6	65.5	1.7	2.3
2899.9	63.3	64.9	66.1	68.2	65.5	65.6	1.8	2.3
2920.2	63.3	64.9	66.2	68.4	65.5	65.6	1.8	2.2
2940.0	63.4	64.9	66.2	68.5	65.4	65.7	1.9	2.2
2959.8	63.4	64.9	66.2	68.6	65.4	65.7	1.9	2.2
2980.0	63.4	64.9	66.3	68.6	65.6	65.7	1.9	2.2
2999.9	63.4	64.9	66.3	68.6	65.7	65.8	1.9	2.2

Appendix B

B(1). Matlab script for run the test using step frequency;

```
% AzimanCompactDAQmxSteppedFrequency
% Matlab interface script to communicate with a NI 9172 chassis populated
with a 9263 signal source
% and multiple 9239 4-channel A/Ds
% Step through the frequencies

% Warning: the transpose function ' is actually the complex conjugate
transpose!

% Status is int32 value error code returned by the function in the event
of an error or warning.
% A value of 0 indicates success.   A positive value indicates a warning.
A negative value indicates an error.

clear all
%clear global
count=0;
NumberOfRXChannels = 4; % Define the number of RX channels being used
NumberOfTXChannels = 1; % Define the number of TX channels being used
InputSamplesPerChannel = 2^17; % Samples to be collected per channel
OutputSamplesPerChannel = 2^17; % Samples to be output per channel
BufferSize = InputSamplesPerChannel;
InputSamplingRate = double(50000);% Input Sampling rate
OutputSamplingRate = double(50000); % Output Sampling rate - normally the
same
ZeroPaddingTime = 0.00; % Zero pad transmission signal to there is a
dead-time to allow for signal to be received and processed without
aliasses
StartingFrequency =100; % sweep from 0Hz to one third of the available
bandwidth
StepFrequency =10;
StopFrequency =3000;
SensorSpacing = 0.03; % accelerometer spacing (assume uniform) in meter
Vmax = 9.99;

NumOfPhaseRotation=1;
EstimatedVelocity=50;

LoopThroughTest = 0; % Test delay from transmit to receive
CrossSpectrumMeasurements = 1;% Collect data for velocity/phase coherence
measurements

NumberOfSnapshots =5; % Number of data collection operations to measure
real data

PassBandFraction = 0.50; % A/D converter passband as a ratio of the
sampling frequency
Bandwidth = OutputSamplingRate*PassBandFraction; % Bandwidth of
transmission signal

% Add experiment information here
```

```
Comment1 = 'One current measuring channel and four accelerometer. Order
from Department: REF,Chan1,Chan2...Chan4';
Comment2 = 'Chan0 measures voltage across 10 0hm resistor, Chans 1 - 4
measure voltage from accelerometers';
Comment3 = 'Add specific comments here';

% Check out valid sampling rate
ValidSamplingRates = 50e3./(1:31); % Search for best fit of sampling rate
[ActualInputSamplingRate ActualInputSamplingRateIndex] =
min(abs(InputSamplingRate-ValidSamplingRates));
ActualInputSamplingRate =
ValidSamplingRates(ActualInputSamplingRateIndex);
if ActualInputSamplingRate~=InputSamplingRate,
    fprintf('Program input sampling rate replaced with actual sampling
rate of %f Hz\n',ActualInputSamplingRate);
    InputSamplingRate = ActualInputSamplingRate;
end
[ActualOutputSamplingRate ActualOutputSamplingRateIndex] =
min(abs(OutputSamplingRate-ValidSamplingRates));
ActualOutputSamplingRate =
ValidSamplingRates(ActualOutputSamplingRateIndex);
if ActualOutputSamplingRate~=OutputSamplingRate,
    fprintf('Program output sampling rate replaced with actual sampling
rate of %f Hz\n',ActualOutputSamplingRate);
    OutputSamplingRate = ActualOutputSamplingRate;
end

fprintf('Observation period = %f
s\n',InputSamplesPerChannel/ActualOutputSamplingRate);


% Predicted input A/D channel latency
PredictedInputLatency = 38.4/InputSamplingRate + 3e-6; % latency measured
in seconds

% Predict output D/A latency
OutputLatency = [3e-6 5e-6 7.5e-6 9.5e-6];
PredictedOutputLatency = OutputLatency(NumberOfTXChannels);

% Measurements imply an extra few samples of delay
AdditionalDelaySamples = 2;
TotalPredictedLatency = PredictedOutputLatency + PredictedInputLatency +
AdditionalDelaySamples/InputSamplingRate + 1.8e-6;

% The IDAQmx DLL functions appear to exist in 'nicaiu.dll'
if ~libisloaded('nicaiu') % checks if library is loaded
    %hfile  =  'C:\Program Files\National Instruments\NI-DAQ\DAQmx ANSI C
Dev\include\NIDAQmx.h';
    %hfile  =  'C:\\Program Files\\National Instruments\\NI-DAQ\\DAQmx
ANSI C Dev\\include\\NIDAQmx.h';
    hfile  =  'NIDAQmx.h';
    [notfound,warnings] = loadlibrary('nicaiu.dll', hfile, 'mfilename',
'mxproto');
    % mxproto contains the function prototypes
end

%% required constants (see NIDAQmx.h)
```

```
% Terminal Configuration
DAQmx_Val_Cfg_Default = int32(-1);              % Default
DAQmx_Val_RSE = int32(10083);                  % RSE
DAQmx_Val_NRSE = int32(10078);                 % NRSE
DAQmx_Val_Diff = int32(10106);                 % Differential
DAQmx_Val_PseudoDiff = int32(12529);           % Pseudodifferential
                                               % Units
DAQmx_Val_Volts = int32(10348);                % Volts
DAQmx_Val_FromCustomScale = int32(10065);      % From Custom Scale
                                               % Active Edge
DAQmx_Val_Rising = int32(10280);               % Rising
DAQmx_Val_Falling = int32(10171);              % Falling
                                               % Sample Mode
DAQmx_Val_FiniteSamps = int32(10178);          % Finite Samples
DAQmx_Val_ContSamps = int32(10123);            % Continuous Samples
DAQmx_Val_HWTimedSinglePoint = int32(12522);   % Hardware Timed Single
Point
                                               % Fill Mode
DAQmx_Val_GroupByChannel = uint32(0);          % Group by Channel
DAQmx_Val_GroupByScanNumber = uint32(1);       % Group by Scan Number
                                                    % Device ID
DAQmx_Val_CompactDAQChassis = uint32(14658);   % CompactDAQ chassis


%% Try getting names of NI cards
DeviceNames = libpointer('stringPtr',blanks(60));
[Status, DeviceNames] =
calllib('nicaiu','DAQmxGetSysDevNames',DeviceNames,uint32(60));
%DAQmxGetSysDevNames(char *data, uInt32 bufferSize);
if isempty(DeviceNames),
    fprintf('No NI DAQ devices found\n');
    unloadlibrary 'nicaiu';                % unload library
    return
end
% There may be multiple device in a comma-separated list
CommaSeparatedVariableCell = textscan(DeviceNames, '%s', 'delimiter',
',');     % Convert to a list of CSV names
% Process each name in-turn
IndividualDeviceNameList = cell(numel(CommaSeparatedVariableCell{1}),1);
for DeviceNameIndex = 1:numel(CommaSeparatedVariableCell{1}),
    IndividualDeviceName =
char(CommaSeparatedVariableCell{1}(DeviceNameIndex));
    fprintf('Device Name = %s    ',IndividualDeviceName);
    ProductType = libpointer('stringPtr',blanks(60));
    [Status,IndividualDeviceName,ProductType] =
calllib('nicaiu','DAQmxGetDevProductType',IndividualDeviceName,ProductTyp
e,uint32(60));
    %int32 DAQmxGetDevProductType(const char device[], char *data, uInt32
bufferSize);
    IndividualDeviceNameList{DeviceNameIndex,1} = char(ProductType);
    fprintf('Product Type = %s\n',ProductType);
end

% Check if required chassis exists in list
DeviceComparison = strcmp(IndividualDeviceNameList,'cDAQ-9172');
if sum(DeviceComparison) == 0,
    fprintf('cDAQ-9172 compact device chassis not found\n');
    unloadlibrary 'nicaiu';                % unload library
```

```
    return
end
% Recover device name of chassis
IndividualChassisName =
char(CommaSeparatedVariableCell{1}(DeviceComparison));

% Check if required input modules exists in list
DeviceComparison = strcmp(IndividualDeviceNameList,'NI 9239');
if sum(DeviceComparison) == 0,
    fprintf('No NI 9239 A/D modules found\n');
    unloadlibrary 'nicaiu';                % unload library
    return
end
% Recover device name of A/D modules
IndividualADNames =
char(CommaSeparatedVariableCell{1}(DeviceComparison));

% Check if required output modules exists in list
DeviceComparison = strcmp(IndividualDeviceNameList,'NI 9263');
if sum(DeviceComparison) == 0,
    fprintf('No NI 9263 D/A modules found\n');
    unloadlibrary 'nicaiu';                % unload library
    return
end
% Recover device name of D/A modules
IndividualDANames =
char(CommaSeparatedVariableCell{1}(DeviceComparison));
%% Determine which input channels are available in device - there may be
multiple modules
for ModuleIndex = 1:size(IndividualADNames,1),
    PhysicalChannels = libpointer('stringPtr',blanks(200));
    [Status,IndividualDeviceName,PhysicalChannels] =
calllib('nicaiu','DAQmxGetDevAIPhysicalChans',IndividualADNames(ModuleInd
ex,:),PhysicalChannels,uint32(200));
    %int32  DAQmxGetDevAIPhysicalChans(const char device[], char *data,
uInt32 bufferSize);
    if Status ~= 0,
        fprintf('Error in DAQmxGetDevAIPhysicalChans.   Status =
%d\n',Status);
        return
    end

    % There may be multiple physical channels in a comma-separated list
    CommaSeparatedVariableCell = textscan(PhysicalChannels, '%s',
'delimiter', ',');     % Convert to a list of CSV names
    % Convert to a full list
    if ModuleIndex == 1,
        IndividualPhysicalChannelName =
cell(numel(CommaSeparatedVariableCell{1}),size(IndividualADNames,1));
    end
    for PhysicalChannelIndex = 1:numel(CommaSeparatedVariableCell{1}),
        IndividualPhysicalChannelName{PhysicalChannelIndex,ModuleIndex} =
char(CommaSeparatedVariableCell{1}(PhysicalChannelIndex));
    end
end

%% Analogue Input configuration string generation
% Make a single string determined by the 'NumberOfRXChannels' requested
```

```
if NumberOfRXChannels > numel(IndividualPhysicalChannelName),
    fprintf('Request number of A/D channels exceeds the number
available\n');
    return
end

% Assume A/D modules are obtained in groups of four
CompleteADModules = floor((NumberOfRXChannels-1)/4);        % e.g.
0,0,0,0,1,1,1,1,2,2,2,2,3,3,3,3
PartialADChannels = mod((NumberOfRXChannels-1),4);          % e.g.
1,2,3,4,1,2,3,4,1,2,3,4,1,2,3,4
if NumberOfRXChannels == 1,
    % single channel
    AIConfigString ={IndividualPhysicalChannelName{1,1}};
else
    % multiple channels
    AIConfigString = '';
    if CompleteADModules >= 1,
        for ModulesIndex = 1:CompleteADModules,
            % Complete group of four channels
            AIConfigString =
strcat(AIConfigString,cellstr([IndividualPhysicalChannelName{1,ModulesInd
ex} ':' IndividualPhysicalChannelName{4,ModulesIndex}]),',');
        end
    end
    % Add in last group
    if PartialADChannels == 0,
        AIConfigString =
strcat(AIConfigString,{IndividualPhysicalChannelName{1,CompleteADModules+
1}},',');
    else
        AIConfigString =
strcat(AIConfigString,cellstr([IndividualPhysicalChannelName{1,CompleteAD
Modules+1} ':'
IndividualPhysicalChannelName{PartialADChannels+1,CompleteADModules+1}]))
;
    end
end
AIConfigString = char(AIConfigString);
fprintf('A/D Configuration String = %s\n',AIConfigString);

%% Determine which output channels are available in device - there may be
multiple modules
for ModuleIndex = 1:size(IndividualDANames,1),
    PhysicalChannels = libpointer('stringPtr',blanks(200));
    [Status,IndividualDeviceName,PhysicalChannels] =
calllib('nicaiu','DAQmxGetDevAOPhysicalChans',IndividualDANames(ModuleInd
ex,:),PhysicalChannels,uint32(200));
    %int32  DAQmxGetDevAIPhysicalChans(const char device[], char *data,
uInt32 bufferSize);
    if Status ~= 0,
        fprintf('Error in DAQmxGetDevAOPhysicalChans.   Status =
%d\n',Status);
        return
    end

    % There may be multiple physical channels in a comma-separated list
```

```
    CommaSeparatedVariableCell = textscan(PhysicalChannels, '%s',
'delimiter', ',');     % Convert to a list of CSV names
    % Convert to a full list
    if ModuleIndex == 1,
        IndividualPhysicalChannelName =
cell(numel(CommaSeparatedVariableCell{1}),size(IndividualDANames,1));
    end
    for PhysicalChannelIndex = 1:numel(CommaSeparatedVariableCell{1}),
        IndividualPhysicalChannelName{PhysicalChannelIndex,ModuleIndex} =
char(CommaSeparatedVariableCell{1}(PhysicalChannelIndex));
    end
end
% Re-arrange into a single row vector
IndividualPhysicalChannelName =
reshape(IndividualPhysicalChannelName,[],1);

%% Analogue Output configuration string generation
% Make a single string determined by the 'NumberOfTXChannels' requested
if NumberOfTXChannels > numel(IndividualPhysicalChannelName),
    fprintf('Request number of D/a channels exceeds the number
available\n');
    return
end

% Assume D/A modules are obtained in groups of four
CompleteDAModules = floor((NumberOfTXChannels-1)/4);        % e.g.
0,0,0,0,1,1,1,1,2,2,2,2,3,3,3,3
PartialDAChannels = mod((NumberOfTXChannels-1),4);          % e.g.
1,2,3,4,1,2,3,4,1,2,3,4,1,2,3,4
if NumberOfTXChannels == 1,
    % single channel
    AOConfigString ={IndividualPhysicalChannelName{1,1}};
else
    % multiple channels
    AOConfigString = '';
    if CompleteDAModules >= 1,
        for ModulesIndex = 1:CompleteDAModules,
            % Complete group of four channels
            AOConfigString =
strcat(AOConfigString,cellstr([IndividualPhysicalChannelName{1,ModulesInd
ex} ':' IndividualPhysicalChannelName{4,ModulesIndex}]),',');
        end
    end
    % Add in last group
    if PartialDAChannels == 0,
        AOConfigString =
strcat(AOConfigString,{IndividualPhysicalChannelName{1,CompleteDAModules+
1}},',');
    else
        AOConfigString =
strcat(AOConfigString,cellstr([IndividualPhysicalChannelName{1,CompleteDA
Modules+1} ':'
IndividualPhysicalChannelName{PartialDAChannels+1,CompleteDAModules+1}]))
;
    end
end
AOConfigString = char(AOConfigString);
fprintf('D/A Configuration String = %s\n',AOConfigString);
```

```
%% Create new tasks
TaskHandle1 = libpointer('uint32Ptr',0);        % VOID task handle
pointers
TaskHandle2 = libpointer('uint32Ptr',0);
InputTaskName = 'AITask';
OutputTaskName = 'AOTask';
[Status,TaskNameText,TaskHandle1]  =
calllib('nicaiu','DAQmxCreateTask',InputTaskName,TaskHandle1);     %
Create a NIDAQmx Task TaskHandle1
% int32 DAQmxCreateTask (const char taskName[], TaskHandle, *taskHandle);
if Status ~= 0,
    fprintf('Error in DAQmxCreateTask - Input Task.   Status =
%d\n',Status);
    return
end
TaskHandle1Numeric = TaskHandle1;
TaskHandle1 = libpointer('uint32Ptr',TaskHandle1);

[Status,TaskNameText,TaskHandle2]  =
calllib('nicaiu','DAQmxCreateTask',OutputTaskName,TaskHandle2);     %
Create a NIDAQmx Task TaskHandle2
% int32 DAQmxCreateTask (const char taskName[], TaskHandle, *taskHandle);
if Status ~= 0,
    fprintf('Error in DAQmxCreateTask - Output Task.   Status =
%d\n',Status);
    return
end
TaskHandle2Numeric = TaskHandle2;
TaskHandle2 = libpointer('uint32Ptr',TaskHandle2);

% Generate a D/A output channels and A/D input channel to be referred to
% later
minVal = double(-10);
maxVal = double(10);

% Generate a D/A output channel
[Status,ChannelNameText,c,d]  =
calllib('nicaiu','DAQmxCreateAOVoltageChan',TaskHandle2Numeric,AOConfigSt
ring,'',minVal,maxVal,DAQmx_Val_Volts,'');
% int32 DAQmxCreateAOVoltageChan (TaskHandle taskHandle, const char
physicalChannel[], const char nameToAssignToChannel[], float64 minVal,
float64 maxVal, int32 units, const char customScaleName[]);
if Status ~= 0,
    fprintf('Error in DAQmxCreateAOVoltageChan.   Status = %d\n',Status);
    return
end

[Status,ChannelNameText,c,d]  =
calllib('nicaiu','DAQmxCreateAIVoltageChan',TaskHandle1Numeric,AIConfigSt
ring,'',DAQmx_Val_Diff,minVal,maxVal,DAQmx_Val_Volts,'');
% int32 DAQmxCreateAIVoltageChan (TaskHandle taskHandle, const char
physicalChannel[], const char nameToAssignToChannel[],
% int32 terminalConfig, float64 minVal, float64 maxVal, int32 units,
const char customScaleName[]);
if Status ~= 0,
    fprintf('Error in DAQmxCreateAIVoltageChan.   Status = %d\n',Status);
    return
```

```
end


%%
% Set up the on-board timing with internal clock source
ActiveEdge = DAQmx_Val_Rising;          % Samplig edge
SampleMode = DAQmx_Val_FiniteSamps;     % Collect a finite number of
samples
%SampleMode = DAQmx_Val_ContSamps;       % Collect samples continuously
%SamplesToAcquire = uint64(InputSamplesPerChannel*NumberOfRXChannels);
% Make buffer size large - several times expected window size
SamplesToAcquire = uint64(BufferSize);
[Status,ClockSource] =
calllib('nicaiu','DAQmxCfgSampClkTiming',TaskHandle1Numeric,'OnboardClock
',InputSamplingRate,ActiveEdge,SampleMode,SamplesToAcquire);
% int32 DAQmxCfgSampClkTiming (TaskHandle taskHandle, const char
source[],float64 rate, int32 ActiveEdge, int32 SampleMode, uInt64
% sampsPerChanToAcquire);
if Status ~= 0,
    fprintf('Error in DAQmxCfgSampClkTiming for TaskHandle1   Status =
%d\n',Status);
    Status = calllib('nicaiu','DAQmxClearTask',TaskHandle1);           %
Clear the task
    return
end


TerminalName = 'ai/StartTrigger';

%  Define the parameters for a digital edge start trigger for output.
Set the analog output to trigger off the AI start trigger. This is an
internal trigger signal.
[Status,a] =
calllib('nicaiu','DAQmxCfgDigEdgeStartTrig',TaskHandle2Numeric,TerminalNa
me,DAQmx_Val_Rising);
% [int32] DAQmxCfgDigEdgeStartTrig (TaskHandle taskHandle, const char
triggerSource[], int32 triggerEdge);
if Status ~= 0,
    fprintf('Error in DAQmxCfgDigEdgeStartTrig.   Status = %d\n',Status);
    Status = calllib('nicaiu','DAQmxClearTask',TaskHandle2Numeric);
% Clear the task
    return
end

%% Make an LFM transmission signal
ZeroPaddingPoints = round(OutputSamplingRate.*ZeroPaddingTime);     %
This is the number of zeros to be added after the transmission has
finished
ActiveTXPoints = OutputSamplesPerChannel - ZeroPaddingPoints;       %
This is the number of samples within the active region of the TX signal
% Weight received signals with a suitable window
WeightingFunction = tukeywin(ActiveTXPoints,0.005)';  % Tukey Window

% Make a single chirp signal for transmission
% Make a complex chirp signal - zero padded
TXSignal = zeros(1,OutputSamplesPerChannel);
TXTimeIndex = 0:ActiveTXPoints-1;
```

```
%TXSignal(1,1:ActiveTXPoints) =
exp(j.*(StartingFrequency*2*pi*TXTimeIndex/OutputSamplingRate +
Bandwidth*2*pi*TXTimeIndex.^2./(2*ActiveTXPoints*OutputSamplingRate)));
FixedFrequency = 500;
TXSignal(1,1:ActiveTXPoints) =
exp(j.*(FixedFrequency*2*pi*TXTimeIndex/OutputSamplingRate));

% scale result
TXSignal(1:ActiveTXPoints) = Vmax .*
WeightingFunction.*TXSignal(1:ActiveTXPoints) / max(abs(TXSignal));
TXSignal('last') = 0;     % Last sample should be zero

% Make a one-sided spectral estimate of the complex TX signal - including
zero padding
DriveFFT2N = conj(fft(TXSignal,2*InputSamplesPerChannel) ./
InputSamplesPerChannel);

% If the signal was generated in a complex form then convert back to a
real number
if ~isreal(TXSignal),
    % Convert back to a real signal (start at zero voltage)
    TXSignal = -imag(TXSignal);
end

% Calculate the spectrum of the transmitted signal
TXSignalFFT = conj(fft(TXSignal));

% Time index for display purposes
TimeIndex = (0:(OutputSamplesPerChannel-1))/OutputSamplingRate;
% Frequency index for display purposes - assuming zero padded
FrequencyIndex = (0:(OutputSamplesPerChannel -
1)).*OutputSamplingRate./OutputSamplesPerChannel;

DisplayThis = 0;
if DisplayThis == 1,
    figure(1)
    plot(TimeIndex,real(TXSignal),'r')
    title('Transmitted waveform')
    xlabel('Time (s)')
    ylabel('Voltage (V)')
    figure(2)

plot(FrequencyIndex,20*log10(abs(fft(TXSignal)./OutputSamplesPerChannel))
);
    title('Spectrum of transmitted signal')
    xlabel('Frequency (Hz)')
    ylabel('Spectrum Level (dB)')
    xlim([0 OutputSamplingRate*PassBandFraction])
end
%%
% Make buffer size same as number of samples transmitted -
SamplesToTx = uint64(BufferSize);
[Status,ClockSource] =
calllib('nicaiu','DAQmxCfgSampClkTiming',TaskHandle2Numeric,'ai/SampleClo
ck',OutputSamplingRate,ActiveEdge,SampleMode,SamplesToTx);
if Status ~= 0,
```

```
    fprintf('Error in DAQmxCfgSampClkTiming for TaskHandle2.   Status =
%d\n',Status);
    Status = calllib('nicaiu','DAQmxClearTask',TaskHandle2Numeric);
% Clear the task
    return
end

%%
LoopThroughLatency = zeros(1,NumberOfRXChannels);
if LoopThroughTest == 1,
    %% Write samples to task
    SamplesPerChannelWritten = libpointer('int32Ptr',0);
    [Status,DAQmxWriteAnalogF64Return1,DAQmxWriteAnalogF64Return2] =
calllib('nicaiu','DAQmxWriteAnalogF64',TaskHandle2Numeric,int32(OutputSam
plesPerChannel),int32(0),double(-
1),DAQmx_Val_GroupByScanNumber,TXSignal,SamplesPerChannelWritten,[]);
    % int32 DAQmxWriteAnalogF64 (TaskHandle taskHandle, int32
numSampsPerChan, bool32 autoStart, float64 timeout, bool32 dataLayout,
float64 writeArray[], int32 *sampsPerChanWritten, bool32 *reserved);
    if Status ~= 0,
        fprintf('Error in DAQmxWriteAnalogF64.   Status = %d\n',Status);
        Status = calllib('nicaiu','DAQmxClearTask',TaskHandle1Numeric);
%#ok<NASGU> % Clear the tasks
        Status = calllib('nicaiu','DAQmxClearTask',TaskHandle2Numeric);
        return
    end
    % Perform loop-through latency check
    for InputSensorIndex = 1:NumberOfRXChannels,
        % Scan through each input channel
        % Prompt user to connect desired loop through
        fprintf('Testing input channel %d\n',InputSensorIndex-1)
        UserReply = input('Connect output to desired input channel and
press enter','s');
        % Collect data
        % Start the tasks - start output before input as the input task
would trigger the output task
        Status = calllib('nicaiu','DAQmxStartTask',TaskHandle2Numeric);
        % int32 DAQmxStartTask (TaskHandle taskHandle);
        if Status ~= 0,
            fprintf('Error in DAQmxStartTask.   Status = %d\n',Status);
            Status =
calllib('nicaiu','DAQmxClearTask',TaskHandle2Numeric);           % Clear
the task
            return
        end

        Status = calllib('nicaiu','DAQmxStartTask',TaskHandle1Numeric);
        % int32 DAQmxStartTask (TaskHandle taskHandle);
        if Status ~= 0,
            fprintf('Error in DAQmxStartTask.   Status = %d\n',Status);
            Status =
calllib('nicaiu','DAQmxClearTask',TaskHandle1Numeric);
%#ok<NASGU> % Clear the tasks
            Status =
calllib('nicaiu','DAQmxClearTask',TaskHandle2Numeric);
            return
        end
        %FillMode = DAQmx_Val_GroupByChannel;
```

```
        FillMode = DAQmx_Val_GroupByScanNumber;                     %
Interleaved samples
        RecoveredInputData =
zeros(InputSamplesPerChannel*NumberOfRXChannels,1);
        Timeout = double(-1);                    % maximum waiting time
before timeout (in secs)
        RecoveredInputDataPtr  =
libpointer('doublePtr',zeros(InputSamplesPerChannel*NumberOfRXChannels,1)
);
        ReadPtr = libpointer('int32Ptr',0);
        ReservedPtr = libpointer('uint32Ptr',[]);


[Status,RecoveredData,DAQmxReadAnalogF64Return1,DAQmxReadAnalogF64Return2
] =
calllib('nicaiu','DAQmxReadAnalogF64',TaskHandle1Numeric,int32(InputSampl
esPerChannel),Timeout,FillMode,RecoveredInputDataPtr,uint32(InputSamplesP
erChannel*NumberOfRXChannels),ReadPtr,ReservedPtr);
        % int32 DAQmxReadAnalogF64 (TaskHandle taskHandle, int32
numSampsPerChan, float64 timeout, bool32 fillMode, float64 readArray[],
uInt32 arraySizeInSamps,int32 *sampsPerChanRead, bool32 *reserved);
        if Status ~= 0,
            fprintf('Error in DAQmxReadAnalogF64.   Status =
%d\n',Status);
        end

        % Stop the tasks
        Status = calllib('nicaiu','DAQmxStopTask',TaskHandle1Numeric);
        % int32 DAQmxStopTask(uint32)
        % int32 DAQmxStopTask (TaskHandle taskHandle);
        if Status ~= 0,
            fprintf('Error/warning in DAQmxStopTask.   Status =
%d\n',Status);
        end
        Status = calllib('nicaiu','DAQmxStopTask',TaskHandle2Numeric);
        if Status ~= 0,
            fprintf('Error/warning in DAQmxStopTask.   Status =
%d\n',Status);
        end

        % If more than one A/D channel is used, then the sampes should be
separated
        RecoveredData =
reshape(RecoveredData,NumberOfRXChannels,InputSamplesPerChannel);



        figure(3)
        plot(TimeIndex,RecoveredData(InputSensorIndex,:))
        title('Raw Input Data')
        xlabel('Time (s)')
        ylabel('Voltage (V)')
        ylim([-1 1])

        RecoveredDataFFT =
fft(RecoveredData(InputSensorIndex,:),2*InputSamplesPerChannel);
        % Calculate the covariance
        RecoveredDataFFT(1) = 0;       % Remove any DC component
        DisplayThis = 1;
```

```
        if DisplayThis == 1,
            figure(4)
            PaddedFrequencyIndex = (0:(2*OutputSamplesPerChannel -
1)).*OutputSamplingRate/OutputSamplesPerChannel/2;
            plot(PaddedFrequencyIndex,20*log10(abs(DriveFFT2N)),'r')
            hold on
            plot(PaddedFrequencyIndex,20*log10(abs(RecoveredDataFFT) ./
InputSamplesPerChannel),'k');
            hold off
            legend('Drive Signal','Sense Signal',0)
            ylabel('Spectral Amplitude (dB)')
            xlabel('Frequency (Hz)')
            title('Linear Spectra of Transmit and Received Signals');
            xlim([0 InputSamplingRate*PassBandFraction]);
            drawnow
        end
        % Calculate the correlation function
        CrossSpectrum = RecoveredDataFFT .* DriveFFT2N;
        CrossCorrelation = ifft(CrossSpectrum);
        [maxval LoopThroughLatency(InputSensorIndex)] =
max(abs(CrossCorrelation));
        % Re-order data - swap frequency portions
        %CrossCorrelation =
[CrossCorrelation(NumberSamples+1:2*NumberSamples) ;
CrossCorrelation(1:NumberSamples)];
        figure(5)
        DisplayTimeIndex2N = (0:(2*InputSamplesPerChannel-
1))/InputSamplingRate;
        plot(DisplayTimeIndex2N,abs(CrossCorrelation),'k')
        title('Cross Correlation Function')
        ylabel('Magnitude')
        xlabel('Time (s)')
        %xlim([0 RXSamplingFrequency/(2*NumberRXChannels)])
        drawnow

        % select a small bit of the correlation output
        SegmentLength = 1000;
        SegmentCrossCorrelation = CrossCorrelation(1:SegmentLength);
        SegmentCrossCorrelation = abs(SegmentCrossCorrelation);
        SegmentTime = DisplayTimeIndex2N(1:SegmentLength);
        % Normalise correlation value
        SegmentCrossCorrelation = SegmentCrossCorrelation ./
max(SegmentCrossCorrelation);
        figure(6)
        plot(SegmentTime,SegmentCrossCorrelation,'k')
        title('Cross Correlation Function')
        ylabel('Magnitude')
        xlabel('Time (s)')

        % Plot the cross spectrum
        % First correct by the guess
        DisplayFrequencyIndex2N =
InputSamplingRate*(0:(2*InputSamplesPerChannel-
1))/(2*InputSamplesPerChannel);
        CompensationFunction =
exp(j*2*pi*DisplayFrequencyIndex2N*TotalPredictedLatency);
        CompensatedCrossSpectrum = CompensationFunction .* CrossSpectrum;
        figure(7)
```

```
plot(DisplayFrequencyIndex2N/1000,angle(CrossSpectrum),DisplayFrequencyIn
dex2N/1000,angle(CompensatedCrossSpectrum))
        title('Cross Spectrum Function')
        ylabel('Phase (rads)')
        xlabel('Frequency (kHz)')
        figure(8)
        plot(DisplayFrequencyIndex2N/1000,abs(CrossSpectrum))
        title('Cross Spectrum Function')
        ylabel('Magnitude)')
        xlabel('Frequency (kHz)')
        %xlim([0 RXSamplingFrequency/(2*NumberRXChannels)])
        drawnow

    end
    % Convert sample values into time
    LoopThroughLatencyTime = DisplayTimeIndex2N(LoopThroughLatency);
    fprintf('Measured Latency = %e secs \n',LoopThroughLatencyTime);
end


%% Normal data collection operation
if CrossSpectrumMeasurements == 1,
    % Prompt user to connect desired loop through
    UserReply = input('Connect output to desired input channel and press
enter','s');
    % Predict effects of D/A sampling zero-order-hold
    % Predicted amplitude & phase compensation value
    AmplitudeFunction = sinc(FrequencyIndex/OutputSamplingRate);
    CompensationFunction = AmplitudeFunction .*
exp(j*2*pi*FrequencyIndex*TotalPredictedLatency);
    % Modify predicted TX spectrum
    TXSignalFFT = TXSignalFFT .* AmplitudeFunction;
    %FillMode = DAQmx_Val_GroupByChannel;
    FillMode = DAQmx_Val_GroupByScanNumber;                    %
Interleaved samples


   %for SteppedFrequencyIndex =
StartingFrequency:StepFrequency:StartingFrequency,
   for SteppedFrequencyIndex =
StartingFrequency:StepFrequency:StopFrequency,

        CrossSpectrum = zeros(NumberOfRXChannels,InputSamplesPerChannel);
        PowerSpectrum = zeros(NumberOfRXChannels,InputSamplesPerChannel);

        % Generate a CW signal
        WeightingFunction = tukeywin(OutputSamplesPerChannel,0.005)';
% Tukey Window

        % Make a single CW signal for transmission
        TXSignal = zeros(1,OutputSamplesPerChannel);
        TXTimeIndex = 0:OutputSamplesPerChannel-1;

        TXSignal =
exp(j.*(SteppedFrequencyIndex*2*pi*TXTimeIndex/OutputSamplingRate));
```

```
        % scale result
        TXSignal = Vmax .* WeightingFunction.*TXSignal /
max(abs(TXSignal));
        TXSignal('last') = 0;     % Last sample should be zero

        % Make a one-sided spectral estimate of the complex TX signal -
including zero padding
        DriveFFT2N = conj(fft(TXSignal,2*InputSamplesPerChannel) ./
InputSamplesPerChannel);

        % If the signal was generated in a complex form then convert back
to a real number
        if ~isreal(TXSignal),
            % Convert back to a real signal (start at zero voltage)
            TXSignal = -imag(TXSignal);
        end

        % Calculate the spectrum of the transmitted signal
        TXSignalFFT = conj(fft(TXSignal));

        % Time index for display purposes
        TimeIndex = (0:(OutputSamplesPerChannel-1))/OutputSamplingRate;
        % Frequency index for display purposes - assuming zero padded
        FrequencyIndex = (0:(OutputSamplesPerChannel -
1)).*OutputSamplingRate./OutputSamplesPerChannel;

        DisplayThis = 1;
        if DisplayThis == 1,
            figure(1)
            plot(TimeIndex,real(TXSignal),'r')
            title('Transmitted waveform')
            xlabel('Time (s)')
            ylabel('Voltage (V)')
            figure(2)

plot(FrequencyIndex,20*log10(abs(fft(TXSignal)./OutputSamplesPerChannel))
);
            title('Spectrum of transmitted signal')
            xlabel('Frequency (Hz)')
            ylabel('Spectrum Level (dB)')
            xlim([0 OutputSamplingRate*PassBandFraction])
        end
        % Write samples to task
        SamplesPerChannelWritten = libpointer('int32Ptr',0);
        [Status,DAQmxWriteAnalogF64Return1,DAQmxWriteAnalogF64Return2] =
calllib('nicaiu','DAQmxWriteAnalogF64',TaskHandle2Numeric,int32(OutputSam
plesPerChannel),int32(0),double(-
1),DAQmx_Val_GroupByScanNumber,TXSignal,SamplesPerChannelWritten,[]);
        % int32 DAQmxWriteAnalogF64 (TaskHandle taskHandle, int32
numSampsPerChan, bool32 autoStart, float64 timeout, bool32 dataLayout,
float64 writeArray[], int32 *sampsPerChanWritten, bool32 *reserved);
        if Status ~= 0,
            fprintf('Error in DAQmxWriteAnalogF64.   Status =
%d\n',Status);
            Status =
calllib('nicaiu','DAQmxClearTask',TaskHandle1Numeric);
%#ok<NASGU> % Clear the tasks
```

```
            Status =
calllib('nicaiu','DAQmxClearTask',TaskHandle2Numeric);
            return
        end

        RecoveredInputData =
zeros(InputSamplesPerChannel*NumberOfRXChannels,1);
        Timeout = double(-1);                    % maximum waiting time
before timeout (in secs)
        RecoveredInputDataPtr  =
libpointer('doublePtr',zeros(InputSamplesPerChannel*NumberOfRXChannels,1)
);
        ReadPtr = libpointer('int32Ptr',0);
        ReservedPtr = libpointer('uint32Ptr',[]);

        InputSensorIndex = 1;       % Process for channel one - this can
be updated later
        for SnapShotNumber = 1:NumberOfSnapshots,
            fprintf('Snapshot number = %d\n',SnapShotNumber);
            % Start the tasks - start output before input as the input
task would trigger the output task
            Status =
calllib('nicaiu','DAQmxStartTask',TaskHandle2Numeric);
            % int32 DAQmxStartTask (TaskHandle taskHandle);
            if Status ~= 0,
                fprintf('Error in DAQmxStartTask.   Status =
%d\n',Status);
                Status =
calllib('nicaiu','DAQmxClearTask',TaskHandle2Numeric);           % Clear
the task
                return
            end

            Status =
calllib('nicaiu','DAQmxStartTask',TaskHandle1Numeric);
            % int32 DAQmxStartTask (TaskHandle taskHandle);
            if Status ~= 0,
                fprintf('Error in DAQmxStartTask.   Status =
%d\n',Status);
                Status =
calllib('nicaiu','DAQmxClearTask',TaskHandle1Numeric);
%#ok<NASGU> % Clear the tasks
                Status =
calllib('nicaiu','DAQmxClearTask',TaskHandle2Numeric);
                return
            end

            % Collect the data
            [Status,RecoveredData,e,f] =
calllib('nicaiu','DAQmxReadAnalogF64',TaskHandle1Numeric,int32(InputSampl
esPerChannel),Timeout,FillMode,RecoveredInputDataPtr,uint32(InputSamplesP
erChannel*NumberOfRXChannels),ReadPtr,ReservedPtr);
            % [int32, doublePtr, int32Ptr, uint32Ptr]
DAQmxReadAnalogF64(uint32, int32, double, uint32, doublePtr, uint32,
int32Ptr, uint32Ptr)
            % int32 DAQmxReadAnalogF64 (TaskHandle taskHandle, int32
numSampsPerChan, float64 timeout, bool32 fillMode, float64 readArray[],
uInt32 arraySizeInSamps,int32 *sampsPerChanRead, bool32 *reserved);
```

```
            if Status ~= 0,
                fprintf('Error in DAQmxReadAnalogF64.   Status =
%d\n',Status);
            end
            % If more than one A/D channel is used, then the sampes
should be separated
            RecoveredData =
reshape(RecoveredData,NumberOfRXChannels,InputSamplesPerChannel);

            % Stop the tasks
            Status =
calllib('nicaiu','DAQmxStopTask',TaskHandle1Numeric);
            % int32 DAQmxStopTask(uint32)
            % int32 DAQmxStopTask (TaskHandle taskHandle);
            if Status ~= 0,
                fprintf('Error in DAQmxStopTask.   Status =
%d\n',Status);
            end
            Status =
calllib('nicaiu','DAQmxStopTask',TaskHandle2Numeric);
            if Status ~= 0,
                fprintf('Error in DAQmxStopTask.   Status =
%d\n',Status);
            end

            % Save results structure to disc for later use
            Date = now;
            FileName = datestr(Date);
            % Replace colons
            for i=1:length(FileName),
                if (FileName(i) == ':')||(FileName(i) == ' '),
                    FileName(i) = '-';
                end
            end
            % Add extra Pre-fix
            FileName = strcat('Aziman-', FileName);
            fprintf('File name to be used = %s\n',FileName);
            save(FileName,
'RecoveredData','Date','TXSignalFFT','NumberOfRXChannels','InputSamplesPe
rChannel','InputSamplingRate','NumberOfSnapshots','SteppedFrequencyIndex'
,'Comment1','Comment2','Comment3')

            DoThis = 1;
            if DoThis == 1,
                % Fourier transform - normally an fft operates on each
colum on the matrix
                RecoveredDataFFT =
fft(RecoveredData,InputSamplesPerChannel,2);
                % Calculate the averaged cross-spectrum
                CrossSpectrum = CrossSpectrum +
RecoveredDataFFT.*repmat(TXSignalFFT,NumberOfRXChannels,1);
                % Calculate the averaged power-spectrum
                PowerSpectrum = PowerSpectrum +
RecoveredDataFFT.*conj(RecoveredDataFFT);
                % Only display on single snapshot usage - takes up too
much time otherwise
                DisplayThis = 1;
                if DisplayThis == 1,
```

```
                    % Display data for channel 1
                    InputSensorIndex = 1;
                    figure(3)
                    plot(TimeIndex,RecoveredData)
                    title('Raw Input Data')
                    xlabel('Time (s)')
                    ylabel('Voltage (V)')
                    %ylim([-1 1])
                    legend('RX0','RX1',0)
                    drawnow

                end
            end
        end

        DoThis = 1;
        if DoThis == 1,
            count=count+1;
            % Normalise by the number of snapshots
            CrossSpectrum = CrossSpectrum ./ NumberOfSnapshots;
            PowerSpectrum = PowerSpectrum ./ NumberOfSnapshots;

            % normalise the cross-spectrum
            %CrossSpectrum = CrossSpectrum ./
(PowerSpectrum.*repmat(TXSignalFFT.*conj(TXSignalFFT),NumberOfRXChannels,
1)).^0.5;
            index=round(SteppedFrequencyIndex/FrequencyIndex(2))+1;
            Rec1(count)=RecoveredDataFFT(1,index);
            Rec2(count)=RecoveredDataFFT(2,index);
            Rec3(count)=RecoveredDataFFT(3,index);
            Rec4(count)=RecoveredDataFFT(4,index);
            CRec1(count)=CrossSpectrum(1,index);
            CRec2(count)=CrossSpectrum(2,index);
            CRec3(count)=CrossSpectrum(3,index);
            CRec4(count)=CrossSpectrum(4,index);
            RecIndex(count)=index;

            phaseDiff1=abs(angle(RecoveredDataFFT(1,index))-
angle(RecoveredDataFFT(2,index)));
            phaseDiff2=abs(angle(RecoveredDataFFT(2,index))-
angle(RecoveredDataFFT(3,index)));
            phaseDiff3=abs(angle(RecoveredDataFFT(3,index))-
angle(RecoveredDataFFT(4,index)));

            phaseDiff1=abs(angle(CrossSpectrum(1,index))-
angle(CrossSpectrum(2,index)));
            phaseDiff2=abs(angle(CrossSpectrum(2,index))-
angle(CrossSpectrum(3,index)));
            phaseDiff3=abs(angle(CrossSpectrum(3,index))-
angle(CrossSpectrum(4,index)));


                DisplayThis = 1; % ctrl R % remove ctrl T
            if  DisplayThis == 1,
                figure(21)
                hold on
```

```
plot(SteppedFrequencyIndex,phaseDiff1,'x','color','blue');
               plot(SteppedFrequencyIndex,phaseDiff2,'x','color','red');

plot(SteppedFrequencyIndex,phaseDiff3,'x','color','green');
               title('PhaseDiff')
               xlabel('Frequency (Hz)')
               ylabel('Phase Diffrent (Rad')
               drawnow;
            end

           RotationThreshold=EstimatedVelocity/(2*SensorSpacing);

NumOfPhaseRotation=floor(SteppedFrequencyIndex/RotationThreshold);

           if phaseDiff1>pi,
               phaseDiff1=((NumOfPhaseRotation+1)*2*pi)-phaseDiff1;
           else
               phaseDiff1=(NumOfPhaseRotation*2*pi)-phaseDiff1;
           end
           if phaseDiff2>pi,
                phaseDiff2=((NumOfPhaseRotation+1)*2*pi)-phaseDiff2;
           else
               phaseDiff2=(NumOfPhaseRotation*2*pi)-phaseDiff2;
           end
           if phaseDiff3>pi,
                phaseDiff3=((NumOfPhaseRotation+1)*2*pi)-phaseDiff3;
           else
               phaseDiff3=(NumOfPhaseRotation*2*pi)-phaseDiff3;
           end

            phaseDiff1=abs(phaseDiff1);
            phaseDiff2=abs(phaseDiff2);
            phaseDiff3=abs(phaseDiff3);


estVelocity1=2*pi*SteppedFrequencyIndex*SensorSpacing/phaseDiff1;

estVelocity2=2*pi*SteppedFrequencyIndex*SensorSpacing/phaseDiff2;

estVelocity3=2*pi*SteppedFrequencyIndex*SensorSpacing/phaseDiff3;
            RecEstVelocity1(count)=estVelocity1;
            RecEstVelocity2(count)=estVelocity2;
            RecEstVelocity3(count)=estVelocity3;
            disp(['Estimated velocity: ' num2str(estVelocity1)]);
            % plot magnitude and phase of cross-spectrum
            DisplayThis = 0;
            if DisplayThis == 1,
                figure(5)
                plot(FrequencyIndex,abs(CrossSpectrum));
                title('Normalised Cross-Spectrum')
                xlabel('Frequency (Hz)')
                ylabel('Spectrum Level')
                xlim([0 OutputSamplingRate*PassBandFraction])
                ylim([0 1.01])
                figure(6)
                plot(FrequencyIndex,angle(CrossSpectrum));
                title('Cross-Spectrum Phase')
```

```
                xlabel('Frequency (Hz)')
                ylabel('Phase (rads)')
                xlim([0 OutputSamplingRate*PassBandFraction])
                figure(7)

plot(FrequencyIndex,angle(CrossSpectrum.*repmat(CompensationFunction,Numb
erOfRXChannels,1)));
                title('Compensated Cross-Spectrum Phase')
                xlabel('Frequency (Hz)')
                ylabel('Phase (rads)')
                xlim([0 OutputSamplingRate*PassBandFraction])
            end
            figure(20)
            hold on;
            if estVelocity1<500,
                plot(SteppedFrequencyIndex,
estVelocity1,'x','color','blue');
            end
            if estVelocity2<500,
                plot(SteppedFrequencyIndex,
estVelocity2,'x','color','red');
            end
            if estVelocity3<500,
                plot(SteppedFrequencyIndex,
estVelocity3,'x','color','green');
            end
            xlabel('Frequency, Hz'); ylabel('Velocity, m/s');
            drawnow;


        end
    end
end

%% Clear the tasks
Status = calllib('nicaiu','DAQmxClearTask',TaskHandle1Numeric);
% int32 DAQmxClearTask(uint32)
% int32 DAQmxClearTask (TaskHandle taskHandle);
if Status ~= 0,
    fprintf('Error in DAQmxClearTask.   Status = %d\n',Status);
    return
end
Status = calllib('nicaiu','DAQmxClearTask',TaskHandle2Numeric);
if Status ~= 0,
    fprintf('Error in DAQmxClearTask.   Status = %d\n',Status);
    return
end

unloadlibrary 'nicaiu';                % unload library


return
```

B(2). Matlab script for processing data captured from step frequency;

```
% AnalyseAzimanStepFrequency
% Script to analyse data collected with Aziman Soil Exp

clear

DisplayCompensatedPhase = 0;
pingCount=1;
SnapShotNumber=1;
if exist('C:\Users\aziman\Documents\MATLAB\AzimanData\','file'),
    PathName = 'C:\Users\aziman\Documents\MATLAB\AzimanData\';
end

FileNameStub = 'Aziman-06-Aug-2010';
% Load data files generated on that day
FileNameList = dir([PathName FileNameStub '*.mat']);

NumberOfFiles = numel(FileNameList);
if NumberOfFiles == 0,
    disp('No files found');
    return
end
disp(NumberOfFiles)
for FileNameIndex = 1:NumberOfFiles,
    % Extract file name
    FileName = [PathName FileNameList(FileNameIndex).name];
    % Open file
    if exist(FileName,'file'),
        fprintf('Processing file %s\n',FileName);
        load(FileName);
    else
        disp('File not found')
        return
    end
    dotPos=strfind(FileName,'.');
    hh(FileNameIndex)=str2double(FileName(dotPos-8:dotPos-7));
    mm(FileNameIndex)=str2double(FileName(dotPos-5:dotPos-4));
    ss(FileNameIndex)=str2double(FileName(dotPos-2:dotPos-1));
    % Reserve and initialise variables on the first data load
    if FileNameIndex == 1,
        NumberOfTXChannels = 1; % Define the number of TX channels being
used
        OutputSamplesPerChannel = InputSamplesPerChannel; % Samples to be
output per channel
        % Predicted input A/D channel latency
        PredictedInputLatency = 38.4/InputSamplingRate + 3e-6;     %
latency measured in seconds

        % Predict output D/A latency
        OutputLatency = [3e-6 5e-6 7.5e-6 9.5e-6];
        PredictedOutputLatency = OutputLatency(NumberOfTXChannels);

        % Measurements imply an extra few samples of delay
        AdditionalDelaySamples = 2;
```

```
        TotalPredictedLatency = PredictedOutputLatency +
PredictedInputLatency + AdditionalDelaySamples/InputSamplingRate + 1.8e-
6;


        % Time index for display purposes
        TimeIndex = (0:(InputSamplesPerChannel-1))/InputSamplingRate;
        % Frequency index for display purposes - assuming zero padded
        FrequencyIndex = (0:(InputSamplesPerChannel -
1)).*InputSamplingRate./InputSamplesPerChannel;

        PhaseSpectrum = zeros(NumberOfRXChannels,InputSamplesPerChannel);
        CrossSpectrum = zeros(NumberOfRXChannels,InputSamplesPerChannel);
        PowerSpectrum = zeros(NumberOfRXChannels,InputSamplesPerChannel);
        AvgDataFFT = zeros(NumberOfRXChannels,InputSamplesPerChannel);
    end

    % Fourier transform - normally fft operates on each column on the
matrix
    RecoveredDataFFT = fft(RecoveredData,InputSamplesPerChannel,2);
    Sensor1Max(SnapShotNumber)=max(RecoveredData(1,:));
    Sensor1Min(SnapShotNumber)=min(RecoveredData(1,:));
    AmplitudeSensor1(SnapShotNumber)=Sensor1Max(SnapShotNumber)-
Sensor1Min(SnapShotNumber);

    Sensor2Max(SnapShotNumber)=max(RecoveredData(2,:));
    Sensor2Min(SnapShotNumber)=min(RecoveredData(2,:));
    AmplitudeSensor2(SnapShotNumber)=Sensor2Max(SnapShotNumber)-
Sensor2Min(SnapShotNumber);

    Sensor3Max(SnapShotNumber)=max(RecoveredData(3,:));
    Sensor3Min(SnapShotNumber)=min(RecoveredData(3,:));
    AmplitudeSensor3(SnapShotNumber)=Sensor3Max(SnapShotNumber)-
Sensor3Min(SnapShotNumber);

    Sensor4Max(SnapShotNumber)=max(RecoveredData(4,:));
    Sensor4Min(SnapShotNumber)=min(RecoveredData(4,:));
    AmplitudeSensor4(SnapShotNumber)=Sensor4Max(SnapShotNumber)-
Sensor4Min(SnapShotNumber);

    RecoveredData1 = fft(RecoveredData,InputSamplesPerChannel,2);

    if SnapShotNumber==NumberOfSnapshots,


        AvgDataFFT = AvgDataFFT + RecoveredDataFFT;

        AvgAmplitudeSensor1=mean(AmplitudeSensor1);
        AvgAmplitudeSensor2=mean(AmplitudeSensor2);
        AvgAmplitudeSensor3=mean(AmplitudeSensor3);
        AvgAmplitudeSensor4=mean(AmplitudeSensor4);

        AmpSensor1(pingCount)=AvgAmplitudeSensor1;
        AmpSensor2(pingCount)=AvgAmplitudeSensor2;
        AmpSensor3(pingCount)=AvgAmplitudeSensor3;
        AmpSensor4(pingCount)=AvgAmplitudeSensor4;
```

```
NormalisedWithSensor11(pingCount)=20*log10(AvgAmplitudeSensor1./AvgAmplit
udeSensor1);

NormalisedWithSensor12(pingCount)=20*log10(AvgAmplitudeSensor2./AvgAmplit
udeSensor1);

NormalisedWithSensor13(pingCount)=20*log10(AvgAmplitudeSensor3./AvgAmplit
udeSensor1);

NormalisedWithSensor14(pingCount)=20*log10(AvgAmplitudeSensor4./AvgAmplit
udeSensor1);

        index=round(SteppedFrequencyIndex/FrequencyIndex(2))+1;

        for chanNum=1:NumberOfRXChannels,
            RecordDataFFT(chanNum, pingCount,
SnapShotNumber)=RecoveredDataFFT(chanNum, index);
        end

        Frequency(pingCount)=FrequencyIndex(index);

        ResultTXSignalFFT(pingCount)=TXSignalFFT(index);

        for chanNum=1:NumberOfRXChannels,

ResultAvgDataFFT(chanNum,pingCount)=AvgDataFFT(chanNum,index);
        end

        AvgDataFFT = zeros(NumberOfRXChannels,InputSamplesPerChannel);

        pingCount=pingCount+1;
        SnapShotNumber=1;
    else
        index=round(SteppedFrequencyIndex/FrequencyIndex(2))+1;

        for chanNum=1:NumberOfRXChannels,
            RecordDataFFT(chanNum, pingCount,
SnapShotNumber)=RecoveredDataFFT(chanNum, index);
        end
        SnapShotNumber=SnapShotNumber+1;

        AvgDataFFT = AvgDataFFT + RecoveredDataFFT;

% Only display on single snapshot usage - takes up too much time
otherwise
        DisplayThis = 0;
        if DisplayThis == 1,
            % Display data for channel 1
            InputSensorIndex = 1;
            figure(3)
            plot(TimeIndex,RecoveredData)
            title('Raw Input Data')
            xlabel('Time (s)')
            ylabel('Voltage (V)')
            ylim([-1 1])
```

```
            drawnow

            figure(4)
            plot(FrequencyIndex,20*log10(abs(TXSignalFFT)),'r')
            hold on
            plot(FrequencyIndex,20*log10(abs(RecoveredDataFFT)),'k');
            hold off
            legend('Drive Signal','Sense Signals',0)
            ylabel('Spectral Amplitude (dB)')
            xlabel('Frequency (Hz)')
            title('Linear Spectra of Transmit and Received Signals');
            xlim([0 InputSamplingRate*PassBandFraction]);
            drawnow
        end
    end
end

% AmplitudeFunction = sinc(Frequency/InputSamplingRate);
 CompensationFunction =  exp(j*2*pi*Frequency*TotalPredictedLatency);
 CrossSpectrum =
ResultAvgDataFFT.*repmat(ResultTXSignalFFT,NumberOfRXChannels,1);
 PowerSpectrum = ResultAvgDataFFT.*conj(ResultAvgDataFFT);
 CompCrossSpectrum =
CrossSpectrum.*repmat(CompensationFunction,NumberOfRXChannels,1);

 phaseCross1=CrossSpectrum(1,:).*conj(CrossSpectrum(2,:));
 phaseCross2=CrossSpectrum(2,:).*conj(CrossSpectrum(3,:));
 phaseCross3=CrossSpectrum(3,:).*conj(CrossSpectrum(4,:));
 figure(18);
 plot(Frequency,angle(phaseCross1));
save('ProcessedData.mat','CrossSpectrum','ResultTXSignalFFT','ResultAvgDa
taFFT','RecordDataFFT','CompensationFunction','Frequency')
```

B(3). Matlab script for calculated coherences and phase velocities for each sensor-pair;

```
clear all
load ProcessedData_28Jul_03  %file name
cohThresh=0.9;
minFreq=190;
maxFreq=2510;
depthFreqStep=5;
SensorSpacing = 0.03;

% LOAD SETNUM ONLY
for setNum=1,
    phaseCross(1,:)=ResultAvgDataFFT(1,:).*conj(ResultAvgDataFFT(2,:));
    phaseCross(2,:)=ResultAvgDataFFT(2,:).*conj(ResultAvgDataFFT(3,:));
    phaseCross(3,:)=ResultAvgDataFFT(3,:).*conj(ResultAvgDataFFT(4,:));

phaseD(1,:)=angle(ResultAvgDataFFT(1,:))-angle(ResultAvgDataFFT(2,:));
phaseD(2,:)=angle(ResultAvgDataFFT(2,:))-angle(ResultAvgDataFFT(3,:));
phaseD(3,:)=angle(ResultAvgDataFFT(3,:))-angle(ResultAvgDataFFT(4,:));
```

```
    [chanNum,freqIndexTotal,avgNum]=size(RecordDataFFT);

    for index=1:freqIndexTotal,
        myCrossCoh(1,index)=(1/(avgNum-
1))*(sum((RecordDataFFT(1,index,:)-
mean(RecordDataFFT(1,index,:))).*conj((RecordDataFFT(2,index,:)-
mean(RecordDataFFT(2,index,:)))))/(var(RecordDataFFT(1,index,:))*var(Rec
ordDataFFT(2,index,:)))^0.5;
        myCrossCoh(2,index)=(1/(avgNum-
1))*(sum((RecordDataFFT(2,index,:)-
mean(RecordDataFFT(2,index,:))).*conj((RecordDataFFT(3,index,:)-
mean(RecordDataFFT(3,index,:)))))/(var(RecordDataFFT(2,index,:))*var(Rec
ordDataFFT(3,index,:)))^0.5;
        myCrossCoh(3,index)=(1/(avgNum-
1))*(sum((RecordDataFFT(3,index,:)-
mean(RecordDataFFT(3,index,:))).*conj((RecordDataFFT(4,index,:)-
mean(RecordDataFFT(4,index,:)))))/(var(RecordDataFFT(3,index,:))*var(Rec
ordDataFFT(4,index,:)))^0.5;
    end



    for comp=1:3,
        for index=1:freqIndexTotal,
            if (abs(myCrossCoh(comp,index))>cohThresh),
                phaseCoh(comp,index)=angle(phaseCross(comp,index));
            else
                phaseCoh(comp,index)=0;
            end
        end
    end

    count=0;
    phaseCross1unwrap=unwrap(angle(phaseCross(1,:)));
    for index=1:freqIndexTotal,
        if (abs(myCrossCoh(1,index))>cohThresh) &
(Frequency(index)>minFreq) & (Frequency(index)<maxFreq)
            count=count+1;
            phaseCoh1(count)=phaseCross1unwrap(1,index);
            freq1(count)=Frequency(index);
        end
    end
    if count>0,
        P1=polyfit(freq1,phaseCoh1,1);
    end
    count=0;
    phaseCross3unwrap=unwrap(angle(phaseCross(3,:)));
    for index=1:freqIndexTotal,
        if (abs(myCrossCoh(3,index))>cohThresh) &
(Frequency(index)>minFreq) & (Frequency(index)<maxFreq)
            count=count+1;
            phaseCoh3(count)=phaseCross3unwrap(1,index);
            freq3(count)=Frequency(index);
        end
    end
    if count>0,
        P3=polyfit(freq3,phaseCoh3,1);
    end
```

```
Vph(1,:)=abs(2*pi*Frequency*SensorSpacing./unwrap(angle(phaseCross(1,:)))
);
%
Vph(2,:)=abs(2*pi*Frequency*SensorSpacing./unwrap(angle(phaseCross(2,:)))
); % (off Vph(2,:) if seismic source in the middle of array)

Vph(3,:)=abs(2*pi*Frequency*SensorSpacing./unwrap(angle(phaseCross(3,:)))
);
        VphCoh12=abs(2*pi*freq1*SensorSpacing./phaseCoh1);
%         VphCoh23=abs(2*pi*freq2*SensorSpacing./phaseCoh2); % (off
VphCoh23 if seismic source in the middle of array)
        VphCoh34=abs(2*pi*freq3*SensorSpacing./phaseCoh3);
        Vph1=transpose(Vph);
        Frequency1=transpose(Frequency);
        xlswrite('Frequency1.xls',Frequency1)
        xlswrite('Vph1.xls',Vph1);
        VphCoh12=transpose(VphCoh12);
        VphCoh34=transpose(VphCoh34);
        xlswrite('VphCoh12.xls',VphCoh12);
%         xlswrite('VphCoh23.xls',VphCoh23);
        xlswrite('VphCoh34.xls',VphCoh34);
        freq12=transpose(freq1);
        xlswrite('freq12.xls',freq12);
%         xlswrite('freq2.xls',freq2);
        freq34=transpose(freq3);
        xlswrite('freq34.xls',freq34);


% this plot for all velocity across the frequency without considered
coherence
drawthis=1;
    if drawthis==1,
        figure(30);

plot(Frequency,abs(2*pi*Frequency*SensorSpacing./unwrap(angle(phaseCross(
1,:)))),'b','linewidth',2);
        hold on
%
plot(Frequency,abs(2*pi*Frequency*SensorSpacing./unwrap(angle(phaseCross(
2,:)))),'g','linewidth',2);
%         hold on

plot(Frequency,abs(2*pi*Frequency*SensorSpacing./unwrap(angle(phaseCross(
3,:)))),'m','linewidth',2);
        hold off
        legend('A-B','C-D',0)
        titleH=title('');
        xLabelH=xlabel('Frequency, Hz');
        yLabelH=ylabel('Phase Velocity, m/s');
        set(xLabelH,'FontSize',18);
        set(xLabelH,'FontWeight','Demi');
        set(yLabelH,'FontSize',18);
        set(yLabelH,'FontWeight','Demi');
        set(titleH,'FontSize',18);
        set(titleH,'FontWeight','Demi');
        set(gca,'XLim',[minFreq,maxFreq]);
        set(gca,'FontSize',18);
```

```
        set(gca,'FontWeight','Demi');
        set(gcf,'PaperUnits','inches','PaperPosition',[0 0 7 4])
        grid on
end


% this plot for only velocity that higher than stated coherence
 drawthis=1;
    if drawthis==1,
        figure(40);

plot(freq1,abs(2*pi*freq1*SensorSpacing./phaseCoh1),'b','linewidth',2);
        hold on
%
plot(freq2,2*pi*freq2*SensorSpacing./abs(phaseCoh2),'g','linewidth',2);
%         hold on

plot(freq3,abs(2*pi*freq3*SensorSpacing./phaseCoh3),'m','linewidth',2);
        hold off
        legend('A-B','C-D',0)
        %titleH=title('Phase velocity of clay');
        xLabelH=xlabel('Frequency, Hz');
        yLabelH=ylabel('Phase Velocity, m/s');
        set(xLabelH,'FontSize',18);
        set(xLabelH,'FontWeight','Demi');
        set(yLabelH,'FontSize',18);
        set(yLabelH,'FontWeight','Demi');
        set(titleH,'FontSize',18);
        set(titleH,'FontWeight','Demi');
        set(gca,'XLim',[minFreq,maxFreq]);
        set(gca,'FontSize',18);
        set(gca,'FontWeight','Demi');
        set(gcf,'PaperUnits','inches','PaperPosition',[0 0 7 4])
        grid on
 end

  drawthis=1;
    if drawthis==1,
        figure(5);
        plot(Frequency,abs(myCrossCoh(1,:)),'b','linewidth',2);
        hold on
%         plot(Frequency,abs(myCrossCoh(2,:)),'g','linewidth',2);
%         hold on
        plot(Frequency,abs(myCrossCoh(3,:)),'m','linewidth',2);
        hold off
        legend('A-B','C-D',0)
        %titleH=title('Typical normalised coherence for both receiver');
        xLabelH=xlabel('Frequency, Hz');
        yLabelH=ylabel('Normalise coherence');
        set(xLabelH,'FontSize',18);
        set(xLabelH,'FontWeight','Demi');
        set(yLabelH,'FontSize',18);
        set(yLabelH,'FontWeight','Demi');
        set(titleH,'FontSize',18);
        set(titleH,'FontWeight','Demi');
        set(gca,'XLim',[minFreq,maxFreq]);
        set(gca,'YLim',[0,1]);
        set(gca,'FontSize',18);
```

```
        set(gca,'FontWeight','Demi');
        set(gcf,'PaperUnits','inches','PaperPosition',[0 0 7 4])
        grid on
    end

  drawthis=1;
    if drawthis==1,
        figure(10)
        hold on
        plot(Frequency,angle(phaseCross(1,:)),'blue','linewidth',2);
%       plot(Frequency,angle(phaseCross(2,:)),'green','linewidth',2);
        plot(Frequency,angle(phaseCross(3,:)),'red','linewidth',2);
        legendH=legend('A-B','C-D',1);
        %titleH=title('Phase difference');
        xLabelH=xlabel('Frequency (Hz)');
        yLabelH=ylabel('Phase difference (radians)');
        set(legendH,'FontSize',14);
        set(legendH,'FontWeight','Demi');
        set(xLabelH,'FontSize',18);
        set(xLabelH,'FontWeight','Demi');
        set(yLabelH,'FontSize',18);
        set(yLabelH,'FontWeight','Demi');
        set(titleH,'FontSize',18);
        set(titleH,'FontWeight','Demi');
        set(gca,'XLim',[minFreq,maxFreq]);
        set(gca,'FontSize',18);
        set(gca,'FontWeight','Demi');
        set(gcf,'PaperUnits','inches','PaperPosition',[0 0 7 4])
        grid on
    end

    drawthis=1;
    if drawthis==1,
        figure(12)
        hold on
   plot(Frequency,unwrap(angle(phaseCross(1,:))),'blue','linewidth',2);

%plot(Frequency,unwrap(angle(phaseCross(2,:))),'green','linewidth',2);

plot(Frequency,unwrap(angle(phaseCross(3,:))),'red','linewidth',2);
        legendH=legend('A-B','C-D',2);
        %titleH=title('Phase difference');
        xLabelH=xlabel('Frequency, Hz');
        yLabelH=ylabel('Unwrapped phase difference, radians');
        set(legendH,'FontSize',14);
        set(legendH,'FontWeight','Demi');
        set(xLabelH,'FontSize',18);
        set(xLabelH,'FontWeight','Demi');
        set(yLabelH,'FontSize',18);
        set(yLabelH,'FontWeight','Demi');
        set(titleH,'FontSize',18);
        set(titleH,'FontWeight','Demi');
        set(gca,'XLim',[minFreq,maxFreq]);
        set(gca,'FontSize',18);
        set(gca,'FontWeight','Demi');
        set(gcf,'PaperUnits','inches','PaperPosition',[0 0 7 4])
        %print(gcf,'-dtiffnocompression',tiffFileName,'-r600');
        grid on
```

```
    end

    drawthis=1;
    if drawthis==1,
        figure(15);
        plot(Frequency, abs(myCrossCoh(1,:)),'linewidth',2);
        titleH=title('Typical normalised coherence (1st set receiver)');
        xLabelH=xlabel('Frequency (Hz)');
        yLabelH=ylabel('Normalised coherence');
        set(xLabelH,'FontSize',18);
        set(xLabelH,'FontWeight','Demi');
        set(yLabelH,'FontSize',18);
        set(yLabelH,'FontWeight','Demi');
        set(titleH,'FontSize',18);
        set(titleH,'FontWeight','Demi');
        set(gca,'XLim',[minFreq,maxFreq]);
        set(gca,'YLim',[0,1]);
        set(gca,'FontSize',18);
        set(gca,'FontWeight','Demi');
        set(gcf,'PaperUnits','inches','PaperPosition',[0 0 7 4])
        grid on
    end
%  drawthis=1;
%     if drawthis==1,
%         figure(15);
%         plot(Frequency, abs(myCrossCoh(2,:)),'linewidth',2);
%         titleH=title('Typical Normalised Coherence (Set with Sand)');
%         xLabelH=xlabel('Frequency (Hz)');
%         yLabelH=ylabel('Normalised Coherence');
%         set(xLabelH,'FontSize',18);
%         set(xLabelH,'FontWeight','Demi');
%         set(yLabelH,'FontSize',18);
%         set(yLabelH,'FontWeight','Demi');
%         set(titleH,'FontSize',18);
%         set(titleH,'FontWeight','Demi');
%         set(gca,'XLim',[490,1410]);
%         set(gca,'YLim',[0,1]);
%         set(gca,'FontSize',18);
%         set(gca,'FontWeight','Demi');
%         set(gcf,'PaperUnits','inches','PaperPosition',[0 0 7 4])
%         print(gcf,'-dtiffnocompression',tiffFileName,'-r600');
%         grid on
%     end

    drawthis=1;
    if drawthis==1,
        figure(20);
        plot(Frequency, abs(myCrossCoh(3,:)),'linewidth',2);
        titleH=title('Typical normalised coherence (2nd set receiver)');
        xLabelH=xlabel('Frequency (Hz)');
        yLabelH=ylabel('Normalised coherence');
        set(xLabelH,'FontSize',18);
        set(xLabelH,'FontWeight','Demi');
        set(yLabelH,'FontSize',18);
        set(yLabelH,'FontWeight','Demi');
        set(titleH,'FontSize',18);
        set(titleH,'FontWeight','Demi');
        set(gca,'XLim',[minFreq,maxFreq]);
```

```
        set(gca,'YLim',[0,1]);
        set(gca,'FontSize',18);
        set(gca,'FontWeight','Demi');
        set(gcf,'PaperUnits','inches','PaperPosition',[0 0 7 4])
        %print(gcf,'-dtiffnocompression',tiffFileName,'-r600');
        grid on
    end


    return
```

B(4). Matlab script for calculated weighted-mean and non-weighted mean phase velocities for each sensor-pair;

```
clear all
load ProcessedData_19Jun7cm3cmSrcStart_11    % File name
cohThresh=0.9;
rxSpacing=[0.03, 0.03, 0.03];

setNum=1;
for setNum=1,
    phaseCross(1,:)=ResultAvgDataFFT(1,:).*conj(ResultAvgDataFFT(2,:));
    phaseCross(2,:)=ResultAvgDataFFT(2,:).*conj(ResultAvgDataFFT(3,:));
    phaseCross(3,:)=ResultAvgDataFFT(3,:).*conj(ResultAvgDataFFT(4,:));

    [chanNum,freqIndexTotal,avgNum]=size(RecordDataFFT);

    for index=1:freqIndexTotal,
        % Note that the Matlab 'var' command normalises by N-1.
        myCrossCoh(1,index)=(1/(avgNum-
1))*(sum((RecordDataFFT(1,index,:)-
mean(RecordDataFFT(1,index,:))).*conj((RecordDataFFT(2,index,:)-
mean(RecordDataFFT(2,index,:))))))/(var(RecordDataFFT(1,index,:))*var(Rec
ordDataFFT(2,index,:)))^0.5;
        myCrossCoh(2,index)=(1/(avgNum-
1))*(sum((RecordDataFFT(2,index,:)-
mean(RecordDataFFT(2,index,:))).*conj((RecordDataFFT(3,index,:)-
mean(RecordDataFFT(3,index,:))))))/(var(RecordDataFFT(2,index,:))*var(Rec
ordDataFFT(3,index,:)))^0.5;
        myCrossCoh(3,index)=(1/(avgNum-
1))*(sum((RecordDataFFT(3,index,:)-
mean(RecordDataFFT(3,index,:))).*conj((RecordDataFFT(4,index,:)-
mean(RecordDataFFT(4,index,:))))))/(var(RecordDataFFT(3,index,:))*var(Rec
ordDataFFT(4,index,:)))^0.5;
    end

    drawthis=0;
    if drawthis==1,
        figure(40);
        plot(Frequency, abs(myCrossCoh(1,:)),'linewidth',2);
        titleH=title('Typical Normalised Coherence (1st Set with
Columns)');
        xLabelH=xlabel('Frequency (Hz)');
        yLabelH=ylabel('Normalised Coherence');
        set(xLabelH,'FontSize',18);
```

```
        set(xLabelH,'FontWeight','Demi');
        set(yLabelH,'FontSize',18);
        set(yLabelH,'FontWeight','Demi');
        set(titleH,'FontSize',18);
        set(titleH,'FontWeight','Demi');
        set(gca,'XLim',[490,1410]);
        set(gca,'FontSize',18);
        set(gca,'FontWeight','Demi');
        set(gcf,'PaperUnits','inches','PaperPosition',[0 0 7 4])
        grid on
    end
end
    minFreq1=190;% Selection of frequencies based on near array effect
    maxFreq1=1200; % Selection of frequencies based on far array effect
    minFreq2=190;
    maxFreq2=1200;
    minFreq3=190;
    maxFreq3=1200;
    depthFreqStep=10;
    count=0;
    for index=1:freqIndexTotal,
        if (abs(myCrossCoh(1,index))>cohThresh) &
(Frequency(index)>minFreq1) & (Frequency(index)<maxFreq1)
            count=count+1;
            phaseCoh1(count)=angle(phaseCross(1,index));
            cohRec1(count)=abs(myCrossCoh(1,index));
            weight1(count)=cohRec1(count)^2/(1-cohRec1(count)^2);
            freq1(count)=Frequency(index);
        end
    end
    phaseCoh1u=unwrap(phaseCoh1);
    VelHard1=abs(2*pi*freq1.*rxSpacing(1)./phaseCoh1u);
    vhmean1=repmat(mean(VelHard1),1,length(VelHard1));
vhweightmean1=repmat(sum(VelHard1.*weight1)/sum(weight1),1,length(VelHard
1));
    if count>0,
        P1=polyfit(freq1,phaseCoh1,1);
    end
    count=0;
    for index=1:freqIndexTotal,
        if (abs(myCrossCoh(2,index))>cohThresh) &
(Frequency(index)>minFreq2) & (Frequency(index)<maxFreq2)
            count=count+1;
            phaseCoh2(count)=angle(phaseCross(2,index));
            cohRec2(count)=abs(myCrossCoh(2,index));
            weight2(count)=cohRec2(count)^2/(1-cohRec2(count)^2);
            freq2(count)=Frequency(index);
        end
    end
    phaseCoh2u=unwrap(phaseCoh2);
    VelHard2=abs(2*pi*freq2.*rxSpacing(2)./phaseCoh2u);
    vhmean2=repmat(mean(VelHard2),1,length(VelHard2));

vhweightmean2=repmat(sum(VelHard2.*weight2)/sum(weight2),1,length(VelHard
2));
    if count>0,
        P2=polyfit(freq2,phaseCoh2,1);
    end
    count=0;
```

```
    for index=1:freqIndexTotal,
        if (abs(myCrossCoh(3,index))>cohThresh) &
(Frequency(index)>minFreq3) & (Frequency(index)<maxFreq3)
            count=count+1;
            phaseCoh3(count)=angle(phaseCross(3,index));
            cohRec3(count)=abs(myCrossCoh(3,index));
            weight3(count)=cohRec3(count)^2/(1-cohRec3(count)^2);
            freq3(count)=Frequency(index);
        end
    end
    phaseCoh3u=unwrap(phaseCoh3);
    VelHard3=abs(2*pi*freq3.*rxSpacing(3)./phaseCoh3u);
    vhmean3=repmat(mean(VelHard3),1,length(VelHard3));

vhweightmean3=repmat(sum(VelHard3.*weight3)/sum(weight3),1,length(VelHard
3));
    if count>0,
        P3=polyfit(freq3,phaseCoh3,1);
    end


    return
```